Electric Technology U.S.S.R.

ЭЛЕКТРИЧЕСТВО

Volume 1, May, 1958

Selected papers from
Elektrichestvo Nos. 1-4, 1957

Published by

PERGAMON PRESS NEW YORK LONDON PARIS LOS ANGELES

for Pergamon Institute, New York and London, a non-profit-making foundation

1958

PERGAMON INSTITUTE

A NON-PROFIT FOUNDATION FOR THE FURTHERANCE
AND DISSEMINATION OF SCIENTIFIC KNOWLEDGE

Joint Presidents of the Board of Governors:

Dr. Detlev W. Bronk

Sir Robert Robinson, O.M., F.R.S.

Executive Director: Captain I. R. Maxwell

4 & 5 Fitzroy Square, London W.1

122 East 55th Street, New York 22, N.Y.

Financial assistance has also been received from A.S.E.A., Sweden

---

958

Elektrichestvo

Editor-in-Chief: N. G. DROZDOV

Deputy Editor-in-Chief: I. A. SYROMYATNIKOV

EDITORIAL BOARD

K. A. ANDRIANOV, N. I. BORISENKO, G. V. BUTKEVICH, M. G. CHILIKIN, A. A. GLAZUNOV, V. A. GOLUBTSOVA, E. G. KOMAR, M. P. KOSTENKO, L. R. NEIMAN, I. I. PETROV, V. I. POPKOV, A. M. FEDOSEEV, M. A. SHATELEN

1958

ELECTRIC TECHNOLOGY, U.S.S.R.

VOLUMES 1–4, 1958

Selected papers from *Elektrichestvo*, No. 1, 1957–No. 2, 1958

EDITORIAL BOARD

H. M. Barlow (London)
F. W. Bowden (San Luis Obispo)
F. Brailsford (London)
G. S. Brown (Cambridge, Mass.)
F. M. Bruce (Glasgow)
C. C. Carr (Brooklyn)
G. W. Carter (Leeds)
A. G. Conrad (New Haven, Conn.)
G. F. Corcoran (College Park, Md.)
J. D. Craggs (Liverpool)
A. L. Cullen (Sheffield)
G. E. Dreifke (St. Louis)
V. Easton (Birmingham)
A. R. Eckels (Vermont)
W. Fishwick (Swansea)
C. Froehlich (New York)
C. G. Garton (Leatherhead)
J. Greig (London)
L. D. Harris (Salt Lake City)
J. D. Horgan (Milwaukee)
E. C. Jones (Morgantown)
E. C. Jordan (Urbana)
I. H. Lovett (Rolla, Missouri)
J. M. Meek (Liverpool)
J. H. Mulligan Jnr. (N.Y.)
W. A. Murray (Blacksburg, Virginia)
J. E. Parton (Nottingham)
H. A. Peterson (Madison)
A. Porter (London)
J. C. Read (Rugby)
W. G. Shepherd (Minneapolis)
W. P. Smith (Lawrence, Kansas)
Philip Sporn (Chairman) (New York)
J. A. Strelzoff (East Lansing)
F. W. Tatum (Dallas, Texas)
C. V. O. Terwilliger (Monterey)
D. H. Tompsett (Stafford)
A. Tustin (London)
S. Reid Warren Jnr. (Philadelphia)
A. R. van C. Warrington (Stafford)
A. H. Waynick (Pa.)
E. M. Williams (Pittsburgh)
F. C. Williams (Manchester)
H. I. Wood (Manchester)
C. M. Zieman (Ohio)

PERGAMON PRESS LTD.

LONDON · NEW YORK · PARIS · LOS ANGELES

ELECTRIC TECHNOLOGY, U.S.S.R.

CONTENTS OF VOLUMES 1–4, 1958

Vol. 1

PAGE

V. I. Veits: Fundamentals of an interconnected power grid for the European part of the Soviet Union 1

I. I. Treshchev: Investigation of variable-speed a.c. machines 18

V. A. Naidis: The use of amplidynes and transistor amplifiers for industrial drives 35

R. I. Karaev: Short-circuit transients on long lines 46

M. M. Belousov: Rates of rise of restriking voltage across circuit-breakers contacts in large power systems 64

S. S. Roizen: Selection of antihunt transformers for amplidyne electric drives 74

I. P. Isaev: A statistical assessment of the stability of induction motor characteristics 83

B. A. Alekseev and V. B. Kulakolskii: The problem of impulse tests of the turn insulation of an h.v. machine 96

V. P. Larionov: Voltage gradients in a long-spark leader channel 106

A. B. Oslon: Measurement of earth resistances 111

L. F. Shkliarskii: Automation of electric drives for bucket-chain dredgers 120

A. D. Drozdov: Differential protection circuits with magnetic restraint 129

E. G. Shramkov, A. V. Mitkevich and N. B. Kovalev: The stabilities of measuring instruments using magnice and alnico 138

L. Z. Shenkman: Effect of exciter saturation on transients in synchronous machines 150

Tszo Khu: The behaviour of relay protection on unsynchronized reclosing 159

A. L. Livshits and I. S. Rogachev: Generators for electric spark-machining of metals . . . 170

Vol. 2–3 (combined volume)

N. I. Sokolov: Steady-state stability of a transmission system with controlled synchronous condensers at the sectionalizing substation 1

O. V. Slezhanovskii: Controlling a mill with separately driven rollers 12

N. N. Belyakov: Investigation of over-voltages due to arcing earth-faults in 6-10 kV systems with insulated neutral 25

V. Gusa and Ya. Tsigelka: Arc-quenching processes in air-blast circuit-breakers 37

M. O. Kamenetskii: Determination of the in-feed currents (from induction motors) to short-circuits in low-voltage systems 44

V. V. Burgsdorf: Wind pressure on overhead transmission line conductors 56

A. N. Kozhin: The protection of a regulating autotransformer 67

I. T. Zherdev: Current in the charge materials of a ferrosilicon furnace 75

Z. B. Neyman: Large synchronous motors with solid poles on the rotor 80

V. V. Titov and Z. B. Kogan: Turbogenerator rotor with direct cooling of the winding conductors 85

1958

A. G. Kraiz: High-voltage autotransformers 93

T. I. Smirnova: A new air-blast circuit-breaker for 220 kV 7000 MVA 103

G. I. Pertsov: A method for thermal calculations of mining combine motors 108

L. V. Karniushin: Velocity-time relations for electric drives for intermittent operation . . 122

S. V. Strakhov: A method of deriving equations for the electromechanical transient in electric circuits 139

A. A. Bal'chitis: The induction law for an electrostatic machine 156

D. P. Morozov and Yu. A. Bortsov: Generalized method of investigating the transient processes in electric drive systems 164

V. D. Kravchenko, V. I. Levitov and V. I. Popkov: Corona losses on live transmission lines 176

L. V. Tsukernik and N. A. Kachanova: Analysis of the static stability of complex power systems by electronic computers 183

G. G. Gimoyan: A practical method for designing relays with rectifiers 196

Yu. A. Glants: The use of load distribution diagrams for the design of urban systems . . 204

L. M. Lopshits: The nomogram for determining protective zones of lightning conductors . . 214

958

Vol. 4

I. N. Chupiatov and V. F. Baiko: Two-commutator rotary amplifier 1

N. A. Markov: The theory of the electrical circuit for the three-phase ore-reduction furnace . 10

V. I. Kliuchev: The universal characteristics of the dynamic braking of asynchronous motors 18

A. S. Maikopar and N. N. Beliakov: Arcing short-circuits on 400 kV transmission lines and methods of dealing with them 27

N. A. Melnikov, A. I. Gershengorn and A. N. Sherentsis: Earthwire earthing systems for long power-transmission lines 39

D. E. Artem'ev and S. S. Shur: Experimental determination of parameters of electro-transmission: Kuibyshev Hydro-electric Power Station—Moscow 52

E. A. Meerovich and V. K. Red'kin: Partial capacities (conductivities) of a system of electrodes and separate fluxes of the resultant field 70

F. F. Sokolov: The heat emission of rectifier stacks made of large selenium cells 78

A. N. Zeiliger and B. P. Novgorodtsev: The use of 220 kV lines with split conductors . . 87

G. G. Kostanian: Calculations of short-circuits in unbalanced phase transmission systems . . 97

D. P. Morozov, M. G. Chilikin, N. G. Lysenkov and L. M. Tverdin: A new circuit for high-speed pulse control in systems containing ionic converters 108

O. M. Kostiuk and V. E. Rybinskii: The controlled phase-type compound winding of synchronous generators with correlation as to voltage 118

A. A. Maslov: Transistor amplifiers of the alloy type 132

V. L. Inosov and V. E. Krutikova: A study of the synchronization process in compound excited motors 142

V. S. Burtakov and M. I. Glazov: The performance of current-measuring transformers under increased power output conditions 150

R. A. Mikaelian: A study of the effect of nozzle parameters on arc extinguishing by a compressed air jet 155

1958

FUNDAMENTALS OF AN INTERCONNECTED POWER GRID FOR THE EUROPEAN PART OF THE SOVIET UNION*

V. I. VEITS

"Krzhizhanov", Power Institute of the Academy of Sciences of the U.S.S.R.

(Received 12 September 1956)

The Sixth Five-Year-Plan initiates a new stage in the development of Soviet power production grid interconnexion of power systems.

When the Kuibyshev and Stalingrad power stations and the transmission systems connecting these Volga giants with the central systems and with the Central Black-earth Region, the South and the Urals have been commissioned during the present Five-Year-Plan the first section of the European U.S.S.R. grid will have been completed.

During this period the creation of a Siberian Grid (from Irkutsk to Novosibirsk) will be initiated. The Bratsk and Krasnoyarsk hydro-electric stations which are under construction will dominate the development of the Siberian Grid similarly to Kuibyshev and Stalingrad in the case of the European U.S.S.R. grid. Large transmission lines will connect Bratsk with the Krasnoyarsk and Irkutsk Cheremkhovsk systems, and Krasnoyarsk with the West Siberian systems. Later, the central Siberian grid will be linked with the European U.S.S.R. grid, thus producing an integrated Soviet grid system. The Caucasian and north-west systems will then be connected and a number of Kazakhstan systems will be connected to the European and Siberian grids. Central-Asian and Far-Eastern power systems will be developed. Nuclear power stations will become more important which will affect the development of the U.S.S.R. grid systems in many ways.

The grid ensures the most efficient use of the various sources and provides maximum flexibility and economy. It is now no longer correct

* *Elektrichestvo* No. 1, 1–8 (1957). [Reprint Order No. EL. 1]

to plan power stations and high-voltage systems without considering their part in the future grid.

Areas of the European U.S.S.R. grid

The first stage of the European U.S.S.R. grid covers the following areas: (Fig.1) The Central, Volga, Central Black-earth Region, South,

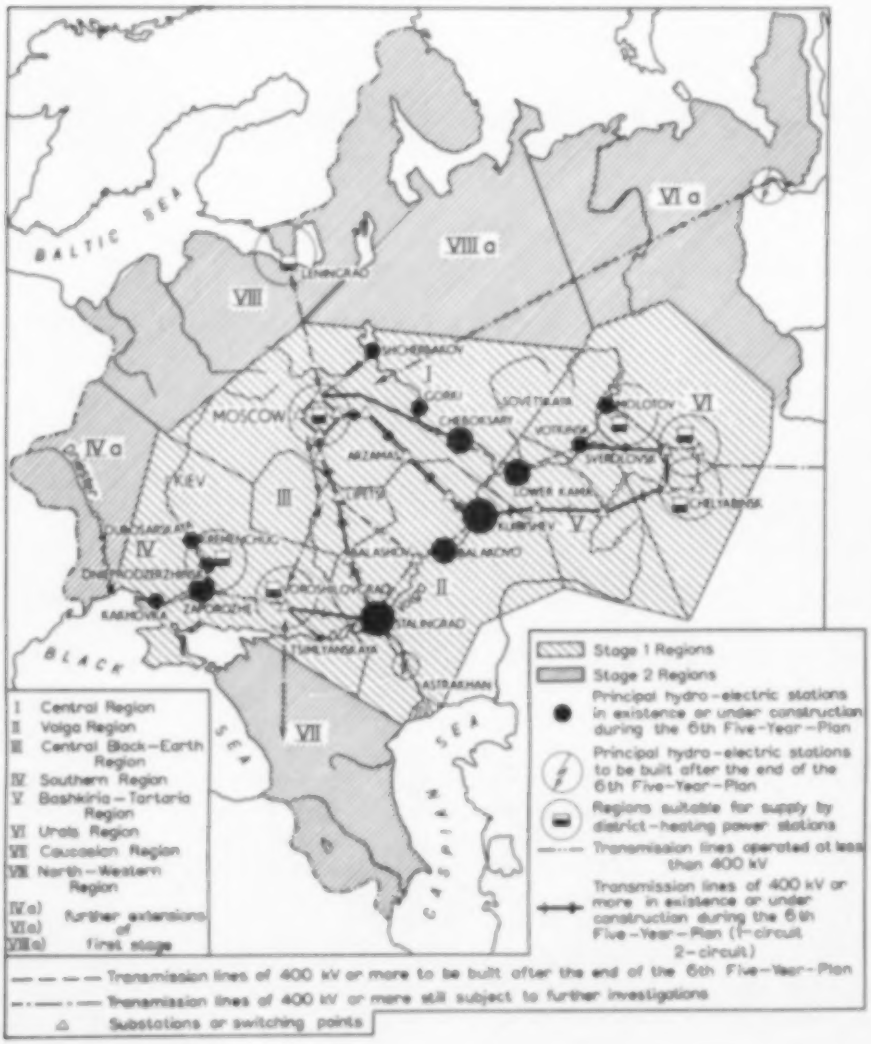
BALTIC SEA
BLACK SEA
CASPIAN SEA
LENINGRAD
MOSCOW
KIEV
VOLGOGRAD
STALINGRAD
ASTRAKHAN
I Central Region
II Volga Region
III Central Black-Earth Region
IV Southern Region
V Bashkiria-Tartaria Region
VI Urals Region
VII Caucasian Region
VIII North-Western Region
IV a) VI a) VIII a) further extensions of first stage
Stage 1 Regions
Stage 2 Regions
Principal hydro-electric stations in existence or under construction during the 6th Five-Year-Plan
Principal hydro-electric stations to be built after the end of the 6th Five-Year-Plan
Regions suitable for supply by district-heating power stations
Transmission lines operated at less than 400 kV
Transmission lines of 400 kV or more in existence or under construction during the 6th Five-Year-Plan (1-circuit, 2-circuit)
Transmission lines of 400 kV or more to be built after the end of the 6th Five-Year-Plan
Transmission lines of 400 kV or more still subject to further investigations
Substations or switching points

Fig. 1.

Bashkiria and Tataria, and Urals areas. The total area is over 2.7 x 10^6 km^2: population 110 million. The maximum east-west distance is over 2700 km, and the maximum south-north 1500 km. In the first section of the European U.S.S.R. grid the present annual output is about 106 x 10^9 kWh or 63 per cent of the total for the country. This is about 40000 kWh per km^2 and 1000 kWh per head.

The future levels and regional characteristics of the energy balance in the U.S.S.R.

The basic layout of the European grid is considered for two different energy levels: 500 and 1000 x 10^9 kWh. The 500 x 10^9 kWh level relates to the output of a substantial part of the Volga, Kama and Dnieper hydroelectric stations and the 1000 x 10^9 kWh to the completed All-Union grid.

500 x 10^9 kWh might be reached in the second half of the next (Seventh) Five-Year-Plan, and 1000 x 10^9 kWh early in the Ninth Plan. In the first stage the output of the first European grid section (without the northwest and Caucasian links) will increase from 106 in 1955 to 240 x 10^9 kWh and in the second stage to 410 x 10^9 kWh, according to our estimates.

On account of the considerable absolute rate of increase of the energy balance in the European grid this rate of increase will be slightly less than the average increase of the All-Union power production. This is due to more rapid expansion of output in areas east of the Urals. Thus the output in the Siberian grid area will increase by a factor 20 when stage 2 is reached, and by 8 – 15 times in other Asian parts of the Soviet Union. The relative output of the European regions (including the Urals) will decrease from 79 per cent to about 52 per cent and that of the Asian regions will increase from 21 per cent to about 48 per cent.

Yet even the European grid will comprise areas with two different rates of development: the older industrial areas in the Central, Urals and southern areas, where the rate of development is smaller than that of the Union as a whole, and the new industrial regions of Bashkiria, Tataria, Central Black-earth Region and Volga, with their rich natural resources and high population density. Here the output will increase faster than that of the Soviet Union as a whole, and their relative output will not decrease, but increase (from 7 – 10 per cent).

The above levels have only been used as a guide. The basic assumptions and the results have been checked with respect to possible deviations from the initially assumed pattern in the levels, rates of development, and general energy balance structures of the individual regions.

Regional characteristics of the energy balance and estimates of future load diagrams

Decrease in the relative industrial load is typical of the European grid. Agriculture, transport and domestic consumers will use more power and the industrial load will decrease from 81 per cent of the total in 1955 to 70 per cent whereas rural power consumption will increase from 2.5 to 6.1 per cent, transport from 3.3 to 8.6 per cent and domestic use from 13.2 to 15.1 per cent.

The load structure varies in the different regions. These variations affect the daily and annual load curves of the regions and of the grid considerably, and thus affect the maximum demand and grid layout.

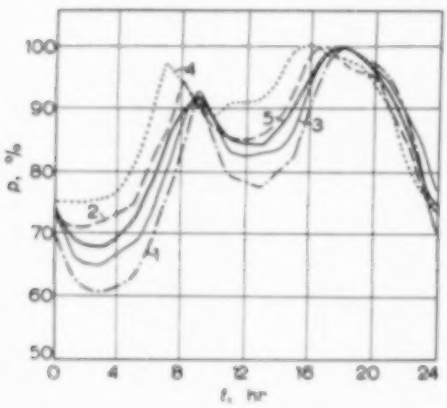

Fig. 2.

Fig. 2 shows the winter load curves for the European grid in the second stage, and the table gives the following:

$\gamma_d^{(w)}$ (load factor of a December day)

$\alpha_d^{(w)}$ (the ratio of minimum off-peak power to the evening peak)

h_a (hours of maximum demand per annum)

Regions	$\gamma_d^{(w)}$	$\alpha_d^{(w)}$	h_m
European grid	0.848	0.679	6300
Central	0.806	0.605	5900
South	0.834	0.653	6200
Volga	0.855	0.710	6400
Central Black-earth Region	0.798	0.592	5600
Tataria and Bashkiria	0.876	0.745	6600
Urals	0.884	0.750	6700

will decrease slightly (by about 1 or 2 per cent) when a 7 hr day is introduced. It would be more complicated to estimate the effect of a 6 hr working day on the load curve; no accurate prediction can be made, since period shift work increases the maximum demand in some industries and decreases it for others.

An upper limit is $h_m = 6300$; this corresponds to higher $\gamma_d^{(w)}$ and $\alpha_d^{(w)}$ in the second stage. Actually h_m may be expected to be 200 – 300 hr less, which must be allowed for in designing the grid structure. By the second stage the diversity effect* for a winter day is about 500 MW.

The structure of the European grid

The maximum demand on the European grid will be about 38 GW (1 GW = 1000 MW) in the first stage and about 65 GW in the second stage. Assuming a minimum spare capacity requirement for frequency, emergency and maintenance purposes†, the total installed capacity of the European grid will be about 42 GW in the first stage and about 72 GW in the second. Fig.3 shows the relative contribution to the total capacity from different types of power station.

The hydro-electric stations form one of the main factors affecting the grid design and determining the intersystem tie line loads.

---

* The difference between the arithmetic sum of the regional maximum demands and the grid maximum demand.

† Problems relating to the magnitude, constitution and distribution of power reserves will not be discussed here.

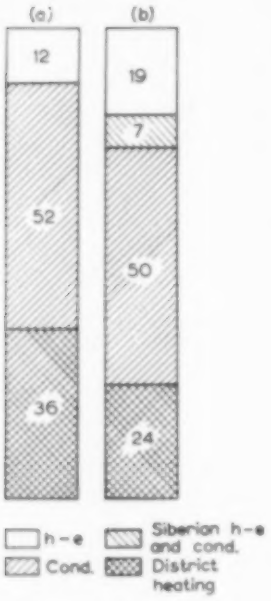

Fig. 3.

The total hydro-electric energy in the first stage of the European grid is planned to be about 66 x 10^9 kWh in a year of average flow.*

The total output in an average year would then be:

11.7 x 10^9 kWh from existing stations,

30 x 10^9 kWh from stations under construction

24 x 10^9 kWh from hydro-electric stations in the design stage.

The hydro-electric schemes in the European grid will produce 16 per cent of the annual output and comprise 19 per cent of the installed capacity in the second stage.

---

* This refers to existing stations and those under construction in various design stages on the Volga and Kama and their tributaries, and on the Dnieper, Don and Dniester. The Volga developments include the lowest barrage at Astrakhan giving 6 x 10^9 kWh. The output of the hydro-electric stations on the Dniester will be about 1.1 x 10^9 kWh. The lower Ob scheme and the so-called "Northern Supply" (direction of the northern river waters into the Volga) are not included.

1958

The part played by the hydro-electric station in covering the load is of great importance in determining the MW-capacity and hence its overall economic effect.

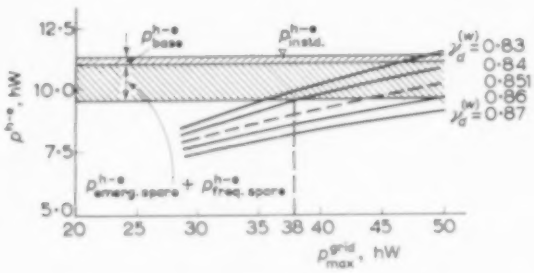

Fig. 4.

Fig.4 shows the effect of changes in the theoretical maximum demand and in the load curve shape for the European U.S.S.R. grid, all other conditions on the total working maximum* of the hydro-electric stations remaining unchanged.

The maximum grid demands are plotted horizontally. The basic figure for the first estimated level is 38 GW, the range of variation being 30 – 50 GW. The hydro-electric capacity is taken as ordinate. $\gamma^{(w)}_d$ ranges from 0.83 – 0.87, the basic value being = 0.851 and $\alpha^{(w)}_d$ = 0.668, the guaranteed hydro-electric output and installed capacity being 4 and 11.3 GW respectively. Below the 11.3 GW level are marked the imposed basic load of the hydro-electric stations (0.3 GW) and the minimum spare (frequency and emergency) capacity (1.5 GW) which may be allocated to the hydro-electric stations. The difference between installed and available capacity due to head variations is less than 0.1 GW.

Fig.4 shows that at the first level, which will be reached by about 1963–64, the total hydro-electric output utilizable without duplication by thermal power stations already constitutes about 9.3 – 9.8 GW† in

---

* The total output of the hydro-electrical stations taking part in the basic and peak-load parts of the load curve.

† The first and second figures refer to the allocation of frequency and emergency spare capacity to the hydro-electric stations, i.e. 1 and 1.5 GW respectively. It should be borne in mind that not all the total planned hydro-electric capacity (11.3 GW) will be in service during that period; some stations will still be under construction.

the first alternative considered (dotted line). If $\gamma_d^{(w)}$ should not be 0.851, but only 0.84, the hydro-electric capacity utilised for the total grid maximum demand would be 9.8 – 10.3 GW. When the maximum grid demand increased by 1/3, with $\gamma_d^{(w)}$ = 0.851 to 0.841,* it will be possible to utilize 11.8 – 12.5 GW of hydro-electric capacity without duplication, i.e., 0.5 – 1.2 GW more than the planned installed hydro-electric capacity.

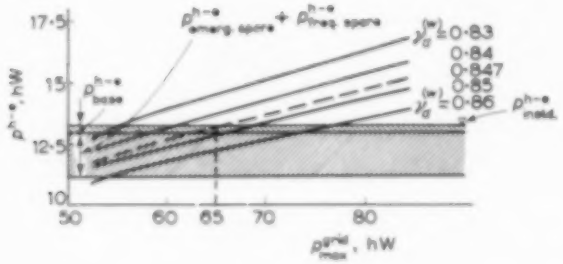

Fig. 5.

The effect of the maximum demand and of the shape of the load curve on the working maximum of the hydro-electric stations appears greater in the diagram Fig.5, where the second estimated level has been considered and where new possible hydro-electric developments (Astrakhan and others) have been taken into account. The total hydro-electric station capacity (13.3 GW) by the time the second estimated level is reached (maximum grid demand 65 GW, $\gamma_d^{(w)}$ = 0.847, minimum essential spare capacity at the hydro-electric stations 2 GW) can be increased by more than 2 GW as compared with the data of the present plan.

We have graphs showing how the installed capacity of the hydro-electric stations of the European grid would vary with deviations of the development of the individual regions from the basic alternative, e.g. the actual rates of maximum demand increase may be lower in the Volga and Central Black-earth regions and higher in the Urals and the South, etc.

The total installed capacity of the above hydro-electric schemes in the European grid is too low. In the investigations and planning work of 1951 and the following years it was found necessary to increase the capacity of the Kuibyshev and Stalingrad power stations beyond their original ratings, i.e. by 1.7 – 2 GW.

At present the capacity installed at these stations is being increased by 700 MW. Further possible increases in the installed capacity must be

---

* Frequency and emergency spare capacity of thermal power stations 1.5 GW.

provided for by performing the appropriate engineering and other works; equipment can be installed later. The capacity installed at Saratov, Lower Kama, Chebokarsk and Astrakhan should be reconsidered in relation to their future part in the development of the European grid.

Of course Figs. 4 and 5 only deal with matters of principle as regards the need to increase the total hydro-electric capacity in the European grid by 2 – 2.5 GW over the present design figure. The individual schemes must be subject to cost analysis. Provision must be made at the design stage for the subsequent installation of additional equipment, otherwise the most efficient and complete use of resources in regions of restricted water supply would be prevented.

These proposals become more important when the link-up between the European and north-west and the Caucasus systems is allowed for, since a tie line will link the European grid with that of Siberia and the "Northern Supply" will become available. These will increase the hydro-electric capacity in the European grid and thus facilitate extension of their working and installed capacities.

The hydro-electric capacities can be assessed for the time when the links connecting the Central, Central Black-earth, Bashkiria, Tataria, Urals and Southern regions are commissioned.

In the second stage thermal stations will supply 75 – 80 per cent of the European grid power, the first including and the second excluding the Siberian hydro-electric stations.

In the second stage the district heating power stations in the European grid will have a capacity of about 17 GW. Their contribution towards covering the maximum demand will depend on their industrial heating load curves.

District heating stations will have dual-purpose turbogenerator sets of increased rating and be larger,* and together with new bleeder-turbine designs with higher efficiencies under various load conditions, application of the "boiler-turbine" unit system, creation of heat supply systems with parallel heat infeed, introduction of efficient heat distribution systems, complex automation and remote control of district-heating power stations.

---

* Unit ratings rising from 12 – 25 MW to 50 – 100 MW, higher input pressures and temperatures will be used. By replacing steam at 90 atm and 500°C by steam at 200 atm and 600°C the heat output per Mcal will be increased by 30 – 50 per cent for 2 atm and 10 atm gauge pressure at the bleed points for heating and industrial steam, respectively.

The regional thermal condensation stations play the largest part in the European grid. Their capacity will be increased to 36 - 41 GW in the second stage.* The major increase (18 out of 27 GW) will occur between the first and the second stages when the water resources in the European grid regions will already be largely utilized. Condensation stations will contribute from 52 to 50 to 57 per cent.*

The grid will facilitate the introduction of stations with sets of 200 - 300 MW and later 500 MW unit rating, with ultra high-pressure steam input and boiler-turbine units.

The siting of the new condensation stations - whether at the fuel source or at the load centres - is of primary importance. The grid will introduce new factors which will greatly influence the solutions adopted. Also the grid layout and design will depend to a great extent on the location of the condensing plant.

Reversible operation in intersystem ties might make it more economic to locate the condensation plant in low-cost fuel areas and substitute electric power transmission for fuel transport by rail.

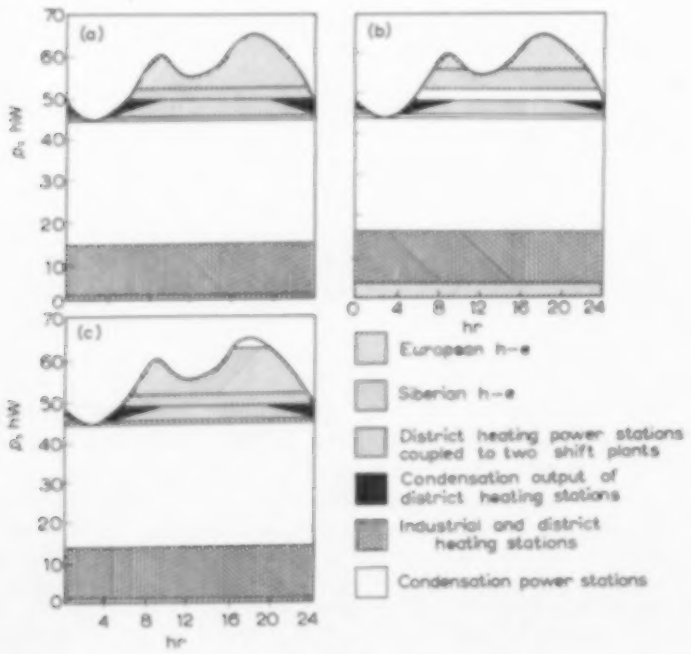

Fig. 6.

* The second figure excludes the Siberian hydro-electric stations.

In some regions stations will be developed in which the fuel will be used for power generation as well as for industrial or technological purposes and will drive gas-turbines, particularly in stations related to underground gasification schemes.

Fig.6 shows three alternative basic plans for covering the winter load curve in a year of low hydro-electric output, corresponding to the second stage in the European grid. The upper part in Fig.6(a) is occupied by the hydro-electric stations on the European rivers, replacing as much power as possible from condensation plant. In this case the total installed capacity (13.2 GW) helps to cover the load curve. Since part of the essential spare capacity may economically be allocated to hydro-electric stations their total capacity should be increased by more than 2 GW. If the hydro-electric station capacities are restricted as in the present plan the total spare capacity must be concentrated in the thermal stations.*

In Fig.6(b) the hydro-electric stations provide 2 GW of reserve capacity, and 11.3 GW covering the winter grid load in a year of low water. This assumes here that 8.3 GW is used for peak load and 3 GW for base load, part of the condensation plant being transferred to peak load, involving lower efficiency.

Fig.6(c) differs from the previous in that 11 GW (i.e. almost all of the hydro-electric power except 300 MW of its inherent base load) is placed just below the peak, but 2.5 GW at the peak is supplied from lower-efficiency steam condensation plant.†

The most favourable conditions for the different types of station in the different seasons and in years of different water availability must be chosen from technical and economic calculations with necessarily complicated conditions of the total energy balance of the grid.

General layout of the European grid

Fig.1 shows the basic layout of the European grid at the second stage. Some new intersystem ties not included in the Sixth Five-Year-Plan are:

---

* This alternative would involve wasting some water, the power loss being 1.4×10^6 kWh. Some 400 MW of hydro-electric power in addition to the 300 MW above must be transferrred from peak to base to avoid this loss. Correspondingly condensation plant would have to be transferred from base to peak, to compensate.

† The Siberian water power contribution to the European grid has also been considered.

Besides the first large 400 kV Moscow-Kuibyshev Hydro - Tatneft - Ufa - Zlatoust trunk line (included in the Sixth Five-Year Plan), a second 400 kV trunk line, viz. Moscow - Chebokarsk Hydro - Lower Kama Hydro - Botkinsk Hydro - Sverdlovsk, is under consideration. The design of the Chebokarsk - Moscow line is linked to that of the Chebokarsk hydro-electric station. The Botkinsk hydro-electric scheme will be connected with Sverdlovsk. It would be incorrect to plan the individual links in these trunk lines in isolation, and the entire trunk line must be designed as one of the main features of the integrated high-voltage grid. The second 400 kV trunk line with its three auxiliary hydro-electric stations (Chebokarsk, Lower Kama and Botkinsk) is 1700 km long. The transmission conditions will vary during construction. In the first stage the flow will be from West to East via two branches: Lower Kama Hydro - Botkinsk Hydro - Sverdlovsk; and Lower Kama Hydro - Tatneft - Ufa - Zlatoust. In the second stage power from the Lower Kama hydro-electric scheme and some from the Lower Yenesei stations will flow along the same line from east to west. The capacity of the second 400 kV trunk line and branches must be determined from the second stage requirements.

1958

The overall plan will ensure that the 400 kV Kuibyshev - Saratov line and the equipment operate at full efficiency. The line should be extended to Stalingrad if the Astrakhan scheme is proceeded with. If not, the extension will not be economic. A 400 kV transmission is being further investigated.

The good industrial and agricultural prospects of the Central Black-earth Region justify the 400 kV Saratov - Central Black-earth Region (Lipetsk substation) transmission system. Use of the hydro-electric station at Saratov to supply the Central Black-earth Region would replace more condensation plant than any other alternative.

The chart also shows a Donbass - Central Black-earth Region - Moscow transmission line. This line will supply the Central Black-earth and Central Regions from stations situated in the Don Basin operating on low-grade residues from coal enrichment processes, or on coal of calorific values below 4000 – 5000 kcal/kg.

The technical and economic aspects of this system will be determined when several supply problems have been resolved, viz. the fuel production of individual regions and the energy available for exchanges with the European grid, etc. Other energy sources competitive with power transmission, must be investigated, particularly nuclear stations.

The basic intersystem grid lines (including those between the 400 kV substations in Moscow and the Urals) comprise about 8700 km of single-circuit line.*

The operating conditions for individual lines will vary with the water supply and during different stages of development. Of the many problems involved only reverse power flow in individual ties will be briefly reviewed since this may be very important for economy in operation.

The essential character of one such operation is illustrated by the Stalingrad - Donbass transmission line.

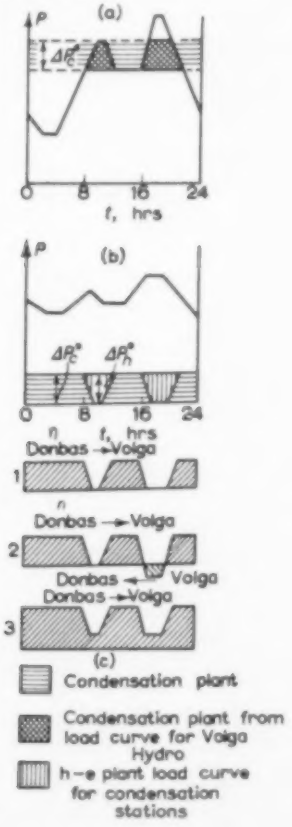

Fig. 7.

* The Donbass- Central Black-earth Region - Moscow and Saratov Stalingrad Hydro Astrakhan Hydro lines are not included. The capacities of the lines connecting the Urals with the Central region may have to be increased if power is received in the European grid from the Yenesei hydro-electric scheme.

Fig.7 shows that two distinct operating conditions alternate because the Stalingrad hydro-electric station supplies power Δp_h^0 to the load curve, the peak of which is determined by the Southern system. During off-peak periods the Donbass supplies Δp_c^0.* Thus the condensation plant in the South has a constant output, the Stalingrad hydro-electric station supplying the peak load at some hours, energy being sent to the Volga at other times.

The operating conditions in the Stalingrad - Donbass tie depend on the structure of the Volga and Southern systems, on the individual station characteristics, on the magnitude and shape of the load peak in the Southern system and the Southern system load allocated to the Stalingrad station, on the Donbass condensation plant capacity, on the contribution to the Volga area load, etc. A winter day flow curve (Fig.7) may be two-way or unidirectional ($\Delta p_c^0 \gtrless \Delta^0 p_h$).

Severe breakdowns in the Southern system may require power to be drawn from the Volga region. Then part or all of the normal Donbass - Volga flow will not be available, and power will have to flow westwards.† The operating conditions in other European grid links will also change during emergencies.

Reversed flow operation has the following advantages: an increase of the coefficient of transformation of the guaranteed power of the hydro-electric stations and, consequently, the possibility of an increase of its installed capacity and output which, in turn, guarantees the economy of the power output of the condensation power stations, fuel economy and reduction of the production cost of the energy, reduction of power and energy losses by intersystem transmission, cost reduction of intersystem transmission in connection with the reduction of the theoretical power flow and reduction of the required transmission capacity.

There are additional ways of increasing the maximum demand covered by the hydro-electric stations and the grid flexibility while retaining the same transmission capacity.

---

* Condensation plant must be installed between the first and second stages in addition to hydro-electric and district-heating stations to accord with long-term plans. This condensation plant will, as usual, supply the Volga region base load. The new condensation plant should be in the Donbass, where coal-enrichment residues are available, and not in the Volga region, for economic reasons.

† This justifies allocating some spare capacity (up to about 300 MW, 2 – 3 sets) at the Stalingrad hydro-electric station to the Southern lines.

1958

Reversed flow operation is of advantage when regions with different times of maximum demand, different load curve shapes and different load structures are interconnected. It facilitates a new approach to the condensing station siting problem.

Another type of reversed flow operation is obtained by using the hydro-electric stations to supply peak loads in the grid when the regional load curves and time zones differ.

Economic efficiency in the European grid

Some approximate round figures for the efficiency of the European grid may be given.

The capital cost of the intersystem lines is about 5.8×10^9 roubles,* and the running cost about 340 million roubles p.a.

The total capital cost of the European grid will be 9.6×10^9 roubles, and running costs 625 million roubles p.a.

The grid will reduce the requirement for condensing stations by 4.8 GW.†

The fuel saved by the additional hydro-electric output (6×10^9 kWh) due to increase in hydro-electric station capacity and the smaller auxiliary consumption is about 2.3 million tons of coal p.a.

The capital saved on generating equipment is 6.7×10^9 roubles and the operating cost is reduced by about 1×10^9 roubles p.a. The additional capital outlay of about 3×10^9 roubles will be saved in less than 8 years by reduced operating costs (375 million roubles p.a.).

These estimates are conservative. The actual effect will be considerably larger. For example, the figures do not allow for concentration of thermal power stations in individual regions which will occur, nor for the savings from the increased guaranteed power from the interconnected Volga, Kama and Dnieper systems. The spare capacity reductions

---

* The Kuibyshev Hydro - Saratov Hydro and Donbass - Central Black-earth Region - Moscow lines are not included.

† About 3.9 GW will be supplied by additional plant at hydro-electric stations; the spare capacity required will be reduced by 0.9 GW when the difference in the auxiliaries at hydro-electric and thermal stations is allowed for.

assumed have been estimated to be 1.5 - 2 times smaller than those predicted by probability formulae.* The same applies to the sum of the individual load curves. The savings produced by coupling the hydro-electric units to the Urals and Southern area before the industrial loads in the Volga and adjacent regions have reached the planned levels (due to water wastage) have not been allowed for. Allowance of these additional factors would shorten the time taken to amortize the cost.

One unfavourable effect not allowed for in the above estimates is the "freezing" of some capital during construction until all the lines can be fully utilized.

The above figures refer to the European grid as a whole. Individual lines vary in economy. For example, the Kuibyshev - Urals and Stalingrad - Donbass lines will take less than 4 years to pay off but the Kuibyshev - Moscow and Stalingrad - Moscow lines will take about 10 years.

1958

The problems of the economic efficiency of the European grid will form the subject of further investigations on the methodological side as well as where the accuracy of the fundamental relations and basic data is concerned. Existing possibilities of further improvement of the economy of the European grid must be explored and utilized.

Connexion of the Caucasian and north western systems with the European grid

The basic problems of developing the Caucasian and North Western Regional grids, and of connecting them to the European grid, have not yet been fully studied.

In a year of medium water supply the hydro-electric potential of the Caucasus has been estimated to be about 180×10^9 kWh. Caucasian rivers have flows which vary in different years and between seasons. Storage lakes are costly and can only partly even out the annual flow. Hydrograph records for the Volga and Dnieper differ considerably from those for the Caucasian mountain rivers which have their largest flows in July and August, due to melting snow.

The Caucasian water power resources would be most efficiently used by linking the Caucasian system with the European grid, particularly with the Southern part. In good years this would reduce the demand on thermal

* The coefficient of availability was assumed as 0.9999; the average maintenance of a unit as 1 per cent, the individual generating units were assumed of 100 MW capacity.

condensation stations in the south and elsewhere. In bad years the flow would be from the southern system to the Caucasus. The Caucasian hydro-electric systems consist of relatively small units, which must be allowed for.

The line connecting the Caucasus with the European grid is about 1000 km long and about 1 GW capacity.

It was originally proposed to connect the north western system to the European grid by a 220 kV line from Leningrad to Moscow, from which the October railway was to be supplied. Such a low-power link (150 - 200 MW) between systems of many million kW capacity is unsatisfactory. It is necessary to envisage other alternatives which would economically justify the creation of a strong power link between the north western Region and the European grid. In particular, it is necessary to consider a line connecting the Lower Ob hydro-electric scheme with Leningrad via the upper Volga region. Such a line would be about 2500 km long and of about 2.5 - 3 GW capacity.

Only a few problems relating to a European grid which have been studied in detail by the Institute of Power Engineering of the U.S.S.R. Academy of Sciences have been dealt with here. In particular the methods of calculating power demand and supply and the economic factors determining basic parameters of the grid have not been touched upon. The Siberian grid, its connection with the European grid, and the future contributions of nuclear power stations will form the subject of separate papers.

INVESTIGATION OF VARIABLE-SPEED A.C. MACHINES*

I. I. TRESHCHEV

Introduction

Modern electrical engineering developments are associated with the continuous increase of machine ratings and operating speeds. Transients then assume an ever greater importance, and are indeed decisive in some practical cases. Cases are known in which a synchronous three-phase generator on dead short-circuit has slowed considerably within a relatively short time. This retardation is due to the braking torque set up by the short circuit, and as the flywheel masses will be different in every concrete case the retardations will differ. The torque speed function must be known in order to determine conditions under which normal operation is rapidly restored.

The maximum short circuit torque must be known in order to determine the mechanical strengths of generator and foundations. But the maximum torque depends on the generator speed changes under these conditions.

The effect of the rate of change of slip on induction motor characteristics is usually neglected in the theory. The power lost on changing the magnetic energy is not considered in the energy balance. Every slip is assumed to have a corresponding well-defined torque independent of the slip variation rate. However, the static mechanical characteristic applies only to the steady state. Even at normal induction motor accelerations the actual torque deviates considerably from its static value. For example, for a type A92–4 motor with a run-up time $t = 2.6\ T_a = 1$ sec, the maximum torque difference will be about 50 per cent of the rated value for small slips.

When the load seizes or jams the retardation is very rapid. If the slip variation rate is considered the effective maximum torque may exceed the maximum steady-state torque by a factor of almost 2, and the rated torque by a factor of almost 5, which must be allowed for in specifying the mechanical strengths of motor and load. A difference

* *Elektrichestvo* 2, 49–55, 1957 (Reprint Order No. EL2)

between these characteristics will also exist when speed control is by frequency variation. The effect of slip variation rate on the motor characteristic is of particular importance in repeated short-time and high-speed processes in connexion with the current general tendency to increased operating speeds. A criterion defining the maximum error in such cases has already been suggested [1].

The short-circuit torque of a synchronous machine can be calculated only if the quadrature components of the currents and flux linkages are known; this complicates matters even if the speed is constant and operational methods are used. On the other hand the short-circuit currents are given approximately by simple formulae which are in satisfactory agreement with experiment.

Great theoretical difficulties also arise when an induction motor is operated at variable speeds.

It will be shown that the power associated with the magnetic energy during a short-circuit may be determined with satisfactory accuracy if the symmetrical current components are known along one axis. These data, together with the energy balance, give the short-circuit torque simply and with the desired accuracy with due allowance for speed changes. Recurrence formulae for the torque of a synchronous machine and the stored magnetic energy will be derived from the energy balance, from which the behaviour under variable speed conditions can be predicted.

Fundamental relationships

The co-ordinate system is assumed at rest relative to the rotor. The voltage equilibrium equations for the stator and (on the usual assumptions) take the form [1],

$$\left.\begin{aligned} u_d &= i_d r_s + \frac{d\psi_d}{dt} - \omega\psi_q ; \\ u_q &= i_q r_s + \frac{d\psi_q}{dt} + \omega\psi_d ; \\ u_0 &= i_0 r_s + \frac{d\psi_0}{dt} . \end{aligned}\right\} \qquad (1)$$

On a per unit basis and for the rotor we get

$$\left.\begin{aligned} u_{rd} &= i_{rd} r_r + \frac{d\psi_{rd}}{dt} \\ u_{rq} &= i_{rq} r_r + \frac{d\psi_{rq}}{dt} \end{aligned}\right\} \qquad (2)$$

where:

u_d, u_{rd}, i_d, i_{rd}, ψ_d, ψ_{rd}, are the components of voltages, currents and flux linkages along the d-axis; u_q, u_{rq}, i_q, i_{rq}, ψ_q, ψ_{rq}, being the components of the voltages, currents and flux linkages along the q-axis;

u_0, i_0, ψ_0 the same for the zero-components;

r_s, r_r the resistances of stator and rotor, respectively;

and ω is the rotor angular velocity.

For simplicity the zero-components will be omitted because they are unrelated to the other components and can easily be considered if necessary. For a normal induction motor $u_{rd} = u_{rq} = 0$ in equation (2), and for a normal synchronous generator without damper these equations degenerate into one along the direct axis for the field winding.

If the generator has a damper in the direct axis, the two equations will relate quantities referring to this axis, viz. one for the field winding and the second for the damper winding. The number of equations in (2) will increase with the number of rotor windings.

Equations (1) and (2) are equivalent to reducing the machine to two transformers with windings about the d and q axes mutually related by the rotational e.m.f. These transformers rotate together with the co-ordinate system, at the rotor speed (Fig. 1).

If we multiply the left hand and right hand sides of (1) and (2) by i_d, i_q, i_{rd} and i_{rq} respectively, and add these parts we get

$$p = p_T + \frac{dW_m}{dt} + \omega M \qquad (3)$$

where p is the total electrical power supplied to the machine or by it; p_T the copper losses in the stator and rotor; $\omega M = \omega(\psi_d i_q - \psi_q i_d)$

is the mechanical power supplied to the rotor or derived from it; dW_m/dt, the power expended on varying the magnetic energy. Also

$$\frac{dW_m}{dt} = \frac{d\psi_d}{dt} i_d + \frac{d\psi_q}{dt} i_q + \frac{d\psi_{rd}}{dt} i_{rd} + \frac{d\psi_{rq}}{dt} i_{rq} . \qquad (4)$$

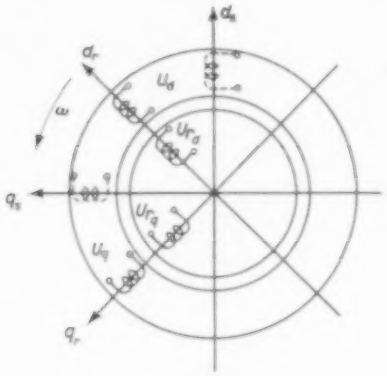

Fig. 1. Reduction of a three-phase machine to two double-wound transformers.

Equation (3) expresses the power balance. It is easy to show that if $dW_m/dt = 0$, no transient electromagnetic processes take place in the machine. Consequently, this term in the over-all power balance (3) determines the effect of transient electromagnetic processes on the behaviour.

If we introduce generalized complex terms for the flux linkages, $\bar{\psi}_s$, $\bar{\psi}_r$, and currents, $\bar{i}_s$, $\bar{i}_r$, of stator and rotor, respectively, (4) takes the form:*

$$\frac{dW_m}{dt} = \left(\frac{d\bar{\psi}_s}{dt} \bar{i}_s^* + \frac{d\bar{\psi}_r}{dt} \bar{i}_r^* \right)_{Re} . \qquad (5)$$

where, $\bar{i}_s^*$, $\bar{i}_r^*$ are the complex conjugates of $\bar{i}_s$, $\bar{i}_r$.

The magnetic energy stored in the machine is

$$W_m = -\frac{1}{2} (\bar{\psi}_s \bar{i}_s^* + \bar{\psi}_r \bar{i}_r^*)_{Re} . \qquad (6)$$

Differentiating (6) and incorporating (5), we find

* Subscript *Re* indicates the real part.

$$\frac{dW_m}{dt} = \left(\bar{\psi}_s \frac{d\bar{i}_s^*}{dt} + \bar{\psi}_r \frac{d\bar{i}_r^*}{dt}\right)_{Re} . \tag{7}$$

Equation (7) offers considerable advantages in approximate work. Equations (5) and (7) are also valid if we use the complex conjugates of the flux linkages instead of those of the currents. Operational methods are usually used nowadays with a.c. machines. This is possible if we assume the rotational speed constant and that the currents vary exponentially. The stator and rotor current vectors $\bar{i}_s$ and $\bar{i}_r$, rotate at variable speeds, and their amplitudes are also variable, i.e.

$$\left.\begin{aligned} \bar{i}_s &= i_{sm} e^{j(\int \omega_s dt + \theta_{s0})} ; \\ \bar{i}_r &= i_{rm} e^{j(\int \omega_r dt + \theta_{r0})} . \end{aligned}\right\} \tag{8}$$

where i_{sm}, i_{rm}, ω_s, ω_r, are the variables.

Substituting (8) into (7) and considering that for a symmetrical machine $[j\bar{\psi}_s \bar{i}_s^*]_{Re} = -[j\bar{\psi}_r \bar{i}_r^*]_{Re}$ we find

$$\frac{dW_m}{dt} = \frac{1}{i_{sm}} \frac{di_{sm}}{dt} [\bar{\psi}_s \bar{i}_s^*]_{Re} + \frac{1}{i_{rm}} \frac{di_{rm}}{dt} [\bar{\psi}_r \bar{i}_r^*]_{Re} -$$

$$- (\omega_s - \omega_r)[j\bar{\psi}_s \bar{i}_s^*]_{Re} . \tag{9}$$

If the currents decay exponentially then

$$\frac{1}{i_{sm}} \frac{di_{sm}}{dt} = -\alpha_s , \quad \frac{1}{i_{rm}} \frac{di_{rm}}{dt} = -\alpha_r ,$$

where α_s and α_r are the stator and rotor damping factors respectively.

When the current and flux linkage vectors lie along one axis, for example the d-axis, or almost so (symmetrical components in a three-phase short-circuit), the first two terms in (9) may be determined with a high degree of accuracy if we consider only the components along the d-axis, since we then get

$$[\bar{\psi}_s \bar{i}_s^*]_{Re} = \psi_d i_d + \psi_q i_q \approx \psi_d i_d ,$$

1958

because when ψ_q and i_q are small $\psi_q i_q$ is a second-order infinitesimal. To determine the last term in (9) the in-phase and quadrature components must be accurately known because

$$[j\bar{\psi}_s \bar{i}_s^*]_{Re} = \psi_d i_q - \psi_q i_d .$$

Herein lies the main difficulty. However, we see from (9) that this term vanishes when $\omega_s = \omega_r$. But if the current vectors rotate at different angular velocities (e.g. if the aperiodic component is considered), the last term in (9) will not vanish. But we need to know the current amplitudes and initial phases only approximately, because the relative phases of the current vectors vary continuously.

This property of dW_m/dt occurs only when variations in the total magnetic energy of the machine are considered. It is no longer true if variations in the magnetic energy of stator or rotor alone are considered.

If the machine is not symmetrical, strictly speaking, (9) no longer applies. However, in most practical cases the error associated with the asymmetry is small. Consequently, the property of dW_m/dt discussed above will occur in asymmetric machines, i.e. synchronous generators with or without damping windings.

For a three-phase dead short-circuit at the terminals of an induction motor, if copper losses are neglected and there is no shaft load the dynamic equation and (3) give

$$W_{m1} - W_{m0} \approx J \frac{\omega_0^2 - \omega_1^2}{2} .$$

The change in magnetic energy is equal to the change in kinetic energy. Applications of the above relations will now be dealt with.

The torque of a synchronous generator on three-phase dead short-circuit

In this case we must put $p = u_f u_f$ in (3).

Consequently

$$M = \frac{1}{\omega}\left(\frac{dW_m}{dt} + p_T - u_f u_i\right) . \qquad (10)$$

We stated above that dW_a/dt and the copper losses are practically completely determined by the currents in stator and rotor. The short-circuit currents can also be satisfactorily calculated from simple formulae based on the assumption that the symmetrical component vectors lie in the direct axis (2,3).

Using these formulae together with equation (4), dW_a/dt is found for a generator without damper winding by assuming that T'_d and T_a (in radians) are relatively large (Appendix)

$$\frac{dW_a}{dt} \approx \omega E_0^2 e^{-t/(T_a)} \sin \beta_\omega \left[\frac{1}{x_d} + \left(\frac{1}{x'_d} - \frac{1}{x_d}\right) e^{-t/(T'_d)}\right] -$$

$$- \omega \frac{E_0^2}{2} e^{-2t/(T_a)} \sin 2\beta_\omega \left(\frac{1}{x'_d} - \frac{1}{x_q}\right). \qquad (11)$$

The main copper loss may be calculated by Lyuter's method (3) by considering the losses to currents set up in the rotor by the aperiodic stator current component. For a generator with damper winding this method, with the same simplifications, gives:

$$\frac{dW_a}{dt} \approx \omega E_0^2 e^{-t/(T_a)} \sin \beta_\omega \left[\frac{1}{x_d} + \left(\frac{1}{x'_d} - \frac{1}{x_d}\right) e^{-t/(T_d)} +\right.$$

$$\left. + \left(\frac{1}{x''_d} - \frac{1}{x'_d}\right) e^{-t/(T''_d)}\right] - \omega \frac{E_0^2}{2} e^{-2t/(T_a)} \sin 2\beta_\omega \left(\frac{1}{x''_d} - \frac{1}{x''_q}\right). \qquad (12)$$

Equations (10 - 12) show that when the generator speed is sharply reduced copper loss effects increase, this causing an additional rise in braking torque.

Where the angular velocity is constant at the synchronous value ω_{syn} i.e. $\omega = \omega_{syn} = 1$ and also if we simplify for T''_d, T'_d and T_a very large the torque formulae coincide with those obtained by Lyuter's method [3]. The more exact treatment used here will only apply to low-rated machines with small time-constants and running at synchronous speed.

Fig. 2 shows the torque curve for a three-phase dead short-circuit in a W999 synchronous generator (28.2 kVA; 220/380 V; 74/43 A) during no-load operation for $E_0 = 1$. and $\alpha = 1500$ rev/min.

The instantaneous copper losses are considered. The braking torque rises very rapidly and reaches almost 10 times its initial value. This causes the generator to lock suddenly which from (10) in turn causes a further increase in the maximum torque as indicated in Fig. 2.

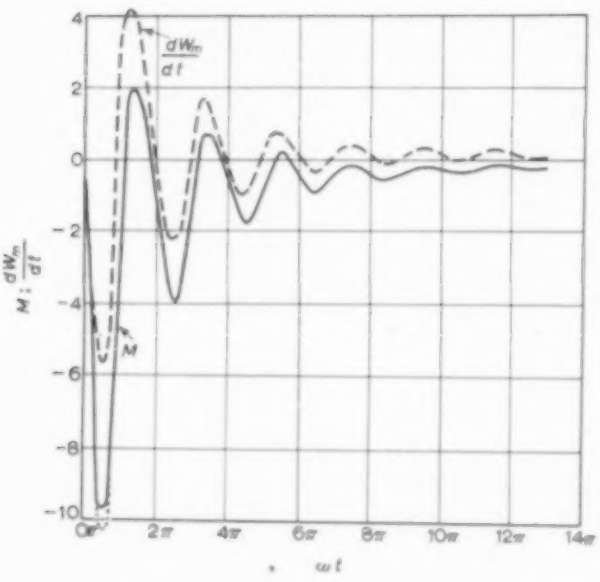

Fig. 2. Torque variation and dW_m/dt curves for a three-phase dead short-circuit across a W999 synchronous generator (28.2 kVA; 220/380 V;) 74.3/43 A; 1500 rev/min under no-load conditions at $E_0 = 1$.

... — is the effect of speed change on M_{max} when $\Delta n = -10$ per cent.

Variable-speed operation of an induction motor

The voltage balance equations for the generator, referred to axes rotating at synchronous speed, take the symbolic form

$$\left.\begin{aligned} \bar{u} &= \bar{i}_s r_s + j\bar{\psi}_s + \frac{d\psi_s}{dt}; \\ 0 &= \bar{i}_r r_r + js\bar{\psi}_r + \frac{d\bar{\psi}_r}{dt}. \end{aligned}\right\} \qquad (13)$$

where $\bar{i}_s$ and $\bar{\psi}_s$ are the complex stator currents and flux linkages

$\bar{i}_r$ and $\bar{\psi}_r$ are the same for the rotor;

r_s and r_r are the resistances of stator and rotor, respectively.

Equation (13) can be solved by numerical integration if we assume $r_s = 0$ when s is variable [4]. But even then special functions have to be used and, if the slip-time relation is linear, series which are not always rapidly convergent. The grapho-analytical method [5] also has some severe drawbacks. This problem, of considerable practical importance, is difficult to solve.

The stator and rotor currents will be written in the following form so that the energy relations can be used:

$$\left.\begin{aligned} \bar{i}_s &= \bar{i}_{se} + \bar{i}_{sv} \; ; \\ \bar{i}_r &= \bar{i}_{re} + \bar{i}_{rv} \; , \end{aligned}\right\} \qquad (14)$$

where i_{se} and i_{re} are the complex stator and rotor currents which approach, and at small rates of change of s are equal to the steady-state currents i_{sss} and i_{rss} ; i_{sv} and i_{rv} are the complex transient equalizing currents of stator and rotor.

If we assume a normal linear relation between currents and flux linkages we get

$$\left.\begin{aligned} \bar{\psi}_s &= \bar{\psi}_{se} + \bar{\psi}_{sv} \; ; \\ \bar{\psi}_r &= \bar{\psi}_{re} + \bar{\psi}_{rv} \; . \end{aligned}\right\} \qquad (15)$$

The magnetic energy changes associated with the flux linkage changes $d\bar{\psi}_{se}/dt$, $d\bar{\psi}_{re}/dt$, are normally small. Then (13), using (14) and (15) splits up into the following four equations.

$$\left.\begin{aligned} \bar{u} &= \bar{i}_{se} r_s + j\bar{\psi}_{se} + \frac{d\bar{\psi}_{se}}{dt} \; ; \\ \bar{i}_{re} r_r + js\bar{\psi}_{re} + \frac{d\bar{\psi}_{re}}{dt} &= 0 \; ; \end{aligned}\right\} \qquad (16)$$

$$\left.\begin{aligned} \bar{i}_{sv} r_s + j\bar{\psi}_{sv} + \frac{d\bar{\psi}_{sv}}{dt} &= 0 ; \\ \bar{i}_{rv} r_r + js\bar{\psi}_{rv} + \frac{d\bar{\psi}_{rv}}{dt} &= 0 . \end{aligned}\right\} \qquad (17)$$

A solution of (17) containing no constant term gives expressions in the form of elementary functions. Equation (16) is solved from the energy balance by successive approximation for the effect of magnetic energy changes on the motor currents. When the currents and flux linkages have been determined we get recurrence formulae for the torque and stored magnetic energy, from which the behaviour of a variable speed induction motor can be predicted (Appendix):

$$M_n = M_e + e^{-\alpha(t)}[\cos \beta_r (M_{n-1} - M_e) - \sin \beta_r (W_{n-1} - W_e)] - i_{sn}^2 r_s ; \qquad (18)$$

$$W_n = W_e + e^{-\alpha(t)}[\cos \beta_r (W_{n-1} - W_e) + \sin \beta_r (M_{n-1} - M_e)]. \qquad (19)$$

where, M_n, W_n and i_{sn} are the torque, stored magnetic energy and stator current for the n-th range of variation of s;

$$M_e = \frac{M_{ss}}{1 + \epsilon} ; \qquad (20)$$

$$\epsilon \approx \frac{M_{ss}}{u^2} \cdot \frac{ds}{dt} \cdot \frac{(x_1 + c_1 x_2')}{\omega} \left(\frac{c_1}{s} + \frac{r_s}{r_r} \right); \qquad (21)$$

is the steady-state torque:

$$\beta_r \approx \beta + \alpha_r' \alpha_s' (t - \beta) ;$$

$$\beta = \int s dt;$$

$$\alpha(t) \approx \alpha_r' t + \alpha_s' s \beta .$$

ds/dt is small for ordinary induction motors under normal operating conditions and so, from (21), $\epsilon = 0$.

Then

$$\left.\begin{aligned} M_e &\approx M_{ss}; \\ W_e &\approx W_{ss} \end{aligned}\right\}. \qquad (22)$$

the torque and magnetic energy stored in the stator are determined by the static characteristics. (18) and (19) may be similarly simplified.

Calculations using (18) and (19) are hardly more difficult than predicting the behaviour from steady-state characteristics, particularly if the stator copper losses are neglected and (22) used.

1958

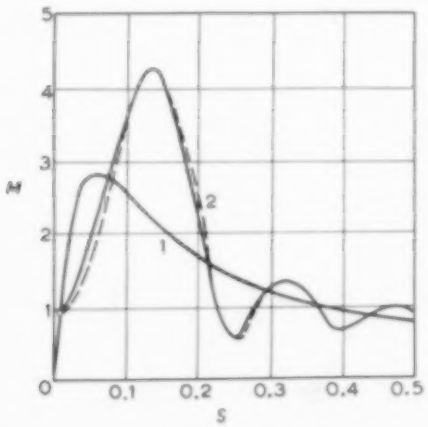

Fig. 3. Induction motor torque curves on braking at constant acceleration ($2a = 1/48\pi$)

1 - steady-state characteristic;

2 - characteristic including electromechanical transients.

To test (18) and (19), Fig. 3 shows torque curves for an induction motor during braking at constant acceleration $2a = 1/48\pi$, the parameters being: $x_s = x_r = 3.07$; $x_m = 2.99$; $r_s = r_r = 0.01$. The figure also shows the result predicted by using a computer [6] (broken curve). Table 1 gives the theoretical results. Where stator resistance is allowed for and M_e and W_e are used instead of M_{ss} and W_{ss} the agreement is satisfactory.

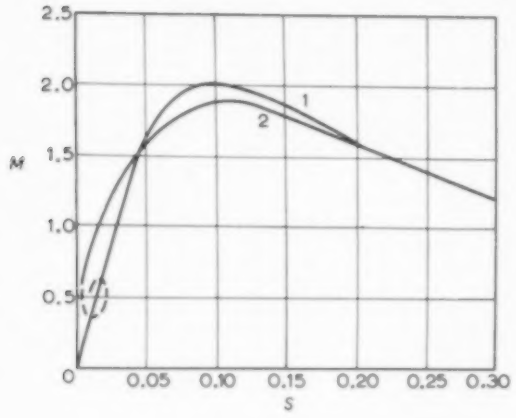

Fig. 4. Torque of a A92–4 induction motor on starting with an acceleration $2a = -1\ \text{sec}^{-2}$,

1 – steady-state characteristic

2 – characteristic including speed variation effects.

Fig. 4 shows the torque curve for a type A92–4 induction motor (100 kW, 1460 r.p.m.) run-up time $t = 2.6\ T_a = 1$ sec and $2a = -1\ \text{sec}^{-2}$ (a typical practical value). Table 2 gives the numerical values. The figure shows that the effect on the motor speed changes on the characteristic is fairly considerable around s_{max} and in the working range.

By considering the aperiodic current and flux linkage components in a similar way, we may predict the conditions during a three-phase dead short-circuit across the terminals of an induction motor.

Conclusions

The transient torque can be determined comparatively simply to the required accuracy by using the energy relations if approximate expressions are available for the currents, particularly the reactive short-circuit currents. This enables us to solve a number of practical problems.

Equations (18) and (19) can be used in simple calculations on induction motors operated at variable speeds where electromechanical transients are involved. These transients may solve many particularly important problems.

A similar study of power surges in synchronous machines and other such detailed processes not considered here may yield equally important results.

Appendix I

The stator currents i_d and i_q as well as the field current i_f during a three-phase dead short-circuit across a generator without damping winding may be expressed approximately by the following formulae [2,3]:

$$\left.\begin{aligned} i_d &\approx E_0\left[\frac{1}{x_d} + \left(\frac{1}{x'_d} - \frac{1}{x_d}\right)e^{-t/(T'_d)}\right] - \\ &\qquad - \frac{E_0}{x'_d}\, e^{-t/(T_a)} \cos \beta_\omega \ ; \\ i_q &\approx \frac{E_0}{x_q}\, e^{-t/(T_a)} \sin \beta_\omega \ ; \\ i_f &\approx i_{f0} + i_{f0}\,\frac{x_d - x'_d}{x'_d}\left(e^{-t/(T'_d)} - e^{-t/(T_a)} \cos \beta_\omega\right) . \end{aligned}\right\} \quad (I,1)$$

where $\beta_\omega = \int \omega dt$.

where E_0 is the no-load e.m.f.

The flux linkages of stator ψ_d and ψ_q and rotor ψ_f will be

$$\left.\begin{aligned} \psi_d &= -E_0 e^{-t/(T_a)} \cos \beta_\omega \ ; \\ \psi_q &= E_0 e^{-t/(T_a)} \sin \beta_\omega \ ; \\ \psi_f &= E_0 x_{af}\left[\frac{1 - e^{-t/(T'_d)}}{x_d} - \frac{1}{x_d - x'_d}\right] . \end{aligned}\right\} \quad (I,2)$$

1958

The magnetic energy variation dW_m/dt, from (4) taking into account (I,2), is

$$\frac{dW_m}{dt} \approx E_0 e^{-t/(T_a)} \left[\left(\omega \sin \beta_\omega + \frac{\cos \beta_\omega}{T_a} \right) i_d + \left(\omega \cos \beta_\omega - \frac{\sin \beta_\omega}{T_a} \right) i_q \right] - \frac{E_0^2 e^{-t/(T_d')}}{T_d' x_d} \left[1 + \frac{x_d - x_d'}{x_d'} \left(e^{-t/(T_d')} - e^{-t/(T_a)} \cos \beta_\omega \right) \right] . \qquad (I,3)$$

T_d' and T_a are some tens or hundreds of radians for normal machines. For simplicity therefore we may neglect terms containing T_d' and T_a in the denominator. After substituting the currents from (I,1) into (I,2) we get (11) for dW_m/dt.

Appendix II

The flux linkages of the stator ψ_{sv} and rotor ψ_{rv} are:

$$\left. \begin{aligned} \bar{\psi}_{sv} &= x_s \bar{i}_{sv} + x_m \bar{i}_{rv} \; ; \\ \bar{\psi}_{rv} &= x_r \bar{i}_{rv} + x_m \bar{i}_{sv} \; . \end{aligned} \right\} \qquad (II,1)$$

where x_s and x_r are the total stator and rotor reactances; x_m is the magnetizing reactance. From (17), (II,1) and (II,7) we get

$$\frac{d\bar{i}_{sv}}{dt} = - \frac{\alpha_s' \alpha_r + j\alpha_s' s + j(\alpha_r' + js)}{j\alpha_s' \alpha_r - \alpha_s' s + \alpha_s' + j} \bar{i}_{sv} , \qquad (II,2)$$

where α_s', α_r' and α_r are the damping factors of stator and rotor Since α_s' and $\alpha_r \approx 0$ (II,2) may be written in the form;

$$\frac{d\bar{i}_{sv}}{dt} \approx - j \frac{j + \alpha_s'}{j + \alpha_s'(1 - s)} s \bar{i}_{sv} - \frac{\alpha_r'}{1 - j\alpha_s'(1 - s)} \bar{i}_{sv} .$$

As $\alpha_s'(1-s)$ has relatively little effect and neglecting second-order infinitesimals, integration gives an approximate expression for the effect of stator resistance.

$$\bar{i}_{sv} \approx Ce^{-j\beta_r}e^{-\alpha(t)} , \qquad (II,3)$$

where

$$\beta_r = \beta + \alpha_r'\alpha_s'(t-\beta) ;$$

$$\beta = \int s\,dt ;$$

$$\alpha(t) = \alpha_r' t + \alpha_s' s\beta .$$

substituting (II,3) into (14), we find

$$\bar{i}_s = \bar{i}_{se} + Ce^{-j\beta_r}e^{-\alpha(t)} \qquad (II,4)$$

When $t = 0$, $\beta_r = 0$, $\alpha(t) = 0$. From (II,4) we find:

$$C = \bar{i}_{s0ss} - \bar{i}_{se} .$$

Consequently

$$\bar{i}_s = \bar{i}_{se} + (\bar{i}_{s0ss} - \bar{i}_{se})e^{-j\beta_r}e^{-\alpha(t)} . \qquad (II,5)$$

The smaller $di_{se}/ds \times ds/dt$ the better (II,5) satisfies the original differential equations. In the working range when ds/dt is comparatively large (II,5) will therefore yield sufficiently accurate results from relatively small ranges of slip variation. For this reason we will transform (II,5) into the following recurrence formula

$$\bar{i}_{sn} = \bar{i}_{se} + (\bar{i}_{s(n-1)} - \bar{i}_{se})e^{-j\beta_r}e^{-\alpha(t)} , \qquad (II,6)$$

where $\bar{i}_{sn}$ and $\bar{i}_{s(n-1)}$ are the complex stator currents for the nth and $(n-1)$th ranges of slip variation.

We then find i_{se} for the given slip, and β_r and $\alpha(t)$ are read every time. (II,6) agrees with a similar formula obtained by another method in (5) when $\beta_r \approx \beta$, $\alpha(t) \approx \alpha_r'\Delta t$ and $i_{se} \approx i_{s\,ss}$.

The complex stator flux linkage ψ_s, when approximate allowance is made for the stator resistance, becomes

$$\bar{\psi}_s \approx \frac{\bar{u}}{j} + j\bar{i}_s r_s \,. \tag{II,7}$$

M_n and W_n are given by

$$\left.\begin{aligned} M_n &= [j\bar{\psi}_{sn}\bar{i}^{*}_{sn}]_{Re} \,; \\ W_n &= [\psi_{sn} i^{*}_{sn}]_{Re} \,. \end{aligned}\right\} \tag{II,8}$$

Substituting (II,6) and (II,7) into (II,8) we get (18) and (19).

To determine i_{se}, M_e and W_e we start from (16) and use (3). As dW_e/dt is small we assume to a first approximation that the current and flux linkage variations follow the steady-state characteristics. If we simplify the equivalent circuit of the induction motor by eliminating the magnetizing circuit, we get

$$\frac{dW_e}{dt} \approx M_{ss}\epsilon \,,$$

where

$$\epsilon \approx \frac{M_{ss}}{u^2}\,\frac{ds}{dt}\,\frac{x_1 + c_1 x_2'}{\omega}\left(\frac{c_1}{s} + \frac{r_s}{r_r}\right).$$

Successive improvement of the term for the effect of magnetic energy variation on the motor currents, and repeated calculation of the energy relations from (3) yield a formula for the torque, viz.

$$M_e = M_{ss}(1 - \epsilon + \epsilon^2 - \epsilon^3 + \ldots) \,. \tag{II,9}$$

The terms in brackets are in geometrical progression; this gives (20). The magnetic energy stored in the stator is

$$W_e \approx \frac{u^2}{c_1 x_m} + \frac{u^2\sqrt{x_m^2 + \epsilon(r_m^2 + x_m^2)}}{c_1(1 + \epsilon)(r_m^2 + x_m^2)} \,,$$

where

$$r_a = r_s + c_1 \frac{r_r}{s} ; \qquad x_a = x_1 + c_1 x_2' .$$

REFERENCES

1. A.V. Ivanov - Smolwnskii; Effect of the rate of slip variation on the torque of an induction motor. *Elektrichestvo* No.6 (1950).
2. M.P. Kostenko; *Electric Machines (Special Part)*. Gosenergoizdat (1949).
3. R.A. Luyter; Prediction of induction motor short-circuit torques. *Elektrosila* No.7 (1950).
4. E. Ia. Kazovskii; Transients in induction motors on load cut-in and cut-out. *Vestnik Elekt. Prom*, No.2 (1949).
5. V.A. Shubenko and I.S. Pinchuk; A graphical method of predicting transients in induction motors. *Elektrichestvo* No.2 (1950).
6. F.I. Maggines and M.R. Shultz; Characteristics of induction motors. *Trans. Amer. Inst. Elect. Engrs.* **63**, 641, (1944).

1958

THE USE OF AMPLIDYNES AND TRANSISTOR AMPLIFIERS FOR INDUSTRIAL DRIVES*

V.A. NAIDIS

Machine Tool Experimental Research Institute

Controlled feed mechanisms driven by d.c. motors supplied by quadrature field controlled amplidynes are now widely used on heavy horizontal and vertical lathes, boring and milling machines.

The motor speed ranges on heavy machine tools feed drives must be large (1:100 upwards) speeds constant to better than ±10 per cent and the automatic control system must be sufficiently fast. The latter arises from the need for the drive to be uniform and stable notwithstanding the varying motor loading from heavy slow moving tool rests, head and tail stocks, etc.

Most heavy electric units use velocity feedback in which the difference between the set and d.c. tachometer voltages is fed to the amplidyne control winding either directly or through an intermediate amplifier.

In 1950 ESRIMCL (Machine Tool Experimental Research Institute) developed the first electric machine tool feed using electronic amplification; this was installed on an experimental vertical lathe type P.521. Such units have been widely used in a series of boring machines produced by "Sverdlov" machine-tool works in Leningrad. Considerable control-circuit gain is required as the speed range is up to 1:1800 and this demands intermediate amplification in the feedback circuit.

Intermediate amplification is also advantageous with much smaller speed ranges (1:100 or less) if the amplifier is sufficiently simple, reliable and of small size.

* *Elektrichestvo* No.3, 5-10 (1957). [Reprint Order No. EL.3]

If the tachometer's output is fed directly to the amplidyne input the amplidyne control winding must be of low resistance to give sufficient gain. The fairly high amplidyne control winding currents required demand tachogenerators and reference sources of rather larger capacity and size. For example, in units made to the designs of the "Elektroprivod" K.D.B. for large lathes, vertical lathes and other machine tools PN-2.5 type d.c. generators built into the feed gearbox are used as tachometers being themselves gear-driven. The voltage references are too large to be fitted on rack panels. Bulky anti-hunt transformers types TS 72-60 and TS 144-110 are used.

Intermediate feedback circuit amplifiers greatly reduce the size, weight and price of tachometer, regulator, etc. Smaller d.c. or a.c. tachometers integral with the motors can be used as well as small speed (references) with or without contactors which can be controlled from several places, e.g. from rack panels, as well as small anti-hunt R-C -circuits.

Intermediate feedback circuit and amplifiers improve the speed stability against load variation, reduce the effect of magnetization in the amplidyne winding, heating, exciter voltages etc. At constant overall gain, the gain of the time-lag element (amplidyne) can be reduced because the gain of the quick response element (intermediate amplifier) is higher, and this produces an improvement in the transient response.

Disadvantages of intermediate electronic amplifiers in units with speed ranges of 1:100 are limited valve life, filament preheating time, etc.

A number of organizations "Elektroprivod", Central Design Bureau, the Leningrad Electrotechnical Institute, together with the "Sverdlov" machine tool factory ESRIMCL, etc. have worked on intermediate magnetic amplifiers powered at 500 and 50 c/s. A 500 c/s magnetic amplifier can replace an electronic amplifier completely, but a frequency changer is required. A magnetic amplifier supplied from 50 c/s mains cannot be made to give a short enough response time. Stability becomes difficult to obtain because there is now an extra time constant. It was quite sufficient in the intermediate amplifier control system to introduce an amplidyne feedback to the intermediate amplifier input via an R-C-circuit. A magnetic amplifier control system also requires a series of derivative feedbacks between the amplifier stages and overall derivative feedback.

Transistor amplifiers

The production (1956) of a 1 W output Germanium transistor (type P.3) by the electronic industry resulted in the development of a transistor amplifier for machine tool control systems. Transistor amplifiers comparable with electronic amplifiers on gain and response time have advantages such as longer life, fewer service faults and smaller size. Transistor amplifiers have lives 10-15 times greater than vacuum valves. Transistors have no heaters and hence no warm-up time. The higher efficiency as compared with the electronic amplifier reduces the size of the supply transformer, rectifier and voltage stabilizer. The complete transistor amplifier is therefore only about half the size of an equivalent electronic amplifier.

The comparatively low input impedances of transistors might appear to be a disadvantage since this restricts the tachometer and reference source resistances and increases the derivative circuit capacitances, but these disadvantages can be avoided by using suitable circuits. The lower input impedance of a transistor amplifier enables one to isolate the input without fear of producing interference and noise. The need to earth the input of an electronic amplifier is disadvantageous especially when the amplifier and the rest of the drive circuit are connected electrically. Current production transistors still show large scatters in parameters; moreover many with high initial collector currents must be rejected as unsuitable for use in d.c. amplifiers.

The main disadvantage of transistors is, however, their sensitivity to ambient temperature variations. For example, in a simple two-stage amplifier with P3A transistor the output current changes by factors of 1.3 – 2 according to the working point used when the ambient temperature varies by 30°C. This causes difficulties in using transistor amplifiers in modern feed controls. Various methods of transistor amplifier temperature compensation are given in foreign journals. Either *p–n–p* and *n–p–n* triodes are used in alternate stages or else the parameters are stabilized by means of nonlinear resistances sensitive to ambient temperature. The first method cannot be used here because Soviet industry does not produce the barrier layer *n–p–n* type transistor. Parameter temperature-compensation circuits have been tested satisfactorily. Their disadvantages lie in the need to adjust the circuit, and the compensation is upset when one parameter changes. Considerably better results are obtained when the temperature compensation is obtained via special interstage circuits.

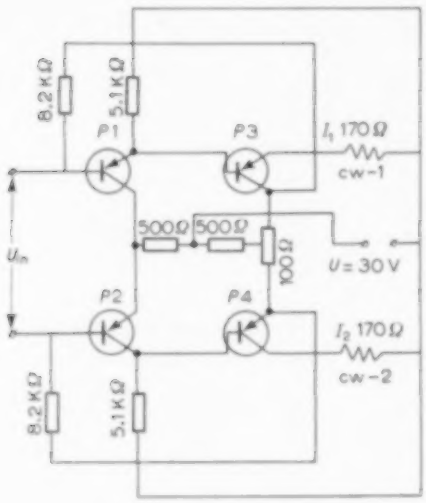

Fig. 1. Outline circuit of a two-stage balanced transient amplifier.
cw 1, *cw* 2 amplidyne control windings.
*P*1 – *P*4 transistors type P3A.

Fig. 1 shows the basic circuit of a two-stage balanced amplifier with P3A transistors which can be used for reversible drives. Temperature compensation is obtained as follows. The collector current increases

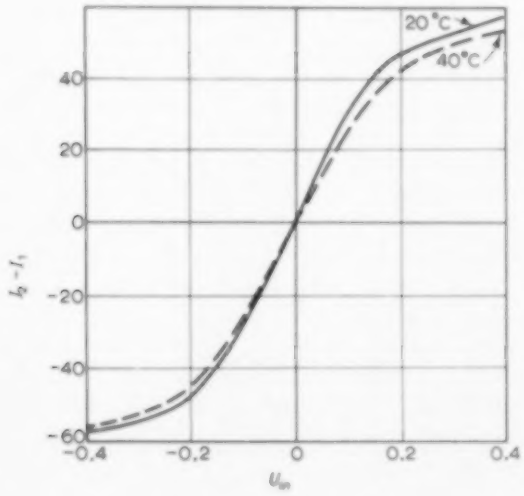

Fig. 2.

with ambient temperature. The collector current increase in stage one causes a decrease in positive emitter-base current in stage two i.e the load current falls. Suitable choice of the resistance controlling the collector-emitter voltage and suitable gain of the first stage and the use of negative feedback gave a characteristic $I_2 - I_1 = f(U_{input})$ almost independent of ambient temperature (Fig.2).

Units using the tachometers

Fig.3 shows the basic circuit of a feed drive for heavy horizontal and vertical lathes developed by the ESRIMCL. In these machines one d.c. motor provides feed movement in two directions at 90°. The feed direction is controlled by four electromagnetic clutches also used for copying work. A simple non-reversing circuit can then be used. The

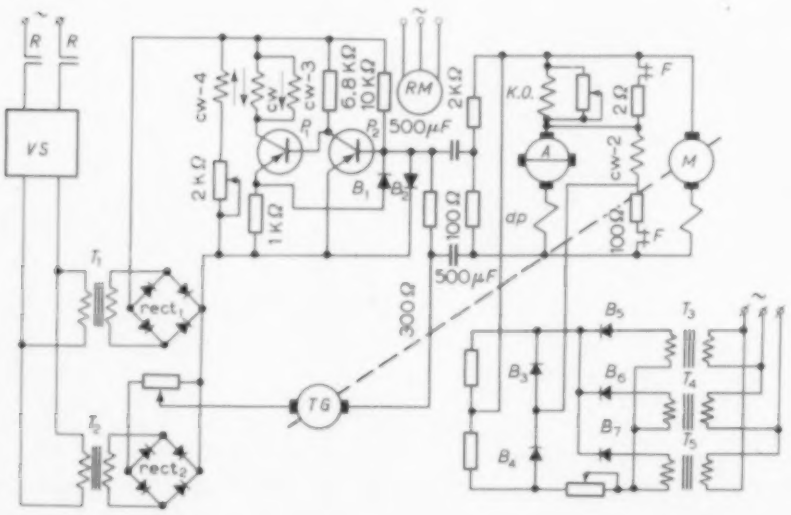

Fig.3 Outline circuit of the feed drives of horizontal and vertical lathes using d.c. tachometers.

IM induction motor, *A* amplidyne type EMU-25, 2.5 kW, 230 V, 2850 rev/min, *M* motor PN-28.5, 4.2 kW, 220 V 22 A, (I_{don} = 13 A at n = 0), *TG* tachogenerator TMG 30P, 250 V, 4000 rev/min, T_1 - T_5 transformers, *VS* voltage stabilizer, *P*1 transistor P3A, *P*2 transistor P1A, B_1, B_2 DG TS 27 diodes.

speed ranges required may be as high as 5000 – 10000. But electro-mechanical control plus gearbox-controlled steps of 1:100 would be more suitable.

A signal proportional to speed is provided by a small permanent-magnet d.c. tachometer *TG*, attached to the motor *M*. The difference between the set voltage and the velocity feedback signal is applied to the transistor amplifier input. The amplifier has r.c. feedback.

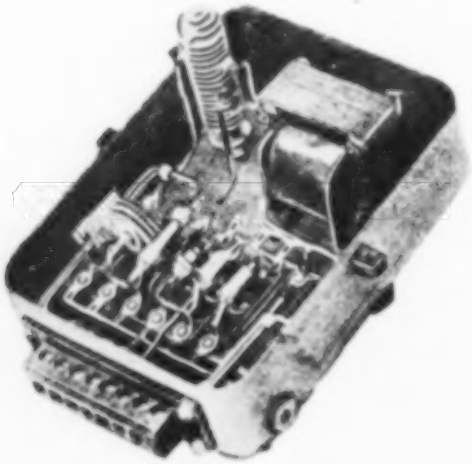

Fig.4 General view of the intermediate transistor amplifier (circuit diagram of Fig.3).

A photograph of the two-stage transistor amplifier shown in Fig.4 forms one of the arms in the circuit of Fig.1. At zero input and positive emitter-base in the first stage the collector current of the input stage is a maximum. The output stage load current is then a minimum (Fig.5). The working point I_w at the minimum motor speed $I_{w'}$ is determined by the control winding flux *cw* 4, and the residual flux in the amplidyne. By varying the resistance in the circuit of *cw* 4 it is possible to adjust this current to ensure maximum amplification at minimum motor speed and to reduce the effects of ambient temperature variations. The input is shunted by germanium diodes B_1 and B_2 to protect the amplifier against large input voltages during transients. B_1 has a voltage limiter protecting against the effects of the forward resistance of the diode in the steady-state conditions.

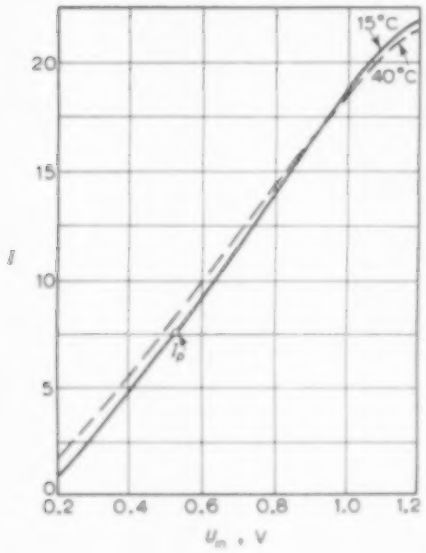

Fig. 5.

The current limitation is not different from that usual in amplidyne circuits of electric drives. The negative voltage feedback in the amplidyne effects braking and demagnetization on switching off and the compensation winding is shunted by a small resistance.

The unit was tested on the test bed and on a vertical lathe over a motor speed range of 1:100 (25 – 2500 rev/min). The set speed was constant within ±10 per cent for load variations from zero to rated load, the exciter voltage variations from 0.85 to 1.1 U_n, ambient temperature change from 10 to 40°C, and amplidyne remanent voltages of –20 to +20 V; temperature rise of the machine during 8 hour continuous operation at rated load, variation of the transistor amplifier supply voltage from 0.85 to 1.1 U_n, of the antihunt circuit leakage resistance by up to 1000 Ω, and successive replacement of both transitors.

Transient tests are equally important in heavy machine tools, especially sudden load change tests. It was stated above that during low-speed saddle feed movements without cutting work being done the load varies periodically. When the load suddenly changes the motor speed varies because of the natural regulation in the drive, recovering after a time dependent on the control system response time.

The initial motor speed change, the tool movement during the transient and the recovery time are all important with machine tools. At present there is no rule covering the permissible values of these quantities. The permissible overshoot under transient conditions should not, however, be more than 0.2 of the minimum feed rate expressed in mm per faceplate revolution.

For heavy horizontal and vertical lathes the minimum feed rate per revolution is supposed to be not less than 0.05 - 0.1 mm/rev and therefore the saddle movement must not be more than 0.01 - 0.02 mm. The reduction ratio from motor to saddle must be taken into account when calculating the permissible armature rotation. In heavy lathes the minimum feed-drive motor speed corresponds to a feed-rate of 0.1 - 10 mm/min depending on the lathe type and size. In the most unfavourable case, viz. 10 mm/min at a minimum motor speed of about 25 rev/min the permissible angular travel is 10 - 20°.

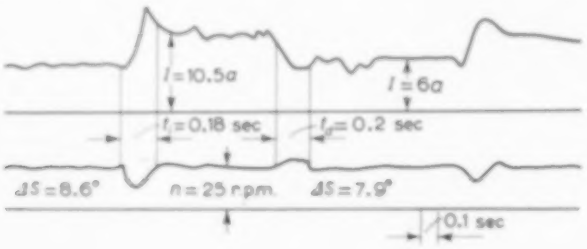

Fig. 6.

Fig. 6 shows an oscillogram for sudden load changes at 25 rev/min (range 1:100). The load change was 75 per cent which is 2 - 3 times more severe than the values usual under actual lathe working conditions. The oscillogram shows that the motor overshoot Δs, did not exceed 10 per cent, i.e. the fundamental requirement was satisfied.

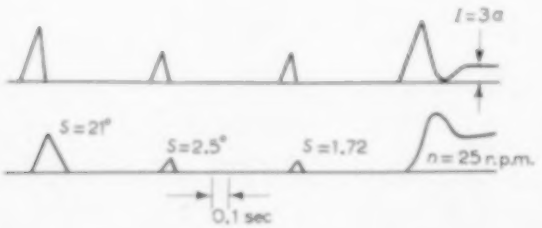

Fig. 7.

When the overshoot as a function of transient time was recorded for a minimum motor speed of 25 rev/min the angular travel (S) was between 2 and 20^{o} which corresponds to saddle movements of not more than 2 - 20 μ (Fig.7) in heavy horizontal and vertical lathes, even under the most unfavourable conditions.

Starting and braking at maximum motor speed are less important with these machine tools since electromechanical clutches are usually used.

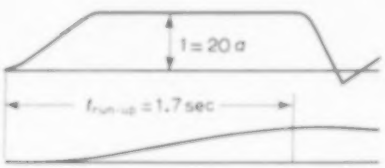

Fig.8

Fig.8 shows an oscillogram for a motor starting under load and running up to a 2500 rev/min. The long run-up time is due to the current being limited to the rated amplidyne current. The transient response time could be reduced considerably by increasing the amplidyne rating to 4.5 kW and the maximum current to 40 A.

Electric feed using an a.c. tachometer

The following advantages follow from replacing d.c. tachometers by a.c. ones: Absence of brushes and slot or commutator ripple on the output, and the possibility of using contactless selsyn regulators, the output being compared directly with the tachometer voltage.

Induction type a.c. tachometers with cup type rotors give outputs of constant frequency (50 c/s) this being their main advantage over synchronous a.c. tachometers, but induction-type tachometers with low induced e.m.f.s are very difficult to make.

The first experimental induction-type a.c. cup type rotor TG-56 tachometer has now been produced at The Moscow Electromechanical Engineering works to ESRIMCL specifications. The induced e.m.f. does not exceed 15 mV in these prototype tachometers the alternating component being 2 - 5 mV for a 60 V rating at 4000 rev/min.

ESRIMCL developed an electric feed unit with a.c. tachometer and transistor amplifier in which control of the feed from a number of

separate locations is particularly required with heavy vertical lathes, where the control must be both from a central panel and from the tool-

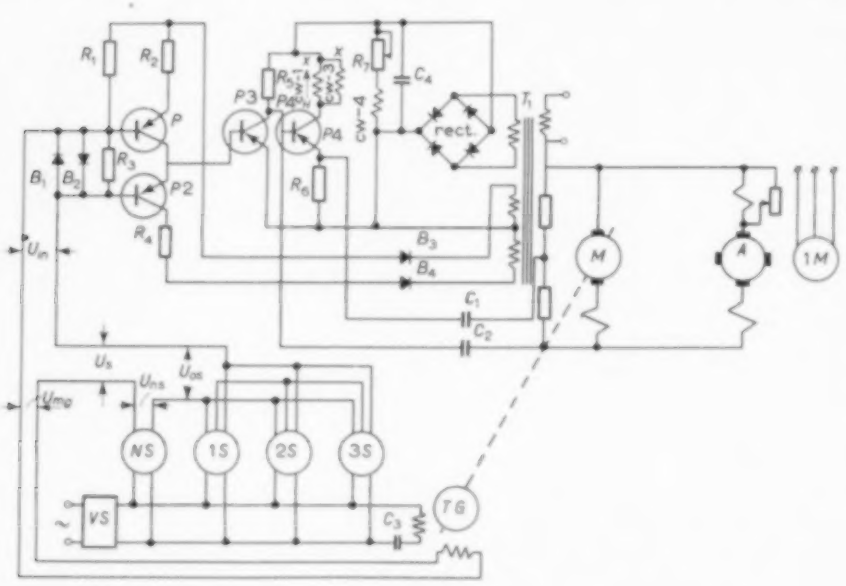

Fig.9 Outline circuit of heavy and turret lathe feed drives using a.c. tachometers.

M d.c. motor, *A* amplidyne, *IM* induction motor, *TG* tachometer, 1*S* – 3*S* selsyns, *NS* non-movable selsyn, *VS* voltage stabilizer, *P*1 – *P*4 transistors, B_1 – B_4 semiconductor diodes, *cw* 1 – *cw* 4, amplidyne control windings.

post control panels. Fig.9 shows the basic circuit without the current limitation, demagnetization and braking feedsback.

Selsyn receivers at appropriate check points transmit the required speed variations. 1*S* – 3*S* Selsyns serve as indicators, their secondary windings giving the required reference voltage.

The voltage U_{ns} from the stationary Selsyn NS on the control panel is subtracted from the output voltage U_{os} from the 1*S* – 3*S* Selsyns (Fig.10a).

1958

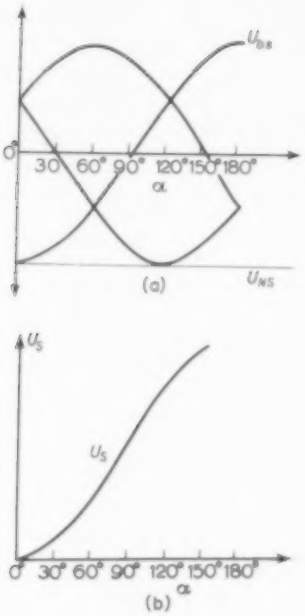

Fig. 10.

The $U_s = U_{os} - U_{ns}$ curve (Fig.10b) gives a convenient scale for the speed recording selsyns (these scales cover unequal ranges). The capacitor C_3 connected to the tachometer primary causes a phase difference of 180° between the speed voltage feedback U_{tg} and U_s. $U_i = U_s - U_{tg}$ is fed to the transistor amplifier input. This differs from the amplifier shown in Fig.3 only in having a preliminary phase-sensitive stage with P1A transistors (P1 and P2). The diodes B_3 and B_4 prevent reverse currents through the transistors.

The a.c. tachometer drives were tested over a speed range of 1:100 the test programme being the same as with the d.c. tachometers. The results were very similar.

Conclusions

Intermediate amplifiers should be used even in automatic speed control systems for heavy machine tool feed drives using small speed ranges (1:100 and less) which could be controlled without them. The intermediate amplifier reduces the sizes, weights and prices of the regulators, tachos and damping circuits required and improves the drive characteristics.

SHORT-CIRCUIT TRANSIENTS ON LONG LINES

R. I. KARAEV*

Molotov Power Engineering Institute, Moscow

1958

When long lines are affected by short-circuits, wave phenomena occur which cannot be obtained in circuits with lumped parameters. Although several papers on this problem have appeared [1,2] only the methods of solution have been described. The solutions are obtained by numerical methods which sometimes lead to tedious calculations involving complex numbers. The classical orthogonal function method (Sturm-Liouville's problem) which is comprehensively treated in works on mathematical physics [3] has not yet been applied to this problem. Sturm-Liouville's treatment assumes self-adjoint boundary conditions at the ends of a system with distributed parameters (open-circuit or short-circuit conditions, or time-independent ones). This condition is not fulfilled in transmission line circuits, especially compensated ones, in which the functions are not orthogonal in the narrow sense as formulated in Sturm-Liouville's problem. But when the system is considered as a whole, the functions will, nevertheless, be orthogonal in loss-free systems. The method described here is based on the orthogonality condition and yields a general solution for every concrete case. Such a solution facilitates analysis of the way individual parameters affect the phenomena without involving laborious calculations. The structure of the solution obtained is connected with the normal co-ordinates (natural oscillations) of the system which is advantageous when protective relay operating conditions are to be predicted.

Only the fault component of the short-circuit current is computed in this method since the normal load conditions can easily be determined. Transient phenomena in a three-phase circuit are considered using $\alpha\beta 0$ components. This is superior to the symmetrical component method under these conditions [2,5]. Thus the problem is reduced to the formulation of the additional sinusoidal e.m.f. in the individual single-phase

* Candidate in Technical Sciences, Molotov Power Engincering Institute, Moscow

component circuits when the initial condition is zero, the circuits being connected in accordance with the varying fault symmetry or asymmetry.

The circuit then has linear parameters, since the voltages in the various parts of the circuit do not increase during the short-circuit, even when the neutral is not effectively earthed. Iron-cored transformers and reactors also continue to operate on the linear parts of their characteristics. This simplifies the problem considerably.

Only the currents and voltages during the first 3 – 5 cycles are of interest at 50 c/s, since after that time the transients on the line have practically decayed. The operating time of the main protective equipment of a long line usually falls within this interval, and during these first 3 – 5 cycles the negative-sequence impedances in turbo-generators and in machines with damping cages, which are usually large hydro electric generators, differ from the positive-sequence values by not more than 20–25 per cent [4]. Moreover, with long transmission lines the generator reactances are of secondary importance, and in practice it is therefore possible to ignore this difference since it would not reduce the accuracy appreciably.

The method may be demonstrated by computing for a single-phase short-circuit at the end of an uncompensated long line supplied at both ends (Fig. 1).

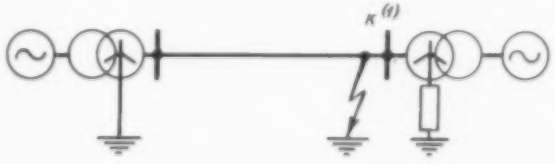

Fig. 1

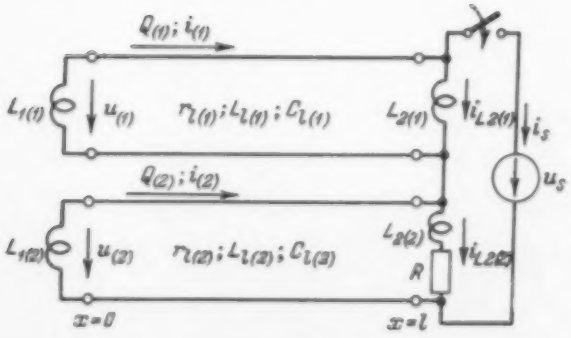

Fig. 2

The equivalent circuits used are shown in Fig.2 the upper representing the α-component, the bottom one the zero-component, the impedances being halved [2]. At first we consider circuits consisting of reactive elements only, but the method will subsequently be extended to include active resistances.

From electromechanical analogies [6] we take the unknown to be the charge $Q(x,t)$, which has passed through a point x on the line at a time t.

Q must satisfy

$$\frac{\partial^2 Q(x,t)}{\partial t^2} = \frac{1}{L_l C_l} \frac{\partial^2 Q(x,t)}{\partial x^2}$$

and is related to the voltages and currents at the point by:

1958

$$u(x,t) = -\frac{1}{C_l} \frac{\partial Q(x,t)}{\partial x} \tag{1}$$

$$i(x,t) = \frac{\partial Q(x,t)}{\partial t} . \tag{2}$$

Separating the variables, we obtain the solution in the form:*

$$Q_{f(m)} = \sum_{k=1}^{\infty} p_{kf} \left[A_{k(m)} \sin \frac{\omega_k}{v_{(m)}} x + B_{k(m)} \cos \frac{\omega_k}{v_{(m)}} x \right] + p_{0f} X_{0(m)} \tag{3}$$

where

$$p_{kf} = n_k \sin \omega_k t + m_k \cos \omega_k t ;$$

$$p_{0f} = n_{0t} + m_0$$

---

* In what follows the subscript (1) indicates quantities relating to the α-component, (2) those relating to the zero-component, and (m) quantities relating to both components; (k) denotes quantities relating to the k-th root of the characteristic equation

the ω_k are the angular frequencies of the natural oscillations;

the $v(m)$ are the electromagnetic wave propagation velocities.

The boundary conditions for the circuit shown in Fig.2 are as follows (quantities corresponding to the root $k = 0$ will be considered later):

$$\left| \frac{1}{C_{l(m)}} \frac{\partial Q_{f(m)}}{\partial x} = L_{1(m)} \frac{\partial^2 Q_{f(m)}}{\partial t^2} \right|_{x=0} \tag{4}$$

$$\left| \frac{1}{C_{l(1)}} \frac{\partial Q_{f(1)}}{\partial x} = -\frac{1}{C_{l(2)}} \frac{\partial Q_{f(2)}}{\partial x} \right|_{x=l} \tag{5}$$

$$\left| \frac{1}{C_{l(1)} L_{2(1)}} \frac{\partial Q_{f(1)}}{\partial x} + \frac{\partial^2 Q_{f(1)}}{\partial t^2} = \frac{1}{C_{l(2)} L_{2(2)}} \frac{\partial Q_{f(2)}}{\partial x} + \right.$$

$$\left. + \frac{\partial^2 Q_{f(2)}}{\partial t^2} \right|_{x=l} \tag{6}$$

Using equation (4) and assuming that

$$p''_{kf} = -\omega_k^2 p_{kf}$$

we get

$$B_{k(m)} = -A_{k(m)} \frac{Z_{s(m)}}{\omega_k L_{1(m)}} = A_{k(m)} \cot \theta_{1k(m)} \tag{7}$$

where

$$\theta_{1k(m)} = \tan^{-1} \frac{\omega_k L_{1(m)}}{Z_{s(m)}} \quad ;$$

$Z_{s(m)}$ is the surge impedance of the line.

Substituting the $B_{k(m)}$ in equation (3), we find that

$$Q_{f(m)} = -\sum_{k=1}^{\infty} p_{kf} \frac{A_{k(m)} \cos\left((\omega_k / v_{(m)})\, x + \theta_{1k(m)}\right)}{\sin \theta_{1k(m)}} + p_{0f} X_{0(m)} \cdot$$

The boundary condition (5) leads to the relation

$$A_{k(2)}Z_{s(2)}\frac{\sin(\omega_k\tau_{(2)}+\theta_{1k(2)})}{\sin\theta_{1k(2)}} =$$

$$= -A_{k(1)}Z_{s(1)}\frac{\sin(\omega_k\tau_{(1)}+\theta_{1k(1)})}{\sin\theta_{1k(1)}}$$

and (6) gives the characteristic equation as:

$$\frac{\omega_k}{Z_{s(1)}}\left[\cot(\omega_k\tau_{(1)}+\theta_{1k(1)})+\frac{Z_{s(1)}}{\omega_k L_{2(1)}}\right]+$$

$$+\frac{\omega_k}{Z_{s(2)}}\left[\cot(\omega_k\tau_{(2)}+\theta_{1k(2)})+\frac{Z_{s(2)}}{\omega_k L_{2(2)}}\right]=0\,, \qquad (8)$$

the roots of which are the natural frequencies of the system. Equation (8) is solved by iteration; the solution is not given here.

Passing from the free components to the actual values of the quantities, we write them in the following way:

$$Q_{(1)} = \sum_{k=1}^{\infty} q_k \frac{\cos(\omega_k/v_{(1)}\,x+\theta_{1k(1)})}{Z_{s(1)}\sin(\omega_k\tau_{(1)}+\theta_{1k(1)})}+p_0X_{0(1)} \qquad (9)$$

$$Q_{(2)} = -\sum_{k=1}^{\infty} q_k \frac{\cos(\omega_k/v_{(2)}\,x+\theta_{1k(2)})}{Z_{s(2)}\sin(\omega_k\tau_{(2)}+\theta_{1k(2)})}+p_0X_{0(2)} \qquad (10)$$

where

$$q_k = -p_kA_{k(1)}Z_{s(1)}\frac{\sin(\omega_k\tau_{(1)}+\theta_{1k(1)})}{\sin\theta_{1k(1)}}\,.$$

Lagrange's equation is used to determine the generalized co-ordinate $q_k (k \geqslant 1)$ (7)

$$\frac{d}{dt}\left(\frac{\partial T}{\partial q_k'}\right)+\frac{\partial V}{\partial q_k}+\frac{\partial F}{\partial q_k'}=f_k \qquad (11)$$

where T is the magnetic field (kinetic) energy of the system as a whole, (Fig.2);

V is the electric field (potential) energy,

F is the electromagnetic energy loss function (in a lossless system $F = 0$)

f_k is a generalized force.

The well-known theorem in algebra, that two homogeneous quadratic functions can be reduced by linear transformations to a sum of squares, can be used to give V and T for a lossless system in a form having no cross-products of co-ordinates (or velocities) but squares only [8, p.201].

With lossless long distance lines the above transformation of V and T is not required if these are considered for the system as a whole, i.e. they will not involve cross-products (of q_k and q_k'). This is also a property of orthogonal functions in general with consideration of the loads which also extends to the direct current component (corresponding to $k = 0$).

It is not necessary to calculate both T and V when considering harmonics since in a lossless system V is obtained by multiplying the corresponding terms in T by ω^2 [8, p.205].

It is simpler to calculate V for Fig.2, this being:-

$$V_{l(n)} = \int_0^l \frac{C_{l(n)} u_{(n)}^2}{2}\, dx = \frac{1}{2C_{l(n)}} \int_0^l \left(\frac{\partial Q_{(n)}}{\partial x}\right)^2 dx =$$

$$= \frac{1}{2} \sum_{k=1}^{\infty} q_k^2\, \omega_k^2\, a_{k(n)}$$

where

$$a_{k(n)} = \frac{\partial V_{l(n)}}{\partial q_k} \frac{1}{\omega_k^2\, q_k} =$$

$$= \frac{2\omega_k \tau_{(n)} - \sin 2(\omega_k \tau_{(n)} + \theta_{1k(n)}) + \sin 2\theta_{1k(n)}}{4\omega_k Z_{s(n)} \sin^2(\omega_k \tau_{(n)} + \theta_{1k(n)})}\,.$$

Adding the energies for both components, we find that V for the system as a whole is

$$V = V_{l(1)} + V_{l(2)} = \frac{1}{2} \sum_{k=1}^{\infty} q_k^2 \omega_k^2 a_k$$

where

$$a_k = a_{k(1)} + a_{k(2)} .$$

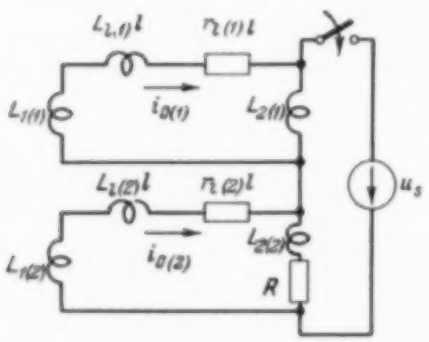

Fig. 3

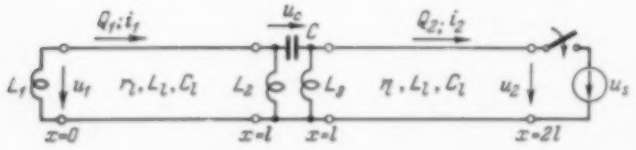

Fig. 4

If the line is capacity-compensated (Fig. 4) the energy stored in the capacitances would have to be added.

Substituting V and T in equation (11) we get

$$a_k(q_k'' + \omega_k'' q_k) = f_k \qquad (12)$$

To find f_k we must determine the energy the generator supplies when q_k changes by Δq_k:

$$f_k = \frac{u_s \Delta Q_{ks}}{\Delta q_k}$$

where

$$u_s = U_{max} \sin(\omega t + \psi) = \text{the switched e.m.f.}$$

Since

$$\int q_k dt = -\frac{q_k'}{\omega_k^2}$$

we obtain

$$i_{L2k(1)} = \frac{1}{L_{2(1)}} \int u_{k(1)} dt \Big|_{x=l} =$$

$$= -\frac{1}{C_{l(1)} L_{2(1)}} \int \frac{\partial Q_{k(1)}}{\partial x} dt \Big|_{x=l} = -\frac{q_k'}{\omega_k L_{2(1)}} . \quad (13)$$

From equations (9) and (13), the charge passing through the source is

$$\Delta Q_{ks} = \frac{\Delta q_k}{Z_{s(1)}} \left[\cot(\omega_k \tau_{(1)} + \theta_{1k(1)}) + \frac{Z_{s(1)}}{\omega_k L_{2(1)}} \right] .$$

And finally the expression for the generalized force is:

$$f_k = \left[\cot(\omega_k \tau_{(1)} + \theta_{1k(1)}) + \frac{Z_{s(1)}}{\omega_k L_{2(1)}} \right] \frac{U_{max}}{Z_{s(1)}} \sin(\omega t + \psi).$$

The integral of (12)[9, equations 5-96] is:

$$q_k = \frac{U_{max} \left[\cot(\omega_k \tau_{(1)} + \theta_{1k(1)}) + (Z_{s(1)}/\omega_k L_{2(1)}) \right]}{Z_{s(1)} (\omega_k^2 - \omega^2) a_k} \times$$

$$\left[\sin(\omega t + \psi) - \sin\psi \cos\omega_k t - \frac{\omega}{\omega_k} \cos\psi \sin\omega_k t \right] . \quad (14)$$

Substituting this in equations (9) and (10) and further in (1) and (2) the formulae are obtained for currents and voltages corresponding to the characteristic equations in (8) for $k \geqslant 1$.

In a lossless system the d.c. components of the free current and potential energy correspond to the root $k = 0$, and are zero. Fig.3, with open-circuited capacitances, also gives this result.

The Lagrange equation (in a lossy circuit) is then written as

$$\frac{d}{dt}\left(\frac{\partial T}{\partial q_0'}\right) + \frac{\partial F}{\partial q_0'} = f_0 \,. \tag{15}$$

From the line current components corresponding to $k = 0$,

$$i_{0(\alpha)} = p_0' X_{0(\alpha)} \,,$$

the current component in the supply is

$$i_{s0} = p_0' X_{0(\alpha)} \frac{L_{1(\alpha)} + L_{l(\alpha)} l + L_{2(\alpha)}}{L_{2(\alpha)}} \,.$$

1958

Assuming that this affects the α- and zero-components in the same way, the generalized co-ordinate is

$$q_0 = p_0 X_0 \frac{L_{1(\alpha)} L_{l(\alpha)} l + L_{2(\alpha)}}{L_{2(\alpha)}} \,.$$

So the generalized force is

$$f_0 = u_s = U_{max} \sin(\omega t + \psi) \,.$$

The magnetic energy component corresponding to $k = 0$ is

$$T_0 = \frac{a_0}{2} (q_0')^2$$

where

$$a_0 = L_{0(1)} + L_{0(2)}$$

and

$$L_{(\alpha)} = \frac{(L_{1(\alpha)} + L_{l(\alpha)} l)\, L_{2(\alpha)}}{L_{1(\alpha)} + L_{l(\alpha)} l + L_{2(\alpha)}} \,.$$

The solution to (15) for a lossless circuit ($F = 0$) is

$$q_0' = \frac{U_{max}[\cos\psi - \cos(\omega t + \psi)]}{\omega a_0} \tag{16}$$

Circuits with losses will now be considered.

The resistances in the equivalent circuits for single-phase and two-phase earth faults are

$$r_{lk} = (r_{ek} + r_c)/2$$

where $r_{ek} = 1.5\pi \cdot 10^{-4} w_k$ ohms/km [10], is the earth impedance per unit length (depending on frequency)

r_c = the conductor impedance per unit length

The line zero sequence inductance is only slightly frequency-dependent, and this effect will not be considered in what follows.

Unlike T and V, cross-products are retained in F and these influence the results somewhat. Assuming that the current distribution depends basically on the reactive elements, the dissipation function $F_{l(m)}$ for the line is:

$$F_{l(m)} = \int_0^l \frac{r_{l(m)}}{2}\left(\frac{\partial Q_{(m)}}{\partial t}\right)^2 dx =$$

$$= \int_0^l \frac{r_{l(m)}}{2}\left[\sum_{k=1}^{\infty}(\pm q_k') \frac{\cos[(\omega_k/v_{(m)})x + \theta_{1k(m)}]}{Z_{s(m)} \sin(\omega_k \tau_{(m)} + \theta_{1k(m)})} + \right.$$

$$\left. + q_0' \frac{L_{2(m)}}{L_{1(m)} + L_{l(m)} l + L_{2(m)}}\right]^2 dx =$$

$$= \sum_{k=1}^{\infty}\left[\frac{b_{k(m)}}{2}(q_k')^2 + \sum_{\substack{n=0 \\ n\neq k}}^{\infty} b_{kn(m)}\, q_k'\, q_n'\right]^*$$

---

* In this formula the positive sign corresponds to $m = 1$ and the negative sign to $-m = 2$.

where

$$b_{k(n)} = \frac{r_{1k(n)}}{L_{1(n)}} \times$$

$$\frac{2\omega_k\tau_{(n)} + \sin 2(\omega_k\tau_{(n)} + \theta_{1k(n)}) - \sin 2\theta_{1k(n)}}{4\omega_k Z_{s(n)} \sin^2(\omega_k\tau_{(n)} + \theta_{1k(n)})} \quad (k \geqslant 1);$$

$$b_{kn(n)} = \frac{r_{1kn(n)}}{L_{1(n)}} \times$$

$$\times \left\{ \frac{1/(\omega_k + \omega_n)\{\sin[(\omega_k + \omega_n)\tau_{(n)} + \theta_{1k(n)} + \theta_{1n(n)}] - \sin(\theta_{1k(n)} + \theta_{1n(n)})\}}{4 Z_{s(n)} \sin(\omega_k\tau_{(n)} + \theta_{1k(n)}) \sin(\omega_n\tau_{(n)} + \theta_{1n(n)})} + \right.$$

$$\left. + \frac{1/(\omega_k - \omega_n)\{\sin[(\omega_k - \omega_n)\tau_{(n)} + \theta_{1k(n)} - \theta_{1n(n)}] - \sin(\theta_{1k(n)} - \theta_{1n(n)})\}}{4 Z_{s(n)} \sin(\omega_k\tau_{(n)} + \theta_{1k(n)}) \sin(\omega_n\tau_{(n)} + \theta_{1n(n)})} \right\} \quad (k \geqslant 1);$$

$$b_{0(n)} = \frac{r_{10(n)} l L_{2(n)}^2}{(L_{1(n)} + L_{1(n)} l + L_{2(n)})^2} \quad (k = 0)$$

$$b_{0n(n)} = \pm \frac{r_{1n(n)}}{L_{1(n)}} \times$$

$$\times \frac{[\sin(\omega_n\tau_{(n)} + \theta_{1n(n)}) - \sin\theta_{1n(n)}]\, L_{2(n)}}{2\omega_n \sin(\omega_n\tau_{(n)} + \theta_{1n(n)})(L_{1(n)} + L_{1(n)} l + L_{2(n)})} \quad (k = 0)\,.$$

The quantity $r_{1kn(n)}$ appearing in the dissipation coefficient is given by

$$r_{1kn(n)} = \frac{r_{1k(n)} + r_{1n(n)}}{2}\,.$$

The current through R (Fig.2) is

$$i_{(R)} = \frac{1}{C_{1(2)} L_{2(2)}} \int \frac{\partial Q_{(2)}}{\partial x\, dt}\bigg|_{x=l} = \sum_{k=1}^{\infty} \frac{q_k'}{\omega_k L_{2(2)}} - \frac{q_0' L_{0(2)}}{L_{2(2)}}$$

---

* In this formula the positive sign corresponds to $n = 1$ and the negative sign to $n = 2$.

The dissipation function for R is:

$$F_{(R)} = \frac{Ri^2_{(R)}}{2} = \sum_{k=0}^{\infty}\left[\frac{b_{k(R)}}{2}(q'_k)^2 + \sum_{\substack{n=0\\ n\neq k}}^{\infty} b_{kn(R)}\, q'_k\, q'_n\right]$$

where

$$b_{k(R)} = \frac{R}{\omega_k^2 L^2_{2(2)}}; \qquad b_{kn(R)} = \frac{R}{2\omega_k\omega_n L^2_{2(2)}};$$

$$b_{0(R)} = \frac{RL^2_{0(2)}}{L^2_{2(2)}}; \qquad b_{0n(R)} = \frac{-RL_{0(2)}}{2\omega_n L^2_{2(2)}}$$

The dissipation coefficient for the circuit as a whole becomes

$$b_k = b_{k(1)} + b_{k(2)} + b_{k(R)}$$

b_{kn} b_0 and b_{0n} are calculated similarly by summing the individual components. For the generalized co-ordinates we substitute V, T and F in equation (11) and obtain a system of $(k+1)$ differential equations:

$$a_k q''_k + \omega_k^2 a_k q_k + b_k q'_k + \sum_{\substack{n=0\\ n\neq k}}^{\infty} b_{kn} q'_n = f_k \quad (k \geqslant 0)\,. \tag{17}$$

By successive approximation [11] we first eliminate the term $\Sigma b_{kn} q'_n$ (which is small compared with the others) from the left hand side. Then equation (17) separates into independent equations:

$$a_k q''_{kI} + \omega_k^2 a_k q_{kI} + b_k q'_{kI} = f_k \tag{18}$$

the solutions being (9, 5–94):

$$q_{kI} = q_{k\max}\left\{-\cos(\omega t + \psi - \Phi_k) + \right.$$

$$+ e^{-\delta'_k t}\left[\frac{\delta_k}{\omega_{kr}}\cos(\psi - \Phi_k)\sin\omega_{kr}t - \right.$$

$$\left.\left. - \frac{\omega}{\omega_{kr}}\sin(\psi - \Phi_k)\sin\omega_{kr}t + \cos(\psi - \Phi_k)\cos\omega_{kr}t\right]\right\}, \tag{19}$$

where

$$q_{k\max} = \frac{U_{\max} \sin \Phi_k \left[\cot(\omega_k \tau_{(1)} + \theta_{1k(1)}) + (Z_{s(1)}/\omega_k L_{2(1)})\right]}{Z_{s(1)}(\omega^2 - \omega_k^2)a_k} \qquad (k \geqslant 1);$$

$$\tan \Phi_k = \frac{\omega_2 - \omega_k^2}{2\delta_k \omega}; \qquad \delta_k = \frac{b_k}{2a_k}; \qquad \omega_{kr} = \sqrt{\omega_k^2 - \delta_k^2}.$$

Further, q'_{kI} is

$$q'_{kI} = q_{k\max}\,\omega\left\{\sin(\omega t + \psi - \Phi_k) - e^{-\delta_k t}\left[\sin(\psi - \Phi_k)\cos\omega_{kr}t + \right.\right.$$

$$\left.\left. + \frac{\omega_{kr}}{\omega}\cos(\psi - \Phi_k)\sin\omega_{kr}t - \frac{\delta_k}{\omega_{kr}}\sin(\psi - \Phi_k)\sin\omega_{kr}t\right]\right\} \quad (k \geqslant 1). \qquad (20)$$

When $k = 0$ we have

$$q'_{0I} = q_{0\max}\,\omega\left[\sin(\omega t + \psi - \Phi_0) - e^{-\delta_0 t}\sin(\psi - \Phi_0)\right] \qquad (21)$$

where

$$q_{0\max} = \frac{U_{\max}\sin\Phi_0}{a_0\omega^2};$$

$$\delta_0 = \frac{b_0}{a_0}; \qquad \tan\Phi_0 = \frac{\omega}{\delta_0}.$$

To find the second approximation, q_{kII}, it is necessary to substitute $q_k = q_{kI} + q_{kII}$ in the main terms and only the first approximation $q_n = q_{nI}$ is necessary in the summation $\Sigma b_{kn} q'_n$. Substituting these values and solving (18) we obtain

$$a_k(q''_{kII} + \omega_k^2 q_{kII}) + b_k q'_{kII} = -\sum_{n=0}^{\infty} b_{kn} q'_{nI} \quad (k \geqslant 0).$$

Applying Duhamel's formula [9, equations 5-116]

$$q_{kII} = \int_0^t \frac{e^{-\delta_k(t-\lambda)}\sin\omega_{kr}(t-\lambda)}{a_k\omega_{kr}}\left[-\sum_{\substack{n=0\\ n\neq k}}^{\infty} b_{kn} q'_{nI}(\lambda)\right] d\lambda.$$

q'_{nI} can be obtained from [20,21] by substituting subscript-n for subscript k.

Since q_{kII} is only a correction to q_{kI}, we assume in the following calculations that $\delta_k \ll \omega_k$.

Then:

$$q_{kII} = \sum_{\substack{n=0 \\ n\neq k}}^{\infty} \frac{b_{kn} q_{n\max} \omega}{a_k \omega_{kr}} \left[\frac{-\omega_{kr} \sin(\omega t + \psi - \phi_n) + \omega e^{-\delta_k t} \sin(\omega_{kr} t + \psi - \phi_n)}{\omega_{kr}^2 - \omega^2} + \right.$$

$$+ \frac{\omega_{kr} \sin(\psi - \phi_n)(e^{-\delta_n t} \cos \omega_{nr} t - e^{-\delta_k t} \cos \omega_{kr} t)}{\omega_{kr}^2 - \omega_{nr}^2} +$$

$$\left. + \frac{(\omega_n/\omega) \cos(\psi - \phi_n)(\omega_{kr} e^{-\delta_n t} \sin \omega_{nr} t - \omega_{nr} e^{-\delta_k t} \sin \omega_{kr} t)}{\omega_{kr}^2 - \omega_{nr}^2} \right] \quad (k \geqslant 0) \quad (22)$$

$$q'_{kII} = \sum_{\substack{n=0 \\ n\neq k}}^{\infty} \frac{b_{kn} q_{n\max}}{a_k} \left\{ \frac{\omega^2}{\omega_{kr}^2 - \omega^2} \left[-\cos(\omega t + \psi - \phi_n) + \right. \right.$$

$$\left. + e^{-\delta_n t} \cos(\omega_{kr} t + \psi - \phi_n) \right] -$$

$$- \frac{\omega \sin(\psi - \phi_n)(\omega_{nr} e^{-\delta_n t} \sin \omega_{nr} t - \omega_{kr} e^{-\delta_k t} \sin \omega_{kr} t) -}{\omega_{kr}^2 - \omega_{nr}^2}$$

$$\left. \frac{- \omega_{nr}^2 \cos(\psi - \phi_n)(e^{-\delta_n t} \cos \omega_{nr} t - e^{-\delta_k t} \cos \omega_{kr} t)}{\omega_{kr}^2 - \omega_{nr}^2} \right\} (k \geqslant 0). \quad (23)$$

q_{kI} (first approximation) gives the reactive current components with adequate accuracy. q_{kII} (second approximation) differs in phase from the first by $\pi/2$ and gives the ohmic current components satisfactorily. These approximations always suffice since in the majority of practical calculations the first approximation is sufficiently accurate, and (22) and (23) need only be used to check the error involved.

The active resistances affect the current distribution mainly via the component corresponding to $k = 0$. Therefore the zero-components of the currents and voltages should be calculated direct from the circuits in very complicated systems with open-circuit capacitances and high active resistances, without applying Lagrange's equation, (15), in order to avoid errors.

Using the generalized co-ordinates and their derivatives, together with equations (9) and (10), the required currents and voltages are found to be:

$$i_{(1)} = \sum_{k=1}^{\infty} q_k' \frac{\cos((\omega_k/v_{(1)})x + \theta_{1k(1)})}{Z_{s(1)} \sin(\omega_k \tau_{(1)} + \theta_{1k(1)})} + \\ + \frac{q_0' L_{2(1)}}{L_{1(1)} + L_{l(1)} l + L_{2(1)}} ; \quad (24)$$

$$u_{(1)} = \sum_{k=1}^{\infty} q_k \frac{\omega_k \sin((\omega_k/v_{(1)})x + \theta_{1k(1)})}{\sin(\omega_k \tau_{(1)} + \theta_{1k(1)})} - \\ \frac{q_0'' L_{2(1)}(L_{1(1)} + L_{l(1)} x) + q_0' L_{2(1)} r_{l(1)} x}{L_{1(1)} + L_{l(1)} l + L_{2(1)}}. \quad (25)$$

$i_{(2)}$ and $u_{(2)}$ are written by analogy by interchanging subscripts (1) and (2) and reversing the sign. The components corresponding to $k = 0$ do not alter in sign.

The known relationships in the $\alpha\beta 0$ system [2] can be used to calculate the phase currents and voltages in the three-phase system. The forced and free components were calculated simultaneously above. Obviously, they can also be found individually by the symbolic method [9].

---

* See (9) and (10).

The formulae for a three-phase fault on a compensated line are given in the Appendix by way of an example. More complicated systems can also be treated by this method.

Appendix

Formulae for use with three-phase faults at the ends of compensated lines (Fig. 4)

Characteristic equation:

$$\frac{1}{\cot(\omega_k\tau + \theta_{1k}) + Z_s/\omega_k L_2} + \frac{1}{\cot \omega_k\tau + Z_s/\omega_k L_3} = \frac{1}{\omega_k C Z_s}$$

Currents and voltages

$$i_1 = \sum_{k=1}^{\infty} q_k' N_k \cos(\omega_k x/v + \theta_{1k}) ;$$

$$i_2 = \sum_{k=1}^{\infty} q_k' \cos(2\omega_k\tau - \omega_k x/v) + i_0 ;$$

$$u_1 = \sum_{k=1}^{\infty} q_k N_k \omega_k Z_s \sin(\omega_k x/v + \theta_{1k}) ;$$

$$u_2 = -\sum_{k=1}^{\infty} q_k \omega_k Z_s \sin(2\omega_k\tau - \omega_k x/v) + u_0 ;$$

$$u_c = \frac{1}{C}\sum_{k=1}^{\infty} q_k \frac{\sin(\omega_k\tau + \theta_{3k})}{\sin \theta_{3k}} + L_3 \frac{di_0}{dt}$$

where

$$i_0 = \frac{U_{max} \sin \phi_0 [\sin(\omega t + \psi - \phi_0) - e^{-\delta_0 t} \sin(\psi - \phi_0)]}{\omega(L_3 + L_l l)} ;$$

$$u_0 = -[L_3 + L_l(x - l)] \frac{di_0}{dt} + r_l(x - l)\, i_0 ;$$

$$N_k = \frac{\sin(\omega_k\tau + \theta_{3k}) \sin\theta_{2k}}{\sin\theta_{3k} \sin(\omega_k\tau + \theta_{1k} + \theta_{2k})} \quad (k \geqslant 1)$$

$$\delta_0 = \frac{r_l l}{L_3 + L_l l} .$$

The amplitudes of the generalized co-ordinates are

$$q_{k\max} = \frac{U_{\max} \sin\Phi_k}{(\omega^2 - \omega_k^2)a_k} \quad (k \geqslant 1) .$$

The coefficients in the differential equations for the generalized co-ordinates are:

$$a_k = \frac{Z_s}{4\omega_k}\left\{N_k^2[2\omega_k\tau - \sin 2(\omega_k\tau + \theta_{1k}) + \sin 2\theta_{1k}] + \right.$$

$$\left. + 2\omega_k\tau - \sin 2\omega_k\tau + \frac{4\sin^2(\omega_k\tau + \theta_{3k})}{\omega_k CZ_k \sin^2\theta_{3k}}\right\} \quad (k \geqslant 1) ;$$

$$b_k = \frac{r_l}{L_l}\frac{Z_s}{4\omega_k}\left\{N_k^2[2\omega_k\tau + \sin 2(\omega_k\tau + \theta_{1k}) - \sin 2\theta_{1k}] + \right.$$

$$\left. + 2\omega_k\tau + \sin 2\omega_k\tau\right\} \quad (k \geqslant 1) .$$

q_{kI}, q'_{kI}, δ_k, Φ_k, Φ_0, ω_{kr} are given by the above formulae.

REFERENCES

1. E.A. Meerovich; Calculation of transient phenomena in complicated electrical systems. *Izv.Akad. Nauk SSSR., otd. tekh. nauk* No. 10 (1950).
2. R.I. Karaev; Transient phenomena in long three-phase lines. *Electrichestvo* No.10 (1954).
3. R. Courant and D. Hilbert; *Methods of Mathematical Physics.* Gos. izd. tekh. i teor. lit. (1951).
4. S.A. Ul'yanov; *Short-Circuits in Electrical Systems.* Gosenergoizdat (1952).

5. E. Gross and L. Rabins; Transient performance of three-phase power systems. *J. Franklin Inst.* (May 1951).
6. K. Teodorchik; Two electromechanical Analogue systems based on Lagrange's equation. *Zh. tekh. fiz.* 8, No.18 (1938).
7. Lord Rayleigh (J.V. Strutt); *Theory of sound.* Gosenergoizdat (1955).
8. E.T. Whittaker; Analytical dynamics. *ONTI NKTP SSSR* (1937).
9. A.V. Neshutil and S.V. Strakhov; *Fundamentals of Electrical Engineering* Part II. Gosenergoizdat (1955).
10. R. Rudenberg; *Transient Performance of Electrical Power Systems NL* (1950).
11. A.N. Krylov; Lectures on approximate calculations. *Gos. izd. tekh. i teor. lit.* (1950).

RATES OF RISE OF RESTRIKING VOLTAGE ACROSS CIRCUIT-BREAKER CONTACTS IN LARGE POWER SYSTEMS*

M. M. BELOUSOV**

Lenin All-Union Electrical Engineering Institute

1958

The rate of rise of the restriking voltage across the contacts of a circuit-breaker clearing a short-circuit is determined by the circuit parameters (neglecting post-arc conductivity). Most determinations of restriking voltage characteristics from theory or experiment comprise values corresponding to various points in existing systems and which are expressed statistically, (by their frequency or by the rate of rise of restriking voltage) and the restriking rate requirements are specified to correspond [1-3].

The design of new circuit breakers must not be governed by present-day operating conditions but should envisage conditions which will probably obtain in 5-10 years time.

The growth of system power is not only due to increase in the number of elements (generators, transformers, transmission lines) but also to increase in their power ratings and to the tendency towards higher operating voltages.

The increase in transformer ratings results in a greater short-circuit MVA at the terminals. To preserve the original operating conditions for a circuit-breaker clearing a fault on the transformer busbars, the increase in the short-circuit MVA would have to be accompanied by a reduction in the restriking voltage frequency. But the frequency does not decrease, and actually becomes slightly higher.

When the system voltage is increased, the number of transmission lines connected to the station busbars is usually reduced. This produces a higher resultant characteristic impedance of all lines connected to these busbars, and also increases the likelihood that a

* *Elektrichestvo* 4, 21-24, 1957 (Reprint Order No. EL5)

** *Candidate in Technical Sciences*

fault occurring at the beginning of one line may be cleared when no other line (or only one) is connected in parallel. In both cases the rate of restriking voltage rise (s) may become high.

Analogue studies of an isolated station with powerful generators (4) indicated values higher than those present in actual systems. It will be shown later that these results are insufficient as criteria of the values in large power systems.

Let us consider, for example, the S value for a 220 kV circuit breaker interrupting a fault at the point K-1, Fig. 1. We will assume

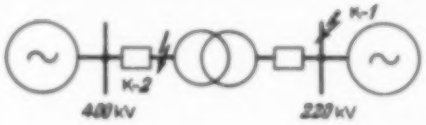

Fig. 1

that the transformer rating is 360 MVA, u_k = 14 per cent, a winding capacitance of 10,000 pF and an external circuit capacitance (busbars and circuit breaker) of 600 pF. Referring one half of the winding capacitance to the line terminal and assuming the h.f. inductance to be 90 per cent of that at 50 c/s, the natural frequency of the restriking voltage becomes

$$f = \frac{1}{2\pi\sqrt{L_t C}} = 9.04 \text{ kc/s}$$

where L_t = transformer inductance

C = capacitance to earth of the transformer line terminal.

Another method is to assume the "high frequency" inductance to be the same as at 50 c/s and to consider only one third of the winding capacitance. Then f = 10.2 kc/s. In what follows the average value of 9.6 kc/s is used. It is obvious that when a short-circuit behind the transformer (K-2) is interrupted we should get the same fundamental frequency if the reactances of the other sources referred to the 220 kV busbars were smaller than the transformer reactance.

The above frequency is much higher than those at which 220 kV circuit-breakers are tested at present; the short-circuit MVA interrupted in Fig 1.can also be considerable (in the example about 2000 MVA).

In determining the S values let us consider only a three-phase fault not involving earth. The amplitude of the 50 c/s recovery voltage is then $1.5U_{ph}\sqrt{2}$.

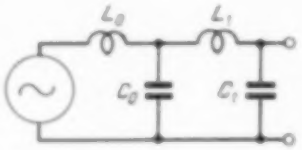

Fig. 2. L_0 is the referred inductance of the system; C_0 is the equivalent parallel capacitance across the left-hand winding of the transformer; L_t the transformer inductance, and C_t the capacitance from live to neutral of the transformer secondary.

If a fault occurs at K-1 the circuit of Fig. 1 can be considered as a double-frequency circuit (Fig. 2). S is then determined by the h.f. component, of amplitude proportional to L_t:

$$s = 4f \times 1.15 \times 1.5U_{ph}\sqrt{2}\,\frac{L_t}{L_0 + L_t}$$

$$= 4 \times 9600 \times 1.15 \times 1.5 \times \frac{220}{\sqrt{3}} \times \sqrt{2} \times 0.835 \times 10^6$$

$$= 9.9 \text{ kV}/\mu\text{sec}$$

(Allowance has been made for a possible increase of 15 per cent in the system voltage.)

An amplitude factor of 1.57, which allows for the damping is introduced when this formula is used for determining the maximum S. The experimental value of this factor is about 1.6 [1].

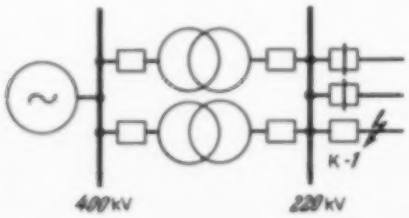

Fig. 3.

Consider the circuit of Fig.3. In this case we assume the short-circuit MVA at the 400 kV busbars to be 15,000 MVA with all the 220 kV lines in circuit and that at the 220 kV busbars to be 10,000 MVA. The transformer parameters are the same as those of Fig.1. Then if all the 220 kV lines are disconnected, the short-circuit MVA interrupted on clearing the fault at K-1 is 364 MVA and $L_t/(L_0 + L_t) = 0.71$. Assuming further that the total capacitances of the busbars and 220 kV switchgear is 6000 pF, the h.f. component frequency becomes

$$f = \frac{1}{2 \times 3.14\sqrt{0.9(0.06/2)\left[2(10000/2) + 6000\right]}}\,10^{-3} = 7.65 \text{ kc/s}$$

and hence

$$S = 4 \times 7650 \times 1.15 \times 1.5\,\frac{220}{\sqrt{2}}\,\sqrt{2} \times 0.71 \times 10^{-6} = 6.72 \text{ kV/}\mu\text{sec}$$

Let us next determine S at the full short-circuit MVA (10,000 MVA) under the least favourable conditions, i.e. when a large short-circuit MVA obtains at a given point (due mainly to generator proximity) and the number of outgoing lines on the busbars is least.

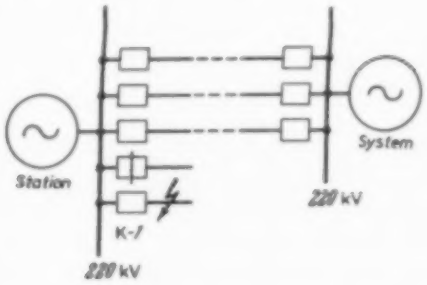

Fig. 4.

Consider a station with five outgoing lines (Fig.4). Three lines connect the station to a large power system, the other two are either spur lines, or may be interconnected with stations which affect the short-circuit currents at K-1 to a negligible extent; one of these lines has been switched off earlier.

Conditions are then most severe when clearing a fault on the spur which had been left in circuit.

For simplicity assume the three lines of the same length (100 km) and that the distant busbars are of infinite capacity. This does not

introduce any serious errors since the line reactances are high by comparison with the referred reactances of the large power system.

Calculating according to the method of [1], we get the restriking voltage curve shown in Fig.5. The restriking voltage is expressed as a relative quantity in this figure, and also in Figs. 6 and 7, the amplitude of the 50 c/s recovery voltage being taken as unity.

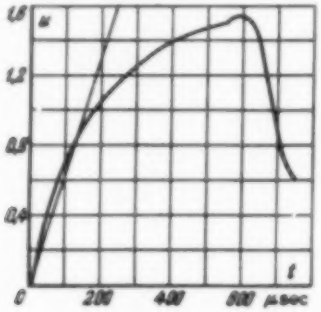

Fig.5.

With this shape of restriking voltage curve it would be incorrect to determine S from the slope of the tangent at the origin. The mean rate of rise to the maximum would also be incorrect, since this would be too low.

We shall take the rate of rise to be the average rate for the interval from the origin to the point corresponding to 80 per cent of the 50 c/s recovery voltage amplitude. The point corresponding to 100 per cent of the 50 c/s recovery voltage amplitude should not be used, since this would give values much too low with nearly-aperiodic curves, and zero rate of rise in the limiting case of complete aperiodicity.

The value of S and the amplitude factor as determined from Fig.5 are 2.05 kV/μsec and 1.53 respectively.

If the number of lines is increased in Fig.4, S will be lowered, e.g. if the number of lines is raised from three to five, S drops from 2.05 kV/μsec to 1.38 kV/μsec.

These relatively high S values are typical for stations and sub-stations working in a large power system where large breaking MVA's are involved. The S values for isolated stations with many lines are considerably lower, even if the stations are of large capacity.

With an isolated station with the same equipment parameters as in the above example, and with five outgoing lines (apart from the line on which a fault is being cleared) we would get the curve shown in Fig.6 and an S of 0.38 kV/μsec when 4000 MVA is interrupted.

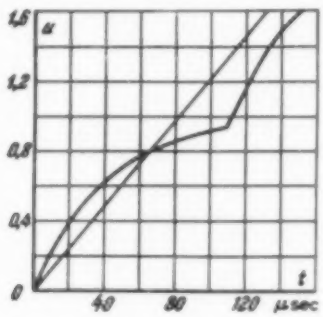

Fig. 6.

Thus it appears that the breaker operating conditions in an isolated station are much easier than in a large power system, and it is therefore incorrect to determine restriking rate requirements for new circuit-breakers from results on an isolated station or its model.

The author has carried out similar calculations for a 110 kV breaker. It was assumed that at full MVA four 30 km lines remained connecting the station busbars to the large power system. The reactance of the 110 kV system was not assumed as zero, as in the 220 kV system example, since the line reactances are considerably lower in this case. The referred reactance of the 110 kV system was taken as 2.01 ohms, which corresponds to a short-circuit MVA of 6000.

No calculations were made for the conditions of Fig.3 for the 110 kV system since at this voltage such a circuit would in practice only be used with relatively small transformers.

The results for the 110 and 220 kV systems are given in the Table 1 below.

Table 1.

Rates of rise of restriking voltage in 110 and 220 kV systems

Circuit diagram	110 kV system			220 kV system		
	MVA interrupted	Rate of rise of restriking voltage, kV/μsec (S)	Frequency, kc/s	MVA interrupted	Rate of rise of restriking voltage, kV/μsec	Frequency, kc/s
Fig.1	2140	8.65	16.4	2140	9.9	9.6
Fig.3	–	–	–	3640	6.72	7.65
Fig.4	6000	1.69	2.73	10,000	2.05	1.65

1958

$$f = \frac{s \times 10^3}{4U} \text{ kc/s}$$

where S = rate of rise of restriking voltage, kV/μsec

U = amplitude of the 50 c/s recovery voltage, kV.

Since the calculations involve a number of assumptions and simplifications they cannot, of course, be expected to be very accurate. Nevertheless, the results can form a basis for selecting restriking voltage requirements for large circuit-breakers of the 110 – 220 kV class.

The present practice of standardizing restriking voltage frequency at 100 and 50 per cent of the ultimate breaking capacity of the circuit breaker should be regarded as unsuitable. Since the restriking voltage parameters depend not on the circuit-breaker but on the power system, they should be chosen in relation to the absolute magnitude of the short-circuit MVA, irrespective of the circuit breaker capacity. Each h.v. circuit breaker intended for operation in a large power system, irrespective of its nominal breaking capacity, should be type-tested at 2000 – 2500 MVA under the conditions represented in Fig.1, since these very conditions produce the highest S values, as well as at its nominal breaking MVA.

Since the foregoing concerns only breakers without contact shunts, let us now examine the effect of shunting. In transmission line circuits (e.g.Fig.4), the circuit breaker contacts are shunted by the characteristic line impedances. Therefore for a shunt to control the restriking voltage its impedance should be comparable with the effective characteristic line impedance. This means that the shunt resistance should not exceed a few hundred ohms (or sometimes maybe only a few tens of ohms). A subsidiary switch or arc-quenched interrupter has then to be fitted into the main body of the circuit-breaker to interrupt the final shunt current.

In Fig.1 the shunt resistance should also be comparable with the characteristic impedance of the circuit. Assuming that the restriking voltage frequency is to be reduced (by using an ohmic shunt) by at least 25 per cent, we get

$$f_1 = \frac{1}{2\pi}\sqrt{\frac{1}{LC} - \left(\frac{1}{2rc}\right)^2} = \frac{0.75}{2\pi\sqrt{LC}}$$

whence

$$r_{sh} \approx 0.755\sqrt{\frac{L}{C}}$$

In particular, with the transformer parameters assumed for Fig.1 r_{sh} becomes 1300 and 2900 Ω for the 110 and 220 kV circuit-breakers respectively.

If the circuit-breaker in Fig.1 has a non-linear shunt having the characteristic $u = ki_{sh}^{\alpha}$ the following equations apply:

$$L\frac{di}{dt} + u = U; \qquad i = C\frac{du}{dt} + \left(\frac{u}{k}\right)^{\alpha^{-1}}$$

After differentiating and rearranging, we get an equation which is not integrable in the general form, viz.

$$\frac{d^2u}{dt^2} = \frac{U}{LC} - \frac{u^{(\alpha^{-1}-1)}}{C\alpha k^{\alpha^{-1}}}$$

Taking a numerical example (transformer 110 kV, 180 MVA, non-linear shunt with $k = 8 \times 10^4$ and $\alpha = 0.25$), we get the curve shown in Fig.7 by numerical integration and iteration. This figure also shows the undamped curve (2) obtained with the same transformer parameters for comparison. In the example the shunt characteristic was so chosen that

the shunt should also be of acceptable size and have a final current which could be interrupted by a simple break in air. It can be seen from Fig.7 that the shunt does not lower S, but only decreases the amplitude and accelerates damping.

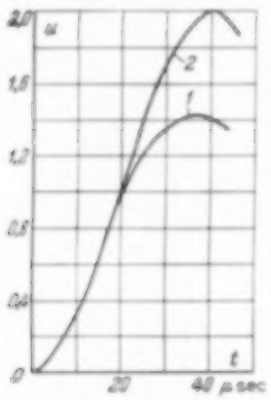

Fig. 7

Thus, shunting the contacts of a h.v. circuit-breaker operating in a large power system can reduce S only if the shunt resistance is sufficiently low. In this case, however, an arc-quenching device is necessary to interrupt the final current, which considerably complicates the design and increases the cost of the circuit-breaker.

Therefore the breaker design in practice should be one which can cope with high S values without resort to contact shunting; light shunting may be used for voltage grading across the gap. The gap should possess a high rate of dielectric strength recovery. It is probably that on interrupting transformer magnetising currents such a breaker would set up high surge voltages.

The surge voltages can be reduced to a permissible level by using a light non-linear shunt having an acceptable size and a small final current which is easy to inetrrupt. However, in all probability, a more suitable solution would be to install valve type surge diverters directly on the transformers (and not on the station busbars).

CONCLUSION

As power systems expand and capacities of generators and transformers increase, the rates of rise of restriking voltage are bound to go up.

New designs for large h.v. circuit-breakers should be based on high rates of rise of restriking voltage. The calculations presented in the present communication may be used to derive standards for the rates of rise of restriking voltage used in circuit-breaker tests.

REFERENCES

1. P. Hammarlund; *Restriking Voltage across the Contacts of a Circuit Breaker*. Gosenergoizdat (1956).
2. Johansen; *CIGRE* Paper no.104, (1952).
3. G.V. Butkevich; Some problems in the design of modern circuit-breakers. *Elektrichestvo* No.2 (1955).
4. Johnson, Schulz and Skeats; *Trans. Amer. Inst. Elect. Engrs.* **111**, 1339 (1953).

SELECTION OF ANTIHUNT TRANSFORMERS FOR AMPLIDYNE ELECTRIC DRIVES*

S.S. ROIZEN†

Tiazhpromelektroprokt

1958

Motor + generator electric drives using amplidynes employ antihunt transformers to secure stability and the required transient characteristics. The transient duration and hence the system quality are determined to a large extent by correct transformer parameter choice in the design stage and correct setting when commissioning the drive.

The solution might appear to be simply to provide the design and erection engineers with the catalogue data, but experience has shown that calculations based on catalogue data for the machines and antihunt transformers give results which do not agree with tests.

The calculated overall maximum gains are usually much higher than the actual ones. For example, the calculated overall gain (K) for a 20 kW system with an EMU-12 A amplidyne and TS–72/60 transformer, was 65, but instability actually sets in at $K = 20$. Allowing for the self and mutual inductances of the amplidyne control windings and the transformer leakage reactance does not produce any considerable difference in the result.

When the system is RC stabilized, the calculated and experimental results are in good agreement. Hence the errors in the transformer calculation are not due to the method but to the transformer data used.

Consider an antihunt circuit including an amplidyne (Fig.1). The following equations can be set up for this circuit:

$$U_{1t} = i_{1t}r_{1t} + w_{1t}p\Phi_t \qquad (1)$$

$$w_{2t}p\Phi_t = i_{2t}(r_{2t} + r_2) \qquad (2)$$

* *Elektrichestvo* 4, 57–59, 1957 (Reprint Order No. EL6)

† *Candidate in Technical Sciences, Tiazhpromelektroprokt*

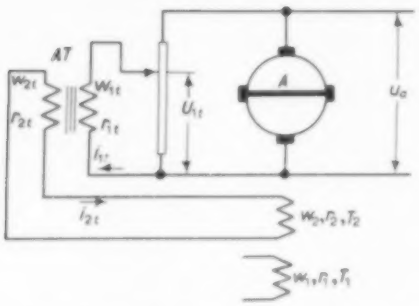

Fig. 1. Circuit diagram of the amplidyne–antihunt transformer unit.

A = amplidyne, AT = antihunt transformer.

$$(i_{1t}w_{1t} - i_{2t}w_{2t}) = \alpha_t\phi_t \tag{3}$$

where ϕ_t is the magnetic flux in the transformer core. The transformer core is usually assumed unsaturated; α_t is also assumed constant. We make the following substitutions:

$$m = \frac{U_{1t}}{U_a}; \qquad T_{1t} = \frac{w_{1t}^2\alpha_t}{r_{1t}}; \qquad T_{2t} = \frac{w_{2t}^2\alpha_t}{r_{2t} + r_2}$$

$$T_s = T_{1t} + T_{2t}; \qquad K_s = m\frac{w_{2t}}{w_{1t}} \cdot \frac{w_2}{R_2} \cdot \frac{T_{1t}}{T_s}$$

$$R_2 = r_{2t} + r_2$$

Solving equations (1) – (3) simultaneously, we obtain the antihunt transformer operator

$$K_s(p) = \frac{i_{2t}w_2(p)}{U_a(p)} = \frac{K_sT_sp}{(T_sp + 1)} \tag{4}$$

The variable feedback amplidyne operator is given by

$$K(p) = \frac{U_a(p)}{F_r(p)} = \frac{K_a(p)}{1 + K_a(p)K_s(p)} \tag{5}$$

where

$$K_a(p) = \frac{K_a}{T_ap + 1}$$

is the amplidyne operator which acts as a simple inertial link, if we assume only one time constant for the cross-field circuit

T_a is the cross-field circuit time-constant,

$K_a = \frac{\Delta U_a}{\Delta F_r}$ the amplidyne transfer coefficient,

F_r is the resultant m.m.f. of the amplidyne.

Substituting the expressions for $K_s(p)$ and $K_a(p)$ into (5) we get

$$K(p) = \frac{K_a(T_s p + 1)}{(T_a p + 1)(T_s p + 1) + K_a K_s T_s} \tag{6}$$

The characteristic vector of the amplidyne plus antihunt transformer can be obtained by replacing p by $j\omega$ and introducing the amplidyne feedback winding parameters;

$$K_{fb} = \frac{F_{fb}}{U_{fb}} = \frac{i_{fb}\omega_{fb}}{i_{fb}R_{fb}} = \frac{\omega_{fb}}{R_{fb}}$$

Some simple transformations and the substitution

$$T_A = T_a + T_s + K_a K_s T_s$$

gave us the characteristic vector of the amplidyne-antihunt transformer unit, viz.

$$W_a(j\omega) = \frac{U_a(j\omega)}{U_{fb}(j\omega)} = \frac{K_a K_{fb}(T_s j\omega + 1)}{T_A j\omega + (1 - T_a T_s \omega^2)} \tag{7}$$

If T_a is neglected the expression becomes much simpler. Then

$$W_a(j\omega) = \frac{K_a K_{fb}(T_s j\omega + 1)}{T_A j\omega + 1} \tag{8}$$

The vector can also be obtained from Morozov's method of following for the self and mutual inductances of the amplidyne control windings. It then takes the form:

$$W_a(j\omega) = \frac{K_a K_{fb}(T_s j\omega + 1)}{j(T_A'\omega - a\omega^3) + (1 - b\omega^2)} \qquad (9)$$

where

$$T_A' = T_s + T_a + T_1 + T_2 + K_a K_s T_s = T_A + T_1 + T_2;$$

$$a = T_s T_a T_1 + T_a T_{1t} T_2;$$

$$b = T_a(T_s + T_1 + T_2) + T_s T_1 + T_{1t} T_2;$$

T_1 and T_2 are the time constants of the corresponding amplidyne windings.

Usually

$$(T_1 + T_2) \ll T_s + T_a + K_a K_s T_s$$

and therefore

$$T_A' \approx T_A$$

When deciding which of these three expressions should be used in practice it should be remembered that medium and large power amplidyne industrial units the amplidyne pass band has a cut-off at $\omega = 8 - 10$ sec^{-1}. This explains why the short amplidyne time constants have little effect on the transients, since normally $T_A\omega \gg a\omega^3$ and $1 \gg b\omega^2$ when $\omega = 8 - 10$ sec^{-1}.

Fig. 2 shows the log frequency characteristics plotted from tests made on a 20.5 kW unit using an EMU-12A amplidyne, and TS-72/60 antihunt transformer. The transformer settings were chosen to give 30 per cent over-shoot and fast damping. Fig. 2 shows that the cut-off frequency is 6 sec^{-1}. The maximum frequency is even smaller with larger units where the generator field winding time constants (T_g) are greater than 0.5 sec.

Only when T_g and the electromechanical time constant of the motor (T_m) are smaller ($T_g < 0.5$ sec, $T_m < 0.05$ sec), does the cut-off frequency increase to 10 sec^{-1}; these values are not typical of large industrial units and will not be considered.

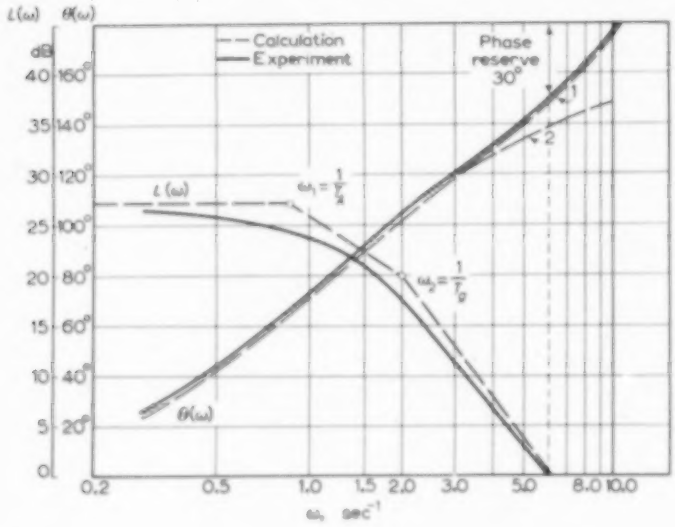

Fig. 2. Frequency characteristics of the motor-generator plus amplidyne system.

1 - Allowing for the armature time constant, T_r;

2 - Without allowance for T_r.

Frequency characteristics have been recorded on various combinations of three types of amplidyne with two types of transformer to prove that small time constants have practically no effect on transient response when the cut-off frequency is not more than 8 - 10 sec^{-1}. Fig. 3 shows the characteristics obtained with an EMU-12A amplidyne and TA-72/60 transformer. These curves (and also (7) and (9)) show that the transient performance of a system with $\omega_c < 8 - 10$ sec^{-1} is completely defined as T_s, T_A and K_a, and that the characteristic vector is given by (10).

T_A and T_s can be easily determined from the asymptotic characteristics via the conjugate frequencies ω_1 and ω_2:

$$T_A = \frac{1}{\omega_1}; \qquad T_s = \frac{1}{\omega_2}$$

T_A and T_s thus obtained are equivalent values if the transformer saturation is taken into account. The most accurate predictions of transient performance calculations are therefore to be expected when the T_A and T_s values used have been determined in the operating voltage range of the unit.

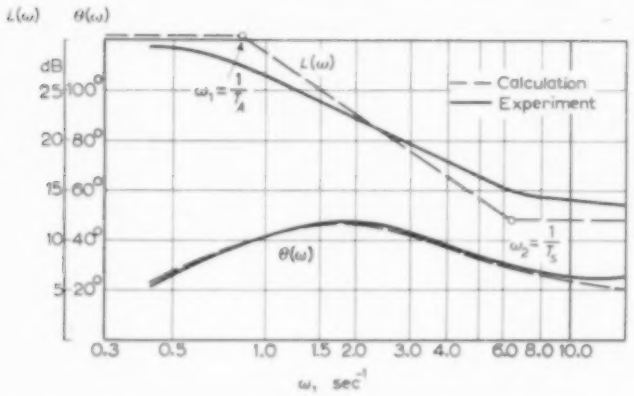

Fig. 3. Log frequency characteristics of an EMU-12A amplidyne plus antihunt transformer (T_s = 0.17 sec, T_A = 1.2 sec).

T_A and T_c, calculated from name-plate data, differ considerably from test values. The data for the EMU-12A plus TS-72/60 may serve as an example. The circuit parameters for Fig. 1 are: $W_1 = W_2 = 900$, $r_1 = r_2 = 145\ \Omega$; $m = 1$.

The name-plate data for the TS-72/60 are $W_{1t} = 4800$; $r_{1t} = 232\ \Omega$; $L_{1t} = 95$ H; $W_{2t} = 1100$; $r_{2t} = 10.3\ \Omega$; $L_{2t} = 5$ H.

These give:

$$T_{1t} = \frac{L_{1t}}{r_{1t}} = \frac{95}{232} = 0.41 \text{ sec};$$

$$T_{2t} = \frac{L_{2t}}{r_{2t} + r_2} = \frac{5}{10.3 + 145} = 0.03 \text{ sec};$$

$$T_s = T_{1t} \quad T_{2t} = 0.44 \text{ sec};$$

$$K_s = m \frac{W_{2t} W_2 T_{1t}}{W_{1t} R_2 T_s} = 1.21;$$

$$K_s T_s = 1.21 \times 0.44 = 0.52$$

The experimental K_a of the EMU-12A (for the m.m.f.) is 5 V/A for armature voltages within the range 30 – 70 V.

But experiments on an EMU-12A plus TS-72/60 gave T_s = 0.17 sec and T_A = 1.2 sec. The frequency characteristics were taken with minimum transformer air gap using the windings fully without additional resistances. The amplidyne armature voltage varied from 30 to 70 V at low frequencies and the transformer's primary current did not exceed 0.3 A.

Thus the name-plate data gave transformer time-constants 2.7 times larger than did experiment. The calculated results with other types of amplidyne and transformer were also considerably different from experiment.

Better results are obtained when frequency test data are used in the calculations. Fig.3 shows the experimental characteristics for a TS-72/60. The shape of the amplitude characteristic confirms that the transformer operator is actually

$$K_s'(p) = \frac{U_2(p)}{U_1(p)} = \frac{K_s' T_s p}{T_s p + 1}$$

1958

The intersection point on the asymptote gives the conjugate frequency ω_c for the component $L_1(\omega) = 20 \log \sqrt{(T_s^2\omega^2 + 1)}$ from which T_s can be determined and the amplitude at 10 - 15 sec^{-1} gives K_s.

When measuring antihunt transformer frequency characteristics it is important to vary the primary voltage over the operating range encountered in circuit with the amplidyne unit. The test then give some effective values of T_s and K_s' which take into account the transformer core saturation. Fig.3 was obtained by using a primary voltage composed of 50 V d.c. and 20 V a.c. The a.c. frequency varied from 0.1 - 2 c/s (ω = 0.68 - 13.6 sec^{-1}). The transformer core had no gap, the windings were used fully and additional resistances were not used.

The data of Fig.4 gave T_s = 0.2 sec; K_s' = 0.2. Then calculation gave

$$K_s = 1.15; \qquad T_A = 1.45 \text{ sec.}$$

These values of T_s and T_A are much closer to the experimental ones.

When T_s and T_A have been determined it is possible to determine the transient performance rapidly with an accuracy sufficient for practical purposes, and hence to check the suitability of the transformer.

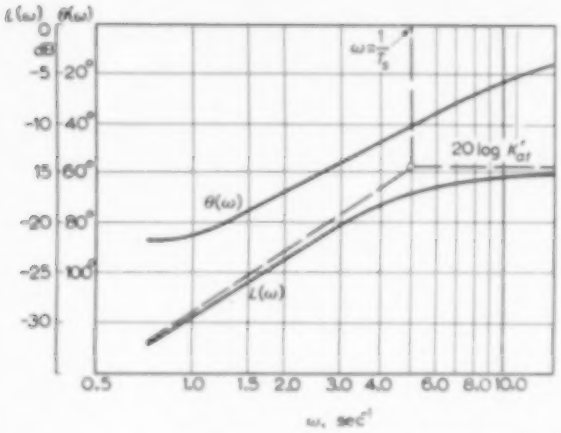

Fig. 4. Log frequency characteristics of TS-72/60 antihunt transformer.

As an example we may consider a 20.5 kW unit with an EMU-12A and a TS-72/60. T_m = 0.1 sec; T_g = 0.5 sec, the armature time-constant T_r is 0.075 sec. K is 23 with 30 – 180 V on the generator; T_s = 0.17 sec and T_A = 1.2 sec.

The characteristic vector of the entire open loop system is equal to the product of those for the amplidyne-transformer and generator-motor units:

$$W(j\omega) = \frac{K(T_s j\omega + 1)}{(T_A j\omega + 1)(T_g j\omega + 1)[T_m j\omega + (1 - T_m T_r \omega^2)]}$$

The log frequency characteristics are:-

Amplitude:

$$L(\omega) = 20 \log K + 20 \log\sqrt{T_s^2\omega^2 + 1}$$
$$-20 \log\sqrt{T_A^2\omega^2 + 1} - 20 \log \sqrt{T_g^2\omega^2 + 1})$$
$$-20 \log\sqrt{T_m^2\omega^2 + (1 - T_m T_r \omega^2)^2} \qquad (11)$$

Phase:

$$\theta(\omega) = \tan^{-1}T_s\omega - \tan^{-1}T_A\omega - \tan^{-1}T_g\omega - \tan^{-1}\frac{T_m\omega}{1 - T_m T_r \omega^2} \qquad (12)$$

Fig.2 shows these characteristics plotted from the above data. The experimental characteristics are also shown. Fig.2 shows that neglect of the armature circuit time constant leads to considerable error in the transient performance because of phase errors.

Tests on several drive units showed that a phase margin of 30° gives entirely satisfactory transient performance.

1958

A STATISTICAL ASSESSMENT OF THE STABILITY OF INDUCTION MOTOR CHARACTERISTICS*

I.P. ISAEV

Moscow Rail Transport Engineering Institute

(Received 14 August 1956)

The problem and essentials of the method

In a number of induction motor applications the stabilities of characteristics dependent on manufacturing tolerances in the parameters have to be assessed.

The actual parameters of identical motors always differ slightly from nominal so the characteristics will also differ from nominal. This shows why motors working in parallel on a single power drive are unequally loaded. Hence follows the practical interest of estimates of divergences in characteristics due to motor parameter differences.

In essence the parameters which determine the motor characteristics are assumed to follow a normal random distribution law, with mathematical expectations and standard deviations for the parameters.

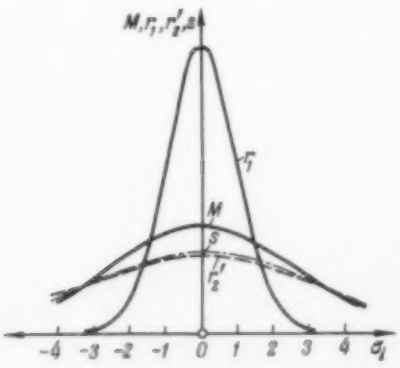

Fig. 1.

* *Elektrichestvo* No. 4, 64–69 (1957). [Reprint Order No. EL. 7]

Statistical analysis of motor tests shows this to be so. By way of example, Table 1 gives the values, and Fig.1 the distribution curves,

TABLE 1

Motor parameters	Theoretical nominal values	Arithmetic means from type tests	Standard deviation, referred to mean value, %
Resistance of stator winding (Ω)	1.385	1.365	2.6
Rotor resistance (assumed) (Ω)	1.440	1.448	10.2
Slip, %	1.67	1.41	10.1
Torque, kg-m	96.0	95.5	7.0

1958

for the stator resistance, rotor resistance (referred), slip and torque of KAMO-133-2 induction motors, as obtained in type tests at the Vladimir Il'ich Works.

Since the graphs are actually normal distribution curves, we may assume that the very general conditions of Lyapunov's theorem for independent variables, or of Bernstein's theorem for weakly dependent variables, are satisfied. According to this some function X of the independent variables $x, v, \ldots z$, with mathematical expectations $\bar{x}, \bar{v}, \ldots \bar{z}$, and corresponding small deviations $k, l, \ldots q$, may be represented accurate to the second order of small quantities, as follows

$$X(x, v, \ldots, z) = X(\bar{x}, \bar{v}, \ldots, \bar{z}) \pm t\sigma \qquad (1)$$

where

$$\sigma^2 = \left(\frac{\partial \bar{X}}{\partial \bar{x}}\right)^2 k^2 + \left(\frac{\partial \bar{X}}{\partial \bar{v}}\right)^2 l^2 + \ldots + \left(\frac{\partial \bar{X}}{\partial \bar{z}}\right)^2 q^2; \qquad (2)$$

t being a certain number.

Considering $X(x, v, \ldots z)$ in (1) as the mathematical expectation of the nominal motor characteristic, we may from equation (2) determine the standard deviation of this characteristic as a function of the deviations in the parameters.

From Lyapunov's theorem it is possible to state that, with a probability $P_t = 1 - Q_t$ the parameters will in practice remain within the bounds $\bar{X} \pm t\sigma_x$.

Stability of characteristics in an induction motor

We will first of all determine the effect of manufacturing tolerances in the resistances on the torque deviations at a given slip.

The torque at the nominal parameter values is

$$M = \frac{mpU_1^2(r_2'/s)}{9.81\omega[(sr_1 + ar_2')^2 + (x_1 + ax_2')^2 s^2]} \quad [k_g - m] \tag{3}$$

The voltage is assumed to be constant at the nominal value and the voltage system to be symmetrical.

Since the parameters are statistically distributed we will assume:

$$r_1 = \bar{r}_1 \pm t\sigma_{r1}; \quad r_2' = \bar{r}_2' \pm t\sigma_{r2}; \quad x_1 = \bar{x}_1 \pm t\sigma_{x1};$$

$$x_2' = \bar{x}_2' \pm t\sigma_{x2}$$

The bars denote the nominal resistances and reactances, respectively, σ being the standard deviation; t is a certain number.

The incremental torque due to small resistance and reactance increments, accurate to quantities of the second order, is

$$dM = \frac{\partial M}{\partial r_2'} dr_2' + \frac{\partial M}{\partial r_1} dr_1 + \frac{\partial M}{\partial x_2'} dx_1 + \frac{\partial M}{\partial x_2'} dx_2'$$

and according to equation (2) the deviation of the motor torque is given by

$$\sigma_m^2 = \left(\frac{\partial \bar{M}}{\partial \bar{r}_2'}\right)^2 \sigma_{r2}^2 + \left(\frac{\partial \bar{M}}{\partial \bar{r}_1}\right)^2 \sigma_{r1}^2 + \left(\frac{\partial \bar{M}}{\partial \bar{x}_1}\right)^2 \sigma_{x1}^2 + \left(\frac{\partial \bar{M}}{\partial x_2'}\right)^2 \sigma_{x2}^2$$

Determining the partial differential coefficients from equation (3) and substituting into them the mathematical expectations for the motor parameters, we find that

$$\sigma_{\bar{m}}^2 = \frac{c^2}{[(\bar{r}_1\bar{s} + a\bar{r}_2')^2 + (\bar{x}_1 + a\bar{x}_2')^2 s^2]^2} \times$$

$$\times \left\{ \left(1 - \frac{2a\bar{r}_2' \cos^2\bar{\phi}}{\bar{r}_1\bar{s} + a\bar{r}_2'} \right)^2 \sigma_{r2}^2 + 4\bar{r}_2'^2 \left[\frac{\bar{s}^2 \cos^4\bar{\phi}}{(\bar{r}_1\bar{s} + a\bar{r}_2')^2} \sigma_{r1}^2 + \right. \right.$$

$$\left. \left. + \frac{\sin^4\bar{\phi}}{(\bar{x}_1 + a\bar{x}_2)^2} (\sigma_{x1}^2 + a\sigma_{x2}^2) \right] \right\}, \qquad (4)$$

where

$$\cos^2\bar{\phi} = \frac{(\bar{r}_1\bar{s} + a\bar{r}_2')^2}{(\bar{r}_1\bar{s} + a\bar{r}_2')^2 + (\bar{x}_1 + a\bar{x}_2')^2 s^2}$$

$$c = \frac{mp\bar{U}_1^2\bar{s}}{9.81\omega}$$

In practical calculations it is sometimes more convenient to use a per unit basis, relating to operation under the nominal conditions. Using the notation $\sigma_{\bar{m}}/\bar{m} = \sigma_{m0}$ (and analogous notations for the partial standard deviations of the other parameters), and dividing the right-hand side of equation (4) by the square of the nominal torque, we get:

$$\sigma_{m0} = \left(1 - \frac{2a\bar{r}_2' \cos^2\bar{\phi}}{\bar{r}_1\bar{s} + a\bar{r}_2'} \right)^2 \bar{r}_2'^2 \sigma_{r20}^2 + 4\bar{r}_2^2 \left[\frac{\bar{s}^2\bar{r}_1^2 \cos^4\bar{\phi}}{(\bar{r}_1\bar{s} + a\bar{r}_2')^2} \sigma_{r10}^2 + \right.$$

$$\left. + \frac{\sin^4\bar{\phi}}{(\bar{x}_1 + a\bar{x}_2')^2} (\bar{x}_1^2 \sigma_{x10}^2 + \bar{x}_2'^2 a^2 \sigma_{x20}^2) \right]. \qquad (5)$$

This relative standard deviation formula for the torque enables us to estimate the effect of changes in the stator and rotor resistances and reactances.

1958

It is clear from equations (4) and (5) that the torque deviation is a variable quantity which depends on the operating conditions to which the deviation is referred.

When the slip is small, i.e. on the stable part of the motor characteristic, we may assume $s^2 \approx 0$ and $\sin^4 \bar{\phi} \approx 0$. Consequently, the torque deviations will be defined by the following equation:

$$\sigma_{m0} = \pm 1 - \frac{2a\bar{r}_2'^2}{\bar{r}_1 s + a\bar{r}_2'} \cos^2 \bar{\phi}\, \sigma_{r2} \qquad (5a)$$

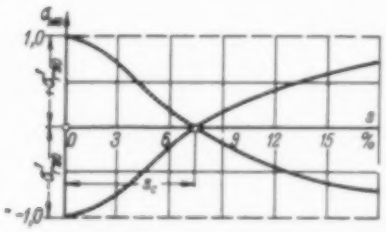

Fig. 2.

As an example, Fig. 2 shows the graph (based on (5a)), for the variation in the standard deviation of the torque of KAMO-133-2 motors with slip, where $r_1 = 1.77$ ohm; $r_2 = 1.565\ \Omega$; $a = 1.03$ and $s_c = 0.075$.

Equation (5a) shows that at small slip the torque deviations are determined, other things remaining equal, by the rotor resistance tolerances. Stability of rotor resistance within reasonable limits is therefore above all else essential if the desired stability is to be obtained.

As methods of stabilising the short-circuit rotor resistances in large induction motors we may recommend the following: (a) selective checking of the rotor bar blank sizes; (b) selective checking of bar material resistivity and (c) use of electric contact welding on the bars instead of autogenous welding, since the latter is liable to leave porosities or cavities at the seams which render the phase resistances unequal.

Equations (4) and (5) show that the torque deviations on starting ($s = 1$) are primarily affected by the tolerances in stator resistance and reactance. In this case the rotor resistance tolerance is of less importance.

The effect of tolerances in any particular type of motor at a given slip may be estimated from equations (4) and (5) for the appropriate mathematically expected parameters.

In general, the standard deviations in the parameters of the various phases may differ. The symmetrical components method, supplemented by statistical considerations, may be used to study the deviations in the characteristics of such an "asymmetric" motor.

However, let us consider the simpler case in which the standard deviations of the phase resistances are assumed to be equal.

Knowing the standard deviations of the parameters, we can determine the standard deviation in the torque. With nominal parameters the maximum torque is given by equation (6), viz.

$$M_m = \frac{C_1}{r_1 + \sqrt{r_1^2 + (x_1 + ax_2')^2}} \tag{6}$$

where

$$C_1 = \frac{mpU_1^2}{2a \cdot 9.81 \cdot 2\pi f}$$

The increment in the maximum torque due to increments in the resistances and reactances is

$$dM_m = \frac{\partial M_m}{\partial r_1} dr_1 + \frac{\partial M_m}{\partial x_1} dx_1 + \frac{\partial M_m}{\partial x_2'} dx_2'$$

and the standard deviation of the maximum torque is

$$\sigma_{M_m}^2 = \left(\frac{\partial \bar{M}_m}{\partial \bar{r}_1}\right)^2 \sigma_{r1}^2 + \left(\frac{\partial \bar{M}_m}{\partial \bar{x}_1}\right)^2 \sigma_{x1}^2 + \left(\frac{\partial \bar{M}}{\partial \bar{x}_2'}\right)^2 \sigma_{x2}^2$$

where σ_{r1}, σ_{x1}, and σ_{x2} are the standard deviations of the corresponding parameters.

Determining the partial differential coefficients from equation (6) and substituting into them the mathematical expectations for the parameters, we get from equation (2) the standard deviation in the maximum torque, viz.

$$\sigma_{M_m}^2 = \frac{\bar{M}_m^2}{\left[\bar{r}_1 + \sqrt{(\bar{r}_1^2 + (\bar{x}_1 + a\bar{x}_2')^2)}\right]^2} \times$$

$$\times\left\{\left[\left[1+\frac{\bar{r}_1}{\sqrt{[\bar{r}_1^2+(\bar{x}_1+a\bar{x}_2')^2]}}\right]^2\sigma_{r1}^2+\right.\right.$$

$$\left.\left.+\frac{(\bar{x}_1+a\bar{x}_2')^2}{[\bar{r}_1^2+(\bar{x}_1+a\bar{x}_2')^2]}\,(\sigma_{x1}^2+a^2\sigma_{x2}^2)\right\}\right]. \qquad (7)$$

Analogously, we may also find the standard deviation in the slip corresponding to this maximum torque. For this purpose we use the expression which defines the critical slip, viz.,

$$s_c = \frac{ar_2'}{\sqrt{[r_1^2+(x_1+ax_2')^2}} \qquad (8)$$

from which we get

$$\sigma_{sc}^2 = \left(\frac{\partial\bar{s}_c}{\partial\bar{r}_1}\right)^2\sigma_{r1}^2+\left(\frac{\partial\bar{s}_c}{\partial\bar{x}_1}\right)^2\sigma_{x1}^2+\left(\frac{\partial\bar{s}_c}{\partial\bar{x}_1'}\right)^2\sigma_{x2}^2+\left(\frac{\partial\bar{s}_c}{\partial\bar{r}_2'}\right)^2\sigma_{r2}^2$$

Determining the partial differential coefficients from equation (8) and using the mathematical expectations applying to their parameters, we get

$$\sigma_{sc}^2 = \bar{s}_c^2\left\{\frac{\sigma_{r2}^2}{\bar{r}_2'^2}+\frac{1}{[\bar{r}_1^2+(\bar{x}_1+a\bar{x}_2')^2]^2}\times\right.$$

$$\left.\times\,[\bar{r}_1^2\sigma_{r1}^2+(\bar{x}_1+a\bar{x}_2')^2(\sigma_{x1}^2+a^2\sigma_{x2}^2)]\right\} \qquad (9)$$

This gives the standard deviation in the slip corresponding to the maximum torque. Comparison with equations (7) and (9) shows that the effect of deviations from nominal in the winding inductances on the critical slip deviation may be neglected in the practice, and that we may consider σ_{sc} as independent of σ_{x1} and σ_{x2}. On the other hand, deviation of the inductances from nominal has a considerable effect on the deviation of the maximum torque.

A lucid representation of the effect of tolerances on the motor characteristic stability is obtained if the origin of a system of orthogonal co-ordinates (s,M) is made to coincide with the point of maximum torque, and the deviations $t\sigma_c$ and $t\sigma_m$ are laid off along the axes (Fig.3). The locus of possible standard deviations in the maximum

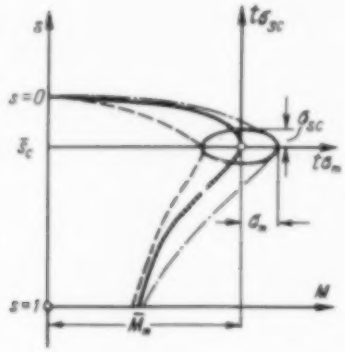

Fig. 3

torque will then in general be represented by the ellipse

$$\left(\frac{s-\bar{s}_c}{\sigma_{sc}}\right)^2+\left(\frac{M-\bar{M}_m}{\sigma_{Mm}}\right)^2=1$$

The locus of the limiting deviations in the maximum torque will also be an ellipse in this system of co-ordinates, being

$$\left(\frac{s-\bar{s}_c}{t\sigma_{sc}}\right)^2+\left(\frac{M-\bar{M}_m^2}{t\sigma_{Mm}}\right)=1$$

obtainable from the previous ellipse by a t-fold increase in the semi-axes.

Parallel operation of induction motors

The deviations in the maximum torque and in the corresponding slip due to deviations in the parameters are responsible for variations in the motor characteristics.

Motors with differing characteristics operating in parallel in the same electrically-driven system will have the load non-uniformly distributed between them, which is usually undesirable.

To assess the effect of deviations in the motor parameters on the non-uniformity of load distribution for operation in the range $0 \lesssim s \lesssim s_c$, we use the equation for the mechanical characteristic, viz.,

$$M = M_m \frac{2(1+\epsilon)}{s/s_c + s/s_c + 2\epsilon} \tag{10}$$

We found above that s_c is a function of the parameters and of the tolerances, given in general as $s_c = \bar{s}_c \pm t\sigma_{sc}$, and that $M_m = \bar{M}_m \pm t\sigma_{Mm}$.

To render the results more general, we will assume that under load the motors show a σ_s not dependent on manufacturing tolerances and determined by the operating conditions. In this case the torque increment for small increments m s, s_c and M_m, is determined by

$$dM = \frac{\partial M}{\partial s} ds + \frac{\partial M}{\partial s_c} ds_c + \frac{\partial M}{\partial M_m} dM_m$$

and, according to equation (2), σ_M becomes

$$\sigma_M^2 = \left(\frac{\partial \bar{M}}{\partial \bar{s}}\right)^2 \sigma_s^2 + \left(\frac{\partial \bar{M}}{\partial \bar{s}_c}\right)^2 \sigma_{sc}^2 + \left(\frac{\partial \bar{M}}{\partial \bar{M}_m}\right)^2 \sigma_{Mm}^2$$

Differentiating (10), we find that σ_m under these conditions is

$$\sigma_M^2 = \left[\frac{2\bar{M}_m(1+\epsilon)}{(\bar{s}^2 + \bar{s}_c^2 + 2\epsilon\bar{s}\bar{s}_c)^2}\right]^2 \left[\bar{s}^2(\bar{s}^2 - \bar{s}_c^2)^2 \sigma_{sc}^2 + \right.$$

$$+ \frac{\bar{s}^2\bar{s}_c^2(\bar{s}^2 + \bar{s}_c^2 + 2\epsilon\bar{s}\bar{s}_c)^2}{\bar{M}_m^2} \sigma_{Mm}^2 + \bar{s}_c^2(\bar{s}_c^2 - \bar{s}^2)\sigma_s^2 +$$

$$\left. + \frac{\bar{s}^2\bar{s}_c^2(\bar{s} - \bar{s}_c)^4}{(1+\epsilon)^2}\left(\frac{\bar{r}_1}{\bar{r}_2'}\right)^2 \sigma_{sc}^2\right] \tag{11}$$

or, in relative units,

$$\sigma_{M0}^2 = \sigma_{Mm}^2 + \frac{1}{(\bar{s}^2 + \bar{s}_c^2 + 2\epsilon\bar{s}\bar{s}_c)^2}\left\{(\bar{s}_c^2 - \bar{s}^2)^2\sigma_{s0}^2 + \right.$$

$$\left. + \left[(\bar{s}^2 - \bar{s}_c^2)^2 + \frac{\bar{s}_c^2}{(1+\epsilon)^2}(\bar{s}^2 + \bar{s}_c^2 - 2\bar{s}\bar{s}_c)^2\left(\frac{\bar{r}_1}{\bar{r}_2'}\right)^2\right]\sigma_{sc}^2\right\} \tag{12}$$

Let us assume that the motors are "ideally" produced, i.e. that their parameters are exactly the nominal ones. In this case we have to put $\sigma_{sc} = \sigma_{Mm} = 0$ in equation (12), derived from equations (7) and (9).

Hence,

$$\sigma_{m0} = \frac{\bar{s}_c^2 - \bar{s}^2}{\bar{s}^2 + \bar{s}_c^2 + 2\epsilon\,\bar{s}\,\bar{s}_c}\,\sigma_{s0} \qquad (13)$$

Consequently, the load divergence will be determined by the slip divergence which, in turn, is determined by the conditions of operation. Conversely, if such a divergence is impossible, i.e. $\sigma_s = 0$, and the motors are produced with due tolerances, the differences in the loadings will be completely determined by the deviations in their parameters, viz.

$$\sigma_{M0}^2 = \sigma_{Mm0}^2 + \frac{1}{(\bar{s}^2 + \bar{s}_c^2 + 2\epsilon\,\bar{s}\,\bar{s}_c)^2}\left\{(\bar{s}^2 - \bar{s}_c^2)^2 + \right.$$

$$\left. + \frac{\bar{s}_c^2}{(1+\epsilon)^2}\,(\bar{s}^2 + \bar{s}_c^2 - 2\bar{s}\,\bar{s}_c)^2\left(\frac{\bar{r}_1}{\bar{r}_2'}\right)^2\right\}\sigma_{sc}^2 \qquad (14)$$

Therefore equations (11) and (12) enable us to solve two practical problems, viz. either by assuming the tolerances as given, to determine the permissible slip divergence from the permissible torque divergence or, conversely, to assume the slip as given and to determine the permissible standard deviations in the parameters from the permissible torque divergence.

By way of example, we shall solve the first of these problems for the induction-type traction motors used in individual-drive a.c. locomotives. We will define the wheel-pair rim tolerances so that the induction motors in the electric locomotive one-hour rated have the same torque divergence as the DPE-400A d.c. motors used in VL-22[m] electric locomotive under the regulations in force (a divergence in the wheel rims of 15 mm produces a divergence of about ±4 per cent in the DPE-400A loadings when the motors are connected in parallel).

This problem has become very important nowadays since various a.c. locomotives are being developed. We use equation (11) in which we assume that

$$\sigma_s = -n_2/n_1\,\sigma_{D0}$$

The standard deviation in the wheel diameters, as related to the parameters of induction-type traction motors and the locomotive operating conditions, is given in the following general form

$$\sigma_{D0} = \sigma_{M0} \frac{\bar{M}(\bar{s}^2 + \bar{s}_c^2 + 2\epsilon \bar{s}\bar{s}_c)^2}{2\bar{M}_m \bar{s}_c(\bar{s}_c^2 - \bar{s}^2)} \cdot \frac{n_1}{n_2}$$

Table 2 gives the diameter differences given by this equation, for three types of electric locomotive with induction-type traction motors, viz. OT, OD-1, and OD-II, designed by the NEVZ-Works "Budennii".

TABLE 2

Type of electric locomotive	Nominal diameter of rim (shrouding) of wheel pair, (mm)	Permissible wheel diameter deviation (mm)
OT	1200	5.0
	1050	4.5
OD-1	1200	3.8
	1050	3.2
OD-2	1200	3.0
	1050	2.8

Equation (14) shows that the load divergence is a variable quantity, dependent on the operating conditions. Let us determine from (14) the slip at which the load difference in parallel operation is a maximum.

The condition to be satisfied is that

$$\frac{\partial \sigma_M}{\partial s} = 0$$

Hence the roots of

$$\frac{\partial}{\partial s} \sqrt{\sigma_{M=0}^2 \bar{M}^2 + 4\bar{M}_M^2 s^2 \frac{(1+\epsilon)^2(\bar{s}^2 - \bar{s}_c^2)^2 \bar{s}^2 + \bar{s}_c^2(\bar{s} - \bar{s}_c)^4}{(\bar{s}^2 + \bar{s}_c^2 + 2\epsilon \bar{s}\bar{s}_c)^4} \sigma_{sc}^2} = 0$$

must be determined.

Carrying out the differentiation and assuming that the terms containing ϵ will involve higher powers of s than the others, we get approximately (subject to the conditions $\sigma_{M_{a0}} = 0$):

$$s^4 - 2s\bar{s}_c^2 + \bar{s}_c^4 = 0$$

whence under operating conditions the maximum value is $s'_M = 0.412\ \bar{s}_c$, i.e. the maximum torque divergence of parallel motors allowing for manufacturing tolerances in their parameters, occurs at about 40 per cent of the critical slip.

When we know s'_M, we can determine $\sigma_{M_{a0}}$ if we substitute $s = s'_a = 0.412\ \bar{s}_c$ into equations (14).

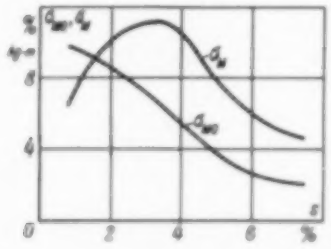

Fig.4.

Fig.4 shows by way of example the relative and absolute standard deviations in the torques of type KAMO-133-2 motors, determined from the following data:

$r_1 = 1.77\ \Omega$; $r'_2 = 1.565\ \Omega$; $s_c = 0.075$; $\sigma_{M_{a0}} = 0.02$; $\sigma_{sc0} = 0.10$.

The above statistical study of the stability in induction motor characteristics enables one to assess the effects of tolerances in various motor parameters scientifically, and to attempt to standardize the tolerances on the basis of the detailed operating conditions and special duties involved.

The statistical method explained above is of general application and may be extended to any other type of motor.

REFERENCES

I.P. Isaev: Effect of manufacturing tolerances on the stability of characteristics in traction motors and electric locomotives. *Elektrichestvo* No.11 (1955).

E.Ya. Kazovskii; Application of probability theory to the design and operation of electric machines. *Trans. LEMI* No.1 (1932).

R. Ruedenberg; Assessment of electrical machines and apparatus by tolerances based on statistical methods. *Z. Angew. Math. Mech.* **9**, No.4 (1929).

958

THE PROBLEM OF IMPULSE TESTS OF THE TURN INSULATION OF AN H.V. MACHINE*

B.A. ALEKSEEV and V.B. KULAKOLSKII

1958

There is so far no practical method of calculating the impulsive voltages in the windings of electric machines, viz. on the sections and turns in any special part of the winding. Theoretical studies in this field have not yet reached a stage where calculations can be based on them [1]. Experimental investigations give a good idea of the maximum pulse voltages on the first turns of the winding [2], but they do not give adequate data on the voltages across the remaining turns. But a knowledge of the pulse voltages on turns in the centre of the winding, though not necessary for surge protection purposes, is indispensable for turn insulation test purposes.

In recent years two basic methods have been used for testing the turn insulation of assembled windings, viz. travelling-wave tests effected by applying impulses to the ends of the winding [3] and tests based on induced pulse voltages; the latter are carried out by inducing these voltages successively in each pair of winding sections, using a special impulse inductor [4,5].

Basically the travelling-wave test is more convenient, particularly when applied to large slow-running machines, because neither withdrawal of the rotor nor successive testing of all sections of the winding is required. On the other hand, this kind of test is usefully applied only when the turn-voltage pulses in any part of the winding are sufficiently high to test the winding insulation effectively and are obtainable with a pulse amplitude not exceeding the permissible test voltages on the frame insulation. For this reason the turn-voltage distribution over the winding affects the choice of turn insulation test method greatly.

The way various factors influence the turn-voltages in the windings of electric machines must, therefore, also be studied. Pulse tests on

* *Elektrichestvo* No.4, 75–79 (1957). [Reprint Order No. EL.8]

machines of various powers and voltage ratings were, therefore, carried out; the most typical results are tabulated below.

Set-up and test method

The data were measured on the machines with a specially designed portable set-up 10 – 1, consisting of a pulse oscillograph with built-in surge generator.

The generator provides pulses of amplitude up to 350 V, with 0.2 – 5μsec fronts and relatively flat tails at a repetition frequency of 50 c/s. The wave is applied to one end of the winding, the other end being earthed.

The time required for the wave to travel along the winding was determined by measuring the voltage at the open end. The period of the voltage oscillations from the time marks was assumed to be equal to four times the travelling time. The characteristic impedance was assumed to equal the resistance connected to the end of the winding, across which the amplitude of the voltage was half the voltage at the open end.

Minimum impulse voltages on sections

The general pulse voltage distribution on the windings of medium-power motors was investigated in the Central Electrical Research Laboratory between 1950-1952; these investigations have been reported [2,6]. In 1954-1955 the voltages set up on the winding sections of larger electrical machines were determined; these windings differ considerably from motor windings in size, of number turns in the sections, etc. The voltage across a section is determined by two factors, viz. the steepness of the wave front and the electrical length of the section. As the wave penetrates into the winding, the steepness of the front is reduced and so the section voltages decrease. Table 1 and Fig.1 illustrate the relationship between the minimum section voltage and the number of winding sections for several electrical machines.

The second factor which influences the minimum section voltages considerably is the electrical length of the section, as is seen in the table.

Therefore, we may assume that for basket (double-layer) wound machines, the section voltages depend, to a first approximation, on the number of sections per phase or parallel branch, and on the wire length in the sections.

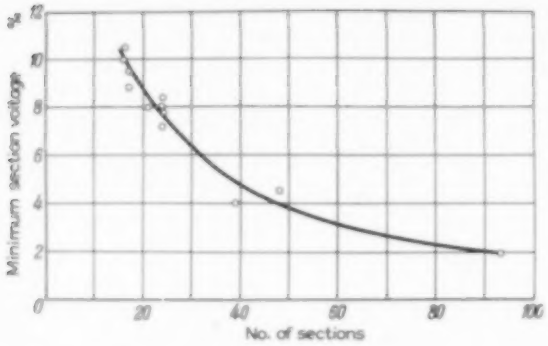

Fig. 1 Relationship between minimum voltage on section and number of sections.

Electric length of section 0.21 – 0.25 μ sec; length of wave front 0.6 μ sec.

1958

The number of turns in the section, length of active steel, etc., do not influence the section voltages directly. But the number of turns in the section is the basic factor determining the turn voltages.

As is well known [2,6,7], pulse voltages are uniformly distributed over the turns of a section. Consequently, the turn voltages are inversely proportional to the number of turns (other things being equal).

Effect of the type of winding

The section voltage distribution in a real machine winding when a pulse is applied differs considerably from that in a circuit consisting of identical *LC* and attenuating elements. The section voltage distribution curve along the winding is not smooth but stepwise, the shape being dependent on the winding circuit and on the spatial disposition of the winding sections.

Inductive coupling between the parts of the winding is the main operative factor.

Tests on a model of part of a medium-power motor stator with inserted winding sections have shown that the sections, and hence the groups, mostly influence one another electromagnetically.

If the section ends are screened electrostatically during the tests, the section voltages are practically unaltered. Sections with sides in the same slot and parallel sections placed in a row interact most strongly. The magnetic couplings are responsible for the way in which the section couplings strongly influence the section voltage distributions. A group of sections round one pole pair has several strongly coupled parallel sections in a row. In impulse winding tests the section voltages appear related in amplitude because the group sections are strongly coupled.

Groups belonging to the various parallel branches of one phase influence one another. Several parallel branches connected to one phase show a certain rise in section voltages relative to a single branch. This is due to the increased number of grouped sections or, which is equivalent, to the stronger magnetic coupling.

When a pulse is applied to two phases, the phases influence one another. This is of great importance because when the turn insulation is tested in a bridge circuit, the pulse is usually applied to the two phases compared. The different current directions in the different phase sections lying close together produces demagnetization while reinforcement takes place when the parallel branches on one phase are used.

Modern machine winding circuits with shortened pitch use different phase sections placed in one slot. Such sections, and also the series and parallel sections of another phase determine the minima of the winding distribution curve. These minima are particularly marked when the ordinal numbers of the sections of the different phases in series are near together. The demagnetization is then caused by current pulses of similar form and amplitude because the windings shape the pulses to the same degree [8].

Fig.2 shows section voltages measured on one phase of a motor when the impulse is applied to one and to two phases. The marked minima correspond to sections placed in the same slot when the second phase sections are in circuit. Fig.2 shows that with two different phase pairs (1–2 and 1–3) the section voltage minima correspond to different phase sections, this being the object of the winding design.

It is possible to avoid section omission due to gaps in the section voltage distribution curve by testing all three phase combinations (1–2, 1–3 and 2–3) successively. In this case, the winding sections (e.g. of phase 2), which are only weakly tested with one phase pair (1–2), will be tested at the normal voltage when the second phase pair (1–3) is used.

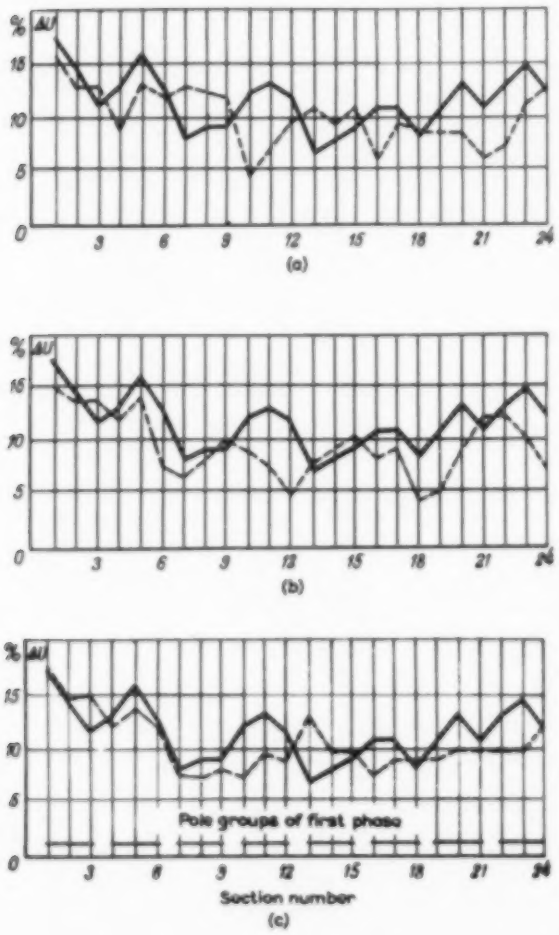

Fig. 2 Section voltages in a 1st phase branch with different testing circuits.

(a) Simultaneous test of 1st and 2nd phases;

(b) Simultaneous test of 1st and 3rd phases;

(c) Simultaneous test of 1st and 2nd phases connected in opposition.

Full lines: tests on 1st phase alone;

Broken lines: simultaneous test of phases.

1958

There is another method by which gaps in the section voltage curve can be avoided, viz. one phase is tested together with another connected in opposition. In this case the different phase conductors in one slot will reinforce and not demagnetize one another.

The variation of minimum section voltage in a motor winding (6 kV, 200 W, 375 r.p.m.) with the test circuit is illustrated by the following data:

TABLE 1

Test	Minimum section voltage of phase 1 (%)
Phase 1 only	6.5
Phases 1 & 2 (equidirectional connexion)	4
Phases 1 & 3 (equidirectional connexion)	4
Phases 1-2 & 1-3 (general result)	7.5
Phases 1 & 3 (connected in opposition)	7.5

The most informative tests are those using two phase pairs or phases connected in opposition. The minimum section voltage then exceeds that involved in testing a single phase.

Turn insulation test voltages required

Turn insulation tests are obviously of value only if the test voltages on the turns are sufficiently high to reveal insulation defects. The voltages adopted for works tests are usually 50 per cent of the minimum breakdown voltage for new insulation of that particular thickness and structure.

There are no generally accepted recommendations for testing the insulation of machines in service. Hence tests were carried out on insulation with artificial defects, which showed that the breakdown voltage of faulty turn insulation was determined by that across the air gap between turns, and remained sufficiently high whatever the damage type. For example, the turn insulation breakdown voltages of single-layer micafolium sections after a fracture in two directions at right-angles did not fall below 900 V.

In other sections, with the turn insulation completely stripped while the conductor spacing had been maintained at the original insulation thickness, the flash-over voltage between turns remained higher than the works test voltages for section turn insulation on sections not in the same slot. Only when the inter-turn gaps are reduced to ~1/100 mm are the works test voltages sufficient to produce spark-over between turns.

At atmospheric pressure the breakdown voltage of an air gap of practically any width is never less than about 350 V max [9]. Extrapolation of an experimental curve of breakdown voltage vs. distance between two parallel 2.5 x 5.5 mm conductors gave about the same value. The curve was taken from 0.03 to 0.1 mm and extrapolated to zero.

We have therefore to consider 350 V max as the lower limit of turn-insulation test voltages; tests at lower voltages can only detect complete short-circuits.

1958

Insulation defects between conductors at spacings up to 0.1 mm can be detected with test voltages of 350–1000 V max. So, tests at these voltages can only detect a fraction of the winding insulation defects occurring in the practice. When the inter-turn spacings are 0.01 mm (having breakdown voltages of the order of several hundred volts) the gaps may be closed by comparatively small forces. For example, the gap between the bare turns of a synchronous condenser section (6.6 kV, 15,000 kVA, 7500 r.p.m.), which had been brought close together in winding (breakdown voltage at the power frequency 480 V) was closed by applying a force of 11.3 kg, despite the considerable cross-section of the turns (sixteen conductors each of 6 mm^2 section).

It is therefore always necessary to try to raise the test turn voltages to about those used in works tests, which are determined by the turn insulation design and thickness. Lower test voltages (but not below 350 V max) are only justified when sufficiently high voltages cannot be produced by methods acceptable in practice.

Ways of turn insulation testing in electric machines

The tabulated data indicate that it is practically impossible to test the turn insulation of electric machines with travelling waves when the number of turns in the individual sections is great (nine to ten, or more). When the applied surge amplitude does not exceed the standard test voltage (i.e. 7 kV for machines rated 3 kV, 14kV for machines rated 6 kV, and 21 kV for machines rated 10 kV), the turn insulation in the centre of

the winding may receive only about 100–200 V, which is obviously insufficient. With these machines it is at present more expedient to test with induced impulsive voltage [4,5].

However, if the machines have few turns per section, travelling-wave tests are often possible. For example, with a synchronous condenser of 6.6 kV, 15,000 kVA, 750 r.p.m. minimum turn impulse voltages of about 750 V may obtain, with a hydrogenerator of 13.8 kV, 55,000 kW, 62.5 r.p.m., about 550 V; in both cases the test voltage amplitude will not exceed the values permissible for frame-winding insulation tests under service conditions.

When each phase is tested twice (in cyclic combination with each of the other two phases) the minimum turn voltages can be raised slightly, as shown above.

Summarizing, machines for which annual rotor withdrawal is not stipulated (generators, synchronous condensers) and on which turn-insulation test induction is consequently difficult to carry out, it is often possible to test by travelling-wave methods, i.e. by applying impulses to the ends of the phases.

The test turn voltages can be predicted by impulse tests during production or on rewinding. If results of such tests are not available, a decision on the advisability of using an impulse bridge-circuit for testing the turn insulation can be obtained by comparing the winding data with previously derived numerical values. Knowing the number of winding sections and the electric length of a section, the probable turn voltages may be predicted from the curve relating the section voltages to the number of sections (corrected for the electric length of a section) (Fig.1).

The above correction is unnecessary since, with sections with compounded insulation and a total conductor length $\geq$ 20 m, the electric length will usually be below 0.3 μ sec.

Determination of the electric length of a section from the wave propagation data for windings given in "Regulations on Surge Protection" may lead to incorrect results; experience shows that the true speeds may differ considerably from the average values given.

For example, for a 55,000 kW, 13.8 kV hydroelectric generator, the velocity of propagation is given as about 15 m/μ sec, but in reality it approaches 75 m/μ sec; for a 5000 kVA, 6 kV synchronous condenser, it is supposed to be about 25 m/μ sec, but is in fact not more than

14 m/μ sec. This is because the relationships on which the data are based are unrelated to the concrete features of each machine, viz. number of parallel branches, number of turns per slot, method of insulation, winding design, etc.

A method of calculation which would give the basic impulse parameters of the windings and, particularly, the wave propagation velocity from the concrete winding and design data of any machine is much to be desired.

Conclusions

(1) The minimum inter-turn test voltages for a given test surge voltage depend above all on the number of turns in the section, on the number of sections in the branch or phase, on the total wire length in the section and on the surge wave propagation velocity in the winding.

1958

The relationship between the latter velocity and the design parameters has not yet been firmly established; in many cases the data in "Regulations on Protection against Surges" will not be sufficiently close to the measured values.

(2) The impulse voltage distribution over the winding sections depends strongly on the group sequence, which controls the strong electromagnetic coupling between winding sections.

In bridge tests using two phases of the winding, the relative disposition of the tested branch or phase sections (particularly if the pitch is shortened) has a great influence, and the current directions in the tested phases, have a marked influence; the currents in the phases or branches must have opposite directions if its section voltages are to be raised. If this is impossible, all three phase combinations must be tested.

(3) Turn insulation tests are of value only at turn voltages $\leq$ 350 V max. The main point in choosing test methods and circuits is to ensure test turn voltages about equal to those used in works tests.

(4) The preferred method for testing large electric machines, particularly hydroelectric generators with many slots, is to apply a surge voltage to the end of the winding (travelling-wave test), if this assures sufficiently high turn voltages.

(5) The inter-turn voltages expected in travelling-wave tests can be calculated approximately from the machine winding data. As a rule, the test voltages will be sufficiently high in machines with few (two to four) turns per section.

REFERENCES

1. V.A. Karasev and Z.G. Kaganov; Wave propagation in the windings of electrical machines. *Elektrichestvo* No.4 (1949).
2. G.N. Petrov and A.I. Abramov; Inter-turn voltages in the windings of electrical machines during wave processes. *Elektrichestvo* No.7 (1954).
3. A.A. Timofeenko; Set-up for testing the inter-turn insulation of electric motors. *Elektricheskie Stantsii* No.6 (1950).
4. N.V. Smirnov; *Checking and Testing Windings in Electric Machines and Apparatus*. Gosenergoizdat, 1955.
5. N.V. Smirnov; Testing the turn insulation of electric motor windings under service conditions. *Elektrichestvo*, No. 5 (1955).
6. Deckans; Investigation of surges in H.V. motors. A.S.E. – Bull. No.35 (1953).
7. G.G. Shvets and S. Gretskii; Experimental investigation of surges in the windings of electric machines. *Electrical Insulation* No.2 (1938).
8. R.C. Robinson; Distribution of impulse voltages in bar-wound high-speed turbogenerators. *Proc.Instn.Elec. Engrs.* No.77 (1953).
9. A.P. Aleksandrov *et al.* *The Physics of Dielectrics*. G.T.T.I. (1932).

VOLTAGE GRADIENTS IN A LONG-SPARK LEADER CHANNEL*

V.P. LARIONOV

The Lenin All-Union Electrotechnical Institute

(Received 11 June 1956)

Komelkov [1] was the first to show that the leader structure is rather complex in a long-gap spark in air. An extensive ionized region occurs at the tip of the narrow leader channel. This region is composed of separate streamers, i.e. thin, long channels so numerous in the case of a positive discharge that the whole ionized region resembles a cascade of luminous filaments issuing from the tip of the leader. The electrons released at the fronts of the streamers rush along the streamer ducts into the leader channel, leaving positive ions in the ionized region. As the leader penetrates more deeply into the interelectrode space, new streamers appear as the old ones are extinguished, giving an immobile space charge envelope around the narrow leader channel.

The narrow leader channel (the "core") in direct contact with the electrode provides a path along which electrons flow to the electrode in a positive discharge. The voltage gradient along the leader channel determines the ionization conditions at its tip and is therefore the most important parameter. However, this parameter has not yet been fully investigated.

The mean longitudinal gradients were studied at the All-Union Institute of Electrical Engineering by producing an artificial step in the leader channel [2]. The current in the step was first assumed to produce a state of arc-conduction in the channel, the second assumption being that the leader tip potential is unaffected by this, i.e. that the abrupt drop in spark-gap voltage at the instant of producing the step determines the voltage across the channel. Thus, the mean gradients were determined as follows:

$$E_{1m} \approx \frac{U'}{l_1} + E_a \qquad (1)$$

where U' is the abrupt drop in spark-gap voltage.
l_1 is the leader length at the moment of producing the step
E_a is the voltage gradient in the arc channel.

* *Elektrichestvo* No. 4, 80–81 (1957). [Reprint Order No. EL.9]

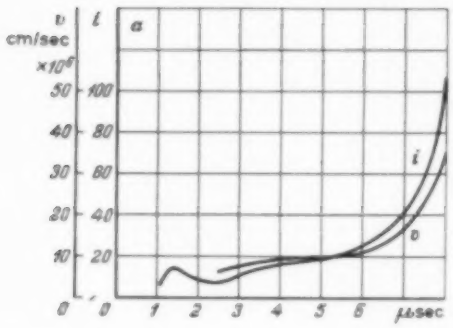

Fig.1 Leader current and leader tip velocity. Spark gap "rod-plane", 100 cm long. Discharge circuit resistance 2.5 kΩ.

While the first assumption is certainly correct, the second is obviously without foundation. Experience shows that where the step has been formed the current and tip velocity increase considerably; this can only be attributed to an increase in field strength at the tip and therefore to an increased potential on the tip itself. The sudden voltage drop at the instant of step formation does not by any means give the full voltage across the leader channel, so the mean longitudinal voltage gradients calculated from this voltage drop are too low. Using a 200 cm rod-plane gap, the lower values obtained by this method for the mean voltage gradient along the positive leader channel when this was 120 – 140 cm long were found to be between 1200 and 1600 V/cm with discharge circuit resistances of between 140 and 400 kΩ respectively [2]. These figures show that the picture if the developing leader as a highly conducting almost equipotential channel (longitudinal gradients $\sim$ 10 V/cm is not consistent with physical facts.

The longitudinal gradients may be expected to decrease in time owing to the increased current heating the leader channel. It is here of interest to consider the final stages of leader development.

The abrupt drop in spark-gap voltage when the main discharge strikes can be regarded as the sum of the voltage across the leader channel and the potential of its tip immediately before reaching the plane. Thus, assuming that the tip potential is zero near earth, it is possible to obtain a value, which we know to be exaggerated, for the mean longitudinal channel gradient at the instant immediately preceding the main discharge. The gradients obtained under the above test conditions were between 1000 and 1600 V/cm, regardless of the discharge resistance (in 42 tests the drop was between 230 and 370 kV).

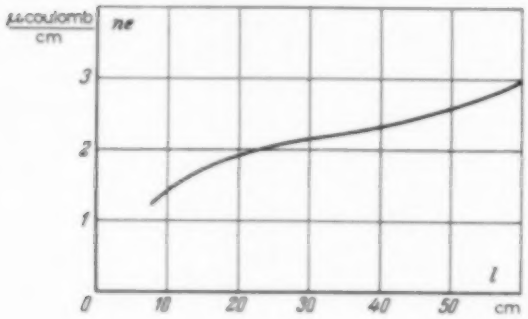

Fig. 2 Distribution of the excess positive charge along the leader (for the discharge of Fig. 1).

Thus, the *lower* limit for the mean channel gradient determined when the leader bridges 60 – 70 per cent of the spark gap is between 1200 and 1600 V/cm, and the *upper* limit, determined immediately before the leader reaches the plane, is between 1000 and 1600 V/cm. This shows that the mean longitudinal gradient decreases considerably during development.

The channel current, i, is given by $i = nev$, where v is the tip velocity, e the electronic charge and n the number of electrons leaving the channel per unit increase in length (ne is numerically equal to the linear excess positive space charge density in the leader envelope). On the other hand, i may be expressed as the number of electrons released during ionization per unit length of the leader, n', and by the electron drift velocity, v' produced by the longitudinal gradients in the channel, viz.

$$i = nev = n'ev', \quad \text{i.e.} \quad nv = n'v' \tag{2}$$

As the tip of the leader approaches the plane, the leader current and the tip velocity increase considerably. Of the two, the current grows more rapidly, which means that the linear density of excess charge increases in the lower part of the leader. The variation in leader current and tip velocity in the rod-plane gap is shown in Fig. 1. In 5 μsec (from 3 μsec to 8 μsec) the current increases ten times, the tip velocity five times, and their ratio $ne = i/v$ two times. The distribution of linear excess charge density along the whole channel for the same discharge is shown in Fig. 2.

v' is less than v [3]. An increase in ne along the leader channel therefore means, in accordance with (2), an increase in n' in the channel plasma.

Let us consider the discharge records for the rod-plane gap shown in Fig.3. The records were obtained with a high-speed rotating camera with a 'Jupiter-3' lens, by the well-known method [1] of photographing simultaneously through a number of slits at different distances from the plane. The records show that at any particular instant (the times are determined by reference to the instant when the main discharge strikes) the channel diameter ("core") is almost constant throughout the length.

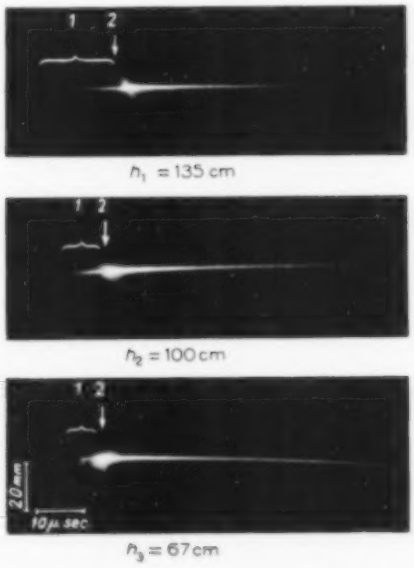

Fig.3 Time-base records for the leader channel. Rod-plane gap, 150 cm long. Discharge circuit resistances 28 kΩ; h = distance, between the leader tip and the plane; 1 - leader stage of the discharge; 2 - main discharge. Side branches round the main channel are visible in the bottom record.

The higher linear electron density in the lower part of the channel (of constant diameter), indicates a higher conductance and a lower longitudinal voltage gradient. The initial voltage gradients therefore vary along the leader channel, being higher at the top, and lower at the bottom. The gradients should fall with time, particularly in the older parts of the channel, owing to thermal ionization.

Since the linear excess positive ion density is constant ($ne = i/v \approx$ const.) Loeb [3] assumes the leader channel homogeneous throughout its length and the voltage gradients constant along the channel.

REFERENCES

1. V.S. Komelkov; The structure and parameters of the leader discharge. *Izv. Akad. Nauk SSSR* (Technical Sciences Section) No.8(1947).
2. V.P. Larionov; The impulse discharge mechanism in a long air gap. *Elektrichestvo* No.7 (1952).
3. L.B. Loeb; Some aspects of breakdown streamers. *Phys. Rev.* **94**, No.2 (1954).

1958

MEASUREMENT OF EARTH RESISTANCES*

A.B. OSLON

Zlatoust

(Received 28 August 1955)

A three-electrode circuit is used to measure the resistances of an earthing system, these being: the earth electrode (earthing circuit), the current electrode and the potential electrode. All quantities referring to the earth electrode are denoted by the K, those referring to the current electrode by subscript T and those referring to the potential electrode by P.

Current is passed through the earth and current electrodes. The potential of the circuit is measured via the potential electrode. The earth resistance equals the measured potential divided by the current passing.

In Fig.1 the voltmeter and ammeter are instruments specially designed for measuring the resistances of earthing systems.

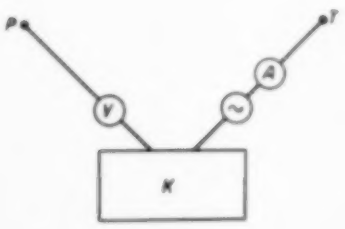

Fig. 1.

It is usually assumed that the current and earth electrodes must be sufficiently far apart not to distort the field and that a sufficiently large zero potential zone remains between them. The potential electrode must be placed in the zero potential zone [1,2].

Let us assume that we already know the earth resistance of the circuit R_K. Is it then possible, having placed the current electrode at an arbitrary point, to so locate the potential electrode that the measured resistance is equal to R_K? If this is possible, how can we determine the 'locus of precise measurements'?

To answer this question we will use the analogy between an electrostatic field and the field due to a current in a conducting medium.

* *Elektrichestvo* No. 2, 56–58 (1957). [Reprint Order No. EL. 10]

Maxwell's equations with potential coefficients for the three electrodes are

$$\phi_K = \alpha_{KK} I_K + \alpha_{KT} I_T + \alpha_{KP} I_P$$

$$\phi_T = \alpha_{TK} I_K + \alpha_{TT} I_T + \alpha_{TP} I_P$$

$$\phi_P = \alpha_{PK} I_K + \alpha_{PT} I_T + \alpha_{PP} I_P$$

Current flow from the electrodes into the ground is taken as positive:

Neglecting the current drawn by the voltmeters we get:

$$I_P = 0, \quad I_T = -I_K$$

The measured resistance is

$$R_{meas} = \left| \frac{\phi_K - \phi_P}{I_T} \right|$$

Assuming $\alpha_{12} = \alpha_{21}$, we have

$$R_{meas} = \alpha_{KK} + \alpha_{TP} - \alpha_{KT} - \alpha_{KP} \qquad (1)$$

The actual earth resistance

$$R_K = \alpha_{KK}$$

If $R_{meas} = R_K$, the following condition must be satisfied:

$$\alpha_{TP} = \alpha_{KT} + \alpha_{KP} \qquad (2)$$

Equation (2) is the answer to our question. From this we can draw the following conclusions:

(a) It is theoretically possible to measure earth resistances accurately when the measuring and earth electrodes are placed arbitrarily close together

(b) When the measuring electrodes have been placed in a certain way, the result of the measurement is independent of which is the current electrode and which the potential electrode.

1958

From (a) it follows that the measurement may be accurate even when the current electrode distorts the field of the earth electrode, and from (b) that the second electrode need not necessarily be placed in a zone of zero potential.

We will demonstrate the usefulness of (b) for any measurement performed by the 'three-point' method used for obtaining potential distributions in the field, measuring the footing-resistances of steel towers connected through earth wires, when the earthing circuit is disconnected from the base of the tower, etc. For this purpose we will represent the measuring circuit as a passive four-terminal network, all elements being linear over the entire current range. In Fig.2, 1′ and 2′ represent the earth electrode, 1 the current electrode and 2 the potential electrode.

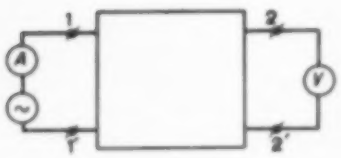

Fig.2

The following relationships apply to such a four-terminal network:

$$U_1 = AU_2 + BI_2, \quad I_1 = CU_2 + DI_2$$

Assuming $I_2 = 0$, we get

$$R_{meas} = \frac{U_2}{I_1} = \frac{I}{C}$$

Let us reverse the current and potential electrodes, (Fig.3). We then get

$$U_2 = DU_1 + BI_1, \quad I_2 = CU_1 + AI_1$$

then $I_1 = 0$ and

$$R'_{meas} = \frac{U_1}{I_2} = \frac{I}{C}$$

Fig.3

The identity $R_{meas} = R'_{meas}$ is the most general demonstration of (b).

We give below examples of electrode sitings satisfying equation (2). In the examples the soil is assumed to be homogeneous and of resistivity ρ.

A concentrated earth electrode

An earth electrode will be termed concentrated if its field is radial and spherical, at a short distance away (~ a few metres). At this distance (2)

$$\alpha_{KM} = \frac{\rho}{2\pi r_{KM}}$$

where r_{KM} is the distance (subscript M denoting any measuring electrode).

Since the measuring electrodes are concentrated electrodes, we always have

$$\alpha_{KP} = \frac{\rho}{2\pi r_{KP}}$$

1958

These expressions and equation (2) show that for the earth resistance measurement to be accurate we must have

$$\frac{1}{r_{TP}} = \frac{1}{r_{KT}} + \frac{1}{r_{KP}} \qquad (3)$$

or

$$r_{TP} = \frac{r_{KT}\, r_{KP}}{r_{KT} + r_{KP}}$$

In practice it is desirable that the total lead length to the measuring instrument ($r_{KT} + r_{KP}$) should be a minimum, this being the case when $r_{KT} = r_{KP}$.

If r_{KT} must not be less than a certain value for some reason, the same condition must be imposed on r_{KP}, since the conditions applying to both electrodes are similar. In this case

$$r_{TP} = \frac{r_{KM}}{2} \qquad (4)$$

The relative positions of the electrodes are indicated in Fig.4.

A radial earth electrode

The equipotential lines of a radial earth electrode on the surface of the ground are ellipses, so

Fig. 4. Recommended positions for the measuring of electrodes when testing a small earth electrode

$r_{TP} = r_{KP}/2 = r_{KT}/2$.

$$\phi = \frac{I\rho}{4\pi c} \ln \frac{a + c}{a - c}$$

where a is the semi-major axis, and "c" the focal distance, equal to the length of the earth electrode l; instead of 8π we took 4π, because the ground represents a half-space.

Hence,

$$\alpha_{KM} = \frac{\rho}{2\pi l} \ln \frac{2a + l}{2a - l}$$

where $2a$ is the sum of the distances from the measuring electrode to the ends of the radial earth electrode.

We will measure r_{KM} from the mid-point of the earth electrode.

When $r_{KT} = r_{KP}$ (Fig. 5)

$$\alpha_{KM} = \frac{\alpha_{TP}}{2} = \frac{\rho}{4\pi r_{TP}} = \frac{\rho}{8\pi x} = \frac{\rho}{2\pi l} \ln \frac{2a + l}{2a - l}$$

where x and y are the co-ordinates of the measuring electrode in the first quadrant.

Hence,

$$x = \frac{l}{4 \ln \frac{a2a + l}{2a - l}}$$

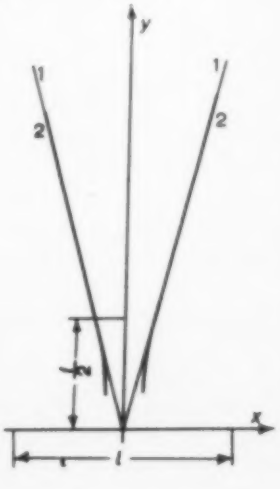

Fig. 5. Resistance measurement for a radial earth electrode. 1. Lines along which equation (4) is satisfied for symmetrically disposed electrodes. For these, $x' = y'\sqrt{15}$; 2. Lines of accurate measurement (columns 3 and 4 of table).

We will find the relation between x and y which assures accurate measurements. From the equation of an ellipse

$$\frac{x^2}{a^2} + \frac{y^2}{b^2} = 1$$

we have

$$y = \sqrt{\frac{b^2(a^2 - x^2)}{a^2}}$$

We have, therefore, obtained a single-valued solution applicable to measuring electrodes disposed symmetrically about the y-axis.

The measured data are given in the first six columns of the following table. As fundamental datum we took the semi-minor axis b of the ellipse.

1958

All distances are in metres.

a/ρ emphasises that the result is independent of the character of the soil (ρ is measured in ohm-metres).

TABLE 1

b	a	x	y	$\frac{a_{PT}}{\rho}$	$\frac{a_{KM}}{\rho}$	x'	$\frac{a'_{PT}}{\rho}$	$\Delta R_K'\%$
2.5	10.6	1.41	2.47	0.00564	0.0282	0.63	0.126	77.4
5	11.2	1.73	4.94	0.0460	0.0230	1.27	0.0625	18.3
10	14.1	2.8	9.8	0.0284	0.0142	2.53	0.0315	3.44
20	22.4	5.2	19.4	0.0154	0.0077	5.0	0.0158	0.45
30	31.6	7.6	29	0.0104	0.0052	7.47	0.0106	0.22

Let us assume that $l = 20$ m, the earth electrode diameter to be $d = 1$ cm, sunk to a depth $t = 50$ cm.

For a radial earth electrode (1)

$$R_K = \frac{\rho}{2\pi l} \ln \frac{l^2}{dt}$$

In our case $R_K = 0.09\rho$.

The table shows that when x has the values given in column 3, we get, with the values of y in column 4, $\alpha_{BT} = 2\alpha_{KM}$ and $\Delta R_K = 0$.

The last three columns show the error of measurements when the electrodes are placed to correspond with equation (4), i.e. on the lines 1 (Fig.5). y' is assumed equal to y, in which case we get practically $\alpha'_{KM} = \alpha_{KM}$.

The table shows that when the electrodes are arranged to correspond with equation (4), distances of $l/2$ from the mid-point of the radial earth electrode to the measuring electrodes are sufficient to assure an accuracy of 5 per cent.

Circuit consisting of linear horizontal segments (polygon, star, etc.)

Each linear segment i sets up a potential

$$\phi_i = \frac{I_i \rho}{2\pi l_i} \ln \frac{2a_i + l_i}{2a_i - l_i}$$

the measuring electrode where $2a_i$ is the sum of the distances from the measuring electrode to the ends of segment i;

l_i being the length of segment i;
I_i the current flowing from it into the ground.

The potential set up at the measuring electrode by the whole circuit becomes

$$\phi_{KM} = \sum \phi_i = \frac{\rho}{2\pi} \sum \frac{I_i}{l_i} \ln \frac{2a_i + l_i}{2a_i - l_i}$$

Let us assume $I_i/l_i = I_K/L$, where $L = \Sigma l_i$. Then,

$$\alpha_{KM} = \frac{\phi_{KM}}{I_K} = \frac{\rho}{2\pi L} \ln \prod_i \frac{2a_i + l_i}{2a_i - l_i}$$

Where Π is the product sign.

We use a rectangular circuit to show that a correct choice of distance from the circuit will give a satisfactory accuracy when the electrodes are placed in accordance with equation (4). Distances are measured from the centre of the circuit.

Fig.6 shows a rectangular earthing system and also two possible locations for the measuring electrodes. We know [3] that for such a system

$$R_K = \frac{\rho}{2\pi L} \ln \frac{8L^2}{\pi bt}$$

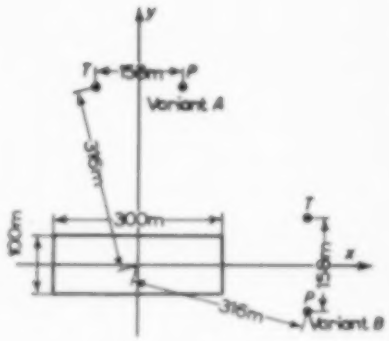

Fig.6. Earth resistance measurement on a rectangular earthing system.

where L is the perimeter of the circuit; b the width of the earthing strip; t the depth to which it is sunk in the earth.

In our case L = 800 m, b = 50 mm, t = 50 cm. With these parameters, $R_K = 3.58 \times 10^{-3}\rho$.

The above formulae give

	α_{KM}/ρ	α_{TP}/ρ	ΔR_K,
Variant A	0.050×10^{-3}	1.06×10^{-3}	1.7
Variant B	0.574×10^{-3}	1.06×10^{-3}	2.5

By using additional internal strips, vertical earth electrodes, etc. the earth resistances may be reduced, but it cannot be less than the resistance of a hemisphere of diameter equal to the circuit diagonal D = 316 m, for which

$$R_K = \frac{\rho}{\pi D} = 10^{-3}\rho$$

In this extreme case the error reaches 8.8 per cent for B. In general an error of 10 per cent is regarded as acceptable [1,3,4].

1958

In the literature [2–4] recommended for use, when measuring the resistance of the earthing of large objects

$$r_{KP} \geqslant 5D; \quad r_{TP} = 40 \text{ m}; \quad r_{KT} \geqslant (5D + 40) \text{ m}$$

These cause exceptionally large errors. Indeed, we would get in our case

$$r_{KP} = 1580 \text{ m}, \quad \alpha_{KP} = \frac{\rho}{2\pi r_{KP}} = 0.1 \times 10^{-3}\rho; \quad r_{TP} = 40 \text{ m}, \quad \alpha_{TP} =$$

$$= \frac{\rho}{2\pi r_{TP}} = 4 \times 10^{-3}\rho$$

$$r_{KT} = 1620 \text{ m}, \quad \alpha_{KT} = \frac{\rho}{2\pi r_{KT}} \approx 0.1 \times 10^{-3}\rho; \quad \Delta R_K = \alpha_{TP} - \alpha_{KP} - 3_{KT} =$$

$$= 3.8 \times 10^{-3}\rho$$

$$\Delta R_{K'} = \frac{\Delta R_K}{R_K} 100 = 3.8 \times 10^{-3}\rho / 3.58 \times 10^{-3}\rho \times 100 = 106\%$$

and in the extreme case for $R_K = 1 \times 10^{-3}\rho$

$$\Delta 3_K = 380 \text{ per cent}$$

So in measuring the earth resistances of large objects the distance between the measuring electrodes and the centre of the system must not be shorter than the diagonal of the earth contact, and the interelectrode distance not less than half this.

REFERENCES

1. K.I. Lur'e; *Testing the Earth Connections of Electrical Plant.* Gosenergoizdat (1950).
2. K.A. Krug; *Fundamentals of Electrical Engineering.* Gosenergoizdat (1946).
3. L.N. Baptiddnov and V.I. Tarasov; *The Electrical Equipment of Power Stations and Sub-stations* Vol. II, Gosenergoizdat, (1948).
4. *Protection of Industrial Plants and Buildings against Lightning* (Edited by I.S. Stekol'nikov) Akad. Nauk SSSR (1951).

AUTOMATION OF ELECTRIC DRIVES FOR BUCKET-CHAIN DREDGERS*

L.F. SHKLIARSKII

Bauman Higher Technical College, Moscow.

1958

Automatic load drive and manoeuvring winch control is a current problem in ensuring maximum dredger productivity.

Attempts† had earlier been made to render the drive control automatic, e.g. in 1937 in the "Primorzoloto" trust [1]. They were based on the use of fluid flywheels with servomotors actuated by current relays in the stator circuit of the bucket chain drive motor. Such a stepwise control could not be widely used in practice††.

Therefore the output control required by the soil variations is performed manually in most induction-motor dredgers, viz. by altering the lateral feed rate. Rheostats are used in the manoeuvring winch rotor circuit, the bucket drive motor speed being constant.

The automatic control system described below is based on the manual one, viz. that the lateral feed rate must change with the soil properties, the bucket drive speed being kept practically constant to ensure maximum productivity.

---

* *Elektrichestvo* No. 1, pp. 22–25, (1957).

† Only a.c. driven dredgers are considered.

†† A design for 0.23 m^3 bucket (1949: "Sibelektromontazh" trust) for both d.c. (generator + motor) and a.c. systems. Provided for automatic rheostat control of the maneouvring winches. But the IZTM works adopted the d.c. drive system for industrial production.

[Reprint Order No. EL. 11]

Field tests by the author in 1951, 1954 and 1955 on excavators in the Northern and Southern Urals gave approximate relationships between power, current and torque for bucket- and manoeuvring-winch drives, from which the winch motor characteristics could be more accurately defined. These requirements are specified below.

When, for example the buckets are incompletely filled during excavation and therefore the bucket motor load is lower, the bucket load must be increased by increasing the pressure on the ground, i.e. by increasing the latersl feed rate. On the other hand when the buckets become too full the lateral feed rate must be reduced.

Moreover, the desirability of limiting the bucket and manoeuvring winch drive overloads on encountering obstacles in the ground also calls for a reduction in lateral feed. The manoeuvring winch drives must therefore have flexible characteristics.

This can be checked from the field tests characteristics, one of which is shown in Fig.1.

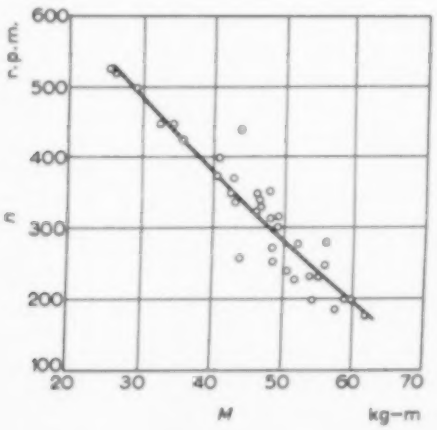

Fig.1. Mechanical characteristics of a manually controlled winch motor on a dredger with 0.38 m^3 buckets. Motor ratings P_n = 25.8 kW, n_n = 575 rev/min, M_n = 44 kg m.

The maximum winch motor torque must not exceed the value permitted by the winch rope strength. This means it must stall at $M_{max} = 1.5\ M_n$.

Thus the characteristic must approximate to hyperbolic, the stalling torque being M_{max} (at $n = 0$).

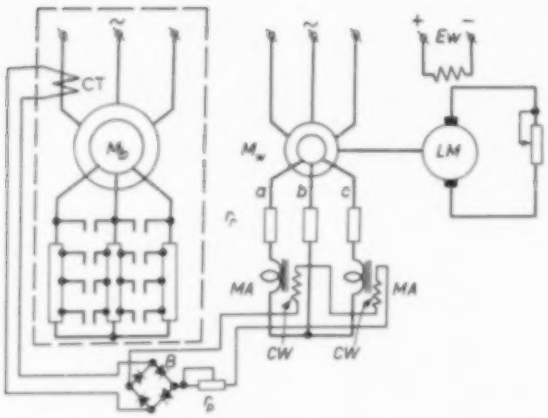

Fig. 2. Basic circuit diagram of the laboratory test set-up.
M_w: winch motor; *LM*: loading machine;
M_b: bucket drive motor replaced by a rheostat in the laboratory.

Control of the winch drive motor with a resistor r_r in series with the rotor and magnetic amplifiers (MA, Fig. 2) is the most suitable as regards motor temperature rise and automatic control of characteristics as a function of bucket drive motor load assuming that slipring-type induction motors are used for driving the manoeuvring winch.

The magnetic amplifier control windings *CW* are fed via a metal rectifier *B* from the current transformer *CT* in the bucket drive stator circuit. The manoeuvring winch motor M_w is controlled automatically by the bucket drive stator current.

This system does not require the existing electrical equipment to be rearranged, and is not very expensive. A number of alternative reactor-controlled slipring motors with different saturable reactors in the rotor circuit have been studied to determine the minimum capital outlay, weight and space requirements. This work led to the two-phase saturable reactor system (two single-phase a.c. windings on a common core, (Fig. 2) being adopted. The curves for M_w at different control currents i_c are shown in Fig. 3.*

---

* The induction motor used in the laboratory tests was a type AK-51-6, P_n = 1.7 kW, n_n = 905 rev/min, U_n = 220/380 V, I_1 = 8.5/3.8 A, η = 0.725, p.f. = 0.72, I_2 = 20.2 A, E_2 = 57 V, stalling torque/normal torque = 2, x_s = 11.3 Ω, r_1 = 5.5 Ω, r_2 = 6 Ω. Ratings of the loading machine: Type PN 28.5, P_n = 2.8 kW, U_n = 220 V, I_n = 15.8 A, n_n = 1500 rev/min.

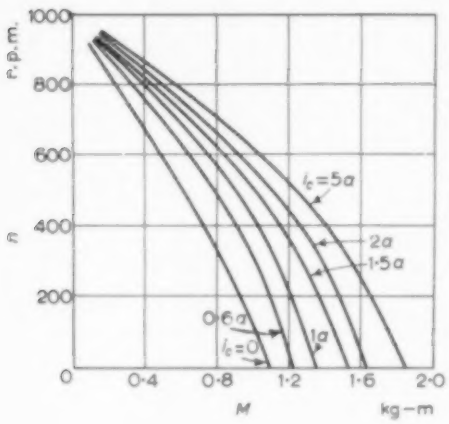

Fig. 3. Experimental mechanical characteristic of M_w in the circuit of Fig. 2 for different control currents, i_c.

The system with asymmetric (two-phase) control reactances (MA) in the rotor circuit may be analysed via the symmetrical components method [2]. Although the general theory of induction motor operation with asymmetry in the secondary circuit has been fully treated in the literature [3–6], no expression for the torque applicable to this case and convenient for practical use has yet been given. Therefore we derive below an expression for the torque as a function of slip, based on the equivalent circuit for a forward rotating field (positive phase-sequence), Fig. 4(a), and for a reverse rotating field (negative phase sequence), Fig. 4(b).

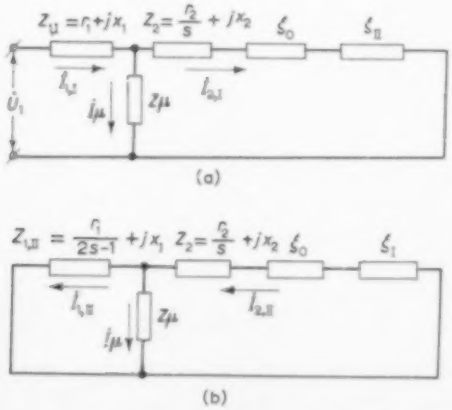

Fig. 4. Equivalent circuit of the induction motor for the direct (a) and the inverse field (b).

The equivalent impedances of the zero, positive and negative phase sequences $\underline{\xi}_0$, $\underline{\xi}_I$, $\underline{\xi}_{II}$, respectively, which are determined by the magnetic amplifier reactances x_a and x_c in the two rotor phases, can be written as follows:*

$$\underline{\xi}_0 = j\frac{x_a + x_c}{3} \tag{1}$$

$$\underline{\xi}_I = j\frac{x_a + a^2 x_c}{3} \tag{2}$$

$$\underline{\xi}_{II} = j\frac{x_a + x_c}{3} \tag{3}$$

From the equivalent circuits of Fig.4, neglecting the magnetizing current ($I_\mu = 0$), some simple steps give the torque as:

from the direct field

$$M_I = K\frac{(r_2/2)(c^2 + b^2)}{(a_c - b^2 + d)^2 + b^2(a + c)^2}\ ; \tag{4}$$

from the inverse field

$$M_{II} = K\frac{\dfrac{r_1}{(2_s - 1)d}}{(a_c - b^2 + d)^2 + b^2(a + c)^2}\ ; \tag{5}$$

where

$$K = \frac{mV_1^2}{9.81\omega}\ ; \qquad a = r_1 + \frac{r_2}{s}\ ;\dagger \qquad b = x_s + \frac{1}{3}(x_a + x_c)\ ;$$

$$c = \frac{r_1}{2s - 1} + \frac{r_2}{s}\ ; \qquad d = \frac{1}{9}\left[(x_a - x_c)^2 + w_a w_c\right]$$

---

* The resistances of the a.c. windings on the magnetic amplifier are neglected.

† r_2 includes the internal resistance of the rotor phase as well as the external series resistances r_r.

The total torque is the algebraic sum of the forward and reverse torques, i.e.

$$M = M_{I} + M_{II} \tag{6}$$

equations (4), (5) and (6) therefore enable us to derive the mechanical characteristics for different signals at the magnetic amplifier inputs which determine the corresponding reactances x_a and x_c.

The experimental curves (Fig. 3) show that there is practically no undesirable torque drop due to core saturation [7–8] in the half-synchronous speed range. The torque drop can therefore be neglected in calculating the mechanical characteristics.

This system (Fig. 2) makes it possible to obtain the desired winch motor characteristic automatically, (e.g. similar to that shown in Fig. 1) and to satisfy the requirements laid down at the beginning of the article.

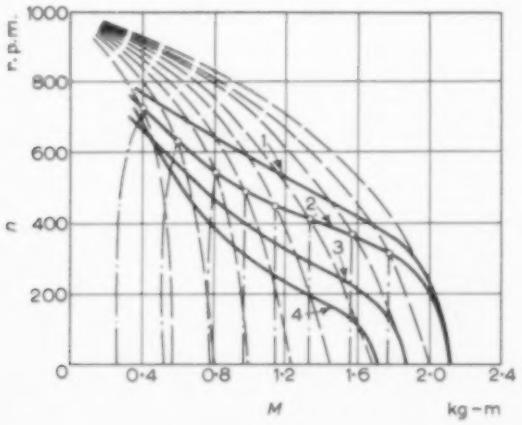

Fig. 5. Characteristics of M_{II} in the circuit of Fig. 2 obtained under laboratory conditions. — . — . — static torque.

Fig. 5 shows several such laboratory test curves obtained with various m.m.f. increments in the magnetic amplifier control circuits. 1 and 2 were obtained with two single-phase amplifiers and 3 and 4 with one two-phase amplifier.

The asymmetric impedances in the rotor give rise to direct and inverse fields, the stator current contains a component of normal frequency f_1 and another of reduced frequency $f_3 = f_1(1 - 2s)$, which cause beating. But Fig. 6 shows that this beat remains slight even at minimum signals

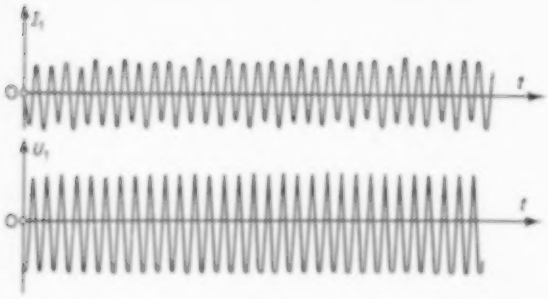

Fig. 6. Oscillograms for I_1 and U_1 in the stator.

($i_c = 0$) when the asymmetry is maximal.* The additional winding temperature rise due to the reduced frequency currents is also very small. The stator terminal voltage is practically unchanged.

The reduced p.f. typical of inductor control systems cannot be considered as hindering the use of this system on dredgers since the winch drives on those with 0.155, 0.21 and 0.38 m^3 buckets are of relatively low ratings (18 – 26 kW). Static capacitors connected to the stator terminals will improve the p.f.

Conclusions

(1) Laboratory and theoretical work has shown that the magnetic amplifier system provides the required winch motor characteristics automatically.

(2) The system is simple. The main electrical equipment need not be rearranged or changed in order to introduce it. The capital cost is low.

(3) The automatic control system would reduce the strain on the operator and increase his productivity.

List of symbols

x and x_c magnetic amplifier inductive reactances in the a and c rotor phases;

a operator rotating vectors through 120^p;

* When $i_c = 0$ the modulus of the coefficient of current unbalance ($\gamma = \dot{I}_{II}/\dot{I}_I$), which specifies the degree of asymmetry in the rotor circuit, was 0.68.

$Z_{1,I}$ positive-sequence impedance of one stator phase;

$Z_{1,II}$ negative-sequence impedance of one stator phase;

Z_2 impedance of one rotor phase;

r_1 and x_1 resistance and inductive reactance of one stator phase;

r_2 and x_2 referred resistance and inductive reactance of a rotor phase;

x_k inductive reactance of one motor phase;

U_1 phase voltage on the stator;

$\dot{I}_{1,I}$ positive-sequence stator current;

$\dot{I}_{1,II}$ negative-sequence stator current;

$\dot{I}_{2,I}$ positive-sequence rotor current;

$\dot{I}_{2,II}$ negative-sequence rotor current;

$m_1 = m_2 = m$ = number of phases in stator and rotor;

ω_0 = synchronous angular velocity of the motor;

s = slip;

w_c and r_c are the number of turns and resistance of the magnetic amplifier control winding respectively.

REFERENCES

1. A.G. Vecheslov and P.K. Shindel'man; Automatic Control of the manoeuvring Winch on a 210 litre Electric Dredger. *Sovetskaya Zolotopromyshlennost'* No.4 (1937).
2. K.A. Krug; *Fundamentals of Electrical Engineering.* Gosénergoizdat (1952).
3. K.F. Wagner and R.D. Evans; *Symmetrical Components.* (1933).
4. G.I. Shturman; *Asymmetry of the Secondary Circuits in Induction Motors.* ONTI (1935).
5. G.B. Merkin and E.D. Nesgovorova; *Induction Motor Operation with Rotor Asymmetry.* Trudy Leningradskogo Industrial'nogo Institute, No.2 (1938).

6. M.P. Kostenko; *Electrical Machines (Special Part).* Gosénergoizdat (1949).
7. S.N. Veshenevskii; *Calculation of Characteristics and Impedances in Electric Motors.* Gosénergoizdat *(1955).*
8. T.H. Barton and B.C. Doxey; Operation of Three-phase Induction Motors with Asymmetric Rotor Circuit Impedances. *Proc. Inst. Elect. Engrs.* A **102**, No.1 (1955).

1958

DIFFERENTIAL PROTECTION CIRCUITS WITH MAGNETIC RESTRAINT*

A.D. DROZDOV

Ordzhonikidze Polytechnical Institute, Novockerkassk

(Received 19 October 1955)

The simple principle of magnetic restraint, known since 1930, has now also been applied to differential protection. We are now well acquainted with the theory of this principle and have evolved methods of eliminating the dependence of relay response on the phase relations of the individual phases; also rational relay designs using one or more restraining windings exist [1 - 4].

The present communication presents methods of synthesizing, transforming and designing differential protection circuits.

Fig. 1(a) shows a symmetrical circuit containing a balance coil and split restraining or premagnetizing coils connected into the arms of the protection circuit. One three-limb core could be used instead of the two two-limb cores shown in Fig.1: tests show that the results obtained with this arrangement are quite similar to those with two-limb cores.

By applying the law of conservation of current the circuit of Fig.1(a) can be simplified without appreciably altering its characteristics. Two coils with different numbers of turns could be used instead of the three coils in series on the outer and central limbs.

Let us remove the coil $w_{na}/2$ on the right-hand limb, and reduce the turns on the working winding by $w_{na}/2$, thus retaining the nett ampere turns, and increase the turns on the left-hand premagnetizing coil by the same number, or, which amounts to the same, let us transfer $w_{na}/2$ turns from the right-hand to the central and left-hand limbs. The new working winding then has $w_w = w'_w - w_{na}/2$ turns.

To maintain the ampere-turns produced in the central limb by I_b we have to increase the balance winding turns by $w_{na}/2$.

* *Elektrichestvo* No. 2, 33-36 (1957). [Reprint Order No. EL. 12]

Furthermore, we will remove $w_{nb}/2$ turns from the left-hand limb and correspondingly reduce the balance turns and increase the right-hand premagnetizing turns. The new number of turns on the balance winding is

$$w_{bl} = w'_{bl} + w_{na}/2 - w_{nb}/2$$

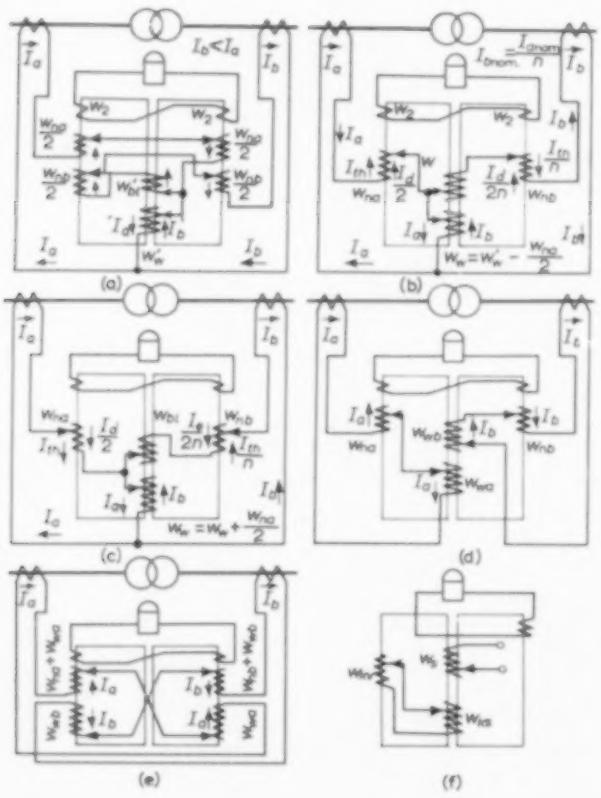

Fig. 1 Differential protection circuits with equal total numbers of ampere-turns.

(a) with separate working and premagnetizing windings;
(b) equivalent circuit with premagnetizing windings partly acting as working coil;
(c) the same, but with reversed senses of the premagnetizing coils;
(d) and (e) with separate circuits.
(f) saturable transformers with short-circuited turns.

1958

Fig.1(b) shows the circuit so obtained. The premagnetizing coils act partly as the working winding. Therefore we may add the turns on the working and balance windings and determine them from the following formulae:

$$w'_w = w_w + w_{na}/2; \quad w'_{bl} = w_{bl} - w_{na}/2 + w_{nb}/2$$

The total may be fractional. We derive below the formulae and give an example of winding calculation for the circuit of Fig.1(b).

The total turns are determined from the ampere-turns found experimentally via the response of an unrestrained relay, viz. F = 70 A:

$$w'_w = cF/I_{sa} = 1.05 \times 70/5 = 14.7$$

where I_{sa} = 5 A is the operate current on the side of the winding a; $c = I_{sa}/I_{so}$ is a factor allowing for the increase in operate current with a unilateral internal fault over the current occurring with a symmetrical bilateral supply. The well-known formula for c for mechanical relays gives

$$c = \frac{2}{\sqrt{4 - k_r^2}}$$

The restraining factor k_r is assumed as 0.6 when c = 1.05. We can determine c for magnetically restrained relays similarly because their characteristics at low currents are similar to those of mechanical relays. w_{na} then is (1, 2)

$$w_{na} = k_r w'_w = 0.6 \times 14.7 = 9$$

The effective k_r will be greater at high currents as may be established experimentally or from the curves of double magnetization (2).

If the ratio of the nominal currents $n = I_a/I_b$ is assumed as 1.46, w_{nb} for the second premagnetizing coil becomes

$$w_{nb} = nw_a = 1.46 \times 9 = 13$$

and w_w is

$$w_w = w'_w - \frac{w_{na}}{2} = 14.7 - 4.5 \approx 10$$

The current in the arms of the protection circuit may be divided into the through-current I_{th} and the differential current I_d. Since I_d flows from the current transformer secondary to the differential circuit from both sides, we get

$$I_a = I_{th} + \frac{I_d}{2}; \quad I_b = \frac{I_{th}}{n} - \frac{I_d}{2n}$$

The magnetizing forces in the right-hand and left-hand circuits due to I_{th} must be equal and opposite, i.e.

$$n(w_w + w_{na}) - w_w - w_{bl} = w_w + w_{bl} + w_{nb} - w_w \qquad (1)$$

from which we can determine w_b

$$w_{bl} = (n-1)w_w + 0.5(nw_{na} - w_{nb}) =$$

$$= 0.46 \times 10 + 0.5(1.46 \times 9 - 13) = 4.67 \approx 5 \qquad (2)$$

The second term 5 on the right-hand side of equation (2) allows for imperfect agreement between the ratios of rounded-off turns and currents for the premagnetizing windings.

Since w_{bl} has been rounded off equation (1) will be satisfied at some current ratio other than nominal, corresponding to the winding parameters adopted and determined from equation (1), viz.

$$\Delta n_{wd} = \frac{w_w + w_{bl} + w_{nb} \times 0.5}{w_w + w_{na} \times 0.5} = \frac{10 + 5 + 6.5}{10 + 4.5} = 1.482 \qquad (3)$$

Hence I_{th} will cause an additional flux unbalance in the two cores, which is equivalent to the unbalance-current increasing by

$$\Delta i_{ub} = \frac{n - n_{wd}}{n_{wd}} 100 = \frac{1.46 - 1.482}{1.482} 100 = -1.5 \text{ per cent}$$

If we assume $w_{bl} = 4$, $n_{wd} = 1.414$; $\Delta i_{ub} = 3.25$ per cent. For an operate current $I = 10$ A, $w_w = 5$; $w_{bl} = 2.22 \approx 2$; $\Delta i_{ub} = 2.1$ per cent; and when $w_{bl} = 3$, so $\Delta i_{ub} = -7.0$ per cent. Even when the choice of w_{bl} is not correct, as in the latter example, the effect of the i_{ub} is fully compensated by the restraint (7 per cent << 60 per cent).

For compensation to be obtained we must have

$$i_{ab} + \Delta i_{ab} < k_r$$

If the restraint is strong enough there is no need for the ratios of the current transformers to be exactly equal.

Fig.1(a) may be modified in yet another way, viz. by transferring $w_{na}/2$ from the left-hand to the centre and right-hand limbs. w_w is then increased, viz.

$$w_w = w'_w + 0.5\, w_{na} = 14.7 + 4.5 \approx 19$$

This gives the circuit of Fig.1(c) which differs from the original in the sense of the premagnetizing windings, which have the same turns as in Fig.1(a).

Equations (1 – 3) may also be applied to Fig.1(c) if the signs of w_{na} and w_{nb} are reversed, viz.

$$w_{bl} = (n-1)w_w - 0.5(nw_{na} - w_{nb}) = 8.7 \approx 9:$$

$$n_{wd} = \frac{w_w + w_{bl} - 0.5w_{nb}}{w_w - 0.5w_{na}} = 1.482$$

$$\Delta i_{ab} = -1.5 \text{ per cent}$$

If we assume $w_{bl} = 8$, $n_{wd} = 1.414$ and $\Delta i_{ab} = 3.25$ per cent. Consequently the figures are unchanged, from which we conclude that Fig.1(b) and (c) are equivalent as regards balancing the secondary currents, although Fig.1(c) would appear to have advantages owing to the greater number of turns.

When other protection circuits are connected to one of this type the secondary circuits may have sometimes to be split. Fig.1(b) may then take the form shown in Fig.1(d). Fig.1(e), obtained by separating the common coils in Fig.1(d) will also serve.

The restraining characteristics of the circuits must be identical if leakage is disregarded. But they actually differ in curvature (2). If the restraining and secondary windings are placed on the same limbs, and the working windings on the opposite limbs (Fig.1,a) the characteristic will become concave and k_r will increase for large currents due to

additional premagnetization in one part of the magnetic circuit. In Fig.1(b) the premagnetizing coils act as working coils so its characteristics will be less concave than those of Fig.1(a). The characteristics of Fig.1(d) and (b) are similar. The concavity for Fig.1(c) is much greater than that for Fig.1(a). Fig.1(e) has approximately linear characteristics because all windings are on the same limbs.

Fig.1(b) is preferable owing to its simplicity, universal usefulness, smaller number of turns and symmetrical characteristics. The premagnetizing coil connections can here be reversed (Fig.1 c) or the circuits may be separated (Fig.1,d). No alterations to the design are required.

Fig.1(b) can be made to give a saturable transformer with short-circuited turns with a lower sensitivity to aperiodic currents. One such circuit is shown in Fig.1(f). Here the right-hand core with its windings is the transformer proper. In the short-circuited circuit of the left-hand core a current partly compensating the effect of the primary (alternating) current on the right-hand core is set up which reduces the number of primary turns, as it were. However, the effect of the constant current is not reduced, which results in a reduced sensitivity. Saturable transformers are more fully treated in (4).

1958

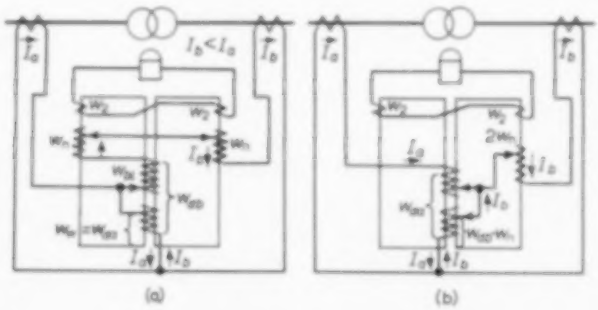

Fig. 2 Differential protection circuits with premagnetizing windings in one arm.
(a) with separate working and premagnetizing windings;
(b) simplified equivalent circuit.

The circuit is simplified if the premagnetizing coils are placed asymmetrically, i.e. in one arm only (Fig.2,a). The circuit is further simplified by transferring the left premagnetizing coil to the central and right-hand limbs, as shown in Fig.2(b). A disadvantage of Fig.2(b) is that the leakage flux is asymmetric when only I_{eh} flows. If i_{ab} and

I_{th} are in phase in the premagnetizing windings ($nI_b > I_a$), both the circuits of Fig.2 are under great restraint, as illustrated by curves 2

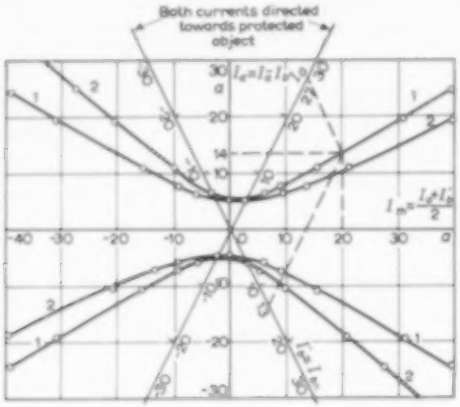

Fig.3 Experimental characteristics of differential protection circuits.

(a) symmetric circuit;

(b) asymmetric circuit.

in Fig.3, which refer to Fig.2(a). Symmetric circuits have symmetric characteristics (curve 1). The curves of Fig.3 are universal and give the currents in the protection circuit arms in terms of the oblique coordinates I_a and nI_b. Curves 2 may be made more symmetric by increasing w_{b1} (Fig.2), but this will normally introduce a flux which is difficult to control.

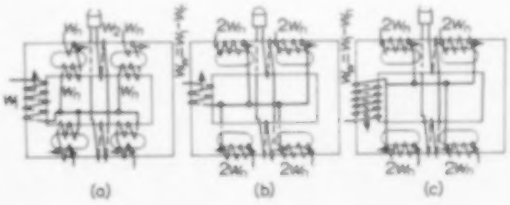

Fig.4 Differential protection circuits of multiply wound transformers with equal total numbers of ampere-turns.

(a) with separate primary and premagnetizing windings windings;

(b) with premagnetizing windings partly acting as primary coil;

(c) with reversed connections to the premagnetizing windings.

The circuits of Fig.2 are simpler than those of Fig.1 but restraints depend on the direction of I_{ub} which is difficult to predict. The location of the restraining coils is also of some importance. Fig.1(b) can easily be converted into the assymetric circuits of Fig.2.

A differential protection circuit with several restraining coils can be designed round a transformer with slots in the magnetic circuits (Fig.4,a). The four premagnetizing coils act here independently. Fig.4(a) may be simplified as above, the equivalent circuit Fig.4(b) in which the premagnetizing windings act partly as primary coils being then obtained. The circuit can also be used with reversed premagnetizer connections (Fig.4,c); the curve is then strongly convex. But Fig.4(b) is preferable because it is simpler and has less turns.

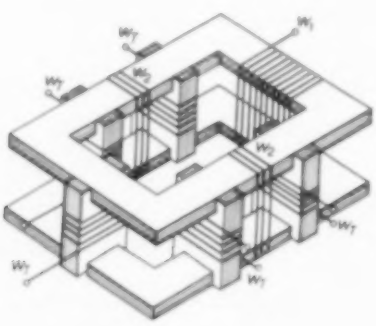

Fig.5 Saturable transformer with 5 premagnetizing coils on the cross-members.

The premagnetizing coils may also be formed by cross-connections (Fig.4), i.e. by threading the turns first through one, and then through the other opening. It is then convenient to use a different core design with cross-members (Fig.5). This has the advantage of simplifying coil winding and facilitating alterations. There is no restraining effect with an internal symmetrically fed fault, this making for reliability of operation. The damping characteristics of this arrangement are effected by a certain dispersion owing to the different arrangement of the coils. The construction of working coil and magnetic system is simpler with the longitudinally slotted magnetic circuit, the whole unit being more rigid and compact. This design may therefore be regarded as more satisfactory.

REFERENCES

1. V.I. Ivanov; *Relays and Relay Protection*. Gosenergoizdat (1932).
2. A.D. Drozdov; Fundamental equations of saturable differential current transformers for relay protection. *Elektrichestvo* No.6 (1954).
3. M.B. Tsfasman; Design of differential protection with magnetic restraint for transformers. *Elekt. Stantsii* No.3 (1955).
4. A.D. Drozdov; Saturable current transformers with short-circuited turns for relay protection. *Elektrichestvo* No.10 (1953).

THE STABILITIES OF MEASURING INSTRUMENTS USING MAGNICO AND ALNICO*

E.G. SHRAMKOV, A.V. MITKEVICH and N.B. KOVALEV

1958

Although permanent magnets made from alloys of iron, nickel and aluminium are extensively used in modern devices, the stabilities of such systems have not been fully studied nor have they been exhaustively treated in the literature. The measuring apparatus used previously has been of low sensitivity and the methods of measurement have not been sufficiently accurate to detect small flux variations and hence prevented a sound appraisal of the way the systems behave.

Some experimental data on Alni and Alnico permanent magnets have been published [1 – 3], which state that flux variations of several per cent were observed. Other papers [4 – 6] mainly give general information with no experimental data. One paper [7] describes a sensitive balance method in which balance is obtained by varying the current through a coil in the air gap of the magnet, though data are only given for a few magnets. Ballistic null-methods for measuring accurately the flux densities in the air gaps of permanent magnets have also been described [8 – 10]. Kronenberg [10] gives data also on the stabilities of Alni and Alnico magnets.

Measuring instruments and magnetic systems investigated

A special type of measuring apparatus based on null-principles was developed to measure relative flux changes of about 10^{-2} per cent. These new instruments were used to study the stability of one kind of magnet system with Alnico and Magnico magnets. Rectangular magnets with pole pieces held together in a silumina diecasting were held in rings of magnetically soft material to complete the flux path. The system differed from those used in electromagnetic instruments only by having a somewhat longer core which was pressed into a brass bush with an external thread to secure the system during the flux measurements. One of the

* *Elektrichestvo* No. 3, 62–67 (1957). [Reprint Order No. EL. 13]

measuring instruments developed consists of a balance with arms having different masses (similar to that described in [7]). The balance beam rests with its knife edges on jewel bearings. One arm bears a pointer which is observed with a telescope. A gear transmission train actuated by a handle is used for positioning the system and balancing is achieved by varying the current through a coil in the air gap. At balance the current in the coil is inversely proportional to the flux density.

The other measuring instrument was developed by N.B. Kovalev. Here two opposing torques acting on a moving system are balanced; one torque is produced by an astatic electrodynamic measuring system and the other by the current in a test coil and the flux of the system. The stationary and the moving coils of the electrodynamic system and the test coil are all connected in series. The moving system is suspended, and carries a mirror. A fixed mirror is placed below the first one so that two images (from the two mirrors) of a scale placed near the telescope can be seen. When the two torques are equal, or when no current flows in the coils, the instrument reads zero, and the two images coincide. When the two torques balance the current in the coils is proportional to the flux density in the air gap. A handle is used to position the magnetic system.

In both measuring instruments the coil current was measured potentiometrically accurate to ~ 0.005 per cent. Since the instruments were designed for making extensive measurements provision was made to ensure accurate resetting of the magnetic systems. The temperature of the instrument room was maintained constant at $22^{\circ} \pm 0.1^{\circ}C$. All readings were made from another room which contained the potentiometer. The reproducibility was estimated to be ~ 0.03 per cent for each instrument. The results given below were obtained mainly with the first instrument; the second instrument was primarily used to verify the readings of the first.

Altogether we investigated 94 systems; 50 were fitted with Magnico magnets (40 were produced in August, 1952 and 10 in February, 1955) and 44 of Alnico (produced in May – September, 1953 and in November, 1954). Only the most typical results will be described.

All 94 systems were magnetized practically up to saturation with a d.c. electromagnet having special pole pieces embracing the system. Magnetic stabilization, i.e. partial demagnetization, was carried out mainly by applying a 50 c/s field which was gradually reduced to zero. For this purpose another electromagnet with laminated sheet steel yoke and pole pieces was used; the pole pieces were arranged as in the d.c. magnetizing electromagnet.

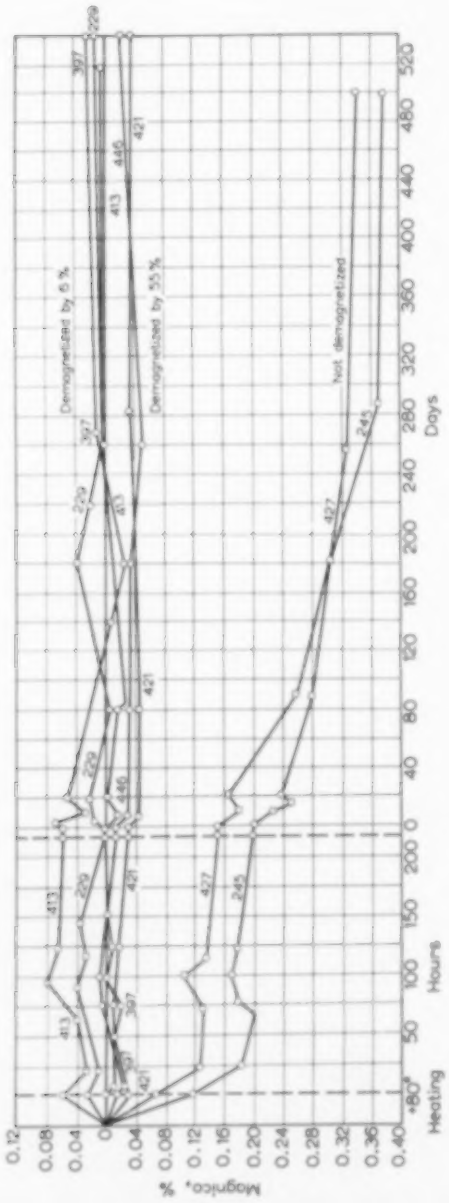
Demagnetized by 6 %
Demagnetized by 55 %
Not demagnetized
Magnico, %
Hours
Heating
Days
0.12
0.08
0.04
0
0.04
0.08
0.12
0.16
0.20
0.24
0.28
0.32
0.36
0.40
+80°
200
150
100
50
0
40
80
120
160
200
240
280
320
360
400
440
480
520

Fig. 1.

1958

Magnetic systems with Magnico alloy magnets

Heat treatment effects following magnetization and stabilization, and the effect of the degree of stabilizing demagnetization on the consequent behaviour were studied on Magnico alloy systems for periods of up to 1½ years.

Fig.1 shows the results obtained on seven systems six months after manufacture (the system numbers are shown against the curves on this and the following figures). The ordinate indicates the percentage flux density variation in the working gap, the abscissae indicating the annealing temperatures and time in hours and days.

All seven systems were magnetized: two were not subsequently demagnetized (lower curves), two others (nos. 446 and 421) were 55 per cent demagnetized using an a.c. electromagnet and the remaining three (nos. 229, 397 and 413) were 6 per cent demagnetized, using the same method. Next, six were treated at +80°C for 1 hr and cooled down to room temperature. (The heating time of about 30 min is not included). One (no. 397) which was 6 per cent demagnetized was not subjected to heat treatment (the curve starts from the vertical dashed line marked "anneal").

The six treated systems were first measured 2 – 3 hr after heating and the unannealed one was first measured approximately 30 min after demagnetization. Fig.1 shows that heating at +80°C led to a flux increase of 0.03 – 0.06 per cent in 6 per cent demagnetized systems, whereas in 55 per cent demagnetized systems a slight weakening of 0.02 – 0.03 per cent resulted. In the systems which were not demagnetized the flux drop was 0.07 to 0.12 per cent. The flux drop was greater following annealing at +80°C; for example, a drop of 0.9 per cent was observed for one non-demagnetized system.

The flux changes were most pronounced during the first few days after heat treatment for the non-stabilized systems. Stabilized systems were stable to within a few hundredths of one per cent.

Systems 6 – 10 per cent demagnetized and given a second heat treatment at +80°C showed flux increases of sometimes up to 0.16 per cent. Treatments subsequent to the second or third were found to have comparatively little effect and the annealing time if > 1 hr, was unimportant; annealing for 1 or 4 hr produced approximately the same effect.

Investigations on systems immediately after manufacture, and some time afterwards showed that annealing at +80°C has more effect on the flux when carried out immediately after manufacture. This is quite possibly due to structural changes in the magnet or to some other changes in the system as a whole.

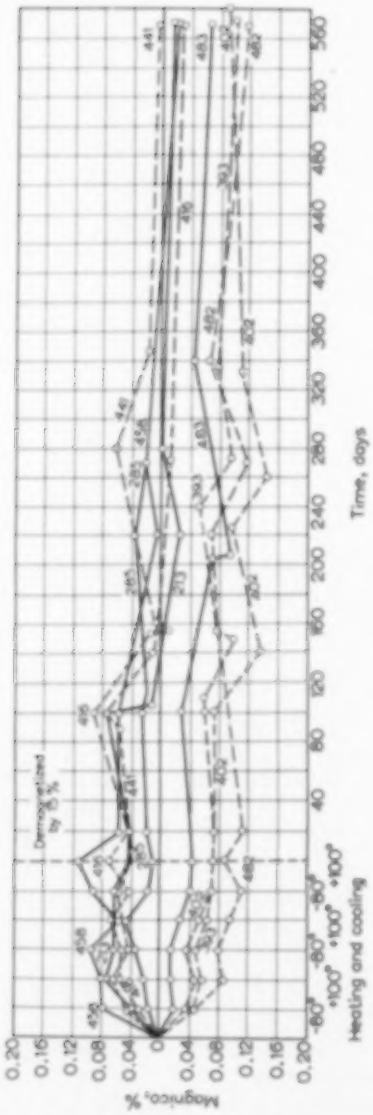
Magnico, %
0.20
0.16
0.12
0.08
0.04
0
Demagnetized by 6 %
Heating and cooling
-80° +100° -80° +100° -80° +100°
Time, days
0
40
80
120
160
200
240
280
320
360
400
440
480
520
560

Fig. 2.

1958

In practice magnetic systems are sometimes conditioned by thermal cycling prior to magnetization. It was desired to elucidate how this treatment would influence subsequent behaviour of the system. Fig.2 gives data for nine systems, five of which (broken lines) were given 10 cycles from $-80^{o}C$ to $+100^{o}C$ before magnetization; each temperature being maintained for 4 hr. The remaining four systems (full lines) did not undergo this treatment. Next, all the nine systems were magnetized and partly demagnetized using an a.c. electromagnet. Five systems were demagnetized 12 – 15 per cent (upper curves in Fig.2) and four 60 – 70 per cent (lower curves). After this all the systems were given 3 cycles from $-80^{o}C$ to $+100^{o}C$, temperature being maintained for 2 hr; the treatment being started with cooling.

The curves show that thermal conditioning produces slight flux increases in 12 – 15 per cent demagnetized systems whereas the flux decreases slightly in systems demagnetized 60 – 70 per cent. Whether the magnet was cooled before or after being annealed made no difference to its subsequent behaviour.

Similar systems, 20 and 45 per cent demagnetized, gave curves which lie between the upper and lower groups in Fig.2.

The data show that preliminary thermal treatment does not affect the subsequent behaviour to any noticeable extent, i.e., this treatment is not essential. All the nine systems studied were about equally stable. A rather important fact is that even those 60 – 70 per cent demagnetized were satisfactorily stable.

Magnetic shunts were applied before magnetization in some cases and, after demagnetization and a few cycles to $+80^{o}C$ the shunts were moved from one limiting position to the other. The stabilities of these systems did not differ from those of systems without shunts.

Systems with Alnico magnets

Fig.3 shows the effects of post-magnetization heat treatment followed by stabilization, and of the degree of stabilizing demagnetization on Alnico systems. Six systems were magnetized and then demagnetized 6 – 10 per cent using an a.c. electromagnet. All these were then subjected to six heat treatments at $+80^{o}C$, each heating being followed by cooling to room temperature. The higher temperature of $+80^{o}C$ was maintained for 1 hr with three specimens (full curves) and 4 hr with the other three (broken curves). As before, the time required to reach $+80^{o}C$ (30 min) is not included in the duration of the heat treatment.

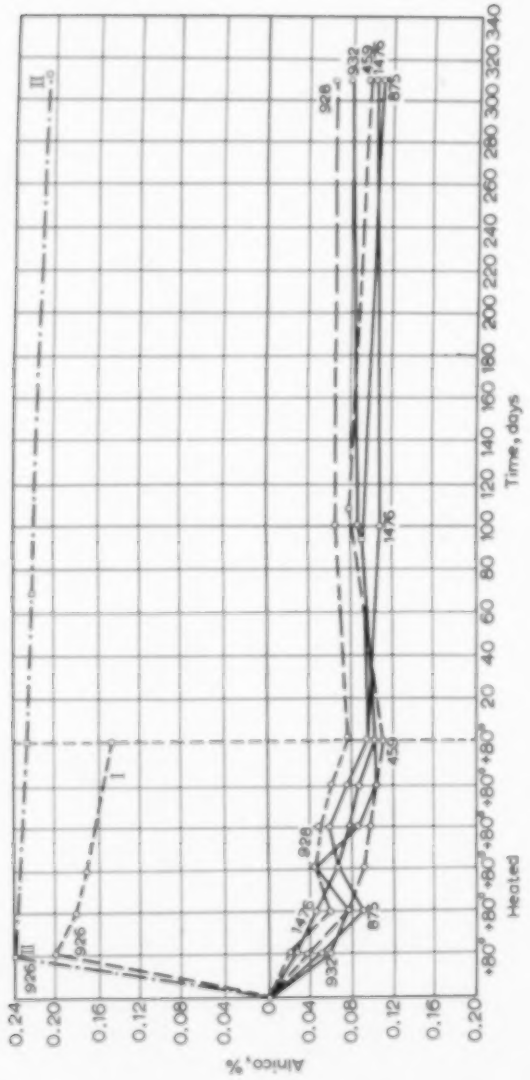
Alnico, %
0.24
0.20
0.16
0.12
0.08
0.04
0
0.04
0.08
0.12
0.16
0.20
Time, days
0
20
40
60
80
100
120
140
160
180
200
220
240
260
280
300
320
340
Heated
+80°
I
II
III
926
932
459
1476
875

Fig. 3.

1958

The curves show that 1 and 4 hr annealing have approximately the same effects. Further treatments beyond the second also have comparatively little effect. One system (top curve, I) stands out from the others. An unusually large flux change was found after the first heat treatment, and therefore the system was subjected to a new series of heat treatments two weeks later (curve II, Fig.3). This confirmed that there was a genuine difference between this system and the others, which did not disappear after the subsequent heat treatments. During the work on Alnico magnets yet another system was discovered which reacted to heating in the same manner as no. 926 (Fig.3). These two which reacted quite strongly to annealing had originally the same flux densities as all the others. So some definitely undesirable irregularity requiring separate investigation occurred here.

Two systems were annealed at +300°C for 4 hr, which caused little change in their subsequent reactions.

A number of systems demagnetized by varying percentages (between 4 and 20 per cent), and one system not demagnetized at all, were subjected to several cycles between +80°C and −80°C. With two exceptions the resulting flux reductions were less than 0.06 per cent. The exceptions were one demagnetized 4 per cent which had its flux reduced by approximately 0.18 per cent and the non-demagnetized system which dropped by approximately 0.7 per cent.

All the partially demagnetized systems were found to be about equally stable and the variations during a year did not much exceed 0.01 per cent (within the limits of experimental error).

The systems were normally magnetized in groups placed between the poles of an electromagnet. Partial demagnetization was carried out using a 50 c/s a.c. electromagnet. The magnets were therefore magnetized and demagnetized under conditions differing from their normal working conditions. A magnet in a 50 c/s field is also more strongly demagnetized near the surface. Consequently various demagnetization methods were studied at the same time as the premagnetization heat treatment.

Five of the eleven systems were given 11 cycles from −80°C to +120°C, each temperature being maintained for 2 hr before magnetization (dashed curves, Fig.4). The remaining six systems were not so treated (full curves, Fig.4). All eleven were magnetized and then demagnetized by 6 – 10 per cent by various methods. Heat treatment at +80°C for 4 hr followed. Three systems were demagnetized using the field of a d.c. electromagnet with pole pieces sufficiently large to enclose the systems.

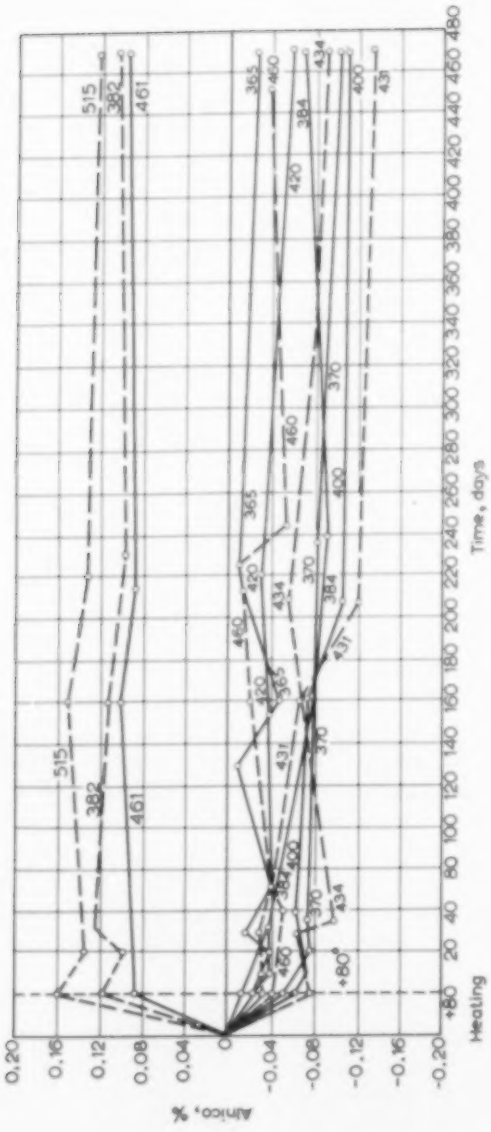
Alnico, %
0.20
0.16
0.12
0.08
0.04
0
-0.04
-0.08
-0.12
-0.16
-0.20
Heating
+80
Time, days
0 20 40 60 80 100 120 140 160 180 200 220 240 260 280 300 320 340 360 380 400 420 440 460 480
515
382
461
365
460
434
384
420
400
431
370

Fig. 4.

1958

The exciting current was smoothly reduced to zero and reversed 1 to 2 times/sec. The curves obtained lie in the upper part of Fig.4. Two systems were demagnetized by d.c. coils placed directly on the magnets. The direction and magnitude of the direct currents in these coils were altered as with the electromagnet. Two other systems were a.c. demagnetized using the same coils. The remaining four systems were demagnetized in the usual way using an a.c. electromagnet. The curves for the last eight systems (lower curves in Fig.4) are more or less similar, the spread in the points being within the limits of experimental error (0.03 per cent). The systems demagnetized with d.c. and a.c. electromagnets were interchanged to check that a different type of curve resulted from demagnetization with the d.c. electromagnet. It was found that the type of curve obtained depended on the method of demagnetization, not on the particular system considered.

Fig.4 shows that the systems demagnetized by means of the coils wound directly on the magnets, i.e. those magnetically stabilized under conditions similar to their working conditions, are affected by subsequent heat treatment and time in approximately the same manner as the systems demagnetized with the a.c. electromagnet; their fluxes show a slight drop. A.C. electromagnet demagnetization is therefore sufficiently reliable. But systems demagnetized with the d.c. electromagnet reacted quite differently to heat treatment; their fluxes increased by up to 0.2 per cent. It would seem that large pole pieces make demagnetization with d.c. electromagnets more difficult than with a.c. electromagnets. The latter method is more similar to the way in which magnets are normally demagnetized during use.

Fig.4 also shows that premagnetization heat treatment has little effect on the subsequent behaviour of Alnico magnet systems and so is not essential. The same conclusion had also been reached for Magnico systems.

The present work also included some tests of the effects of magnetic shunts. Magnetic shunts were fitted to six of the above eleven systems before magnetization, and after demagnetization and heat treatment at $+80^{\circ}C$ these shunts were transferred between extreme positions. Nos. 365, 400, 461, 515 and 420 had shunts fitted after annealing, i.e. moved to have maximum shunting effect, while no. 431 had its shunt removed. Fig.4 shows that the stabilities are approximately the same with or without shunts. Only in no. 431 did the flux decrease by ~ 0.09 per cent during the first six months after the de-shunting, and this has remained stable for the last nine months.

Effects of temperatures, vibration and external magnetic field

These effects were studied mainly on magnetically and thermally stabilized Alnico and Magnico magnets, .i.e. ones which had undergone temperature cycle conditioning after magnetization and demagnetization.

The systems were demagnetized by varying percentages (5 – 10 per cent) and after demagnetization were thermally cycled a number of times (+80°C to +20°C) and subsequently annealed at either +50°C or –50°C for 5 hr. The flux changes after this treatment were within the limits of experimental error.

Magnico magnets heat-treated after stabilization, but only annealed at 50°C retained their fluxes practically unchanged for one year after stabilization.

Vibration at 30 c/s and accelerations of 7g produced no effect on Magnico and Alnico magnets demagnetized by 6 – 10 per cent.

These systems were subjected to an external uniform d.c. field of 4 ampere/turns/cm and also to a 50 c/s a.c. field of 4 ampere-turns/cm peak. No changes were produced by this test.

A flux increase of up to 0.09 per cent was observed in some cases when a 50 c/s field of amplitude 40 ampere-turns/cm had acted on Alnico magnets demagnetized by 6 – 10 per cent by an a.c. electromagnet. Those demagnetized 6 – 10 per cent by a d.c. electromagnet showed even greater flux increases, namely 0.1 – 0.4 per cent.

The causes of the flux increases found in the Alnico systems used in the earlier tests were investigated by demagnetizing them in a weak 50 c/s field from coils wound direct on the magnets. The fluxes decreased.

In a second test the systems were demagnetized in the same type of field but with the coil wound on the ring completing the magnetic circuit. In this case the flux in the air gap was increased.

It seems possible that in the first case only the actual magnets become demagnetized, causing flux reduction in the air gap, whereas in the second the comparatively weak alternating field affects the properties of the ring completing the circuit more than the actual magnets. It is also possible that applying the demagnetizing coil to the ring (which was originally magnetized in the opposite sense to the magnets) improves the properties of the magnetic circuit and thus increases the air gap flux.

1958

It is suggested that the flux increase found when the system has been subjected to a comparatively weak external field (40 ampere-turns/cm), is associated with the way this field affects the magnet keeper ring.

Conclusions

The work on Magnico and Alnico magnets largely solved a number of problems relating to their stabilities against various external factors and indicated rational technical means of stabilizing them satisfactorily.

The results apply to a considerable extent to other such items. But as the shape of the circuit and the material influence the stability to some degree more general deductions can only come from further work with various designs.

REFERENCES

1. A.S. Zaimovskii, P.I. Denisov, E.S. Berkovich and N. Ia. Drozdov; Improving the magnetic properties of iron-nickel-aluminium alloys. *Elektrichestvo* No.20, 22 (1937).
2. A.A. Kuznetsov, A.S. Naimovskii and V.V. Usov; *Metals and Alloys in Electrical Engineering* p.280. Gosenergoizdat (1949).
3. L.M. L'vova, A.S. Zaimovskii and V.V. Usov; *Ibid.* p.282.
4. K. Hoselitz; Modern hard magnetic materials. *J. Sci. Instrum.* **23**, 65 (1946).
5. J.H. Goss; Permanent magnet materials. *Mech.Engng., N.Y.* **70**, 671 (1948).
6. A.J. Tyrrell; The performance and stability of permanent magnets. *J. Brit.Instn.Radio Engrs.* **10**, 182 (1950).
7. S.F.Knight; A sensitive balance for stability tests on permanent magnets. *Proc.Inst.Elec.Engrs.* **96**, 635 (1949).
8. R.K. Tenzer; A contribution to the ballistic null-method for precise measurement of magnetic flux densities. *Arch.Elektrotech.* **40**, No.7, 406 (1952).
9. R.K. Tenzer; A precision measuring circuit for research on the ageing of permanent magnets. *Arch.Tech.Messen* No.239, 285 (1955).
10. K.J. Kronenberg; An investigation of ageing in permanent magnets. *Z. Angew.Phys.* **9**,321 (1953).

EFFECT OF EXCITER SATURATION ON TRANSIENTS IN SYNCHRONOUS MACHINES*

L.Z. SHENKMAN

1958

It has been repeatedly stated [1,2] that the exciter affects transients in synchronous machines. Short-circuit and voltage recovery tests with the exciter connected to the generator rotor winding give a time constant T_d' somewhat smaller than that obtained by field-switching tests with the exciter disconnected. Exciter effects must therefore be allowed for when a more accurate knowledge of transients in synchronous machines is required.

Analytical solution of the differential equations for transients in a synchronous machine plus those for exciter transients is rather complicated and is possible only if the equations are linearized by neglecting exciter saturation [2]. This linearization causes considerable errors and vitiates the results. We have analysed transients in a system of synchronous machine plus exciter (allowing also for saturation) by integrating the equations numerically using the no-load exciter characteristic.

Theoretical formulae

As is usual when setting up the equations [2] we neglect the stator transient and stator resistance, the speed changes and also the effect of damper windings. The differential equation for the transient can then be written [3 - 4]:

$$E_{det} = E_d + T_d' \frac{dE_d}{dt} \qquad (1)$$

where

E_{det} is the steady-state e.m.f. determined by the excitation current corresponding to the exciter terminal voltage;

* *Elektrichestvo* No.1, 35-38 (1957). [Reprint Order No. EL.14]

E_d is the e.m.f. determined by the excitation current;

T'_d is the transient time constant

$$T'_d = T_{d0} \frac{x'_d}{x_d}$$

The stator current equation for a three-phase stator short circuit has the same form:

$$I_{det} = I_d + T'_d \frac{dI_d}{dt} \tag{2}$$

I_d being related to E_d on a per unit basis by the following obvious relation:

$$I_d = \frac{E_d}{x_d}$$

The exciter transient differential equation can be representated with a satisfactory degree of accuracy by that for e.m.f. equilibrium in the exciter winding [5 - 6]:

$$U_e = i_e r_e + 2pw\sigma \frac{\Phi_n}{E_{en}} \cdot \frac{dE_e}{dt} \tag{3}$$

where

E_e and U_e are the e.m.f. and terminal voltage of the exciter,

i_e is the current in the exciter winding,

$2p$ is the number of exciter poles,

w is the number of turns per pole in the field winding

Φn and E_{en} are the rated effective magnetic flux and corresponding rated e.m.f.

σ is the magnetic flux leakage coefficient for the main exciter poles, equal to the ratio of total to effective flux ($\sigma > 1$)

To integrate nonlinear equations numerically we write them in finite difference form. The synchronous machine transient equation is

$$E_{d2} = \frac{2\Delta t}{2T'_d + \Delta t} E_{\text{det}} + \frac{2T'_d - \Delta t}{2T'_d + \Delta t} E_{d1} \tag{4}$$

Neglecting saturation we can write on a per unit basis:

$$E_{\bullet d} = I_{\bullet r}$$

where

$I_{\bullet r}$ is the ratio of the rotor current to the no-load value.

Then

$$I_{r2} = \frac{2\Delta t}{2T'_d + \Delta t} I_{\text{ret}} + \frac{2T'_d - \Delta t}{2T'_d + \Delta t} I_{r1} \tag{5}$$

The equation for the exciter transient is:

$$\frac{U_{e1} + U_{e2}}{2} = \frac{i_{e1} + i_{e2}}{2} r_e + k \frac{E_{e2} - E_{e1}}{\Delta t} \tag{6}$$

where

$$k = \frac{2pw\sigma\Phi_n}{E_n}$$

Exciter armature reaction is allowed for by subtracting γI_r from i_e (2)

$$\delta E_{\text{arm.react.}} = c\sigma I_r \gamma \tag{7}$$

where

γ is the armature reaction coefficient

c is the gradient of the exciter no-load characteristic, $c = f(E_e)$ (Fig.1).

1958

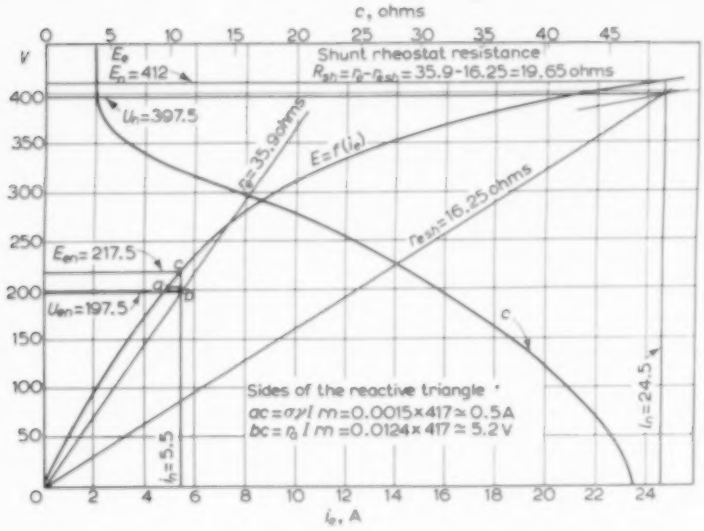

Fig. 1

The relation between exciter terminal voltage and e.m.f. can be from equation (7) expressed simply as

$$U_e = E_e - (c\sigma\gamma + r_a)\, I_r \tag{8}$$

where

r_a = resistance of the exciter armature, made up of the armature, compoles and compensating winding resistances and the equivalent brush contact resistance.

Introducing (8), (6) becomes:

$$\frac{E_{e1} + E_{e2}}{2} - (c\sigma\gamma + r_a)\frac{I_{r1} + I_{r2}}{2} =$$

$$= \frac{i_{e1} + i_{e2}}{2} r_e + k\frac{E_{e2} - E_{e1}}{\Delta t} \tag{9}$$

So the exciter e.m.f. and current can be expressed in terms of their previous values as:

$$E_{e2} + i_{e2} r_e \frac{\Delta t}{2k - \Delta t} = E_{e1} \frac{2k + \Delta t}{2k - \Delta t} -$$

$$- i_{e1} r_e \frac{\Delta t}{2k - \Delta t} - (I_{r1} + I_{r2})\, r_e \frac{\Delta t}{2k - \Delta t} \qquad (10)$$

where

$r_e = c\sigma\gamma + r_a$ is the equivalent exciter resistance.

When field-forcing is automatic we assume that the whole or part of the exciter field rheostat is cut out from the beginning of the transient.

$$(r_e = r_{e.sh} - \Delta R_{sh})$$

When compounding is used a term proportional to the stator current is introduced on the right-hand side of (9):

$$c\, k_i\, I_d$$

where k_i is the compounding coefficient [2].

Thus the problem is reduced to the simultaneous numerical solution of equations (5) and (10) with the exciter no-load characteristic $E_e = f(i_e)$, (Fig.1), whereby

$$I_{ret} = \frac{U_e}{R_r I_{e0}} \qquad (11)$$

where

R_r is the rotor resistance,

I_{e0} is the rotor current at no-load, and $U_e = E_e - (c\sigma\gamma + r_a)\, I_r$

Transient calculation

Consider a three-phase short-circuit at the stator terminals of a T-2-25-2 turboalternator with a model B 4-120-3000 exciter.

The T-2-25-2 turboalternator parameters are* [7]

P_n = 25 MW x_d'' = 12.9% Rotor currents

U_n = 10.5 kV x_d' = 23.3% I_{r0} = 164 A

I_n = 1720 A x_d = 199% I_{rn} = 417 A

$\cos\phi$ = 0.8 R_r = 0.473 Ω I_{1r} = 267 A

T_{d0} = 9.9 sec r_a = 0.19% $T_d' = 9.9 \frac{0.233}{1.99} = 1.16$ sec.

The parameters of the model B4-120-3000 exciter are: P = 120 kW, U = 230 V, I_a = 520 A.

$2p$ = 4, number of parallel field windings,

a = 1, number of turns per pole of this winding,

w = 600, number of turns per pole of the armature winding,

w_a = 23.

Exciter resistance r_e = 16.25 Ω, compoles, r_c = 0.0021 Ω, armature, r_a = 0.0053 Ω.

Flux at the rated load, $\Phi_n = 2.58 \times 10^6$ maxwell.

E.m.f. at rated load, E_n = 238 V. Resistance of the armature circuit† $r_a(75^\circ C) = 0.0124$ Ω.

Leakage coefficient σ = 1.15 [6]. Coefficient of armature reaction γ = 0.001 [2].

The no-load exciter characteristic $E_e = f(i_e)$ is shown in Fig.1. The shunt rheostat resistance determined from the no-load characteristic (Fig.1) is R_{sh} = 19.65 Ω.

---

* The resistances are given at 75°C, except those for compoles and armature, which are given at 15°C.

† We assume a brush contact drop of 1.5 V.

On introducing the numerical values (5), (8), (10) and (11) become:

$$I_{r2} = \frac{2\Delta t}{2.32 + \Delta t} I_{ret} + \frac{2.32 - \Delta t}{2.32 + \Delta t} I_{r1} \tag{5a}$$

$$U_e = E_e - (0.0015\ c + 0.0124)\ I_r \tag{8a}$$

$$\left.\begin{aligned} E_{e2} + i_{e2} \frac{35.9\Delta t}{0.598 - \Delta t} &= \\ = E_{e1} \frac{0.598 + \Delta t}{0.598 - \Delta t} - i_{e1} \frac{35.9\Delta t}{0.598 - \Delta t} &- \\ - (I_{r1} + I_{r2}) \frac{(0.0015c + 0.0124)\Delta t}{0.598 - \Delta t} & \end{aligned}\right\} \tag{10a}$$

$$I_{ret} = U_e/77.5 \tag{11a}$$

The compounding coefficient was estimated to be $k_1 = 0.00278$ [2]. The calculation can proceed when Δt is assigned a value. The tabulated form of calculation is most convenient. The results, viz. curves of stator and rotor currents as functions of time, are shown in Fig.2.

Conclusions

(1) Comparison of the stator and rotor current during generator transients found when exciter saturation is allowed for (Fig.2) with those obtained from the linearized differential equations (cf [2], Fig.5) shows that exciter saturation has a considerable effect on the transient especially in its final stages. For example, the exciter effect becomes apparent from the fact that after 10 sec the rotor current with compounding falls by $\Delta I_r = 0.24\ I_{r0}$ is the no-load rotor current.

The linearized system gives $\Delta I_r = 1.2 I_{r0}$ (cf.2, Fig.5).

The large discrepancy (a factor 5) is explained by the armature reaction being assumed to remain constant at its initial value throughout the transient (linearized no-load characteristic) in the linearized system.

1958

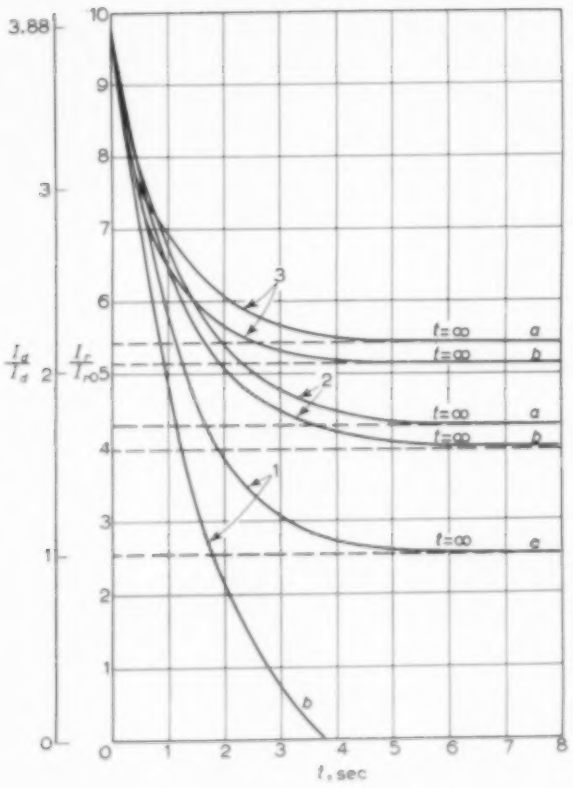

Fig. 2. (a) Neglecting the effect of the exciter

(b) Including the effect of the exciter

1 – without additional measures on the exciter,

2 – with compounding,

3 – with automatic field forcing.

The equivalent armature circuit resistance is here large $r_e = 0.2\,R_r$, [2]. This causes a large drop in exciter terminal voltage and therefore a large fall in the rotor current.

Neglect of exciter saturation thus makes its apparent effect on the transient considerably greater than the real one.

(2) The greatest distortions of the transient picture due to neglect of exciter saturation occur when automatic field-forcing or compounding is used. In this case the exciter voltage rapidly approaches its limiting value (within 0.5 – 0.7 sec), complete exciter saturation

occurs and armature reaction becomes very small. The effect of the exciter on the transient is then noticeable only during the initial stage when the exciter voltage has not yet risen to its limiting value. The exciter affects the steady-state rotor-current only via the voltage drop in r_a, which is 15 per cent of $r_{e\ max}$.

Again we notice the beneficial effect of compounding on the whole transient process.

(3) No great differences are introduced when non-linearity is allowed for in the absence of automatic field-forcing and compounding. For example, under the conditions obtaining when T'_d is determined experimentally, the exciter works on the unsaturated part of its characteristic and appears to be highly effective. As has been stated [2] considerable demagnetization or remagnetization can then occur. This can be observed if for some reason the exciter armature resistance or the armature reaction are increased.

The author is indebted to L.G. Mamikoniants Cand.Tekh.Nauk for valuable advice and suggestions during the preparation of this article.

REFERENCES

1. L.G. Mamikoniants; Improving the accuracy of synchronous machine parameters. *Elekt. Stantsii* No.11 (1949).
2. L.V. Tsukernik; Transients systems in synchronous machine + exciter systems. *Elektrichestvo* No.10 (1954).
3. S.A. Ul'yanov; *Short-Circuits in Power Systems*. Gosenergoizdat (1952).
4. P.S. Zhdanov; *Power System Stability*. Gosenergoizdat (1948).
5. V.T. Kas'yanov; Theoretical calculation of exciter voltage rise rates. *Elektrosila* No.9 (1951).
6. V.T. Kas'yanov; *Design of Salient-Pole Synchronous Generators*. (1951).
7. *Electrical Engineering Reference Book*. Gosenergoizdat (1952).

THE BEHAVIOUR OF RELAY PROTECTION ON UNSYNCHRONIZED RECLOSING*

TSZO KHU

Molotov Power Engineering Institute, Moscow

(Received 14 March 1956)

Unsynchronized automatic reclosing of individual transmission lines of power systems has lately assumed increasing importance on account of its simplicity and effectiveness. However, this must not be taken as meaning that all the problems associated with this use of automatic reclosing have been sufficiently studied and solved. In particular, one of these problems is the behaviour of relay protection and prevention of its incorrect operation during unsynchronized reconnexion [1]. We will consider this problem below with reference to systems having large earth-fault currents.

It is well-known that unsynchronized closing of a transmission line may result in a synchronous operation and power swings and, consequently, (owing to the varying power angles between e.m.f. vectors of the generators) variations of the phase currents, voltages and other electrical quantities may occur, similar to those occurring in the case of power swings caused by disturbances to the static or dynamic stability of the system.

Immediately after unsynchronized reconnexion negative and zero phase-sequence components may appear for a short time due to partial reclosures resulting from the sequential making of the circuit-breaker contacts.

We will assume equal positive and negative sequence impedances and also that the station e.m.f's NM (Fig.1a) have the same magnitude. Referring to the equivalent circuits (Fig.1d), the negative and zero-sequence currents will be: when a single phase is closed:

$$I_2^{(1)} = I_0^{(1)} = 2 \sin \frac{\delta}{2} \frac{1}{2z_{1t} + z_{0t}} \qquad (1)$$

* *Elektrichestvo* No. 1, 42-51 (1957). [Reprint Order No. EL. 15]

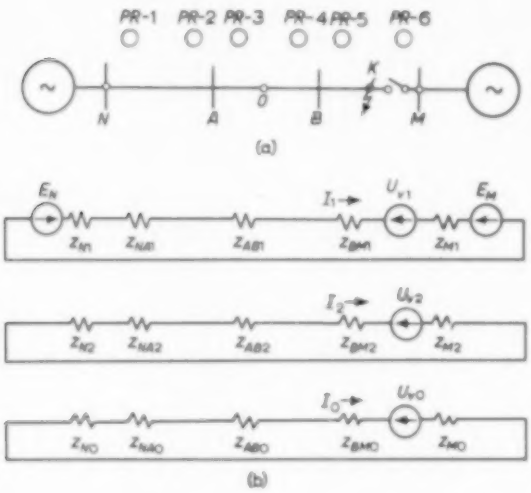

Fig. 1. Actual circuit and equivalent circuits of various phase-sequences during unsynchronized automatic reclosing.

when two phases are closed

$$I_2^{(II)} = 2 \sin \frac{\delta}{2} \frac{z_{0t}}{z_{1c}(2z_{0t} + z_{1t})} \tag{2}$$

$$I_0^{(II)} = 2 \sin \frac{\delta}{2} \frac{1}{2z_{0t} + z_{1t}} \tag{3}$$

where

z_{1t} and z_{0t} are the total impedances of the positive and zero sequences of the whole system;

δ is the difference of the e.m.f. vector angles of the generators in partially reclosed operation. If we assume that δ can reach 180° during unsynchronized reconnexion the maximum negative and zero sequence currents will, according to equations (1), (2) and (3) be determined in the following way:

When $z_{1t}/z_{0t} > 1$

1958

$$I_{2max} = \frac{2}{2z_{1t} + z_{0t}} \tag{4}$$

$$I_{0max} = \frac{2}{2z_{0t} + z_{1t}} \tag{5}$$

When $z_{1t}/z_{0t} < 1$

$$I_{2max} = \frac{2z_{0t}}{z_{1t}(2z_{0t} + z_{1t})} \tag{6}$$

$$I_{0max} = \frac{2}{2z_{1t} + z_{0t}} \tag{7}$$

The above expressions for electrical quantities as functions of δ after unsynchronized reconnexion are the same equations as in the case of power swings or loss of stability when the oscillations are initiated by a short-circuit. The only difference between unsynchronized reconnexion and power swings following short-circuit is that δ may take values up to 180^{o} (in the first case) whereas in the second case δ, being initially the angle under the operating conditions preceding the short-circuit, cannot change discontinuously and will become large only a certain time after the oscillation starts.

Incorrect operation of relay systems during oscillations is due to the fact that unsynchronized automatic reclosing may occur at large values of δ and, after reclosing, asynchronous operation and oscillations may take place.

The behaviour of distance relays on a line, the circuit of which is indicated in Fig.1(a), is considered as an example of the behaviour of such protective systems after unsynchronized reclosing. We analysed the response of the relay units RZ-4, RZ-5 of this system. The analysis was carried out in the complex impedance plan (Fig.2). The results of the analysis may be summarized as follows.

The distance protection operating with an impedance relay and a directional power relay, may operate incorrectly on unsynchronized reclosing if the electrical centre of the system is situated inside the protected zone or in its immediate neighbourhood. In cases in which the electric centre of the system during the unsynchronized

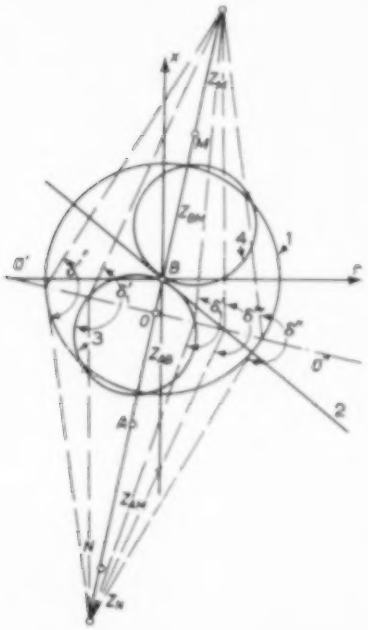

Fig. 2. Analysis of the behaviour of distance protection during unsynchronized reclosing, represented in the complex resistance-impedance plane.

(1) Characteristic of the impedance relays of the protection units PR-4 and PR-5 (Fig. 1);

(2) Characteristic of the directional power relays PR-4 and PR-5;

(3) and (4) Characteristics of the directional impedance relays of PR-4 and PR-5. The straight line $0'\,0''$ is the locus of the impedance vectors at the terminals of the relays PR-4 and PR-5.

reclosing is behind the busbars of the sub-station in which the protection is installed, the possibility of an incorrect operation may be eliminated by using, for example, for a protection relay PR-5 (Fig. 2) an impedance relay having a directional distance element.

It follows that we arrive at the same conclusions as resulted from the analysis of the behaviour of distance protection under power swings [2].

Protection systems responding to negative and zero-sequence components and acting without time-lag may also operate incorrectly on unsynchronized reconnexion.

An instantaneous zero-sequence relay may operate if its setting current is smaller than the maximum zero-sequence current at unsynchronized reconnexion (cf. expressions (5) and (7)). The behaviour of a directional instantaneous zero-sequence relay during unsynchronized reconnexion depends on the behaviour of its directional power element. If, on unsynchronized reconnexion the zero-sequence current at the location of the relay set for the direction towards the busbars leads the voltage of the same phase-sequence, the directional power element will not respond and, consequently, neither will the directional zero-sequence relay. This, for example, corresponds to the behaviour during unsynchronized reconnexion of the protective equipment PR-4 in the section BM (Fig.1a). The zero-sequence relay can be rendered insensitive to the effects of partially reclosed operation by the use of an auxiliary relay with delayed action, having a time-lag slightly greater than the time required for closing the contacts of all three phases of the circuit breaker.

During unsynchronized reconnexion it is also possible for incorrect operation to occur in directional protection with carrier-current, lock-out, for example, a protection of type RZ-164. At the inception of the asymmetric conditions the protection is started, and when the asymmetry disappears, the directional elements of the protection are switched over to phase current and line voltage; the protection can then operate just as in the case of symmetric short-circuits on the protected element. The protection located in the section reclosed out of synchronism may operate also before the disappearance of the asymmetry if the voltage transformers are connected to the busbars, and the unsynchronized automatic reclosing is carried out by a circuit-breaker requiring a comparatively long time for closing the contacts of all three phases (e.g. a circuit-breaker with individual drives for each phase).

Differential current protective systems of all types, including phase comparison systems, should in principle never operate incorrectly on unsynchronized reconnexion.

Most of the devices, nowadays widely used, for lock-in protection systems in the case of power swings are based on two principles, viz. (1) on the use of the different character of variation of the electrical quantities in the case of short-circuits and power swings respectively and (2) on the principle of starting the protection at

the appearance of negative or zero-sequence components for a time sufficient for its operation. The devices based on the first principle prepare the relay circuit for tripping in the case of a sudden discontinuous variation of the phase or line currents and/or voltages. The devices based on the second principle prepare the relay circuit for tripping when asymmetrical conditions arise. Both types of device terminate the operation of the protection before the angular phase difference, δ, between the generators rises to a dangerous value (i.e. from the viewpoint of a possible incorrect operation of the protection).

Since in the case of unsynchronized reconnexion a sudden discontinuous variation of the currents and voltages of all phases, as well as negative and zero-sequence components may occur, the lock-in devices mentioned above may be activated just as in the case of short-circuits. Consequently, the protection may operate in the case of unsynchronized reconnexion until its operation is terminated by the lock-in devices. However, we should not conclude from this fact that it is impossible to use lock-in devices for preventing incorrect operation of the protection during unsynchronized automatic reclosing.

1958

Let us consider the possibility of using for this purpose lock-in devices based on the principle of having the protection started by negative-sequence components of the voltage and current (U_2, I_2).

Lock-in devices used for preventing a response of the protection to power swings may also be used for preventing such an incorrect operation in the case of unsynchronized automatic reclosing. For this purpose the voltage or current setting of the starting element of such a device must be greater than the negative-sequence voltage or current associated with unsynchronized reconnexion at the location of the device.

This method of selection is conditional on

$$U_{2\ \mathrm{sh.c.min}}/U_{\mathrm{set}} > k_{\mathrm{sen}} \tag{8}$$

where

$U_{2\ \mathrm{sh.c.min}}$ is the minimum negative-sequence voltage at the location of the protection in the case of a short-circuit in the protected zone; k_{sen} the required coefficient of sensitivity.

It should be noted that this condition is more easily satisfied in cases where the relays are located at points remote from the enclosed section.

Lock-in devices with time-controlled lock-out may be used to prevent incorrect operation of the protection of any section of the system, except the one reconnected, if unsynchronized automatic reclosing is carried out after the clearance of a short-circuit, i.e. after the operation of the relay protection.

It is well-known that in a system equipped with automatic reclosing gear the resetting time of the lock-in devices with time-controlled lock-out is selected after consideration of the time required for clearing a persisting short-circuit after unsuccessful reclosing. Consequently, the lock-out device started at the inception of a short-circuit and terminating the operation of the protection after a short time, may lock it in the case of unsynchronized reconnexion. If this principle is used it is advisable to use more sensitive starting elements.

For reliable locking, for example, of the protection RZ-3 at unsynchronized reconnexion of the line section BM (Fig.1), the following condition must be satisfied

$$U_{2A\ \text{sh.c.min}} > k_{\text{rel}}\, U_{\text{set}} \tag{9}$$

where $U_{2A\ \text{sh.c.min}}$ is the minimum negative-sequence voltage at the location of PR-3, set-up by a short-circuit in section BM; k_{rel} is the coefficient of reliability ($k_{\text{rel}} > 1$).

A lock-out device with time-controlled lock-out may be used to prevent incorrect operation of a protection in the case that the protection is located not far from the reconnected section.

The use of a combination of negative and zero-sequence components for starting the lock-out devices may in some cases slightly improve the reliability of locking the protection in the case of unsynchronized reconnexion.

To prevent incorrect operation of the protection on unsynchronized reconnexion it is desirable to desensitize the starting elements of the lock-out device where possible. It will then be possible to use lock-out devices with time-controlled, as well as with high-speed, lock-out and also to use a circuit for automatic asynchronous reclosing started by a "discrepancy circuit".

Let us consider the lock-out characteristics of the protection for line sections which may be reconnected unsynchronized.

It is well known that in cases in which the lines are equipped with automatic reclosing gear the lock-in circuits must be designed so that the protection is rapidly reset after a clearance of a short-circuit in the protected zone. The protection reset after the clearance of a short-circuit may respond to asynchronous reclosing in the same way as in the case of unsuccessful reclosing. For this reason lock-in devices with time-controlled lock-out of the conventional type cannot in this case prevent incorrect operation of the protection. Desensitization of the starting elements of the lock-out devices may in this case find only very limited application. The minimum negative sequence voltage or current at the location of the protection will frequently be smaller during short-circuits in the protected section than during unsynchronized reconnexion of this section. This can be partly explained by the fact that on unsynchronized reconnexion the whole negative-sequence current passes through the reclosed section, whereas in the case of a short-circuit the current is divided into two parts. If it is impossible to render the protection insensitive to the effect of unsynchronized reclosing by desensitization of the starting elements of the lock-out device, the reclosing must be carried out in the following way.

1958

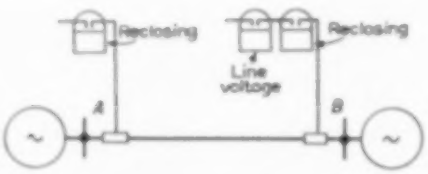

Fig.3 Sequence of the unsynchronized reclosing of the line section *AB*. The contact of the line voltage relay is closed when the line is live.

The line is first reclosed from end *A* (Fig.3) in the absence of an opposing voltage. Reclosing from end *B* is carried out only when the closing from the end *A* is successful, i.e. if there is no sustained fault on the line. After successful reclosing from end *A*, the protection is made inoperative and reclosing from the end *B* is carried out after the protection has been made inoperative. To render the use of this method possible it is necessary in addition to making ineffective the protection at the end *A*, to use at the end *B* the lock-out device operating in the case of power swings with time-controlled deblocking and prevention of rapid resetting of the protection after the clearance of the short-circuit.

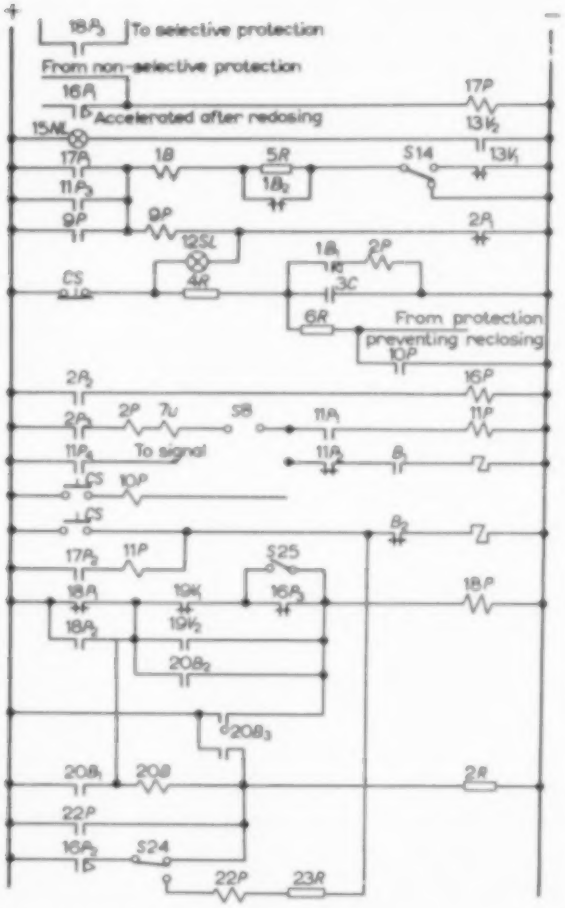

Fig. 4 A possible modification of the circuit for unsynchronized automatic reclosing.

1B, 2P, 3C, 4R, 5R, 6R, elements of relay EVP. 285;

7U signalling relay;

12SL incandescent lamp;

15NL neon lamp;

S8, S14, S24, S25 change-over switches;

18P, 19N, 20V, 21R, Lock-out devices with time-controlled deblocking;

13V voltage relay type EN. 529;

CS control switches;

9P, 17P, 22P intermediate relay type EP. 101;

11P intermediate relay type EP. 131;

10P intermediate relay with series winding;

16N intermediate relay, Type EP. 106;

23R series resistance.

The contacts as shown in the positions occupied by them when the line is closed and the circuit ready for operation.

A possible modification of the automatic reclosing gear, satisfying the conditions discussed is shown in Fig.4. This circuit is based on the commercial circuit APV-2, but is started by the relay protection. It contains change-over arrangements enabling the line to be tested from either end.* The change-over arrangements in the circuit of Fig.4 are shown in the position for testing the line. Relay 13H is designed for carrying out the detection of an opposing voltage, rendering the protection ineffective at end *A* after successful test of the line is carried out in the following way.

Simultaneously with the despatch of a closing signal to the circuit breaker, relay 16P starts operating. Its normally open contact $16P_2$ is closed and shunts the time relay 20V, whereas its normally closed contact $16P_3$ opens and interrupts the circuit of relay 18P. The relay 20B returns then into its initial position and cannot operate until the contact $16P_2$ of relay 16P drops off, and relay 18P biases the protection circuits and the windings of relay 20 EV. When the circuit-breaker contacts have closed, the armature of relay 16P drops off with a certain time lag. Owing to this, relay 20V will operate once more and the protection will become ineffective after its contact $20V_3$ has closed. In this way the lock-out device blocking the protection in the case of power-swings may be used for the same purpose during unsynchronized automatic reclosing.

The circuit contains further an intermediate relay 22P, for rapid deblocking of the protection when the circuit is used for reclosing from end *B*. This ensures rapid isolation of the line in the case of asymmetric short-circuits, when owing to an irregularity in the automatic reclosing circuit reclosing from end *B* takes place earlier than that from end *A*.

Conclusions

(1) Protection systems having to operate under the asymmetrical conditions produced for a short while during unsynchronized reclosing, can be neutralized against these effects by the use of an auxiliary relay with slightly delayed action.

(2) The lock-out devices neutralizing the protection against the effects of power swings may also be used to prevent incorrect operation of the protection on unsynchronized automatic reclosing.

---

* Testing is to be taken as meaning automatic reclosing of the line from one end in the absence of an opposing voltage.

In some cases this is obtained by desensitizing the starting elements of the lock-out devices and in others by using more sensitive starting elements and providing them with time-control deblocking devices.

(3) Incorrect operation of the protection of an unsynchronized reclosed section may be prevented in all cases.

REFERENCES

1. L.G. Mamikonyats; Use of asynchronous operation of generators for improved reliability of the power supply. *Elektrichestvo* No. 8 (1955).
2. A.M. Fedoseev; *Relay Protection of Power Systems*. Gosenergoizdat (1952).

GENERATORS FOR ELECTRIC SPARK-MACHINING OF METALS*

A.L. LIVSHITS AND I.S. ROGACHEV

1958

In electric methods of machining metals the metal is cut or its structure and durface finish altered thermally or chemically by an electric current supplied direct to the tool or work. Electro-erosion is a special type of electrical machining based on joule heating.

Three fundamental conditions must be satisfied if electrical erosion is to give true-scale machining and if the blank is to reproduce the tool electrode shape faithfully.

(1) The current pulses supplied must be sufficiently short, the "feed rate" being determined by the distance between the elementary portions of the electrodes. The maximum pulse durations $t_1 < 10^{-4}$ sec [1] and $t_1 < 10^{-3}$ sec [2] recommended in the literature cannot be confirmed. The precision of the tool-shape reproduction and the cutting rate are increased, and the tool wear and power consumption reduced, if the pulse duration is between 10^{-3} and 10^{-2} sec. Only under "soft" operating conditions, in machining hard alloys and for delicate work should the pulse duration be reduced to 0.15×10^{-3} sec [3,4], or less.

(2) The area between electrode and work to which the pulse is supplied must be fairly small to obtain the required energy concentration together with acceptable finished maximum surface-roughnesses.

The area varies with the working cond tions from 10^{-4} mm^2 to several mm^2 and the maximum surface roughness from 10^{-3} to 0.5 mm.

(3) The pulses must be supplied continuously at the requisite frequency and space-mark ratio.

* *Elektrichestvo* No. 3, pp. 19–23, (1957). [Reprint Order No. EL. 17]

The pulse repetition frequency in electro-erosion lies within the audio range. The pause space mark ratio varies from 1.1 to $10–10^2$.

The above conditions are satisfied by supplying the electrodes through a discharge channel (making arc or spark) or through a contact between micro-roughnesses of the electrodes moving relatively to one another (breaking arc or spark) [3]. In the first case a special voltage pulse source is required, viz. an impulse generator; in the second case, a mechanical device which produces a relative electrode displacement (rotation, vibration, etc. is required, the electrodes being connected into a d.c. or a.c. circuit. Combined electrical and mechanical generation systems are also possible.

The load on the impulse generator is the erosion gap, i.e. a short arc or sparking and arcing discharge between the electrodes. The distances between the electrode sections, the volume and surface concentrations of the erosion products in the working zone, the conditions of particle and gas removal, etc., may all vary during the operation. Different types of generators will react differently to such variations. If the amplitude, duration and frequency of the impulses supplied by the generator do not depend on the physical conditions in the erosion gap, they are termed *independent*. If this is not so, they are referred to as *dependent*. Certain generators have some parameters (e.g. polarity, mark–space ratio) which depend on the conditions in the erosion gap, whereas others (e.g. the frequency) do not.

The method of generation, the type of generator, type of current, working fluid, polarity, tool material, etc., imply certain differences between electro-erosion methods. For example, the spark-cutting method uses electrical generation, a *dependent* (relaxation) generator, asymmetric pulses of alternating polarity, an insulating fluid, direct polarity (tool–cathode, work–anode). The new electric– impulse method [3] also uses electrical generation, an insulating liquid, but an *independent* generator, *unipolar* current pulses, and reversed polarity (in working steel). The mechanical–anodic method uses mechanical generation via a dependent generator, unipolar current pulses, an electrolyte (waterglass) and direct polarity. The electric-contact method differs from the mechanical–anodic method in the preferred use of pulses of alternating polarity and in the working medium (air, water, less frequently oil). Because the two latter methods involve relative motion the chances of reproducing the shape of the tool electrode are restricted.

Electrical erosion is polar in nature, i.e. with given electrode materials, working medium and pulse parameters, there is a definite pulse polarity which gives the maximum rate of removal of metal from the work and the minimum from the tool. Also if an unsuitable polarity is used solid pyrolytic residues from the liquid medium deposit on the electrodes, which disrupts the steady erosion process and spoils the surface of the work. So electro-erosion should employ unipolar impulses.

Machining by unipolar impulses of considerable duration increases the rate of removal of material by a factor 10, reduces the relative wear by factors of 5 – 20, and the energy consumption by factors of 3 – 5 relative to alternating-polarity impulses produced by a dependent relaxation generator [3].

Hence a new branch of electrical engineering had to be developed, viz. the production of *strong unipolar impulse currents at low voltages at audio-frequencies*. It is very difficult to generate such currents because there are no suitable generators. This led to a number of compromise solutions, taking the form of dependent relaxation generators of asymmetrical alternating current and voltage impulses (of types RC, RCL, RCLL, etc.) used to supply spark-machining units [3], and of rotary generators for asymmetrically alternating impulse voltages [5].

1958

In principle, sources of unipolar voltage pulses can be based on:

(a) current interruption; (b) rectification of sinusoidal or pulse-type alternating voltages; (c) superposition of direct and alternating e.m.f.'s of different wave-forms; (d) direct generation; (e) various combinations of the foregoing principles.

Two types of unipolar pulse generator using current interruption exist: (a) with turbo-type mercury-jet interrupters, first realized in the Odessa Polytechnical Institute in 1951, similar to the well-known systems used in radio engineering [6] and (b) with electrolytic interrupters [7], designed specially for electro-impulse machining. Both types of interrupters can produce currents of some 10 A at frequencies up to 100 pulses/sec. Their use is limited to "soft" operating conditions.

Independent pulse generators, based on half-wave rectification of sinusoidal voltages at power or higher frequencies using semi-conductor (selenium) rectifiers were produced between 1950 and 1955 for frequencies of 50 – 500 pulses/sec. and currents up to 100 A at mean voltages of up to 50 V. The advantages of such systems are their

simplicity and reliability and the possibility of supplying several independent circuits simultaneously by using both half-waves. Drawbacks of selenium rectifier generators are the inverse current half-wave due to the inverse conductivity of the barrier layer and its considerable capacitance, furthermore the need for special voltage supply at frequencies above 50 pulses/sec. (frequency converter, or for mark-space ratios exceeding 2, a generator of alternating pulses).

When selenium is replaced by new semi-conductor rectifiers (germanium, silicon, etc.) considerable current densities can be used, the capacitances being also small and the back-resistances high; this extends the useful frequency and current ranges considerably, and has added advantages of high efficiency and small dimensions. Electronic systems could give any frequency but are out of the question because of the small attainable currents. Ionic rectifier systems (thyratrons without grid-control) could furnish frequencies up to 3 - 5 kc/s [4], but only at low efficiencies, and would also be unduly bulky, even if only required to supply currents of around 0.1 A. The use of mercury power rectifiers is limited by their frequency range (500 - 700 pulses/sec) and low efficiency at the low voltages required.

The simplest way of obtaining unipolar pulses by superposing direct and alternating e.m.f.'s of different forms is to use a sinusoidal alternating e.m.f. In this case the direct component must equal the peak alternating voltage; however, the relative pulse duration obtained by interrupting an arc discharge at 20 - 30 V will be very large, this being undesirable for work in an erosion gap. To obtain a pulse of shorter relative duration we require an asymmetrical pulse voltage source, obtained from special rotary generators or electronic or ionic apparatus. A drawback of superposed voltages is the need to use two supplies of specially chosen and matched characteristics. The limiting frequencies and currents are determined by the characteristics of the voltage sources.

Unipolar pulses can be generated directly by using ionic or electronic apparatus and rotary generators.

Ionic generators are preferable owing to their relatively simple construction when powerful unipolar pulses of low frequency (up to 150 pulses/sec) of controllable amplitude, relative duration and frequency are required. The power from ionic generators is practically unlimited, so the rate of removal of the metal is also unlimited. For example, with the ionic generators developed in 1950-1951 in the Ministry of the Machine Tool Industry [3], a rate of removal of material was $\sim$ 6000 mm^3/min, this being 8-10 times higher than the limiting rate of removal in spark-machining. Disadvantages of independent ionic generators are their much

more complicated circuits for obtaining high frequencies, their low p.f.s and efficiencies, high transformer ratings and non-sinusoidal mains load currents.

Pulse generators using valves can provide low currents and high frequencies. This is because there are no hard valves designed for currents around 10–100 A (RMS) at voltages around 10 V. The development of controllable germanium or silicon power rectifiers will greatly improve this type of generator. Combined electronic and ionic unipolar pulse generators may also be considered [4].

The rotary pulse generators form a new branch of electrical engineering opened up only since 1951. We can distinguish machines for generating unipolar pulses directly and machines generating alternating pulse voltages, subsequently rectified either within or outside the machine.

Commutatorless d.c. machines must involve the circuit being altered in time by continuously introducing new circuit elements via sliding contacts. This is the principle on which a unipolar commutatorless d.c. machine is based. One of the authors [8] has suggested that this principle could also be used for producing unipolar pulses.

Let us imagine that the air gap in a unipolar d.c. machine varies periodically in width around the armature periphery, due to the arrangement of stator teeth (Fig.1). The flux density in the air gap will then

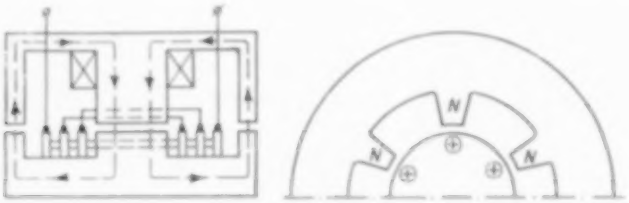

Fig. 1. General system of the unipolar generator.

also vary periodically. When the armature rotates at constant speed, e.m.f.'s will be induced in the bars of that armature winding, the instantaneous values of which will be proportional to the flux densities under the bars. If the ends of the bars are connected to slip rings running under brushes, the e.m.f. between the brushes will always have the same direction. By appropriate choice of air gap and stator slot dimensions, the minimum e.m.f. can be kept sufficiently small and the pulses will be practically unipolar and of a quite satisfactory form.

The frequency of the unipolar impulses is

$$f = zn/60 \tag{1}$$

where z is the number of stator teeth; n the rotor speed in rev/min.

The maximum e.m.f. is

$$E_{max} = kB_{max}lv \tag{2}$$

where k is the number of series-connected bars in the winding (no. of pairs of slip rings);

B_{max} = maximum flux density in the air gap,

l = active length of a bar, m;

v = peripheral speed of the armature, m/sec.

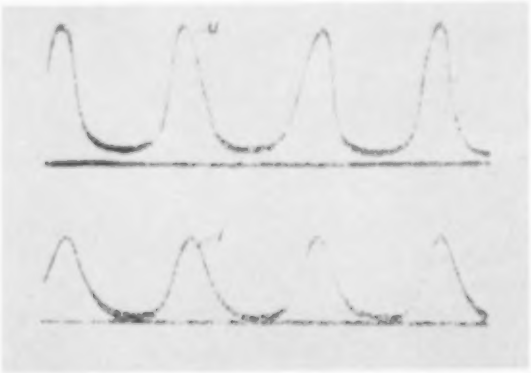

Fig.2. General view of a unipolar pulse generator.

The Department of Electrical Machinery at Kharkov Polytechnical Institute carried out the design and testing of an experimental unipolar generator for a mean current of 150 A, mean voltage of 15 – 20 V and a frequency of 800 pulses/sec on behalf of the Ministry of the Machine Tool Industry in 1953–55; it was produced by the Kharkov Electrical Machine Works [9]. Fig.2 is a view of this generator, Fig.3 showing oscillograms of the voltage and current.

The second group of rotary pulse generators are those which generate alternating pulse voltages, subsequently rectified.

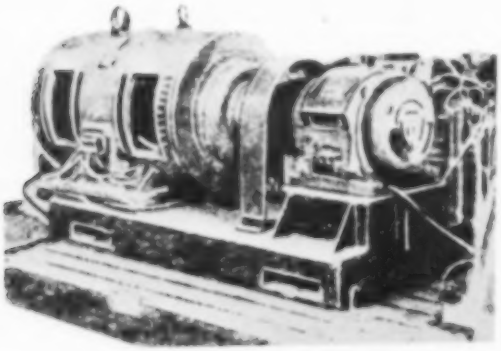

Fig.3. Voltage (u) and current (i) oscillograms for the unipolar pulse generator.

One style of self-rectifying pulse generator was suggested by the authors jointly with Perchik and Borisenko [10,11], and designed by the Department of Electrical Machinery at the Kharkov Polytechnical Institute. This consists of a pole-changing magnetic system and poles formed on the stator or rotor, and an armature winding, situated, correspondingly, on the rotor or stator. The ends of the armature winding are led out to the commutator consisting of two systems of bars arranged alternately and insulated from one another. The number of bars equals the number of poles. The bars of each system are electrically interconnected, and each system is connected to one end of the winding. Two systems of brushes run on the commutator, so arranged that the brushes of either polarity are simultaneously only on one system of bars and have a relative displacement corresponding to the width of a bar. The pole arc/pitch ratio is chosen much smaller than normal (lower than 0.5), and the armature winding is arranged under the poles in narrow segments. This design produces an e.m.f. of very marked pulse character. Fig.4 shows diagrammatically

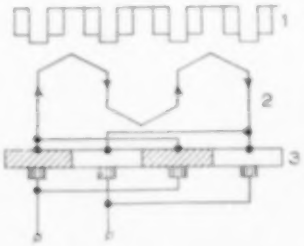

Fig.4. Theoretical circuit of commutator-type pulse generator.
1)- Stationary poles with field winding;
2 - Rotating armature winding;
3 - Commutator.

a generator with a four-pole stationary magnetic system 1 and rotating armature coil 2, placed in four slots. The ends of the winding are led out to the commutator 3, consisting of four bars on which the brushes run. It is easy to design this generator for the desired voltage which, with given dimensions and speed, is determined by the number of armature conductors connected in series.

The frequency is

$$f = pn/30 \tag{3}$$

where p is the number of pole pairs, n being the rev/min.

Since the armature winding occupies only a small part of the periphery, two or more independent windings can be used, each having its own commutator which can be connected to separate loads.

Experimental generators of this type were produced in the Kharkov Polytechnical Institute and in the Experimental Machine Tool Research Institute and were found to work very satisfactorily with an erosion-machining load. The Kharkov Polytechnical Institute designed and investigated a number of generators of a type suggested by the Experimental Machine Tool Research Institute and built by the Kharkov Electrical Machine factory, for frequencies up to 1000 pulses/sec, mean currents up to 300 A, mean voltages up to 40 V, and also designed a batch of experimental generators producing 400 pulses/sec, mean currents of 80 A and mean voltages of 30 V [12] from tests carried out

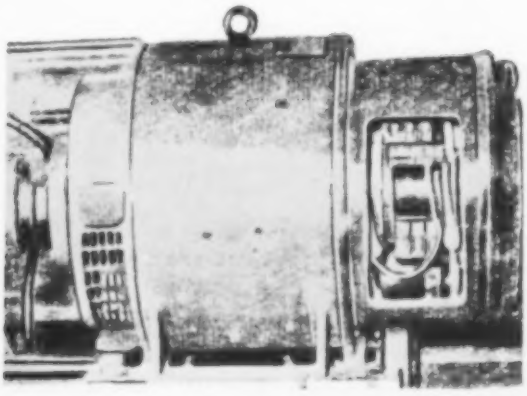

Fig. 5. General view of commutator-type pulse generator.

at the Experimental Machine Tool Research Institute. Fig.5 is a general view of such a machine, Fig.6 showing current and voltage oscillograms of one of the generators.

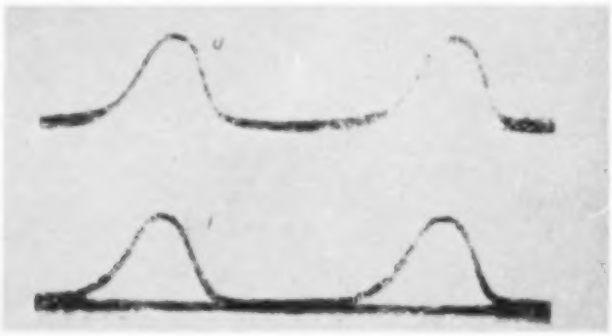

Fig.6. Voltage (u) and current (i) oscillograms for the commutator-type pulse generator.

1958

The commutator-generator is most suitable for currents from 10 – 20 to 500 – 600 A and for frequencies from 150 to 1000 pulses/sec.

The generator may alternatively be connected to a rectifier inside or outside the machine.

This type of commutator-generator with full-wave rectifier may also be provided with a half-wave rectifier. For this purpose the ends of the windings are also brought out to slip-rings. The load is connected between the ring and the commutator. This halves the pulse frequency and the relative duration is considerably reduced. Two independent loads can then also be supplied simultaneously. This kind of operation was investigated with one of the generators and proved to be quite reliable, apart from the increased stability of the operation in the gap, due to the smaller relative pulse duration.

Comparison of these rotary generators with other types of independent generator indicates that in the ranges 10 – 600 A and range 150 – 1000 pulses/sec they exhibit considerable advantages, viz. the conversion from mains a.c. to unipolar current impulses is shortened from three stages to two, the efficiency is increased by a factor 1.5 – 2, the p.f. being also increased; the number of units is reduced by a factor 1.5 – 2, the working conditions are considerably simplified and the reliability improved.

Rotary unipolar impulse generators are at present the best source of supply for electric pulse-machining installations. The Ministry

of the Electrical Industry has now released the first series of generators for electric-impulse broaching and copying machines.

REFERENCES

1. B.R. Lazarenko and N.I. Lazarenko; *Electric Spark-Machining of Metals*. Gosenergoizdat (1950).
2. B.R. Lazarenko and N.I. Lazarenko; Electric spark-machining of metals. *Elektrichestvo* No.8 (1955).
3. A.L. Livshits and V. Ya. Rassokhin; Present state and development prospects in electric methods of metal shaping and working. *Stanki i Instrument* No.11 (1954); No.1 (1955).
4. A.L. Livshits, N.I. Blitshtein *et al;* Improvement of the productivity of electric-erosion-machining of metals in soft operating conditions. *Technical Report ENIMS-KB*. MSiIP (1955).
5. Yu. V. Mordvinov; Inductor-type impulse generator. Author's affidavit No.95245 (1952); No.97622 and No. 97623 (1953).
6. *Technical Encyclopedia* Vol.26, pp.484-492. OGIZ RSFSR (1934).
7. L.A. Goncharski; Rotating electrolytic contact-breaker, *Elektrichestvo* No.4 (1954).
8. A.L. Livshits; Commutatorless unipolar pulse generator. Author's affidavit No. 880 MSiIP (1951).
9. I.S. Rogachev, L.D. Perchik *et al; Unipolar pulse generator.* Technical Report of the Kharkov Polytechnical Institute "V.I. Lenin" (1955).
10. I.S. Rogachev and A.L. Livshits and L.D. Perchik; A rotary generator for unipolar current pulses. Author's affidavit No. 101332, (1952).
11. I.S. Rogachev, A.L. Livshits, L.D. Perchik and N.I. Borisenko; Synchronous generator with mechanical rectifier. Author's affidavit No. 98751, (1953).
12. I.S. Rogachev, L.D. Perchik *et al;* Development and investigation of rotary pulse generators. Technical Reports of the Kharkov Polytechnical Institute "V.I. Lenin" (1953-1955).

1958

STEADY – STATE STABILITY OF A TRANSMISSION SYSTEM WITH CONTROLLED SYNCHRONOUS CONDENSERS AT THE SECTIONALIZING SUBSTATION*

N.I. SOKOLOV

(Received 11 June 1956)

One of the first (chronologically) methods suggested for improving the transmitting capacity of long transmission lines was their sub-division into sections and the erection of synchronous condensers in the intermediate sub-stations. The original publication of this method, subsequently known as Baun's circuit took place in 1921 [1]. The basic assumption was that the stability of each section of the line could be considered as independent of that of the other sections.

Further experimental and theoretical work on the subject revealed that the increase of the transmitting capacity has to be bought by particularly high rating of the synchronous condensers [2]. It was mainly due to the fact that on transmission lines with synchronous condensers were not actually erected.

In 1937 S.A. Lebedev [3] showed that in the presence of an automatic regulation of the excitation it is basically possible to reduce the rating of the intermediate synchronous condensers to economically justifiable values. Analogous calculations were also carried out for the case of synchronous condensers fitted with compounding-gear [7].

The necessary kVA for intermediate synchronous condensers are determined by the requirement of keeping the voltage at the ends of each section constant when the limiting power is transmitted over the line. The latter will be greater, the greater the active power transmitted through the line in comparison with the natural power of the line. When the natural power is transmitted, the synchronous condensers work on no-load.

However, the usual excitation regulators (electronic regulator of the All-Union Electrotechnical Institute, compounding-gear with corrector, etc), cannot assure constancy of the voltage at a given point when angle swings occur, since in this case large amplification factors and high-speed action are required. The best to be obtained from ordinary excitation regulators is the constancy of the e.m.f.

* *Elektrichestvo*, No. 5, 25 – 30, 1957 [Reprint Order No. EL 18].

behind the transient reactance of the generator. The limiting transmitting capacity is in this case considerably smaller.

S.A. Lebedev's investigations demonstrated the possibility of a transmission through a sectionalized line of large powers with intermediate synchronous condensers of relatively small rating if sensitive automatic high-speed excitation regulators are used, and if their regulation is controlled by derivatives of the controlled quantity. The introduction of the first derivative of the voltage enabled the limit of the constancy of the e.m.f. behind the transient reactance to be surpassed and constancy of the voltage at the generator terminals approached.

The investigations of the stability of the synchronous condensers referred to dealt only with an idealized regulation without considering the transient processes in the generators and the time lags in the excitors and regulators. Yet they were still the first to reveal the real possibility of a very considerable increase of the transmitting capacity of transmission systems.

Up to the present time there were not regulators perfect enough to permit a regulation according to the deviation of the controlled quantity and its derivatives. The regulators used by S.A. Lebedev in 1937 in his laboratory experiments were imperfect and that was why his experiments did not yield realistic results.

In recent years comprehensive investigations into the stability of synchronous generators working on long transmission lines were carried out and regulators designed of equality assuring during the transient process not only constancy, but even an increase of the flux-linkages of the rotor without provoking hunting phenomena. These regulators may maintain the voltage at given system points constant, thereby considerably improving the steady-state stability of the transmission systems. They are now known as strong-action regulators and usually respond not only to a deviation, but also on the first and second derivatives of the deviation. The strong-action regulators were investigated theoretically and on electric models [4] and [5], and were tested under operating conditions.

Investigations and tests of strong-action regulators on the generators showed that they are likewise useful for synchronous condensers erected in the sectionalizing sub-stations. However this calls for an additional theoretical clarification of the effect of the transient processes in the generator on the regulation of the synchronous condenser, the combined regulation of generators and synchronous condensers, and furthermore, an investigation of the stability of the regulation with unchanged coefficients of the regulation and changes of the loading of the line within a wide range; also, the possibility of increasing the transmitted power with a minimum rating of the synchronous condensers and of their concentration in one sectionalizing substation should be examined.

All these problems were theoretically investigated in the Central Electrotechnical Research Laboratory of the Ministry of Power Stations.

The investigations of the effect of intermediate synchronous condensers on system stability were based on the method of small oscillations; simplified equations of the synchronous machines (without transformer e.m.f's) were used and the resistances in the stator circuits were neglected. Since the relation between the electro-magnetic torques of the machines and the angles between the e.m.f.'s is non-linear, the equations were linearized in the range of small deviations.

Let subscript 1 denote quantities referring to the sending-end station, subscript 2 those referring to the receiving system, 3 those referring to the sectionalizing substation. Let us, furthermore, consider the power of the receiving system as infinite. The equations of motion may then be written for every station (not considering mechanical friction and the effect of damping) as follows:

$$\Delta P_1 + T_{j_1} p^2 \delta_{12} = 0; \quad \Delta P_3 + T_{j_3} p^2 \Delta \delta_{32} = 0;$$
$$p^2 \delta_1 = p^2 \delta_{12}; \quad p^2 \delta_3 = p^2 \delta_{32} \tag{1}$$

The deviations of the powers are a function of the relative angles and e.m.f.'s of the generators (cf. appendix) and may be expressed linearly by the partial derivatives with respect to the corresponding variables. Using also the expressions of the deviations of the torques by the deviations of the synchronous and transient e.m.f.'s and introducing the well-known relationship between them, viz

$$\Delta E_{dc_1} = \Delta E_{d_1} + T_{d_1} p E'_{d_1}$$
$$\Delta E_{dc_3} = \Delta E_{d_3} + T_{d_3} p E'_{d_3} \tag{2}$$

We get the characteristic equation of the system of the three stations, not considering the regulation, viz

$$Q_1 Q_4 - Q_2 Q_3 = 0 \tag{3}$$

where Q_1, Q_2, Q_3, Q_4 are third order polynomials depending on the parameters of the transmission system as well as on the power transmitted or the angle

To consider the regulation of the excitation of the generators of the sending-end station and the synchronous condensors we introduce into the equations the transmission functions of the regulators: the characteristic equation of the system then takes the following form:

$$\left[Q_1 + \frac{M(p)_1}{Z(p)_1}\right]\left[Q_4 + \frac{M(p)_3}{Z(p)_3}\right] - Q_2 Q_3 = 0 \tag{4}$$

It is clear that in such a relatively complicated system (of three stations) the coefficients of the characteristic equation will have a very involved structure and their investigation in a general form will therefore be laborious. The problem can, however, be greatly simplified by substituting numerical values into the initial expressions. The result is still of a sufficiently general character to enable the analysis of a number of cases important for the practice to be carried out.

In considering actual transmission systems it is convenient to plot the ranges of stability vs. two variable coefficients of regulation, for example, the coefficients

for the first and second derivatives. The other coefficients remain fixed. The method of graphing these ranges from the characteristic equation is not described here because it is sufficiently well-known [8].

For the generator as well as for the synchronous condenser the analysis was carried out for regulation according to the angle between the e.m.f. of the generator and the voltage of the receiving system; the coefficients of the regulation according to deviation were chosen on the condition of the constancy of the voltage at the h.v. busbars of the sending-end station and sectionalizing substation. The regulation based on the angle was adopted only for convenience of the analysis. We may state that with a correct choice of the coefficients, regulation based on current, voltage or on both combined, leads to the same limit of the power transmitted as a regulation based on the angle. The theoretical analysis showed that by a close regulation on generators and synchronous condensers the limit of the power transmitted may be considerably increased, i.e. up to the ;ower limit of the weakest section. For example, the limit of the power transmitted through the line Kuibyshev Hydro-Electric Power Station – Moscow, may be increased to 1800 MW when the condensers are placed in the central sub-station, without the use of longitudinal compensation. The angle between the vectors of the e.m.f. of the sending-end station and the voltage of the receiving system goes in this case up to 150°. We note that the theoretical limit of the transmitted power without intermediate synchronous condensers and without longitudinal compensation, but with close regulation on the generators of the Kuibyshev H.E.S., is 1150 – 1200 MW.

1958

The limit of the transmitted power could be further increased and the angle brought up to 180° if the location of the central substation could be chosen from the condition of equality of the angles between the voltage vectors of the busbars of the sending-end station and the intermediate sub-station, and also at the intermediate sub-station and the receiving end. In our consideration of the case we adopted the location of the sub-station foreseen in the project of the transmission system.

The ranges of stability for various angles between the vectors of the e.m.f. of the sending-end station and the voltage of the receiving system are in a concentrical position (Fig.1). This fact indicates that there is no necessity for altering the coefficients of the regulation when the transmitted power varies. The investigation also showed that regulation according to derivatives need only be used on the synchronous condensers, whereas on the generators it is sufficient to regulate according to the deviation without any stabilizing gear. Comparison of Fig.1 and 2 shows that use of regulation according to derivatives also on the generators leads only to a displacement of the stability range which may be useful in certain operational circumstances.

We see from the Table, the data of which were obtained without considering the shunting reactors, that the kVAr of the synchronous condensers required for keeping the voltage at the 400 kV busbars of the intermediate sub-station constant,

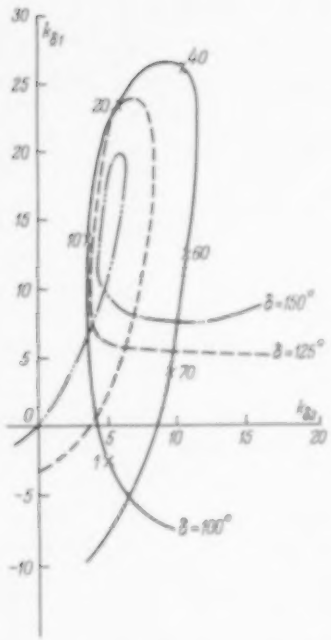

FIG.1. Stability ranges at angles $\delta = 100°$, 125° and 150° and control (regulation) on the generators only from deviation and on the synchronous condensers according to deviations of the angle and its two derivatives.

The figures against the points of the curves indicate $2\pi\omega$, where ω is the frequency of the free oscillations.

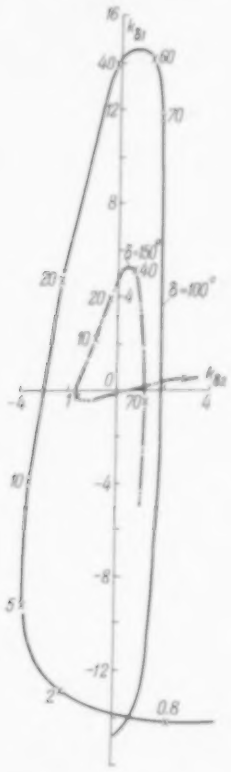

FIG.2. Stability ranges for angles $\delta = 100°$, 150° and regulation according to derivatives on generators and synchronous condensers.

The coefficients of regulation on the generators are assumed to be constants, viz. $k\delta_0 = 1; k\delta_1 = 3; k\delta_2 = 2$.

TABLE 1

Angle	100°	120°	150°
Power transmitted through the line MW.....	1300	1600	1800
Required rating of the synchronous condensers MVA	225	525	1425

depend to great extent on the power transmitted through the line. It is clear that with 750 MW installed power of the synchronous condensers and

without longitudinal compensation the system can continuously transmit 1600—1650 MW. After faults in the system short-time transmission of 1800 MW is possible when the synchronous condensers work with 100 per cent overload. Considering that a synchronous condenser works under normal conditions almost on no-load, the duration of this overloading should not exceed 1 min. This time will be sufficient to permit the automatic load-shedding devices to reduce the loading of the system to the permissible limit.

The investigation of the characteristic equation also showed that in the absence of an excitation control of generators on synchronous condensers the latter will produce practically no increase of the transmitting capacity of the line, even if their rating is fairly high (750 MW).

The use of a strong-action excitation control makes great demands on the high-speed action of regulators and excitors. If the time constant of the exciter exceeds 0.1 sec, the efficiency of the control is already considerably reduced. The use of a rigid feedback comprises the excitor enabling the time constant to be appreciably reduced, if the latter is mainly due to the parameters of the excitor winding itself. Time lags introduced by eddy currents in the massive poles, and also by currents passing through the auxiliary windings placed on these poles cannot be eliminated.

An increase of the mechanical time constant of the synchronous condensers has a beneficial effect on the stability at small deviations, N.A. Kachanova [7] has shown that an increase of the mechanical time constant is very useful in the case of large disturbances.

The results of the theoretical investigations were corroborated by tests on the model of the Central Electrotechnical Research Laboratory of the Ministry of Power Stations in the Karamyshev H.E.S [6].

For the model tests two hydrogenerators of the station, of ratings 1360 kW (1700 kVA) and an artificial line consisting of four reactors, capacitors and resistors, were used. The circuit of the model (Fig.3) permits the parameters of the system to be altered within certain limits.

The time constant of the rotor and the mechanical constant of the generators of the Karamyshev station differ from the corresponding constants of the generators of the Kuibyshev. For this reason the results of the experimental investigation are more useful in a qualitative than in a quantitative respect.

The model circuit was so assembled that one of the generators of the Karamyshev's H.E.S. represented the sending-end station and the second the synchronous condenser. Corresponded to the actual line, the place of erection of the synchronous condenser would not coincide with the mid-point of the line, and its position on the line model was somewhat less favourable.

Both generators were provided with regulators of the Central Electrotechnical Research Laboratory enabling regulation to be carried out either according to the

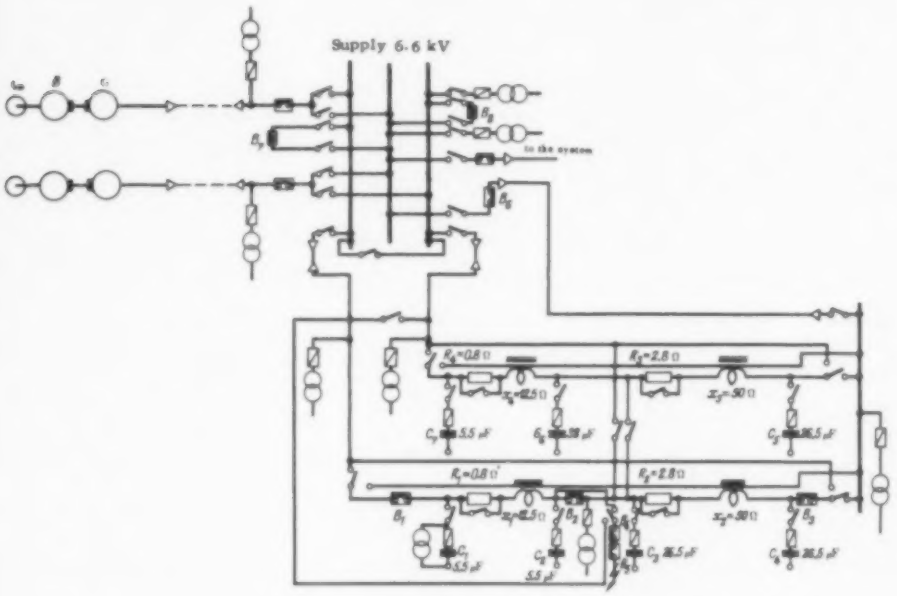

FIG.3. Diagram of the model on the Karamyshev HES. Am – angle-measuring machine; B – exciter; G – generator.

angle and its derivatives, or according to voltage and the derivatives of the angle. In the first tests the generator was regulated according to the angle and its derivatives, the condenser during one test series according to the angle and its derivatives, and during other tests, according to the voltage and the derivatives of the angle relative to the receiving end. The latter method of regulation was found to be more favourable in the practice, since it led to a higher limit of the transmitted power. This is explained by the fact that with an invariable coefficient of regulation according to the angle the relationship between the voltage in the sectionalizing sub-station and the angle is non-linear owing to which the voltage varied considerably at load changes and loss of stability of the section of the transmission line sometimes occurred. The maximum angle that could be obtained in steady operation was 145°; in this case, the angle between the voltage vectors at the ends of the section was almost 90°. A further increase of the load resulted in loss of stability due to the stability limit of the section being exceeded. The character of this loss of stability was a vehement increase of the angle not preceded by any hunting phenomena.

When the intermediate synchronous condenser was regulated according to the voltage variations and to the derivatives of the angle, and the generator only according to variations of the angle, practically the same results were obtained.

Conclusions

The limit of the power transmitted over long transmission lines can be efficiently increased by the use of synchronous condensers erected in sectionalizing sub-stations; their use is particularly indicated where it is necessary to tap off power at points along the line. In this case the use of synchronous condensers will not involve any complications of the lay-out of the sub-stations and in most cases not even the installation of additional transformers.

The points of erection of the synchronous condensers along the line and their rating are determined by technical and economic considerations.

Sub-stations may consume kVAr, thereby reducing, or even eliminating the need for shunting reactors.

Appendix

Characteristic equation of a transmission system with synchronous condensers in one sectionalizing substation. The power of the generating station may be expressed in the following way by the generator e.m.f.'s and the angles between the e.m.f. vectors:

$$\left.\begin{aligned} P_1 &= \frac{E_{q1}E_{q2}}{x_{12}}\sin\vartheta_{12} + \frac{E_{q1}E_{q3}}{x_{13}}\sin\vartheta_{13};\\ P_2 &= \frac{E_{q2}E_{q1}}{x_{12}}\sin\vartheta_{21} + \frac{E_{q2}E_{q3}}{x_{23}}\sin\vartheta_{23};\\ P_3 &= \frac{E_{q3}E_{q1}}{x_{31}}\sin\vartheta_{31} + \frac{E_{q3}E_{q2}}{x_{32}}\sin\vartheta_{32};\\ \vartheta_{12} &= -\vartheta_{21};\quad \vartheta_{13} = -\vartheta_{31};\quad \vartheta_{18} = \vartheta_{13} - \vartheta_{23}. \end{aligned}\right\} \qquad (A,1)$$

In the system of equations (A,1) only two equations are independent. We take δ_{12} and δ_{13} as independent variables. For station 2 .... $E_{q2} = E_{d2}$. In terms of deviations, after linearization, we get

$$\left.\begin{aligned} \Delta P_1 &= A_1\,\Delta E_{q1} + B_1\,\Delta E_{q3} + C_1\,\Delta\vartheta_{12} + D_1\,\Delta\vartheta_{13};\\ \Delta P_3 &= A_3\,\Delta E_{q1} + B_3\,\Delta E_{q3} + C_3\,\Delta\vartheta_{13} + D_3\Delta\vartheta_{23} \end{aligned}\right\} \qquad (A,2)$$

where

$$A_1 = \frac{\partial P_1}{\partial E_{q1}} = \frac{E_{q2}}{x_{12}}\sin\vartheta_{12} + \frac{E_{q3}}{x_{13}}\sin\vartheta_{13};$$

$$B_1 = \frac{\partial P_1}{\partial E_{q3}} = \frac{E_{q1}}{x_{13}}\sin\vartheta_{13};$$

$$C_1 = \frac{\partial P_1}{\partial\vartheta_{12}} = \frac{E_{q1}E_{q2}}{x_{12}}\cos\vartheta_{12} + \frac{E_{q1}E_{q3}}{x_{13}}\cos\vartheta_{13};$$

1958

$$D_1 = \frac{\partial P_1}{\partial \delta_{12}} = -\frac{E_{q1} E_{q3}}{x_{13}} \cos \delta_{13};$$

$$A_2 = \frac{\partial P_2}{\partial E_{q1}} = \frac{E_{q3}}{x_{21}} \sin \delta_{21};$$

$$B_2 = \frac{\partial P_2}{\partial E_{q3}} = \frac{E_{q1}}{x_{21}} \sin \delta_{21} + \frac{E_{q2}}{x_{23}} \sin \delta_{23};$$

$$C_2 = \frac{\partial P_2}{\partial \delta_{12}} = -\frac{E_{q3} E_{q1}}{x_{21}} \cos \delta_{21};$$

$$D_2 = \frac{\partial P_2}{\partial \delta_{32}} = \frac{E_{q3} E_{q1}}{x_{21}} \cos \delta_{21} + \frac{E_{q3} E_{q2}}{x_{23}} \cos \delta_{23}.$$

From equations (A,2) and (1) we get,

$$\left.\begin{aligned} A_1 \Delta E_{q1} + B_1 \Delta E_{q3} &= -(C_1 + T_{j1} p^2) \Delta \delta_{12} - D_1 \Delta \delta_{32}; \\ A_2 \Delta E_{q1} + B_2 \Delta E_{q3} &= -C_1 \Delta \delta_{12} - (D_2 + T_{j3} p^2) \Delta \delta_{32}. \end{aligned}\right\} \qquad (A,3)$$

The system of equations (A,3) must be solved with respect to the variables E_{q1} and E_{q3}. To consider the magnetic asymmetric of the machine we write down the relationships between the quantities E_d and E_q, viz.

$$\left.\begin{aligned} E_{d1} &= \left(1 + \frac{x_{d1} - x_{q1}}{x_{11}}\right) E_{q1} - \frac{(x_{d1} - x_{q1})}{x_{13}} \cos \delta_{12} E_{q2} - \\ &\quad - \frac{x_{d1} - x_{q1}}{x_{13}} \cos \delta_{13} E_{q3}; \\ E_{d3} &= -\frac{x_{d3} - x_{q3}}{x_{13}} \cos \delta_{21} \cdot E_{q1} - \\ &\quad - \frac{x_{d3} - x_{q3}}{x_{23}} \cos \delta_{23} \cdot E_{q2} + \left(1 + \frac{x_{d3} - x_{q3}}{x_{23}}\right) \cdot E_{q3}; \\ E'_{d1} &= \left(1 + \frac{x'_{d1} - x_{q1}}{x_{11}}\right) E_{q1} - \\ &\quad - \frac{(x'_{d1} - x_{q1})}{x_{13}} \cos \delta_{12} \cdot E_{q2} - \frac{x'_{d1} - x_{q1}}{x_{13}} \cos \delta_{13} \cdot E_{q3}; \\ E'_{d3} &= -\frac{x'_{d3} - x_{q3}}{x_{13}} \cos \delta_{21} \cdot E_{q1} - \\ &\quad - \frac{x'_{d3} - x_{q3}}{x_{23}} \cos \delta_{23} \cdot E_{q2} + \left(1 + \frac{x'_{d3} - x_{q3}}{x_{23}}\right) E_{q3}. \end{aligned}\right\} \qquad (A,4)$$

x_{11}, x_{12}, etc., are the self and mutual inductive reactances in the equivalent representation of the generators by the quadrature components of the synchronous reactances.

The system of equations (A,4) may also be written in terms of the partial differentials of the deviations, viz.

$$\left.\begin{aligned}
\Delta E_{d1} &= E_1 \Delta E_{q1} + F_1 \Delta E_{q3} + G_1 \Delta \delta_{12} + H_1 \Delta \delta_{32};\\
\Delta E_{d3} &= E_3 \Delta E_{q1} + F_3 \Delta E_{q3} + G_3 \Delta \delta_{12} + H_3 \Delta \delta_{32};\\
T_{d1} \Delta E'_{d1} &= E'_1 \Delta E_{q1} + F'_1 \Delta E_{q3} + G'_1 \Delta \delta_{12} + H'_1 \Delta \delta_{32};\\
T_{d3} \Delta E'_{d3} &= E'_3 \Delta E_{q1} + F'_3 \Delta_{q3} + G'_3 \Delta \delta_{12} + H'_3 \Delta \delta_{32}.
\end{aligned}\right\} \qquad (A,5)$$

The partial differentials E_1, F_1, E_3, F_3, E'_1, F'_1, F'_3, E'_3 remain equal to the coefficients of E_q of the corresponding columns of the system of equations (A,4), for example

$$E_1 = \frac{\partial E_{d1}}{\partial E_{q1}} = 1 + \frac{x_{d1} - x_{q1}}{x_{11}} \quad \text{etc.}$$

The partial differentials of the deviations of the angles are.

$$\left.\begin{aligned}
G_1 &= \frac{\partial E_{d1}}{\partial \delta_{12}} = + \frac{x_{d1} - x_{q1}}{x_{12}} \sin \delta_{12} E_3 + \\
&\quad + \frac{x_{d1} - x_{q1}}{x_{13}} \sin \delta_{12} E_{q3};\\
H_1 &= \frac{\partial E_{d1}}{\partial \delta_{32}} = - \frac{x_{d1} - x_{q1}}{x_{13}} \sin \delta_{12} E_{q3};\\
G_3 &= \frac{\partial E_{d3}}{\partial \delta_{12}} = \frac{x_{d3} - x_{q3}}{x_{13}} \sin \delta_{12} E_{q1};\\
H_3 &= \frac{\partial E_{d3}}{\partial \delta_{32}} = - \frac{x_{d3} - x_{q3}}{x_{13}} \sin \delta_{12} E_{q1} + \\
&+ \frac{x_{d3} - x_{q3}}{x_{32}} \sin \delta_{32} E_3;\\
G'_1 &= T_{d1} \left(\frac{x'_{d1} - x_{q1}}{x_{12}} \sin \delta_{12} E_3 + \right.\\
&\quad \left. + \frac{x'_{d1} - x_{q1}}{x_{13}} \sin \delta_{12} E_{q3} \right);\\
H'_1 &= T_{d1} \left(- \frac{x'_{d1} - x_{q1}}{x_{13}} \sin \delta_{12} E_{q3} \right);\\
G'_3 &= T_{d3} \left(\frac{x'_{d3} - x_{q3}}{x_{13}} \sin \delta_{12} E_{q1} \right);\\
H'_3 &= T_{d3} \left(- \frac{x'_{d3} - x_{q3}}{x_{13}} \sin \delta_{12} E_{q1} + \right.\\
&+ \left. \frac{x'_{d3} - x_{q3}}{x_{23}} \sin \delta_{32} E_3 \right).
\end{aligned}\right\} \qquad (A,6)$$

Substituting into equation (2) the values of the e.m.f.'s, we get from equations (A,5):

$$\left.\begin{aligned}
\Delta E_{de1} &= (E_1 + pE'_1) \Delta E_{q1} + (F_1 + pF'_1) \Delta E_{q3} + \\
&\quad + (G_1 + pG'_1) \Delta \delta_{12} + (H_1 + pH'_1) \Delta \delta_{32};\\
\Delta E_{de3} &= (E_3 + pE'_3) \Delta E_{q1} + (F_3 + pF'_3) \Delta E_{q3} + \\
&\quad + (G_3 + pG'_3) \Delta \delta_{12} + (H_3 + pH'_3) \Delta \delta_{32}.
\end{aligned}\right\} \qquad (A,7)$$

The deviation of the voltage on the rotor rings resulting from the action of the regulator may be expressed as follows:

$$\left.\begin{aligned}\Delta E_{dc1} &= \frac{M(p)_1\,\Delta\delta_{12}}{(1+pT_{e1})(1+pT_{reg1})} = \frac{M(p)_1}{Z(p)_1}\,\Delta\delta_{12};\\ \Delta E_{dc2} &= \frac{M(p)_2\,\Delta\delta_{22}}{(1+pT_{e2})(1+pT_{reg2})} = \frac{M(p)_2}{Z(p)_2}\,\Delta\delta_{22}.\end{aligned}\right\} \qquad (A,8)$$

We have for, $$Z(p) = (1 + pT_{ex})\ (1 + pT_{reg});$$

where T_{ex} is the time constant of the excitor;
T_{reg} is the time constant of the regulator. With regulation by an angle $M(p) = k_0 + k_1 p + k_2 p^2$.

Substituting the values E_{q_1}, E_{q_2} obtained from the solution of the system of equations (A,3), into equations (A,7) and considering the expression (A,8), we get two equations involving $\Delta\delta_{12}$ and $\Delta\delta_{22}$, viz,

$$\left.\begin{aligned}\left(Q_1 + \frac{M(p)_1}{Z(p)_1}\right)\Delta\delta_{12} + Q_3\,\Delta\delta_{22} &= 0;\\ Q_2\,\Delta\delta_{12} + \left(Q_4 + \frac{M(p)_2}{Z(p)_2}\right)\Delta\delta_{22} &= 0.\end{aligned}\right\} \qquad (A,9)$$

In equations (A,9) the coefficients of the deviations of the angles were obtained by substitution.

The determinant composed of the coefficients of the angle deviations yields the characteristic equation (4) required. In stability investigations the characteristic equations must be written in explicit form and arranged in descending powers of p.

REFERENCES

1. F.G. Baum; *Voltage Regulation and Insulation for Large Power Long Distance Transmission Systems, Trans. AIEE*, 40, p. 1017 (1921).
2. P.S. Zhdanov; *The 1000 MW Transmission System Kuibyshev–Moscow, Elektrichestvo*, No.13 (1936).
3. S.A. Lebedev; *Investigation of artificial Stability, Reports of the All–Union Electrotechnical Institute*, No.40, *Gosenergoizdat* (1940).
4. M.M. Botvinnik; *Excitation Regulation and steady-state Stability of the synchronous Machine, Gosenergoizdat* (1950).
5. V.A. Venikov and I.V. Litkens; *Effect of the Excitation Regulation on the Transmitting Capacity of long Transmission Lines, Elektrichestvo*, No.11 (1955).
6. E.L. Bronshtein and M.S. Fezi-Zhilinskaya; *Model of a long Transmission Line, Reports of Central Electrical Research Laboratory*, No.2, *Gosenergoizdat* (1954).
7. N.A. Kachanova and V.E. Krutikova; *Investigation of the Methods of Improving the Stability of long Transmission Systems (A.C.)* (1955).
8. M.A. Aizerman, *Theory of automatic Control of Motors, State Publishing House of technical and theoretical Literature* (1952).

CONTROLLING A MILL WITH SEPARATELY DRIVEN ROLLERS*

O.V. SLEZHANOVSKII

(Received 12 December 1956)

The separate drive of the rollers of large rolling mills, though possessing considerable advantages over group drives, complicates the control system and introduces some novel requirements, of which the basic one is the necessity of securing rolling without bending with a sufficiently uniform distribution of the loads between the roll-drive motors. Most existing systems do not satisfy these requirements; moreover, the systems are also unnecessarily complicated and do not ensure a satisfactory transient response. A new system proposed by the author (Fig. 1) is sufficiently simple and eliminates the above disadvantages.

1958

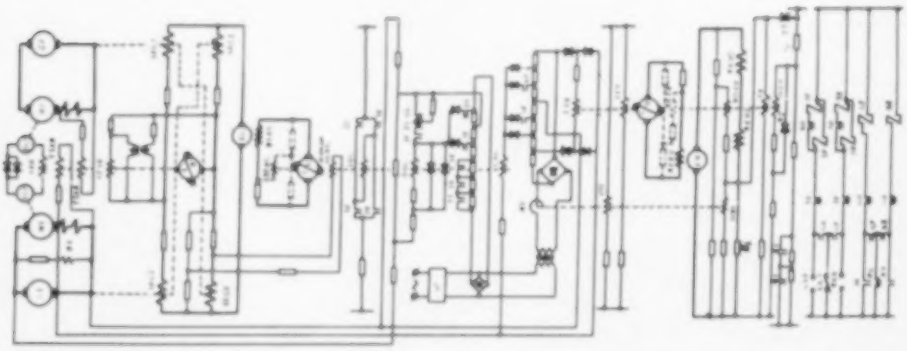

FIG. 1. Elements of the control circuit of a mill with individual roll-drives.

The field windings of the generators are connected to a bridge ciruit fed by the common exciter EG†). The regulator *AR* co-ordinating speed and current of the roll-drive motors is connected in the diagonal arm of the bridge. When the control acts, the field of one generator increases and that of the other decreases. The regulator

* *Elektrichestvo* No. 5, 12 – 20, 1957 [Reprint Order No. EL 19].

† The bridge circuit may also be formed by windings and ohmic resistances or by two windings and armatures of the exciters where two exciters are used.

windings are connected to the voltage drops in the sections of the main circuit of each of the roll-drive motors and to the voltage difference of the tachogenerators. The field windings of the motors receive their supply from the exciter *EM* whose excitation is provided by the amplidyne *AM*, so that the character of the transient processes comes near the possible optimum. This is achieved by arranging the m.m.f. of the input winding *IAM* in the positive direction, a "cut-off" of the field current by the differential winding *DAM*, and a positive feedback of the field currents *PB*. The m.m.f.'s are denoted by F_{im}, F_{dm} and F_{pf}.

The m.m.f. of the input winding determines the polarity of the exciter in the steady-state. The differential winding is connected to the difference of two voltages, viz. a voltage proportional to the field current of the motor and the voltage of the calibrating potentiometer. The rectifier *R*1 in the circuit of the differential winding prevents its action when the exciting flux of the motor increases, but towards reducing the field current. The rectifier *R*2, shunting the winding, limits its m.m.f. during periods of decreasing flux of the excitation.

The steady-state characteristics of the control system of the excitation of the generators and of the roll-drive motors are shown in Fig. 2a and b. The method of plotting them is similar to that described in [1]. The analysis of the steady-state characteristics confirms in principle the usefulness of the system adopted. The resulting m.m.f. of the amplidyne *AG* of the generators is in all cases determined within narrow limits, and the m.m.f. of the amplidyne *AM* of the motors changes in such a way that it creates favourable conditions for the forcing of processes of decreasing or increasing the fluxes of the roll-drive motors.

By altering the amplification factor of the positive feedback for the motor field current and the m.m.f. of the input winding it is possible to adjust the character of the increase of the exciting flux in the most appropriate way to suit the actual conditions of operation of the drive. If the machines of the main drive have a low voltage between segments, a small flywheel moment and a large magnetic time constant, it is expedient to increase the m.m.f. of the input winding. Increased flux forcing at the beginning of the process is so obtained and the braking conditions are also established correctly from the viewpoint of energy economy, since the speed is first reduced by the strong increase of the motor field and then by the reduction of the generator voltage. Cases are possible where during a forced increase of the field the load regulator, tending to limit the current of the main circuit, also slightly increases the generator voltage above its rating.

With machines having a large voltage between segments, which would not permit the voltages to exceed the rated values during braking periods, it is necessary to decrease the m.m.f. of the input winding and to increase the positive feedback of the field current. By this re-arrangement the initial forcing of the motor field is reduced to the correct value and the forcing increased subsequently as the motor flux increases, in accordance with the requirements set out in [1] and [2].

Rotating machines are not used as sources of reference voltages in the circuit suggested. The generator of the reference voltage of the voltage regulator is re-

placed by a voltage stabilizer and the generator of the reference voltage of the power regulator by a magnetic amplifier. Flexible feedbacks of the generator voltage and field current are provided by a Birfeld differential-bridge circuit without stabilizing transformers.

The use of this circuit introduces several novel characteristics. Fig. 3a shows that the transfer function $K(p)$ of of the (ideal) differential bridge without load can be found as follows:

$$U_0 = U_i \frac{r_2}{r_1 + r_2} \frac{r_4}{r_3 + r_4} \frac{1}{(1 + pT)}$$

In the balanced bridge

$$\frac{r_2}{r_1 + r_2} = \frac{r_4}{r_3 + r_4} = Kbb,$$

then

$$K(p) = \frac{U_0}{U_i} = K_{bb} \frac{pT}{(1 + pT)} \qquad (1)$$

where

$$T = \frac{L}{r_3 + r_4}.$$

Comparing the expression with the transfer function of the stabilizing transformer (Fig. 3b):

$$K(p) = \frac{U_0}{U_i} =$$

$$K_S \frac{p}{p^2 T_1 T_2 (1 - \sigma^2) + p(T_1 + T_2) + 1}$$

where

$$K_S = \frac{MR}{R_1(R + R_2)}; \sigma^2 = \frac{M^2}{L_1 L_2}; T_1 = \frac{L_1}{R_1}; T_2 = \frac{L_2}{R + R_2}.$$

Neglecting leakage, i.e. assuming $\sigma = 1$, and introducing $T_1 + T_2 = \tau$; $K_{st} = \frac{K_S}{\tau}$ we obtain

$$K(p) = K_{cm} \frac{p\tau}{(1 + p\tau)}. \qquad (2)$$

It follows that on the assumptions made the transfer functions of the bridge and of the stabilizing transformers have the same form. Since, however, the time constants of the stabilizing transformers differ in most cases from the time constants in the circuits of the machine windings forming the branches of the bridge, the effects of the use of the circuits compared will also be different.

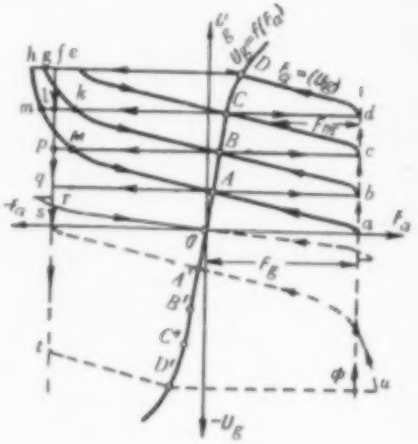

FIG. 2. Steady-state characteristics of the field control of the generators and motors.

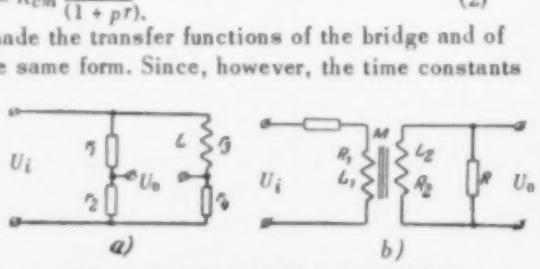

FIG. 3. Stabilizing bridge and stabilizing transformers.

It is easy to show that this difference may be intrinsic. If the input voltage U_i is the exciter voltage U_{eg} of the generators, we find from the relation $U_{eg} = E_g \frac{(1+pT_g)}{K_g}$ that when the bridge circuit is used, $U_0 = U_{eg} K_{bb} \frac{pT_g}{(1+pT_g)} = \frac{K_{bb}}{K_g} T_g p E_g$.

Denoting $\frac{K_{bb}}{K_g} T_g = \alpha$, we obtain

$$U_0 = \alpha p E_g. \tag{3}$$

The m.m.f. of the amplidyne supplied with the output voltage is approximately

$$F_{bg} \approx K_{bg} p E_g \approx K_{bg} p U_g, \tag{4}$$

where

$$K_{bg} = K_{bb} \frac{W_w}{r_w}.$$

When the stabilizing transformer is used the following expression results for the output voltage U_O:

$$U_0 = \frac{K_{st}}{K_g} \tau \frac{(1+pT_g)}{(1+p\tau)} p E_g = \beta p E_g \frac{1}{(1+p\tau)} + \gamma p^2 E_g \frac{1}{(1+p\tau)}. \tag{5}$$

Analysis of the expressions for U_O shows that the bridge circuit enables a feedback proportional to the net first derivative of the generator e.m.f. to be obtained whereas the stabilizing transformer gives with the same input voltage two components the first of which is proportional to the first derivative of the generator voltage, and the second to the second derivative. Also an additional time delay element is introduced which is determined by the denominator $(1 + p\tau)$.

To obtain an expression similar to (5) by the bridge circuit, it is necessary to have at the input of the bridge the voltage U_{ag} of the amplidyne, and not that of the exciter.

Indeed, since in this case $U_0 = U_{ag} K_{bb} \frac{pT_{eg}}{(1+pT_{eg})}$,

we get by transition from U_{ag} to E_g,

$$U_0 = \frac{K_{bb}}{K_{eg} K_g} T_{eg} (1+pT_g) p E_g = \mu p E_g + \varepsilon p^2 E_g. \tag{6}$$

The m.m.f. of the amplidyne winding connected to U_O will be

$$F_{be} \approx K_{be} (1+pT_g) p E_g \approx K_{be} (1+pT_g) p U_g. \tag{7}$$

where

$$K_{bc} = \frac{K_{bb}}{K_{eg} K_g} T_{eg} \frac{W_w}{r_w}.$$

Comparison of the equations (5) and (6) shows that for small values of τ they practically coincide.

It is obvious that with relatively small values of τ and with divergences between τ and T the effects of flexible feedback obtained by means of stabilizing transformers and bridges respectively, are very much different for the same input voltage. Under these conditions the flexible bridge feedback acts like the feedback of a stabilizing transformer connected to the output of the following cascade.

The above considerations enable us to explain the advantages of the accepted

method of increasing the anti-hunting time constant τ to values equal to the time constant T_g of the generator [3].

In the generator - motor system considered [3] with amplidynes the expression for the flexible feedback assumes in the case of $\tau = T_g$ a form similar to that obtained for the bridge circuit (4), and since by means of the feedback pE_g, the derivative of the generator e.m.f., is controlled, we obtain conditions resulting in uniformly accelerated transient processes of field control of the generator. However, the great varying values of time constants T_g encountered render it difficult to maintain the condition $\tau = T_g$ by the use of stabilizing transformers. This difficulty is obviated by the use of the differential bridge circuit where the problem resolves itself since $T = T_g$.

There is a fair number of systems in which control by the first derivative of the generator e.m.f. is advisable. The control system of the excitation of the generators of the main drives belongs to these. In developing the circuit, a basic flexible link was provided by the bridge circuit connected to the field winding of the generators. The use of an intermediate feedback, shown dotted in Fig. 1, should be avoided or its effect reduced to the minimum necessary with regard to the stability conditions.

1958

Determination of the parameters of the flexible feedback and character of the control operations

For the generator voltage (not considering the action of the regulator, neglecting the time constants of the control windings of the amplidyne, eddy current effects and assuming a linear magnetization characteristic of the machines) the following equation can be written:

$$U_g = F_{ag} K \frac{1}{(1 + pT_a)(1 + pT_{eg})(1 + pT_g)}, \tag{8}$$

where $K = K_a K_{eg} K_g$, the amplification factor of the system:

$$K_a = \frac{\Delta U_{ag}}{\Delta F_{ag}}; \quad K_{eg} = \frac{\Delta U_{eg}}{\Delta U_{ag}}; \quad K_g = \frac{\Delta U_g}{\Delta U_{eg}}; \quad T_a, \; T_{eg}, \; T_g -$$

T_a, T_{eg}, T_g time constants of the amplidyne, exciter and generator respectively; $F_{ag} = F_i - F_{dg} - F_{bg} - F_{be}$ the m.m.f. of the amplidyne AG; F_i, F_{bg}, F_{be} the m.m.f.'s of the input and stabilizing windings; $F_{dg} = K_{dg}(U_g - U_{co})$ the m.m.f. of the differential windings;
Hence

$$F_{ag} = F_i + K_{dg} U_{co} - U_g \{K_{dg} + p[K_{bg} + K_{be}(1 + pT_g)]\}.$$

Substituting the expression for F_{ag} in equation (8), we obtain:

$$U_g = (F_i + K_{dg} U_{co}) \frac{1}{(1 + pT_a)(1 + pT_{eg})(1 + pT_g) + K\{K_{dg} + p[K_{bg} + K_{be}(1 + pT_g)]\}} \tag{9}$$

Up to the cut-off of the forcing, i.e. when the differential winding is not connected:

$$U_g = F_i K \frac{1}{(1 + pT_a)(1 + pT_{eg})(1 + pT_g) + Kp[K_{bg} + K_{be}(1 + pT_g)]} \tag{10}$$

Neglecting the action of the intermediate feedback ($K_{be} = 0$) and bearing in mind that

the time constants of the links included by the flexible feedback can be neglected when the time constant of the transfer function of the feedback is many times larger than the time constant of these links, we find for an approximate calculation:

$$U_g = (F_i + K_{dg} U_{co}) \frac{K}{(1 + K_{dg} K)} \frac{1}{1 + p \frac{T_g + K_{bg} K}{1 + K_{dg} K}} \tag{11}$$

or

$$U_g = (U_{go} - U_{g.fin}) \exp^{-\frac{t}{T_{g.red^1}}} + U_{g.\,fin}, \tag{12}$$

and before cutting-off the forcing with zero initial conditions

$$U_g = F_i K \frac{1}{1 + p (T_g + K_{bg} K)} \tag{13}$$

or

$$U_g = F_i K \left(1 - \exp^{-\frac{t}{T_{g.red^2}}}\right) \tag{14}$$

In the expressions (12) and (14) $T_{g.red^1} = \frac{T_g + K_{bg} K}{1 + K_{dg} K}$ and $T_{g.red^2} = T_g + K_{bg} K$ are the reduced time constants of the generator after "cutting-off" forcing and before, when the circuit is open. U_{go} and $U_{g.fin}$ are the initial and final values of the voltage, determined by the change of the cut-off voltage U_{co}.

Assuming the control time $t = t_r$ we can find the coefficient of the feedback K_{bg} from the above equations. Beginning from the conditions of starting before "cutting-off" forcing (14), we obtain

$$K_{bg} = \frac{1}{K} \left[\frac{t_r}{\ln \frac{F_i K}{F_i K - U_{co}}} - T_g \right]. \tag{15}$$

The right choice of K_{bg} can be checked by calculating the transient process by the complete equation.

The equation and the parameters of the field control of the roll-drive motors are set up in a similar way:

$$i_m = F_{am} K_m \frac{1}{(1 + pT_a)(1 + pT_{em})(1 + pT_m)}, \tag{16}$$

where $K_m = K_{am} K_{em} K_m$, the amplification coefficient of the system; T_a, T_{em}, T_m – the time constants of the amplidyne, the exciter and the motor respectively;

$$K_{am} = \frac{\Delta U_{am}}{\Delta F_{am}}; \quad K_{em} = \frac{\Delta U_{em}}{\Delta U_{am}}; \quad K_m = \frac{\Delta i_m}{\Delta U_{em}} = \frac{1}{\Sigma R};$$

$F_{am} = F_{im} + F_{pf} - F_{dm} - F_b$ the m.m.f. of the amplidyne AM:

$$F_{am} = F_{im} + K_{dm} i_{coc} + i_m [K_{pf} - K_{dm} - p (K_{bem} + K_{bm} + K_{bem} p T_m)],$$

where

$$F_{pf} = K_{pf} i_\partial; \quad K_{pf} = \frac{R_t}{\Sigma r_{pf}} w_{pf};$$

$$F_{dm} = K_{dm} (i_m - i_{coc});$$

$$K_{dm} = \frac{F_{im} + \frac{i_{mn}}{K_m}(K_{pf}K_m - 1)}{i_{mn} - i_{co}}\ ;\ i_{co} = \frac{U_s}{R_p} \cdot \frac{r_p}{R_t}\ ;$$

$$F_b = F_{bem} + F_{bm} = pi_m[K_{bem}(1 + pT_m) + K_{bm}],$$

where U_s is the system voltage; R_p is the total effective resistance of the standard potentiometer, $F_b = F_{bem} + F_{bm}$ the m.m.f. set up by the two flexible feedbacks.

Substituting these expressions in (16) we obtain $i_m = (F_{im} + K_{dm}i_{co})\,K_m$.

$$\frac{1}{(1 + pT_a)(1 + pT_{em})(1 + pT_m) + K_m\{K_{dm} - K_{pf} + p[K_{bm} + K_{bem}(1 + pT_m)]\}} \qquad (17)$$

In the period of increasing flux up to the instant of "cutting-off" forcing the differential winding does not take part in the operation.

Therefore, assuming $K_{dm} = 0$, we obtain for the given condition:

$$i_m = F_{im} \cdot K_m \frac{1}{(1 + pT_a)(1 + pT_{em})(1 + pT_m) + K_m\{p[K_{bm} + K_{bem}(1 + pT_m)] - K_{pf}\}} \qquad (18)$$

or

$$i_m = F_{im}K_m \frac{1}{T_aT_{em}T_mp^3 + [T_m(T_{em} + T_a + K_mK_{bem}) + T_aT_{em}]\,p^2 + [T_a + T_{em} + T_m + K_m(K_{bm} + K_{bem})]\,p - (K_mK_{pf} - 1)} \qquad (19)$$

Usually $K_mK_{pf} \gg 1$. In this condition one root of the characteristic equation is positive, which indicates the increasing rate of rise of the field current. When the current i_m has reached the cutting-off value, it is necessary to use (17).

In order to use the analytical formula for zero initial conditions for the calculation of the excitation flux increase, the calculation is suitably made not for the current itself but for the field current increment, i.e. the co-ordinate origin must be transferred to the point corresponding to the initial steady-state excitation current of the given state of excitation. In this case we have always to calculate first the initial theoretical effective value F_{im}.

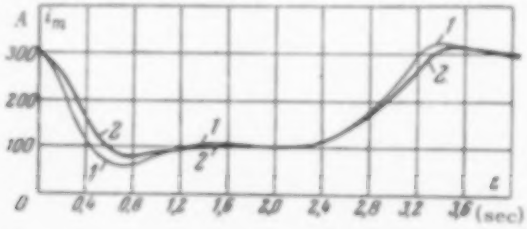

FIG. 4. Conditions of the control of the excitation flux of the roll-drive motors 300 ... 100 ... 300 A. $i_{mn} = 300$ A; $i_{co} = 240$ A; $i_{min} = 100$ A; $F_{im} = 20$ AT; $K_m = K_aK_{em}K_m = 5.2, 5.2 = \lambda\pi$ A/AT; $k_{pf} = 0.6$ AT/A; $K_{dm} = 3$ AT/A; $T_a = 0.1$ sec; $T_{em} = 0.3$ sec; $T_m = 6$ sec. 1 - with $K_{bm} = 0.18$; $K_{bem} = 0$; 2 - with $K_{bm} = 0.1$; $K_{bem} = 0.005$.

$$F_{imr} = F_{imo} + \frac{i_{mr}}{K_m}(K_m K_{pf} - 1), \tag{20}$$

where F_{imo} is the m.m.f. of the input winding; i_{mr} is the motor field current corresponding to the initial state of excitation.

For a more precise determination of the effect of the positive feedback of the excitation current and of the flexible feedbacks on the transient control process calculations were carried out for two values of the coefficient of the positive feedback K_{pf} and for two different methods of obtaining the flexible feedback:

a) $K_{bm} \neq 0$; $K_{bem} = 0$;

b) $K_{bm} \neq 0$; $K_{bem} \neq 0$.

Diagrams of the calculated transient processes are shown in Figs. 4 and 5.

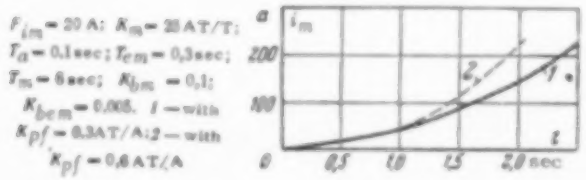

FIG. 5. Increase of the excitation flux of the roll-drive motors.
F_{im} = 20 A; K_m = 25 A/AT;
T_a = 0.1 sec; T_{em} = 0.3 sec;
T_m = 6 sec; K_{bm} = 0.1;
K_{bem} = 0.005.
1 - with K_{pf} = 0.3 AT/A;
2 - with K_{pf} = 0.6 AT/A.

When the intermediate flexible feedback is in action, the time constants T_a and T_{em} can no longer be neglected, since owing to the inclusion of a large resistance in the field circuit of the exciter, the time constant T_{em} is relatively small. The calculations must be made according on the complete third-order equation. However, in some cases it is possible to confine it to the second order. Just as in the field control of the generators, the intermediate flexible feedback is not absolutely necessary here. In this case

$$K_{bm} = \frac{1}{K_m}\left\{\frac{(K_{pf}K_m - 1)t}{\ln\left[\frac{i_m}{F_{im}K_m}(K_{pf}K_m - 1) + 1\right]} - T_m\right\}. \tag{21}$$

But in the field control system of the motors the intermediate flexible feedback results in an improvement of the transient performance when the flux is increased, although the performance deteriorates slightly when the flux is decreased.

Fig. 6 shows an oscillogram of the control processes of the motor field ob-

tained on a laboratory model with only one intermediate flexible feedback in operation. The character of the change of the flux Φ is entirely satisfactory. The over-regulation of the flux is small, the over-regulation of the field current i_m reaches 17%. This discrepancy between current and flux is explained by the effect of eddy currents.

It is recommended to provide the controller for balancing the loads and speeds with a non-linear resistor in the circuit of the winding connected to the difference of the tachogenerator voltages. The function of this resistor is not to prevent the regulator from balancing the motor loads. Owing to the non-linearity the winding begins to act effectively only from a certain permissible difference in speed onwards.

The m.m.f. of the regulator AR, produced by the current windings, is proportional to the difference of the load currents $F_{\Delta I} = K_I \Delta I$.

The m.m.f. of the winding connected to the difference of the tachogenerator voltages is $F_{\Delta n} = K_n \Delta n$.

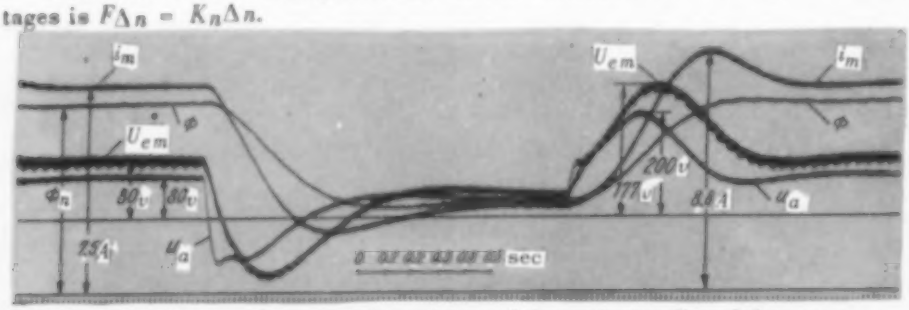

FIG. 6. Oscillogram of the control conditions of the excitation flux of the motors of the laboratory model. i_{mn} = 7.5 A; i_{co} = 4.9 A; i_{min} = 3 A; K_m = 1.5 A/AT; K_{pf} = 8.33 AT/A; T_a = 0.05 sec; T_{em} = 0.117 sec; T_m = 1.06 sec; K_{dm} = 29.8 AT/A;

The speed difference produced by the rolling process determines the unavoidable difference of the loads under conditions of equality of the initial value of the generator e.m.f.'s $E_{g1} = E_{g2}$ and of the e.m.f.'s of the motors $E_{m1} = E_{m2}$. In this case

$$F_{\Delta n} = K_n \frac{R_{arm}}{C\Phi} (1 + pT_{arm}) \Delta I,$$

where R_{arm} and T_{arm} are the resistance and time constant of the armature respectively, C is the motor constant.

The m.m.f. of the error signal of the controller F_e consists of two components $F_{\Delta I}$ and $F_{\Delta n}$.

$$F_e = F_{\Delta I} + F_{\Delta n} = \Delta I \left\{ K_I - K_n \frac{R_{arm}}{C\Phi} (1 + pT_{arm}) \right\}$$

or

$$F_e = \Delta I \left\{ \left(K_I - K_n \frac{R_{arm}}{C\Phi} \right) - K_n \frac{R_{arm}}{C\Phi} pT_{arm} \right\}.$$

Denoting $\frac{R_{arm}}{C\phi} = A$ with $T_{arm} = 0$, we obtain: $F_e = \Delta I (K_I - K_n A)$.

This equation shows that the presence of the winding setting up $F\Delta n$ prevents the balancing of the loads. On the other hand, it is obvious that this winding can prevent the possibility of the development of a large discrepancy of speeds which is especially undesirable during the gripping of ingots by the rolls.

The load controller is designed according to well established principles. The m.m.f. of the current winding of the amplidyne AG decreases the acceleration of the motors during the overloading on starting and retards the reduction of the generator voltage during braking periods. The m.m.f. of the current winding of the amplidyne AM increases the excitation flux of the motor when the current exceeds the set value. As the speed of the motor rises, the setting is reduced by the amplidyne, one of which is connected to a voltage proportional to the field current. The amplification factor must be chosen for the extreme case viz. overloading in the beginning of the weakening of the excitation flux of the motor. The m.m.f. of the current winding must discontinue initiating a decrease of flux and effect its increase [2]. During this period the motor current may exceed the setting (error of the steady-state regulator) by a value ΔI, smaller than the difference between the setting of the first stage protection and the setting of the regulator.

In some cases, where it is desirable to have a large amplification coefficient of the regulation and to improve the characteristic of the drive, it is recommended to use an amplidyne in conjunction with a magnetic amplifier and filters similar to the arrangement shown in [4]. The large number of control windings of the magnetic amplifier enables all the feedbacks described to be connected up. When an amplidyne system without a magnetic amplifier is used, where the number of control windings (four windings) is not sufficient, the introduction of feedbacks into the motor field control system can be achieved by means of stabilizing transformers connected to the output of the amplidyne, which corresponds to the intermediate feedback and to the unbalanced bridge circuit connected to the field winding of the motor. The unbalanced system furnishes a m.m.f. consisting of two components one of which is proportional to the field current and the second, to the rate of change of the flux.

Testing the new system

The basic solutions of the new system passed a laboratory test; successful introduction of the new system into the industry has begun. On the plate mill 2800 at Voroshilovsk operating station the system shown in Fig. 7 has been used. The drive of the upper and the lower rolls was obtained from virtually independent systems, connected only through the windings of the amplidynes AG 1 and AG 2. The windings were connected to the difference of the voltage drops in the interpoles and the compensating windings of the motors, and also to the difference of the voltages of the two tachogenerators. The amplification factors of these amplidynes were very low, otherwise, there would have been a danger of loss of stability. On the other hand, a reinforcement of the stabilizing devices would lead to an inadmissible reduction of the intensity of the forcing of the basic transient processes owing to the common control channels. The balancing members operated very unsatisfactorily after the "cut-off" of the forcing when the voltage control system prevented its ac-

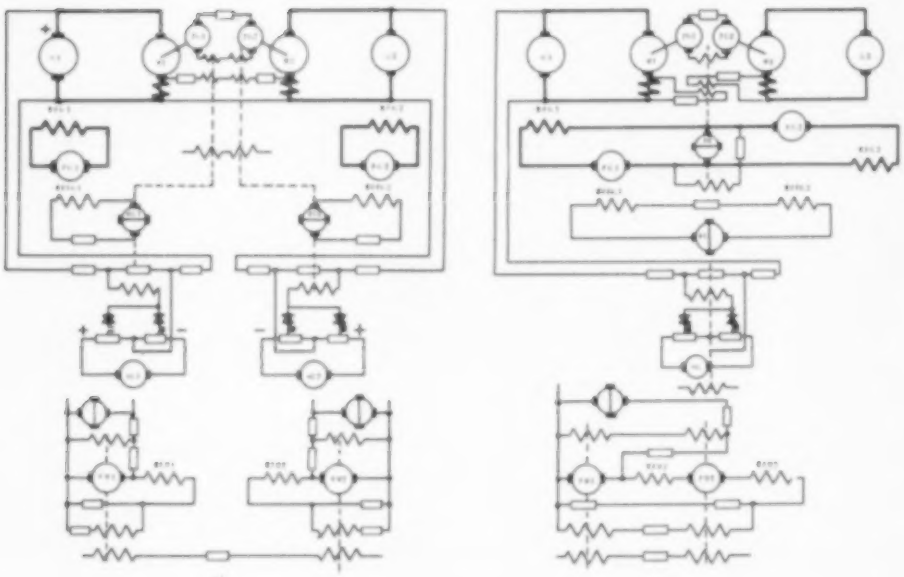

FIG. 7. Elements of the control system of the mill 2800.
a) before b) after modernization.

tion.

As a result of these shortcomings inadmissible bending of the ingots was observed during rolling and the difference in the motor loads reached 50 - 60% of the rating, and sometimes even higher values.

On our recommendations the system was altered to that shown in Fig. 7b. The exciters used in the original circuit and part of the amplidynes were retained. In the modernized ciruit the controller was connected into the diagonal arm of the bridge formed by the windings of the generators and the armatures of the exciters.

The system as a whole was considerably simplified, one amplidyne. one setting generator, scveral stabilizing transformers and other elements being eliminated as no longer required.

The positive results of the combination of the controls of the basic processes and the regulator performance are shown in the oscillograms Fig. 8.

Fig. 8a shows the rolling with disconnected regulator; the difference of the loads I_1 and I_2 was in this case smaller than that observed before modernization.

Fig. 8b shows the rolling with the regulator operating but with the winding acting on the difference in speeds disconnected. It follows from an analysis of the oscillogram that as a result of the regulator action the steady-state motor currents

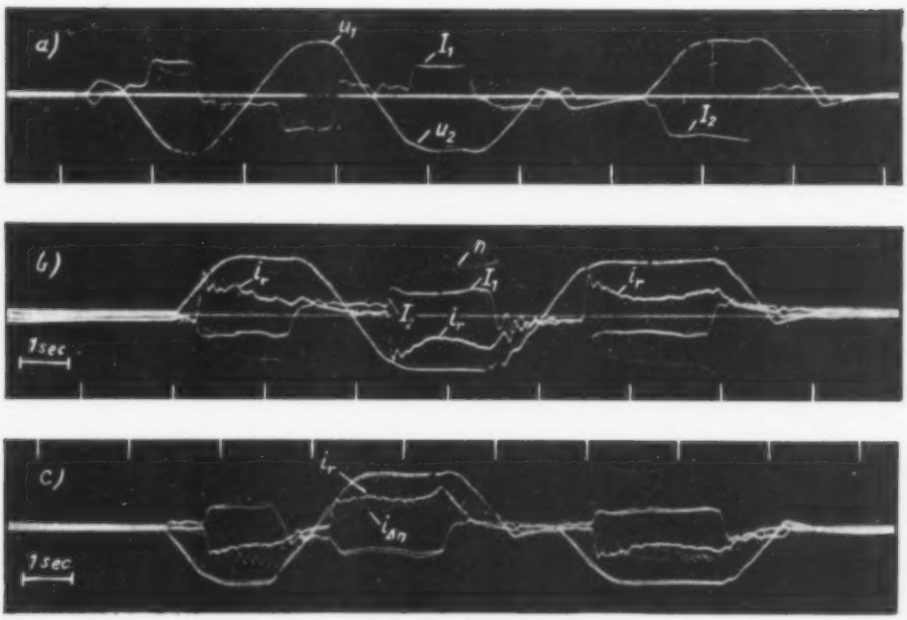

FIG. 8. Oscillogram of rolling operation on the 2800 mill after modernization. a - regulator disconnected b - regulator connected, but without the winding speed balancing c - regular connected with all its windings. U_1, U_2 - generator voltages; I_1, I_2 - motor currents; I_r - armature current of the amplidyne (regulator current) $i_{\Delta n}$ - current of the windings of the amplidyne AR connected to the difference of the tachogenerator voltages; n - motor speed.

during the rolling are sufficiently close together. The largest discrepancy between I_1 and I_2 is observed immediately after the gripping of the metal by the rolls, which is explained by the difference in speed between the upper and the lower roll during gripping. The regulator current i_r caused by the difference of the motor currents rises fairly steeply and leads to the balancing of the loads.

Fig. 8c shows the operation of the system with the regulator in action, all its windings being connected. It can be seen that as a result of the action of the windings responding to the difference of speeds (current $i_{\Delta n}$ shown) the generator voltages U_1 and U_2 differ very little in no-load conditions and, consequently, the difference of speeds and the difference of the motor currents I_1 and I_2 is negligible.

The increase of the difference of the currents in steady-state conditions of rolling, caused by the effect of the speed-balancing windings is small and does not impair its positive effect under other conditions.

The results of the analysis of the control system of the rolling mill with independent drives of the rolls, the tests of the component circuits and also the experience with the modernization of the electric drive of the rolling mill 2800 at the Voroshilovsk works enable the new system to be recommended for newly planned or

reconstructions of existing rolling mills. The replacement of stabilizing transformers by differential-bridge circuits simplifies the control system and can improve the transient (dynamic) features of certain types of drives.

REFERENCES

1. O.V. Slezhanovskii; *Analysis of control systems of blooming mills by means of drooping characteristics. Elektrichestvo*, No. 3, (1953).
2. O.V. Slezhanovskii, *Analysis of the control system of a reversing rolling mill. Elektrichestvo*, No. 5, (1955).
3. V.V. Imedadze; *Investigation of systems of automatic regulation and control of the auxiliary mechanisms of blooming mills and large excavators*. Thesis (1953). *Lenin Library*.
4. A.G. Efanov,and Yu.R. Reungol'd, *Electric drives of large excavators. Elektrichestvo*, No. 4, (1956).

1958

INVESTIGATION OF OVER-VOLTAGES DUE TO ARCING EARTH-FAULTS IN 6-10 kV SYSTEMS WITH INSULATED NEUTRAL *

N.N. BELYAKOV

(Received 4 September 1956)

The mechanism of the formation of over-voltages at arcing earth-faults in systems with insulated neutral or neutral earthed across high active or inductive resistance and the possible magnitude of these over-voltages is still not sufficiently known. It is believed that arcing fault over-voltages can reach 4-5 times the phase voltage and perhaps more.

In the power systems of the Soviet Union the over-voltages due to arcing earth faults are considered to be harmless for normal insulation i.e. insulation that withstands operational test voltages [1]. Actually, experience shows that with systematically conducted prophylactic tests and with planned routine maintenance of the system earth-faults on one phase are not followed by faults on the other phases. But deductions of the magnitude of the over-voltages from the puncture or flashover voltages of the insulation require caution. A wrong opinion of the magnitude of the over-voltages and their increased danger may be formed in poorly insulated systems, tems, especially cable systems in the absence of prophylactic tests [3].

The principle of the formation of the over-voltages during arcing was discovered by Petersen [4] who also estimated the maximum magnitude with consideration of the majority of the influencing factors including phase to phase capacitance and attenuation.

The behaviour of the arc is important, especially the moment of restrike and extinction, for a realistic estimate of over-voltages. The theories of the formation of over-voltages through arcing earth-faults put forward by different authors [4-7] are based on different assumptions of the arc properties. Petersen assumes that the arc extinguishes at the zero passage of the current of the natural oscillations ($i_{osc} = 0$) and strikes again at the next maximum of the power frequency voltage. Such idealization of the arc properties gives the severest possible conditions and therefore the upper limit of the over-voltages obtained by Petersen is doubtless correct.

* *Elektrichestvo* No.5, 31-36, 1957 [Reprint Order No. EL 20].

But none of the proposed theories has been verified by tests. One can often find in oscillograms the extinction of the arc in accordance with Petersen's theory ($i_{osc} = 0$) or with that of Peters-Slepian (at zero passage of the power frequency current i_p). For example oscillogram in Fig. 1 shows that the arc extinguishes several times at $i_p = 0$ (points 1, 3, 6), once at $i_{osc} = 0$ (point 5). Besides that extinctions after zero passage of the oscillating current are observed (point 4).

Thus the forms of behaviour of the capacitive arc are manifold. And the existing theories do not explain the phenomena actually occurring. The laws governing the extinction of the intermittent arc remain unexplained.

Ch. M. Dzhubarly did not obtain over-voltages exceeding 3 U_{ph} [8] in tests carried out at the TsNIEL, but his theoretical explanation of the limitation of the arc over-voltages is not convincing.

The purpose of the present article is to determine the properties and the behaviour of the capacitive arc in 6-10 kV systems from systematical tests and to establish the over-voltage level on the basis of these data.

1958

Arc and over-voltage tests were made on system models with lumped capacitances. The basic 6 kV system was supplied through a 5600 kVA transformer 35/6 kV. Tests were also made in a 6 kV cable system without load.

The models permitted a variation of the test conditions over a wide range and the obtained over-voltages include a certain margin since in actual system condition the distributed capacitance and the attenuation will further reduce the over-voltages.

Greatest attention was given to systematical tests of the arc in air, drawn out by an isolator. Other tests were made with the arc across a pin-type insulator, in the slot of a machine, in a cable, under oil, in a cable joint, etc.

The extinction conditions of the capacitive arc

The character of the recovery of the voltage in capacitive circuits has a strong effect on the arc behaviour. The phenomena connected with the extinction of the capacitive arc may be considered for the case of the single-phase circuit, Fig. 2a.

The voltage at the unfaulted capacitance may be U_0 at the moment of zero passage of the current, when extinction takes place. After extinction the system neutral is displaced by the voltage value $U_{dis} = \frac{1}{2} U_0$. The voltage of the system generator is superposed to this. But the transition from the original condition ($U_f = 0$) to this new condition takes place in form of the extinction oscillations with the frequency $\omega_{osc} = 1/\sqrt{LC/2}$. In half a cycle of such oscillation ($T_{osc}/2$) after the zero passage of the current, the voltage across the arc gap reaches its first high-frequency maximum U_{om} (Fig. 3). The voltage reaches its second

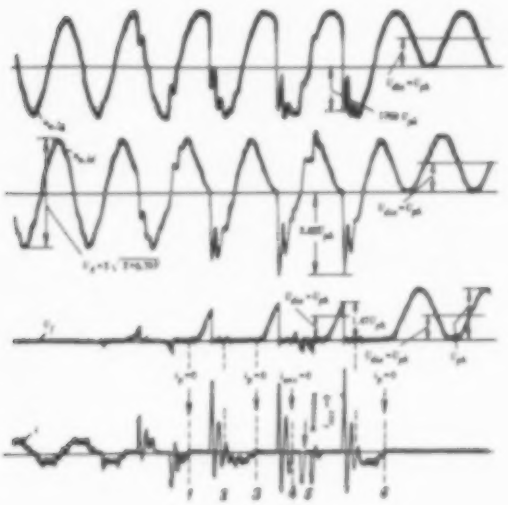

FIG. 1. Earth-fault in a three-phase system with insulated neutral.

Voltage 6 kV, Capacitive earth fault current $I_c = 105$A, phase-earth capacitance $C = 28.8\ \mu$ F, phase-phase capacitance $C_m = 0$. Transformer 5.6 MVA, 35/6 kV.
u_a, l_g voltage of the unfaulted phase, lagging behind
u_b, l_d - voltage of the unfaulted phase, leading the faulty phase.
u_f - voltage of the faulty phase.
i - arc current.

maximum as a result of the change of the generator voltage of power frequency.

The magnitude of the high-frequency maximum of the restriking voltage equals twice the difference between the displacement voltage and the phase voltage

$$U_{om} = 2\,(U_{dis} - U_{ph}) \tag{1}$$

Fig. 2a, shows that the voltage on the capacitance of the unfaulted phase at the moment of arc extinction differs from the generator voltage by the voltage drop across the inductance of the circuit, therefore

$$U_{dis} = \frac{U_0}{2} = \frac{2U_{ph} + L\left(\frac{di}{dt}\right)_{i=0}}{2}.$$

Substituting U_{dis} in (1) we obtain

$$U_{om} = L\left(\frac{di}{dt}\right)_{i=0}, \tag{2}$$

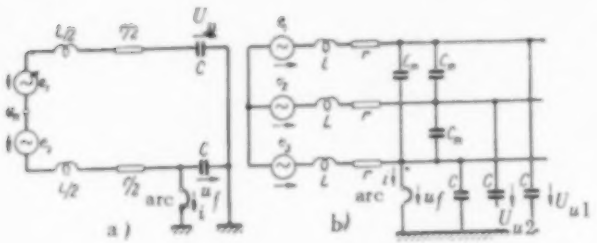

FIG. 2. Circuit diagram of the system with insulated neutral.
a - single-phase. $e_1 = U_{ph} \sin(\omega t + \psi)$ $e_2 = -U_{ph} \sin(\omega t + \psi)$
b - three-phase. $e_2 = -U_{ph} \sin(\omega t + \psi)$ - e.m.f. of faulty phase.
$e_1 = -U_{ph} \sin(\omega t + \psi - 120^0)$.
$e_3 = -U_{ph} \sin(\omega t + \psi + 120^0)$ - e.m.f. of the unfaulted phase.

i.e. the high frequency maximum of the restriking voltage equals the inductive voltage drop of the circuit at the moment of zero passage of the current. The relation (2) remains correct at any phase of the e.m.f. of the generating source at the extinction moment.

The recovery of the voltage after extinction of the earth-fault arc in a three-phase system with insulated neutral (Fig. 2b) has also the character shown in Fig. 3.

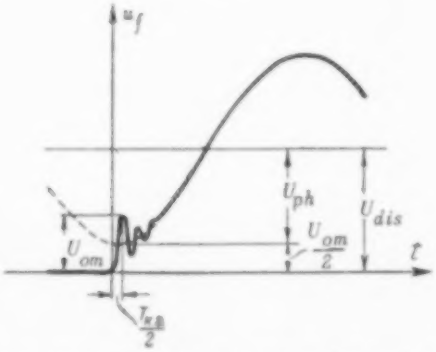

FIG. 3. Recovery of the voltage on the faulty phase after extinction of the capacitive current.

A more thorough examination of the arc extinction process by means of c.r.o. permitted to establish the following essential fact: The extinction of an open capacitive earth-fault arc takes place at each zero passage of the current but the arc strikes again within a small fraction of the natural oscillation cycle. The formation of the arc takes place following the breakdown of the gap before the first maximum (Fig. 4, points 1 - 5). With a large rate of rise of current this breakdown takes place long before the restriking voltage has reached its first maximum. This breakdown voltage may be designated as U_{bd}. The existence of the extinction and the rapidly following restrikes is also ahown by the fact that the current in the

oscillograms in every new half-cycle of the h.f. oscillations has a steep front which is explained by the surge of the discharge current of the capacitance of the faulty phase.

The conditions where the capacitive arc extinguishes after a long time interval (after a greater part of the power frequency cycle) are of major interest. Experiments show that this type of extinction is possible only when the first maximum of the restriking voltage does not exceed a certain critical value:

$$U_{om} \leq U_{cr} \tag{3}$$

This critical value U_{cr} obviously depends on the dielectric strength of the gap for the time interval of one half-cycle of the natural oscillations. If the condition (3) is not fulfilled the extinction is not achieved, i.e. the arc strikes again (Fig. 5).

In order to determine the numerical value of the critical voltage U_{cr} from the oscillograms it is necessary to determine the magnitude of U_{om} or U_{bd} for every passage of current zero. Fig. 6 shows the distribution of the frequency of occurrence of these values in general for all capacitive currents since the magnitude of the current has practically no effect on this distribution. The maximum values of U_{om} and U_{bd} differ only slightly from each other and it is possible to ascribe a common upper limit of 1800 V for both. This limit determines also U_{cr}.

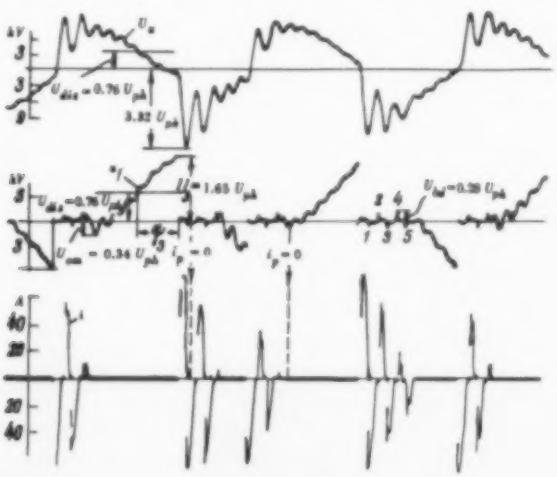

FIG. 4. Arcing earth-fault in the single-phase circuit with insulated neutral.
Arc on the isolator, $I_c = 4.4$ A, $C = 2\ \mu$F, $C_m = 0$,
Transformer 5.6 MVA, 35/6 kV.

The experiments show that the velocity of drawing out the arc with the iso-

lator affects only the rise of the restriking voltage but not the extinction conditions. The fact that the current magnitude and the velocity of drawing out the arc have no effect on the extinction conditions of the capacitive arc is explained by the same growth in electrical strength of the gap in all cases during the short time intervals which possibly indicates the importance of the electrode effects and the thermal inertia of the arc column. All oscillograms with relatively high values of U_{om} and U_{bd} were used in the analysis of the test results. Besides that our distribution contains oscillograms of which more than 12,000 extinctions have been recorded with values of U_{om} and U_{bd} below the obtained maximum.

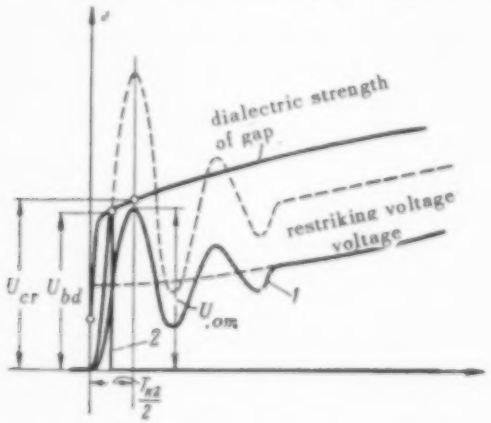

FIG. 5. Extinction and restriking of the arc. 1 - extinction achieved, 2 - extinction not achieved.

The task is to determine the upper limit U_{cr}. Therefore, one has to set out from the minimum oscillating frequency possible in practice. The above value of U_{cr} was obtained from tests in which this frequency was reduced down to $\omega_{osc} = 5\ \omega$ although in actual systems this value is ten times the power frequency or more.

The above value of U_{cr} is $0.37\ U_{cr}$ for 6 kV and $0.22\ U_{ph}$ for 10 kV systems. For simplification of the calculations and also for inclusion of some margin in the estimate of the possible over-voltages we assume for 6 and 10 kV systems $U_{cr} = 0.4\ U_{ph}$ *

We see that

$$U_{om} \leq 0.4\ U_{ph} \qquad (4)$$

The tests with the arc across a pin-type insulator, in the machine insulation, in a cable, under oil and in a cable joint give a relation between U_{om} and U_{ph} close to that obtained with the arc across the isolator. Therefore, the magnitude of the h.f. maximum of the restriking voltage U_{om} remains the limit under different conditions of striking the arc and the maximum over-voltages are the same as with the arc across the isolator.

The arc in the cable and in the machine insulation has a low striking voltage

* Our rounding off means in the case of 10 kV systems an increase in the over-voltage magnitude of 3%.

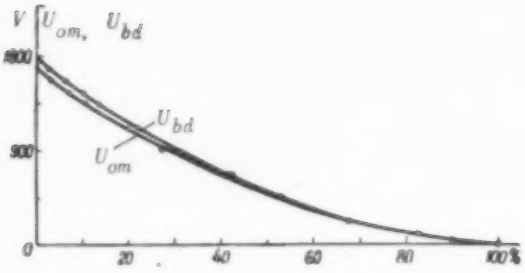

FIG. 6. Distribution curve of the values of U_{om} and U_{bd} (plotted on the basis of 2800 extinctions).

($U_s < U_{ph}$) and its magnitude hardly changes while the arc is burning. The arc can stay for a very long time.

Maximum over-voltages

The important value of the displacement voltage U_{dis} of the neutral (the general potential of the system with respect to earth after arc extinction) is limited owing to the limitation of the voltage U_{om}. Actually Fig. 3 shows that

$$U_{dis} = U_{ph} + \tfrac{1}{2} U_{om} \tag{5}$$

and since $U_{om} \leq 0.4\, U_{ph}$, that always

$$U_{dis} \leq 1.2\, U_{ph} \tag{6}$$

Equations (5) and (6) are valid for single-phase and three-phase systems. The magnitude of the over-voltages can be determined from the formula

where
$$U_{max} = U_{fin} + (U_{fin} - U_{in}) \frac{C}{C + C_m}(1 - d), \tag{7}$$

U_{fin} and U_{in} are the final and initial voltages;

C and C_m are the phase-earth and phase-phase capacitances

$\frac{C}{C + C_m}(1 - d)$ -- is the coefficient taking account of the decrease in amplitude owing to phase-phase capacitance and attenuation.

The tests show that the main cause of attenuation is not the loss in the arc, as it was considered to be by some investigators [8], but the losses in the other parts of the circuit. With metallic fault connection no decrease of the attenuation was observed as compared with the intermittent arc. With the drawn out arc the arc

voltage drop was very often considerably smaller than the source-voltage (50 - 100 V against 6000 V) even up to the moment of final extinction. Thereby the coefficient $(1-d)$ may be about 0-98 - 0.99 [7, p. 530]. During the tests on the models the highest value of $(1-d)$ was 0.9. This value should be taken for the determination of the maximum over-voltage since the attenuation in actual systems is even greater.

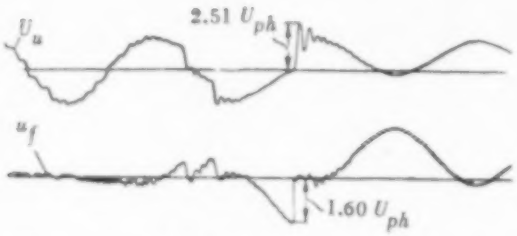

FIG. 7. Arcing fault in a single-phase system with insulated neutral (arc under oil).
$I_c = 11$ A, $C = 5\ \mu$F, $C_m = 0$. Transformer 3.2 MVA, 35/6 kV; u_u voltage of the unfaulted phase, u_f voltage of the faulty phase.

The tests show that restriking can take place at any moment including the moment for which the over-voltage becomes highest.

Thus, knowing the magnitude of the displacement voltage and the attenuation coefficient and assuming that the restriking takes place at the moment which produces the highest over-voltage, one can determine the maximum over-voltage.

Assuming that restriking takes place at the moment of maximum e.m.f. of the faulty phase with the same sign as the displacement voltage we obtain for the single-phase circuit and for $C_m = 0$

$$U_{in} = U_{ph} - 1{,}2U_{ph} = -0{,}2U_{ph}$$

and

$$U_{max} = 2U_{ph} + [2U_{ph} - (-0{,}2U_{ph})]\,0{,}9 \approx 4U_{ph}$$

Applying (7) to the three-phase circuit we consider that the e.m.f. of the faulty phase changes according to the law $e_f = -U_{ph} \sin(\Omega t + \psi_s)$ whereby the time is counted from the moment of restrike. We determine the magnitude of the positive over-voltage on the unfaulted phase ($U_{max} > 0$) which is lagging behind the faulty phase. Considering that for the formation of such over-voltage the restrike must occur with negative e.m.f. of the faulty phase and that with a negative displacement voltage ($U_{dis} < 0$) we obtain

$$U_{inv} = -U_{ph}\sin(\psi_3 - 120°) + U_{dis} =$$
$$= U_{ph}\cos(30° - \psi_3) + U_{dis}$$
$$U_{fin} = \sqrt{3}U_{ph}\sin(\psi_3 + 30°);$$
$$U_{max} = \sqrt{3}U_{ph}\sin(\psi_3 + 30°) + \quad (U_{ph}\sin\psi_3 - U_{dis})\,\frac{C}{C + C_m}(1 - d). \qquad (8)$$

The maximum over-voltage occurs on restrike at

$$\psi_s = \tan^{-1}\left[\frac{2}{\sqrt{3}}\frac{C}{C+C_m}(1-d)+\sqrt{3}\right].$$

With $C_m = \frac{1}{3} C$, which is characteristic for 6-10 kV cable systems and $(1-d) = 0.9$ and more, the maximum over-voltage would occur on restrike at $\psi_s = 68°$, i.e. when restriking occurs somewhat before the maximum of the voltage. Substituting in (8) the values: $(1-d) = 0.9$, $C = 3C_m$, $\psi_s = 68°$ and $U_{dis} = -1.2\ U_{ph}$, we obtain for the maximum overvoltage:

$$U_{max} = 3.2\ U_{ph}.$$

On the faulty phase the over-voltage may reach the value:

$$U_{max,f} = U_{dis} + U_{ph} = 2.2\ U_{ph}.$$

The formation of the maximum over-voltage in a three-phase system is illustrated in Fig. 8.

For verification of the calculated maximum over-voltage mass observations were made with c.r.o. with very small time scale. An oscillogram thus obtained in a single-phase circuit is shown in Fig. 9.

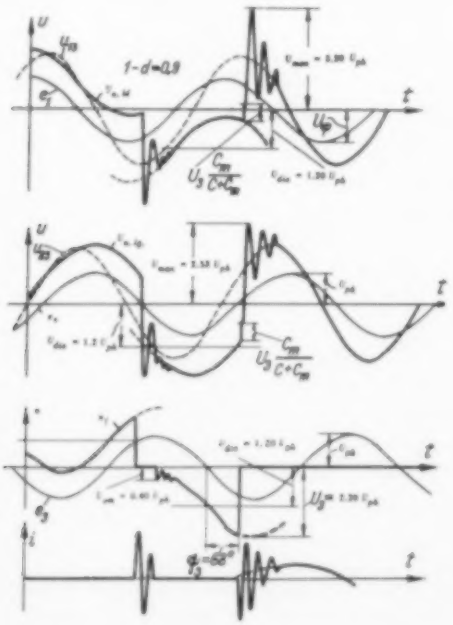

FIG. 8. Formation of the maximum possible over-voltage in a three-phase system with insulated neutral.
Symbols (u_u, $lg\ u_u$, ld, u_f, i) as in Fig. 1.

The calculated and measured over-voltage values for the three-phase circuit are given in the table, which shows that the measured values are in good agreement with the calculated ones. The maximum over-voltages are practically independent of the capacitive current and are relatively rare since several conditions must coincide for their formation.

		$I_c = 7.5$ A $C = 2\mu$F		$I_c = 23$ A $C = 6\mu$F		$I_c = 45$ A $C = 12\mu$F		$I_c = 100$ A $C = 30\mu$F		
Calculated Values	C_m μF	U_{max}	$U_{max,f}$	U_{max}	$U_{max,f}$	U_{max}	$U_{max,f}$	U_{max}	$U_{max,f}$	Number of faults
3.62	0	3.45	2.00	–	–	–	–	–	–	200
3.62	0	–	–	3.30	2.02	–	–	–	–	100
3.20	2	–	–	2.91	2.15	–	–	–	–	200
3.62	0	–	–	–	–	3.50	2.10	–	–	200
3.20	4	–	–	–	–	3.05	2.14	–	–	300
3.62	0	–	–	–	–	–	–	3.44	2.12	100

1958

The actual mechanism of the formation of the over-voltages

Extinction takes place when the h.f. maximum of the restriking voltage is sufficiently small and therefore also the rate of change of the current is sufficiently small at the zero passage. This is the case for the first zero of the oscillating current (usually with small striking voltage) and after some attenuation of the transient process. Arc extinction is also possible after transition of the oscillating current into the power frequency current, especially when the latter goes through zero.

For the formation of the maximum over-voltage it is not necessary to have a number of restrikes. Therefore, it is sufficient for its determination to consider one cycle extinction-restrike. In that cycle the extinction must take place at the moment of maximum e.m.f. of the faulty phase and at the maximum rate of change of the current permitted for the extinction, and the following restrike must occur somewhat before the voltage peak. The cause of the often observed increase of the over-voltage towards the end of the arcing time is not the cumulative effect (i.e. the increase of the displacement voltage) but the gradual increase of the striking voltage owing to the increased arc length.

The increase of the displacement voltage of the neutral is connected with the simultaneous increase of the h.f. maximum of the restriking voltage. The actual arc gap cannot withstand a rapid increase of the restriking voltage so that the possible maximum of the oscillation is limited and consequently also the displacement voltage. Thus, the limit to the over-voltage is set by the finite and relatively low electric strength of the arc gap which by the very nature of the phenomenon

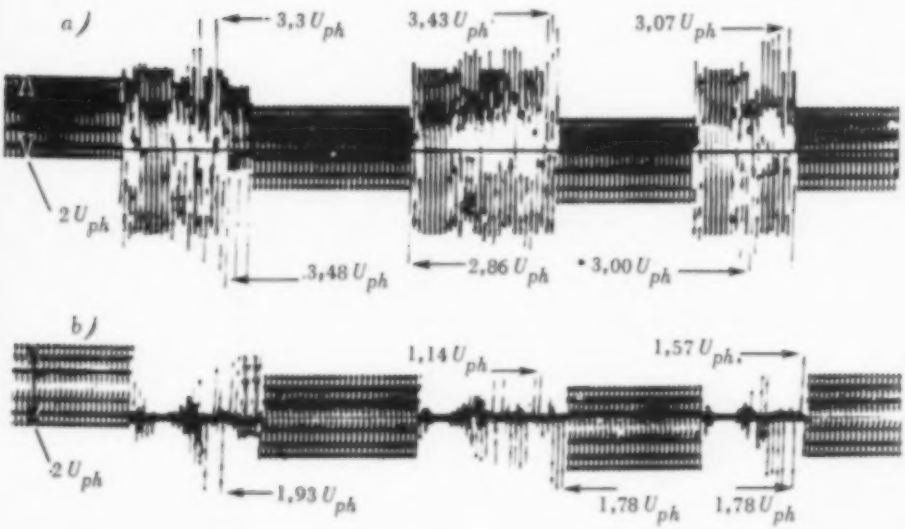

FIG. 9. Values of the over-voltages in the single-phase circuit with insulated neutral. $I_c = 55$ A, $C = 25.3\ \mu F$, $C_m = 0$. Transformer 3.2 MVA, 35/6 kV. a - voltage of the unfaulted phase, b - voltage of the faulty phase.

cannot de-ionize instantly.

The attenuation coefficient (1 - d), obtained in a cable system of 6 kV, with load, is 0.7 - 0.75. It is naturally smaller than on the model. The resistance of the current path of the natural oscillations has a strong effect on the attenuation in actual systems. The effect can be so strong that the actual system may be incapable of oscillating. This is the case when the earth-fault in a system with high capacitive current occurs at a point remote from the centre. This is illustrated by the oscillogram, Fig. 10, *) obtained in a system with a capacitive earth-fault current of 100 A. The earth-fault occurred at a point in the system remote from the supplying busbars. The transient process after striking is aperiodic. The voltage of the unfaulted phase did not exceed the phase-earth voltage, i.e. over-voltages did not occur.

Conclusion

The laws governing the extinction of the intermittent earth-fault arc and the possible magnitude of the over-voltages under different conditions of the arc (including different system voltages) are found by determination of the electric strength of the arc gap immediately after extinction and its comparison with the magnitude of the h.f. maximum of the restriking voltage.

* The oscillogram was kindly offered by F.A. Likhachev (ORGRES).

The extinction of the capacitive arc is not controlled by the frequency of the natural oscillations nor by the power frequency. Extinction takes place if the h.f. maximum is below a certain value. The extinction conditions set a limit to the displacement voltage of the neutral.

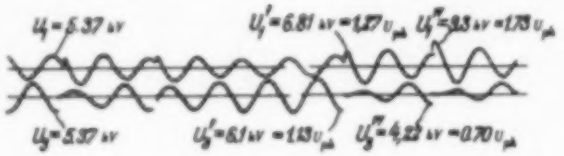

FIG. 10. Arc fault on an insulator in a compensated system, 6 kV, with load.
U_1 voltage of the unfaulted phase, U_3 voltage of the faulty phase. Degree of mistuning $v = -9$ per cent. Earth fault current $I_e = 9.6$ A.

Since the check tests under different conditions of arc formation agree with the results of arc tests on an isolator, a general conclusion can be drawn on the magnitude of the over-voltages caused by earth-fault arcs in 6 - 10 kV systems with insulated neutral. The maximum values of these over-voltages do not exceed 3.2 U_{ph} and they are not directly dependent on the magnitude of the capacitive current. They occur relatively rarely since for their formation several conditions must be fulfilled simultaneously. With large capacitive currents the arc may remain more stable and thus reduce the over-voltages.

The author is indebted to V.V. Burgsdorf for a number of valuable suggestions in the preparation of the present article.

REFERENCES

1. *On the operating conditions of the neutral earthing and the protection against earth-faults in 6 - 35 kV systems. A solution of the Technical Department of the Ministry of Electric Power Plants*, No. 89/3 of 28.5.1949. *Elekt. Stantsii*, No. 10, (1949).
2. I.A. Syromatnikov; *Operating conditions of the system with small earth-fault currents. Elekt. Stantsii*, No. 2, (1951).
3. N.N. Belyakov; *Analysis of damage from earth-faults in cable systems. Elekt. Stantsii*, No. 6, (1952).
4. W. Petersen; *Der aussetzende Erdschluss. ETZ*, No. 47, 553, No. 48, p. 564, (1917).
5. J.F. Peters, J. Slepian; *Voltages induced by arcing grounds, Trans. AIEE*, p. 478, (1923).
6. P. Steinmetz; *Frequency conversion by arcing class conductor and mechanism of the arcing ground. Trans. AIEE*, p. 470, (1923).
7. R. Rudenberg; *Transient processes in electric power systems. Izdatel'stvo inostrannoi literatury*, (1955).
8. Ch. M. Dzhuvarly; *On the theory of over-voltages from earth-fault arcs in systems with insulated neutral. Elektrichestvo*, No. 6, (1953).

1958

ARC-QUENCHING PROCESSES IN AIR-BLAST CIRCUIT-BREAKERS*

V. GUSA and Ya. TSIGELKA

(Received 1 August 1956)

The increasing powers of modern electrical systems account for a corresponding increase of the breaking capacity of the h.v. circuit-breakers, particularly the air-blast breakers, the use of which is spreading all the time. The present communication proposes to investigate the factors influencing the quenching of the arc in air-blast circuit-breakers and the practical methods available for increasing the breaking capacity of these breakers.

The experiments were carried out on circuit-breakers of type SR, rated at 10 kV. The design of the quenching arrangement of this breaker type is shown in Fig. 1 and the main parameters given in the following Table.

Breaker type	Rated air pressure abs. atm.	Nozzle diameter (d) mm	Travel of moving contacts. (l) mm
SR205 – 10/600	12	22	185
SR405 – 10/600	12	35	210
SR605 – 10/600	21	45	225

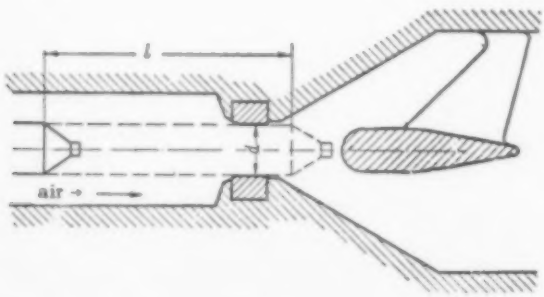

FIG. 1.

* *Elektrichestvo* No. 5, 37-39, 1957 [Reprint Order No. EL 21].

Tests on the clearance of single-phase short-circuits, carried out at 9 kV and at a frequency of the restriking voltage of 4.5 kc/s produced results which can be represented by the following empirical formula,

$$I_{sh} = 5.35\, p^{0.30} F^{0.34}, \qquad (1)$$

where, I_{sh} is the amplitude value of the limiting short-circuit current cleared, kA;
p the air pressure in the air receiver of the circuit-breaker, abs. atm.;
F cross-sectional area of the nozzle, cm².

This relationship is graphed for the pressures of 12 and 21, abs. atm. in Figs. 2 and 3.

The limiting breaking current, represented by (1) corresponds to the current at which the nozzle of the breaker is pluged by the thermal energy evolved by the

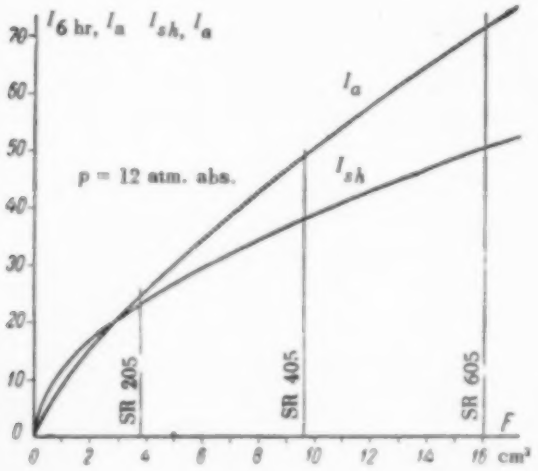

FIG. 2.

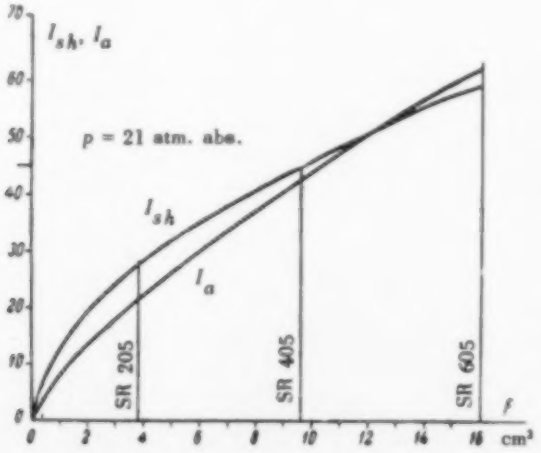

FIG. 3.

arc. This phenomenon is generally interpreted in the following way.

Evolution of heat by the arc reduces, as it were, the cross-section of the nozzle, this reduction of the effective cross-section being the greater, the higher the current passing through the circuit breaker. The reduction of the cross-section of the nozzle entails a corresponding reduction of the air supply for arc quenching, so that at a certain magnitude of the short-circuit current the circuit breaker will no longer be able to interrupt this current; in other words, the nozzle of the circuit-breaker is plugged.

It is clear that for equal values of the breaking-current the phenomenon of nozzle-plugging will be more marked at smaller nozzle diameters, i.e. smaller nozzle diameters will reduce the breaking capacity of the given circuit-breaker.

However, experiments showed that the magnitude of the limiting breaking current does not always correspond to the volume given in (1). For example, a breaker of type SR205 at pressure 21 abs. atm. of the quenching air can interrupt a current of 42 kA as against 19.5 according to (1).

To find the causes of this surprising increase of the breaking current during the circuit-breaker tests, we carried out measurements of the voltage drops in the arc. These measurements showed that for the short-circuit current of 30 kA the voltage drop in the arc after the zero-passage of the current begins to rise steeply, falling again with similar abruptness after reaching a certain value, to rise again only immediately before the end of the half-period of the current curve (Fig. 4,a). At a current of 15 kA there are no such "breaks" in the curve of the voltage in the arc (Fig. 4,b). This phenomenon may be interpreted as follows. At every instant the diameter of the arc depends on the current in the arc at that instant and so long as the arc diameter is small, the arc will burn, being drawn out to a comparatively great length (Fig. 5,a). The voltage drop in the arc will then have a certain value. When the current increases, there will be an instant at which the actual diameter becomes equal to the diameter of the nozzle, in this case the length of the arc is considerable reduced and the arc fills out completely the nozzle opening. This is the instant at which the nozzle is plugged by the arc column (Fig. 5,b). This causes a considerable decrease of the voltage drop in the arc.

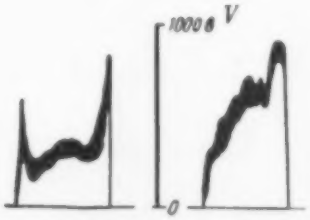

FIG. 4.

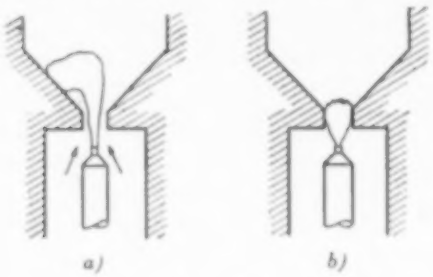

FIG. 5.

Later on the current, having passed through its peak value, falls with a simultaneous reduction of the diameter of the arc column and at a certain value of the current the arc diameter becomes again smaller than the diameter of the nozzle opening. At this instant the air pressure detaches the arc from the walls of the nozzle and draws the arc out; the voltage drop in the arc increases again.

The plugging of the nozzle interrupts the air flow, as the result of which the pressure of the air before the nozzle increases to the value of the pressure in the air receiver. The great difference of the pressures before and behind the nozzle quickly restores the maximum velocities of the air flow once the nozzle is free again, which leads to rapid arc-quenching.

We find, therefore, that the plugging of the nozzle by the arc column is a positive factor acting towards an increase of the limiting breaking-current. It is by this phenomenon that we can explain the increase of the limiting breaking current of the circuit breaker type SR205 at the pressure 21 abs. atm. as against the value obtained from (1).

On the other hand, we have to consider that at an increase of the short-circuit current the time interval between nozzle opening and zero-passage of the current is reduced which, in the last result prevents the velocity of the air flow from reaching the values required for arc-quenching, so that the circuit-breaker can no longer clear the short-circuit currents.

Let us analyse the phenomenon of the nozzle-plugging by the arc column. We assume that the arc is a cylindrical absolutely black body whose temperature, and consequently, charge density is constant over the cross-section. The stage of ionization of the gas in the column may be expressed in Saha's equation

$$\frac{x^2}{1-x^2} \cdot p = 3.2 \cdot 10^{-7} T^{2.5} e^{-\frac{\epsilon E_i}{kT}}, \qquad (2)$$

where x is the stage of ionization of the gas;
p the gas pressure, abs. atm.;
E_i the ionization potential, V;
T the temperature, °K;
ϵ the electron charge, coulomb;
k Boltzmann's constant.

In (2) the quantity x^2 may be neglected against unity. The justification of this assumption will be shown below. The relation between the stage of ionization and the current density in the arc may be found from the following equations

$$x = n/N \text{ and } n = j/\epsilon E b^-$$

where n is the number of electrons in 1 cm³ of gas;
N the initial number of neutral atoms in 1 cm³;
j the current density in the arc;
E the electric gradient in the plasma;
b the electron mobility.

Remembering that,

$$b^- = \sqrt{\frac{T}{T_0}} \cdot \frac{p_0}{p} b_0^- \quad \text{и} \quad N = \frac{T_0}{T} \cdot \frac{p}{p_0} N_0,$$

where $P_0 = 1$ abs. atm.;
$T_0 = 273°K$;
$b_0 = 5.9 \times 10^3$ cm²/V. sec;
$N_0 = 2.7 \times 10^{19}$ 1/cm³, or considering that for nitrogen $\epsilon E_i/k = 1.68 \times 10^5$ we get after rearrangement the equation of the arc current, viz

$$I_\partial = 238 \cdot EF \frac{1}{\sqrt{p}} T^{0.75} e^{-\frac{8.4 \cdot 10^4}{T}} \tag{3}$$

where F is the cross-section of the arc in cm².

The energy radiated from the surface corresponding to unit length of the arc is determined by Stephan-Boltzmann's law on the assumption that convection at high temperatures is so insignificant as against radiation, that it may be neglected, viz.

$$EI_\partial = CT^4 \cdot \pi d \cdot 10^{-7} = 2CT^4 \sqrt{\pi F} \cdot 10^{-7}, \tag{4}$$

where d is the diameter of the arc in cm;
$C = 5.73 \times 10^{-8}$.

Considering that the arc current $I = jF$ and solving simultaneously equations, (3) and (4) we get

$$I_\partial = 6.94 \cdot 10^{-5} p^{-0.25} F^{0.75} T^{2.375} e^{-\frac{4.2 \cdot 10^4}{T}}. \tag{5}$$

The results of measurements carried out on a circuit-breaker of type SR205 at a pressure of the quenching air of 21 abs. atm., showed that the plugging of the nozzle by the arc column occurs at the instant at which the instantaneous value of the short-circuit current is 21.2 kA. Assuming that up to the instant of complete plugging of the nozzle the air pressure before the nozzle rises to the value of the pressure in the air receiver of the circuit-breaker, i.e. that $p = 21$ abs. atm., and that the section of the arc is then equal to the section of the nozzle i.e. $F = 3.8$ cm² we find from (5) that the arc temperature equals 13070°K.

Since we may assume that the temperature of the free arc is independent of the value of the arc current, we find by substituting the above value of the temperature into (5) the following relationship between arc current, its cross-section F and the pressure of the quenching air, p

$$I_a = 16.65.p^{-0.25} F^{0.75}$$

This relationship is plotted in Figs. 2 and 3 for the pressures 12 and 21 abs. atm.

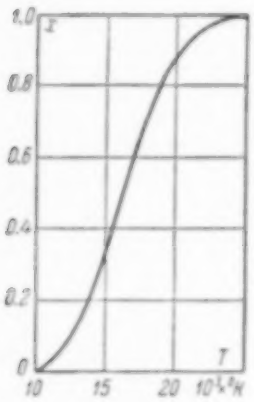

FIG. 6.

From Fig. 6 we can determine that for nitrogen at the temperature $T = 13070$°K the degree of ionisation $x = 0.117$. It follows that our assumption of the smallness of x^3 in equation (2) by comparison with unity is justified.

Fig. 2 also shows that for sections smaller than 12 cm² curve I_a is below curve I_{sh}. This means that for these cross-sections the plugging of the nozzle of the circuit-breaker by the arc column precedes the clearance of the short-circuit current. In the range of cross-sections greater than 12 cm², curve I_a is above the curve I_{sh}. This indicates that within this range no plugging of the nozzle by the arc colum takes place.

1958

From Fig. 2 follows furthermore, that the cross-section of the nozzle of the circuit-breaker SR205 falls into the range where the phenomenon of plugging of the nozzle by the arc column takes place. For a nozzle corresponding to that of the circuit-breaker SR405 the difference between the currents at which either plugging of the nozzle by the arc column or plugging by the effect of the heat liberated in the arc takes place, becomes insignificant and the short-circuit current is, therefore, determined by the curve I_{sh}. The cross-section of the circuit-breaker SR605 falls into the range of plugging of the nozzle as an effect of the heat evolved by the arc.

In the light of the various phenomena of plugging of the nozzle of the circuit-breaker considered here the pressure of the quenching air has an effect in the following direction. With increasing air pressure the point of intersection of the curves I_{sh} and I_a shifts towards the range of larger sections of the nozzles and the distance between these curves on the left and their point of intersection increases (Fig. 2 and 3). Consequently, in this range of sections the conditions of arc-quenching improve. This fact explains, in particular, the comparatively greater increase of the breaking capacity of the circuit-breaker type SR205 when the pressure is increased from 12 to 21 abs. atm. than is obtained for the circuit-breakers of types SR405 and SR605.

We may conclude from the above fact that the density of circuit-breakers should select its parameters with a view to obtaining plugging of the nozzle of the breaker by the arc column before the nozzle is plugged by the heat liberated in the arc. It must also be borne in mind that during the plugging of the nozzle by the arc column that the nozzle itself is scorched. For this reason an arc-quenching device in which the nozzle represents simultaneously one of the circuit-breaker contacts is unsuitable. In particular, the experimental part of the present study which was carried out on circuit-breakers with such a nozzle designed (Fig. 1). The deterioration of the contact characteristics by the clearance of a particularly high short-circuit-current may be of such an order that on the subsequent closing of the breaker no sufficiently reliable contact-making can be achieved. The design of the quenching device should be such that the nozzle serves exclusively the purpose of arc-quenching. A further indispensible condition is that the arc route should, right from the beginning, be situated in the critical cross-section of the model.

In the case that the section of the arc increases to a value equal to the cross-section of the nozzle and the current still continues to rise, the arc can no longer increase its section with increasing current. Owing to this, the current density rises as well as the degree of ionization and, as follows from equation (5), so does the arc temperature. For exactly this reason stabilized electric arcs used for a number of scientific investigations have higher temperatures than the arcs in circuit-breakers.

DETERMINATION OF THE IN-FEED CURRENTS (FROM INDUCTION MOTORS) TO SHORT-CIRCUITS IN LOW-VOLTAGE SYSTEMS *

M.O. KAMENETSKII

(Received 28 May 1956)

1958

It is a peculiarity of the short-circuit conditions in power systems operated at voltages below 1000 V that when the voltage falls induction motors send for a certain time current to the point of the fault; this has become known as "in-feed current from induction motors".†

This peculiarity is not fully considered by the methods of short-circuit current calculations in h.v. systems. The determination of the in-feed currents from the induction motors was therefore based on various recommendations, so that they are determined in very many different ways.

An experimental determination of the short-circuit currents in an actual 380 V industrial system was carried out by the Projecting and Experimental Department of the Leningrad "Tyazhpromelektroproekt". Together with the use of the method described below the ratings of the induction motors taking part in the in-feed were determined; for the calculation of the short-circuit currents the resistances and reactances of the 380 V system were measured and compared with data in reference books.

The magnitude of the in-feed currents depends on the power rating of the motors connected to the system at the time of the fault and on their distance from the point of the fault. Other basic data for the calculation of the in-feed currents (ratio of starting current and e.m.f. of the motors) can be considered as constant for a given motor group.

No method for the determination of the power rating of induction motors which send in-feed current to the fault point has yet been suggested. The separation of this power from the total installed power of all the motors connected to the system by direct observation is very laborious and with a large number of operating motors distributed over a wide industrial area it is impracticable. The present recommendations for the calculation of the fault current in systems

* *Elektrichestvo* No.5, 40-45, 1957 [Reprint Order No. EL 22].

† The transient electromagnetic processes taking place in the motor during this period are described in [1].

up to 1000 V ignore, as a rule, this problem; this cannot be justified where a large number of motors is connected to an industrial supply system and is dealt with summarily. The method of determining the power rating of the motors connected to the system at the instant of fault by arbitrary coefficients referred to the rating of the step-down transformers has not found a wide introduction since these coefficients cannot be reliably determined. Nor does this method consider the system impedances through which the in-feed currents flow.

In the calculations carried out in parallel with the experiments it was found convenient to determine the required power rating of the motors on the basis of the load before the fault. This power was determined (at the junction points) for the groups of motors, which are replaced by equivalent motors. The procedure suggested by S.A. Rinkevich [2] for determining the total power connected (rated power at the shaft) of a group of induction motors from their reactive power demand may serve as a basis for the adoption of the above method.

Assuming that the reactive power absorbed by the induction motors at different loads (60 – 80 per cent) is constant, S.A. Rinkevich introduces the concept of the "relative VAr" of all the motors (ratio of the VAr to the power installed

$$q_{\text{rel}} = \frac{Q}{P_n},$$

which on the assumptions made, which are analysed in the appendix, can also be considered to be a constant quantity.

S.A. Rinkevich determined experimentally values of the relative kVAr. He measured the kVAr demand of a motor group at no-load and then determined from these data and the (total) kVA rating of the motors of the group their relative kVAr.

It is easy to show that the relative kVAr can also be determined analytically, for which purpose the kVAr demand and the rated power should be expressed in terms of the kW demand, viz,

$$Q = \sqrt{3} U_n I \sin \varphi_i = P_a \tan \varphi_i;$$

$$P_n = \frac{P_a}{k_c} = \frac{P_a \eta_i}{k_i};$$

$$q_{y\partial} = \frac{Q}{P_n} = \frac{P_a \tan \varphi_i k_i}{P_a \eta_i} = k_i \frac{\tan \varphi_i}{\eta_i}, \qquad (1)$$

where

η_i is the efficiency of a given motor if P_a and Q are the powers at its terminals;

k_c is the demand factor of the group of motors;

k_i is the relative load of the given motor.

As follows from (1), the relative kVAr can be determined for a value of tan ϕ and the efficiency corresponding to the given load of the (equivalent) motor. In view of the arbitrariness of the assumption of the constancy of the relative kVAr q_{rel} may be determined for greater accuracy at loads near the rated values. The values of efficiency and power factor at different loads of motors of different ratings and nominal parameters (no-load current, speed etc.) and also kVAr of motors are given in reference books [3 and 4].

Thus according to the parameters of the motors, the relative kVAr can be calculated for the "average" motor of the given group, this being characterized by several values of rated efficiency and power factor.

Once the relative kVAr and the kVAr demand are known, it is easy to determine the rating of the equivalent motor and its short-circuit current:

$$I_s = K_{st}\, I_n = K_{st}\, \frac{P_n}{\sqrt{3}\, U_l\, \eta_n \cos \phi_n},$$

1958

where

K_{st} is the ratio of the starting current to rated current.

If the system impedance is neglected, the in-feed current from the equivalent motor is approximately equal to the short-circuit current directly at its terminals:

$$I_{sm} = \frac{E_0}{z_m} = \frac{aU}{z_m};$$

where

E_0 is the phase e.m.f. of the stator of the motor (V);
U the phase voltage of the motor (V);
a the ratio of the e.m.f. to the voltage;
z_m the motor impedance.

During a fault, not at the terminals of the equivalent motor but at some other point of the system, the in-feed current must be determined from the formula:

$$I_{sm} = \frac{E_0}{z} = \frac{aU}{z};$$

where z is the resulting impedance of the windings of the equivalent motor and of the parts of the system (per phase) to the point of the fault (ohms).

The formula for the determination of the in-feed current in the special case of a radial system takes the following form:

$$I_{sm} = \frac{aU}{\sqrt{(r_c + r_m)^2 + (x_c + x_m)^2}} ;$$

where

r_c and x_c are the resistance and reactance of the system respectively;
r_m and x_m the resistance and reactance respectively of the motor.

The resistance of an induction motor can be approximately determined from the following formula:

$$r_m = 0.5 \frac{U}{I_n} (1 - \eta)$$

or from the exact formula

$$r_m = z_m \cos \phi_{st}$$

The reactance of the motor is

$$x_m = \sqrt{z_m^2 - r_m^2} .$$

The relation of the e.m.f. to the voltage can be determined according to an investigation by V.S. Mogil'nikov ([1], who showed theoretically and experimentally that for an induction motor

$$E_0 = 0.93 - 0.95\ U.$$

For the experimental determination of the fault current one section of the distribution busbars of a step-down transformer substation was disconnected from the system. The section was supplied through a 1000 kVA, 6/0.4 kV transformer, to which one feeder of the workshops and two of the boiler house were connected (Fig. 1). The substation 6/0.4 kV was supplied from the main 35/6 kV substation of the works which was connected to the power system. The short-circuit capacity was the 35 kV system 330 MVA, that at the 6 kV busbars 85 MVA.

The main consumers of the system were the induction motors. The normal load of the industrial system was 500 – 600 A, that of the boiler house 450 – 500 A.

Faults were applied (Fig. 1) at the substation distribution panel (1), at the entrance to the workshops (2), at the power cubicle (3) and at the busbar assembly (4).

For the subdivision of the total fault current into in-feeds from the system and in-feeds from the motors, the currents were recorded by oscillograph at the

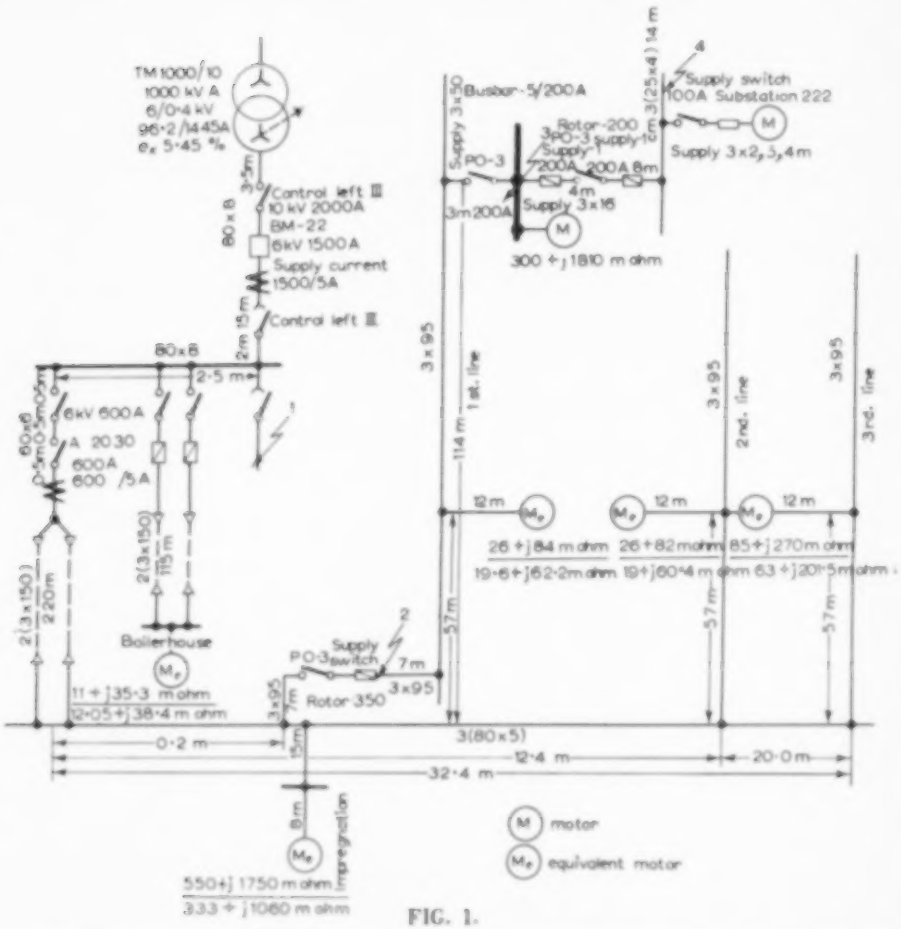
TM 1000/10
1000 kV A
6/0·4 kV
96·2/1445A
e_x 5·45 %
Control left III
10 kV 2000A
BM-22
6kV 1500A
Supply current
1500/5A
Control left III
80×8
2·5 m
6kV 600A
600A 20.30
600 /5A
2(3×150)
220m
2(3×150)
115 m
Boilerhouse
11 + j35·3 m ohm
12·05+j38·4 m ohm
Busbar-5/200A
Supply 3×50
PO-3
Supply-1
200A 8m
4m
Supply 3×16
3m 200A
300 + j 1810 m ohm
Supply switch
100A Substation 222
Supply 3×2,3,4m
3(25×4) 14 m
Rotor-200
3PO-3 supply-1
3×95
1st. line
2nd. line
3rd. line
114 m
12 m
26 + j 84 m ohm
19·6+j62·2m ohm
26 + 82 m ohm
19+j60·4 m ohm
85+j 270 m ohm
63 + j201·5 m ohm
57 m
PO-3 switch
7m
Rotor 350
0·2 m
15m
3(80×5)
12·4 m
20·0 m
32·4 m
8m
550+j 1750 m ohm
333 + j 1060 m ohm
impregnation
M motor
M_e equivalent motor

FIG. 1.

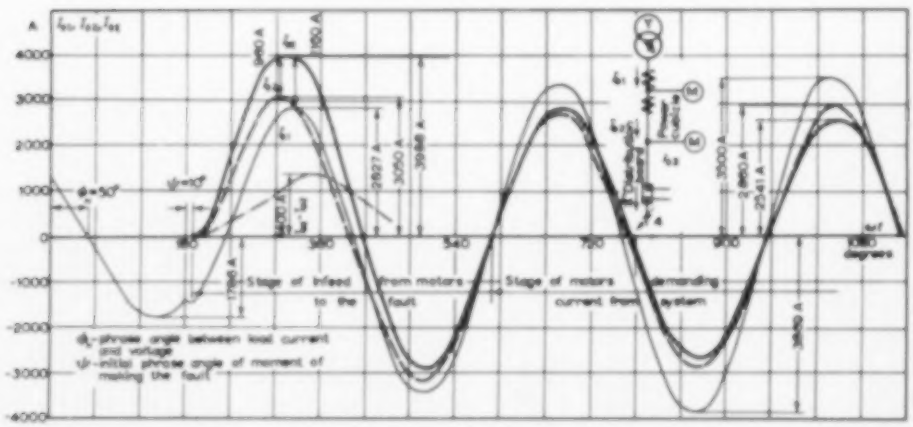
A
4000
3000
2000
1000
0
-1000
-2000
-3000
-4000
ϕ=50°
ψ=10°
2627 A
3050 A
3966 A
1760 A
1760 A
2460 A
2041 A
3500 A
3850 A
Stage of infeed to the fault
Stage of motors current from system
ϕ_k-phase angle between load current and voltage
ψ-initial phase angle of moment of making the fault

FIG. 2.

fault points, at the substation and also at intermediate points of the system through which the in-feed currents from the motors were passing.

An electronic device was used for the control of the instant of the application of the fault (within the period)in order to obtain maximum impulse current. At the substation and at the point of the fault the short-circuit currents were recorded in all three phases.

For example, Fig. 2 shows the oscillogram and the test connexions of a three-phase fault at the point 4. The oscillogram shows that the initial phase angle at the moment of making the short-circuit was 10 electrical degrees. (The voltage curve passing through the coordinate origin is not shown in the figure.) The recorded load current (I_{bl}) at a phase angle of 180° (before inception of the fault) may have been caused by the start at that instant of a motor of a crane or a similar drive.

The short-circuit current has various phase angles according to the fraction of motor in-feed currents it contains. At the moment of the first current peak the in-feed at the point of the fault was 1160 A, but the maximum value of the in-feed current reached 1400 A (after the maximum of the total fault current).

Beginning from the second stage of the process, the fault current measured at the transformer exceeded the current at the fault point owing to the motor current (starting and working).

For the calculation of the fault currents the impedances of the system sections were determined by direct measurements and the impedances of some parts were taken catalogue data. The measurements confirmed the catalogue data for the equipment installed in the given system.

For the determination of the rated power of the motors contributing to the in-feed currents the efficiency of the "average" motor was assumed as 0.9, the rated power factor 0.84, and the relative reactive power (at 75 per cent load) 0.6 kVAr/kW.

The calculations of the power rating of the motors sending in-feed current to the fault were checked wherever possible by visual inspection. The difference between the observed and calculated values for the different fault points was 3 – 11 per cent. (Table 2).

The ratio of starting current to rated current of the equivalent motor was assumed to be 6, the e.m.f. of the motor 205 V. To determine the motor in-feed at every fault current an equivalent circuit diagram of the system sections and the equivalent motors was drawn up from which the resultant impedances were determined. The total current at the point of the fault was determined by the arithmetic superposition of the current in-feeds from the system and the in-feeds from the motors *

* Owing to the fact that in the test circuit the short-circuit making device constituted

(continued)

TABLE 1.

Designation of section	Impedance of section in milliohms					
	Resistance		Inductive Reactance		Total Impedance	
	from catalogue data	measured	from catalogue data	measured	from catalogue data	measured
From transformer to substation distribution panel (fault point 1)	2.83	4.97	11.66	13.28	11.95	14.10
From transformer to entrance of workshops (fault point 2)	19.63	20.46	20.20	20.26	28.2	28.9
From transformer to Power cubicle (fault point 3)	50.19	44.37	47.28	49.44	69.0	66.2
From transformer to busbar assembly (fault point 4)	116.45	88.97	79.88	120.43	141.5	149.9

Note. The impedance calculated from catalogue data included the reduced impedance of the h.v. system of 1.87 milliohms.

The measured impedance included also the impedance of the fault-making device equal to $0.84 + j\ 1.305$ milliohm (in phase *A* during faults at points 1 and 2) and $0.944 + j\ 0.975$ milliohm (in phase *C* during faults at points 3 and 4).

Reference data of the individual elements of the l.v. system have been obtained mainly from the work of the Rostov department of the Tyazhpromelektroproekt (1953).

1958

TABLE 2.

Designation of the equivalent motor	Oscillogram Data				Connected capacity of equivalent motors kW	
	load current (*A*)	phase voltage (*V*)	sin ϕ	kVAr	from kVAr	from inspection
Fault at point 1						
Workshop feeder . . .	556	220	0.819	300	500	–
In particular						
1st line	–	–	–	–	220	–
2nd line	–	–	–	–	215	–
3rd line	–	–	–	–	65	–
impregnating . . .	–	–	–	–	10	–
1st boiler feeder	288	220	0.707	134	480	497
2nd boiler feeder	272	220	0.806	154		
Fault at point 2						
Workshop feeder . . .	547	236	0.982	380	630	–
In particular						
1st line	220	236	0.945	149	248	280.5
2nd line	–	–	–	–	–	289.1
3rd line	–	–	–	–	–	87.0
impregnating . . .	–	–	–	–	–	16.5
Boilers	–	–	–	–	–	455
Fault at point 3						
Power cubicle (in mine)	–	–	–	–	–	60
Fault at point 4						
Busbar assembly by . .	–	–	–	–	–	67.5
motor connected to cubicle.	–	–	–	–	–	10

Note. Resistances and reactances of the motors are shown directly in Fig. 1 in numerator for fault point 1, and in denominator for fault point 2.

TABLE 3.

Fault point	Number of fault point	≤ System phase voltage prior to fault	Symmetrical fault current					First peak of fault current									Ratio of first peak of fault current at fault point to that at transformer
			from system			from motors	at fault point, calculated	from system			from motors (in-feed)			at fault point			
			calculated	test	ratio	calculated		calculated	test	ratio	calculated	test	ratio	calculated	test	ratio	
0.4 kV busbars	1	220	15,600	15,300	0.97	6,610	22,210	29,350	27,160	0.925	9,310	7,400	0.795	38,660	33,240	0.865	1.225
Workshop feeder	2	236	8,160	7,560	0.93	6,710	14,860	12,200	10,200	0.845	9,470	9,050	0.96	21,670	19,250	0.885	1.80
Branch from workshop feeder to power cubicle	3	216	3,260	3,230	0.985	545	3,805	4,940	4,400	0.895	768	650	0.847	5,708	6,250	1.09	1.42
Distribution busbar assembly	4	214	1,635	1,900	1.32	745	2,180	2,260	2,830	1.25	1,055	1,850 960 1,160 (1,400)	2.4 0.91 1.1 (1.32)	3,315	3,990	1.2	1.41

Notes. 1. Test values of the first peak of the fault current in-feeds from motors (*graph 13*) are determined as the difference of measured current at the fault from that at the transformer. An exception is point 1, where the in-feed from the motor is measured directly. For points 3 and 4, where the in-feed takes place from motors between fault point and supply, two values are given; the first is the in-feed from motors on the other side of the fault compared with calculated values the second is the in-feed from all motors (Fig. 2). Owing to the lack of a practical method of calculating short-circuit currents at system points where the e.m.f. of the motor equals that of the system, the in-feed currents from motors between the fault and the supply point were not calculated in cases of fault points 3 and 4.

2. During faults at the end of the circuit 4 the test values of the symmetrical component of the fault current and of the first current peak (from the system and at the fault point) were larger than the calculated values, obviously because the reduction during the fault of the resistance and reactance of the steel busbars of the distribution panel against the values as measured at the rated current (due to the skin effect in ferromagnetics) were neglected.

1958

The results of the calculation of the impedance of the system sections to the short-circuit points are given in Table 1. The determination of the equivalent ratings of the motors is detailed in Table 2; and the short-circuit currents are given in Table 3.

The difference between the experimental and the calculated values of the fault currents is about 10 – 15 per cent. This comprises the errors in measurements, estimated at about 6 – 10 per cent, the increase in the impedance of the experimental system at the time of the fault by the formation of the arc in the fault-making device and by the approximative character of the mathematical description of the short-circuit processes. But, as can be seen, the difference is within the limits of experimental and calculating errors. In individual cases Table 3 gives a short explanation of the causes of the discrepancy.

Conclusions

Experiment and calculation confirm that, when the system impedances during fault conditions and the rating of the motors sending current to the fault, are correctly estimated, the results of short-circuit current calculations are entirely satisfactory in cases in which the fault takes place near the supply point of the low-voltage system. For medium and long distances to the fault point the calculated values of the in-feed currents from the motors may be too small because the in-feed of some motors on the supply side of the fault point is neglected.

The in-feed currents attenuate rapidly and need be taken into account only for the first peak of the short-circuit current at the fault. For medium and long distances the motors located between fault and supply point rapidly cease to end current to the fault and soon will require to be supplied with current again; During faults at points 3 and 4 the value of the current therefore measured at the transformer (at the input end of the circuit) became larger than at the first fault current peak.

The in-feed currents from the induction motors have a considerable magnitude especially at medium and long distances from the fault in the system shown in Fig. 1 the first fault current peak exceeded the corresponding current of the supply transformer by 22 – 80 per cent.

The resistances and reactances of the low-voltage system have a considerable effect on the magnitude of the fault currents. In the system shown in

* *(Continued)*
a common impedance for currents from both sources, strictly speaking the calculations should have been made with different distances of the sources (consideration of self and mutual impedances). However, such a calculation is very complicated and would have rendered, according to a check, the result only about 3 – 5 per cent more accurate than the calculation made individually from each in-feed source.

Fig. 1 the current at the far end of the system was 10 times smaller than that at the busbars.

It is possible to calculate the in-feed currents from a given group of motors fairly exactly by using a value of the rating of the motors sending current to the fault determined from the load before the fault and from the value of the relative kVAr determined analytically.

Appendix

The kVAr Demand. The assumption of constant kVAr demanded from the system at different loads of induction motors is based on the following considerations:-

The total kVAr demand by a motor comprises the kVAr for magnetization Q_o and the kVAr for the leakage reactance Q_D. The magnetization kVAr are virtually independent of the motor load and are determined by the equation:

$$Q_o = \sqrt{3}\, U_l\, I_o\,,$$

where

U_l is the line voltage of the system (V);

I_o the no-load current (A).

The total kVAr demand from the system in particular at the rated load can be determined from the expression:

$$Q_n = \sqrt{3}\, U_l\, I_n \sin \phi_n\,,$$

where

I_n is the rated stator current (A).

It is easy to show that the magnetizing kVAr are equal to the total kVAr in the special case that the stator current is equal to no-load current and the phase displacement between the current and the voltage is 90°.

The specific value of the magnetizing kVAr, independent of the loading of the motor, is given by the ratio:

$$\frac{Q_o}{Q_n} = \frac{\sqrt{3}\, U_l\, I_o}{\sqrt{3}\, U_l\, I_n \sin \phi_n} = \frac{I_o}{I_n \sin \phi_n}\,,$$

If the no-load current is expressed by the rated stator current [5]

$$I_o = I_n \left(\sin \phi_n - \frac{\cos \phi_n}{2\, b_n}\right.$$

then the ratio

$$\frac{Q_o}{Q_n} = \frac{I_n \left(\sin \phi_n - \frac{\cos \phi_n}{2\, b_n}\right)}{I_n \sin \phi_n} =$$

$$= \frac{\sin \phi_n - \frac{\cos \phi_n}{2b_n}}{\sin \phi_n} = 1 - \frac{\cot \phi_n}{2b_n},$$

where

b_n is the ratio of the maximum torque to the rated torque of the motor.

Substituting likely values of cot ϕ_n and b_n it is easy to determine the limits of the ratio

$$\frac{Q_o}{Q_n}$$

In [4] it is shown that for induction motors the relative value of no-load kVAr become, owing to the fact that the motors are not fully loaded, practically as follows: For a rated p.f. of 0.91 – 0.93 approximately 85 per cent and for rated p.f. of 0.77 – 0.79 approximately 90 per cent.

REFERENCES

1. V.S. Mogil'nikov, *Pull-out of induction motors during short-circuits in the system. Elektrichestvo*, No. 11, (1954).
2. S.A. Rinkevich, *On the individual power demand of metal-cutting lathes in mechanical engineering works. Sbornik informatsionnykh materialov Energosbyta Lenenergo (Information Handbook of the Power Sales Department of the Leningrad Power Authority)*, 3rd Edition, (1948).
3. M.P. Kostenko, *Electric machines. Gosenergoizdat* (1944).
4. L.V. Litvak, *Problems of raising the power factors in industrial plants. Gosenergoizdat* (1950).
5. I.A. Syromatnikov, *Operating conditions of induction motors. Gosenergoizdat* (1955).

WIND PRESSURE ON OVERHEAD TRANSMISSION LINE CONDUCTORS*

V.V. BURGSDORF

(Received 9 January 1957)

The correct assessment of wind pressure on conductors is of great importance in the design of transmission lines. This applies particularly to double-circuit lines and lines equipped with release clamps and safety (swivelling or collapsible) cross-arms, since in these cases there is an upper limit imposed for the maximum permissible wind loading. In designing large installations, it is necessary to know accurately the aerodynamic characteristics of conductors and the distribution of wind pressure.

As is well known, strong winds are always of turbulent nature and consist of fast-and slow-moving air masses. In other words, the wind velocity is never uniform along the front of a gust. The total load on a long object is therefore determined not by the maximum, but by some mean value, of the wind velocity. For spans longer than 200 m this lack of uniformity may be of considerable importance.

The first experimental investigations to ascertain the extent of the non-uniformity in the distribution of the wind velocities affecting the total load on conductors date back over 25 years [1] and [2]. These tests showed that for wind speeds up to 20 m/sec. this non-uniformity can be neglected for spans up to 100 m. long, but that it becomes sufficiently noticeable on spans about 200 m. long.

Later investigations carried out in Sweden in 1939 revealed a possibility of reducing the design value of wind load because of the finding that the wind pressure becomes less uniform with velocity [3]. Similar experiments were also carried out in other countries: France in 1951 [4] and [5], Australia in 1949 [6]; Belgium in 1952 [7]. Recently investigations were made in West Germany [8] and in the U.S.S.R. where eight experimental stations were erected with span lengths from 220 to 350 m.

The reduction co-efficient considering the non-uniform distribution of the pressure along the span was introduced in the Soviet Regulations for Trans-

* *Elektrichestvo* No.5, 47-52, 1957 [Reprint Order No. EL 23].

mission Lines in 1947 [9]. These regulations recommend the following formula

$$P = aC_x \frac{v^2}{16} \tag{1}$$

where P is wind pressure in kg/m² of projected area;
a is the reduction co-efficient;
C_x is the head resistance of conductor;
v is the wind speed in m/sec.

In the above formula the wind speed is taken usually as the maximum velocity registered by a meteorological station, for a period of 5 to 10 years. The head resistance of the conductor which can be referred to conductor diameter and wind speed, is normally taken as 1.2 [10]. The coefficient a is 0.85.

The coefficient a depends not only on the conditions existing in a given locality, but also on the method of measurement of the wind velocity.

It should be pointed out that the anemometers used in the U.S.S.R. were of the pressure-plate type whereas those used abroad were generally of the pressure – tube type (i.e. working on the Pitot-tube principle). The latter anemometers can register the velocity of a wind gust lasting 10 to 15 sec. whereas the pressure-plate instrument, according to the instruction book, should register a mean position of the plate for 2 min. It is obvious that the maximum velocities as recorded by low-inertia anemometers should be higher than those recorded with the pressure-plate anemometers. This, in fact, explains the various statements on low wind speed prevailing in the U.S.S.R.

The wind load on conductors is usually computed from the measurement of the angle of swing of the insulator string or the coupling link from which the conductor is suspended. This gives directly the horizontal force on the tower and the reduction of the clearance to the tower. To determine the maximum wind loading for a given period of time, continously recording instruments were used in Sweden, Germany, and U.S.S.R. and maximum-swing indicators were used in France and Belgium. The deflection angles thus obtained were checked against records of the maximum wind velocities measured in the immediate vicinity of the experimental span or at a near-by meteorological station.

A visual method of measuring the angle of deflection of the conductor at midspan was used in Australia. Readings were taken "only when the conductor was fairly steady" obviously because such a method is not particularly suitable for measuring maximum deflections. Moreover, the readings were checked against wind velocities measured by a cup-type anemometer and consequently, in this investigation, one can speak only of some average conductor deviation and wind speed. A simultaneous underestimation of conductor deflection and wind speed leads to the cancellation of the error. Thus, such results cannot be accepted as being characteristic of maximum wind loadings and will not be utilized in the following considerations.

In the U.S.S.R. the wind velocity was invariably recorded by means of

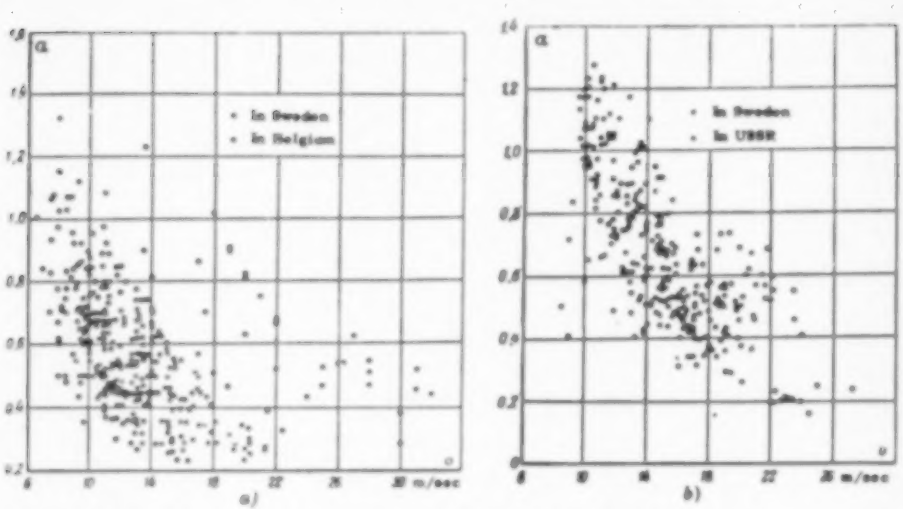

FIG. 1. Relationship between the coefficient a and wind velocity
a — measurements in Sweden (inland regions): d = 25 to 27.7 mm, l = 155 to 300 m; measurements in Belgium: d = 9.5 mm, l = 120 and 190 m;
b — measurements in Sweden: d = 15.8 mm, l = 200 m; measurements in U.S.S.R. (coastal area): d = 19.1 mm, l = 250 m.

pressure plate anemoters, except in one case in which a pressure-tube instrument was used.

The results of various investigations are presented in different ways. For example, Swedish publications give the measured wind pressure on conductors as a fraction of the wind pressure on a large plane ($C_x = 2$), i.e. the measured pressure is characterized by a quantity which is less than the coefficient a; in French investigations the results are expressed in terms of the ratio of the measured to calculated angle of conductor deflection (the calculations being performed in accordance with the method accepted in France). In order to compare the results from various countries the data were recalculated on a common basis. The quantities calculated were the coefficient a from (1) and the effective load per square metre of the projected area normal to the direction of wind*. For each particular case the head resistance was taken as depending on the type of conductor and wind speed in accordance with the results of tests in wind tunnels carried out in the U.S.S.R. [10]. In this way it was possible to arrive at more accurate values of the coefficient a.

The results of this re-calculation are shown in dotted lines on the accompanying figures. Figs. 1,2 and 3 show the values of the coefficient a for the various countries, and Fig. 4 the envelopes drawn through the points of maximum value. Two points differing from the others are shown in Fig. 4 separately.

* It is regretted that the results of German investigations could not be recalculated because of the insufficiency of published data.

1958

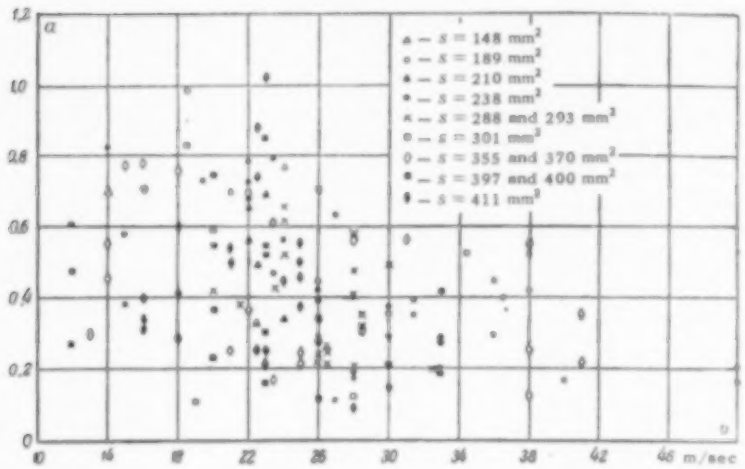

FIG. 2. Relation between the coefficient a and wind speed according to the results obtained in France.

When analysing results of measurements, apart from the non-uniform distribution of the wind speed along the span, one should also consider the case when the wind speed at the span is higher than that at the point of location of the anemometer. In this case the coefficient a becomes greater than unity. It is characteristic that for high wind speeds (20 m/sec and more) no such case has been observed in practice.

The manner in which the experimental points are distributed allows us to establish beyond any doubt the fact that the wind pressure becomes less uniform along the span as the wind becomes stronger. Also, the influence of the different physical and geographical factors pertaining to different geographical areas is clearly brought out. Moreover, this is true not only for coastal and inland regions within one country such as, for example, Sweden. The first measurements carried out in the Leningrad area with low-inertia instruments yielded values * for the coefficient a greater than those obtained for a coastal region in Sweden. Even greater values of the coefficient were obtained in Belgium and yet greater values in France.

In France values between 0.5 and 0.55 were obtained for the coefficient a for wind velocities up to 38 m/sec. It is regrettable that no information is available on the experimental span lengths but it can be taken that in France the span length for conductors of 300 mm² or more† cross-sectional area, is, as a rule, more than 400 m and only rarely 350 m.

* Here and later on the values of the coefficient a are taken for the same, and not for the maximum wind speeds, recorded in the given localities.

† It can be shown that for a wind speed of 34.5 m/sec, $a = 0.52$ (Fig. 2) was recorded on a span 462 m long.

The coefficients a obtained from measurements in the U.S.S.R. by using pressure-plate anemometers with loaded plate (Fig.3) correspond mainly to wind speeds of up to 20 – 25 m/sec. However, there is enough experimental data to establish the fact that the coefficients obtained in this way are greater than those resulting from measurements with low-inertia instruments. One fact stands out, viz. the large number of points whose values are considerably greater than unity for wind speeds up to 18 m/sec and also the number of points having values of the order of 0.8 for wind speeds of about 25 m/sec for long spans.

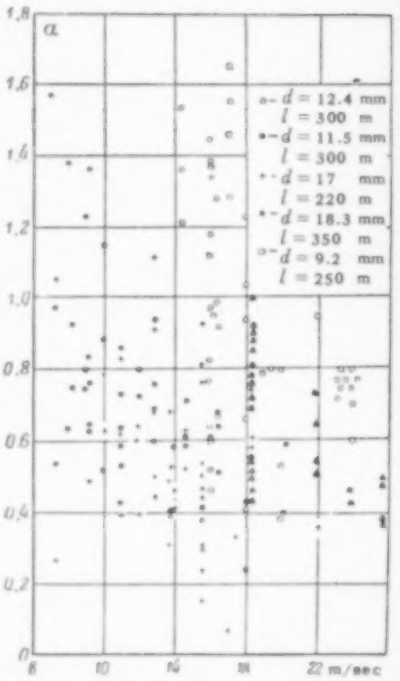

FIG. 3. Relation between coefficient a and wind speed according to results obtained in the U.S.S.R.

A comparison of the curves shown in Fig. 4 indicates that the coefficient a depends on the degree to which a given district is exposed to high winds. In this respect the comparison of the Swedish data for coastal and inland regions and of the Belgian and French data are characteristic. From Fig. 4 it is seen that the curves of the reduction coefficient obtained for different regions are shifted with respect to each other, and the coefficients a for districts subjected to stronger winds are higher than those for districts with less intense winds for a given wind speed. Therefore, if a coefficient a is obtained for a region with strong winds, it cannot be extended to maximum wind speeds of regions with moderate winds. For example, the value of a at 25 m/sec for the region with the design wind speed of 30 or 35 m/sec cannot be applied to a line erected in a region where the design wind speeds is 25 m/sec, since in this latter case the value of a is smaller.

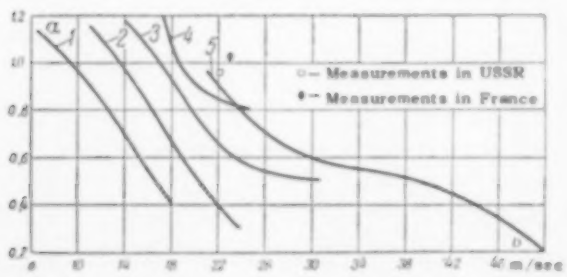

FIG. 4. Relation between greatest values of coefficient a and wind speed as measured in different countries:
1 – in Sweden (inland regions);
2 – in Sweden (coastal regions);
3 – in Belgium;
4 – in U.S.S.R; 5 – in France.

To facilitate further analysis, mean values of wind pressure on a conductor for one span recorded at various wind speeds are plotted in Figs. 5 – 7. The distribution of these points is typical. The curves shown in these figures are drawn from (1) for $C_x = 1.2$ and

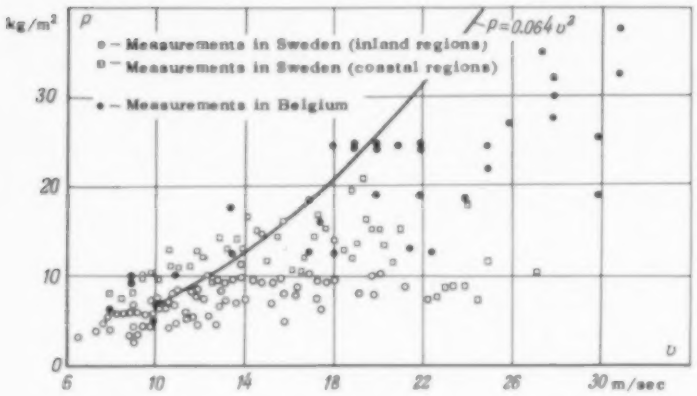

FIG. 5. Relation between wind pressure on conductor projection area normal to wind direction and wind speed according to measurements in Sweden and Belgium.

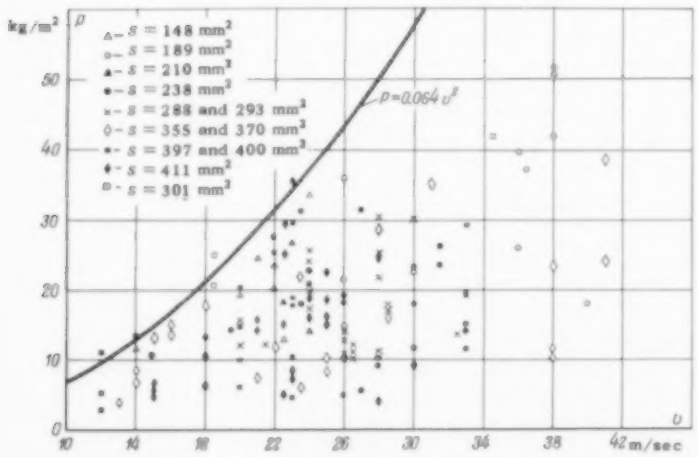

FIG. 6. Relation between wind pressure on conductor projection area normal to wind direction and wind speed according to measurements in France.

$a = 0.85$ in accordance with the recommendations given in the Regulations for the Erection of Electrical Installations [9].

The practical conductor loading in Sweden (especially in inland regions) is noticeably lower than it is in Belgium and this, in turn, is lower than in France. For wind speeds up to 15 m/sec the experimental points lie not infrequently above the design curve and for velocities of 15 to 20 m/sec they are, in general,

the same as the higher values observed in Belgium and France. At still higher wind velocities the measured wind load is smaller than the calculated one which is obviously due to the lowering of the coefficient a.

Of a similar character is the distribution of experimental points obtained from short-period tests in the U.S.S.R., though the quantitative relations are here different *: wind pressures greater than those given by (1) occur often at speeds of up to 18 or 19 m/sec, and at 25 m/sec they are almost as high as the highest values recorded.

The material presented demonstrates convincingly the importance of the correction factor for wind pressure at high wind speeds. This coefficient should be different for speeds measured with the low-inertia and the pressure-plate anemometers.

The West European investigators working with low-inertia anemometers suggest a value of 0.5 for the reduction coefficient; they are also referring to a considerable local wind speed of 35 m/sec. The investigators in Sweden, where the wind speed has also been measured with low-inertia anemometers, recommend the coefficient $a = 0.4$ on the basis of a wind speed of 28 m/sec. Such a lowering of the coefficient appears to be justifiable on the ground that undoubtedly the winds in Sweden are not so strong as those in Belgium and France.

1958

The value of the coefficient a should be greater if this is worked out from the data on wind velocities obtained with the method which is accepted in the U.S.S.R. The relation between the coefficient obtained with the two types of anemometer is given by

$$\left(\frac{v_{li}}{v_{pp}}\right)^2,$$

where v_{li} is the speed measured with the low-inertia, and v_{pp} with the pressure-plate anemometers. At the present time work is being done to determine this ratio, but it can be said even now that no great reduction can be expected in the present value (0.85) of the coefficient a. Indeed, taking the West European coefficient $a = 0.5$, the ratio

$$\frac{v_{li}}{v_{pp}} = \sqrt{\frac{0.85}{0.5}} = 1.3$$

which may be regarded as a sufficiently realistic figure for the ratio of short duration (10 to 20 sec) to one minute maximum wind velocity.

The above statement is verified by the damages to transmission lines occur-

* This is obviously connected with the different method of measurements (pressure-plate anemometers) used in the U.S.S.R.

ring at strong winds when the effective wind pressure on conductors is nearly 60 kg/m² and the wind speed (measured by pressure-plate anemometer) 32 to 35 m/sec.

A more substantial reduction of the coefficient a can be expected for regions where the design wind speed is 35 m/sec or more, and also where the repetition rate of the assumed design speed comes near the highest observed.

To give a fuller picture of practices in various countries the tables 1 and 2 of design wind loadings on conductors and metal supports were compiled.*

It is seen from Table 1 that the conductor loading used in the U.S.S.R. is about the same, or even sometimes lower, than in other countries.† The lowest wind loading is applied in Finland where, as in the Leningrad district and Karelian A.S.S.R., the wind speeds are not very high due to favourable geographical conditions.

Recent research on the effects of non-uniform wind pressures is now being accepted as a basis for the reduction of the design wind loadings in Belgium and France, where until recently these loadings have been excessively high.

The design wind loadings on supports are invariably higher abroad than in the U.S.S.R., sometimes by as much as 50 or even 100 per cent.

It appears from the foregoing that the design values used in the U.S.S.R. for wind loading are in every respect more modern than in most other countries where only recently the regulations were slightly eased-up, which brings the foreign design values nearer to the Soviet values. It should be made clear, however, that this does not preclude the possibility of a future reduction in the design wind loading for transmission lines.

This further reduction should be well substantiated by more extensive investigations to determine realistic loadings for various regions and to obtain more accurate aerodynamic characteristics of conductors and supports and the possible values of the coefficient a.

From experiments which have been carried out up to now it is possible to reduce the design head resistance to 1.1 for the values of the product $vd \geq 400$ m/sec. mm. It is also possible to take the coefficient $a = 0.75$ if the supports are checked for the highest wind loads ††. This relaxation of the design conditions can be extended also to localities with the design wind velocity of

* In the U.S.S.R. the loads are taken for the average wind speed of 25 m/sec.

† The accepted thickness of ice for Sweden varies between 1.3 and 3.2 cm. Therefore the resulting wind load on tower becomes considerably greater than in the U.S.S.R.

†† The speeds considered are the maximum values for a given region, occurring once in 5 years, and not the design speeds.

TABLE 1. Design wind loadings on conductor projection area without ice used in various countries.

	Country	USSR	Great Britain	Belgium	Germany	Italy	Canada	USA	Sweden	Switzerland	Finland	France
Design load	kg/m²	40	39	72*** / 45	44-53	72	39	44	25*	50	25	72** / 48
	%	100	97.5	180*** / 112.5	110-130	180	97.5	110	–	125	62.5	180** / 120

* With and without ice load.
** Numerator – present standards; denominator – standards recommended at the present time, publications referred to
*** Numerator – present standards; denominator – proposed new standards with $C_x = 1.2$.

TABLE 2. Design wind loadings on flat tower sections used in various countries.

	Country	USSR	Great Britain	Germany	Italy	Canada	USA	Sweden	Switzerland	Finland	France
Design load	kg/m²	54.9	120	77	120	63	70.5	100	100	100	120
	%	100	220	140	220	115	128	182	182	182	220
Pressure on leeward face %		100	–	81	60-80*	100	100	80/100**	60-80	100	60-80*

* Depending on projected tower area.
** Depending on distance between tower sides.

1958

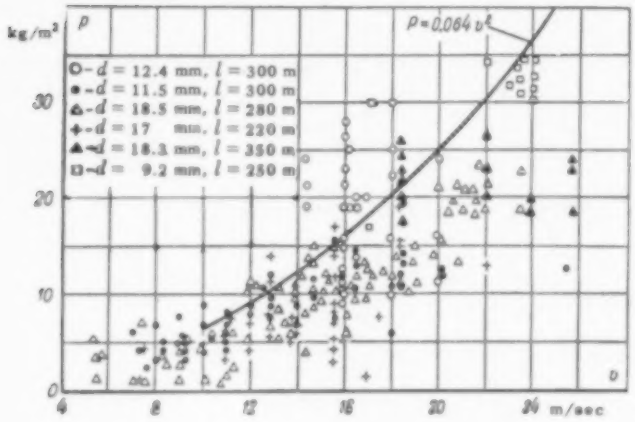

FIG. 7. Relation between wind pressure on conductor projection area normal to wind direction and wind speed according to measurements in the U.S.S.R.

35 to 40 m/sec, except for the regions adjacent to large water areas. The question of specifying more precise value for the coefficient a will be decided from the results of experiments now being carried out in the U.S.S.R.

It is also necessary to consider more closely the actual conditions under which a line is expected to operate. In particular the present practice of extending the design wind speed of 25 m/sec. to regions with light wind should be abandoned. In all cases the design wind speeds should be chosen in accordance with observations. For lines passing through woodlands the design speed should be taken at least 5 m/sec. less than the speed for the main region.

REFERENCES

1. W.D. Tuck, *Variation in Distribution of Wind Pressure on Overhead Lines. Brit. Electr. a. All. Indust. Research Assoc. Tech., rep.* X (1934).
2. R.H. Sherlock and M. Stont, *Storm Loading a. Strength of Wood Pole Lines a. Study of Wind Gusts. Edis. El. Inst.* (1936), *University of Michigan, Ann Arbor.*
3. O.P. Zetterholm and S. Sandin, *Wind Pressure on Overhead Transmission Line Conductors.* CIGRE Rep., 202 (1954).
4. R. Poyart, *Effect of High-Velocity Winds on Overhead Line Conductors. Bull. Soc. France des electriciens,* XI (1953).
5. P. Schuepp *et al, Investigation of Mechanical Overload in Insulators of Transmission Lines Under Normal Service Conditions. Rev. Gen. Electr.*, No. 2 and 3 (1955).
6. H.C. Harrison, *Factors Affecting the Mechanical Design of Transmission Lines.* Pt. 1,CIGRE. Rep. 218 (1956).
7. L.H. Marchal *et al, The Action of Wind on Overhead Line Conductors.* CIGRE. Rep. 206 (1956).
8. H. Mors *et al, Wind Pressure on Overhead Transmission Line Conductors.* CIGRE., Rep. 220 (1956).

REFERENCES (*continued*)

9. *Recommendations for Erection of Electrical Installations. Gosenergoizdat* (1947).
10. V.V. Burgsdorf, *Fundamental Problems in Erection of Overhead Transmission Lines. Trudy Central Scientific Research Electrochemical Laboratory.* 5th Edition.

Note:

(CIGRE *stands for Conference Internationale des Grands Reseaux Electriques.)*

1958

THE PROTECTION OF A REGULATING AUTOTRANSFORMER*

A.N. KOZHIN

(Received 23 March 1956)

The voltage regulation on load in the h.v. systems of the USSR is increasingly carried out by transformers with booster groups. The use of autotransformers with regulating gear for this purpose is spreading.

Fig.1 is the diagram of a power transformer with a booster group. The latter consists of a regulating autotransformer (or transformer) and a transformer in series with it.

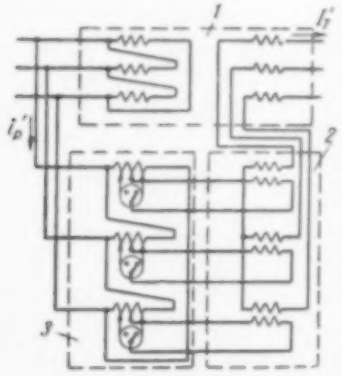

FIG.1. Schematical representation of a transformer with on-load voltage-regulating gear.
1-Main Transformer; 2-Series Transformer; 3-Regulating Autotransformer.

The present communication considers the protection of a regulating autotransformer (or transformer) against phase-phase faults and short-circuits between the lead-outs of its secondary winding. Our considerations will deal more specifically with the protection of autotransformers. However, they can be extended to include the case of a regulating transformer, and also other circuits comprising a power transformer or autotransformer with a booster group.

For a regulating autotransformer high-speed protection is desirable. Yet the use of the simplest types of high-speed protection entails certain difficulties.

The difficulty in using a tripping coil ("current cutout") consists in the fact that the currents set up at faults inside the autotransformer and at external faults may be of the same order. This makes it impossible to design a protection system of satisfactory sensitivity and operate from the short-circuit currents at external faults.

The difficulty in using a differential protection resides in the fact that the

* *Elektrichestvo* No. 5, 52–56, 1957 [Reprint Order No. EL24].

transformation ratio of the autotransformer varies between wide limits. The operating current of the protection, selected with allowance for the unbalance current set up by a variation of the transformation ratio of the autotransformer, may become so high that it may be impossible to assure the required sensitivity to short-circuits in the protected zone.

An inclusion of the autotransformer in the zone protected by the differential protection of the main transformer requires the sensitivity of this protection to be reduced. Also, the fault current in the autotransformer will, as a rule, be negligible in comparison with the operating current of the relay and the protection will then not operate in the case of such a fault.

A.A. Gevorkov suggested, in 1935, for the protection of autotransformers a special type of overcurrent relay connected to current transformers inserted into the primary circuit of the regulating autotransformer. At external short-circuits the protection is locked out by current relays connected into the circuit of the main transformer [1]. However, this protection system suffers from substantial disadvantages which will be considered below. For some types of autotransformers it is altogether unsuitable.

To protect a regulating autotransformer against phase-phase short-circuits and short-circuits between the lead-outs of an individual phase of its secondary winding the author of the present paper developed a new overcurrent protection with restraining characteristic (Fig.2). The current relays of this protection are connec-

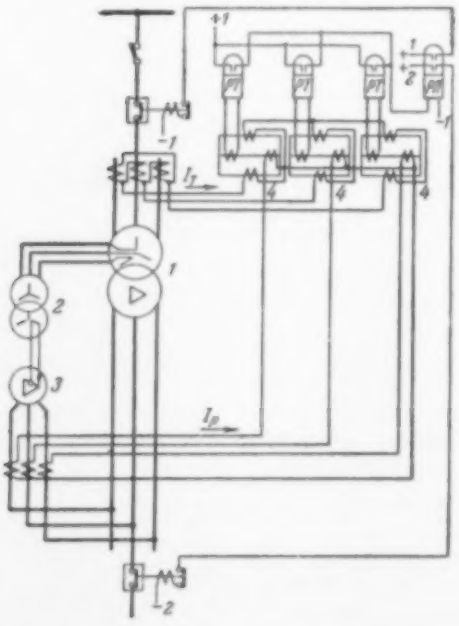

FIG.2. Protection of regulating autotransformer. 1-Main Transformer; 2-Series Transformer; 3-Regulating Autotransformer; 4-Interposing Saturable Transformers.

1958

ted into the primary circuit of the regulating autotransformer.

To obtain magnetic restraint, the interposing transformer has in addition to its operating and secondary windings a restraining winding (Fig.3) connected to the current transformers inserted into the circuit of the winding of that side of the main transformer on which voltage regulation is carried out.

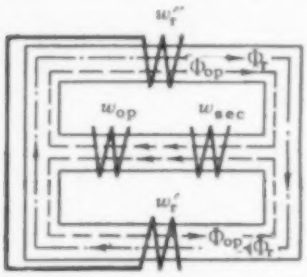

FIG.3. Interposing Saturable Transformer. w_r' and w_r'' restraining windings; w_{sec} secondary winding; w_{op} operating winding; Φ_r - flux set up by restraining windings; Φ_{op} - flux set up by operating winding.

When no current flows through the restraining windings the interposing transformer operates as an ordinary saturable transformer. The magnetic flux produced by the restraining windings when current passes through them is closed through the outer limbs, it does not enter the middle limb nor does it set up an e.m.f. in the secondary winding, but it saturates the magnetic circuit and deteriorates the conditions of transformation of the operating current. The higher the restraining current, the greater must be the current in the operating winding in order to obtain in the secondary winding a current equal to the operating current of the relay.

To show the advantages of the new system over the protection with a lock-out, we will consider the sequence of the selection of the parameters of both systems.

The operating current of the lock-out relay in the protection working with lock-out must be greater than the maximum operating current and the maximum short-circuit current in the zone protected by the relay. The latter is assumed equal to the maximum current at the point of erection of the locking relays for short-circuits on the secondary lead-outs of the autotransformer.

There are therefore two conditions for the selection of the operating current of the blocking relays, viz.

$$1)\ I_{op.bl.r} \geq K_r I_{t.op.max},$$

$$2)\ I_{op.bl.r} \geq K_r I_{sh.max},$$

where K_r is the coefficient of reliability, $I_{t.op.max}$ the maximum operating current in the winding of that side of the power transformer where the voltage is regulated, $I_{sh.max}$ the maximum current in the same winding of the power transformer at an internal short-circuit in the regulating autotransformer.

As a rule, the second condition is the decisive one. For this reason the operating current of the blocking relays becomes greater than the rated current of the autotransformer

$$I_{op.bl.r.} > I_{r.rat.} \qquad (1)$$

At through short-circuits and under normal conditions the primary current of the regulating autotransformer is

$$I_r = KI_t \tag{2}$$

where K is a proportionality factor and I_t the current in the winding of the power transformer on the side at which the regulation is carried out.

The proportionality factor K may be determined with satisfactory accuracy as the product of the transformation ratios of the regulating autotransformer and series transformer, respectively, viz.,

$$K = k_r k_s \tag{3}$$

The theoretical value of this factor K will be greater than its actual value.

Fig.4 represents the relationship $I_r = f(I_t)$ and the characteristic of the protection according to Fig.2.

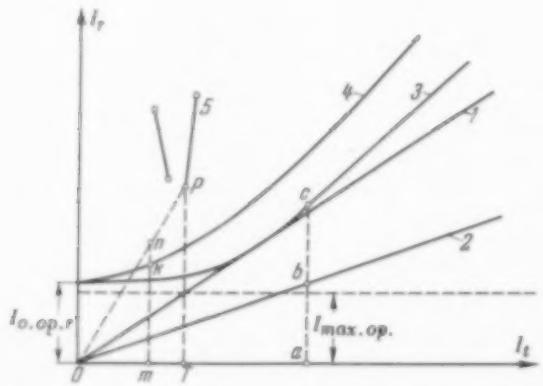

FIG.4. Relationship between Current in primary Winding of Autotransformer and Current in Winding of Main Transformer.
1 – ideal Characteristic of Protection; 2 – $I_r = KI_t$;
3 – $I_{op.r(I)} = f(I_t)$; 4 – $I_{op.r(II)} = f(I_t)$; 5 – $I_{r.sh.} = f(I_t)$.

For a selective action of the protection at external short-circuits the following relation must hold between the operating currents of the blocking and protective relays

$$I_{op.pr.r.} = K_r' I_{op.pr.r.} \tag{4}$$

where K_r' is the coefficient of reliability ($K_r' > 1$). Consequently,

$$I_{op.pr.r.} > I_{rat.r.} \tag{5}$$

Practical calculations showed that $I_{op.pr.r.} \gg (1.5–2)\, I_{rat.r.}$ i.e. the protection is of low sensitivity.

A protection with locking-out device may fail to operate at short-circuits in

the autotransformer where the current in the blocking relay exceeds the maximum of the theoretical short-circuit current. Also, it does not operate at phase-phase short-circuits on the lead-outs of the primary winding of the autotransformer because in this case the short-circuit current on the side where the blocking relays are placed is greater than the operating current of the latter. It may be equal to the current set up in the case of short-circuits on the low-voltage side.

Failure to respond of the protection in the cases mentioned will require the installation of a stand-by protection or the inclusion of the autotransformer into the zone protected by the differential protection of the main transformer. The latter method meets with certain design difficulties in some cases.

When the autotransformer (without its tap-changing gear) is included in the zone protected by the differential protection of the main transformer, the operating current of the blocking relays may be reduced by matching to the operating current of the differential relays; this increases the sensitivity of the protection to short-circuits in the autotransformer.

The ideal characteristic of a current protection with restraint may be represented by a straight line, whereas its actual characteristic is curved (Fig.4). Also, according to the angle α between the vectors of the currents in the operating and restraining coils of the relay, the restraining characteristic may be above or below the characteristic for $\alpha = 0°$, i.e. at the same value of I_t the operating current may have different values.

To calculate the selectivity of the protection the characteristic $I_{op.r}(I) = f(I_t)$ corresponding to the angle at the minimum restraint is selected.

To prevent non-selective operation of the protection when its secondary circuits are interrupted, the operating current of the relay without restraint $I_{0.op.r.}$ is assumed greater than the operating current of the autotransformer.

The quotient of the ordinate ac (Fig.4) of the characteristic of the relay $I_{op.r}(I) = f(I_t)$ adopted for calculating the selectivity by the ordinate ab of the straight line $I_r = KI_t$ for the same current I_t determines the margin of selectivity or the coefficient of reliability K_r.

The minimum value of this coefficient should not be less than 1.2.

In the case of short-circuits in the autotransformer the curve relating the current of the autotransformer $I_{r.sh.}$ with the current in that winding of the main transformer on whose side the regulation takes place is higher up than the curve $I_r = KI_t$. On a three-phase short-circuit on theconnections between regulating and series transformers fed only from the h.v. side, the above relation takes the following form

$$I_{r.sh.} = k_t I_t \qquad (6)$$

where k_t is the transformation ratio of the main transformer.

As a rule, the coefficient k_t is considerably greater than the coefficient K. Consequently, for the same value current I_t is greater than current I_r.

To calculate the sensitivity we assume the characteristic for an angle between the vectors of the operating and restraining currents corresponding to maximum restraint. The minimum coefficient of sensitivity K_{sen} is determined by the quotient of the ordinate mn of the curve $I_{r.sh.} = f(I_t)$ corresponding to the current $I_{r.sh.}$ calculated under consideration of the fault resistances, by the ordinate mk of the curve $I_{op.r}(\text{II}) = f(I_t)$ for a restraining current also calculated under consideration of the fault resistances.

The consideration of the fault resistances in the calculation of the fault currents may be carried out by reducing the currents of a dead short-circuit by factors of 1.5–2. The coefficient of sensitivity of the protection at the minimum fault current must not be below 1.2–1.3.

The minimum coefficient of restraint of the protection K_{rest} is determined as the tangent of the angle of slope of the tangent to the characteristic of restraint $I_{op.r}(\text{I}) = f(I_t)$, drawn from the origin of the coordinates. It is found from the following expression

$$K_{rest} = K_r I_{op.}/I_{rest} = K_r K n_t/K_{cc} n_{t.r} \qquad (7)$$

where K_r – is the coefficient of reliability, $I_{op.}$ –the current in the operating winding of the interposing transformer, I_{rest} –the current in the restraining coil of the interposing transformer, K –the theoretical value of the coefficient of proportionality between the currents $I_{op.}$ and I_{rest}, n_t –the transformation ratio of the current transformers in the circuit of the main transformer, $n_{t.r.}$ –the transformation ratio of the current transformers in the circuit of the primary winding of the regulating autotransformer, K_{cc} –the coefficient of the circuit connections of the current transformers in the circuit of the main transformer.

By contrast to a protection with blocking relay the protection with a relay with restraint is intrinsically a high-speed protection, i.e. its reliable operation in the case of external short-circuits can be assured without introducing an additional time-lag.

Saturable interposing current transformers are also used for offsetting against magnetizing current rushes occurring when the transformer is connected under no-load conditions.

Fig.5a shows a single-line diagram of a variant of an autotransformer whose stationary lead-out is fixed at the mid-point of the winding. In this case the short-circuit currents are limited by the resistance of the winding at any position of the moving lead-out.

Fig.5b shows another variant of the autotransformer; the stationary lead-out of this is fixed at one end of the winding. When the moving lead-out is at the

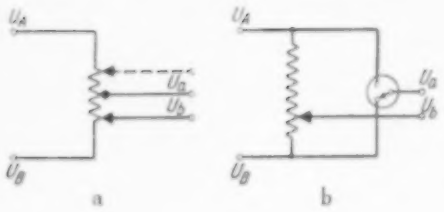

FIG.5. Variants of the Location of the stationary Lead-out of Autotransformers. a - stationary lead-out fixed at midpoint of winding; b - stationary lead-out fixed at ends of winding.

opposite end of the winding, the short-circuit currents are not limited by the resistance of the autotransformer and are of the same magnitude as on external short-circuits on the side to which the regulating element is connected. To such an autotransformer a protection with blocking relays cannot be applied since at the maximum regulation the values of the currents at the location of the blocking relays are of the same order in the cases of external short-circuits and of short-circuits at the lead-outs of the secondary winding of the autotransformer. Also, the protection with lockout may fail to respond at overload currents of the main transformer exceeding the operating current of the blocking relays.

A protection with restraining characteristic has none of the disadvantages mentioned; also, it may be made more sensitive and has a larger protected zone.

Fig.6 shows a comparison of the characteristics of the protection systems.

To simplify the analysis, the effect on the characteristic of the protection of the angle between operating and restraining currents is not considered. In the shaded areas A and B the protection with lockout does not operate, but the protection with restraint does. Area A corresponds to faults with small, area B to faults with large short-circuit currents.

The zone protected by the protection with restraint includes the regulating autotransformer, the connexions between autotransformer and series transformer, and parts of the series transformer. As current relay a relay of type ET-520 may be used.

It should be noted that the protection may be designed not only

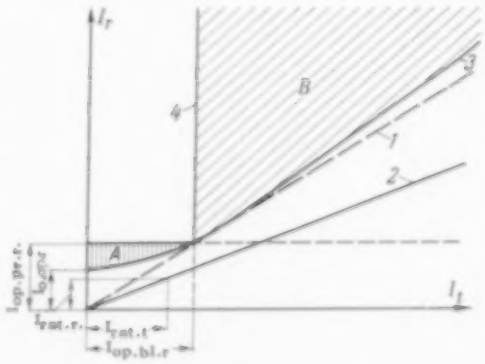

FIG.6. Comparison of Characteristics of Protection Systems for a Regulating Autotransformer.

1 - Ideal Characteristic; 2 - $I_r = KI_t$; 3 - characteristic of protection with restraint; 4 - characteristic of protection with lockout. $I_{op.op.r.}$ — operating current of operating relay; $I_{op.bl.r.}$ — operating current of blocking relay; $I_{rat.r.}$ — rated current of regulating autotransformer; $I_{rat.t.}$ — rated current of main transformer.

for the type of relays with restraint described above, but also with relays with independent restraining coils.

The difficulty of using commercially available relays with restraint consists in the fact that for the protection of a regulating autotransformer a relay with a high restraining factor is required. Orientating calculations show that the minimum restraining factor should be of the order of 1.5 – 2, whereas the commercial relays have only restraining factors of the order of 0.2 – 1.

Conclusions

The protection of a regulating autotransformer or transformer, using relays with a restraining characteristic has a number of advantages over a protection using blocking current relays. The protection with restraint is sufficiently sensitive for faults in a regulating autotransformer or transformer. For some types of regulating autotransformer only a protection with restraint may be used. The use of relays with restraining characteristic renders it possible to offset the relays against fault currents of external short-circuits and load currents. The protection with restraint is intrinsically a high-speed protection. It also requires fewer pieces of relay apparatus than the system with blocking relays.

1958

REFERENCES

1. B. Ya. Smelyanskaya and A.B. Chernin; *Relay Protection of auxiliary transformers for longitudinal voltage regulation under load. Elektrichestvo* No.5 (1954).

CURRENT IN THE CHARGE MATERIALS OF A FERROSILICON FURNACE*

I.T. ZHERDEV

(Received 24 November 1957)

The type of iron-alloying furnace most frequently used nowadays is the circular-shaft three-phase type of furnace with continuous electrodes arranged in a triangle symmetrically to the axis of the furnace (Fig. 1). In normal operation the lower part of the electrodes plunges into the charge materials with which the working space of the furnace is filled. The power is supplied to the electrodes by a special furnace transformer enabling the value of the lower voltage to be altered. For any selected voltage of the transformer the load regulation is carried out by a vertical displacement of the electrodes or by altering the resistance of the charge continuously introduced through the top of the furnace.

Despite the apparent simplicity of the plant and the considerable successes achieved where equipment and operation of alloying furnaces is concerned, there is as yet very little in the way of a theory of the processes taking place in these furnaces. For this reason the main parameters of new furnace designs are usually selected by analogy with furnaces already successfully operating. For the same reason, the choice of rational operating conditions and the rapid correction of deviations from the normal course of the process requires highly skilled and experienced personnel.

That knowledge of the processes in alloying furnaces is still insufficient is also confirmed by the fact that up to the present there is no generally accepted view on the distribution and main paths of the current in the working space of the furnace and, consequently, no generally accepted views on the most suitable equivalent circuit for such a furnace.

That current passes through the charge materials of alloying furnaces was pointed out a fairly long time ago by M.S. Maksimenko [1] and Vochke [2]. In a discussion organised by the *All-Union Central Scientific Research Institute* in 1954, the view that a charge current virtually does not exist was expressed.

This considerable divergence of opinions on one of the fundamental questions associated with the problem of the correct representation of the phenomena in the

* *Elektrichestvo* No. 5, 65 – 67, 1957 [Reprint Order No. EL 25].

sondes being open;

I_1' – the current in the charge between the blades when the external circuit of the sondes is closed;

I_1'' – the current in the external circuit of the sondes when it is closed;

r_0 – the resistance of the part of the charge through which the current passes between the electrode and through the nearest blade;

r_1 – the resistance of the part of the charge through which the current passes from one blade to the other;

s – area of the blade of the sonde.

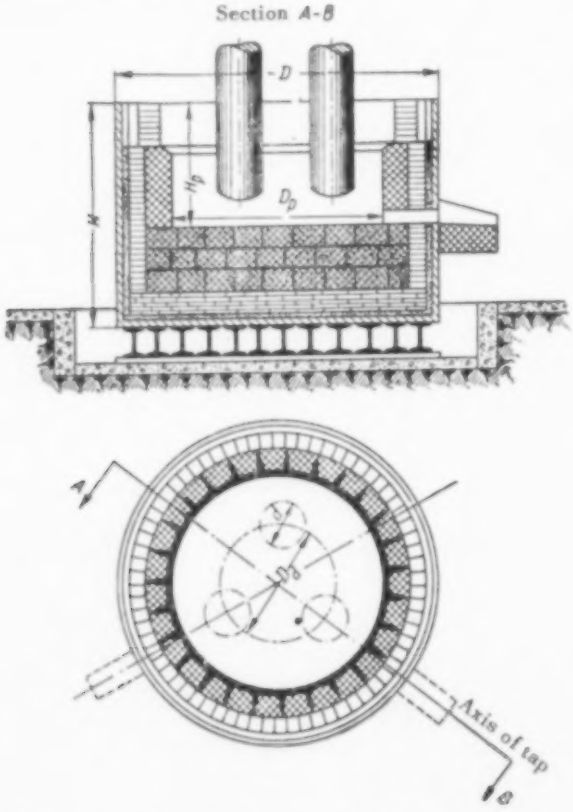

FIG. 1. Schematic plan and cross-section of a modern 3-phase alloying furnace.

Having calculated the p.d. between the blades of the sondes for open and closed external circuit of these sondes, we can express the current I_1' by the current I_1, viz:

$$I_1' = I_1 \frac{U_1 - U_2}{U_{10} - U_{20}}. \qquad (1)$$

Having determined the p.d. between the electrode and the blade of the sonde

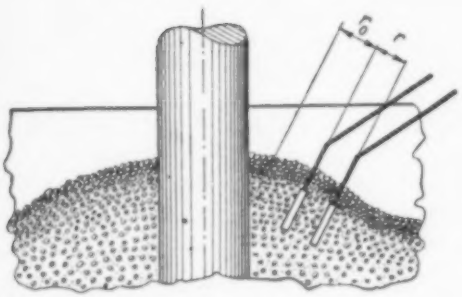

FIG. 2. Diagram of the location of the blades of the sondes for determining the current density in the charge materials.

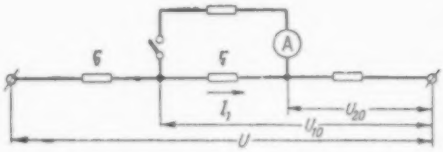

FIG. 3. Equivalent circuit for the current in the charge materials passing through the blades of the sondes.

nearest to it for open and closed external sonde circuit, we calculate the sum of the currents $I_1' + I_1''$, viz:

$$I_1' + I_1'' = I_1 \frac{U - U_1}{U - U_{10}}. \tag{2}$$

Substituting the value of current I_1 from (1) into (2), we get

$$I_1 = \frac{I_1''}{\frac{U - U_1}{U - U_{10}} - \frac{U_1 - U_2}{U_{20} - U_{10}}} \tag{3}$$

Equation 3 enables us to calculate the value of the current in the part of the charge between blades of the sondes under normal operating conditions of the furnace.

The mean current density in the charge materials in the volume enclosed by the surfaces of the blades of the sondes will be

$$j = \frac{I_1}{S}$$

From the current density and the p.d. it is easy to calculate the mean resistance of the charge between the blades of the sondes. The table brings together the results of measurements carried out by means of sondes in an actual furnace, and also the calculated current densities and resistances of the charge materials.

The above method of determining the current densities in the charge materials cannot claim to yield very accurate measuring results. In addition to the errors introduced by the basic assumptions, additional errors arise in the measurements on an actual furnace by incorrect arrangement of the blades of the sondes (deviation of the surface of the sonde from the equipotential surface), imperfect contact between the charge materials and the blades of the sondes, reduction of the area of the blades by their partial melting, etc.

It is, therefore, difficult to determine the magnitude and the character of the experimental error and the measured values of the current density shown in the table have, therefore, to be considered as purely orientating.

electric circuit of an alloying furnace is due to the absence of direct experimental demonstrations in favour of one or the other point of view.

The difficulties of carrying out experiments on an actual alloying furnace owing to the high temperature of the open top are well-known. However, it is possible to demonstrate the existence of a charge current and approximately to determine the current density in the charge materials in different parts of the working space of the furnace under conditions of industrial operation of such furnaces.

We give below a description of the method and the results of the experimental determination of current density in the charge of a ferrosilicon furnace. The measurements were carried out on a furnace (Fig. 1) producing 45 per cent ferrosilicon.

To measure the current densities in the charge we used sondes of a special form, produced from steel rods of 18 - 20 mm diameter and about 6 m length. One of the ends of each steel rod, about 300 m long, was bent to an angle of 60° and a blade of sheet steel about 10 mm thick and of an area of 200 - 300 cm^2 was welded to it.

1958

The ends of the steel rods were inter-connected through a current transformer by means of clamps and flexible cables. When the cables were connected, the current of the external circuit of the sondes could be measured. The blades were plunged into the viscous charge materials in the working space of the furnace near the electrodes. The equivalent circuit of the blades is shown in Fig. 2.

To determine the current densities in the charge, the potentials of each blade relative to the neutral point of the furnace (its hearth) were measured on the sonde circuit which was opened and closed on the current transformer. In addition, the phase voltage of the electrode near which sondes were placed, and also the current in the external circuit of the sondes when it was closed, were measured.

All the following calculations to determine the densities of the charge current are based on assumptions that the resistances of the parts of the charge along the paths of the current passing through the sondes blades retain their value whether the external circuit of the sondes is open or closed; moreover, it was assumed that all the resistances in the paths of the charge mentioned and in the sonde circuit are purely active. In this case the equivalent circuit of the actual circuit of the charge current through the blades of the sondes may take the form represented in Fig. 3.

It is not difficult to calculate the current in the charge flowing in the region of the blades of the sondes when the external circuit of these sondes is open. We introduce the following symbols:

U – is the potential of the electrode relative to the neutral point of the furnace;

U_{10} and U_{20} are the potentials of the first and second blades of the sondes relative to the neutral point of the furnace when the external circuit of the sondes is open;

U_1 and U_2 are the potentials of the same blades relative to the neutral point of the furnace when the external circuit of the sondes is closed;

I_1 – is the current in the charge between the blades, the external circuit of the

Area of the blade of the sonde (cm^2)	Distance between sonde blades (cm)	Distance from electrode to nearest sonde blade (cm)	Measured with the external sonde circuit open (V)			Measured with external circuit of the sondes closed				Calcu-current density, j (A/cm^2)	Calcu-resis-tivity (ohm. cm)
			U	U_{10}	U_{20}	$U(V)$	$U_1(V)$	$U_2(V)$	$I_1(A)$		
310	20	41	64	38	10	64	20	10	180	0.43	3.3
310	20	28	72	49	32	72	48	36	90	0.87	1.0
310	20	28	72	50	25	72	47	26	100	1.1	1.2
200	10	37	58	27.5	18.5	58	26	20	40	0.52	1.7
200	15	31	78	35	24	78	22	18	150	0.80	0.9

Nevertheless, the data in the table make it possible to trace a certain regularity in the variation of the current density in the charge materials. The current density in the charge decreases with increasing distance from the electrodes; a similar relationship should also be observed for the working space of the furnace since the area of the current-carrying cross-section of the charge materials increases with increasing distance from the electrodes.

The method of measurement by means of sondes buried in the charge materials we put forward enabled us to determine the order of magnitude of the densities and resistivities of the charge of a working ferro-silicon furnace. These experimental results confirmed the necessity of considering the conductivity current of the charge in the study of the electric circuit of a ferrosilicon furnace.

REFERENCES

1. M.S. Maksimenko; *Vliiganic raspredeleniya sil toka na induktionoe soprotivlenie pechnoga kontura pechi Mige (Effect of Current Distribution on the Inductive Reactance of the Circuit of a Mige furnace)*, *Metallurg*, No. 9 (1938).
2. I. Vochke; *The Electric Smelting Furnace*, *United and Technical Publishing Houses*, 346 and 361 (1936).

LARGE SYNCHRONOUS MOTORS WITH SOLID POLES ON THE ROTOR*

Z.B. NEYMAN

(Received 4 February 1957)

For the drive of some high-speed mechanisms, e.g. blowers, pumps etc., large electric motors are required for a speed of 1500 rev/min. The use of induction motors with squirrel cage rotor is uneconomic because of the reduced p.f. It also must be considered that with increasing power of the drive and therefore, of the motor, the energy dissipated in the short-circuited rotor winding during starting increases more than the heat capacity of the rotor. With large motors it is therefore difficult to keep the temperature conditions of the rotor within the permitted limits. A further problem is how to provide sufficient mechanical strength for the rotor. These factors limit the maximum rating of induction motors with squirrel cage rotors to about 2000 kW.

Better economic characteristics are obtained by the use of synchronous salient-pole motors with a short-circuited winding for starting, located in the pole shoes. But long experience with the operation of such motors shows that they often fail because of damage to the joints and breakage of the rods of the starter winding. The fundamental difficulty of a reliable design of the rotor of the synchronous motor with starter winding on the poles is the great amount of heat developed during starting which leads to excessive heating of the winding, especially with drives having a large flywheel moment.

For driving high speed mechanisms a series of synchronous motors of 1300, 2000 and 3000 kW has been developed by the "Ural-Elektroapparat" Works with solid rotor and solid pole shoes. These motors have no special short-circuit windings which makes them very reliable in service.

The starting of the motor as induction motor is done in the same way as with synchronous machines with short-circuited winding on the pole shoes, i.e. by across-the-line starting or through a reactor with a reduced voltage of 70 per cent of the rated value.

At the beginning of the starting process the current is distributed over the surface of the solid pole shoes, since at a frequency of, or about, 50 c/s the depth of

* *Elektrichestvo* No. 6, 32 – 35, 1957 [Reprint Order No. EL 26].

penetration of the current is small. The current runs parallel to the rotor axis and is terminated in a tangential direction at the edges of the pole shoes. The pole shoes are interconnected on both sides of the rotor by copper rings so that a part of the current circuit may be closed through these rings. With increasing rotor speed the frequency of the pole shoe current decreases and the current penetrates more deeply into the steel.

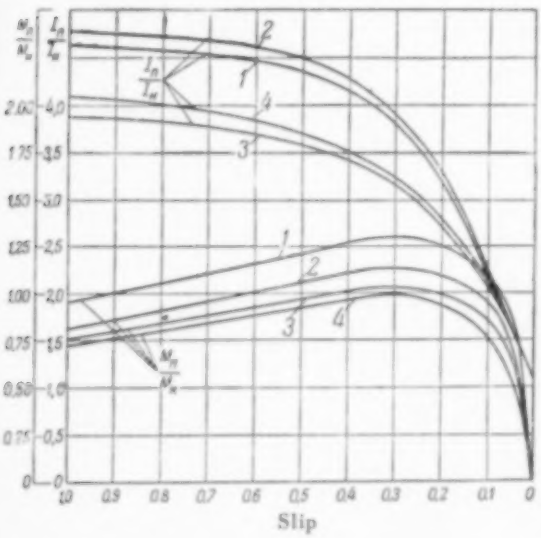

FIG. 1. Starting characteristics of the motor type DSP 116/49-4 (1300 kW, 6000 V, 1500 rev/min)
1 - rotor closed across discharge resistor, pole shoe faces connected through copper rings.
2 - rotor short-circuited, pole shoe faces connected through copper rings.
3 - rotor closed across discharge resistor, pole shoe faces open (copper rings removed).
4 - rotor short-circuited, pole shoe faces open (copper rings removed).

Fig. 1 shows the starting characteristics of the motor type DSP 116/49-4 (1300 kW, 6000 V, 1500 rev/min). These chacteristics correspond to starting at full voltage with the field winding of the motor short-circuited or closed across a discharge resistor. In order to check the effects of the rings connecting the faces of the pole shoes the starting characteristics were taken with and without these rings.

Fig. 1 shows that the asynchronous torque is considerably higher with the rings. The tests also showed that under asynchronous conditions the motor worked with better stability and pulled into synchronism more safely. As could be expected, the presence of the discharge resistor in the field circuit has a marked effect on the increase of the asynchronous torque.

The starting characteristics in Fig. 2 of a motor connected to a fan drive of the type D 3500-11 again show the favourable effect of the copper rings connecting the faces of the pole shoes.

The starting characteristics of the motor type DSP 140/74-4 (3000 kW, 6000 V, 1500 rev/min), also with solid pole shoes on the rotor, are reproduced in Fig. 3.

It should be noted that there are as yet no practical methods for determining the starting chacteristics of motors with solid poles on the rotor with the accuracy required. The method of calculating the starting process suggested by Kh. R. Bal'yan [1] yields somewhat low values of the starting characteristics.

It is known that with laminated poles the pole face losses are insignificant. But with solid poles, especially when the ratio of stator slot width to air gap is larger

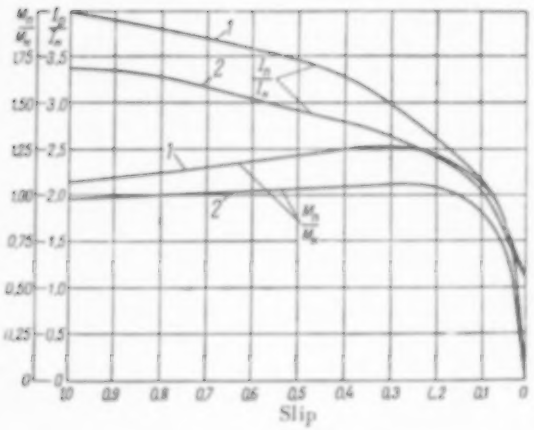

FIG. 2. Starting characteristics of the motor type DSP 116/49-4 connected with an exhauster type D 3500-11 (start on across the line with exhauster valve closed).
1 - rotor closed across discharge resistor, pole shoe faces connected through copper rings,
2 - rotor closed across discharge resistor, pole shoe faces open (copper rings removed).

than unity these losses increase considerably. On the motors of the series DSP this ratio is slightly larger than unity and therefore the effect of the surface losses on the total steel losses is insignificant. On an average, the pole face losses of these motors do not exceed about 8 per cent of the total losses in the machine.

The temperature rise of the pole shoes of the rotor during starting was determined by tests on a 1300 kW motor driving a fan type D 3500-11. During the start of the motor with resistors in the field circuit the temperature rise in the pole shoes was 100 - 130°C and in the connecting rings 140 - 180°C for an initial temperature of 50 - 60°C. Starting took about 16 sec. With direct connection of the field winding to the exciter, the temperature rise of the pole shoes was about 30 per cent higher than the above values.

These experimental data agree satisfactorily with values of the pole shoe temperature calculated from the duration of the start and the magnitude of the relative losses in the pole shoes at the instant of connecting the motor to the system. (Data of the Central Electrical Research Laboratory given in [2 and 3]).

The motors of the DSP series are of the fully-enclosed type and have two-way radial and axial ventilation. The air circulation in the machines is maintained by the rotation of the salient poles of the rotor and by two fans of the propeller-blade type mounted on the shaft at both ends of the rotor. (Fig. 4). The intake of the cool air is below the machine and so also the outlet of

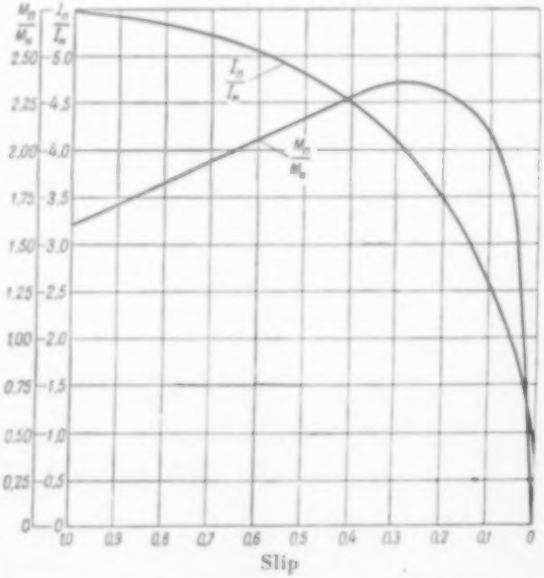

FIG. 3. Starting characteristics of the motor type DSP 140/74-4 (3000 kW, 6000 V, 1500 rev/min).

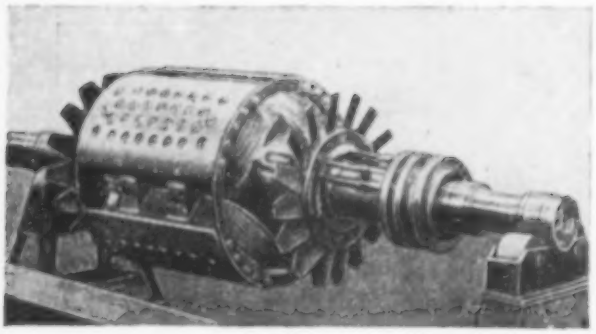

FIG. 4. Rotor of the motor type DSP 140/74-4 of 3000 kW.

the warm air through ducts of of the stator.

A special feature of the rotor design of the 1300 kW motor is its cross-shaped frame made of strong steel plates to which the four pole shoes are bolted. The copper rings are also bolted to the ends of the pole shoes.

For reasons of mechanical strength the rotors of the 2000 and 3000 kW motors are steel forgings. The rotor windings consist of bare copper strips. The turn insulation consists of varnished asbestos.

The stator bodies are of welded construction. The core is made of highly-alloyed dynamo sheets. The stator windings have reinforced mechanical clamping to ensure reliable service of the machine in transient conditions and during starting. The coil insulation is compounded mica.

The motors have bracket-type bearings with self-adjusting bushings; the working surfaces of the bearings are babbitted. The bearings of the motor have ring lubrication. The 3000 kW motors are also designed for forced-oil-lubrication. The bearings are provided with reliable oil-seals.

The excitation of the motors is obtained from directly-coupled exciters of type PN. The value of the field current for the motors of 1300 and 3000 kW is 370 and 490 A respectively. (Exciters type PN-205 and PN-400 are used.)

The motors with solid poles on the rotor have more favourable weight figures than synchronous and induction motors for 1500 - 300 rev/min (Fig. 5). Bearing in mind the weight of the exciter, which in the range considered amounts to about 5-6 per cent of the total weight of the motor, we find that the weights of the synchronous motors with solid poles are more favourable than those of four-pole induction motors. The efficiency of the synchronous motors of the series DSP is also higher than that of four-pole induction motors (Fig. 6).

The experience gained on design and operation of the four-pole synchronous machines of the type DSP of the "Ural-Elektroapparat" Works enables us to to state that the range of applications of high-speed synchronous machines of the series DSP could still be usefully extended.

Solid-pole synchronous condensers equipped with high-speed field regulation must be considered as a very promising application of the new design. Good starting characteristics of the motor with solid poles would render it possible to start the condensers at a very much reduced voltage and the presence of the large air gap between

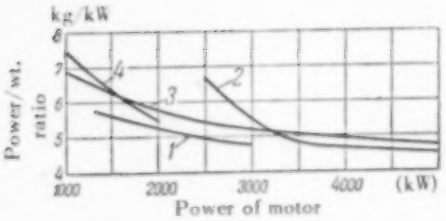

FIG. 5. Relative weights of the electric motors
1 - synchronous motors of the DSP-series, 1500 rev/min.
2 - synchronous motors of the CM-series, 3000 rev/min.
3 - induction motors 1500 rev/min.
4 - induction motors of the ATM-series, 3000 rev/min.

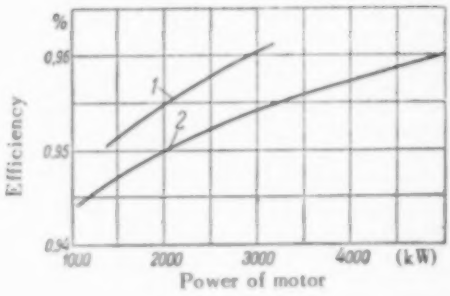

FIG. 6. Efficiencies of electric motors
1 - synchronous motors 1500 rev/min.
2 - induction motors, 1500 rev/min.

stator and rotor virtually suppresses the effect of the pole shoe face losses at the starting of the motor.

It is also suggested to develop a series of small condensers of the 2000-5000 kVA range at 1500 rev/min based on the design of the four-pole machines of the DSP series.

The experience gained in recent years with the operation of high-speed synchronous motors with solid poles on the rotor has confirmed the possibility of their wider use in place of smaller machines with laminated poles and with squirrel-cage windings in the pole shoes.

REFERENCES

1. R.Kh. Bal'yan, *On the design of the solid rotor. Elektrichestvo*, No. 6, (1955).
2. I.A. Syromatnikov; *Operating conditions of synchronous generator. Gosenergoizdat* (1952).
3. *Report No.* 1-113 *Central Electrical Research Laboratory* (1954).

TURBOGENERATOR ROTOR WITH DIRECT COOLING OF THE WINDING CONDUCTORS*

V.V. TITOV and Z.B. KOGAN

(Received 18 January 1957)

In the instructions of the Sixth Five-Year Plan for the development of the national economy of the U.S.S.R. for 1956 - 1960 by the 20th Congress of the Communist Party of the U.S.S.R. suggestions on the design and construction of large generators of ratings up to 300 MW were included.

In the course of the development of new types of large turbogenerators the "Elektrosila" Works designed and produced an experimental rotor with direct hydrogen-cooled conductors. This rotor was installed in an actual set of 30 MW rating in one of the Leningrad power stations in 1956 and was tested in service on load.

Design of the Rotor Winding

In the project the design of the rotor was based on the principle of self-ventilation with inlets and outlets for the cooling gas distributed over the whole length of the rotor. This leads to the most uniform distribution of the copper temperature along the machine.

The principle of introducing the cooling gas into the rotor directly from the air gap of the machine is well known; it is used by the American General Electric Co. In the generators of this firm the gas circulates in the longitudinal or the axial direction of the rotor through ducts formed by the hollow rotor conductors. The length of the sections of these ducts is about 500 - 600 mm. The gas enters and leaves each conductor through a system of openings in the rotor teeth and slot wedges. The gas flow in a rotor of this design is shown schematically in Fig. 1.

The "Elektrosila" Works used an original construction and layout of the ducts in the rotor conductors. The coils in the slotted part of the rotor consist of conductors of the usual rectangular cross section. On the lateral faces of the coils oblique channels 18 mm wide are milled all along the slotted part of the rotor. At either side of each coil the channels are inclined at the same angle to the axis of the conductors, but slope in different directions. The gas enters a channel

* *Elektrichestvo* No. 6, 35 - 38, 1957 [Reprint Order No. EL 27].

through an opening in the wedge, flows along and down the coil to the bottom of the slot, passes under the bottom turn, up through a channel on the other side of the coil, and into the air gap through an outlet opening also in the wedge. Inlet and outlet gas zones alternate on each side of the coil. The width of a zone equals the spacing between the inlet and outlet openings of the connected ducts. The distribution of the channels is shown in Fig. 2.

The bottom of the rotor slot is semi-circular in shape and is filled with an insulating packing which is grooved to allow the gas to flow from one side of the coil to the other. The end connectors or parts of the coils outside the rotor body are of hollow section. Each conductor consists of two U-shaped bars forming an internal duct in the conductor which is linked to a sloping channel in the slotted part of the rotor. The gas, having passed through the duct in the end connector, is discharged through the lateral sloping channel into the air gap. Provided a sufficiently high velocity of gas flow through the ducts and channels is assured, this design will result in a good heat dissipation and in practically uniform copper temperature all along the winding.

FIG. 1. Schematical diagram of gas flow along rotor winding conductors. General Electric Company.

FIG. 2. Schematical representation of gas flow along winding conductors of rotor of "Elektrosila" Works.

The gas velocity in the ducts and channels is greatly affected by the shape and dimensions of the inlet and outlet openings for the cooling gas. On the experimental rotor the openings in the wedge were designed in the simplest manner which would still enable smooth inlet and outlet passage between the gap and the slot to be obtained (Fig. 3.). In the gas inlet zone the slot wedge was provided with a lip projecting slightly above the surface of the rotor. The channels in the slot wedges through which the gas enters the slots are arranged alternately in the leading and trailing edge, thus assuring a uniform distribution of the gas on both sides of the coil in every slot. The rotor teeth opposite the inlet openings in the wedges are chamfered in a radial direction. In the gas outlet zone the openings in the wedges are arranged on a slightly smaller diameter and the wedges do not project above the surface; the outlet openings also face annular grooves turned with a uniform pitch at the rotor surface. During the tests it was found that the gas velocity in a channel was on an average 20-25 per cent of the peripheral speed of the rotor.

The manufacture of the experimental rotor made it possible for the new design to be thoroughly tested. In contrast to the production processes required for a rotor of normal design the production of the coils and their insertion into the slots required the development of many specialized techniques. The U-shaped copper end connections were wound as coils and cut into four parts. The individual parts and the rectangular strips for the slots were fitted in a template and welded together. The finished half-turns were checked on the template, where they were formed to their final shape. When the inter-turn insulation had been applied, they were inserted into the rotor slots and welded together.

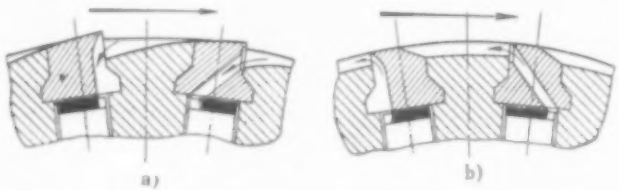

FIG. 3. Section through teeth and slot wedges a-gas inlet zone; b-gas outlet zone

The slot insulation was made of glass-textolite. The forming and stoving process of the coils did not take long, although the insertion and matching of the turns was very difficult. The machining of the rotor surface was not very difficult, since the gas inlet and outlet openings were not in the teeth, but in the slot wedges. In future it is proposed to use pressure cast wedges of a light and strong alloy. This will enable suitable shaped openings to be obtained with a satisfactory surface finish without further processing.

Owing to the fact that the rotor end connector is a hollow bar and is deeper than in a normal design, the total number of turns per pole is smaller, and the exciting current is correspondingly increased. If the exciting current on load in an ordinary turbogenerator rotor of 30 MW rating is 470-490 A, the corresponding current in the experimental rotor with direct-cooled conductors is about 1500 A. This required the rotor brush gear and slip rings to be correspondingly larger. The width of the brush contact surface of the slip rings was doubled in comparison with the normal design (cuts of worm wheel shape being also made in their middle parts), with a view to improving the cooling of the rings. The contact area between the current carrying studs and the slip rings, and the slip ring lead in the rotor bore were also enlarged.

The generator in which the experimental rotor was tested was provided with a new excitation system. A direct driven synchronous high-frequency generator supplied to a system of semi-conductor rectifiers, the rectified current being supplied to the rotor slip rings. The new excitation system is now being subjected to tuning-up and service tests.

The new design of rotor is mechanically stiffer than a normal rotor for the same turbogenerator. This is due to the reduction in weight of the rotor winding owing to the internal cooling of the conductors, and to the reduced over-hang of the end connectors resulting from reduced inter-coil spacing and solid packing of the end turns. In the new design it was possible to increase slightly the diameter of the rotor shaft under the end connectors and as a result, the deflection of the rotor shaft is reduced, thus relieving the stresses in the bearings.

Assembly and Operation

In recent years, sufficient data on the operation of turbogenerators with a hydrogen pressure of 0.05 - 0.1 atm gauge have become available. There are, furthermore, some operational results available at still higher pressures. For example, as early as 1953 tests were carried out on a set of 30 MW rating with special radial seals for operation at a gas pressure of 0.5 atm. Continued operating experience enables us to conclude that this type of seal is the most convenient and would make it possible to raise the gas pressure to 2 - 3 atm.

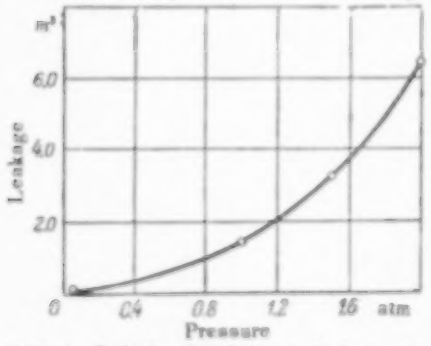

FIG. 4. Relationship between hydrogen leakage per day and pressure.

During a long period of operation it was also found that the oil pressure on the seals must exceed the gas pressure in the machine by not less than 0.3 atm. At a gas pressure of 0.05 atm the impellar-type oil pump of the turbine, producing an oil pressure of 0.3 - 0.35 atm at the seals, assures normal operation of the unit. When the gas pressure is raised, it is necessary to adjust the oil pumps, which must run continuously.

On the generator considered, two oil pumps were provided, viz. the working pump and a stand by pump, with a head of 3.5 atm gauge. The stand-by pump is automatically started when the oil supply to the sealing bearings fails or if the oil pressure falls below a pre-set value.

To improve the performance of the oil seals the rotor shaft has a conical part immediately behind the seal to prevent the oil from creeping along the shaft. After a period of operation of the generator in air, an inspection was carried out in which complete absence of oil on the surface of the shaft behind the seals was established. It should be noted that if the temperature of the sealing bearings was previously found to be of the order of 50 - 57°C., this was reduced by the new design to 45 - 46°.

Before the installation of the experimental rotor designed to work at a hydro-

gen pressure of 2 atm gauge, the stator of the machine was tested by compressed air at a pressure of 3 atm gauge. Points of gas leakage were carefully observed and removed by scaling the individual micro-cracks by welding. This considerably reduced the gas leakage from the generator during operation. It is recommended that in future compressed air tests on stators should be carried out in the works, as this results in a considerable improvement in the quality of the machines delivered and also facilitates and accelerates the change-over of newly erected generators to hydrogen cooling.

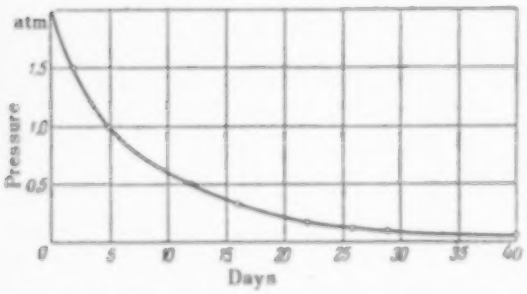

FIG. 5. Reduction of gas pressure in a turbogenerator.

The operation of the generator at higher hydrogen pressures required a number of alternations in the gas circuit to be carried out. In particular, the design becomes more convenient, if the liquid relay is removed from the hydrogen panel and erected separately. A new system of automatic hydrogen supply was also installed.

Sustained operation of the set on full load at a hydrogen pressure of 0.05 atm gauge showed that the hydrogen leakage was of the order of 0.10-0.12 m^3 per day. When the gas pressure is raised, the gas leakage increases considerably (Fig. 4). Since an analysis of the gas sampled from the oil detraining pipe does not reveal any changes of its composition at various gas pressures, we must assume that the leakage is not confined to the seals, but also finds its way through leaks in the casing of the machine.

At pressures of 0.5-2 atm gauge the purity of the hydrogen hardly varies at all and keeps within limits of 95.7-95.3 per cent.

The quality of the hermetic sealing of the machine is indicated by Fig. 5, which shows that in a period of 40 days the gas pressure fell from 2 to 0.5 atm gauge in the running machine in the complete absence of a further supply (topping up). During these tests the relationship between the oil consumption of the seals and pressure was established (Fig. 6).

Results of the Thermal Tests

Fig. 7a shows that when the temperature rise of the rotor copper is 105°C., i.e. the maximum permissible temperature rise of insulation of class VS, a rotor with surface cooling by air may be loaded to 420A (curve 1). If, however,

the load of the generator is 30 MW and the power factor 0.8, the exciting current will be 490A and the temperature rise of the copper will be about 140°C.

The direct cooled rotor running in air and with an exciting current of 1450A, corresponding to the same load of 30 MW, has a temperature rise of 62.5°C. (curve 1. Fig. 7b) i.e. only 45 per cent of the figure applying to surface cooling. We see, therefore, that even with air cooling the new rotor assures reliably the full output of the generator. The test results obtained on the rotor showed that if the hydrogen pressure is not increased, the temperature rise of the copper under the rated conditions of operation will also be 45 per cent of the value obtaining for surface cooling by hydrogen (curves 2 and 4 of Fig. 7).

If, however, the hydrogen pressure is 2 atm gauge, the temperature rise of the copper under the rated operating conditions is only 16 per cent of the temperature rise for surface cooling by hydrogen at a pressure of 0.05 atm gauge.

1958

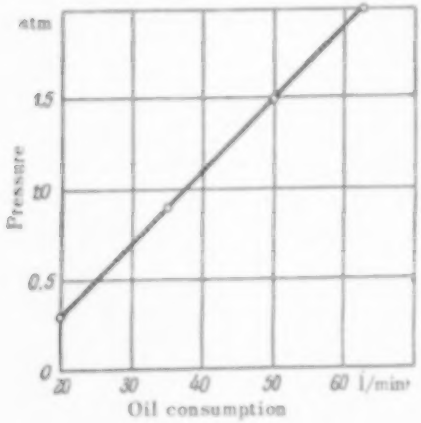

FIG. 6. Relation between hydrogen pressure and oil flow through seals.

If we keep the temperature of the copper at the previous level, the maximum rotor current could be increased by a factor of 2.5. However, since the insulation of the rotor winding and, particularly, the inter-turn insulation of direct cooled conductors works under more severe conditions, it is preferable to maintain the average temperature of the winding at a slightly lower level with a view to reducing the thermal deformation of the turns. This is particularly important from the viewpoint of the reliable operation of a generator under conditions of repeated shorttime overloads and forced excitation on short-circuits. The increased current density in the rotor winding (approximately double the usual value) causes considerable short-time temperature rises which must not impair the dielectric strength of the inter turn insulation.

Assuming the average temperature rise of the copper, measured by the resistance method, as equal to 65-70°C., we can obtain with the same dimensions of the active part of the rotor a total rotor current 2.0-2.2 times higher than with

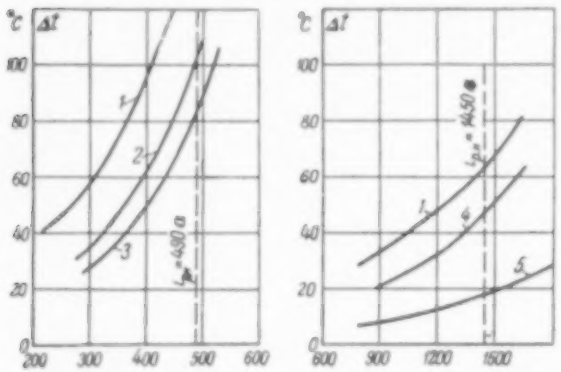

FIG. 7. Temperature rise of rotor winding above ambient temperature
a) rotor with surface cooling; b) rotor with direct cooled winding.
1) air cooling; 2) hydrogen cooling, $p = 0.35$ atm gauge;
2) id., $p = 0.5$ atm gauge; 4) id., $p = 0.05$ atm gauge;
5) id., $p = 2$ atm gauge.

surface cooling of the winding. The possible increase of the exciting current vs. hydrogen pressure is plotted in Fig. 8.

CONCLUSIONS

1. The experience gained in manufacture and the results of thermal tests on the experimental rotor designed by the "Elektrosila" Works permit us to expect that this method of direct cooling of the rotor conductors may be used in the design of turbogenerators rated at 200 to 300 MW.

2. The calculations show that the utilization of the materials in a turbogenerator with a rotor of the new design and a conventional stator is improved on an average by 60 per cent as against the most fully utilised machines of normal design. Also, the operating temperature of the rotor winding is then not more than 80 per cent of the permissible temperature for the rotor insulation with the usual cooling system.

3. The new design of rotor winding may be used successfully for hydrogen cooled turbogenerators of 30-150 MW rating; this means that though the main operational parameters of the machine are unchanged, its weight and dimensions can be reduced by 30-35 per cent against those of existing machines. This is a considerable advantage from the point of view of reducing the production costs of generators. and also to facilitate transport and installation.

4. The manufacturing processes for the new design of rotor winding are undoubtedly more difficult than those of the conventional machine. However, if the technique is appropriately developed and carried out with the use of special, but not referred to unit output of the machine, may not on the whole be greater than with the present design.

5. For generators working at higher hydrogen pressure the use of shaft seals of a special type is recommended.

6. The stators of hydrogen cooled turbogenerators should be tested in the works with compressed air.

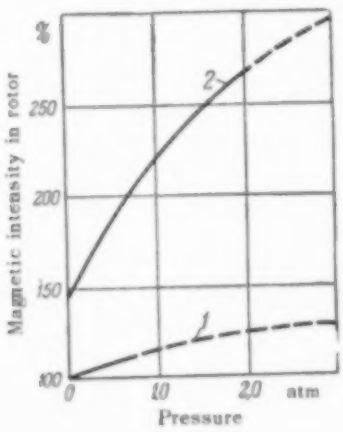

FIG. 8. Rotor ampere-turns vs. hydrogen pressure for various methods of cooling rotor winding.

1958

HIGH-VOLTAGE AUTO-TRANSFORMERS*

A.G. KRAIZ

(Received 17 January 1957)

The present communication considers some characteristic features of the operation and design of H.V. auto-transformers. The basic circuit diagram of an auto-transformer is shown in Fig. 1. The H.V. winding and the M.V. winding are taken conventionally as the series and the common windings, respectively.

Conditions of operation of auto-transformers

The most important conditions of operation are the following:

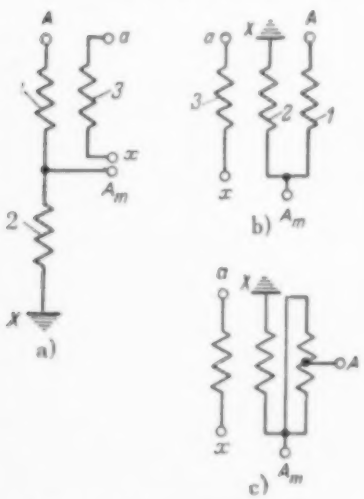

FIG. 1. Basic diagram of an auto-transformer. a) schematic arrangement of windings; b) actual arrangement of windings, H.V. bushing at end of winding; c) actual arrangement of windings, M.V. bushing at midpoint of winding. 1-H.V. winding; 2-M.V. winding- 3-L.V. winding.

a) *Operating conditions H.V.-M.V. and M.V.-H.V.* This case refers to pure auto-transformer operation. A step-down auto-transformer with H.V. and M.V. windings arranged in series will, as a rule, deliver to the load its full rated kVA. With a step-up auto-transformer having the L.V. winding placed between the H.V. and M.V. windings it is sometimes necessary to limit output below the auto-transformer rating, to avoid an excessibely additional iron loss due to magnetic flux leakage. The short-circuit loss will under these conditions be 60-70 per cent of the maximum loss.

b) *Operating conditions H.V.-L.V. and L.V.-H.V.* Under these conditions the machine operates as a pure transformer and the output kVA is equal to the kVA rating of the L.V. winding. The short-circuit loss is about 55 per cent of the maximum loss.

c) *Operating conditions M.V.-L.V. and L.V.-M.V.* Operation as a pure transformer with output kVA equal to the rated kVA of the L.V. winding. The short-circuit loss is 45-55 per cent of the maximum loss (for a step-down auto-

* *Elektrichestvo* No. 6, 39 – 44, 1957 [Reprint Order No. EL 28].

transformer).

d) *Combined transformer-auto-transformer operation H.V. - M.V.* simultaneously with L.V. - H.V. Under these conditions there is the greatest short-circuit loss. The maximum permissible load is limited by the current in the H.V. winding which should not exceed the rated current I_{1n}. If the load on the L.V. side is $S_3 = 0$, the machine operates as a pure auto-transformer (conditions H.V. - M.V. and M.V. - H.V.). If S_3 increases, there should be a corresponding decrease of S_2 on the M.V. side to avoid overloading the H.V. winding.*

To determine the permissible loads S_2 and S_3 for different values of the power factor, let us consider the current vector diagram of an auto-transformer operating under combined conditions and supplied on the H.V. side (Fig. 2a). Also, let us assume that the rated current I_{1n} flows in the H.V. winding, i.e. that the auto-transformer is being supplied with (or supplies) on the H.V. side its rated kVA. On this vector diagram $I'_2 = I_2/k_{12}$ and $I'_3 = I_3/k_{13}$ represent currents referred to the H.V. side; $k_{12} = U_{1n}/U_{2n}$ is the transformation ratio between the H.V. and M.V. sides and $k_{13} = U_{1n}/U_{3n}$ is the ratio between the H.V. and L.V. sides.

1958

From the vector diagram it follows that

$$I'^2_2 + I'^2_3 + 2I'_2 I'_3 \cos(\varphi_2 - \varphi_3) = I^2_{1n}. \tag{1}$$

Multiplying (1) by $(U_{1n})^2$, we get an expression for kVA loads.

$$S'^2_2 + S'^2_3 + 2S'_2 S'_3 \cos(\phi_2 - \phi_3) = S^2_{1n} \tag{2}$$

Dividing both sides of (2) by S^2_{1n}, we get an equation relating the relative loads (i.e. loads expressed as fractions of rated output of the auto-transformer) $S'_2 = S_2/S_n$ and $S'_3 = S_3/S_n$.

$$s^2_2 + s^2_3 + 2s_2 s_3 \cos(\varphi_2 - \varphi_3) = 1. \tag{3}$$

By the use of this equation it is possible to determine the permissible loads on the M.V. and L.V. sides for different values of the power factors $\cos\phi_2$ and $\cos\phi_3$. Fig. 3 gives curves plotted from (3) for $\cos\phi_2 = 1$ and $\cos\phi_3$ varying between 0 to 1.

As stated above (3) and the curves of Fig. 3 were obtained for the condition of full-load on the H.V. winding i.e. for $I_1 = I_{1n}$. It is of interest also to determine for this case the current I_{MV} passing through the common part of the auto-transformer winding (the M.V. winding). Let $I_{*MV} = I_{MV}/I_{MVn}$ denote the relative magnitude of this current referred to the rated current of the M.V. winding, $I_{MVn} = I_{1n}(k_{12} - 1)$. It is not difficult to obtain an expression for the current I_{*MV} from the vector diagram.

$$I_{*MV} = \sqrt{s^2_2 + \left(\frac{s_3}{k_{12} - 1}\right)^2 - \frac{2s_2 s_3}{k_{12} - 1}\cos(\varphi_2 - \varphi_3)}. \tag{4}$$

If $k_{12} = 2$, (4) assumes the following form:

$$I_{*MV} = \sqrt{s^2_2 + s^2_3 - 2s_2 s_3 \cos(\varphi_2 - \varphi_3)}. \tag{5}$$

Fig. 4 shows curves plotted from (5). These curves represent the current in the M.V.

* All quantities referring to the H.V., M.V., and L.V. sides will be denoted by subscripts 1,2 and 3, respectively.

winding at cos $\phi_2 = 1$ for different values of cos ϕ_3 and for different loads on the L.V. winding. In the particular case when the loads on the M.V. and L.V. sides are non-reactive, and with the L.V. winding fully loaded ($s_3 = 0.5$), $I_{*MV} = 0$, i.e. although the M.V. winding supplies in this case a load equal to one-half of the rated output of the auto-transformer, it does not carry any current.

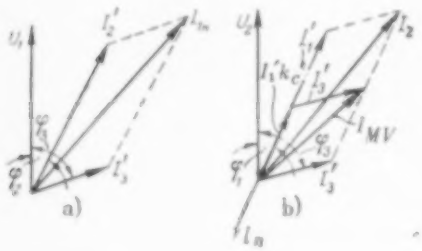

FIG. 2. Vector diagrams of the auto-transformer. a) Conditions H.V. - M.V. simultaneously with H.V. - L.V. b) Conditions M.V. - H.V. simultaneously with M.V. - L.V.

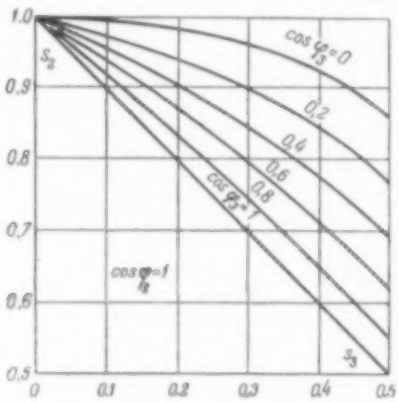

FIG. 3. Curves of permissible loads s_3 and s_1 for an auto-transformer operating under conditions H.V. - M.V. simultaneously with H.V. - L.V.

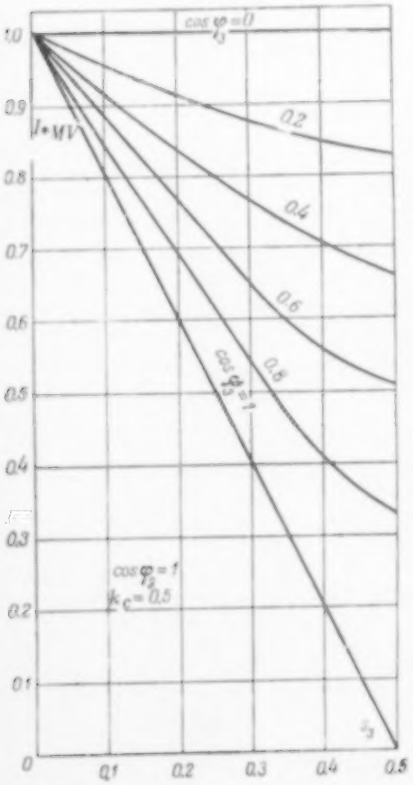

FIG. 4. Relative current in M.V. winding against L.V. winding load. Conditions of operation H.V.-M.V. simultaneously with H.V. - L.V.

e) *Combined transformer-auto-transformer operation* H.V. - M.V. simultaneously with L.V. - M.V., or M.V. - H.V. simultaneously with M.V. - L.V. Under these conditions the greatest input or output kVA on the M.V. side are limited by the current I_{MV}. Let us assume that the M.V. winding is fully loaded, i.e. the current carried by it is

$$I_{MV} = I_{MVn} = k_c I_{2n} = I_{1n}(k_{12} - 1), \quad (6)$$

where

$k = 1 - \frac{1}{k_{12}}$ is the auto-transformer transformation co-ratio, or the capacity coefficient.

The case when the M.V. winding is the primary is represented by the vector diagram of Fig. 2b.

According to this diagram the rated current of the M.V. winding is

$$I_{MVn} = \sqrt{(I_1' k_c)^2 + I_3'^2 + 2 I_1' I_3' \cos(\varphi_1 - \varphi_3)}, \tag{7}$$

where

$$I_1' = I_1 k_{12} \text{ and } I_3' = \frac{I_3}{k_{23}}.$$

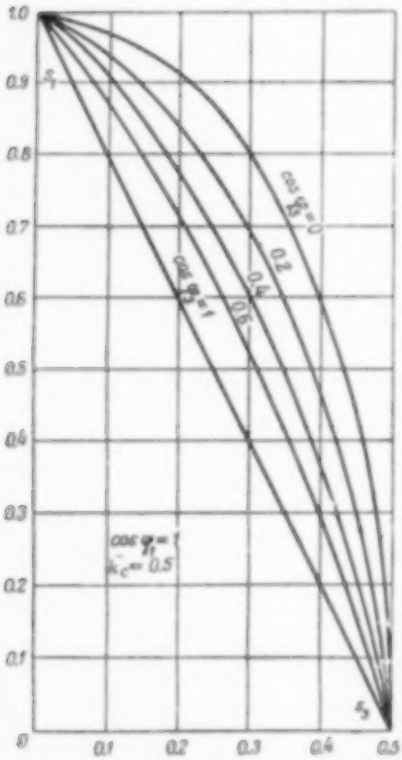

FIG. 5. Curves of permissible loads s_1 and s_3 for auto-transformer operating under conditions M.V. - H.V. simultaneously with M.V. - L.V.

From (7) we get after simple transformations and using the expressions for the relative loads,

$s_1 = \frac{S_1}{S_n}$ and $s_3 = \frac{S_3}{S_n}$,

$$s_1^2 + \left(\frac{s_3}{k_c}\right)^2 + \frac{2 s_1 s_3}{k_c} \cos(\varphi_1 - \varphi_3) = 1. \tag{8}$$

This equation enables for the operating conditions considered the permissible loads s_1 and s_3 of the primary and tertiary windings to be determined, if the corresponding power factors are known.

Equation (8) takes the following form if $k_c = 0.5$. (for 220/110 kV auto-transformers).

$$s_1^2 + 4 s_3^2 + 4 s_1 s_3 \cos(\varphi_1 - \varphi_3) = 1. \tag{9}$$

Using (9) the graphs of Fig. 5 were constructed for $\cos \phi_1 = 1$ and for different values of $\cos \phi_3$.

Voltage regulation

On-load voltage regulation by means of a boosting unit connected between the common neutral point of the H.V. and M.V. windings and earth is provided nowadays for auto-transformers of home production (Fig. 6). This type of construction results in "tied" voltage regulation in these windings since the e.m.f. of the series transformer adds to the e.m.f.'s of both the H.V. and M.V. windings at the same time.

Using the diagram of Fig. 6, let us find the relation between the additional e.m.f. and the primary and secondary voltages for a step-down auto-transformer.

$$E_{add} = \frac{U_2}{k_c} - \frac{U_1}{k_{12} - 1} \tag{10}$$

Expressing the voltages and the additional e.m.f. as percentages, viz.,

$$e_{add}\% = \frac{E_{add}}{U_{1n}} 100\%; \quad u_1\% = \frac{U_1}{U_{1n}} 100\%; \quad u_2\% = \frac{U_2}{U_{2n}} 100\%,$$

we get

$$e_{add}\% = \frac{u_2\% - u_1\%}{k_{12} - 1}. \tag{11}$$

Equation (11) allows us to determine the additional e.m.f. (in per cent of the rated H.V. winding voltage) for given values of u_1 and u_2. Substituting into (11) for $u_2\% = 100\% = \text{const}$, we get the additional e.m.f. necessary to maintain rated voltage on the secondary of the auto-transformer when the voltage on the primary changes (under no-load conditions).

Substituting $u_1\% = 100\% = \text{const}$, we get the additional e.m.f. necessary to obtain a given secondary voltage while the primary voltage is kept at its rated value.

Fig. 7. shows curves for both the above cases. It is seen that the additional e.m.f. becomes greater as the transformation of the auto-transformer, k_{12}, decreases.

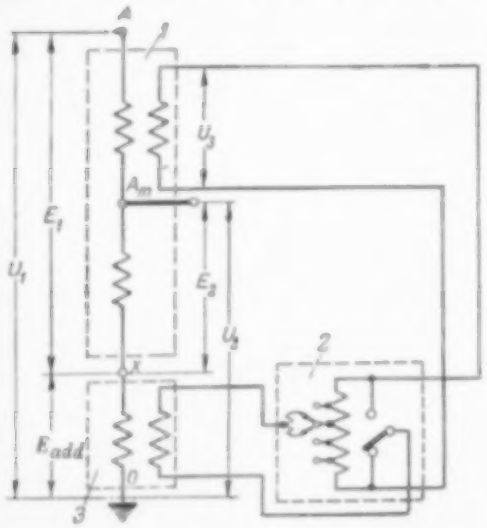

FIG. 6. Circuit diagram of auto-transformer with boosting unit connected to the common neutral point of the H.V. and M.V. windings. 1 - main auto-transformer; 2 - regulating auto-transformer; 3 - series auto-transformer.

The coefficients k_{12} and k_c used above are collected in Table 1, for various auto-transformer standard voltage ratings.

TABLE 1.

U_{1n}/U_{2n}	k_{12}	k_c
150/110	1,365	0,267
220/150	1,47	0,32
400/220	1,82	0,45
220 110	2,00	0,50
400/150	2,67	0,63
110.35	3,14	0,68
400/110	3,64	0,73

The system of voltage regulation by means of a boosting unit connected to the neutral point of the auto-transformer leads in some cases to over-excitation of the latter, in others to under-excitation. Auto-transformer over-excitation expressed in absolute values is given by $\Delta E_1 = E_1 - E_{1n}$

or in percentage values $\Delta e_1\% = \dfrac{E_1}{U_{1n}}\ 100\%$.

The percentage excitation can be calculated using the following formula

$$\Delta e_1\% = \frac{1}{k_c}\left(u_1\% - \frac{u_2\%}{k_{12}}\right) - 100. \qquad (12)$$

Fig. 8 gives curves constructed from (12). The curves show auto-transformer excitation for various values of k_{12} and for various differences between the applied primary voltage on the H.V. side and the rated voltage.

For example, if a voltage of 242 kV ($u_1\% = 110\%$) is applied to the H.V. winding of the 220/110 kV auto-transformer ($k_{12} = \dfrac{220}{110} = 2$; $k_c = 0.5$), the overexcitation is

$$\Delta e_1\% = \frac{1}{0.5}\left(110 - \frac{100}{2}\right) - 100 = 20\%$$

which would lead to an excessive increase in the no-load loss and current.

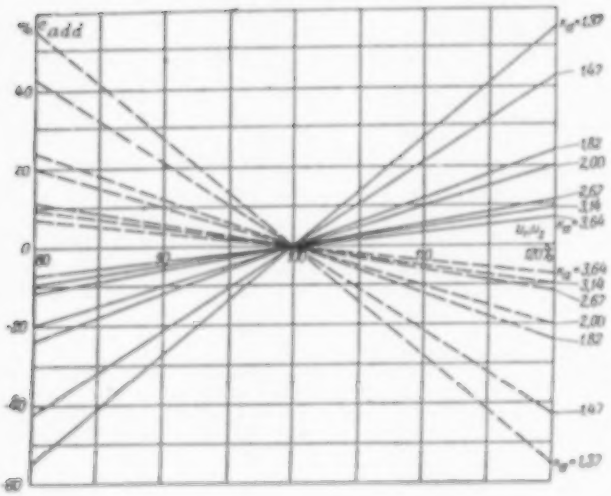
%
e_{add}
40
20
0
-20
-40
-60
80
60
40
20
0
20
40
60
80
100
120
140
160
180
200
220
240
260
280
300
320
340
360
380
400
420
440
460
480
500
520
540
560
580
600
620
640
660
680
700
720
740
760
780

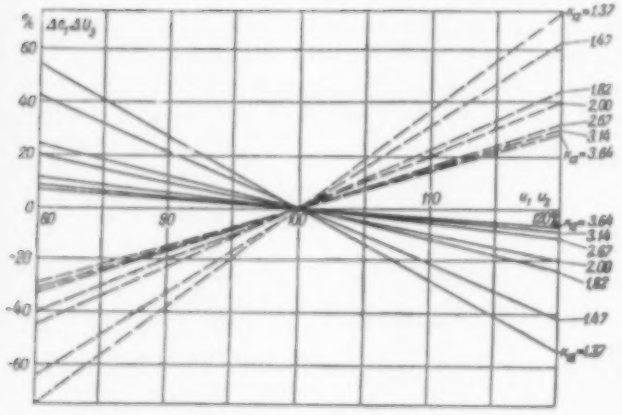

FIG. 8. Auto-transformer overexcitation $\Delta e_1\%$ and the deviation of the tertiary voltage from the rated voltage, $\Delta u_3\%$ against the voltage on the H.V. or M.V. side (for "tied" regulation).
Continuous lines - $\Delta e_1\% = \Delta u_3\% = f(u_2\%)$ for $u_1\% = 100\% = \text{const}$.
Broken lines - $\Delta e_1\% = \Delta u_3\% = f(u_1\%)$ for $u_2\% = 100\% = \text{const}$.

Thus, from (12) and (13) and the graphs of Fig. 8 we can also determine the deviation of the tertiary voltage from its rated value.

An examination of Fig. 8 reveals yet another shortcoming of the "tied" regulation. If the voltage $u_2\%$ on the M.V. side is increased while keeping $u_1\% = \text{const} = 100\%$, the voltage on the L.V. side drops ($\Delta u_3\%$ is negative).

If, however, $u_2\% = 100\%$ is kept constant, the voltage on the L.V. side varies as the applied voltage u_1 changes.

The drawbacks of the "tied" regulation can be avoided by connecting the boosting unit in the H.V. or M.V. line, or between the common and the series windings of the auto-transformer. Such systems are not entirely free from disadvantages either. These, however, cannot be discussed here because of lack of space.

It may be stated that the best solution to the problem of voltage regulation is to insert the regulating equipment always in the main auto-transformer provided that this is possible from considerations of transport requirements.

Surge phenomena in auto-transformers

The differences in the surge behaviour of transformers and auto-transformers are due to the fact that there is a direct electrical connexion between the H.V. and M.V. windings.

A surge can impinge on the H.V. winding either from the side of its line end (end A, Fig. 1) or from the opposite side - the M.V. line (end A_m, Fig. 1). In both cases the initial (capacitive) voltage distribution along the H.V. winding (the steepness of which determines the amplitude of the following oscillations) is different since it depends on the ratio of the series (coil-to-coil) to shunt (coil-to-earth) capacitances. The least steepness of the curve of the initial voltage distribution occurs when the wave enters the winding at the line end A. Thus, the effect of surges on auto-transformers should be considered for the above two cases.

In Table 2 a comparison is made between the voltages on line terminals of windings for 220/110/11 kV step-down and step-up transformers and auto-transformers impulsed with the 1.5/40 μsec full wave. The data shows that with the impulse applied to the terminal A (220 kV) the voltage on the terminal Am (110 kV) is $0.25 \times 945 = 236$ kV_{max} for step-down transformers and $0.68 \times 945 = 644$ kV_{max} for step-down auto-transformers, the full-wave impulse voltage test level being only 480 kV_{max} for the 110 kV insulation class (945 kV_{max} for the 220 kV class).

TABLE 2.

	Impulse voltage applied to terminal A			Impulse voltage applied to terminal Am		
	A—O, (%)	Am—O (%)	Am—O (kV_{max})	O—Am (%)	A—O (%)	A—O (kV_{max})
Transformer:						
a) step-down	100	25	236	100	117	561
b) step-up	—	—	—	100	220	1 030
Auto-transformer:						
a) step-down	100	68	644	100	219	1 050
b) step-up	100	100	945	100	300	1 440

With the impulse applied to Am (110 kV) we get, correspondingly, $1.17 \times 480 = 561$ kV_{max} for transformers and $2.19 \times 480 = 1050$ kV_{max} for auto-transformers which also exceeds the full-wave impulse test level for 220 kV insulation class (945 kV_{max}).

To prevent breakdown of auto-transformer insulation under surges, the H.V. and M.V. line terminals should be protected by valve-type surge diverters of appropriate ratings regardless of whether the auto-transformer is connected to the line or not.

Table 3 shows the effects of surges on the series insulation of transformers and auto-transformers. It is seen that the maximum gradients in the oil ducts between coils are approximately the same for transformers and auto-transformers when tested with either full or chopped waves. The exception is only the region of the tap changer where the gradient between the adjacent tappings is considerably greater for auto-transformers than for transformers. This is due to the fact that with the same percentage regulation the fraction of the number of disconnected turns to the number of turns in the H.V. winding (the series part) is twice as high for auto-transformers (with $k_{12} = 2$) than for transformers.

TABLE 3.

	Full wave, 1.5/40 μsec		Chopped wave $\tau = 2$–3 μsec
	Maximum gradient in one oil duct	Maximum gradient in the tap changer region	
Transformer . . .	20	19.5	18
Auto-transformer	16	34	14

The overvoltages which appear on the tertiary winding due to impulse stressing of the H.V. and M.V. windings, are induced in it electrostatically and electromagnetically, i.e. in the same manner as in transformers.

Condition of the neutral point

High-voltage auto-transformers of home produce cannot be operated with the

neutral point disconnected from earth. This will be made clear from the following consideration. In a system with effectively earthed neutral point the voltage on the unearthed neutral of a transformer or an auto-transformer rises during one-phase-to-earth fault to a value given by

$$U_{n0} = \frac{x_0}{x_1 + x_2 + x_0} U_{ph\,1}, \tag{14}$$

where x_1, x_2, and x_3 are positive-, negative-, and zero-sequence reactances.

Assuming $x_1 = x_2$ and substituting $\alpha = \frac{x_0}{x_1}$ and $\beta = \frac{\alpha}{2 + \alpha}$ we get

$$U_{n0} = \beta U_{ph1} = \frac{\beta}{\sqrt{3}} U_1, \tag{15}$$

where U_1 and U_{ph_1} are the line and phase voltages of the H.V. winding respectively.

At the same time the voltage of the sound phases is

$$U_{10} = \frac{U_1}{\sqrt{3}} \sqrt{1 + \beta + \beta^2}, \tag{16}$$

while the voltage at the line terminals of the M.V. winding of the auto-transformer is

$$U_{20} = \frac{U_1}{\sqrt{3}} \sqrt{\frac{1}{k_{12}^2} + \frac{\beta}{k_{12}} + \beta^2} \tag{17}$$

Taking, for example, the 220 kV voltage class and assuming $\alpha = 4$ and $\beta = \frac{4}{2 + 4} = 0.67$ we see that during one-phase-to-earth fault the voltage on the neutral and the voltage on the H.V. line terminal will not exceed the permissible levels of the respective surge diverters RVS-110_{earth} and RVS-220_{earth}, while the voltage on the 110 kV M.V. line terminal will rise to $U_{20} = 141.5$ kV and will therefore exceed the permissible voltage for the RVS-110_{earth} surge diverter by 47 per cent.

This explains the necessity of earthing the neutral points of 220/110 kV auto-transformers, since the insulation of their M.V. windings is coordinated with the protective characteristics of the RVS-110_{earth} surge diverter.

Construction

The constructional design of high-voltage auto-transformers is basically the same as that of transformers for the same voltage class. The characteristic differences are formed in the design of the connexions to the winding ends (the external connexions between windings and between windings and bushings). Also, there are some differences regarding connexions to the ends of the internal windings and regarding some main clearances. Fig. 9 shows a possible method of arranging the windings for the 220/110/6-10 kV step-down auto-transformer with the H.V. bushing connected to mid-point of the H.V. winding. This figure shows that the upper end of the M.V. winding (neutral X) is brought out and so has to be insulated against earth, L.V. winding, and one end of the H.V. winding. On the other hand, construction of the lower part of the auto-transformer is considerably simplified on account of the electrical connexion between the H.V. and M.V. windings since their common point A_m can be brought out directly from the H.V. winding. In the case of a transformer with separate windings, the construction of the connexion to the lower end of the M.V. windings would be the same as that to the upper end.

Also, the existence of the electrical connexion between windings in an auto-transformer makes it possible to reduce the end clearances since, in this case, the

electric field configuration is more favourable.

For a step-up auto-transformer having its M.V. winding placed next to the core instead of between the H.V. and L.V. windings, the construction of the connexions to the ends of the M.V. winding is the same as that for a transformer. The number of high-voltage bushings in a single-phase auto-transformer is one less than that in a transformer.

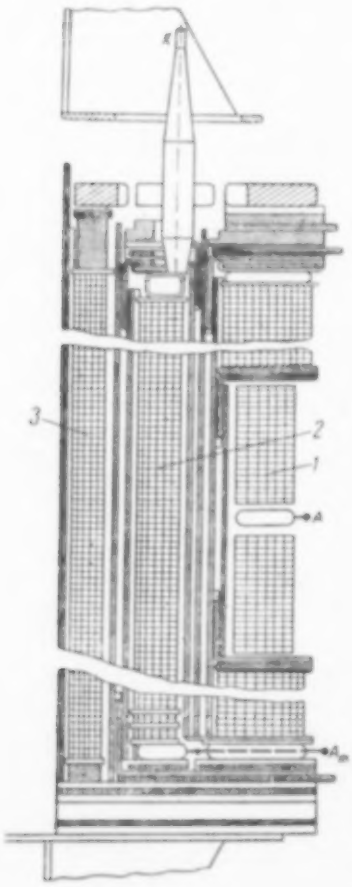

FIG. 9. Construction of 220/110/6 - 10 kV auto-transformer. 1 - H.V. winding; 2 - M.V. winding; 3 - L.V. winding.

1958

A NEW AIR-BLAST CIRCUIT BREAKER FOR 220 kV, 7000 MVA*

T.I. SMIRNOVA

(Received 24 December 1956)

The All-Union Electrotechnical Institute "Lenin" has developed an experimental air-blast circuit breaker rated 220 kV/7000 MVA (Fig. 1), which is an improvement on the 5000 MVA circuit breaker as manufactured at present by the electrical industry.

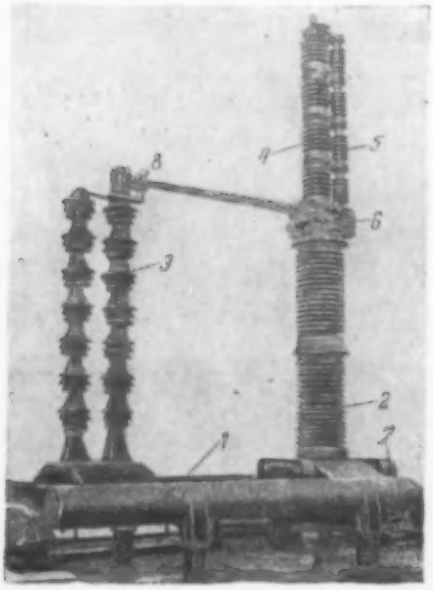

FIG. 1. One phase of the 220 kV, 7000 MVA air-blast circuit breaker.
1 – compressed air tank;
2 – column of support-insulators;
3 – column of pin-insulators;
4 – arc chamber;
5 – voltage divider;
6 – pneumatic drive of the isolator;
7 – control cubicle.

Design of the circuit breaker

Three porcelain tubes are arranged inside the supporting insulate of the breaker; one of 120 mm diameter, leads the compressed air to the arc chamber

* *Elektrichestvo* No. 6, 48-50, 1957 [Reprint Order No. EL 29].

and the two others, of 25 mm diameter, supply the compressed air to the drive of the isolator. The arc chamber is mounted on the drive of the isolator and consists of four identical elements, each of which contains a hollow porcelain insulator, a fixed and a moving contact with the pneumatic mechanism. Both fixed and moving contacts are hollow and communicate with the exhaust ducts of the flanges.

A voltage divider consisting of four metal resistors connected in parallel to the elements of the chamber is arranged beside the arc chamber. The total resistance of the voltage divider is 720,000 ohms.

The isolator drive is connected with a mechanism of switching block contacts with porcelain rods. Two insulator columns support the contact of the isolator, each of the columns consisting of insulators type IShD-35.

For remote and automatic operation each of the phases of the circuit breaker is equipped with two electromagnets. Three-phase operation can be achieved by either series or parallel connexion of the three magnets for which two different sets of coils are used. For manual operation a special pneumatic device is provided whose control buttons are arranged in a control cubicle. In this case the phase cannot be operated individually.

To prevent freezing of the air ducts in the insulators continuous air circulation is provided by means of special reduction valves in the control cubicle. Each phase of the circuit breaker is provided with an indicator, showing the state of the ventilation. The control cubicle also contains contact pressure gauges which interrupt the operating circuits at inadmissible losses of pressure in the air tanks.

The operating columns of the circuit breaker does not differ from that of the air-blast circuit breaker for 220 kV, 5000 MVA*.

Principal characteristics of the circuit breaker:	
Rated voltage	220 kV
Rated current	1000 A
Rated breaking current	18.4 kA
Rated breaking capacity, allowing for rapid reclosing	7000 MVA
Max. "through" short-circuit current,	
amplitude	65 kA †
r.m.s. value	38 kA
Thermal short-circuit rating (10 seconds)	15 kA
Voltage rating of the operating magnets	220 V d.c.

* O.V.V. Afanas'ev and N.A. Makarova; Air-blast circuit breaker 220 kV, 1000 A, 5000 MVA. *All-Union Electrotechnical Institute* No. 6 (1954).

† These values have been obtained experimentally at the All Union El. Institute. The "Elektroapparat" Works recommend 55 and 32 kA, respectively.

Permissible limits of voltage variations on the operating magnets	65 – 120 per cent
Opening time (from instant of giving the tripping signal to inception of contact separation) not more than	0.06 sec.
Max. arc-duration	0.02 sec.
Total-break-time (from instant of giving the tripping signal to final arc extinction) not more than	0.08 sec.
Making time (from "On" signal to the moment of making contact with the fixed contact of the isolator) not more than	0.45 sec.
Duration of the contactless interval of the arc chamber (from opening to closing of the contact)	0.25 – 0.35 sec.
Time from signal to separation of the isolator from the fixed contact	0.14 sec.
Max. velocity of the movement of the contact knife of the isolator during making and breaking	18 – 22 m/sec
Rated air pressure	20 atm
Max. permissible air pressure in the tanks	21 atm
Min. air pressure at which the capacity of the circuit breaker is not reduced	18 atm
Capacity of the basic storage tank of one phase	1214 litres
Capacity of the additional storage tank of one phase	1214 litres
Pressure drop in the tanks during breaking	2.25 – 2.5 atm*
Air consumption for one breaking operation	5500 – 6100 ltr.†
Air consumption for one making operation about	400 litres
Pressure drop with automatic reclosing followed by breaking	4 – 4.5 atm
Air consumption for automatic reclosing	9700 – 10,900 ltr.
Air consumption for ventilation	900 ltr/hr
Weight of one phase appr.	6000 kg.
Weight of control cubicle appr.	350 kg.

Results of circuit breaker duty tests

Mechanical tests consisting of 1000 making and breaking operations were carried out with a pressure of 20 atm. In addition, 25 duty cycles were carried out at a pressure of 21 atm and 25 cycles at 15 atm. Inspection of the individual part and of the assembly of the circuit-breaker after the mechanical tests showed that its main elements were in good condition and that the circuit-breaker remained in full working order. The mechanical characteristics are shown in Fig. 2.

The tests showed that the voltage distribution on the arc chambers is as

* The magnitude of the pressure drop shown takes account of the installation of the additional storage tanks.

† The figures for air consumption are given for one phase and refer to atmospheric pressure.

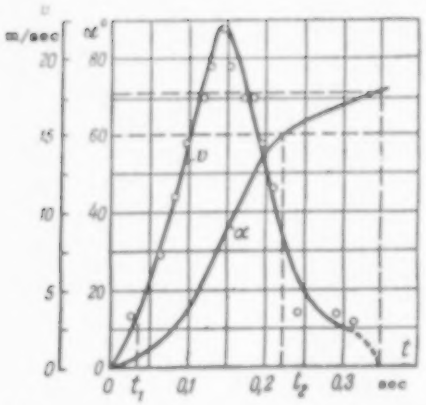

FIG. 2. Mechanical characteristics of the breaking operation.
Pressure in the tank 20 atm.
v – linear velocity of the knife end;
t_1 – moment of separation of the knife from the isolator contact
t_2 – moment of making contact in the arc chamber.

follows: The first (bottom) element takes 24 per cent of the total voltage, the second 23.6 per cent, the third 22.9 per cent and the fourth 29.5 per cent. This sufficiently uniform distribution of the voltage enables tests of the breaking capacity to be carried out on individual elements.

1958

The rated voltage for each circuit-breaker element is 45 kV_{max}. The magnitude of the test voltage is determined by the conditions of a three-phase short-circuit and equals 1.5 x rated voltage, i.e. 67.5 kV_{max}.

For the test of the circuit-breaker with interruption of 50 per cent of its interruption capacity (Fig. 3) the amplitude factor of the restriking voltage was assumed to be 1.6, i.e. the magnitude of the restriking voltage at one breaker element must be 108 kV_{max}. The frequency of the natural oscillations of the restriking voltage was assumed to be 2000 c/s.

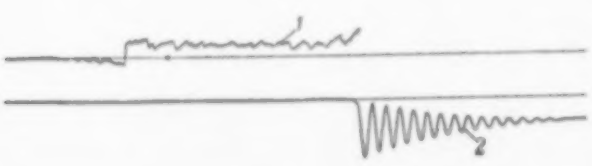

FIG. 3. Oscillogram obtained during breaking of 50 per cent of the breaking capacity of the breaker; p = 18 atm.
1 – arc voltage drop (duration of the arc 0.0138 sec)
2 – restriking voltage (frequency 2000 c/s.

The tests consisted of the check of the interruption capacity of each individual breaker element. An oscillatory circuit was used as the current source, but the restriking voltage was obtained from a surge voltage generator. These tests showed that with a pressure in the tank of 17 – 18 atm each element easily

performed its duty of the interruption of 50 per cent of the breaker capacity with a value of the restriking voltage of 110 – 130 kV_{max}. The average rate of rise of the restriking voltage was 1.65 – 1.81 kV/μ sec.

During the tests it was found that with a tank pressure of 16 atm sometimes restriking occurred at a voltage of the order of 90 – 100 kV_{max}. In order to achieve the necessary electric strength, i.e. 108 kV_{max}, it proved to be essential to raise the preasure in the storage tanks to 17 – 18 atm. Hence follows that auxiliary storage tanks of the same size as the main tanks are required if reclosing is to be provided.

For interruption of 100 per cent of the rated interruption capacity (Fig. 4) the amplitude factor of the restriking voltage was assumed to be 1.2, i.e. the restriking voltage on each breaker element must be 80.5 kV_{max}. The frequency of the natural oscillations of the restriking voltage was assumed to be 400 c/s.

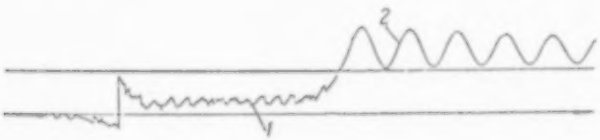

FIG. 4. Oscillogram taken during breaking of 100 per cent of the interruption capacity of the breaker; p = 16 atm.
1 – arc voltage drop (duration of the arc 0.0135 sec)
2 – restriking voltage (frequency 400 c/s).

The tests showed that with a tank pressure of 16 atm the breaker interrupts 100 per cent of its capacity with an amplitude of the restriking voltage of 83 – 90 kV and an average rate of rise of the restriking voltage of 0.3 – 0.35 kV/μ sec.

Tests were also made with respect to the interruption of capacitive current. The breaker interrupts a distributed capacitance of 3.2μF (corresponding to a line of 100 km length) with a voltage across one element of 2 x 1.3 x 45 = 117 kV_{max} (the coefficient 1.3 takes into account the increase of the voltage on the two unfaulted phases during line-earth fault with restriking arc and also the increase of the voltage at the end of a line).

The trials proved that the three lower breaker elements successfully interrupted this capacitive current with a pressure of the storage tanks of 16 atm. For the fourth element (the top one) it has been necessary to raise the pressure to 18 atm.

A METHOD FOR THERMAL CALCULATIONS OF MINING COMBINE MOTORS*

G. I. PERTSOV

(Received 10 December 1956)

Mining combines are driven by enclosed induction motors with squirrel-cage rotors. The main design features of the frames of these motors are shown in Figs. 1 and 2.

The motor represented in Fig.1 has a frame with cooling fins with internal air circulation; Fig. 2 shows a motor with a frame with cooling fins with internal air circulation and external blower-cooling.

Heat is generated in the motors in the stator winding, in the steel of stator and rotor, bars and short-circuiting rings of the rotor, in the internal fan and the sealed bearings. These parts of the machine are connected by thermal conductivities.

The heat energy of the individual parts of the motor is dissipated into the surroundings not through one homogeneous surface, but through several surfaces presenting different conditions for the air-cooling. For this reason it is not permissible to consider an electric machine for thermal calculation as a homogeneous body of infinite thermal conductivity because calculations on this basis lead to considerable discrepancies between theoretical and experimental results.

The results of calculations will be unsatisfactory also in the case that not the temperature rise of the whole machine, but only that of its winding is considered and influences of other parts are only considered by some empirical coefficients. These coefficients, found by experiment, apply only to a given motor and, strictly speaking, only to well-defined operating conditions of the machine.

In thermal calculations based on the theory of the temperature rise of two homogeneous bodies, the heating processes of stator and rotor are considered indepenently of each other.

According to the thermal energy balance for steady operating conditions and for constant heat losses we may write down the following equations.

* *Elektrichestvo* No. 6, 58-64, 1957 [Reprint Order No. EL 30].

$$\left.\begin{aligned} P_1 &= \tau_1\lambda_1 + (\tau_1 - \tau_2)\,\lambda_{12}; \\ P_2 &= \tau_2\lambda_2 + (\tau_2 - \tau_1)\,\lambda_{21}, \end{aligned}\right\} \tag{1}$$

where τ_1 and τ_2 are the temperature rises of the copper (body 1) and steel (body 2), above the temperature of the ambient medium;
λ_1 and λ_2 are the thermal conductivities of bodies 1 and 2, respectively;
λ_{12} and λ_{21} are the mutual thermal conductivities of the bodies 1 and 2, respectively.

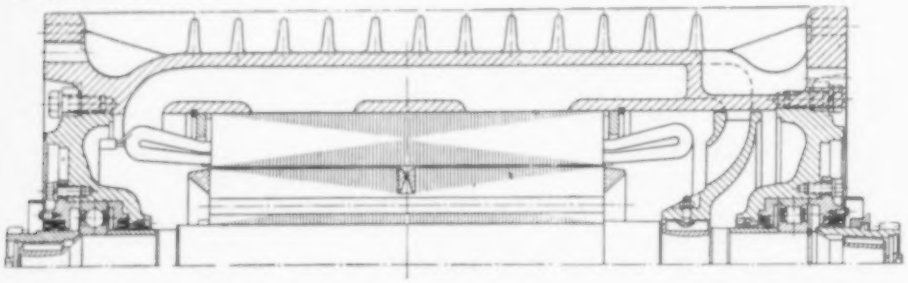

FIG. 1. Enclosed induction motor with ribbed frame and internal ventilation.

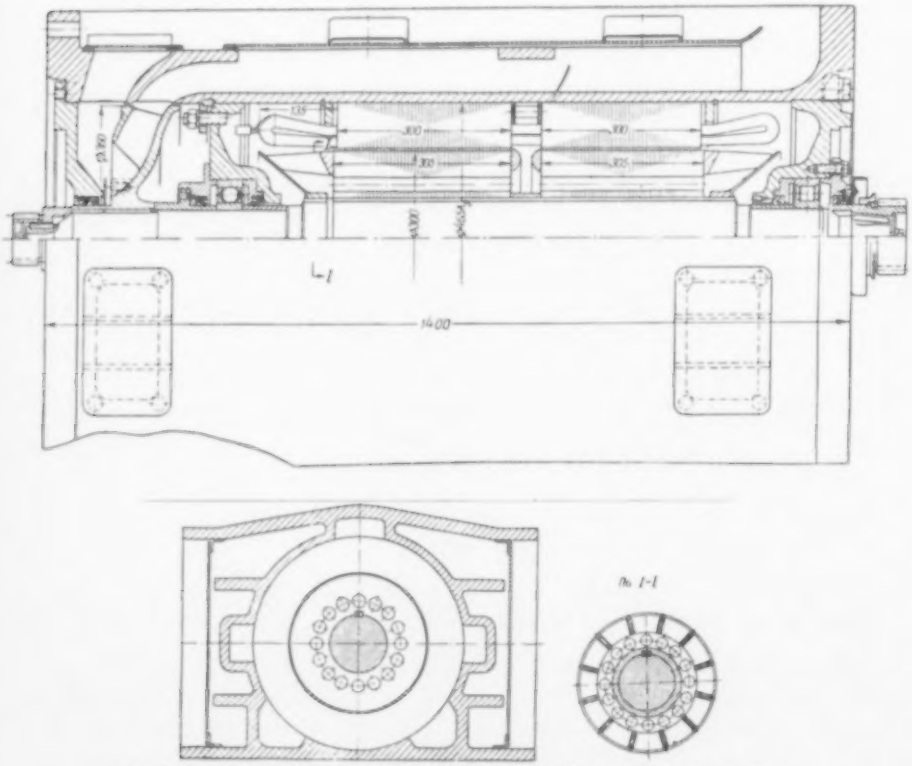

FIG. 2. Enclosed induction motor with internal air circulation and external forced ventilation.

An amount of thermal energy P_1 or P_2 of the given bodies is expended (a) by transfer to the ambient medium; (b) by transfer to the other body.

We get, therefore, a system of two linear equations. This explains the efforts of a number of authors to consider the heating-process of an electrical machine simplified as the temperature rise of two bodies. Experience has shown that the theory of the heating of two bodies yields satisfactory results in the case of a machine with a large air gap. However, in machines with a small air gap the thermal interaction of stator and rotor becomes considerable.

For this reason the theory of the heating of two bodies cannot be applied to induction motors. To take into account the influence of the rotor on the temperature rise of the stator windings B.P. Aparov suggested, on the basis of special investigations, to add to the losses in the stator copper 30 – 50 per cent of the losses in the rotor. The arbitrary addition to the copper losses of 30 – 50 per cent of the rotor losses leads to an incorrect rating of the installed power of the motor, and for this reason B.P. Aparov's method of thermal calculation is not acceptable.

1958

Thermal calculations based on the theory of the heating-up of three homogeneous bodies considered the temperature rise of the copper and steel of stator and rotor (the rotor being regarded as a homogeneous body).

According to the thermal energy balance for steady operating conditions and constant heat losses we may write down the following equations:

$$\left.\begin{aligned} P_1 &= \tau_1\lambda_1 + (\tau_1 - \tau_2)\lambda_{12} + (\tau_1 - \tau_3)\lambda_{13};\\ P_2 &= \tau_2\lambda_2 + (\tau_2 - \tau_1)\lambda_{21} + (\tau_2 - \tau_3)\lambda_{23};\\ P_3 &= \tau_3\lambda_3 + (\tau_3 - \tau_1)\lambda_{31} + (\tau_3 - \tau_2)\lambda_{32}, \end{aligned}\right\} \qquad (2)$$

where τ_1, τ_2 and τ_3 are the temperature rises of the copper (body 1), stator steel (body 2) and rotor steel (body 3) above the ambient temperature;

λ_1 λ_2 and λ_3 are the thermal conductivities of the bodies, 1, 2 and 3;
λ_{12}, λ_{21} and λ_{31} are the mutual thermal conductivities of the bodies 1, 2 and 3.

Amounts of thermal energy P_1, P_2 and P_3 of the three homogeneous bodies are expended

(a) in transfer to the two other bodies;

(b) in transfer to the ambient medium.

To the system of equations (2) corresponds a definite thermal equivalent circuit, represented in Fig. 3.

Our analysis showed that in thermal calculations the temperature rise of the stator winding practically does not change, if the heat flow from the rotor to the stator copper is ignored. This heat flow is considerably less than the heat flow from the rotor to the stator steel owing to the negligible thermal conductivity of the air and the wedge in comparison with that of the steel. The effect of

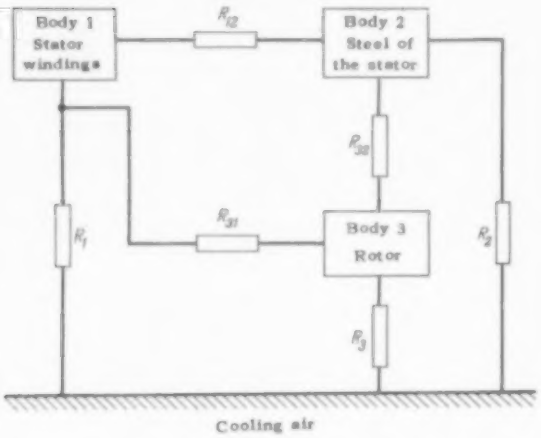

FIG. 3.

the rotor on the temperature rise of the stator winding does not manifest itself directly, but through the thermal flux from the rotor to the stator steel.

The stator steel is additionally heated by the losses in the rotor, owing to which the heat exchange from the stator copper to the steel deteriorates and, consequently, the copper temperature rises. These conditions are represented by the correct thermal equivalent circuit shown in Fig. 4.

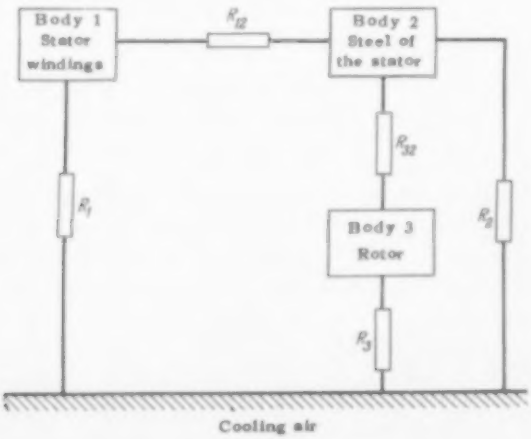

FIG. 4.

For the altered circuit we may write down the following equations in accordance with the thermal energy balance:

$$\left.\begin{aligned} P_1 &= \tau_1\lambda_1 + (\tau_1 - \tau_2)\,\lambda_{12};\\ P_2 &= \tau_2\lambda_2 + (\tau_2 - \tau_1)\,\lambda_{11} + (\tau_2 - \tau_3)\,\lambda_{23};\\ P_3 &= \tau_3\lambda_3 + (\tau_3 - \tau_2)\,\lambda_{32}. \end{aligned}\right\} \qquad (3)$$

The temperature excuss of the stator winding may be determined from the following expression:

$$\tau_1 = \frac{P_1}{aB} + \frac{P_2\lambda_{12}}{aAB} + \frac{P_3\lambda_{23}\lambda_{12}}{aABc},$$

where

$$a = \lambda_1 + \lambda_2; \quad b = \lambda_2 + \lambda_{21} + \lambda_{23};$$
$$c = \lambda_3 + \lambda_{32}; \quad A = \frac{bc - \lambda_{23}\lambda_{32}}{c};$$
$$B = \frac{Aa - \lambda_{12}\lambda_{21}}{Aa}.$$

The thermal calculation based on the concept of three homogeneous bodies for some types of squirrel-cage induction motors results in satisfactory agreement with experimental data. As regards motors of the type used for mining combines, numerous tests and calculations have established that the temperature excess of the stator windings due to the losses in the steel represents:

(a) About 75 per cent of the total temperature rise of the winding at the rated power for closed types of the motor without external forced cooling (Fig. 1);

(b) About 50 per cent of the total temperature rise of the winding at the rated power for closed types of the motor with external fan-cooling (Fig. 2).

Consequently, the temperature rise of the stator only due to the losses in the stator and rotor copper is of the order of 25 per cent for closed types without external forced cooling, and 50 per cent of the total temperature excess of the winding at the rated power for closed types with external forced cooling. When the temperature of the winding rises above the permissible value, for example, by 10 per cent, it is necessary for reducing this temperature to reduce the copper losses by 40 per cent for motor types without external cooling and by 20 per cent for motor types with external forced cooling. The useful output of closed motors of the type designed for mining combine motors varies, therefore, for a type without external forced cooling proportionately to the square of the variation of the overall temperature, and for the types with external forced cooling, approximately in a linear manner.

The thermal calculation based on the theory of three homogeneous bodies constitutes a considerable improvement in comparison with the theory of the temperature rise of two homogeneous bodies, and yet it cannot be recommended for motors for mining combines in which a considerable temperature rise of the stator winding occurs under no-load conditions owing to the constant losses. It is, in this case, necessary also to consider the following circumstances:

1. The losses in the stator winding consist of the losses in the copper of the zone of the slots and of the copper losses in the end connexions of the winding. Depending on the system of cooling of the motor and on its operating conditions, the end-connexions of the winding may dissipate the heat liberated in them in the ambient medium. In addition to this, they may absorb part of the heat liberated in the winding in the zone of the slots or inversely, pass on to the winding in the slot zone part of the heat liberated in themselves. The theory of the temperature rise of three homogeneous bodies considers the stator winding as a homogeneous body having the same temperature with all its parts.

2. The specific thermal fluxes in the steel at the back and the teeth of the stator are inhomogeneous and, consequently, the temperatures of the teeth and the back of the stator will also be unequal. The theory of the temperature rise of three homogeneous bodies regards the steel of the stator as a homogeneous body having all its parts at the same temperature.

3. Sources of heat in the rotor are: the rotor steel, the aluminium of the slotted part of the rotor and the short-circuiting rings. All these parts of the rotor are not at the same temperature, wherefore, it cannot be regarded as a homogeneous body.

4. In closed induction motors a fan is generally used for the internal circulation of the air. This internal fan is, on the one hand, a generator of heat, and on the other hand, responsible for the transfer of heat from the rotor to the frame and to the ambient medium. This fact is not considered by the equations of the temperature rise of three homogeneous bodies.

The above considerations show that for determining the rating of motors of mining combines it is necessary to introduce into the thermal calculation based on the theory of the temperature rise of three homogeneous bodies the additions enumerated above sub 1 – 4.

We suggest *a branched thermal equivalent circuit, based on eight generators of heat,* interconnected by finite thermal conductivities (Fig. 5).

Heat is liberated:

(a) in the copper of the winding in the slots;
(b) in the copper and connexions of the winding;
(c) the steel at the back of the stator;
(d) the steel at the stator teeth;

(e) the rotor steel;
(f) the aluminium of the slot part of the winding;
(g) the short-circuiting rings of the rotor;
(h) the internal fan (internal ventilation losses).

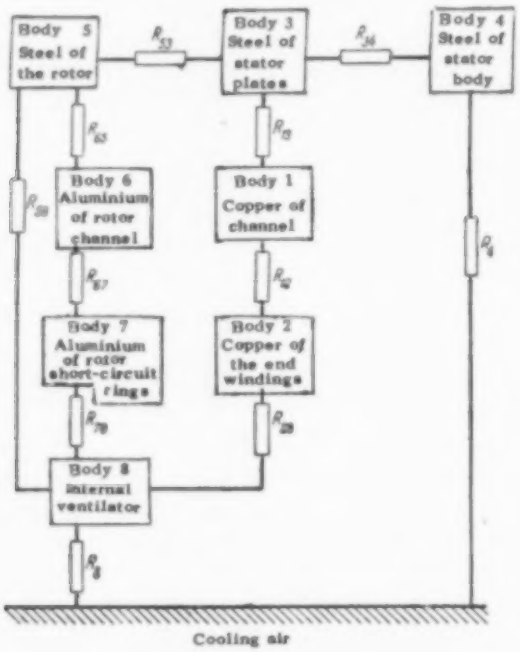

FIG. 5.

To the branched thermal equivalent network represented in Fig. 5 corresponds the following system of equations:

$$\left.\begin{aligned}
P_1 &= (\tau_1 - \tau_2)\lambda_{18} + (\tau_1 - \tau_2)\lambda_{12};\\
P_2 &= (\tau_2 - \tau_1)\lambda_{21} + (\tau_2 - \tau_8)\lambda_{28};\\
P_3 &= (\tau_3 - \tau_4)\lambda_{34} + (\tau_3 - \tau_5)\lambda_{35} +\\
&\quad + (\tau_3 - \tau_1)\lambda_{31};\\
P_4 &= \tau_4\lambda_4 + (\tau_4 - \tau_3)\lambda_{43};\\
P_5 &= (\tau_5 - \tau_8)\lambda_{58} + (\tau_5 - \tau_3)\lambda_{53} +\\
&\quad + (\tau_5 - \tau_6)\lambda_{56};\\
P_6 &= (\tau_6 - \tau_5)\lambda_{65} + (\tau_6 - \tau_7)\lambda_{67};\\
P_7 &= (\tau_7 - \tau_6)\lambda_{76} + (\tau_7 - \tau_8)\lambda_{78};\\
P_8 &= (\tau_8 - \tau_5)\lambda_{85} + (\tau_8 - \tau_7)\lambda_{87} +\\
&\quad + (\tau_8 - \tau_2)\lambda_{82} + \tau_8\lambda_8,
\end{aligned}\right\} \qquad (4)$$

where P_1 and τ_1 are the losses and temperature excess of the stator winding in the slots;

P_2 and τ_2 – the losses and temperature excess of the end-connexions of the stator winding;

P_3 and τ_3 – the losses and temperature excess of the steel at the stator teeth.

P_4 and τ_4 – losses and temperature excess of the steel at the back of the stator;

P_5 and τ_5 – losses and temperature excess of the rotor steel;

P_6 and τ_6 – losses and temperature excess of the aluminium of the slotted part of the rotor;

P_7 and τ_7 – losses and temperature excess of the short-circuiting rings of the rotor;

P_8 and τ_8 – the friction losses of the internal fan and the temperature excess of the air inside;

$\lambda_2, \ldots, \lambda_8$ – the thermal conductivities of bodies 2 . . . 8;

$\lambda_{12}, \ldots, \lambda_{87}$ – the mutual thermal conductivities of bodies 1 and 2, . . . , 8 and 7.

In practice it is required to simplify the methods of thermal calculations.

We must determine the temperature excess of the winding according to the actual physical processes taking place in the machine, even if we introduce the well-known simplifying assumptions. In setting-up the branched thermal equivalent circuit represented in Fig. 5, we make the following assumptions:

1. The thermal fluxes in the stator and rotor steel have only radial direction.

2. The thermal flux from the rotor to the stator copper is very small compared with the thermal flux directed from the rotor to the stator steel; for this reason we neglect it.

3. The outer surface of the motor frame is regarded as an equipotential surface.

In the branched thermal equivalent circuit shown we considered all the thermal flows capable of influencing the temperature rise of the stator winding. The simplifications introduced do not refer to the initial conditions, but consist in neglecting second-order quantities. The precision of the thermal calculations based on the thermal circuit shown, and assuming 8 sources of heat, is quite sufficient for determining the ratings of the fully-enclosed motors of mining combines.

A solution of the systems of equations presented above, though not intrinsically difficult, is yet very laborious and inconvenient for practical purposes.

We recall that the object of the present communication was to evolve a practical method of thermal calculations of fully-enclosed induction motors with a view to determining the rating of such motors. The rating of squirrel-cage induction motors is determined by the temperature rise of the stator winding. As re-

gards the other parts of the motor such as the stator and rotor steel, rotor aluminium, etc., their temperature rise is not limited. Consequently, it is only necessary to determine the temperature rise of the stator winding in order to establish the rating of the motor. Considering the thermal equivalent circuit with eight sources of heat which we evolve, it is only necessary to simplify the determination of the over-temperature of the stator winding; this renders it necessary to reduce the number of equations forming the system.

We explain below the suggested method of thermal calculation for enclosed motors of mining combines. It comprises the following stages:

1. Setting-up a branched thermal equivalent circuit based on the assumption of 8 sources of heat.

2. Determination of the directions of the thermal fluxes from the rotor from the stator windings.

Thermal fluxes from the rotor

There are four directions of thermal fluxes in the rotor, viz:

(a) The losses in the rotor, transmitted through the air gap to the stator steel;

(b) Losses in the rotor carried off through the axial ducts in the rotor and by the air passing through them;

(c) Losses in the slotted part of the rotor aluminium, transmitted to the rotor steel;

(d) Losses in the slotted part of the rotor aluminium, carried off to the short-circuiting rings of the rotor.

Thermal fluxes from the stator winding

In the stator winding there are two directions of the thermal fluxes from the stator winding, viz:

(a) Losses transmitted from the winding in the slots of the stator to the steel of the stator;

(b) Losses transmitted from the stator winding in the slot to the end connexions. If these values happen to be negative, the losses will be directed from the end-connexions to the part of the winding in the slots.

3. Determination of the required numerical values of the six thermal fluxes from the rotor and stator winding. To determine these we put down a system of six equations. We obtain these equations on the basis of the following conditions:

(a) The algebraic sum of all the thermal fluxes towards and from any point equals zero;

(b) The magnitude of the temperature drop between two points does not depend on any particular path through the thermal circuits comprising these points.

4. Determination of the actual thermal fluxes in all the sections from the stator winding to the ambient air. The thermal flux through the stator steel to its external surface consists of: a heat flow of constant magnitude, directed from the rotor to the stator steel; a heat flow of constant magnitude directed from the stator winding to the stator steel; the heat flow proper, set up by the losses in the steel at the teeth and the back of the stator.

5. From the actual heat flows in the various parts of the motor and from design data, it is possible to determine the temperature drops and the temperature excess of the stator winding.

It is, therefore, necessary, in order to determine the temperature excess of the stator winding according to the method suggested, to solve a system of six equations. The number of equations must be equal to the number of possible directions of heat flows from the rotor and from the stator winding. The use of external forced cooling of the frame of the motor does not alter the number of directions of the heat flows from the rotor and from the stator winding; only the coefficient of heat dissipation is altered. To determine the numerical values of the heat flows enumerated, we will carry out the calculation in the individual sections below.

Example of a system of equations

Corresponding to the branched thermal equivalent circuit of Fig. 5 ;

$$\left.\begin{aligned}
P_{x1}+P_{x2}&=P_n;\\
P_{y3}+P_{ar}&=P_{y1}+P_{y2};\\
P_{y3}+P_{y4}&=P_{a.sl.}\\
(P_{x1}+P_{y1}+P_a)R_{34}+&\\
+(P_{x1}+P_{y1}+P_{a_t}^{t}+P_{ab})R_4&=\\
=P_{x2}R_{12}+(P_{x2}+P_e)R_{28}+&\\
+(P_{x2}+P_e+P_{fr})R_8;&\\
P_{y3}R_{65}+P_{y2}R_{58}=P_{y4}R_{67}+(P_{y4}+P_{shr})R_{78};&\\
P_{y3}R_{65}+P_{y1}R_{53}+(P_{y1}+P_{a_t}+P_{x1})R_{34}+&\\
+(P_{y1}+P_{a_t}+P_{x1}+P_{ab})R_4=P_{y4}R_{67}+&\\
+(P_{y4}+P_{shr})R_{78}+(P_{y4}+P_{shr}+P_e)R_8,&
\end{aligned}\right\} \qquad (5)$$

where P_{x1} – are the losses transmitted from the winding in the stator slots to the steel of the stator;

P_{x2} – losses transmitted from the stator winding in the slots to the end-connexions; when P_{x2} has a negative value, the losses will be directed from the end-connexions to the winding in the slots;

P_{s1} – losses in the stator winding in the slots;
P_{y1} – losses in the rotor transmitted through the air gap to the stator steel;
P_{y2} – losses in the rotor transmitted through the axial ducts of the rotor and by the air passing through them;
P_{y3} – losses transmitted to the rotor steel from the aluminium parts in the rotor slots;
P_{y4} losses transmitted to the short-circuiting rings of the rotor from the aluminium in the rotor slots; when P_{y4} is negative, the losses will be directed from the short-circuiting rings of the rotor to the winding in the rotor slots;
$P_{s.r.}$ – losses in the steel of the rotor;
$P_{a.sl.}$ – losses in the aluminium in the rotor slots;
P_t – losses in the stator teeth;
P_e – losses in the end connexions of the stator winding.
$P_{fr.}$ – friction losses between internal fan and air;
P_{shr} – losses in the short-circuiting rings of the rotor;
P_{slo} – losses in the back of the stator;
R_4 and R_8 thermal resistances between the bodies 4 and 8 and the ambient medium;
R_{12}, R_{13} etc. – mutual thermal resistance of the bodies 1 and 2, 1 and 3, etc.

Analysis of experimental data and their comparison with theoretical results

We will analyse the experimental data of a motor EDK-120, designed for the drive of a mining combine, and compare them with results obtained by thermal calculations on the method described above.

The main parameters of the motor EDK-120 are: Continuous output 55 kW; voltage U_l = 660 V; I = 64 A; speed on load n = 1485 rev/min; enclosed with ribbed frame and internal air circulation (Fig. 1); overall dimensions : length 1250 mm, with 780 mm, height 500 mm.

In the thermal tests the motor was placed on rails fixed to the bed and connected to the shaft of the loading generator. Owing to this the lower part of the surface of the frame of the motor could not freely radiate into the surroundings. The thermal tests of the motor were not carried out in a special insulating chamber, but in the test bay of the works. Despite the fact that the tested motor was during its thermal-duty tests separated from the loading generator by a special wooden screen, and at some distance from the other machines working simultaneously in the test bay, the ambient air around the fram of the motor was still slightly agitated.

The thermal-duty tests of motors for mining combines and coal cutters produced by the industry are carried out in the testing stations generally in a

similar way. It is for this reason that even though the frame of the motor may correspond to the type without external forced cooling, there will always be a certain slight cooling effect owing to the agitation of the air in the test bays. To measure the intensity of this external air flow by any instrument was impossible owing to the extremely low air velocity. However, the presence of an even very slight air circulation increases considerably the coefficient of heat transfer and, consequently, reduces the temperature excess of the frame of the motor. The temperature excess of the stator winding, Δt_w, on the other hand, is determined by the temperature drop Δt_f, between the stator winding and the frame and the temperature drop Δt_a between the frame and the ambient air, i.e.

$$\Delta t_w = \Delta t_f + \Delta t_a.$$

Our analysis of the experimental results obtained with enclosed motors of mining combines and coal cutters enabled us to establish the following approximate relations:

$$\Delta t_f / \Delta t_w = 0.25 \ldots 0.3 \text{ and } \Delta t_a / \Delta t_f = 0.75 \ldots 0.7$$

Consequently, for temperature excess of the stator winding $\Delta t_w = 95°C$, the temperature excess of the frame of the motor (assuming the frame to be a thermal equipotential surface) will be $\Delta t_{fr} = 67 \ldots 71°C$.

According to the tests the maximum temperature excess of the motor frame is $\Delta t_{fr} = 85°C$.

The existence of a slight air current around the frame during the thermal-duty tests of the motor is also confirmed by the fact that a thread held near the frame is deflected from the vertical direction.

Tables 1 and 2 collect experimental and theoretical data on the thermal-duty of a motor EDK – 120.

TABLE 1.

	Rating (kW)	Voltage (V)	Current (A)	Slip (%)	Velocity of external air current (m/sec.)
Test results	56.5	660	66	1.2	Owing to the low air speed, the intensity of the external ventilation could not be measured.
Results of calculation	55	660	64	0.89	1 m/sec

TABLE 2.

	Losses						Temperature excesses		
	In steel (W)	Copper (W)	Aluminium (W)	Additional (W)	Windage (W)	Sum of heat losses (W)	Of winding, from resistance (°C)	Of winding, by thermo-couple (°C)	Of frame, by thermo-couple (°C)
Test results	1800	865	700	368	250	3923	98	107	85 (maximum)
Theoretical values	2120	810	500	300	230	3960	93	–	70 (mean)

1958

Conclusions

1. The existing methods of thermal calculations are briefly reviewed and a new method of thermal calculations of enclosed induction motors to be used for the drives of coal cutters and mining combines is presented.

2. The method of thermal calculations suggested may form a basis for a practical method of designing enclosed induction motors to be generally accepted.

3. More research work is required on the coefficients of heat exchange of induction motors.

REFERENCES

1. B.P. Aparov; *Investigation of Temperature Rise of Induction Motors under unsteady conditions. All-Union Electrotechnical Institute* 10-11 (1939).
2. A. Dembo and B. Kuznetsov; *Thermal Testing of Induction Motors. Tr. Leningrad Industrial Inst.* No. 2 (1937).
3. A.P. Ioffe; *Temperature Rise of Squirrel-cage Motors Under Repeated Starts and Stops. All-Union Electrotechnical Institute* No. 3 (1951).
4. I.M. Postnikov; *Projecting Electrical Machines. Gostekhizdat* SSSR (1952).

VELOCITY - TIME RELATIONS FOR ELECTRIC DRIVES FOR INTERMITTENT OPERATION*

L.V. KARNIUSHIN

(Received 17 December 1956)

The theory of motor drive presented below is of practical importance for designing and operating a reversible unit consisting of an electric motor and a driven mechanism which operates intermittently with frequent starting and braking.

Depending on the design, and types of operation performed, the choice of velocity-time relations (or the corresponding load diagrams of the motor and driven mechanism) can be based on various criteria [1-3]. The criteria adopted in the present work are based on the fact that the relation between the output of the machine and the rating of the motor (the latter being fully utilized according to thermal loading) is dependent mainly on the choice of the velocity-time relation of the motor [2,3].

Thus, in the case of machines having a given duty cycle whose operating member moves through a given fixed distance (e.g. a colliery winder), the first condition for the choice of the best velocity-time curve of the driving motor is that *a given output must be secured with the smallest horse-power rating.* (First criterion). It will be shown later that this condition is equivalent to securing the maximum output with a given installed horse-power.

In a number of cases a second criterion is of importance, which is *securing the maximum output with a given rated motor torque.* This is equivalent to securing a given output at the minimum motor temperature rise.

The functional relation between the motor horse-power (or torque), the velocity-time law, and the output power can be found by solving the simultaneous equations for the velocity law of the motor, the heating of the motor, and the angular displacement of the machine shaft. If this relation is found, the question of finding the best velocity-time relation (in accordance with the first or second criterion) amounts to finding mathematically either the extremum of a certain function (for a given form of tachogram) or of the functional.

The solution of this kind of problem (when both criteria are satisfied) is

* *Elektrichestvo* No. 6, 64-71, 1957 [Reprint Order No. EL 31].

given in the literature only for one particular type of motor velocity-time curve, namely when this curve is trapezoidal [2, 4]. A more general solution, when not only the parameters, but also the shape of the velocity-time curve have to be found, is given in [3, 5, 6]. This applies to cases in which only the second criterion is satisfied. The problem of the existence of a velocity-time curve satisfying the first criterion has never been fully investigated [7].

It should be pointed out that there is still at the present time no definite opinion on the practical significance of the best velocity-time curve of the motor drive. This is because sufficiently detailed investigations covering the whole subject have not been carried out.

In preparing this paper the following assumptions have been made:

(a) the temperature rise of the motor is assumed to vary with the r.m.s. torque;

(b) the following quantities, referred to the motor shaft, are constant:- the resistance torque, T_r, the total moment of inertia, J, and the transmission efficiency, η;

(c) the following factors which impose limitations on the voltage-time laws of motor drive are neglected:- type of process, robustness of construction of the machine, conditions for supporting moveable parts, permissible mechanical overloading of motors, and electrical overloading of the supplying converter (the influence of these factors will be considered when comparing the tachograms).

The best trapezoidal velocity-time curves of the driving motor

Only symmetrical trapezoidal curves will be considered, since these are more advantageous with regard to motor heating than the asymmetrical curves [2].

For a given angular displacement, β, the time during which the motor is rotating, t_m, and time of rest, t_o, there is a certain steady (established) angular velocity of the motor, ω_{e2} (or the corresponding acceleration ϵ_2), at which the r.m.s. value of the motor torque for the interval $t_m + t_o$), T_{eq2}, (the equivalent torque) is a minimum [4]. Also there is a steady velocity ω_{e1} (or ϵ_1) at which the motor output permitted by temperature rise is a minimum. This output is given by:

$$P_{eq1} = \frac{\omega_{e1}\, T_{eq1}}{102}. \qquad (1)$$

It is shown in [4] that irrespective of the magnitude of the resistance torque of the machine (T_r = const) and the efficiency of the mechanical transmission (η = const), the minimum T_{eq2} always occurs at $\omega_{e2} = 0.75\,\omega_\Delta$ (or at $\epsilon_2 = 1.125\,\epsilon_\Delta$) where ϵ_Δ and ω_Δ are acceleration and maximum velocity in the case of

a triangular velocity curve at the same β, t_m, and t_o.

The velocity ω_{e1} which corresponds to the minimum P_{eq1} depends on the magnitude of the coefficient of dynamic loading.

$$d = \frac{1}{\mu} = \frac{J\epsilon_\Delta}{T_r}, \tag{2}$$

and lies within the limits

$$0.5 < \frac{\omega_{e1}}{\omega_\Delta} \leq 0.625 \text{ [4].}$$

The ratios of r.m.s. values of torques and outputs with trapezoidal and triangular velocity-time curves for the same values of β, t_m, and t_o are given by

$$\frac{T_{eq}}{T_{eq\Delta}} = \sqrt{\frac{\frac{z^3}{2z-1} + \mu^2}{1+\mu^2}}; \tag{3}$$

$$\frac{P_{eq}}{P_{eq\Delta}} = z\frac{T_{eq}}{T_{eq\Delta}}, \tag{4}$$

where $z = \dfrac{\omega_e}{\omega_\Delta}$

The function $P_{eq}/P_{eq\Delta}$ is a minimum at a certain value of $z = z_o$ which depends on the numerical value of μ and is given by one of the real roots of the following equation:

$$8z^4 - 5z^3 + 8\mu^2 z^2 - 8\mu^2 z + 2\mu^2 = 0 \tag{5}$$

in the region $0.5 \leq z \leq 0.625$.

By assigning different values to μ (in the majority of cases they lie within the limits $0 < \mu < 3$), it is not difficult to find from (5) the corresponding values of $z_p = \omega_{e1}/\omega_\Delta$. This also gives the optimum velocity at which the minimum required output is attained,

$$\omega_{e1} = z_o\omega_\Delta = 2z_o\frac{\beta}{t_a}, \tag{6}$$

1958

where t_a is the duration of the accelerating period.

Having established the values for $\omega_{e\,1}$ and $\omega_{e\,2}$, we can now determine the parameters of the optimum (according to the first and second criteria) rectangular curves of the motor torque for the periods of accelerating and braking.

$$T_{a,b} = J \frac{\omega_{e\,1.2}}{t_{a\,1.2}} \pm T_r ; \tag{7}$$

$$t_{a\,1.2} = t_{b\,1.2} = t_m - \frac{\beta}{\omega_{e\,1.2}} , \tag{8}$$

where t_b is the duration of the braking period.

The optimum velocity-time relations for the drive

The time function $\omega\,(t)$, representing the required velocity-time relations, should increase steadily during the accelerating period, decrease steadily during the braking period, and pass through the points

$$\omega\,(0) = \omega\,(t_m) = 0 \tag{9}$$

With given values for the displacement β and the duration of the cycle $t_c = (t_m + t_o)$, the required rated torque, T_n and the rated horse-power, P_n of the motor working under intermittent load conditions, are given by

$$P_n = \frac{\omega_n T_n}{102} ,$$

$$T_n = \sqrt{\frac{\int_0^{t_a} T_a^2\,dt + T_r^2\,t_e + \int_{t_a+t_e}^{t_m} T_b^2\,dt}{a_1 t_u + a_2 t_0}} , \tag{10}$$

where t_e – period of constant velocity, a_1 and a_2 – coefficients to allow for poorer motor cooling at $\omega < \omega_n$, ω_n – rated angular velocity of the motor rotor.

The motor torques during the accelerating and braking periods are

$$T_a = J\epsilon + T_r \text{ and } T_b = J\epsilon - T_r . \tag{11}$$

Substituting (11) into (10) and considering the condition given by (9)

$$\int_0^{t_a} \epsilon\,dt = \int_{t_a+t_e}^{t_m} \epsilon\,dt$$

and

$$J^2 \int_0^{t_a} \epsilon^2\, dt + J^2 \int_{t_a+t_e}^{t_m} \epsilon^2\, dt = J^2 \int_0^{t_m} \epsilon^2\, dt\ ,$$

we can find the relation between P_n, T_n, the output $\Pi \equiv 1/t_c$, and the velocity-time law:

$$102^2 P_n^2 (a_1 t_m + a_2 t_0) = I_1 ; \tag{12}$$

$$T_n^2 (a_1 t_m + a_2 t_0) = I_2\ , \tag{13}$$

where

$$I_2 = T_r^2 t_m + J^2 \int_0^{t_m} \epsilon^2\, dt\ ; \tag{14}$$

$$I_1 = \omega_n^2 I_2 = \left(\int_0^{t_a} \epsilon\, dt\right)^2 I_2\ . \tag{15}$$

As is seen from (12) and (13), for a given output (i.e. for given values of t_m, t_0, and β), the minimum value of the required motor torque, $T_{n.\min}$, is given by a velocity-time law that minimizes the functional I_2. The minimum value of the rated output, P_n, will be obtained with a different velocity law which minimizes the functional I_1. If T_n (or P_n), β, and t_m (or t_0) are given, the highest output will be obtained with these laws (i.e. the shortest period t_0 (or t_m) and therefore, $t_{c.\min}$).

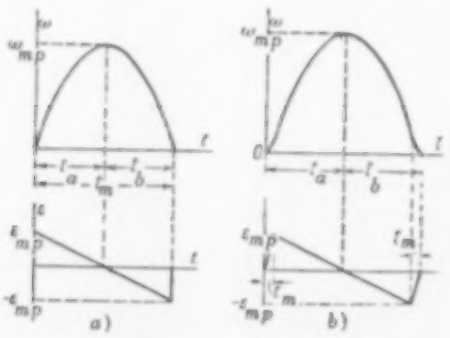

FIG. 1. a) Parabolic velocity curve with sudden change of acceleration;
b) with periods of uniform change of acceleration.

Thus the mathematical determination of the velocity-time relationships for a driving motor can be reduced to two similar isoperimetric variational problems, that is, determination of the function $\omega\,(t)$ which minimizes the functional I_1 (or I_2) and satisfies the boundary conditions given by (9), as well as satisfying an additional condition

$$\int_0^{t_m} \omega\, dt = \beta\,. \tag{16}$$

To determine the function $\omega\,(t)$ which minimizes the functional I_2 is easily done by setting up and solving Euler's equations [5,6]. The required velocity-time law for the drive motor satisfying the second criterion is a symmetrical parabola, Fig. 1a.

$$\epsilon = \epsilon_{mp}\,(1 - 2\,\frac{t}{t_m})\;; \tag{17}$$

$$\omega = \omega_{mp}\,t\,(1 - \frac{t}{t_m})\;, \tag{18}$$

where

$$\epsilon_{mp} = 6\,\frac{\beta}{t_m^2} = 1.5\epsilon_{\Delta}\;;\; \omega_{mp} = 1.5\,\frac{\beta}{t_m} = 0.75\omega_{\Delta}\,. \tag{19}$$

For the same β, t_m, and t_o, the ratio of the r.m.s. value of torque for the parabolic velocity curve to the torque for the trapezoidal velocity curve is given by

$$\frac{T_{eq\,q}}{T_{eq}} = \sqrt{\frac{(0.75 + \mu^2)\,(2\,z - 1)}{z^3 + \mu^2\,(2z - 1)}}\,. \tag{20}$$

Also, the ratio of corresponding outputs is

$$\frac{P_{eq\,p}}{P_{eq}} = \frac{0.75\,T_{eq\,p}}{z\;T_{eq}}\;; \tag{21}$$

The ratio of accelerations is

$$\frac{\epsilon_{mp}}{\epsilon} = \frac{1.5\,(2z - 1)}{z^2} \tag{22}$$

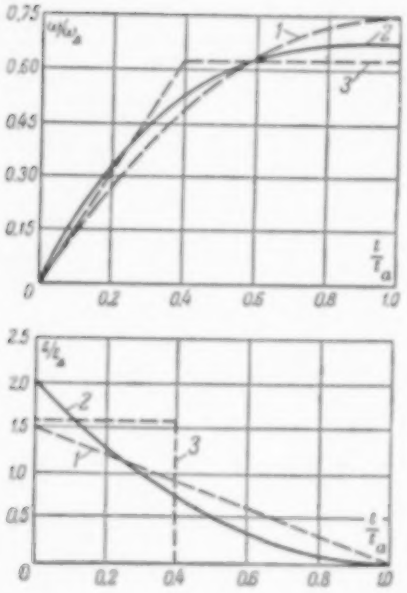

FIG. 2. Diagrams of velocity and acceleration for one-half period of displacement.
1—with "parabolic acceleration";
2—with the optimum velocity law (with respect to output);
3—with the optimum trapezoidal velocity-time curve (with respect to output) ($\mu = 0$).

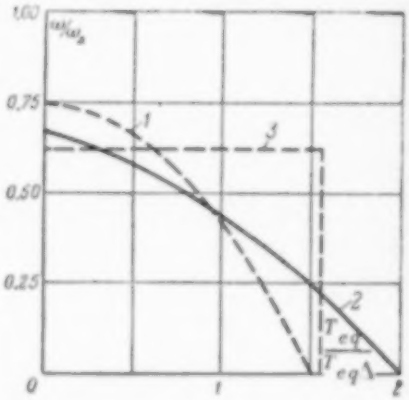

FIG. 3. Characteristics of motor necessary to obtain velocity-time curves of Fig. 2.
1—with "parabolic acceleration";
2—with the optimum velocity law (with respect to output);
3—with the best trapezoidal velocity-time curve (with respect to output).

The load diagram for the parabolic velocity curve and for $T_r = \text{const.}$ is of triangular shape,

$$T = T_r + J\epsilon = T_r + J\epsilon_m \left(1 - 2\frac{t}{t_m}\right) \tag{23}$$

(the ratio of mean height of curve to maximum height is 0.5).

The usual variational method of setting up Euler's equations is not applicable to finding the function $\omega(t)$ which minimizes the second functional, I_2. Therefore, it is necessary to use a direct variational method.

We shall assume a symmetrical velocity curve of the motor. To solve the problem, it is then sufficient to consider only the first half-period of the displacement from $t = 0$ to $t = 0.5\ t_m$, since it is obvious that if the conditions (9) are

satisfied, the required law will also be valid for the second half-period.

Thus, this law of motion can be found for any predetermined relation between T_r and J. We shall, however, confine ourselves to considering only the case when the frictional resistance can be neglected ($T_r \to 0$). The solution to this case will enable us to evaluate the greatest effect which can be achieved by using the law which conforms to the first criterion.

With the assumption made the problem is reduced to finding a function $\omega(t)$ minimizing a functional which is simpler than the functional I_1 and is given by

$$I_3 = \left(\int_0^{0.5t_m} \epsilon\, dt\right)^3 \cdot \int_0^{0.5t_m} \epsilon^3\, dt \tag{24}$$

for the following conditions: a) $\omega(0) = 0$; b) $\omega'(0.5t_m) = 0$;

$$\text{c)} \int_0^{0.5t_m} \omega\, dt = \frac{\beta}{2}; \quad \text{d)} \ \omega'(t) \geq 0 \text{ for } 0 \leq t \leq 0.5\, t_m.$$

Condition d) represents the requirement that $\omega(t)$ is to increase steadily, while condition b) follows from the natural limiting condition for the end of the curve $\omega(t)$ which has a locus $t = t_a$, parallel to the ω axis.

The solution to this problem [7] gives as a first approximation the following optimum (with respect to the equivalent output) laws for the first half of the displacement when $\mu = 0$.

$$\omega = \epsilon_{mo} t \left(1 - 2\frac{t}{t_m} + \frac{4t^2}{3t_m^2}\right); \tag{25}$$

$$\epsilon = \epsilon_{mo}\left(1 - 4\frac{t}{t_m} + 4\frac{t^2}{t_m^2}\right), \tag{26}$$

where $\epsilon_{mo} = 8\dfrac{\beta}{t_m^2} = 2\epsilon_\Delta$ and $\omega_{mo} = \dfrac{4}{3}\dfrac{\beta}{t_m} = \dfrac{2}{3}\omega_\Delta$. (27)

The curves of velocity and acceleration drawn from (25) and (26) are shown on Fig. 2. The same figure also shows for comparison (with the same β, t_m, and $\mu = 0$) the parabolic curve and the optimum trapezoidal curve with respect to output. Fig. 3 shows the torque characteristics of the motor which are necessary to obtain the velocity-time curves shown in Fig. 2.

The r.m.s. value of the torque for the period of $0.5\, t_m$ when the motor acceleration follows the optimum law in accordance with the first criterion, is given by

$$T_{eq0} = \sqrt{2\frac{J^2}{t_m}\int_0^{0.5t} \epsilon^2\, dt} = 3.576\, J\, \frac{\beta}{t_m^2} = 0.894\, T_{eq\Delta}\,. \qquad (28)$$

The equivalent output is found from (27) and (28)

$$P_{eq0} = \frac{2}{3}\, 0.894\, P_{eq\Delta} = 0.596\, P_{eq\Delta}\,. \qquad (29)$$

The ratio between mean and maximum height of the load torque curve when the optimum law (25) is obeyed is given by

$$k_z = \frac{\int_0^{0.5t_m} J\dot{\epsilon}\, dt}{J\epsilon_{m0}\, 0.5t_m} = \frac{1}{3}\,.$$

1958

The use of optimum tachograms with variable path of displacement

Because of the geometrical relationship between the displacement, β, of the operating member of the driven mechanism and the remaining parameters of the tachogram, ω, ϵ and t_m, these parameters vary with β. Also the tachogram should be corrected for permissible velocities and accelerations.

Since in the case of a varying cycle of operation the choice of the best motor tachograms is influenced by a great number of different conditions, this problem must be considered separately for each particular case of the motor drive.

In the case when a uniform regular cycle of operation and a number of fixed paths of displacement are given, the problem consists of either finding optimum tachograms corrected for ω and ϵ, for each displacement, using the condition for the maximum P_{eq} (or T_{eq}) or the maximum output π for the whole cycle.

For mechanisms with an arbitrary path of displacement (e.g. the main mechanisms of an excavator) either the first or the second criterion must be satisfied for the most typical cycle of operation; for other paths of displacement, the highest output permitted by the motor heating must be secured. For this purpose it is expedient to devise a scheme of automatic re-adjustment of the control system of the motor drive which will ensure that the optimum velocity and acceleration are achieved for each displacement.

With a constant standstill period, t_o, the effect which can be achieved with such a scheme cannot be very great. This is clearly seen in the example of the driving motor for the turning mechanism of the walking excavator type ESh – 14/75 for which the duration of the turning operation is up to 85 per cent of the duration of the whole cycle.

If the parabolic tachogram is used, the angle of turn, β, at which the motor

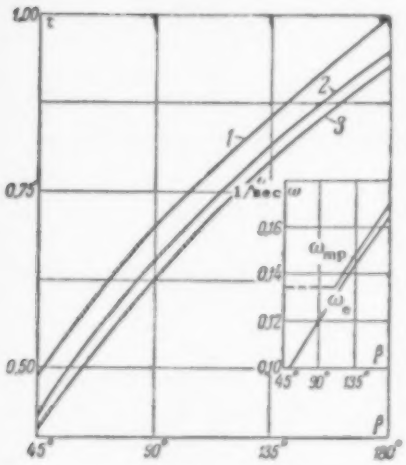

FIG. 4. Relative time of turning against angular path for the excavator type ESh – 14/75.

1 – with trapezoidal velocity-time curve, $\beta > 125°$, and fixed acceleration and velocity (the motor is fully utilized only at $\beta = 125°$);

2 – with the best (in accordance with the 2nd criterion) trapezoidal velocity-time curves for each angle of turning;

3 – with parabolic velocity-time curves and full utilization of the motor with regard to heating at $\beta \geq 110°$.

and the mechanism are fully utilized (the first with respect to heating and the second with respect to permissible acceleration; $\epsilon_{perm.} = 0.025$ 1/sec²) is 110°. If $\beta > 110°$, while keeping $T_{eqp} = \text{const}$, the acceleration ϵ_{mp} decreases. If $\beta < 110°$, the duration of the excavator cycle is limited by the action of the lifting mechanism [1].

We shall denote $\tau = \dfrac{t_m}{t_{m.m}}$, where t_m is the time of turning through the angle β and $t_{m.m}$ is the time of turning through 180° when the velocity-time curve used is of trapezoidal form and ϵ and ω_e are fixed and such that the motor can be fully utilized from the point of view of heating only at $\beta = 125°$.

Fig. 4 shows calculated curves $\tau = f(\beta)$ for different kinematic condition of operation of the motor drive when the period of digging is constant, $t_d = 10$ sec. It is seen from this figure that if the rotation of the driving motor follows the optimum tachogram for each angle of turn, the output of the excavator is increased by 4 to 5 per cent. The advantages of the parabolic over the best trapezoidal curve judged by the second criterion are, in this case, negligible.

Comparison of optimum tachograms for electric drive

In this comparison we shall assume that the cycle of operation consists of one period of displacement and one period of standstill; the path of displacement, β, being constant.

To assess the usefulness of the optimum velocity-time laws both in design and in practice, the following two principles should be applied:

1) *The principle of equal output.* This means that the operating member of the mechanism should move through a given path β in the same time t_m, with the same duration of time during which the motor is switched on, θ. The basic quantities which are compared using this principle are the required motor parameters.

2) *The principle of equal rated motor torque.* This means that the rated torque is maintained constant while either the time of the period of standstill, t_o, or the time of displacement, t_m, (and so π and θ) is changed. The basic quantities which are compared are the durations of the cycles for various velocity-time relations.

Apart from comparing the basic quantities, we shall also compare the mechanical overloading of the motor and the maximum velocity and acceleration of the tachograms. Moreover, we shall take into account the effects of the static resistance torque, T_r, and the total moment of inertia J referred to the motor shaft, using reasonably probable values for the dynamic index μ.

Under actual starting conditions the motor torque (and acceleration) cannot attain maximum instantaneously. (Fig. 1a). If, for example, a parabolic tachogram is used, the end parts of the curve will be slightly distorted (Fig. 1b) due to an initial smooth variation of acceleration. The existence of this initial variation of acceleration is desirable from the points of view of stability and wear of the mechanism. Since similar distortions will occur with any selected velocity-time law, their effect can be neglected for the purpose of the present comparison.

1958

To determine numerical values of the ratios of the equivalent torques, outputs and accelerations for different values of μ and z, we shall use the expressions previously obtained.

In the case of equal outputs the ratio of the required maximum percentage overloads can be found from the velocity-time equation for the period of starting and from relation (20). Thus, we get

$$\lambda_\Delta T_{eq\Delta} = J\epsilon_\Delta + T_r \quad \text{and} \quad \lambda_p T_{eqp} = J\epsilon_{mp} + T_r ,$$

whence

$$\frac{\lambda_p}{\lambda_\Delta} = \frac{(1.5+\mu)}{(1+\mu)} \frac{T_{eq\Delta}}{T_{eqp}} = \frac{(1.5+\mu)}{(1+\mu)} \sqrt{\frac{1+\mu^2}{0.75+\mu^2}} . \tag{30}$$

In a similar way

$$\frac{\lambda_p}{\lambda_{1.2}} = \frac{(1.5+\mu)}{\left(\frac{\epsilon_{1,2}}{\epsilon_\Delta}+\mu\right)} \frac{T_{eq1.2}}{T_{eqp}} . \tag{31}$$

In the case when the duration of cycle is decreased by reducing the standstill period, t_o, while keeping the same duration of the period of displacement, t_m, we have $T_{eq\Delta} = T_{eqp}$ Therefore, equations (30) and (31) become

$$\frac{\lambda_p}{\lambda_\Delta} = \frac{1.5+\mu}{1+\mu}, \tag{32}$$

and

$$\frac{\lambda_p}{\lambda_{1.2}} = \frac{1.5 + \mu}{\frac{\epsilon_{1.2}}{\epsilon_\Delta} + \mu} . \tag{33}$$

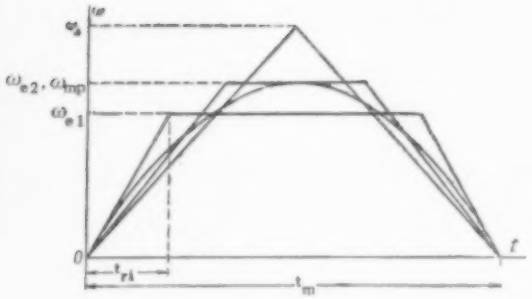

FIG. 5. Triangular, parabolic, and optimum trapezoidal velocity diagrams for the same paths and times of displacement and with $\mu = 0$.

The relative increase, $\Delta\pi$, of the output due to the reduction of the standstill period, t_o,* can again be easily found from the condition that the rated motor torque should be the same. For example, when changing from triangular to parabolic velocity-time diagram, remembering that the ratios previously found for equivalent torques over time t_c will be numerically the same as the ratios over the time t_m with the same t_m and t_o, we find that

$$\left(\frac{T_{eqp}}{T_{eq\Delta}}\right)^2 = \frac{\pi\Delta}{\theta_p} = \frac{t_{cp}}{t_c\Delta} ,$$

and thence

$$\Delta\pi = \left(\frac{\pi_p}{\pi\Delta} - 1\right) 100 = \left(\frac{t_c\Delta}{t_{cp}} - 1\right) 100 = \left(\frac{T^2_{eq\Delta}}{T^2_{eqp}} - 1\right) 100 . \tag{34}$$

* The calculations of the increase of the output and the maximum relative percentage motor overload when t_m is reduced and t_o is constant, are not given. In this case, the time during which the motor is switched on, θ, is given by the velocity-time curve considered [6]. The calculations involve graphical solutions of complex equations. Also, since the r.m.s. torque and the required output of the motor increase much more quickly than the output (e.g., if $T_r = 0$ and $\theta = 100$ per cent, reducing t_m k times increases P_n and T_n k^3 and k^2 times respectively) these means of increasing the output by changing from one type of velocity-time curve to another become so ineffective for $\theta < 60$ per cent that they cannot be applied in practice [6].

TABLE 1. Comparison between the parabolic and optimum (as judged on torque basis) trapezoidal tachograms

$$\left(\frac{\omega_{mp}}{\omega_{e2}} = 1; \frac{\epsilon_{mp}}{\epsilon_2} = 1.33 \text{ for the same } \beta \text{ and } t_m\right)$$

Basis of comparison	Equal output			Equal T_{eq}, β, and t_m)		
μ	P_{eqp}/P_{eq2}	T_{eqp}/T_{eq2}	λ_p/λ_2	$\Delta\Pi$ (%)	$P'_{eqp}/P'_{eq2} = \omega_{mp}/\omega_{e2}$	λ_p/λ_2
0	0.942	0.942	1.41	12.7	1	1.33
0.5	0.956	0.956	1.28	9.4	1	1.23
1	0.975	0.975	1.20	5.6	1	1.18
2	0.990	0.990	1.14	2.0	1	1.12
3	0.995	0.995	1.10	1.0	1	1.09

TABLE 3. Comparison between the 1st criterion optimum, parabolic, and the optimum judged on power basis, trapezoidal velocity-time diagrams, $\mu = 0$

Basis of comparison	The same β and t_m		Equal output			Equal T_n, β, and t_m		
Index, %	$\Delta\omega_{mo}$	$\Delta\epsilon_{mo}$	ΔP_{eq0}	ΔT_{eq0}	$\Delta\lambda_0$	$\Delta\Pi_0$	ΔP_{eq0}	$\Delta\lambda_0$
Compared with best trapezoidal curve	6.7	28.0	-3.6	-9.5	42	22.0	-6.7	28.0
Compared with parabolic curve	-11.1	33.3	-8.3	3.2	29	-6.2	-11.1	33.3

TABLE 2. Comparison between the parabolic and optimum (as judged on power basis) trapezoidal tachograms

Basis of comparison	The same β and t_m			Equal output			Equal T_n, β, and t_m		
μ	z_0	$\omega_{el}/\omega_{mp} = z_o/0.75$	ϵ_1/ϵ_{mp}	P_{eqp}/P_{eq1}	T_{eqp}/T_{eq1}	λ_p/λ_1	$\Delta\Pi$ (%)	$P_{eqp}/P_{eq1} = \omega_{mp}/\omega_{e1}$	λ_p/λ_1
0	0.625	0.833	1.042	1.05	0.877	1.10	30.0	1.20	0.96
0.5	0.611	0.815	1.119	1.09	0.885	1.04	27.7	1.23	0.92
1	0.587	0.783	1.318	1.15	0.901	0.93	23.1	1.28	0.84
2	0.555	0.740	1.867	1.25	0.926	0.79	16.5	1.35	0.73
3	0.538	0.717	2.516	1.32	0.943	0.71	12.5	1.40	0.67

The results of calculations to compare the velocity-time diagrams of Fig. 5 are given in Tables 1 and 2. Table 3 collects data showing comparisons between the optimum, according to the first criterion, velocity-time curve and the best trapezoidal and parabolic tachograms judged on the power basis (Fig. 2).

Conclusions

1. There are two kinds of extremum velocity-time law of the motor drive operating under intermittent conditions of load with full utilization of the motor with respect to heating:

a) the velocity-time law (25) which gives the minimum rated motor output of the mechanism.

b) the velocity-time law (18) which gives the minimum rated motor torque which is necessary for a given output of the mechanism.

By using these laws we can achieve for a given motor the highest possible output permitted by the heating of the motor.

1958

The parameters of the first kind of the velocity-time law are dependent on the coefficient of dynamic loading (2), whereas those of the second kind of the law are independent of it.

2. As can be seen from Table 2, the efficiency which can be obtained by using the optimum velocity-time curves depends on the relation between the static and dynamic components of the load (i.e. on the coefficient μ) and becomes a maximum for the purely dynamic load. In the case when the static load is predominant, these curves (and also the corresponding armature-current diagrams) have no substantial advantage over the best trapezoidal curves.

3. In the case when the dynamic load is predominant, the following effects can be achieved over to the optimum velocity laws:

a) If the output of an electro-mechanical device for cyclic operation is specified, considerable lowering of the installed horse-power (and consequently lowering of the cycle energy loss) can be obtained by using the velocity-time law (25).

b) If the motor is specified (or has already been installed) a substantial increase of the mechanical output can be achieved without overheating of the motor by shortening the period of rest.

However, in this case the dynamic loading of the mechanism and the percentage overload of the motor are increased.

When the output is specified or needs to be increased by reducing the duration of the period of running without altering the temperature rise of the motor, the advantages of the parabolic velocity-time diagram (18) over the best trapezoidal diagram judged on torque basis are small (Table 1).

The advantages of the optimum in accordance with the first and second

criteria velocity laws are as follows:

a) a much more uniform energy consumption during the starting period;

b) the mechanical characteristics of the driving motor (Fig. 3) which are necessary when these laws are consistent with the kind of relation between the permissible percentage overload and the speed which is peculiar to the d.c. motor;

c) it is not necessary to have a high ratio between the mean height and the maximum height of the load-current (or load-torque) curve of the motor.

4. In order to make use of the advantages presented by the best velocity-time curves in the case when the path of displacement of the operating member of the mechanism is variable, it is expedient to provide an automatic re-adjustment of the control system of the motor drive that will ensure the optimum velocity and acceleration for each displacement. The question of the establishment and application of the optimum velocity-time laws when the path of displacement is variable necessitates additional elaboration depending on the type of the motor drive.

5. The ratio between the mean height and the maximum height of the armature current curve should not be used as a criterion for assessing the usefulness of the drive control system in cases when the motor is fully utilized with respect to heating. The degree of usefulness of a control system is determined by the extent to which a most simplified and reliable system approximates the optimum velocity laws. The ratio of mean to maximum height of the current curve characterizes the usefulness of the control system only in cases in which it is necessary to use the highest acceleration permitted by the mechanism in order to achieve the shortest period of starting or the highest output, irrespective of the required motor output. Therefore, the optimum velocity law is that which gives a constant acceleration [1].

6. The various aspects of the use of the optimum velocity-time laws for motor drives should be considered not only when designing the driving motor and its automatic control system, but also when designing the driven mechanism. In particular, when establishing the permissible accelerations of the mechanisms, an allowance should be made for a possibility of using the optimum velocity-time relations for the motor drive.

The stability of the characteristics of motor drives is of great importance when using the optimum velocity-time laws.

When the motor is fully utilized with respect to heating and specified output, its required rated output and torque depend not only on the type of velocity law but also on the reduction gear ratio [1]. In connexion with this the following additional conclusions drawn from the present investigation are of interrest:

a) The smallest rated motor torque is required by using the velocity law (18) minimizing the equivalent motor torque, and a rated motor speed cor-

responding to the optimum reduction gear ratio.

b) The smallest rated motor output is required when using the velocity law (25) minimizing the motor horse power, and a rated motor speed which should preferably be less than the speed corresponding to the optimum reduction gear ratio.

REFERENCES

1. F.A. Goraiko and L.V. Karnyushin; *The choice of reducing gear ratio for motor drives for lift-conveyer mechanisms and excavators. Transactions of Scientific and Technical Session on Motor Drive for Lifting-and-Conveying Mechanisms. Gosenergoizdat* (1955).
2. M.M. Fedorov; *The best dynamic conditions of operation for some types of ore-lifting equipment. Coal and Steel*, 11 ,12 and 14 (1956).
3. S.A. Press; *Electrical equipment for excavators.* State United Publishing House of Science and Technology (1938).
4. F.A. Goraiko; *The best suitable parameters of the motor-drive velocity-time diagram with three periods. Scientific Reports of Lvov Polytechnical Institute*, Electrotechnical Series, Vol. 40 No. 9 (1956).
5. L.V. Karnyushin; *The best velocity-time laws for a motor drive operating under starting and braking conditions. Scientific Reports of Lvov Polytechnical Institute*, Electrotechnical Series, Vo. 40. No. 9 (1956).
6. K.I. Kozhevnikov; *The current diagram for the motor for the auxiliaries of rolling mills. Elektrichestvo*, No. 6 (1956).
7. L.V. Karnyushin; *Motor drive transient velocity law minimizing the required motor output. Reports of Lvov Polytechnical Institute* Vol. II, 2nd edition (1957).

1958

A METHOD OF DERIVING EQUATIONS FOR THE ELECTROMECHANICAL TRANSIENT IN ELECTRIC CIRCUITS*

S.V. STRAKHOV

(Received 5 October 1956)

There are basically two methods of investigating the transient electromechanical processes in electric circuits, viz:

1. Physical modelling.
2. Mathematical modelling, this comprising two sections, viz:
   (a) the section using physical analogs;
   (b) the section using digital computers (integrators) with continuous and discrete action.

The method of physical modelling, comprehensively treated in papers of V.A. Venikov [1-3], M.P. Kostenko [4-6] and of other authors, consists in the replacement of large rotating electric machines and hydraulic turbines by similar units of small ratings with due consideration to the laws of similitude. Transmission lines, tranformers, saturable reactors and static loads are replaced by assemblies of capacitances and inductances, networks with repeated members being used for transmission lines. In other words, in this case the physical character of the model and of the original are the same.

Among the advantages of the method of physical modelling, where rotating machines are concerned, we should mention the possibility of considering eddy currents, saturation, hysteresis, the actual distribution of stator and rotor windings in space, and of other factors. A drawback of this method is the difficulty of varying the parameters of individual machines, usually necessitating the availability of a number of inter-changeable rotors for them. It is, therefore, more convenient to use the method of mathematical modelling in cases where the parameters of the machines must be variable; because this method can deal in a much more simple way with such variations. However, physical modelling will still be preferable in all cases in which the system of differential equations describing the process is very complicated.

* *Elektrichestvo* No. 7, 5-10, 1957 [Reprint Order No. EL 32].

Referring to the first section of the method of mathematical modelling [1, 7 and 8], we note that rotating machines are replaced by equivalent devices (electronic circuits, electrodynamical apparatus), i.e. physical analogs according to the similar structure of their differential equations. In this case the model has a different physical character from the original. If the system contains static elements, for example, transmission lines, they are represented in the same way as in the preceding method, i.e. to these physical modelling is applied. An advantage of this method is the greater convenience of varying the individual parameters of the rotating machines, because it amounts only to a variation of comparatively easily adjustable parameters of the electronic circuits or the physical analogs. On the other hand, since the static elements of circuits consist of assemblies of coils and capacitors, no differential equations have to be set up for them. This is a great advantage of the first section of the method of mathematical modelling over the second section.

The second section of the method of mathematical modelling, consisting of the use of computing mechanisms (integrators) for the investigation of the transient electromechanical processes in the electric circuits, is nowadays widely used. Its importance is still increasing with the growing production of relatively inexpensive computor types suitable for the integration of systems of non-linear differential equations of an over-all order up to 20 – 30.

1958

This method makes it particularly easy to vary the system of parameters within a wide range by an easy regulation of the blocks collecting the coefficients of the individual equations.

This method is suitable not only for the solution of electrical engineering problems, but also for the solution of systems of non-linear differential equations met in physics, mechanics, hydrodynamics, heat engineering, etc. In this sense it is a universal method.

A disadvantage of this method is the necessity of using a whole number of blocks of the integrator for considering the differential equations of the static circuit elements and, in particular, of long lines, since often the greater half of the overall order of the system of differential equations of the circuit is accounted for by the static circuit elements.

However, the integrators may be designed in such a way as to enable the differential equations of only one part of the whole circuit to be represented, whereas the remaining part is actually present in life-size or represented by physical models. The latter condition considerably extends the range of possible users of integrators of this type for investigations of the transient processes in interconnected systems.

Method of setting-up system of differential equations

In order to use the integrator, the system of differential equations of the circuit has to be set up, first of all, in the simplest and the most rational form.

We will then consider the differential equations of the synchronised generator, referred to all coordinate systems rigidly connected with its rotor, the equations of an induction motor and of all the static circuit elements (loads, transformers, transverse capacitances, compensating coils and lines with longitudinal compensating capacitances) referred to coordinated system rotating at an arbitrary speed, as given.

All the equations given below refer to the positive directions of the currents shown in figures.

When setting up the differential equations for any actual system it is, above all, important to choose the most rational system of rotating coordinates to which then the equations of all static circuit elements have to be referred. For symmetrical circuits the equations of the static elements may be referred to axes rigidly connected to the rotor of any of the generators [9], which follows from the symmetry of the circuit.

We will illustrate the method of setting up the system of equations on the example of the circuit of Fig. 1, being practically symmetrical.

We will refer to equations of all elements of the circuit of Fig. 1 (except *SG*2) and the equations resulting from Kirchhoff's first law, to coordinate axes rigidly connected to the rotor of the synchronous generator *SG*1.

The equations for *SG*1 are [10 and 11]:

$$
\left.
\begin{aligned}
u_{1d} &= -r_{C1} i_{1d} + \frac{d}{dt}(-L_{d1} i_{1d} + M_{f1} i_{1f} + M_{g1} i_{1g}) - \\
&\quad -(-L_{q1} i_{1q} + M_{h1} i_{1h}) \frac{d\theta_1}{dt}; \\
u_{1q} &= -r_{C1} i_{1q} + \frac{d}{dt}(-L_{q1} i_{1q} + M_{h1} i_{1h}) + \\
&\quad +(-L_{d1} i_{1d} + M_{f1} i_{1f} + M_{g1} i_{1g}) \frac{d\theta_1}{dt}; \\
u_{10} &= -r_{C1} i_{10} - L_{01} \frac{di_{10}}{dt}; \\
u_{1f} &= r_{f1} i_{1f} + \\
&\quad + \frac{d}{dt}\left(-\frac{3}{2} M_{f1} i_{1d} + L_{f1} i_{1f} + M_{fg1} i_{1g}\right); \\
0 &= r_{g1} i_{1g} + \\
&\quad + \frac{d}{dt}\left(-\frac{3}{2} M_{f1} i_{1d} + L_{g1} i_{1g} + M_{fg1} i_{1f}\right); \\
0 &= r_{h1} i_{1h} + \frac{d}{dt}\left(-\frac{3}{2} M_{h1} i_{1q} + L_{h1} i_{1h}\right);
\end{aligned}
\right\} \qquad (1)
$$

$$T_{\partial 1} - \frac{3}{2}\left[(L_{d1} - L_{q1})\, i_{1d}\, i_{1q} - M_{f1}\, i_{1f}\, i_{1g} - \right.$$

$$\left. - M_{g1}\, i_{1g}\, i_{1q} + M_{h1}\, i_{1h}\, i_{1d}\right] = J_1 \frac{d^2\theta_1}{dt^2}\,.$$

In an analogous way, by altering subscript 1 to subscript 2, we write the equations for *SG2*, since we refer to its equations to axes rigidly connected to its rotor.

The equations for *IM1* [10 and 12] are:

$$U_{1d} = r_{\partial 1}\, i_{\partial 1d} + L_{C11}\frac{di_{\partial 1d}}{dt} + L_{ad1}\frac{di_{1pd}}{dt} -$$

$$-(L_{C11}\, i_{\partial 1q} + L_{ad1}\, i_{1pq})\frac{d\theta_1}{dt}\,;$$

$$U_{1q} = r_{\partial 1}\, i_{\partial 1q} + L_{C11}\frac{di_{\partial 1q}}{dt} + L_{ad1}\frac{di_{1pq}}{dt} +$$

$$+(L_{C11}\, i_{\partial 1d} + L_{ad1}\, i_{1pd})\frac{d\theta_1}{dt}\,;$$

$$U_{10} = r_{\partial 1}\, i_{\partial 10} + L_{C01}\frac{di_{\partial 10}}{dt}\,; \qquad (2)$$

$$0 = r_{p1}\, i_{1pd} + L_{p11}\frac{di_{1pd}}{dt} + L_{ad1}\frac{di_{\partial 1d}}{dt} -$$

$$-(L_{ad1}\, i_{\partial 1q} + L_{p11}\, i_{1pq})\left(\frac{d\theta_1}{dt} - \omega_{\partial 1}\right);$$

$$0 = r_{q1}\, i_{1pq} + L_{p11}\frac{di_{1pq}}{dt} + L_{ad1}\frac{di_{\partial 1q}}{dt} +$$

$$+(L_{ad1}\, i_{\partial 1d} + L_{p11}\, i_{1pd})\left(\frac{d\theta_1}{dt} - \omega_{\partial 1}\right);$$

$$0 = r_{p1}\, i_{1p0} + L_{p01}\frac{di_{1p0}}{dt}\,;$$

$$\frac{3}{2}L_{ad1}\,(i_{1pd}\, i_{\partial 1q} - i_{1pq}\, i_{\partial 1d}) - T_{C1} = J_{\partial 1}\frac{d\omega_{\partial 1}}{dt}\,.$$

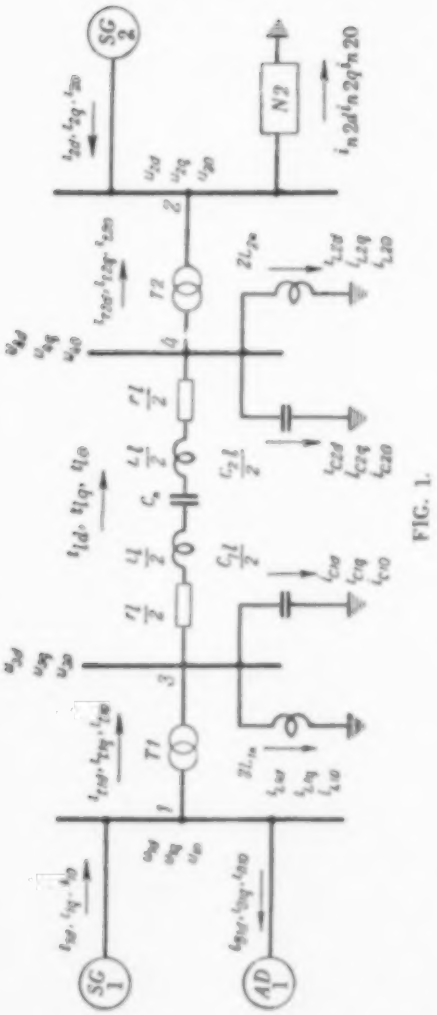

FIG. 1.

The equations following from Kirchhoff's first law [*cf.* (1)] are as follows:

$$\begin{aligned} i_{1d} - i_{\partial 1d} - i_{t1d} &= 0\,; \\ i_{1q} - i_{\partial 1q} - i_{t1q} &= 0\,; \\ i_{10} - i_{\partial 10} - i_{t10} &= 0\,. \end{aligned} \tag{3}$$

The equations for static load [9 and 10] are:

$$\begin{aligned} &U_{2d}\cos(\theta_2 - \theta_1) - U_{2q}\sin(\theta_2 - \theta_1) - \\ &- r_{n2}\, i_{n2d} - L_{n2}\frac{di_{n2d}}{dt} + L_{n21}\, i_{n2q}\frac{d\theta_1}{dt} = 0\,; \\ &U_{2d}\sin(\theta_2 - \theta_1) + U_{2q}\cos(\theta_2 - \theta_1) - \\ &- r_{n2}\, i_{n2q} - L_{n21}\frac{di_{n2q}}{dt} - L_{n21}\, i_{n2d}\frac{d\theta_1}{dt} = 0\,; \\ &U_{20} - r_{n2}\, i_{n20} - L_{n20}\frac{di_{n20}}{dt} = 0. \end{aligned} \tag{4}$$

The occurrence of the factor $\cos(\theta_2 - \theta_1)$ and $\sin(\theta_2 - \theta_1)$ is due to the fact that the terminal voltage of *SG*2 is referred to axes rigidly connected to its rotor.

The equations expressing Kirchhoff's first law [9], considering the positive directions of the currents as assumed in Fig. 1 will be:

$$\begin{aligned} &i_{t2d} + i_{2d}\cos(\theta_2 - \theta_1) - i_{2q}\sin(\theta_2 - \theta_1) - \\ &- i_{n2d} = 0\,; \\ &i_{t2q} + i_{2d}\sin(\theta_2 - \theta_1) + i_{2q}\cos(\theta_2 - \theta_1) - \\ &- i_{n2q} = 0\,; \\ &i_{t20} + i_{20} - i_{n20} = 0\,. \end{aligned} \tag{5}$$

It should be noted that if the equations of the static load N2 are referred to axes rigidly connected to the rotor of $SG2$, equations (5) will become complicated to the extent equations (4) will be simplified.

Indeed, if we refer the equations of the static load N2 to axes rigidly connected to the axes of the rotor $SG2$ we get [9 and 10] :

$$U_{2d} - r_{n2}\, i_{n2d} - L_{n21}\frac{di_{n2d}}{dt} + L_{n21}\, i_{n2q}\frac{d\theta_2}{dt} = 0\,;$$

$$U_{2q} - r_{n2}\, i_{n2q} - L_{n21}\frac{di_{n2q}}{dt} - L_{n21}\, i_{n2d}\frac{d\theta_2}{dt} = 0\,; \tag{4a}$$

$$U_{20} - r_{n2}\, i_{n20} - L_{n20}\frac{di_{n20}}{dt} = 0\,.$$

Under the same conditions the equations of Kirchhoff's first law [*cf.* (2)] are written as follows :

$$i_{t2d} + i_{2d}\cos(\theta_2 - \theta_1) - i_{2q}\sin(\theta_2 - \theta_1) - i_{n2d}\cos(\theta_2 - \theta_1) + i_{n2q}\sin(\theta_2 - \theta_1) = 0\,;$$

$$i_{t2q} + i_{2d}\sin(\theta_2 - \theta_1) + i_{2q}\cos(\theta_2 - \theta_1) - i_{n2d}\sin(\theta_2 - \theta_1) - i_{n2q}\cos(\theta_2 - \theta_1) = 0\,; \tag{5a}$$

$$i_{t20} + i_{20} - i_{n20} = 0\,.$$

We will further consider in the equivalent circuit of the transformer $T1$ the branch of the no-load current (Fig. 2). For the branches 1 – 7 of the primary winding we get [9 and 10] :

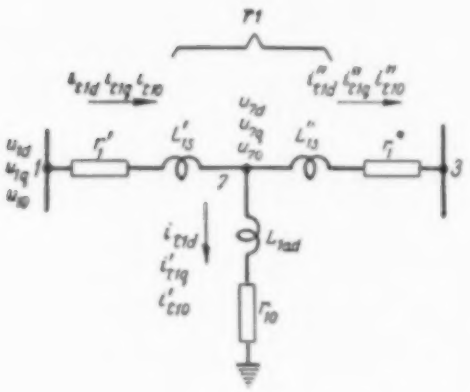

FIG. 2.

$$U_{7d} = U_{1d} - r_1' i_{1d} - L'_{1s1} \frac{di_{1d}}{dt} + \\ + L'_{1s1} i_{1q} \frac{d\theta_1}{dt};$$

$$U_{7q} = U_{1q} - r_1' i_{1q} - L'_{1s1} \frac{di_{1q}}{dt} - \\ - L'_{1s1} i_{1d} \frac{d\theta_1}{dt}; \qquad (6)$$

$$U_{70} = U_{10} - r_1' i_{10} - L'_{1s0} \frac{di_{10}}{dt}.$$

Similarly, we get for the branches 7 – 3 of the secondary winding:

$$U_{3d} = U_{7d} - r_1'' i_{1d}'' - L''_{1s1} \frac{di_{1d}''}{dt} + \\ + L''_{1s1} i_{1q}'' \frac{d\theta_1}{dt}; \qquad (7)$$

$$U_{3q} = U_{7q} - r''_1 i''_{t1q} - L''_{1s1} \frac{di''_{t1q}}{dt} -$$

$$- L''_{1s1} i''_{t1d} \frac{d\theta_1}{dt} ; \qquad (7)$$

$$U_{30} = U_{70} - r''_1 i''_{t10} - L''_{1s0} \frac{di''_{t10}}{dt} .$$

For the no-load branch we get :

$$0 = U_{7d} - r_{10} i'_{t1d} - L_{1ad1} \frac{di'_{t1d}}{dt} +$$

$$+ L_{1ad1} i'_{t1q} \frac{d\theta_1}{dt} ;$$

$$0 = U_{7q} - r_{10} i'_{t1q} - L_{1ad1} \frac{di'_{t1q}}{dt} - \qquad (8)$$

$$- L_{1ad1} i'_{t1d} \frac{d\theta_1}{dt} ;$$

$$0 = U_{70} - r_{10} i'_{t10} - L_{1ad0} \frac{di'_{t10}}{dt} .$$

Equations of Kirchhoff's first law [*cf*(7)] are :

$$i_{t1d} - i'_{t1d} - i''_{t1d} = 0 ;$$

$$i_{tq} - i'_{tq} - i''_{tq} = 0 ; \qquad (9)$$

$$i_{t10} - i'_{t10} - i''_{t10} = 0 ;$$

The equations for the compensating coil $2L_{1k}$:

$$0 = U_{3d} - 2r_{1k} i_{L1d} - 2L_{1k1} \frac{di_{L1d}}{dt}$$

$$+ 2L_{1k1} i_{L1q} \frac{d\theta_1}{dt} ; \qquad (10)$$

$$0 = U_{2q} - 2r_{1k}\, i_{L1q} - 2L_{1k1}\, \frac{di_{L1q}}{dt} -$$

$$- 2L_{1k1}\, i_{L1d}\, \frac{d\theta_1}{dt}\ ; \tag{10}$$

$$0 = U_{30} - 2r_{1k}\, i_{L10} - 2L_{1k0}\, \frac{di_{L10}}{dt}\ .$$

We consider above the branches of the primary and the secondary windings of transformer $T1$, its no-load branch and the branch of the compensating coil as rL-circuits. If the mutual inductance between the phases of these branches may be neglected, the expressions of the parameters after simplying [10] for example, for the compensating coil $2L_{1k}$ we get :

$$L_{1k} = L_{1k1} = L_{1k0}. \tag{11}$$

The equations for the capacitance $C_{1l}/2$ may be obtained from the identities (3, 5) . . . . (3, 7), given in [10] if we substitute in them

$$C_3 = C1l/2,\ i_{C3d} = i_{C1d},\ i_{C3q} = i_{C1q}, i_{C30} = i_{C10}$$

and $\theta_3 = \theta_1$ since at 3 (Fig. 1) the synchronous generator is not connected, and the voltage u_3 is directly referred to axes rigidly connected with the rotor of $SG1$, viz :

$$U_{3d} = \frac{2}{C_{1l}} \int i_{C1d}\, dt + \int U_{3q}\, \frac{d\theta_1}{dt}\, dt\ ;$$

$$U_{3q} = \frac{2}{C_{1l}} \int i_{C1q}\, dt - \int U_{3d}\, \frac{d\theta_1}{dt}\, dt\ ; \tag{12}$$

$$U_{30} = \frac{2}{C_{1l}} \int i_{C10}\, dt.$$

The equations of Kirchhoff's first law [*cf* (3)] are as

$$i''_{t1d} - i_{L1d} - i_{C1d} - i_{ld} = 0\ ;$$

$$i''_{t1q} - i_{L1q} - i_{C1q} - i_{lq} = 0\ ; \tag{13}$$

$$i''_{l10} - i_{l10} - i_{C10} - i_{lo} = 0. \tag{13}$$

We may get the equations for the line (r_l, L_l) with the compensating capacitance C_{com} connected to it, for example, from the identities (7) and (12), viz:

$$\begin{aligned} U_{4d} = U_{3d} - r_l i_{ld} - L_{ld} \frac{di_{ld}}{dt} + \\ + L_{l1} i_{lq} \frac{d\theta_1}{dt} - \frac{1}{C_k}\int i_{ld}\, dt + \\ + \int (U_{4q} - U_{3q} + r_l i_{lq} + L_{l1} \frac{di_{lq}}{dt} + \\ + L_{l1} i_{ld} \frac{d\theta_1}{dt}) \frac{d\theta_1}{dt}\, dt; \end{aligned} \tag{14}$$

$$\begin{aligned} U_{4q} = U_{3q} - r_l i_{lq} - L_{l1} \frac{di_{lq}}{dt} - \\ - L_{l1} i_{ld} \frac{d\theta_1}{dt} - \frac{1}{C_k} i_{lq}\, dt - \\ - \int (U_{4d} - U_{3d} + r_l i_{ld} + L_{l1} \frac{di_{ld}}{dt} - \\ - L_{l1} i_{lq} \frac{d\theta_1}{dt}) \frac{d\theta_1}{dt}\, dt; \end{aligned} \tag{15}$$

$$U_{40} = U_{30} - r_l i_{l0} - L_{l0} \frac{di_{l0}}{dt} - \frac{1}{C_k}\int i_{l0}\, dt. \tag{16}$$

The equations for the capacitance $C_{2l}/2$ of the line will be analogous to (12), viz :

$$U_{4d} = \frac{2}{C_{2l}}\int i_{C2d}\, dt + \int U_{4q} \frac{d\theta_1}{dt}\, dt; \tag{17}$$

$$U_{4q} = \frac{2}{C_{2l}} \int i_{C2q}\, dt - \int U_{4d} \frac{d\theta_1}{dt}\, dt$$

$$U_{40} = \frac{2}{C_{2l}} \int i_{C20}\, dt. \tag{17}$$

The equations for the compensating coil $2L_{2\,com}$ will be analogous to (10) viz :

$$0 = U_{4d} - 2r_{2k}\, i_{L2d} - 2L_{2k1} \frac{di_{L2d}}{dt} +$$

$$+ 2L_{2k1}\, i_{L2q} \frac{d\theta_1}{dt};$$

$$0 = U_{4q} - 2r_{2k}\, i_{L2q} - 2L_{2k1} \frac{di_{L2q}}{dt} - \tag{18}$$

$$- 2L_{2k1}\, i_{L2d} \frac{d\theta_1}{dt};$$

$$0 = U_{40} - 2r_{2k}\, i_{L20} - 2L_{2k0} \frac{di_{L20}}{dt}.$$

The equations of Kirchhoff's first law [*cf* (4)] are

$$i_{1d} - i_{C2d} - i_{L2d} - i_{t2d} = 0;$$

$$i_{1lq} - i_{C2q} - i_{L2q} - i_{lq} = 0; \tag{19}$$

$$i_{l0} - i_{C20} - i_{l20} - i_{t20} = 0.$$

Since the way of considering the no-load current in the equivalent circuit is shown for transformer $T1$, we will write down the equations for transformer $T2$ without considering this factor. These equations may be obtained from the identities (1, 17) . . . . (1, 19) adduced in [10], if we consider that the voltage [*cf* (4)] is referred directly to coordinate axes rigidly connected with the rotor of $SG1$; we have therefore to assume $\theta_3 = \theta_1$. Also having brought the symbols in Fig. 1, 1 of [10] and Fig. 1 of the present paper into agreement, we get

$$U_{3d} = U_{4d};\ U_{3q} = U_{4q};\ U_{30} = U_{40}; \tag{20}$$

$$r_{t2} = r_{t2}\,;\; L_{t2p} = L_{t21}\,;\; L_{t20} = L_{t20}\,;$$
$$i_{t2d} = i_{t2d}\,;\; i_{t2q} = i_{t2q}\,;\; i_{t20} = i_{t20}\,. \tag{20}$$

We then get the branch of transformer $T2$

$$U_{2d}\cos(\theta_1 - \theta_2) + U_{2q}\sin(\theta_1 - \theta_2) =$$
$$= U_{4d} - r_{t2}\,i_{t2d} - L_{t21}\,\frac{di_{t2d}}{dt} + L_{t21}\,i_{t2q}\,\frac{d\theta_1}{dt}\,;$$
$$-U_{2d}\sin(\theta_1 - \theta_2) + U_{2q}\cos(\theta_1 - \theta_2) = \tag{21}$$
$$= U_{4q} - r_{t2}\,i_{t2q} - L_{t21}\,\frac{di_{t2q}}{dt} - L_{t21}\,i_{t2d}\,\frac{d\theta_1}{dt}\,;$$
$$U_{20} = U_{40} - r_{t2}\,i_{t20} - L_{t20}\,\frac{di_{t20}}{dt}\,.$$

Since the equations of the individual circuit elements may be assumed to be known, the whole system of equations can be put together from the individual equations referring to its blocks, which we can immediately write down for each of the circuit elements.

Should it be necessary to consider in any of the synchronous generators or compensating coils the dependence of the inductance on the state of saturation of the steel, this circuit element should be separated and its differential equations be re-written in the proper form, based on the character of the magnetisation curve.

It should be noted that the equations for all the zero-sequence components form a separate system, to be solved independently of the other equations. Their number is 18 in the case of the circuit of Fig. 1.

Determination of the total order of system of non-linear differential equations from structure of circuit

On the above considerations it is possible to determine from the structure of the scheme, without writing down the actual differential equations, the total order to the latter. In doing this we have to bear in mind the following circumstances:

1. For a synchronous machine (generator, synchronous condenser or motor) with in-phase or quadrature damper windings the total order of the equations is

7*, if the circuit contains apart from this at least one more synchronous machine, i.e. a machine of magnetic or electric asymmetry (equations of system (1), except the third).

The order of the equation of motion of the rotor of each of the synchronous machines is 2.

If the circuit contains only one synchronous machine, the total order of the equations for it will be six, because in this case the differential equation of the motion of the rotor will be of the first order and the angle θ will not occur in one of them (by change of the variables $d^2\theta/dt^2 = d\omega/dt$ and $d\theta/dt = \omega$ the order is reduced by one).

2. Neglecting each of the damper windings of the synchronous machine reduces the total order of its defferential equations by one.

3. The total order of the differential equations of an induction machine is 5. This means that each induction machine connected to the system increases the total order of the system of differential equations by 5.

4. The equations of Kirchhoff's first law for the branching points are not differential equations and therefore, do not increase the total order of the equations of the system.

5. The stator circuits of the machines (stationary circuits) must be divided into the simplest independent circuits and their differential equations have to be set up for the in-phase as well as for the quadrature components. This doubles the order of the differential equations for each individual circuit.

6. If a line, system or static load are represented by a coil with resistance and inductance, its series-connexion with the stator of any of the machines does not increase the total order of the differential equations of the system.

7. If the circuit comprises a transformer whose no-load current is not considered, it is represented by a coil. If, however, the no-load current is considered, the equivalent circuit contains a no-load branch (additional circuit), which, together with the necessity of considering the equations of the in-phase and quadrature components, increases the total order of the differential equations of the circuit by 2.

8. If there are no synchronous machines in the circuit (e.g. if one or several induction motors for static loads, etc., are supplied from busbars of infinite power), it is not necessary to set up the equations separately for in-phase and quadrature components. If the complex instantaneous values of currents and voltages are introduced, a static load or transmission line (each of them separately) will be represented by first-order differential equations, and an induction

* This does not take into account the differential equations for the zero-sequence components.

1958

motor by a third-order differential equation. In this case, the connexion of any further induction machine to the circuit increases the total order of the system of differential equations by 3.

Let us determine the total order of the system of differential equations for the circuit of Fig. 3.

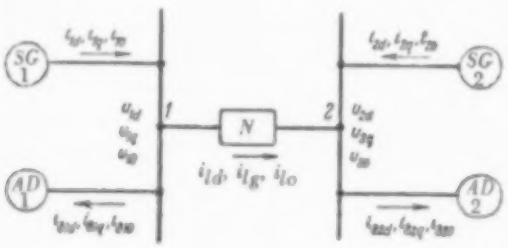

FIG. 3.

In Fig. 3. the stationary part of the circuit is resolved into three circuits, viz:

(a) The stator $SG1$ – stator $IM1$;

(b) Stator $IM1$ – line – stator $IM2$;

(c) Stator $SG2$ – stator $IM2$; for each of which, if the in-phase and quadrature components have to be considered, the differential equation is of the second order, this resulting in the total order of six. Each of the synchronous machines makes a total order of the order of the remaining equations 5, and each of the induction machines involves a total order 3. The total order of the differential equations for the whole circuit will therefore be 22.

In Fig. 1, if the no-load currents of the transformers $T1$ and $T2$ have to be considered, the stationary part of the circuit is resolved into 9 simpler circuits, for example, as follows.

(a) Stator $SG1$ – stator $IM1$ (if it is necessary to consider in-phase and quadrature components, the order of the equations will be 2);

(b) Stator $IM1$ - no - load branch of the equivalent circuit of transformer $T1$ (Fig. 2) (order of the equations-2);

(c) No-load branch of equivalent circuit of transformer $T1$-compensating coil $2L_{1\ com}$ (order of the equations-2);

(d) Compensating coil $2L_{1\ com}$-capacitance of the line $C_{1l}/2$;

(e) Capacitance of the line $C_{1l}/2$ - line - capacitance of the line $C_{2l}/2$ (order of the equations-4).

(f) Capacitance of the line $C_{2l}/2$-compensating coil $2L_{2\ com}$ (order of the equations-4);

(g) Compensating coil $2L_{2\ com}$ -no-load branch of equivalent circuit of transformer $T2$ (order of equations-2);

(h) No-load branch of equivalent circuit of transformer $T2$-static load $SL2$ (order of equations-2);

(i) Stator $SG2$-static load $SL2$ (order of equations-2); this adding up to a total order 24. From this figure the fraction concerning transformers $T1$ and $T2$, lines and loads $SL2$, i.e. the static circuit elements amounts to a total order 18. For the two synchronous generators the total order of the determining equations is 10; for the induction motor, 3.

We see, therefore, that the total order of the differential equations for the whole system will be 37.

If the line is not represented by one member but by several T – or π-type members, the fraction of the line elements (series, connected inductances and shunt-capacitances) in the total order of the system of the differential equations of the circuit will increase still further. This fact is very important in the choice of the method for solving the resulting system of differential equations.

1958

If the in-phase and quadrature damper windings of both synchronous generators are not considered, the total order of the equations will be reduced by 4, i.e. to 33. If, furthermore, we neglect the no-load branches in the equivalent circuits of the 2 transformers, the total order of the equations is again reduced by 4, i.e. to 29. If the two compensating coils $2L_{1\ com}$ and $2L_{2\ com}$ are also neglected, the total order of the equation is again reduced by 4, i.e. to 25.

It is worth noting that in the last case again both synchronous and one induction machine together result in a decrease of the total order of differential equations by 13; the remainder, 12, refers as before to the transmission line.

REFERENCES

1. V.A. Venikov; *The adoption of the theory of similarity and physical modelling in electric technology* Gosenergoizdat (1949).
2. V.A. Venikov and A.V. Ivanov-Smolenskii; A synchronous generator for the dynamic modelling of electrical systems. *Elektrichestvo*, No. 8 (1951).
3. V.A. Venikov *et al.*; *A brief description of dynamic models for electrical systems*, Moscow Power Institute (1955).
4. M.P. Kostenko and E.D. Treivish; Modelling of electrical machinery and transformers in experimental research on the stability of parallel work in power stations. *Transactions of the Leningrad Power Institute* No. 1 (1946).
5. M.P. Kostenko; Electrodynamic model for the study of stability. *Elektrichestvo* No.9 (1951).
6. M.P. Kostenko; The modelling of electrical machinery equipment in the study of stability of parallel work on power systems, linked with long-distance transmission lines *Izv. Akad. Nauk SSSR, Otd. tekh. nauk* No. 12 (1953).

7. V.L. Lossievskii; *The use of the similarity theory and dynamic analogies in problems connected with the modelling of objectives and regulation processes*, Gosenergoizdat (1951).

8. V.A. Trapeznikov; Mathematical modelling of dynamic systems *Elektrichestvo* No. 8 (1955).

9. S.V. Strakhov ; Selection of the co-ordinating systems for calculation of transition processes in chains with synchronous machine *Elektrichestvo* No.6 (1954).

10. S.V. Strakhov; The equating of transition processes in static and rotating elements in electrical chains. *Report on scientific research work. Moscow Power Institute* (1956).

11. R.E. Vowels; Transient Analysis of Synchronous Machines. *Proc. Inst. El. Eng.*, vol. 99 part IV, No. 3 (1952).

12. A.A. Yanko-Trinitskii; The equating of transition electromagnetic processes of an asynchronous motor and their solution. *Elektrichestvo* No. 3 (1951).

958

THE INDUCTION LAW FOR AN ELECTROSTATIC MACHINE*

A.A. BAL'CHITIS

(Received 19 December 1956)

Introduction

The fundamental equations of the classical theory of electrodynamics, the first and second equations of Maxwell point to two possible methods of conversion of mechanical into electrical energy. For example, by the first equation of Maxwell†

$$\operatorname{curl} \bar{H} = \gamma \bar{E} + \frac{\partial \bar{D}}{\partial t} \tag{1}$$

such a conversion is possible when an electric field changes with time, i.e. by mechanical action on the electric field it is possible to obtain the magnetic field connected with it in space.

According to the second equation

$$\operatorname{curl} \bar{E} = -\frac{\partial \bar{B}}{\partial t} \tag{2}$$

it is possible to obtain an electric field by changing the magnetic field associated with it.

The second equation of Maxwell was the generalized form of Faraday's experimental law of electromagnetic induction, viz.

$$E = B\, l\, v, \tag{3}$$

which was discovered in 1831 and forms the basis of the design of a large variety of electric machines, covered by the general term "electromagnetic machines".

Machines working on the principle of a mechanical change of an electric field (Maxwell's first equation) are not nearly so widely used; they are known as *electrostatic* machines. These machines are used for obtaining high and very high voltages for research purposes.

For a long time electrostatic machines did not find practical uses. The suc-

* *Elektrichestvo* No.7, 11 – 14, 1957 [Reprint Order No.EL33].

† All equations are given in terms of the absolute practical rationalized system of units.

cesses in the development of the electromagnetic machines relegated the electrostatic machines to the background. The development of electrostatic machines was also hampered by the absence of a satisfactory theory, since attempts at providing such a theory were based on the electrostatic theory. The electrostatic machine is a converter of one form of energy into another and to apply to it the laws of electrostatics is useless since the electrostatic field is characterized by the fact that energy conversion is impossible in it.

The electrostatic machine has a number of valuable characteristics. Electromagnetic d.c. machines for voltages over 15 kV are very difficult to produce. However, electrostatic machines of much simpler design for voltages of 5 to 5000 kV and more can be built. Their ratings can reach several hundred MW at a very high efficiency.

Soviet scientists have made important contributions to the research on electrostatic machines. A.F. Ioffe and V.M. Gokhberg developed a lucid theory of the electrostatic generator and designed a number of interesting electrostatic machines which found practical application [1].

A.E. Kaplyanskii presented in 1938 a general analytical theory of electromagnetic and electrostatic machines based on suggestions by Olendorf.

In his paper [2] on a general theory of electric machines A.E. Kaplyanskii started from the equations of Lagrange and proved that the conversion of mechanical into electrical energy and vice versa is only possible by variable inductances or capacitances.

The purpose of the present article is to obtain a fundamental law, the law of induction for the electrostatic machine, on the basis of an analysis of the operation of an existing type of such a machine.

Maxwell's first equation must obviously be a generalization of this law.

Operating principle and the working cycle of electrostatic machines

Nearly all modern electrostatic machines work on the principle suggested by Topler [3]. Let us consider the operation of the simplest electrostatic machine with independent excitation (Fig.1).

The electrostatic machine works on the principle of varying (by rotation of the rotor) capacitances, its main elements are therefore the electrodes 1 and 2 of the stator and the rotor, forming the variable capacitance of the machine. It is possible to design the rotor and the stator electrodes i.e., the active surfaces of the machine, in the form of cylinders, discs or rods [4].

The commutators 3 and 4 are on the rotor shaft with the adjacent brushes 5 and 6.

The voltage $-U_1$ is applied to the rotor for the excitation of the machine.

A.F. Ioffe recommended a working cycle for the electrostatic machine in the co-ordinates C, U or Q, U. Such a cycle is similar to the cycle of the ideal four-stroke steam engine.

The co-ordinate system C, U (Fig.2) provides a clear representation of the potential variations of the conductor system representing the electrostatic machine during the variation of its capacitance.

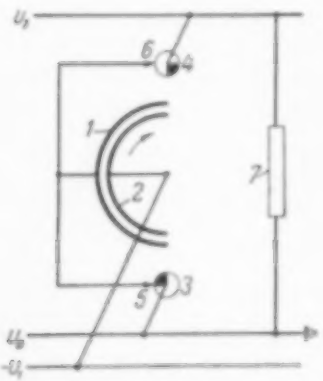

FIG.1. Basic circuit diagram of an electrostatic machine with independent excitation.
1 and 2 stator and rotor electrodes respectively, 3 and 4 commutators, 5 and 6 brushes, 7 load.

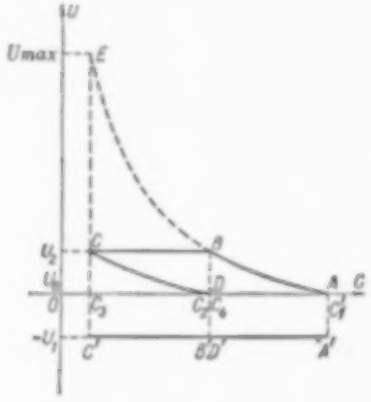

FIG.2. Working cycle of the electrostatic machine in the C, U co-ordinate system.

The co-ordinates Q, U (Fig.3) enable the variations of the magnitude of the charges in the system to be represented in relation to the capacitance of the system.

In the position of the rotor of the machine shown in Fig.1 the capacitance of the system stator-rotor has its maximum, viz. C_1. The potential of the rotor is $-U_1$ and the potential of the stator U_0. As a result of the electrostatic induction the charge q_1 appears on the stator surface, equal in magnitude to the charge on the rotor surface but opposite in sign. To this position of the machine correspond the points A and A' respectively, of the representations in the C, U and Q, U co-ordinates (Fig.2 and 3). Point A determines the value for the stator surface and point A' the corresponding value for the rotor surface.

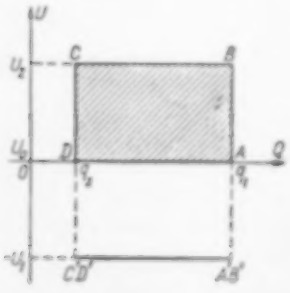

FIG.3. Working cycle of the electrostatic machine in the Q, U co-ordinate system.

Rotation of the rotor in a clockwise direction alters the capacitance of the system. Since

the brushes 5 and 6 are insulated the potential of the stator will rise. During this process the charges on the stator and the rotor remain unchanged, viz. equal to C_1U to which the part AB of the cycle in the co-ordinates Q, U corresponds. The voltage and capacitance vary, therefore, according to a rectangular hyperbola.

During a ¼ revolution of the rotor the capacitance of the system decreases to

$$C_2 = \frac{C_1}{2},$$

and the potential of the system rises to the value

$$U_2 = \frac{q_1}{C_2} = \frac{2q_1}{C_1} = 2U_1,$$

corresponding to point B of the operating cycle of the machine.

When the rotor continues its revolution, the stator electrode, whose potential is now U_2, is connected through the brush 6 and the commutator 4 to the h.v. terminal. When the capacitance decreases to its minimum value C_3, the charge decreases to

$$q_1 - q_2 = (C_2 - C_3)U_2$$

(point C).

The stator is then disconnected from the terminal. The capacitance of the system with unchanged charge q_2 increases to the value C_4, and simultaneously the potential drops to the value U_0 (point D).

During the last part of the operating cycle of the machine, (section DA) while the capacitance increases from C_4 to C_1, a charge equal to $q_1 - q_2$ is absorbed from the low voltage source.

During a full working cycle a charge equal to $q_1 - q_2$ passes therefore from the source at potential U_0 to the h.v. electrode at potential U_2.

The mechanical energy required for the transfer of charges from the equipotential surface U_0 to the surface U_2 is given by

$$W = (q_1 - q_2)\,(U_2 - U_0).$$

The electrostatic machine is reversible and the whole cycle can be carried out in the reverse direction. In this case the h.v. source gives off its charge and the low voltage terminal receives it. The difference of the energy values of the h.v. and the l.v. sources is converted into mechanical energy.

We have considered the operating cycle of an ideal electrostatic machine. In an actual machine it is necessary to consider the losses determined by friction, ohmic and dielectric losses in the conductors and insulators respectively, etc.

The magnitude of the maximum voltage U_{max} developed by the generator

(point E, Fig.2) is determined by the minimum possible capacitance C_3, while the system is disconnected from the high voltage terminal from the condition:

$$C_1U_1 = C_3U_{max} = \text{const.}$$

The current at maximum voltage is zero because then $C_2 = C_3$, whence

$$q_1 - q = (C_2 - C_3)U_2 = 0.$$

Thus, U_{max} is the no-load voltage of the machine.

According to the general theory of electric machines, the equations determining the electrical condition of the machine are the voltage equations for machines based on the principle of electromagnetic induction, and the current equations for electrostatic machines. If the internal losses of the electrostatic generator are neglected, a current is induced in it. Its voltage depends on the load.

Thus, if after one cycle of the electrostatic machine the charge delivered at the high voltage terminal is, a charge equal to nq will have been delivered after q revolutions per 1 second. The load current is calculated from the equation

$$i = nq = (C_2 - C_3)\, n \cdot U_2. \tag{4}$$

When U_2 and the speed remain constant, the tenerator will supply a mean current of constant magnitude.

Equation (4) can be simplified by putting $C_3 = 0$ which is the case in an ideal machine:

$$i = C_2 \cdot n \cdot U_2. \tag{5}$$

The induction law for the electrostatic machine

Equations (4) and (5) yield the mean value of the current induced by the electrostatic machine. To obtain the instantaneous value of the current, it is necessary to separate section BC from the working cycle (Fig.2) since the current flows into the external circuit load only at this instant. During this part of the working cycle of the machine the instantaneous value of the current is determined by the equation

$$i = U_2 \frac{dC}{dt},$$

or in the general case,

$$i = U \frac{dC}{dt}, \tag{6}$$

which has also to be used as a basis for deriving the induction law for the electrostatic machine.

The working capacitance of the machine is determined by its geometric dimensions and by the value of the dielectric constant, $\varepsilon\varepsilon_0$, of the insulation which fills the gap, δ, of the machine:

$$C = \frac{\varepsilon\varepsilon_0 s}{\delta} = \varepsilon\varepsilon_0 \frac{a \cdot \Delta b}{\delta},$$

where $s = a.\Delta b$ is the overlap area of stator and rotor electrodes,
a the linear extension of the electrode at right angles to the direction of rotation,
Δb the increment of the linear extension of the electrodes in the direction of rotation.

Substituting the value of C in (6) we obtain:

$$i = U \frac{dC}{dt} = \frac{\varepsilon\varepsilon_0 U}{\delta} a \frac{d(\Delta b)}{dt}$$

or

$$i = \frac{\varepsilon\varepsilon_0 U}{\delta} a \frac{db}{dt}. \tag{7}$$

Equation (7) can be considerably simplified and put into a form analogous to the electromagnetic induction law, viz.

$$i = D \cdot a \cdot v, \tag{8}$$

where $D = \varepsilon\varepsilon_0 E = \frac{\varepsilon\varepsilon_0 U}{\delta}$ is the electric displacement (induction) in the working gap of the machine;
$v = \frac{db}{dt}$ the linear velocity of the rotor electrode.

Equation (8) represents the induction law for the electrostatic machine.

The similarity of the law of the electromagnetic induction (3) and the induction law for the electrostatic machine (8), is not incidental since, similarly to Maxwell's first and second equation, they express the same physical electromagnetic process of the field in which the forces of electric and magnetic nature appear.

When the overlap of the stator by the rotor electrodes varies by the amount

$$ds = a\, db$$

the corresponding change of the flux of the electric displacement vector N is

$$dN = D\, ds = D\, a\, db.$$

In unit time the flux of the electric displacement vector varies by

$$\frac{dN}{dt} = D.a\frac{db}{dt} = D.a.v. \tag{9}$$

Comparison of equations (8) and (9) yields a new expression of the induction law for the electrostatic machine

$$i = \frac{dN}{dt}, \tag{10}$$

i.e. the current induced in the machine equals the rate of change of the flux of the electric displacement vector in the working gap of the machine.

Equation (10) is easily related to Maxwell's first equation (1). Therefore Maxwell's first equation is the most general expression of the induction law (current induction) for the electrostatic machine.

In the general case, when the electrode-conductor has an arbitrary shape and moves in a non-uniform electric field we can write the expression for an infinitely small current di induced on the part $d\bar{a}$ of the electrode surface. Let $d\bar{a}$ be a vector at right angles to the conductor axis in the direction defined as positive and of magnitude equal to the width of the surface considered. If the velocity vector makes an angle α with vector $\bar{a}$ (Fig. 4), the area traced out by the conductor section da during the time dt is $ds = v\,dt\,da\sin\alpha$.

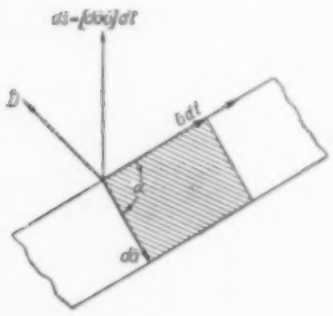

FIG. 4.

Representing this area by the vector $d\bar{s}$ in a direction perpendicular to it, we can write

$$d\bar{s} = [d\bar{a}\ \bar{v}\ dt] = [d\bar{a}\ \bar{v}]\,dt,$$

where $[d\bar{a}\ \bar{v}]$ is the vector product of $d\bar{a}$ and $\bar{v}$.

The flux of electric displacement

$$dN = \bar{D}\,.\,d\bar{s} = \bar{D}[d\bar{a}\,.\,\bar{v}]\,dt,$$

incident on this area induces in the segment $d\bar{a}$ during the movement of the conductor in time dt the current

$$di = \frac{dN}{dt} = \bar{D}\,[d\bar{a}\ \bar{v}]. \qquad (11)$$

Assuming as positive direction of the vector of the electric induction that pointing towards the surface of the conductor, the direction of the induced current in the conductor coincides with the direction of the change of the electric field with respect to the conductor.

The current in the external circuit of the machine is set up as a result of the "displacement" of the stator charge during the decrease of the capacitance of the stator-rotor system; for this reason it makes no sense to ascribe a certain direction to the current in the stator electrode of such a machine.

Conclusions

The electrostatic machine considered, with a working cycle similar to that of a steam engine clearly illustrates the present state of the development of the theory of these machines. Only a small part of the working cycle is used for generating electric current, the rest being taken up by preparatory operations.

Further developments of the theory of electrostatic machines should lead to the

production of new and improved designs of such machines, to be used not only in physical research laboratories but also for industrial purposes, particularly in the field of long-distance d.c. power transmission.

Definition of symbols

$\overline{B}$ vector of the magnetic flux density;
$\overline{D}$ vector of the electric displacement;
$\overline{E}$ vector of the electric field strength;
$\overline{H}$ vector of the magnetic field strength;
W energy;
$\overline{v}$ velocity vector;
γ conductivity.

REFERENCES

1. A.A. Vorob'ev; *Extra high electric voltages. Gosenergoizdat* (1955).
2. A.E. Kaplyanskii; *Introduction to the general theory of electric machines. Gosenergoizdat* (1941).
3. Karel Malek; *Electrostatic generators and their use as h.v. sources for particle accelerators. Elektrotechnický* obzor, 3 (1956).
4. Zdenek Zán; *Design types of modern electrostatic machines. Elektrotechnický* obzor, 7 (1956).

GENERALIZED METHOD OF INVESTIGATING THE TRANSIENT PROCESSES IN ELECTRIC DRIVE SYSTEMS*

D.P. MOROZOV and YU.A. BORTSOV

(Received 28 November 1956)

The investigation of the transient processes in various and complicated systems of electric drives enables the optimum operating conditions of the driven mechanisms as regards the economy and output to be selected. To reduce the differential equations of these processes for circuits with rigid and flexible closed loops is a difficult task which often confronts the designer. It is particularly so where the general differential equation of the transient process of an electric drive has to be written down for different initial conditions. For example, starting, reversal and braking of a motor at a steady speed take place with what is known as "natural" initial conditions. In this case only the initial values of the variable and of one or two of its higher derivatives cannot be zero. However, when the value of a disturbing effect or of any circuit parameter varies at a time at which the system was still in a transient state, all the initial conditions will differ from zero. Examples are to be found in braking before the speed is steady, or the action of "cut-offs", etc.

We will make a few preliminary remarks, viz,

1) The coupling coefficient between control windings placed on a common core in an electric machine is according to experimental findings considerable, viz. of the order 0.85-0.9. The resultant flux then varies with a time constant approximately equal to the sum of the time constants of all the control windings.

2) In an amplidyne the time constant of the first stage may be comparable to the time constant of its short-circuited circuit. It is, therefore, necessary to consider the parameters of both stages of the amplifier in writing down the differential equation.

3) In setting up the basic equations it is not necessary to use the coefficients of mutual inductance between the windings. The derivation becomes simpler and more lucid if the setting up of these equations is based on the resultant magnetic flux [1 and 2].

* *Elektrichestvo* No. 7, 19-24, 1957 [Reprint Order No. EL 34].

4) In setting up the general differential equation of the system for various operating conditions it is recommended to use a method according to which

a) all the variables are written in the form of an algebraic sum of the initial value of the given quantity obtaining at the end of the preceding state of operation, and the increment of this variable quantity during the new stage of the transient process. For example, speed and current of the motor are written as follows: $n = n_0 + n'$; $i_a = I_{a0} + i'_a$, where n_0 and I_{a0} are speed and armature current of the motor, respectively, e.g., at a "cut-off", and n' and i'_a the increments after this instant;

b) the equations of the preceding operating conditions are calculated from equations put together in a similar way. As a result, the system of differential equations for the deviations is obtained; this can then be solved with respect to the required variables (current, e.m.f., speed of the motor, etc.).

The setting-up of the differential equations is based on operating conditions characterised by "natural" initial conditions, i.e. the conditions of "standstill". In the general case they may also be non-zero, for example, for conditions of braking and reversal from steady conditions. This case is the simplest one. The circuit shown in Fig. 1 is used for a number of mechanisms in the metallurgical and mechanical industries. The desired voltage U is supplied by a potentiometer; all the control windings link with the total resultant flux Φ_c.

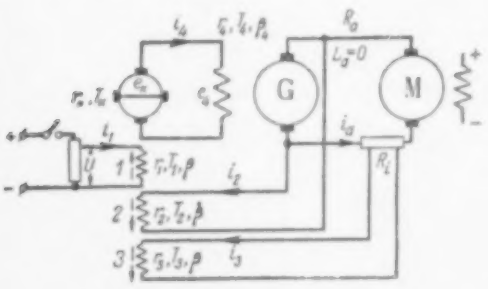

FIG. 1. Circuit generator-motor with negative rigid feedbacks of generator voltage and motor current.

Parameters of the reprint winding: r_1 resistance; b_1 susceptance; w_1 number of turns; L_1 inductance; T_1 time constant; β proportionality factor between ampere-turns of control, winding and e.m.f. of the short-circuited circuit e_{sh}; $k_1 = w_1\beta$ proportionality factor between control current and e.m.f. of the short-circuited circuit e_{sh}; $m_1 = w_1\beta / r_1$ voltage amplification factor (gain).

The parameters of the second and all the other windings are denoted similarly. Other symbols used: R_a total resistance of the armature circuit generator-motor; $\theta = GD^2 R_a / 375\, c_e c_m$ electromechanical time constant.

Let us set up the equations for zero initial conditions, characterising no-load starting of the motor ($M_c = 0$). In doing so,

a) we neglect the leakage of all the magnetizing windings;
b) we linearise the magnetization curves of all the machines;

c) we neglect the electromagnetic time constant of the main circuit;

d) we do not consider the active resistance of the generator in setting up the fundamental equations of the feedback circuits.

The equations are as follows:

$$U = i_1 r_1 + w_1 \frac{d\Phi_c}{dt}; \tag{1}$$

$$e_z = i_2 r_2 - w_2 \frac{d\Phi_c}{dt}; \tag{2}$$

. . . . . .

$$i_a = \frac{GD^2}{375\, c_m} \cdot \frac{dn}{dt}. \tag{3}$$

From this system of equations we derive the general differential equation involving the current and the motor speed. Considering that $d\Phi_c/dt = 1/k_c \cdot de_{sh}/dt$, (1) may be written for the first winding in the following form

$$U = i_1 r_1 + \frac{w_1}{k_c} \frac{de_{sh}}{dt}. \tag{4}$$

Divining all the terms of (4) by r_1 and multiplying into $\omega_1 \beta$, and furthermore considering that $\omega_1^2 \beta / k_c r_1 = L_1/r_1 = T_1$, we get

$$m_1 U = i_1 w_1 \beta + T_1 \frac{de_{sh}}{dt}. \tag{5}$$

For the circuit of winding 2 we get an analogous equation, viz.

$$m_2 e_z = i_2 w_2 \beta - T_2 \frac{de_{sh}}{dt}. \tag{6}$$

Let us note that the negative sign before the second term in (6) and (2) indicates that the e.m.f. induced in the winding 2 by the resultant flux Φ_c sets up a current opposing the flux increase. Consequently, the e.m.f. in winding 2 coincides with the direction of e_g (for rigid negative feedback). The same is the case in the negative current feedback loop.

To complete the setting-up of the general equation it is convenient to cast it in operator form [3], viz.

for the first control winding

$$m_1 \bar{U} = \bar{i}_1 w_1 \beta + T_1 p \bar{e}_{sh}; \tag{7}$$

for the second control winding

$$m_2\bar{e}_g = \bar{i}_2 w_2 \beta - T_2 p\bar{e}_{sh}; \tag{8}$$

for the third control winding

$$m_3\bar{i}_a R_i = \bar{i}_3 w_3 \beta - T_3 p\bar{e}_{sh}. \tag{9}$$

From (7) we subtract (8) and (9) term by term and, considering that $(\bar{i}_1 w_1 - \bar{i}_2 w_2 - \bar{i}_3 w_3 - \beta = \bar{\varepsilon}_{sh}$, we get

$$\bar{e}_g = \frac{m_1\bar{U} - m_2\bar{e}_g - m_3\bar{i}_a R_i}{1 + (T_1 + T_2 + T_3)\,p}. \tag{10}$$

Furthermore, using (1) - (3), we find successively e_ω, e_g and, lastly, i_a:

$$\bar{i}_a = \frac{m_1 m_g m_4 \theta b_a p\bar{U}}{(1+T_c p)(1+T_{sh}p)(1+T_4 p)(1+\theta p) + m_2 m_{sh} m_4 (1+\theta p) + R_i b_a \theta m_3 m_{sh} m_4 p}. \tag{11}$$

The speed of the motor is found from (3), viz.,

$$\bar{n} = \frac{\bar{I}_a}{\theta b_a c_e p} = \frac{m_1 m_g m_4 \bar{U}/c_e}{(1+T_c p)(1+T_{sh}p)(1+T_4 p)(1+\theta p) + m_2 m_{sh} m_4 (1+\theta p) + R_i b_a \theta m_3 m_{sh} m_4 p}. \tag{12}$$

We will show that (11) and (12) may also be used for considering the transient process on braking the motor from some steady speed n_0. We will not only set up the equations for the same drive system, but also consider the initial conditions; as such we assume constant values of the fluxes (or currents) and e.m.f.'s which existed in the motor circuit when the motor operated at a steady speed.

We get

$$0 = (I_{10} + i_1')\,r_1 + w_1 \frac{d\,(\Phi_{c0} + \Phi_c')}{dt}; \tag{13}$$

$$E_{g0} + e_g' = (I_{20} + i_2')\,r_2 - w_2 \frac{d\,(\Phi_{c0} + \Phi_c')}{dt}; \tag{14}$$

. . . . . .

$$I_{a0} + i_a' = \frac{GD^2}{375 c_m} \frac{d\,(n_0 + n')}{dt}. \tag{15}$$

The equations of the "statics", characterizing the preceding process of braking conditions of the motor ($E_{g0} = I_{20} r_2$, etc.) are subtracted from the corresponding equations of the system (13) - (15). Considering that all the differentials of the constant values $d\Phi_{c0}/dt$, dI_{sh0}/dt,.....dn_0/dt vanish, we get the following system of equations for the deviations of the variables:

$$0 = (I_{10} + i_1')\, r_1 + w_1 \frac{d\Phi_c'}{dt}; \tag{16}$$

$$e_2 = i_2 r_2 - w_2 \frac{d\Phi_c'}{dt}; \tag{17}$$

$$i_a' = \frac{GD^2}{375 c_m}. \tag{18}$$

Let us denote $I_{10} r_1 = U_0$; equation (16) is then written as follows:

$$-U_0 = i_1' r_1 + w_1 \frac{d\Phi_c'}{dt}.$$

As a result we get the solution of the system of equations (16) - (18) with respect to i_a':

$$i_a' = \frac{-m_1 m_c m_4 \theta b_a p \bar{U}_0}{(1 + T_c p)(1 + T_{sh} p)(1 + T_4 p)(1 + \theta p) + m_2 m_{sh} m_4 (1 + \theta p) + R_1 b_a \theta m_3 m_{sh} m_4 p} \tag{19}$$

In substituting the numerical values of the parameters into (19) we have to consider:

a) that in the denominator the time constant of the variation of the direct-axis flux $T_c = T_1 + T_3 + T_5$ assumes a new value, since the constant T_1 increases with decreasing resistance r_1;

b) in the numerator the variation of r_1 during braking acts differently on U_0 and m_1. When r_1 increases, the leap in the effect of U_0 also becomes greater. Simultaneously, the second factor, viz. the voltage amplification factor m_1, decreases in the same ratio. Thus, the value of the numerator as a whole remains unchanged. Only its sign changes, indicating that the armature current in the main machines has now the opposite direction to that during starting.

This method may also be used in investigating processes such as the reversing of a motor from any steady speed to a given speed in the opposite direction and any other analogous cases characterised by "natural" initial conditions.

It is more difficult to investigate processes with non-zero initial conditions throughout. Let us examine one of these cases.

One of the frequently occurring operating conditions of motors driving certain mechanisms (operating train of a reversing rolling mill, traversing mechanism of the table of a planing machine, etc.) is the braking from an unsteady speed, taking place at an instant at which the running-up of the motor is not yet completed and the cutting-out of the reference input voltage or the change of its polarity has occurred.

To set up the general differential equation of the current and the speed of a motor operating in a generator-motor system with closed loops (Fig. 1) we use the

system of equations (13) - (15). Each variable was written as a sum of the initial values and its deviations. However, allowance has now to be made for the fact that in all the circuits containing inductances the voltages (e.m.f.'s) applied are balanced not only by the active voltage drops, but also by the self-induced e.m.f.'s.

The solution of the simultaneous equations (13) - (15) with respect to i_a' leads to the following expression:

$$\bar{i}'_a = \frac{\theta b_a p\,[m_4\,(\bar{E}_{x0} - \bar{I}_{x0} r_4)\,(1 + T_x p)\,(1 + T_y p) + \;\rightarrow}{(1 + T_y p)\,(1 + T_x p) \times}$$

$$\rightarrow \frac{+ m_x m_4\,(\bar{E}_{x0} - \bar{I}_{x0}\, r_x)\,(1 + T_y p) - m_x m_4 \bar{E}_{x0} - m_2 m_x m_4 \bar{E}_{z0} - m_3 m_x m_4\,\bar{I}_{a0} R_i] - \;\rightarrow}{\times (1 + T_4 p)\,(1 + \theta p) + m_2 m_x m_4\,(1 + \theta p) + \;\rightarrow}$$

$$\rightarrow \frac{- \bar{I}_{a0}\,[(1 + T_y p)\,(1 + T_x p)(1 + T_4 p) + m_2 m_x m_4]}{+ R_i b_a \theta m_3 m_x m_4 p}. \qquad (20)$$

Hence, by use of (15), transformed to the form $\bar{I}_{a0} + \bar{i}'_a = \theta b_a c_e p \bar{n}'$, we get the following expression for $\bar{n}'$

$$\bar{n}' = \frac{\bar{I}_{a0} + \bar{I}'_a}{\theta b_a c_e p} = \frac{\bar{I}'_a}{\theta b_a c_e p} + \frac{\bar{I}_{a0}}{\theta b_a c_e p}. \qquad (21)$$

It should be noted that (20) and (21), set up for the special case of braking from an unsteady speed, may be used as general differential equations of a typical control circuit with amplidynes and with current and voltage feedbacks. * It is possible to get from them without derivation the equations describing any desired transient process such as starting, braking, reversal, etc. in circuits

a) with negative or positive current and voltage feedbacks or only one of these);

b) with "cut-off" of voltage, and current feedback;
c) with separate current and voltage "cut-offs";
d) with current "cut-off" and voltage feedback;
e) with an amplidyne working as generator in a generator-motor system;
f) with an ordinary d.c. machine working as an exciter of a generator.

From the general differential equation it is easy to obtain the equations for operating conditions with zero initial conditions, which were set up above for

* For this purpose it is only necessary to add the term $m_1 m_{sh} m_4 \theta b_a p U$ in the numerator of (20); this expresses the presence of the reference quantity U at the input of the control system.

starting and braking from steady-speed operation; *Cf.* (11), (12) and (19). The setting-up of the equation of the transient processes in circuits with "cut-offs" must be carried out by stages according to whether the circuit elements are connected up or not. The initial conditions have to be determined separately for each stage.

Starting a motor in a generator-motor system with negative current feedback and voltage "cut-off"

Let us set up the differential equation and represent the transient processes $n(t)$ and $i_a(t)$ for the circuit of the drive shown in Fig. 2. In this case the whole starting period has to be divided into two stages.

First stage, i.e. up to the establishment of the voltage feedback, when the opposing voltage ΔU of the potentiometer is greater than the rising generator voltage e ; we have zero initial conditions, viz., $E_{g0} = E_{s0} = E_{sh0} = 0$, $I_{a0} = I_{s0} = I_{sho} = 0$; there is no voltage feedback ($m_3 = 0$); the time constant of the first amplifier circuit $T_c = T_1 + T_3$; the reference (input) voltage is U.

Under these conditions we obtain from (20) and (21)

$$\bar{i}_a = \frac{m_1 m_g m_4 \theta b_a p \bar{U}}{(1+T_y p)(1+T_g p)(1+T_4 p)(1+\theta p) + R_i b_a \theta m_3 m_g m_4 p} \tag{22}$$

$$\bar{n} = \frac{\bar{i}_a}{\theta b_a c_e p} = \frac{m_\partial \bar{i}_a}{\theta b_a p} =$$

$$= \frac{m_\partial m_1 m_g m_4 \bar{U}}{(1+T_y p)(1+T_g p)(1+T_4 p)(1+\theta p) + R_i b_a \theta m_3 m_g m_4 p} . \tag{23}$$

The second stage, i.e. after the "cut-off" has begun to act, when e_g is greater than ΔU, and their difference $(e_g - \Delta U)$ begins to supply the demagnetizing ampere-turns of the voltage feedback (winding 2). The initial conditions (E_{g0}, E_{s0}, ..., I_{sh0}) will be non-zero. When the effect of the "cut-off" begins, $E_{g0} - \Delta U = 0$, and the term $\bar{E}_{g0} m_3 m_{sh} m_4$ in (20) is zero; the time constant $T_c = T_1 + T_3 + T_3$; the input voltage U remains as before.

Under these conditions we get from (20) and (21)

$$\bar{i}'_a = \frac{\theta b_a p [m_4 (\bar{E}_{s0} - \bar{I}_{g0} r_4)(1+T_{sh} p)(1+T_c p) +}{(1+T_c p)(1+T_{sh} p) \times} \rightarrow$$

$$\rightarrow \frac{+ m_g m_4 (\bar{E}_{g0} - \bar{I}_{sh0} r_{sh})(1+T_y p) + m_1 m_{sh} m_4 \bar{U} -}{\times (1+T_4 p)(1+\theta p) +} \rightarrow$$

$$\rightarrow \frac{-m_{\text{г}} m_4 \overline{E}_{\text{sh0}} - m_3 m_{\text{sh}} m_4 I_{a0} R_i] -}{+ m_2 m_{\text{sh}} m_4 (1 + \theta p) +} \rightarrow$$

$$\rightarrow \frac{-\overline{I}_{a0} [(1 + T_y p)(1 + T_{\text{г}} p)(1 + T_4 p) + m_2 m_{\text{г}} m_4]}{+ R_i b_a \theta m_3 m_{\text{sh}} m_4}; \tag{24}$$

$$\overline{n}' = \frac{\overline{I}_{a0} + \overline{i}'_a}{c_e \theta b_a p} = \frac{m_{\text{m}} \overline{i}'_a}{\theta b_a p} + \frac{\overline{I}_{a0}}{\theta b_a c_e p}. \tag{25}$$

Determination of the initial conditions. To determine the initial conditions it is necessary to know the values of the variables involved at $t = t_0$, i.e. the time of the "cut-off". This requires the functions $e_g(t)$, $e_4(t)$ and $e_{sh}(t)$ to be calculated. We use the system of equations (1) - (3), thus,

$$\overline{e}'_z = \frac{\overline{i}'_a (1 + \theta p)}{\theta b_a p} = \frac{m_1 m_{\text{sh}} m_4 \overline{U} (1 + \theta p)}{\theta_1 (p)}; \tag{26}$$

$$\overline{e}'_4 = \frac{\overline{i}'_4}{b_4} (1 + T_4 p) =$$

$$= \frac{\overline{e}'_z}{m_4} (1 + T_4 p) = \frac{m_1 m_{\text{sh}} \overline{U} (1 + T_4 p)(1 + \theta p)}{\theta_1 (p)}; \tag{27}$$

$$\overline{e}'_{\text{г}} = \frac{\overline{i}'_{\text{г}}}{b_{\text{г}}} (1 + T_{\text{г}} p) = \frac{m_1 \overline{U} (1 + T_{\text{sh}} p)(1 + T_4 p)(1 + \theta p)}{\theta_1 (p)}, \tag{28}$$

where $\theta_1 (p)$ is the characteristic equation of the system during the first stage of the start.

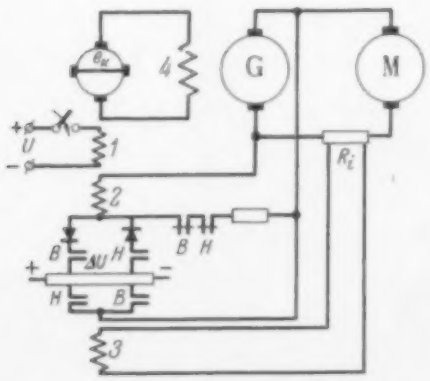

FIG. 2. Generator-motor system with negative current feedback and voltage "cut-off".

The variation of the individual variables in a closed automatic control system

follows the same characteristic equation. This fact also exists in the case considered, and simplifies the calculation of the roots on determining the initial conditions.

We find the initial conditions from (26) - (28) for $t = 0$, viz.,

$$E_{g0} = [e'_g]_{t=t_0}; \quad E_{40} = [e'_4]_{t=t_0}; \quad E_{sh0} = [e'_{sh}]_{t=t_0}; \tag{29}$$

$$I_{40} = \frac{E_{40}}{k_4} = \frac{E_{40}}{m_4 r_4}; \quad I_{sh0} = \frac{E_{40}}{k_{sh}} = \frac{E_{40}}{m_{sh} r_{sh}}. \tag{30}$$

Example. It is required to determine the transient speed and current processes on starting a roll-train driving motor in a generator-motor system with negative feedback and voltage "cut-off" (Fig. 2).

Data of the electric machines: two series-connected separately-excited motors of type MP-82, $P_n = 100$ kW, $U_n = 220$ V, $n_n = 475$ rev/min., $I_n = 500$ A; generator rating $P_n = 320$ kW, $U_n = 460$ V, $n_n = 485$ rev/min; $I_n = 700$ A; amplidyne rating $P_n = 4.5$ kW, $U_n = 230$ V, $n_n = 2935$ rev/min, $I_n = 19.6$ A, $I_{sh} = 5.9$ A, $r_{sh} = 0.85$ Ω.

The basic data of the static calculation are collected in the table.

We will assume that the static torque, only due to the friction losses, is zero, this being a characteristic feature of the drive of a rolling train and enabling equations (22) - (25) to be used without any change.

First stage. $T_c = T_1 + T_3 = 0.0214 + 0.0143 = 0.0357$ sec; $m_3 = 0$.

Substituting the values of the parameters into (23) we get:

$$\bar{n} = \frac{1\,010}{p(0{,}00092p^4 + 0{,}0417p^3 + 0{,}51p^2 + 3{,}37p + 1)} = \frac{A(p)}{pB(p)}.$$

The roots of the characteristic equation: $p_1 = -0.305$; $p_2 = -30.5$; $p_{3,4} = -7.25 \pm j8.04$.

Using a well-known expansion theorem, we find the original, viz.,

$$n(t) = \frac{A(0)}{B(0)} + \sum_{i=1}^{i=4} \frac{A(p_i)\, e^{p_i t}}{[B'(p)]_{p=p_i}} =$$

$$= 1\,010 - 1\,055e^{-0.305t} + 2.18e^{-30.5t} +$$

$$+ 45.1e^{-7.25t} \cos 8{,}04t + 12.85e^{-7.25t} \sin 8{,}04t.$$

1958

Considering that $i_a = GD^2/375c_m \times dn/dt$, we find the expression for the current during the first stage of starting, viz.,

$$i(t) = 885e^{-0,305t} - 260e^{-30,5t} - 530e^{-7,25t}\cos 8,04t - \\ - 1\,280e^{-7,25t}\sin 8,04t.$$

The expressions $n(t)$ and $i(t)$ are represented in Fig. 3.

Determination of the initial conditions. We will assume that the "cut-off" becomes effective at the motor speed $n = 0.8n_n = 380$ rev/min., this corresponding to the time $t = t_0 = 1.78$ sec, when the current $I_{a0} = 520$ A, and the generator e.m.f. $E_{g0} = I_{a0}R_a + c_e n_0 = 365$ V. To solve the equation for the start at the second stage, it is still necessary to know the initial values of E_{a0} and E_{sh0}. Their determination is carried out by finding the originals of expressions (27) and (28). For $t = t_0 = 1.78$ sec, $E_{a0} = 161$ V, $E_{sh0} = 3.6$ V.

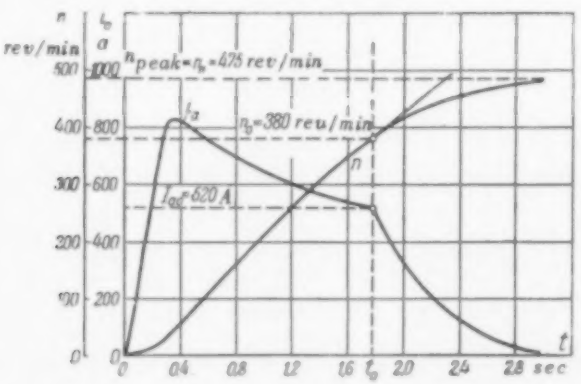

FIG. 3. Curves of the transient process on starting the motor in a generator-motor system with current feedback and voltage "cut-off".

From (30) we get

$$I_{a0} = E_{g0}/m_a r_a = 365/3.83 \times 6 = 16 \text{ A},$$
$$I_{sh0} = E_{a0}/m_{sh} r_{sh} = 3.95 \text{ A}.$$

Second stage. We use (24) and substitute the numerical values of the parameters into it. We consider also the value $T_e = T_1 + T_2 + T_3 = 0.0477$ sec.

The solution of this equation furnishes an expression for the current of the motor during the second stage of the start, viz.,

$$i_a(t) = I_{a0} + i'_a(t) = 489e^{-2.3t} + 30.8e^{-31.3t} - \\ - 10.7e^{-5.95t}\cos 7.54t + 6.2e^{-5.95t}\sin 7.54t.$$

$n(t)$ can also be obtained by graphical integration of the curve of $i_a(t)$ (Fig. 3).

It is possible to draw some conclusions as to the nature of the circuit and the correct values of the parameters from the plotted curves of current and speed of the motor. For example, the duration of the transient process is, without any doubt, excessively long. To obviate this shortcoming, the forcing must be considerably increased and the voltage amplification and other parameters of the control circuit altered accordingly. It is advisable to use separate current and voltage "cut-offs" instead of the basic circuit considered.

The method discussed was investigated experimentally on several variants of the control circuit. Comparison of the theoretical and experimental results revealed differences of the order of 10 - 20 per cent.

Conclusions

1. A method of setting up the differential equations of controlled electric drive circuits for operational conditions characterized by various initial conditions is presented.

2. The differential equation is derived for a number of types of electric drives with rigid feedbacks and "cut-offs" of voltages and current. The equation is suitable for the case of a constant load at the motor shaft.

3. It is proposed to extend the investigation to setting up the equations for circuits with flexible feedbacks.

TABLE 1.

Time constants (sec)	$T_1 = 0.0214$	$T_2 = 0.012$	$T_3 = 0.0143$	$T_{3\text{Д}} = 0.2$	$T_4 = 1.5$	$\theta = 0.086$
Amplification factors	$m_1 = 0.0455$	$m_2 = 0.0272$	$m_3 = 0.24$	$m_{3\text{Д}} = 48$	$m_4 = 3.83$	$m_q = 1.1$
Other parameters	$R_a = 0.0396\ \Omega$	$b_a = 25.2$	$R_i = 0.016\ \Omega$	$U = 110$ V	–	–

REFERENCES

1. A.G. Iosifyan, *et al; Theory of an amplidyne-selsyn synchronous follower system, Elektrichestvo,* No. 3, (1946).
2. D.P. Morozov; *Excitation of electric machines in automatic circuits with amplidynes, Elektrichestvo,* No. 9, (1948).
3. D.P. Morozov; *Method of setting up the differential equations of complicated circuits of electric drives of mechanisms, Trans. Molotov., Institute of Power Engineering.,* No. 22, *Gosenergoizdat,* (1956).

CORONA LOSSES ON LIVE TRANSMISSION LINES*

V.D. KRAVCHENKO, V.I. LEVITOV and V.I. POPKOV

(Received 7 February 1957)

The corona loss on an energized transmission line constitutes only a small fraction of the transmitted energy and is commensurable with or sometimes even smaller than the heat loss. Therefore, it is practically impossible to determine this loss by separating the current component which corresponds to the corona loss from the total line current as measured by conventional methods.

The corona loss is due to the cross currents, that is, the currents that flow between the conductors and between the conductors and earth. If it were possible to measure quantities which are proportional to these currents, or to their corresponding charges this would be the best solution of the problem of measuring the corona losses on energized lines.

Fig. 1 shows an arrangement consisting of a single phase-conductor, 1, and an aerial, 2, which is earthed through a measuring element Z connected to the middle of the aerial.

The e.m.f. induced electromagnetically in an aerial isolated from earth is so distributed that it is zero at the middle of the aerial [1]. Therefore, if this point is earthed through a measuring element Z, no current can flow in the element owing to the magnetic field of the line. The current which flows in the element is determined only by the electrostatic coupling between the line and the aerial.

The minimum height at which conductors are suspended on conventional lines is 7 – 8 m. At this height the space charge in the region G (Fig. 1) is distributed practically symmetrically with respect to the conductor axis, i.e. the space charge density depends only on the distance from the axis of the conductor of the element of charge considered. Consequently, the integrated electrostatic effect of the space charge on the aerial is the same as that of a linear charge of equal magnitude placed at the axis of the conductor.

For sufficiently small values of the impedance Z the relation between the charge on the aerial and the total charge of the conductor is given by:

$$\alpha_{12}q_1 + \alpha_{22}q_2 = 0 \qquad (1)$$

* *Elektrichestvo* No. 7, 31 – 34, 1957 [Reprint Order No. EL 35].

or

$$q_2 = -\frac{\alpha_{12}}{\alpha_{22}} q_1, \tag{2}$$

where $\alpha_{12} = \frac{1}{2\pi\varepsilon_0} \ln \frac{r'}{r}$ - mutual potential coefficient of the aerial and conductor; $\alpha_{22} = \frac{1}{2\pi\varepsilon_0} \ln \frac{2h}{a_0}$ - self potential coefficient of the aerial (a_0 is the radius of the aerial wire); $q_1 = q_c + q_s$ - total charge of conductor per unit length (q_c is the charge on conductor surface and q_s is the integrated space charge); q_2 - charge per unit length of aerial.

Thus, the charge on the aerial which is earthed at its middle point is proportional to the total charge enclosed in the region G, i.e. is determined by both the charge on the conductor surface and the space charge due to corona.

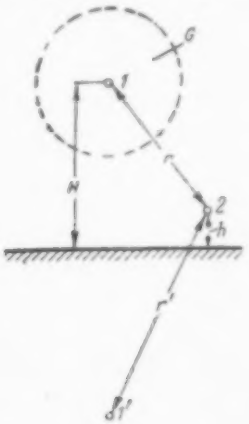

FIG. 1.

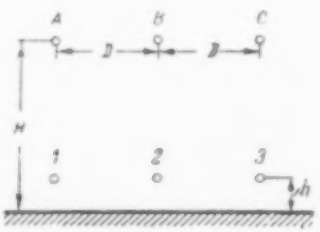

FIG. 2.

Also, the coefficient of proportionality α_{12}/α_{22} is a constant quality depending only on geometrical dimensions of the conductor-aerial arrangement. These circumstances make it possible to use aerials for corona loss measurements.

Three aerials are necessary for measurement on three-phase lines. Fig. 2 shows a possible arrangement of aerials placed directly under the three phase conductors. In this case the relation between the total charges on phase conductors q_A, q_B and q_C and the charges on earthed aerials q_1, q_2 and q_3 is given by the following system of equations:

$$\left.\begin{aligned} -(\alpha_1 q_1 + \alpha_2 q_2 + \alpha_3 q_3) &= \alpha_I q_A + \alpha_{II} q_B + \alpha_{III} q_C; \\ -(\alpha_2 q_1 + \alpha_1 q_2 + \alpha_2 q_3) &= \alpha_{II} q_A + \alpha_1 q_B + \alpha_{II} q_C; \\ -(\alpha_3 q_1 + \alpha_2 q_2 + \alpha_1 q_3) &= \alpha_{III} q_A + \alpha_{II} q_B + \alpha_1 q_C, \end{aligned}\right\} \tag{3}$$

where $a_1 = a_{11} = a_{22} = a_{33}$; $a_2 = a_{12} = a_{21} = a_{23} = a_{32}$; $a_3 = a_{13} = a_{31}$; $a_1 = a_{1A} = a_{2B} = a_{3C}$; $a_{11} = a_{1B} = a_{2C} = a_{3B} = a_{2A}$; $a_{111} = a_{1C} = a_{3A}$ are self and mutual potential coefficients determined from the geometrical dimensions.

By solving the system of equations (3) with respect to conductor charges q_A, q_B and q_C, we get

$$\left.\begin{aligned} q_A &= A_1' q_1 + A_2' q_2 + A_3' q_3; \\ q_B &= B_1' q_1 + B_2' q_2 + B_3' q_3; \\ q_C &= C_1' q_1 + C_2' q_2 + C_3' q_3. \end{aligned}\right\} \qquad (4)$$

The coefficients A'_i, B'_i and C'_i are composed of potential coefficients a_i which appear in (3). For example,

$$A_1' = \frac{A_1}{\Delta}; \quad A_2' = \frac{A_2}{\Delta}; \quad A_3' = \frac{A_3}{\Delta},$$

where $\Delta = a_1(a_1^2 - a_{III}^2) - 2a_{II}^2(a_1 - a_{III})$ - the determinant of the system of equations (3);

$$A_1 = -a_1(a_1^2 - a_{II}^2) + a_2(a_1 a_{II} - a_{II} a_{III}) - \\ - a_3(a_{II}^2 - a_1 a_{III});$$

$$A_2 = -a_2(a_1^2 - a_{II}^2) + a_1(a_1 a_{II} - a_{II} a_{III}) - \\ - a_2(a_{II}^2 - a_1 a_{III});$$

$$A_3 = -a_3(a_1^2 - a_{II}^2) + a_2(a_1 a_{II} - a_{II} a_{III}) - \\ - a_1(a_{II}^2 - a_1 a_{III}).$$

It follows from (4) that the sum of the products of charges on the three aerials, q_1, q_2 and q_3, into their corresponding coefficients A'_i, B'_i and C'_i give the total charges on the phase conductors, q_A, q_B and q_C.

Either capacitors or resistors can be used as the measuring elements. In the first case, the voltages across the elements are proportional to the total charges of phase conductors and in the second case, to their time derivatives, that is to the cross-currents of the line. However, it is preferable to choose capacitors since in this case the measurement will be practically unaffected by the possible h.f. pick-ups of the aerial.

The voltages on the measuring capacitors are given by:

$$U_i = \frac{q_i l}{C} \qquad (5)$$

where U_i - voltages on the aerials; q_i - charges per unit length of the aerials; l - lengths of aerials; C - measuring capacitances.

If follows from (5) that the input voltage to the measuring circuit depends not

1958

only on the coefficients a_i (which are determined by the geometry of the conductor-aerial arrangement) but also on the lengths of aerials and on the values of the me measuring capacitors. The choice of the ratio l/c is governed by the magnitude of the voltage required at the input to the measuring circuit, i.e. it depends on the sensitivity of the measuring device.

The length of the aerial should be such that the part of the conductor catenary which is above the aerial can be taken as being parallel to the ground.* For example, for 220 and 400 kV lines with spans of 450 m this condition is satisfied by an aerial 50 m long placed at mid-span. With this aerial suspended at a height of 0.5 m and with measuring capacitances of the order of 0.1 μF the voltage on the aerial is about 8 to 15 volts.

From the above, a block circuit diagram may be drawn for a device for measuring the corona loss on energized lines. Such a diagram is shown in Fig. 3; A, B and C are line conductors; 1, 2 and 3 aerials; C_u measuring capacitances; $1A$, $1B$ and $1C$ voltage transformers or voltage dividers;

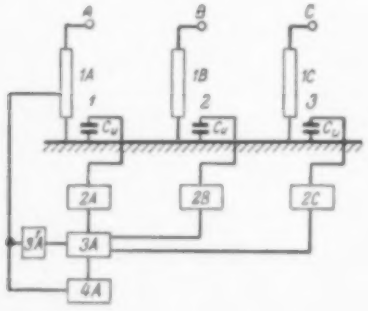

FIG. 3.

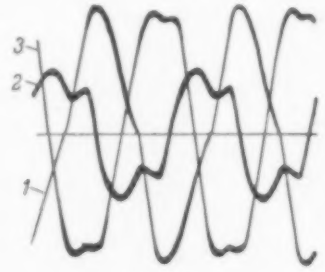

FIG. 4.

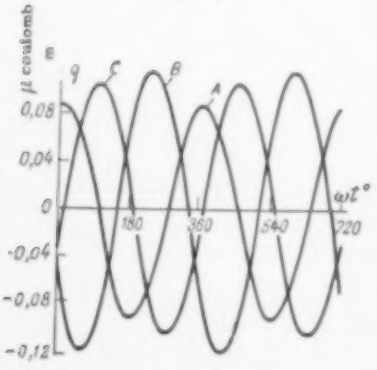

FIG. 5.

$2A$, $2B$ and $2C$ are elements multiplying the voltages corresponding to aerial charges q_1, q_2 and q_3 by their corresponding coefficients A'_i, B'_i and C'_i; $3A$ is an element carrying out the summation of the above products. As a result of this summation we get a voltage (or current) out put proportional to the total charge of phase conductor A; $4A$ is a wattmeter of some sort.

To increase the accuracy of corona loss measurements, particularly at small values of loss, it may be necessary to compensate for the reactive component of the charge q_A.

* In general this condition is not essential, since the effect of the catenary can be taken into account, when calculating potential coefficients. However, it simplifies calculation, if this condition is fulfilled.

Such a compensating voltage may be applied to the integrating element 3A by a suitable device indicated by 3'A.

For simplicity the measuring circuit is drawn for one phase only, the circuits for the remaining two phases are identical.

The assumption made above about the symmetrical distribution of the space charge due to corona with respect to the conductor axis was varified experimentally in the laboratory. A three-phase transmission line model having the following dimensions was set-up: viz. line length - 14.5 m; height of conductor suspension 2 m; interphase clearances - 1.3 m; diameter of polished steel conductors - 1 mm. As aerials copper conductors of 0.83 mm dia, having the same length as the model line were used. One aerial was placed under each phase conductor at a height of 0.27 m above the ground and was earthed through a capacitor. The voltages on the capacitors which are proportional to the charges on the respective aerials were applied in turn (using a special synchronizing device) to the deflecting plates of the CRO and photographed on the same plate. Each oscillogram contains therefore three voltage records. A sample oscillogram obtained with a phase-to-earth voltage of $U = 64\ \mathrm{kV}_{max}$ is shown in Fig. 4.

It is seen from this oscillogram that the curves of the charges on the aerials are irregular and differ from each other. The amplitudes of the charges on the external aerials are approximately the same, but the amplitude of the charge on the middle aerial is about one-half of that of each of the outer aerials. By multiplying the ordinates of the curves by their respective coefficients A'_i, B'_i and C'_i, and adding, we get curves corresponding to equations (4) which are shown on Fig. 5.

It follows from the above that the curves of Fig. 5 should be identical with the curves of the total charges of the experimental conductors in corona conditions. To compare these two sets of curves, an oscillographic record of the volt-coulomb characteristic was obtained for each of the three line conductors. The recording circuit for one phase only is shown in Fig. 6. In this figure the voltage across the capacitor C_q, which is proportional to the total conductor charge, was applied to one pair of deflecting plates of the CRO and the voltage across one arm (C_1) of the capacitance potential divider which is proportional to the voltage of the h.v. transformer T, was applied to the other pair of deflecting plates of the CRO.

With such a circuit the trace on the CRO screen has the form of a closed loop which is known as the volt-coulomb characteristic. The area enclosed by the loop is proportional to the energy loss due to corona for one cycle of the alternating voltage [2].

The volt-coulomb characteristics obtained for the conductors of the experimental line by direct measurement at a phase-to-earth voltage of $U_{ph} = \mathrm{kV}_{max}$ are shown in Fig. 7 (curves drawn in continuous lines). The curves drawn in broken lines represent volt-coulomb characteristics constructed from the data obtained from the aerial measurements (the curves of Fig. 5 and oscillograms of phase-to-earth voltages on the conductors recorded simultaneously with the records of the charges on the aerials), using the same voltage applied to the line.

1958

A good measure of agreement is shown between the volt-coulomb characteristics obtained by the two methods considering the amount of error introduced by the intermediate calculations and constructions in deriving the final curve from the experimental data. The two sets of characteristics agree well as regards the amplitude of the

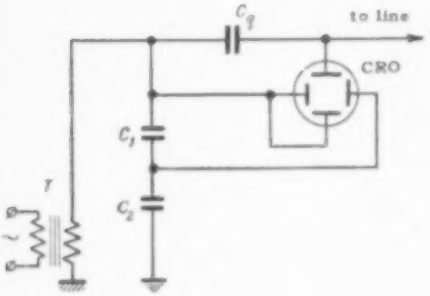

FIG. 6.

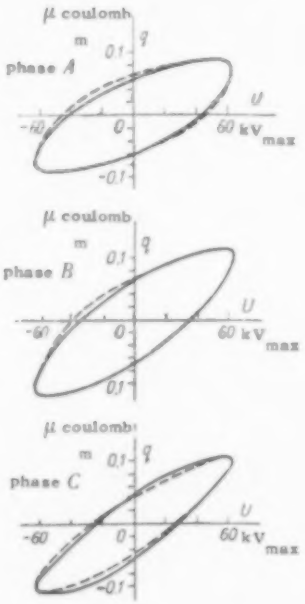

FIG. 7.

charge, the shape of the curve, and the area enclosed by the curve (the last factor being of importance from the point of view of corona loss measurement by means of aerials).

The construction of total charge and volt-coulomb curves was performed for different phase voltages up to a value exceeding three times the critical corona inception voltage. In this way values of corona loss were obtained for the experimental line for a wide range of voltages. These losses are indicated by crosses on Fig. 8 on which are also plotted corona losses derived from the volt-coulomb characteristics obtained by direct measurement. It is seen from this figure that the losses obtained by both methods are practically identical.

Thus, experimental investigations confirm the possibility of measurement of corona loss on live lines by means of aerials and also of verifying the correctness of the assumptions made.

In conclusion it should be mentioned that apart from its application to corona loss measurement the method presented can also be used for investigating other problems; for

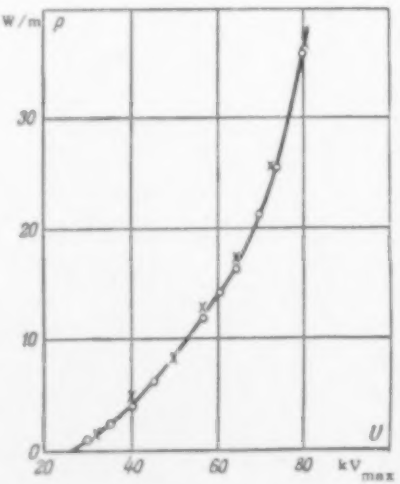

FIG. 8.

example, the distribution of losses along the conductor span, the measurement of charges, etc.

REFERENCES

1. M.I. Mikhailov; *The protection of communication lines. Svyaz'izdat* (1939).
2. H.I. Ryan and H.H. Henline; *The hysteresis character of corona formation. Trans. Amer. Inst. Elect. Engrs.* **43** (1924).

1958

ANALYSIS OF THE STATIC STABILITY OF COMPLEX POWER SYSTEMS BY ELECTRONIC COMPUTERS*

L.V. TSUKERNIK and N.A. KACHANOVA

(Received 7 January 1957)

In the lay-out of installations for the automatic control of the operating conditions of power systems, particularly having regard to their interconnection and the erection of long-distance transmission systems, stability investigations have to be carried out very thoroughly; this refers particularly to the methods of preventing "hunting" under certain operating conditions of the system and as an effect of a possible variation of the system parameters. For such an analysis electronic computers can be used with great advantage.

It is obvious that this has not to be understood in the sense of a preference of electronic digital computers to network analysers which are very suitable indeed for the solution of such problems.

Principles of programming stability calculations

The problem of analysing the steady-state stability of a complex, automatically regulated power system may be divided into the following main stages:

1) Calculation of the coefficients of the characteristic equation of the system;

2) Calculation of the stability criteria;

3) Determination of the limits of the stability range in the space of the given parameters.

The calculation of the coefficients of the characteristic equation is preparatory, but a very significant and a difficult part of the work. It is convenient to represent the equations of the disturbed movement of the power system in matrix form, after which it is easy to obtain an algorithm for programming. The elements of the initial matrices are determined directly from the data of the usual electrical calculation of the initial conditions of the power system and from the parameters of the machines and automatic regulators.

The writing-down of the equations of the disturbed movement of the power

* *Elektrichestvo* No.7, 39–45, 1957 [Reprint Order No.EL 36].

system, the transformation into matrix form and the method of finding an algorithm for programming were described in detail in special papers [1 and 2]. We only note here that the programme of the calculations on an electronic digital computer comprises the development of the characteristic determinant, whose order equals the number of stations in the equivalent circuit used and whose elements are operator polynominals with real coefficients.

The calculation of the stability criteria will preferably follow a programme corresponding to Routh's well-known algorithm [3] because having thus obtained a sequence (recurrence) of simple arithmatical operations remaining equal for characteristic equations of any order. In this respect stability criteria in the form of Hurwitz determinants [3] are less suitable for programming.

However, in analysing the stability of systems with automatic regulation it is desirable not only to test the stability under given conditions but above all, to clarify the effect of various factors (the parameters of the automatic regulators, parameters of the main equipment, etc), for which it is necessary to determine the limits of the stability range in the space of the parameters of interest for the analysis. It is most convenient to use for the solution of this problem two-dimensional representation as functions of two selected parameters. Series of such diagrams obtained by varying the other parameters, the influence of which we want to investigate, may be collected to form an "album of stability ranges".

1958

The determination of the limits of a stability range in the plane of the given parameters is programmed by using "logical" operations to be carried out on an electronic digital computer, with systematic use of the calculation of Routh's criterion as a "sub-programme". The scheme of the programme is as follows.

We feed into the machine as initial data the coefficients of the characteristic equation, represented as function of two parameters, for example the coefficients of the regulation of the excitation of the generators of the power system. In the automatic mechanical calculation process these parameters are given successive number of numerical values with a fairly small numerical difference (step). For each pair of values Routh's criterion is calculated continuously. Simultaneously the change of sign of Routh's criterion is automatically checked. As a result we obtain from the machine pairs of values of the parameters varied for the beginning and end of the interval in which the criterion changes sign. These values are the limiting coordinates between which the required boundary or limit of the stability range exists. The determination of the distribution of the stability and instability ranges with respect to this limit is also carried out on the basis of the calculations of Routh's criterion mentioned above.

This method of determining the limit of the stability range is much more convenient for programming than the well-known method of D-resolution [3]. For a non-linear relation between the coefficients of the characteristic equation and the parameters in the plane of which the *D*-resolution is carried out, the use of the method of *D*-resolution meets, in some cases, very great difficulties. The

calculation of the points of the limit of the stability range in the plane of two parameters (k' and k'') for one of the existing varients of the programme is made clear (Fig.1). We mark up first the extreme values of the parameters k' and k'', determining the sides of the rectangle $ABCD$ inside which we require to find the limit of the stability range. In general, we have a fair idea of the sign and order of the quantity or of realisable values k_a', k_b' and k_a'', k_b'' (Fig.1); if not, they are marked arbitrarily. Also we consider possible limitations of the values k', k'', related to the condition that all the coefficients of the characteristic equation should be positive. The magnitude of the computing interval along the axes k', k'' is then chosen.

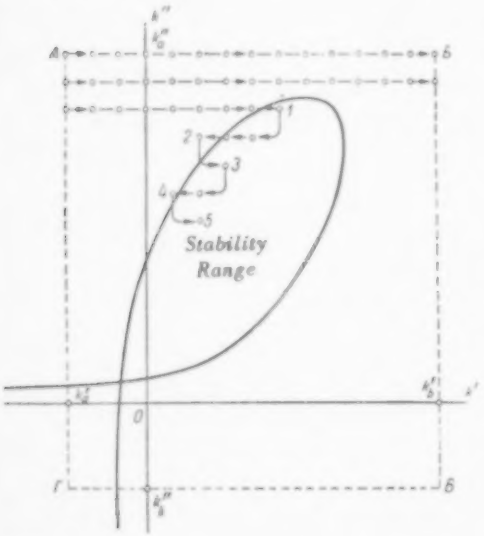

FIG.1. Scheme of the programme of tracing the boundary of the stability range (only the points indicated by the numbers in order are printed).

The calculation may be started at any point, e.g. at A. For this point the machine computes Routh's criterion storing (memorising) the result, without issuing (printing) it from the machine. Then a computing step is made in the direction of k', Routh's criterion computed again, and the result compared with the preceding one. If the sign of the criterion did not change a new computing step is made, etc., not if the sign of the criterion changed, i.e. if the limit of the stability range was over stepped, the machine prints the coordinates of the point considered (k', k''). This fixes point *1* (Fig.1).

Hereafter, the machine begins to follow the limit automatically. For this purpose, it makes twice a computing step in the direction perpendicular to the previous one, and calculations of Routh's criterion in the inverse direction of the original one, so long as the sign of the criterion changes. The coordinates of point 2 are then printed, this fixing the first interval $1-2$ through which the required limit passes. The calculation then proceeds similarly.

If the extreme values of k' are reached in the calculation without change of sign of Routh's criterion, the machine begins to calculate again in the same direction of k', moving through the computing interval along the side AD of the rectangle (Fig.1). If the limit of the range is not found within the rectangle $ABCD$, the computing interval may be reduced sufficiently to verify whether or not the stability range may not be found within a rectangle with sides equal to the original computing interval (for sake of clarity the computing interval was made very large in Fig.1).

The described scheme of a "tracking" programme was evolved by the Mathematical Institute of the USSR Academy of Science [4] for the purpose of providing a possibility of continuous outlining of the boundaries of a stability range of closed configuration.

By grouping the parameters in the plane of which the limit of the stability range is tracked, in pairs, and also by successful variation of other initial data we can obtain the "album of stability ranges" mentioned above.

Calculation of the steady-state stability of a power system

In 1954–1956 the Institute of Electrical Engineering and Mathematics of the Ukrainian Federal Republic Academy of Science carried out a number of calculalations of the stability and electro-mechanical transient process of the transmission system Kuibyshev GES – Moscow (on instructions of the technical administration of the Ministry of Power Stations) with an electronic computer. The present communication will give a brief outline of the content of the calculations of the steady-state stability*.

1958

Three types of automatic regulation of the excitation of the generators of the Kuibyshev GES were considered (*Cf.* Appendix):-

1) According to deviations of voltage and current and also according to the first and second derivatives of the current;

2) According to deviations of voltage and current, and also to slip and acceleration relative to an axis rotating at the synchronous speed of normal operation;

3) According to deviations of voltage and current, viz. compounding ($T_I = 0$), and delaying electromagnetic voltage corrector ($T_U = 3$ sec), connected to the main or booster exciter.

In considering the first type of regulation the time-lag of the generator ($T_{go} = 5.5$ sec), of the booster exciter ($T_{ex} = 0.12$ sec), the regulator ($T_{reg} = 0.1$ sec) and the presence of a rigid negative feedback of the exciter voltage was considered in the structural diagram. This type of automatic excitation control corresponds basically to a strong-action regulator with which the majority of the generators of the Kuibyshev GES is to be provided.

The second type of excitation control is analogous to the first and differs from the "strong action" regulator responding to angle and first and second

* All the calculations were carried out in relative units (U_{bas} = 400 kV, P_{bas} = 1150 MW, time in radians). The computer calculates with six and prints the results in five significant digits. Consequently the accuracy of the calculation depends on the accuracy of the data fed to the computer. All the calculations on the computer were duplicated, control variance being calculated after recording the programme. The programming of typical problems took about 10 – 20 hr and the calculation of one curve 15 – 45 mins.

derivatives of the angle, designed by the Central Electrical Research Laboratory of the Ministry of Power Stations by the fact that there is no necessity of telemetering the angle in this regulator. The slip and acceleration relative to an axis rotating at a synchronous speed of the initial operating conditions may be measured by a special instrument with a memory-element.

The automatic control of the third type was installed on the first generator of the Kuibyshev GES as main regulation, and on the following generators as stand-by. by. The possibility of a control according to individual generator currents was investigated. The Kuibyshev GES was in this investigation represented by two equivalent controlled generators (Fig.2, circuit 1). The characteristic of the system according to this circuit is of the tenth order. The parameters of the regulation according to current (k) or to voltage shown, or to the first and second derivatives (k', k''), in the plane of which the limit of the stability range was determined, are contained in most of the coefficients of the characteristic equation in a higher than the first degree, viz. as squares and products. In such cases a D-decomposition by the ordinary method involves very laborious calculations.

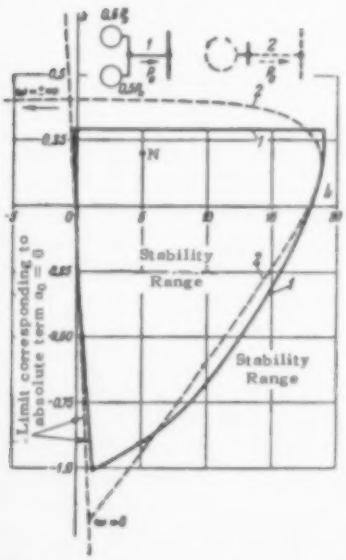

FIG.2. Stability ranges ($P_0 = 1.0$). For representations of the Kuibyshev GES by two equivalent generators (1) and one equivalent generator (group control) (2).

The calculations on the electronic computer showed that there is no stability range for the first type of automatic excitation control, which was also confirmed by analytic calculation and agrees with the results of tests on the electro-dynamic model of the Molotov Institute for Electrical Engineering [5]. It follows that for this type group regulation is required, for example, based on the mean current of generators working in parallel. The stability ranges for group regulation are shown in Fig.3 a and 4 a below.

For an automatic control of the third type a stability range exists, as is shown in Fig. 2 (curve 1). The same figure shows the stability range for group regulation (circuit 2, curve 2). Point N corresponds to the normal setting of the regulator. A comparison shows that group regulation increases the stability margin. The calculations did not consider the mechanical damping of the machine and, consequently, the actual stability margin will be slightly larger.

The margin of stability according to power transmitted was determined and the possibility of cumulative hunting in various loadings of the transmission

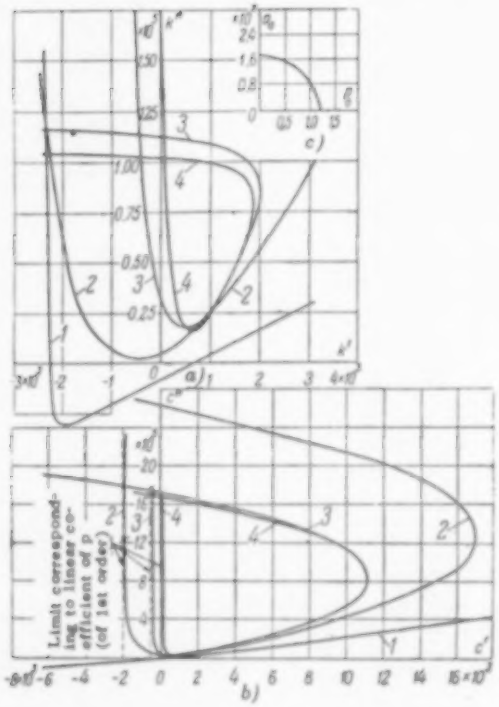

FIG.3. Stability ranges ($k = 0.2$, $b = 5.0$). a) Automatic excitation control of first type; b) Automatic excitation control of second type; c) Graph of the variation of a_0 vs. P. $1 - P_0 = 0$; $2 - P_0 = 0.5$; $3 - P_0 = 1.0$; $4 - P_0 = 1.1$

system was considered.*

For this purpose series of stability ranges were calculated for automatic excitation control of the first and second types (group regulation according to current) and a variation of a power transmitted from 0 to 1.1 for the case that there is no series compensation and the transmitting capacity of the line (ideal power limit), 1.15.

For comparison we entered in Fig.3 the results of the stability ranges in the plane of the coefficients of regulation according to slip and acceleration c', c''. The graph of Fig.3 shows that in both cases the power transmitted may be raised to the value of the transmitted capacity of the line, if the coefficients of the regulations are within the limits of the common stability ranges.

We may suppose that for equal regulation coefficients (in relative units) the design parameters of regulators of the first and second types may be approximately equal. The difference will consist only in the input elements, viz. in the case of a regulator of the second type an angle-measuring element in a memory-element. We may, therefore, conclude that an automatic regulation of the second type has, according to the operating characteristics determined by the graphs of Fig.3 advantages over a regulation of the first type because in the latter type the ranges of the permissible regulation coefficients are considerably increased. Also for load changes of the transmission systems the common part of the stability ranges for regulation by slip and acceleration becomes greater than for regulation according to derivatives of the current; for example, Fig.3 shows that in the first case for the transition from $P_0 = 1.0$ to P_0 1.1 the common part of the stability range 4

* The calculation relating to the measures to be taken to prevent self-excitation and cumulative hunting on no-load and at small loads of the transmission system are not included in the present, because they are not essential where two limiting power transmitted is concerned and mostly to be carried out by simpler methods.

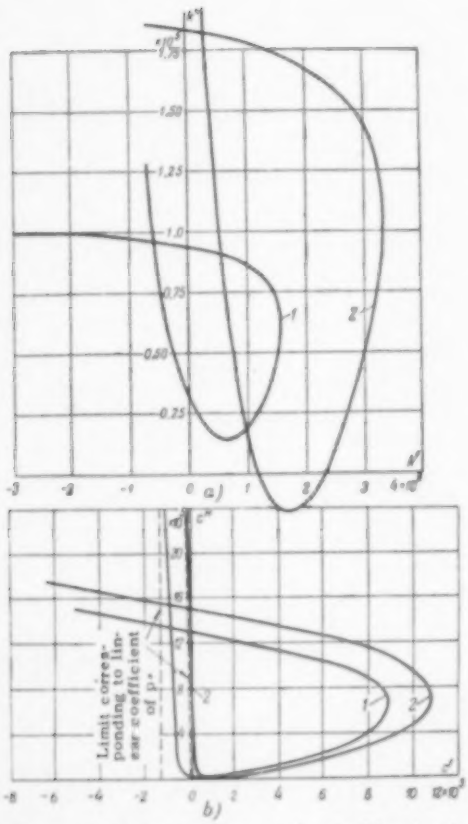

FIG.4. Stability ranges of: double-circuit transmission system ($P_0 = 1.0$; $k = 0.2$; $b = 25.0$). a) Automatic control of the first type; b) Automatic control of the second type. 1 – All the sections of both circuits of the line and series and parallel compensation gears are connected; 2 – One circuit of the head section of the line and parallel compensation gears are connected.

amounts to about 95 per cent of range 3, but in the second only to about 70 per cent.

From the position of the origin of the coordinates relative to the stability ranges (Fig.3) we may draw the conclusion that $P_0 > 0.4$ and in regulation without derivates of the operational parameters no stability can be achieved.

The possibility of cumulative hunting subsequent to alteration of the circuit of the transmission system was assessed. Fig.4 represents the stability ranges for a double-circuit line, calculated for $P_0 = 1.0$ and the same types of automatic excitation control as the stability ranges in Fig.3. The curves *1* refer to the case where all the sections of both circuits are connected as well as series and parallel compensation gears, and the curves 2 to the case where the circuit of the head section of the transmission and compensating gear are disconnected. In Fig.4 we see that with the regulation of the second type the coinciding part of the stability ranges is greater than for the regulation of the first type. Therefore, it is much easier to assure steady operation of the transmission system for possible changes in its circuits with regulation by slip and acceleration without readjustment of the regulation. This agrees very well with the results of tests on the dynamic model of the Molotov Institute of Electrical Engineering [5].

The curves of Fig.4 also show that the stability ranges of the compensated line (curves 1) are under otherwise equal conditions much smaller than the stability ranges of the uncompensated line. This indicates that in the presence of compensation the danger of cumulative hunting is greater. This fact must be considered in a project design and an actual operation.

However, we have to bear in mind not only a margin of stability with respect to cumulative hunting, but also as regards the "aperiodic limit". It is quite obvious that in the example considered the transmitting capacity and the aperiodic limit of the system stability are much higher for a compensated than for an uncompensated line. In the first case, the transmitted capacity of the line including the transformers at the far end, is $P_{max} = 1.87$, in the second $P_{max} = 1.03$. Consequently, when analysing the variation of the stability ranges for different configurations, we must extend our analysis to the character of the variation of the absolute term a_0 of the characteristic equation of the system (Fig.3 c) or else compare the values of the transmitting capacity of the line.

The analysis of the effect of the coefficient of the regulation according to the voltage and current deviations on the stability when "strong-action" is used, was carried out by direct comparison of a series of calculations, as shown, e.g. in Fig.5. We conclude that a variation of the coefficient k within wide limits has but a small influence on the stability ranges in the plane of k' and k'' (Fig.5 a) whereas a variation of the coefficient b has a more marked effect (Fig.5 b). If we bear in mind that a minor instability of the coefficients k and b is still possible after the adjustment of the regulator, there is no reason to assume that this instability may lead to hunting of the system. A simultaneous increase of the coefficients k and b (Fig.5 c) will slightly reduce the variation of the stability range due to an increase of the coefficient b only.

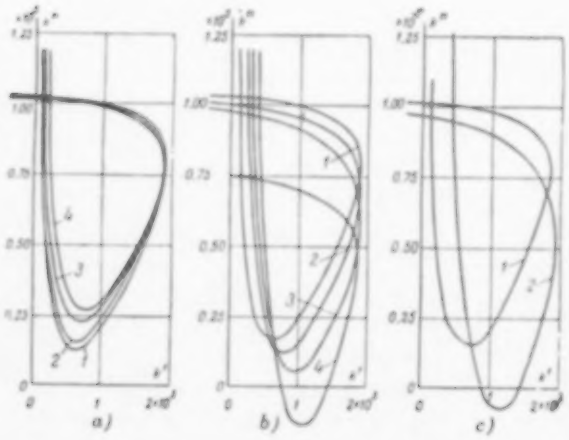

FIG.5. Stability ranges ($P_0 = 1.1$). a) When coefficient of regulation varies with the current ($b = 5$): $1 - k = 0.1$; $2 - k = 0.2$; $3 - k = 0.6$; $4 - k = 1.0$. b) When coefficient of regulation varies with the voltage ($k = 0.2$): $1 - b = 5$; $2 - b = 10$; $3 - b = 15$; c) When coefficients k and b vary simultaneously: $1 - k = 0.2$, $b = 5$; $2 - k = 1.0$, $b = 2.5$.

An increase of the coefficients k and b entails an increase of the absolute term of the characteristic equation and, consequently, an increase of the margin of stability with respect to the aperiodic limit.

The stability ranges in the plane of the coefficients of regulation according to deviations of voltage and current, were calculated, e.g. for $k' =$ var and $k'' =$ const. as shown in Fig.6. Two straight lines correspond to each of the ranges, viz. the line $a_0 = f(b, k) = 0$ and the line which with increasing k' turns anticlockwise from position *1* into position *5*; during this rotation the point of inter-

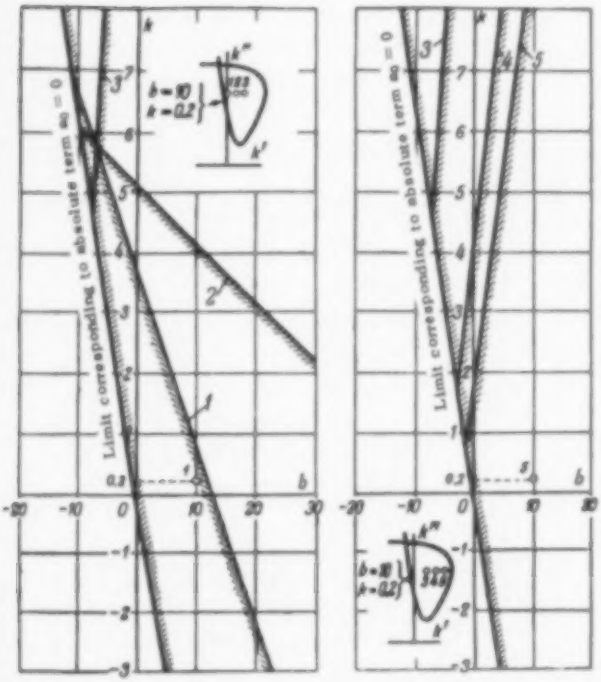

FIG.6. Stability ranges ($P_0 = 1.0$, $k'' = 0.75 \times 10^6$). $1 - k' = 0$; $2 - k' = 0.4 \times 10^6$; $3 - k' = 0.75 \times 10^6$; $4 - k' = 1.6 \times 10^6$; $5 - k' = 1.8 \times 10^6$.

section with the straight line $a_0 = 0$ moves downwards.

For a clear demonstration we entered in Fig.6 the stability range in the plane of k' and k'' on a reduced scale (for $b = 10$ and $k = 0.2$), in which we indicated the intersection studied. Considering for example, point *5* near the limit of the stability range plotted in the plane of the parameters k' and k'', we find that on the graph plotted in the plane of the parameters b and k the proximity of the limit of the stability range is not noticeable. This is as could be expected, for the reason that the stability ranges vary only slightly with a variation of the parameters b and k within fairly wide limits (Fig. 5).

We may, therefore, conclude that the fundamental analysis is better carried out by plotting the stability ranges in the plane of the parameters of regulation according to derivatives than in the plane of parameters of regulation according to deviations.

Stability calculations were carried out for transmission systems with intermediate synchronous condenser, on the assumption that the synchronous condenser of 375 MVA rating is erected in the sectionalizing substation of the transmission system Kuibyshev GES - Moscow and that the line has no series compensation. When the excitation of the synchronous condenser was controlled by a regulator of the first type, no stability range was found even in the presence of a considerable mechanical damping torque ($D = 2$). With a regulation of the third type, supplemented by regulation according to slip and acceleration, stability ranges were obtained (Fig.7) for three cases, viz. $D = 0$; 1; 2. The curves of Fig.7 show the favourable influence of the mechanical damping torque, which is often neglected in calculations, in the stability.

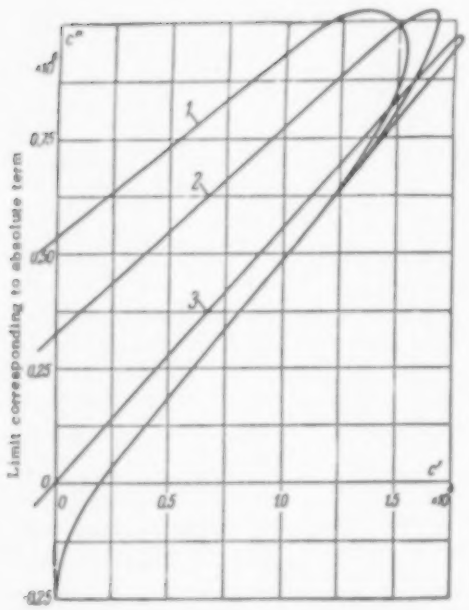

FIG.7. Stability ranges for a transmission system with intermediate synchronous condenser: ($P_0 = 1.0$, $k = 0.12$, $b = 25.0$). Damping torque of condenser: $1 - D = 2.0$; $2 - D = 1.0$; $3 - D = 0$. Stability range bounded by each of the curves 1,2 and 3.

Direct comparison of the results of calculations of typical variants enables us to examine the permissibility of some simplifications in the stability calculations.

With automatic excitation control of the generator groups of the Kuibyshev GES we may neglect the salient-pole character of the generators (Fig.8 a).

The replacement of the receiving system by infinitely powerful busbars does not alter the stability ranges substantially (within the range of positive values of the coefficients of regulation according to derivatives) by comparison with its replacement by an equivalent power state and load (Fig.8 b). In all the cases investigated the stability ranges were inside those obtained for a system with fixed angle coordinates. That means that the fixing of the angles corresponds to necessary, but not sufficient, conditions of stability [1 and 2]. These simplified calculations may sometimes by useful for preliminary assessment of the schemes (rectangle *ABCD*), and for the elimination of definitely unsatisfactory variants. In comparative calculations, we may neglect the time constant of the booster exciter. When the negative feedback of the exciter voltage is weakened in the calculations, we assumed a weakening by a factor (Fig.8). However, it should be borne in mind that for operating conditions near the limit of the stability range this simplification may introduce a considerable error whether by exaggerating or by unduly reducing the stability range (Fig.8 c).

Appendix

Generalised Structural Diagram of a Composite System Considering Automatic Excitation Control of the Synchronous Machines

The transmission functions: of the exciter $\overset{*}{F}_{ex}$, of its feedback $\overset{*}{F}_{fb}$, of the regulation according to angle deviation $\overset{*}{F}_{\delta}$, of the regulation according to deviation of voltage F_v and according to deviation of current F_I [3];

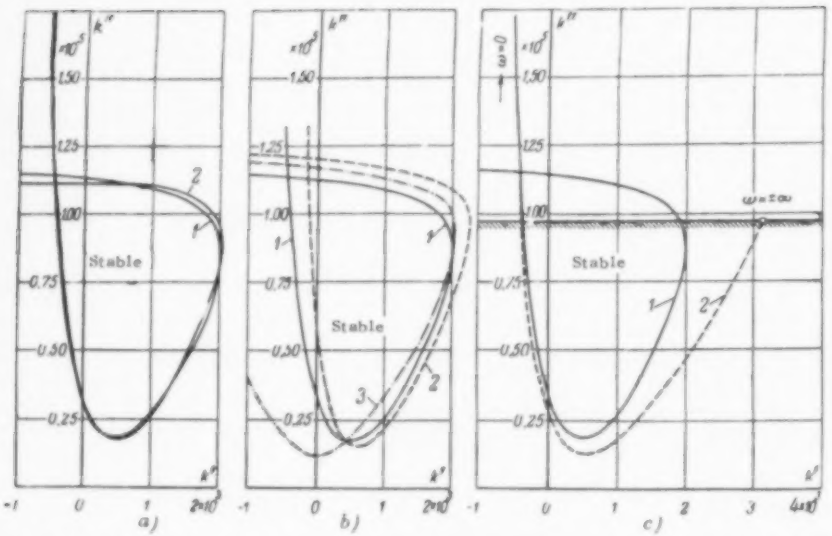

FIG.8, Stability range ($P_0 = 1.0$, automatic control of the first type: $k = 1.2$; $b = 5$). a) 1 – Considering the salient-pole generators of the Kuibyshev GES; 2 – Without considering the salient-pole character. b) 1 – At the end of the line busbars of infinite power; 2 – Receiving system represented by a load and an equivalent station for which $E' = \text{const}$ and $M = \infty$. 3 – The receiving system is represented by a load and an equivalent station for which $E' = \text{const}$ $M \neq \infty$. c) $1 - T_{ex} = 0.12$ sec; $2 - T_{ex} = 0$.

For automatic regulation of the excitation of the first type,

$$\overset{*}{F}_{ex} = \frac{1}{1 + T_{ex}\,p}; \quad \overset{*}{F}_{fb} = -d; \quad \overset{*}{F}_{\delta} = 0;$$

$$\overset{*}{F}_{v} = \frac{-b}{1 + T_{p}p}; \quad \overset{*}{F}_{I} = \frac{k + k'p + k''p^2}{1 + T_{p}\,p}.$$

For automatic regulation of the excitation of the second type,

$$\overset{*}{F}_{ex} = \frac{1}{1 + T_{ex}\,p}; \quad \overset{*}{F}_{fb} = -d; \quad \overset{*}{F}_{\delta} = \frac{c'p + c''p^2}{T_{p}\,p};$$

$$\overset{*}{F}_{U} = \frac{-b}{1 + T_{p}\,p}; \quad \overset{*}{F}_{I} = \frac{k}{1 + T_{p}\,p}.$$

For automatic regulation of the excitation of the third type,

$$\overset{*}{F}_{ex} = \frac{1}{1 + T_{ex}\,p}; \quad \overset{*}{F}_{fb} = 0; \quad \overset{*}{F}_{\delta} = 0;$$

$$\overset{*}{F}_u = \frac{-b}{1 + T_u p}; \quad \overset{*}{F}_I = k.$$

For the synchronous machines, the number of which may be in general n, we considered additionally to the equations of the electro-magnetic transient process in the field winding, represented in Fig.9, the equation of the mechanical movement,

$$(Mp^2 + Dp)\,\Delta\delta = -\Delta p\,.$$

The system connecting the synchronous machines is represented by self and mutual impedances.

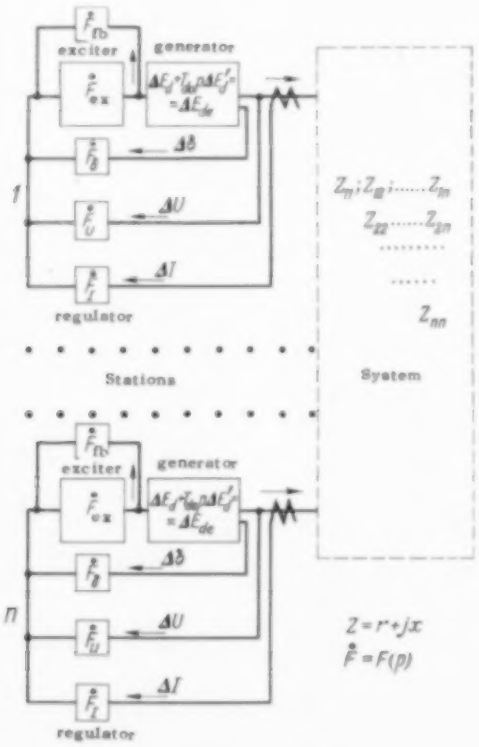

FIG.9. Generalised structural diagram of a power system, considering the automatic excitation control of the synchronous machines.

REFERENCES

1. L.V. Tsukernik; *Differential equations of Disturbed Operation of a Composite Power System for Analysing its Steady-State Stability.* I zv. Otn. A.N.S.S.S.R., 3 (1956).
2. L.V. Tsukernik; *Generalised Equations of Dynamics of a Composite Power System and Use of Electronic Computer for Analysing its Stability. Automatika i Telemekhanika,* 1 (1957).
3. A.A. Voronov; *Elements of the Theory of Automatic Regulation.* 2nd Ed., *Voengiz* (1954).
4. V.S. Korolyuk and D.L. Yushchenko; *Determination of Equipotential Lines of Functions of Two Variables on High-Speed Electronic Computers. Monograph Problems of the Design of High-Speed Computers,* 2, *Akad. Nauk Ukr. SSR* (1955).
5. V.A. Venikov and I.V. Litkens; *The effect of the Excitation Control on the Transmitting Capacity of Long Transmission Systems. Elektrichestvo,* No.11 (1955).

A PRACTICAL METHOD FOR DESIGNING RELAYS WITH RECTIFIERS*

G.G. GIMOYAN

(Received 3 December 1956)

Recent developments in relay engineering are characterized by rapid spreading of the use of semiconductor-type rectifiers in protection and automatic control systems. Design and construction of relays so equipped are still complicated by the fact that they constitute non-linear dipoles for the a.c. circuit. For example, single-coil relays or relays with two magnetically decoupled relays (such as balance relays) are represented in Fig. 1; relays with two inductively coupled and mutually opposing coils in Fig. 5b. There are still other circuits which, however, will not be considered in the present communication.

An analytical determination of the relations of the electrical quantities at input and output of the rectifiers used in these circuits requires involved transcendental equations to be solved. For this reason it is preferable to represent them for practical calculations by linear dipoles (Fig. 7a), obeying Ohm's law.

The determination of the correction factors required for such a transformation is the object of the present paper.

This determination is carried out by the method of linearization [1]; assuming the voltage at the rectifier input as linear,† its current is resolved into harmonic components for each of which a separate equivalent circuit is drawn and the correction factors are found.

For practical calculations it is sufficient to consider the equivalent circuit for the first harmonic only, since the accuracy is sufficiently high and the error does not exceed 5-10 per cent [1-3].

Operation of rectifiers with single-coil relays

For ideal rectifier units and with an input voltage

$$u = \sqrt{2}\, U_1 \sin \theta \qquad \theta = \omega t \tag{1}$$

* *Elektrichestvo* No. 7, 50 – 53, 1957 [Reprint Order No. EL 37].

† Structure and parameters of the equivalent circuit depend on whether the rectifier works in conditions of sinusoidal current or voltage. The operation of the circuits in Fig. 1 and 4b is considered only for sinusoidal voltage, because in relay circuits the resistance of the supply is assumed small [3], to reduce consumption and increase the sensitivity of the arrangement.

where U_1 is the effective value of the fundamental (there being no other harmonic in this case) of the rectifier input, ω the angular frequency of the fundamental. The operation of the rectifier of the circuit of Fig. 1 may be in two different modes, for each of which the relationships between the instantaneous values of currents and voltages are different.

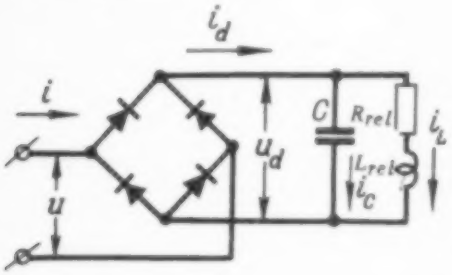

FIG. 1. Equivalent circuit or single-coil relay.

Since a capacitor is connected to the output of the rectifier, the rectified voltage never drops to zero owing to the charge of the capacitor. At the input side of the rectifier, however, the voltage varies sinusoidally and during certain fractions of the period it becomes very small (when changing its direction). During these fractions of the period the following relations hold

$$u_d > |u|;\ i = 0;\ i_d = 0 \qquad (2)$$

where u, i and u_d, i_d are the instantaneous values of voltage and current at input and output of the rectifier.

The mode of operation to which condition (2) applies is known in the literature as the R-state (in the absence of current) [1]. In this state the a.c. and d.c. circuits appear to be absolutely independent because they are separated by the rectifier bridge. According to the line-diagram of voltages and currents (Fig. 2) the circuit operates in the R-state when

$$\begin{aligned} &0 < \theta < \theta_1;\\ &\theta_2 < \theta < \pi + \theta_1;\\ &\pi + \theta_2 < \theta < 2\pi \end{aligned} \qquad (3)$$

When the absolute instantaneous value of the voltage at the rectifier input has reached the value of output voltage, the rectifier begins to conduct, this state being known in the literature as N-state, instead of the R-state.

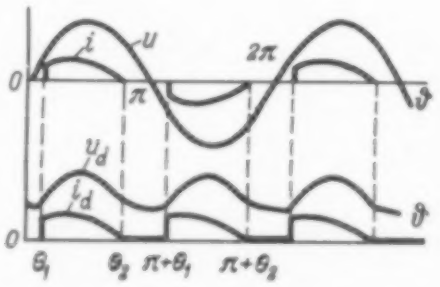

FIG. 2. Line diagrams of voltages and currents at rectifier input (u, i) and output (u_d, i_d).

In the N-state the following identities apply:

$$u_d = |u|;\ i_d = |i|. \qquad (4)$$

The fractions of the period during which the rectifier operates in the N-state correspond to the time intervals

$$\theta_1 < \theta < \theta_2;\ \pi + \theta_1 < \theta < \pi + \theta_2 \qquad (5)$$

The coefficients of equivalent conductance and susceptance are determined by

the formulae

$$\gamma_1 = \frac{\sqrt{2}R_p}{2\pi U_1}\int_0^{2\pi} i \sin\vartheta d\vartheta; \tag{6}$$

$$\beta_1 = \frac{\sqrt{2}R_p}{2\pi U_1}\int_0^{2\pi} i \cos\vartheta d\vartheta. \tag{7}$$

The expressions under the integral sign in (6) and (7) are the instantaneous values of the input current of the rectifier, i, where the input voltage U_1 is given. The relation between the given quantities depends on the circuit parameters. Owing to the large number of unknowns (R_{rel}, L_{rel}, C) it is difficult to determine this relationship by the usual methods of circuit theory. To facilitate the solution of this problem it is useful to carry it out at first for the boundary conditions $R_{rel}/\omega L_{rel} = \infty$ and $R_{rel}/\omega L_{rel} = 0$, and then to find the required solution by comparing the results for the two limiting cases, so that we get an approximate solution for $0 > R_{rel}/\omega R_{rel}$.

The operation of the rectifier of Fig. 1 in the limiting case $R_{rel}/\omega L_{rel} = \infty$ is analysed in [1].

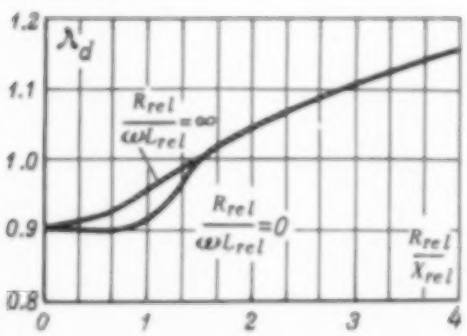

FIG. 3. Values of coefficients determining mean value of rectified voltage.

In the limiting case $R_{rel}/\omega L_{rel} = 0$ the steady-state current passing through the branch with resistance and inductance, i_L, practically remains constant during the period. Since under these conditions the current passing through the capacitive branch has no steady (d.c.) component, the current i_L is practically equal to the mean value of the current at the rectifier output, I_d. The instantaneous values of the output current of the rectifier are therefore determined by the following differential equations:-

in the R-state

$$\frac{1}{X_c}\cdot\frac{dU_d}{d\theta} + I_d = 0 \tag{8}$$

in the N-state

$$i_d = \frac{1}{X_c}\cdot\frac{dU_d}{d\theta} + I_d = \frac{\sqrt{2}\,U_1\cos\theta}{X_c} + \frac{U_d}{R_{rel}} \tag{9}$$

The commutation angles θ_1 and θ_2 and the coefficient of the constant voltage component may be found from (1), (8) and (9) as follows:

$$\theta_2 = \cos^{-1}(U_d X_c / \sqrt{2}\, U_1 R_{rel}); \tag{10}$$

$$\sin\theta_1 = \sin\theta_2 - (U_d X_c / \sqrt{2}\, U_1 R_{rel})(\pi + \theta_1 - \theta_2) \tag{11}$$

$$\lambda_d = U_d/U_1 = \frac{\sqrt{2}}{\pi}\{\cos\theta_1 - \cos\theta_2 + \sin(\pi + \theta_1 - \theta_2) - \\ - \frac{U_d}{\sqrt{2}\,U_1} \cdot \frac{X}{R_{rel}}\left[\frac{(\pi + \theta_1)^2 - \theta_2^2}{2} - \theta_2(\pi + \theta_1 - \theta_2)\right]\} \tag{12}$$

The quantities θ_1, θ_2 and λ_d as functions of the ratio X_c/R_{rel} are determined by grapho-analytic solution of the last three equations [3].

The coefficients of the equivalent conductance γ_1 and susceptance β_1, respectively, are found from (6) and (7), when (9) is considered, thus,

$$\gamma_1 = \frac{1}{\pi}\left[\lambda_d(\cos\theta_1 - \cos\theta_2) + \left(\frac{R_{rel}}{X_c}\left(\frac{\cos 2\theta_1 - \cos 2\theta_2}{2}\right)\right)\right]; \tag{13}$$

$$\beta_1 = \frac{1}{\pi}\left[\lambda_d(\sin\theta_2 - \sin\theta_1) + \frac{R_{rel}}{X_c}\left(\theta_2 - \theta_1 + \frac{\sin 2\theta_2 - \sin 2\theta_1}{2}\right)\right] \tag{14}$$

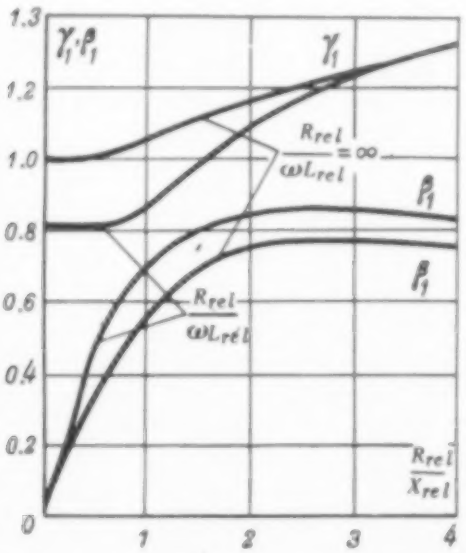

FIG. 4. Theoretical coefficients for the design of automatic control and protection gear using single-coil relays.

The relationships $\lambda_d = f(X_c/R_{rel})$; $\gamma_1 = f(X_c/R_{rel})$ and $\beta_1 = f(X_c/R_{rel})$ for the two mentioned limiting cases are drawn in Fig. 3 and 4. The curves show that the presence of the inductance affects the values of λ_d, γ_1 and β_1 at small values of X_c/R_{rel}.

Operation of rectifiers having relays with two coils

We will consider the operation of rectifiers having a relay with two magnetically coupled coils on the example of a distance relay for h.v. transmission lines [3]. According to the diagram of Fig. 5a the operating (OP) and restraining (OT) coils of this relay are supplied by the rectifiers BP and BT, the input voltages of which are U_P and U_T, respectively. Considering that in any real relay the coupling coefficient of the coils varies, viz. $0 < M_{rel}/L_{rel} < 1$ (where L_{rel} and M_{rel} are self- and mutual-inductances of the relay winding), it will be convenient to examine the operation of the circuit of Fig. 5a for the two limiting cases, viz.

$$M_{rel}/L_{rel} = 0 \text{ and } M_{rel}/L_{rel} = 1.$$

In the limiting case $M_{rel}/L_{rel} = 0$ each relay winding may be imitated by the circuit of Fig. 1 analysed above.

In the limiting case $M_{rel}/L_{rel} = 1$ and under the condition that the ratio X_c/R_{rel} is such as to permit an operation of both rectifiers only in the N-state, the relay circuit may be represented by the linear four-terminal network of Fig. 5c, the input and output voltages of which are U_P and U_T, respectively.

1958

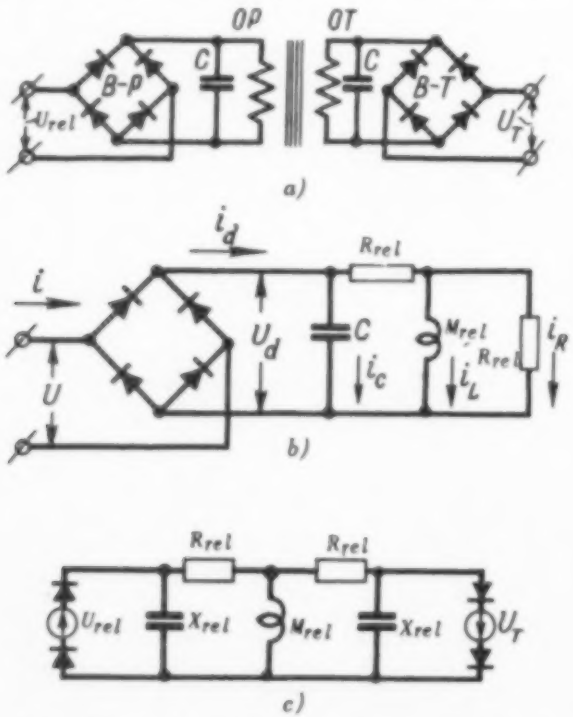

FIG. 5. a) Basic circuit of a distance relay; b) Equivalent circuit of two-coil relays; c) Equivalent circuit of this relay for ideal magnetic coupling of the coils.

The calculation for such a four-terminal network is more conveniently carried out by the method of superposition, i.e. by representing it in the form of two dipoles (Fig. 5b), the rectifiers* of which operate in the N-state.

If we take into account that in reality the inductive reactance of the relay windings is considerably larger than their resistance, it is fairly easy to find by Kirchhoff's laws an expression for the output current of the rectifier [3]:

$$i_d = \sqrt{2}\, U_1 \cos \theta / X_c + \sqrt{2}\, U_1 \sin \theta / 2R_{rel} + U_d / 2R_{rel} \qquad (15)$$

The critical value of $(X_c/R_{rel})_{crit}$ at which the rectifier operates in the N-state, can be found from the last equation by the substitutions

$$i_d = 0;\ \theta = \pi \text{ and } U_d/\sqrt{2}\, U_1 = 2/\pi;$$

Hence $$(X_c / R_{rel})_{crit} > \pi.$$

We note that in the limiting case $M_{rel}/L_{rel} = 0$, $(X_{rel}/R_{rel})_{crit} \geq \pi/2$.

The values of the equivalent coefficients γ_1 and β_1 are plotted against X_c/R_{rel} for both limiting cases in Fig. 6.

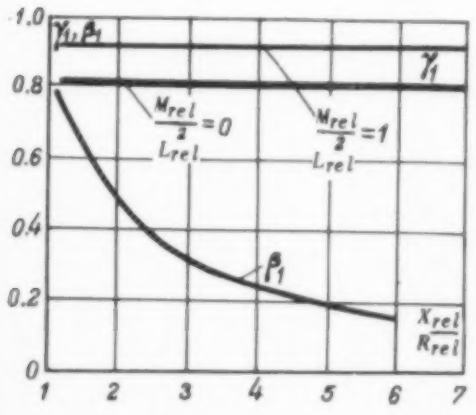

FIG. 6. Design factors for automatic control and protective gear using two-coil relays.

For the limiting case $M_{rel}/L_{rel} = 1$ they were determined from (6), (7) and (15).

The curves indicate that when the mutual inductance is considered, the conductance is slightly reduced, whereas the susceptance remains unchanged.

Appendix

The design of protective and automatic control relays with semiconductor rectifiers centres on the determination of the optimum circuit parameters resulting in the maximum sensitivity and minimum power consumption of the relays, and also in their reliable operation and compact construction.

It is clear that the purpose and the sequence of the calculations will differ according to the type and use of the relay [1-3]. We will solve, by way of example, the following problem. To find the parameters of the other circuit elements (rectifier, supply transformer, etc) when the relay parameters (P_{mean}, R_{rel}, I_{mean}) and the reactance of the capacitive filter X_c are given.

* The rectifier of Fig. 5b may in general operate, analogously to the rectifier of Fig. 1, in the R- and N-states. We use the superposition method only when the N-state exists.

1. As first approximation, viz. assuming ideal rectifier units according to the curves $\gamma_1 = f(R_{rel}/X_c)$ and $\beta_1 = f(R_{rel}/X_c)$, we determine γ_1 and β_1, and from these the resistances and reactances of the equivalent circuit:

$$R_{eq} = \frac{\gamma_1}{\gamma_1^2 + \beta_1^2} R_{rel} \text{ and } X_{eq} = \frac{\beta_1}{\gamma_1^2 + \beta_1^2} R_{rel}.$$

2. From the given value of I_{mean} we determine the mean values of the output current and voltage of the rectifier, viz. $I_d = K_{ser} I_{mean}$ (K_{ser} being the coefficient of reliability of service) and $U_d = I_d R_{rel}$.

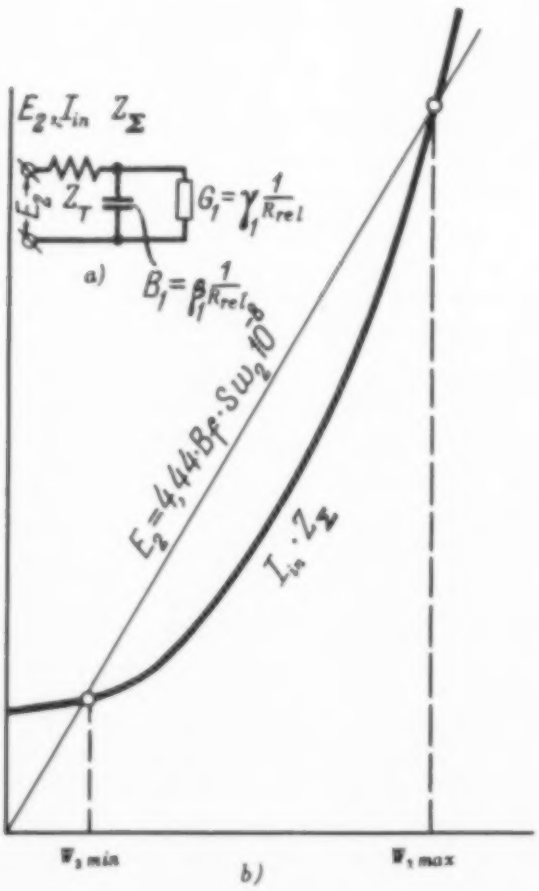

FIG. 7. a) Equivalent circuit of the relay considering internal resistance of supply; b) Graphical solution of the equation of the relay operation.

3. From the value of U_d we find the input voltage U_{in} and current I_{in} of the rectifier, viz.

$$U_{in} = U_d/\lambda_d ; I_{in} = U_{in}/\sqrt{R_{eq}^2 + X_{eq}^2}$$

(λ_d being found from the curve of Fig. 4).

4. From I_d, U_d, I_{in} and U_{in} we determine the number of rectifier elements to be connected in parallel (a) and series (n) into a bridge arm [1 and 2], and with these resultant resistance of the elements of the rectifier $R_a = 2nr_u/a$ (r_u being the resistance of a single rectifier unit).

5. Adding R_a to the resistance R_{rel}, we repeat the calculation for the actual rectifier units, i.e. assume the load resistance to be $R_d = R_{rel} + R_a$.

6. The minimum turns number of the interposing transformer assuring reliable relay operation is found from the condition of equality of the e.m.f. E_2 induced in the secondary winding of the transformer and the voltage drop in the equivalent circuit (Fig. 7a).

$$E_2 = I_{in} Z_{\Sigma} \tag{I.1}$$

where Z_{Σ} is the total impedance of the equivalent circuit

$$E_2 = 4.44\ B.S.f.w_2\ 10^{-8} \tag{I.2}$$

$$Z_{\Sigma} = \sqrt{(C_R\omega_2^2 + R'_{eq})^2 + (C_X\omega_2^2 = X'_{eq})^2} \tag{I.3}$$

In the last equation $C_R\omega_2^2$ and $C_X\omega_2^2$ are the resistance and reactance, respectively, of the secondary winding of the interposing transformer; for a given type of core stampings of the transformer they depend only on ω_2 [3]; R'_{eq} and X'_{eq} are resistance and reactance, respectively, of the equivalent circuit of the rectifier, considering the self-resistance of the latter.

The value of ω_{2min} is determined by the bi-quadratic equation obtained from (I.1), when (I.2) and (I.3) are considered, or by solving equation (I.1) graphically (Fig. 7b).

REFERENCES

1. V.G. Komar; *Operation of Semiconductor Rectifiers in Control Circuits, Gosenergoizdat* (1952).

2. I.L. Kaganov; *Electronic and Ionic apparatus, Gosenergoizdat* (1950).

3. G.G. Gimoyan; *Distance Protection using Semiconductor Rectifiers, Dissertation. Moscow Electrotechnical Institute* (1954).

THE USE OF LOAD DISTRIBUTION DIAGRAMS FOR THE DESIGN OF URBAN SYSTEMS*

YU. A. GLANTS

(Received 12 October 1956)

The character of the distribution of the loads in a system has a great influence on its design and operation. This factor becomes very important for the design of low-voltage systems especially in urban areas.

The choice of the system arrangement for one or other type of distribution of loads must be made on the basis of technical and economical considerations. The proposed method of plotting the load distribution diagrams facilitates these calculations and the derivation of the economic optimum design of the system. We owe the idea of plotting these diagrams to V.P. Khashchinskii [1].

Let us first consider a radial line feeding the loads distributed along its route. The diagram of the distribution of these loads along the line may be presented as shown in Fig. 1.

The area of the diagram, Fig. 1, can be determined by the sum of the load moments:

$$\Sigma P_i l_i = P_1 l_1 + P_2 l_2 + P_3 l_3 + P_4 l_4$$

or

$$\Sigma p_i l'_i = p_1 l'_1 + p_2 l'_2 + p_3 l'_3 + p_4 l'_4,$$

where

P_1, P_2, P_3 and P_4 are the values of power sent through the line sections;
l_1, l_2, l_3 and l_4 are the lengths of the line sections;
p_1, p_2, p_3 and p_4 are the loads connected to the line;
l'_1, l'_2, l'_3 and l'_4 are the distances of the connected loads from the supply source.

Since each of the sums of the load moments represents the same area it can be written:

* *Elektrichestvo* No. 7, 45-50, 1957 [Reprint Order No. EL 38].

$$\Sigma\ P_i l_i = p_1 l_1' \tag{1}$$

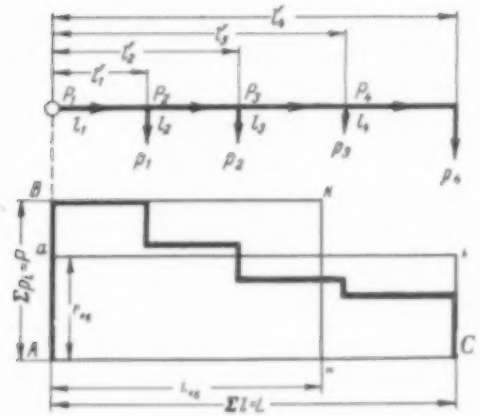

FIG. 1.

The stepped diagram shown in Fig. 1 can be replaced by an equivalent rectangular diagram. There are two alternative methods of such a replacement: 1) The stepped diagram is replaced by the rectangle $AabB$ with the base of the rectangle equal to the length of the line $\Sigma\ l_i = L$; 2) the stepped diagram is replaced by the rectangle $ACkm$ with the height of the rectangle equal to the total load of the line $\Sigma\ p_i = P$.

In the first case we obtain the possibility of replacing the total load by one equivalent load connected to the end of the line. The equivalent load is

$$P_{eq} = \frac{\Sigma p_i l_i'}{L} \tag{2}$$

In the second case we also obtain the possibility of replacing the distributed load by a concentrated one, but in contrast to the preceding case, the latter although equal to the total load, is at an equivalent distance from the supply point given by

$$L_{eq} = \frac{\Sigma p_i l_i'}{P} \tag{3}$$

We now change to relative values of equivalent load P_{eq}^* and of equivalent distance L_{eq}^*, of which the first is considered to be a fraction of the total load and the second a fraction of the line length. It is not difficult to see that

$$P_{eq}^* = L_{eq}^* = \frac{\Sigma\ p_i l_i'}{P L} = \alpha \tag{4}$$

V.M. Khrushchov [2] was the first to introduce this coefficient α. He called it the coefficient describing the distribution of the load and derived this formula for its determination.

The value of the coefficient α may vary between 0 and 1, where the upper limit refers to the case that power is transmitted through the line to a load concentrated at its end, and the lower limit to the case that the load is directly at the supply point.

The coefficient α can be determined graphically if the load distribution diagram is plotted in relative units with unity load being the total load and unity distance the total line length. The coefficient α is determined by the ordinate $Aa = Bb$, or by the abscissa $Am = Ck$ (Fig. 1).

In a similar manner a diagram can be plotted for the squares of the loads, which can be replaced by an equivalent rectangle in the same way as it was done above. The height of this equivalent rectangle plotted on the same base, the line length, is equal to the equivalent square load. The base of the equivalent rectangle whose height is the square of the total load equals the equivalent distance of the connection point of this load from the supply point.

In a similar way as the coefficient α was determined for the load distribution diagram, a coefficient β can be found as follows

$$\beta = \frac{\Sigma\, P_i^2\, l_i}{P^2 L} \,. \tag{5}$$

If the diagram is plotted in relative units,

$$\beta = \Sigma\, P_i^2\, l_i$$

It should be noted, that, if the line has the same conductor size along its entire length, for purely active power the coefficient β will be proportional to the power loss of the line and the coefficient α proportional to the voltage regulation.

Having the values of the coefficients α and β, one can replace the distributed loads by the concentrated loads and thus simplify the design calculations.

It follows from (4), (5) and (1) that the sum of the moments of the distributed loads is

$$\Sigma\, P_i l_i = \Sigma\, p_i l_i' = \alpha\, P L \tag{6}$$

and the sum of the moments of the square loads

$$\Sigma\, P_i^2 l_i = \beta\, P^2 L \tag{7}$$

1958

With the change from the system with distributed loads to the system with concentrated loads it is necessary for the determination of the voltage regulation to arrange at the end of the line a load equivalent to αP or for determination of the power loss a load equivalent to $\sqrt{\beta}\,P$.

Diagrams with the same value of α can have different values of the coefficient β. With diagrams of the same coefficient α it is possible to have two extreme cases: 1) the diagram has the shape of a rectangle with unit base but a height of α 2) the diagram has the shape of a rectangle with the base α but unit height. In the first case $\beta = \alpha^2$ and in the second $\beta = \alpha$.

The diagram of the load distribution along a ring line is obtained from two conjugated diagrams, of which one is obtained by considering the line as a radial feeder supplied from one end. One of the diagrams would correspond to the feeding in the direction 0-1-2-3-4, and the other in the direction 0-4-3-2-1 (Fig. 2). The area of the first diagram is shaded and that of the second one is not shaded. The areas of the two diagrams supplement each other to the rectangle $ACDB$ with the base equal to the line length and the height equal to the total load of the line.

Ring feeders supplied from both ends can be divided at the point of current reversal into two branches. The point of current reversal on the line can be determined graphically from the following conditions: 1) the voltage regulation in each of the branches must be equal, that means the areas of the two load distribution diagrams must be the same; 2) the sum of the loads at the supply point must be equal to the total line load.

For the determination of the point of current reversal it is necessary in the diagram of Fig. 2 to lay a line ab parallel to the abscissa so that the areas $aBbdef$ and $cCmkighf$ cut out by it from the two conjugated diagrams are equal to each other. These diagrams are then also the load distribution diagrams of the two branches of the ring feeder.

The line ac divides the rectangle $ACDB$ into two parts: The area of the lower part $AacC$ is equal to the shaded area of the conjugated diagram, and the upper part $BacD$ is equal to the unshaded part of that diagram. Therefore, the rectangle $AacC$ is equivalent to the shaded diagram, and the rectangle $BacD$ is equivalent to the unshaded diagram.

The maximum ordinates of the branch diagrams aB and cC represent the magnitude of the power flow at the point of supply in each of the branches of the ring feeder. Each load power flow is

$$P_b = \alpha' P \tag{8}$$

where

α' is the coefficient of the load distribution determined for each branch from its conjugated diagram (for the left branch from the unshaded

diagram, and for the right branch from the shaded diagram);
P is the total load of the ring feeder.

It is possible to plot diagrams of the distribution of the square of the loads from the diagram of the load distribution of the branches of the ring feeder by using the square of the ordinates. The one permits the determination of the voltage regulation and the other that of the power losses of the ring feeder.

The area of the load distribution diagram of the branches of the ring feeder will be designated in the following by M_r and the sum of the areas of the diagrams of the distribution of the squares of the loads in both branches by N_r.

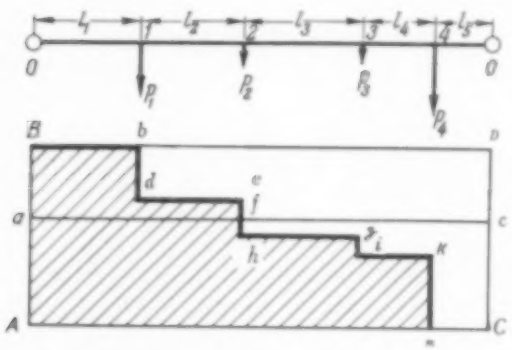

FIG. 2.

The value of N_r can be determined in another way. For this purpose we consider two diagrams, Fig. 3a and 3b which have a different configuration but whose coefficients α and β are respectively equal.

Considering any of the load distribution diagrams Fig. 3a or 3b we transform it into a two-stepped diagram whose first step is unity and whose second is α (Fig. 3c, diagram *Bbcdef*).

If one changes from that equivalent diagram to the square one, then the first step of the latter is also unity, but the second is α^2.

The length of the first step of the equivalent diagram (Fig. 3c), whose ordinate is unity, is designated by x, and the length of the second step, whose ordinate is α, by y. Then, as follows from Fig. 3c, the area of the equivalent diagram, plotted in relative units, is

$$\alpha = x + \alpha y,$$

and the area of the square diagram

$$\beta = x + \alpha^2 y.$$

Solving jointly these two equations we obtain

$$x = \frac{\beta - \alpha^2}{1 - \alpha} \tag{9}$$

$$y = \frac{\alpha - \beta}{\alpha - \alpha^2} \tag{10}$$

The area of the part $aCcd$ of the equivalent diagram (Fig. 3c) is $x(1-\alpha)$. Consequently, on the basis of (9) it is $(\beta - \alpha^2)$. This area changes with a change in the shape of the equivalent diagram. It goes towards zero, if the equivalent diagram approaches the single-stepped diagram $AacC$ with the ordinate α. This corresponds to the extreme case when the total load is supplied directly from the source. It will go towards its maximum value, if the equivalent diagram adopts the shape of the single-stepped diagram $ABkm$ with unity value of the ordinate. The area $aBbd$ has in that case the value $\alpha(1-\alpha) = \alpha - \alpha^2$. This corresponds to the extreme case that the concentrated load is supplied through the ring feeder.

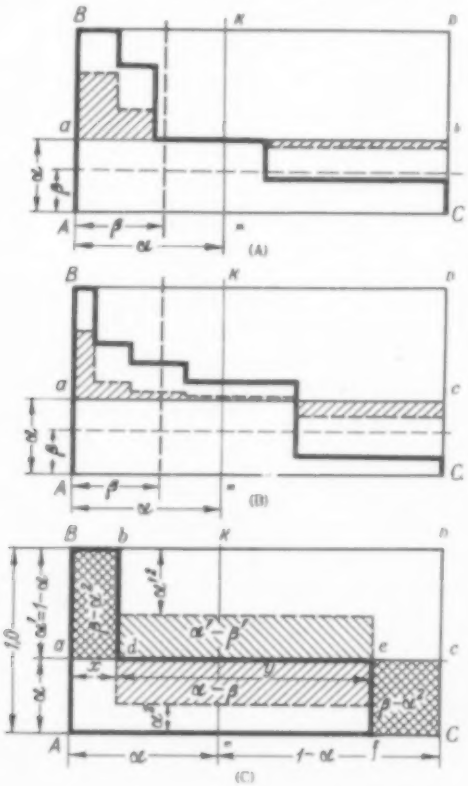

FIG. 3.

In the latter extreme case the area of the square diagram of one branch of the ring feeder is $(1-\alpha)^2\alpha$, and that of the other branch $\alpha^2(1-\alpha)$. The sum of the areas of the square diagrams of the branches is

$$N_r = (1-\alpha)^2\alpha + \alpha^2(1-\alpha) = \alpha - \alpha^2.$$

Since in the considered case $\beta = \alpha$

$$N_r = \beta - \alpha^2 \qquad (11)$$

i.e. the sum of the areas of the square diagrams of the branches equals the area $aCcd$.

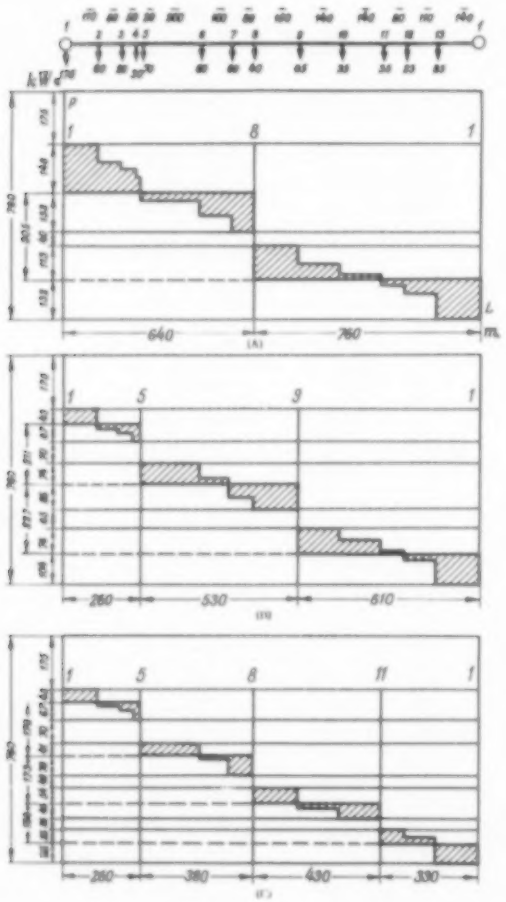

FIG. 4.

Analysis of a large number of diagrams shows that the sum of the areas of the square diagrams of the branches of ring feeder is always equal to the area *aBbd*. Thus, the value of N proportional to the power losses in the ring system can be determined from the magnitude of the area *aBbd* or the equal area *fecC*. This permits the determination of N_r from (11), i.e. without plotting the diagram, if the coefficients α and β are known for one of the conjugate diagrams of the ring system.

It follows from (11) that the power losses in a feeder for feeding from both ends differ from the losses with feeding from one end by α^2. The ratio of these losses is

$$\frac{\beta - \alpha^2}{\beta} = 1 - \frac{\alpha^2}{\beta}; \qquad (12)$$

that means the change to feeding from both ends is the more effective in reducing the losses, the larger is the term (α^2/β).

The above derived relationship of the coefficients of the diagram of the ring system is interesting, because it facilitates the determination of the power losses for feeding from both ends, if the losses for feeding from one end are known. Besides, it is not necessary to calculate both conditions of single-end feeding and it is sufficient to calculate only one of these conditions since one diagram of load distribution also determines the conjugate diagram. Thus one calculation is sufficient for all three supply conditions of the ring feeder.

It follows from the determination of the conjugate diagram that

$$\alpha' = (1 - \alpha) \tag{13}$$

and, since both shaded areas in Fig. 3c are equal:

$$\alpha - \beta = \alpha' - \beta'.$$

Consequently, the coefficient for the conjugate diagram is

$$\beta' = \beta + (1 - 2\alpha) \tag{14}$$

The above conclusions are to be applied to a concrete example.

The coefficients for the case of a ring feeder supplied from one end may be $\alpha = 0.4$ and $\beta = 0.3$, and the power losses $\Delta P = 2.15$ kW. Then

$$\beta' = 0.3 + (1 - 2\times 0.4) = 0.5$$

Consequently, for feeding the line from the other end the losses are

$$\Delta P = 2.15\frac{0.5}{0.3} = 3.58 \text{ kW}.$$

For feeding from both ends

$$N_r = 0.3 - 0.4^2 = 0.14$$

and the power losses

$$\Delta P_r = 2.15\ \frac{0.14}{0.3} = 1 \text{ kW}.$$

An urban ring system often comprises one or several districts and is supplied from several sources. The calculations for the determination of the voltage regulation and especially of the power losses in such systems with a large number of loads are complicated and laborious. The use of load distribution diagrams in a given case can considerably shorten the calculations and make them clearer.

Consider, for example, a ring system connecting a group of consumers, e.g. houses. Fig. 4 shows three diagrams of the load distribution in such a system: the first, Fig. 4a, for the case of two; the second, Fig. 4b, for three, and the third, Fig. 4c, for four supply points.

The supply points can be located in such a manner that the areas cut out of the conjugate diagrams of the sections of the system and representing the load

TABLE 1.

Items	Sections of system with three supply points (Fig. 4b)				Sections of system with four supply points (Fig. 4c)				
	1-5	5-9	9-1	Total	1-5	5-8	8-11	11-1	Total
Total load (kW)	110	160	180	450	110	120	100	110	440
Total length (m)	260	530	610	1 400	260	380	430	330	1 400
Load moment ($kW \cdot m \times 10^3$)	28.6	84.8	110	—	28.6	45.5	43	36.3	—
Square moment ($kW^2 \cdot m \times 10^6$)	3.14	13.6	19.7	—	3.14	5.46	4.3	4.0	—
Load moment of the diagram ($kW \cdot m \times 10^3$)	17.6	45.2	63.7	—	17.6	30	19.95	18.2	—
Square moment ($kW^2 m \times 10^6$)	1.58	6.25	9.23	—	1.58	3.24	1.67	1.77	—
Coefficient α	0.615	0.534	0.578	—	0.615	0.66	0.464	0.5	—
Coefficient β	0.503	0.458	0.458	—	0.503	0.594	0.388	0.442	—
Coefficient N_r	0.126	0.174	0.135	—	0.126	0.16	0.173	0.19	—
Coefficient M_r	0.163	0.195	0.152	—	0.163	0.18	0.187	0.212	—
Cable size (mm^2)	50	95	120	—	50	70	50	50	—
Resistance (Ω)	0.109	0.118	0.107	—	0.109	0.114	0.18	0.139	—
Equivalent load for determining the power losses (kW)	39	67	66.2	—	39	48	41.7	48	—
Equivalent load for determining the voltage regulation (kW)	17.9	31.2	27.4	—	17.9	21.6	28.2	23.3	—
Power losses (kW)	1.14	3.65	3.2	7.99	1.14	1.82	2.16	2.2	7.32
Voltage regulation (V)	5.12	9.7	7.7	—	5.12	6.45	8.8	8.5	—
Copper volume (dm^3)	39	151	219	409	39	80	65	50	234

distribution diagrams for the individual branches are as small as possible. After that the load flow from the supply points can be determined, the conductor size of the individual sections of the system chosen, the voltage regulation and the power losses determined. Such calculations are given below for the system with three (Fig. 4b) and four (Fig. 4c) supply points. The basic data and the results of the calculations are entered in the table.

The load, distributed along the branches of the sections of the ring system between the supply points was replaced by a concentrated load at the end of the branch. For the determination of the voltage regulation the concentrated load at the end of the branch used in the calculation is $P_v = M_r P$, and for the determination of the power losses $P_p = \sqrt{N_r P}$.

The voltage at all supply points of the system was assumed to be 380 V.

The cable sizes were checked with respect to the thermal ratings corresponding to the maximum permissible load with consideration of the conditions of laying and of the ambient soil temperature. The possibility of feeding each section from one end in emergency conditions was taken into account for the choice of the cable size.

It can be seen from the table that with the change from three to four supply points the copper volume of cables is reduced by 175 dm^3 and the power losses by 0.67 kW. The maximum voltage regulation on all sections of the system with three and four supply points is very reasonable at about 2.5 per cent.

The transformer loads with three supply points are:
322; 211 and 227 kW; and with four supply points 273; 178; 173 and 136 kW.

As the above example shows the method of plotting load distribution diagrams permits a clear and simple determination of the approximate load flow in the system, of the voltage regulation and power losses. Thus it reduces the labour of calculations for the purpose of technical and economical considerations.

In cases where it is not suitable to use the same cable size on a section of the system and where at the supply end twin cables are used, the calculation with the graphical method becomes somewhat more complicated. The twin cable section in that case is to be represented by equivalent data of the basic cable size between the two supply points.

REFERENCES

1. V.P. Khashchinskii; *Distribution of electric energy. Commission for improving living conditions of students, Leningrad* (1926).
2. V.M. Khrushchov; *Electric systems and lines*, Part 1. *Gosenergoizdat* (1932).

THE NOMOGRAM FOR DETERMINING PROTECTIVE ZONES OF LIGHTNING CONDUCTORS*

L.M. LOPSHITS

(Received 24 April 1956)

This nomogram supersedes an earlier one (*Elektrichestvo*, No. 10, 1947) and is deemed necessary because of the distinction made in the latest instruction book on overvoltage protection of electrical installations for 3 - 220 kV (Gosenergoizdat, 1954) between the formulae for lightning conductors up to and above 30 m.

The nomogram is constructed for single and double lightning conductors up to 150 m using an emphirical formula based on laboratory test results and on the assumption that orientation of the lightning stroke onto the lightning conductor takes place at the height of H = 600 m (for an open country).

The use of the nomogram is explained with three examples.

1958

That part of the latest Code of Practice on protection against overvoltages [1] which deals with protection against direct lightning strokes is based on laboratory investigations carried out at the V.I. Lenin All Union Electro-technical Institute, and differs from the earlier edition of the Code [3] in that in it a distinction has been introduced between the formulae for rod lightning conductors up to 30 m high and above 30 m high. Thus, the earlier nomogram for determining protective zones, constructed for lightning conductors up to 60 m has become obsolete and now may be used only for lightning conductors up to 30 m.

Figs. 1 and 2 give curves constructed from the data included in [2] which describe protective zones of single and double lightning conductors respectively. The geometrical sense of the parameters of the protective zone a, h, ha, h_x, b_x, and r_x is clear from Fig. 4; by H is denoted the height at which orientation of the lightning channel onto the lightning conductor takes place for open country.

For taller lightning conductors, $h > 30$ m, H was taken as 600 m, and for shorter lightning conductors, $h < 30$ m, the constant ratio of $H/h = 600/30 = 20$ was taken. It should be mentioned here that the Code of Practice does not set definite limits within which its recommendations are valid but merely states that the value of $H = 600$ m can be used for "very tall lightning conductors".

The curves given in Figs. 1 and 2 can be applied in these cases when the height of the lightning conductor does not exceed 150 m ($H/h = 4$), which corres-

* *Elektrichestvo* No. 7, 76 – 78, 1957 [Reprint Order No. EL 39].

ponds to the greatest height of chimneys built in power stations.

With the above value assumed for the height at which orientation of the lightning channel takes place, the following empirical expressions can be written for the relations represented on Figs. 1 and 2.

$$\frac{r_x}{h_a} = \frac{1.6}{1 + \frac{h_x}{h}} \cdot p_1(h); \tag{1}$$

$$\frac{a}{h_a} = 7 \sqrt[1.3]{1 - \left(\frac{b_x}{r_x}\right)^{1.4}} \cdot p_2(h), \tag{2}$$

where $p_1(h)$ and $p_2(h)$ are coefficients depending on the height of the lightning conductor (Fig. 3).

It should be noted that in order to simplify calculations the following assumption is made in the Code of Practice*: $p_1(h) = p_2(h) = p(h)$,

where $$p(h) = \sqrt{\frac{30}{h}} \quad (\text{for} \quad h \geqslant 30 \text{ m}).$$

The relation $p(h)$ is shown in Fig. 3 by the curve drawn in a broken line.

Eliminating r_x from (1) and (2) one gets the following formula for the double lightning conductor:

$$\left(\frac{b_x}{1.6 h_a \cdot p_1(h)}\right)^{1.4} \times \left(1 + \frac{h_x}{h}\right)^{1.4} + \left(\frac{a}{7 h_a \cdot p_2(h)}\right)^{1.3} - 1 = 0$$

which if $a = 0$, becomes also valid for the single lightning conductor.

The calculation of the lightning conductor height using this formula is lengthy and tedious; the present nomogram (Fig. 4) removes this disadvantage. The following examples explain the use of the nomogram and illustrate its scope.

Example 1. The given object has the shape of a parallelepiped with the base 48×48 m² ($b_x = 24$ m) and the height 15 m. It is located between two lightning rods 49 m high in such a way that a line drawn through the centres of the lightning rods coincides with the axis of symmetry of the object. It is required to verify that the object is protected if the distance between the lightning rods is 60 m.

Place one point of a pair of dividers at the point $a = 60$ m on the abscissa (the scale of centres). Bring the other point to $b_x = 24$ m on the ordinate. Keeping the first point unmoved and without altering the distance between the two points place the second point on the curve $h_x = 15$ m.

Through this point of the nomogram the curve $h_a = 32$ m also passes. Thus, the necessary height of the lightning conductor is $h = h_x + h_a = 15 + 32 = 47$ m. Therefore, with $h = 49$ m the object lies within the protective zone of the lightning conductor.

* There are errors in Figs. 4 and 5 of the Code. Instead of $h_x = 0.7h$ and $h_x = 0.9h$ it should be $h_x = 0.6h$ and $h_x = 0.7h$ respectively.

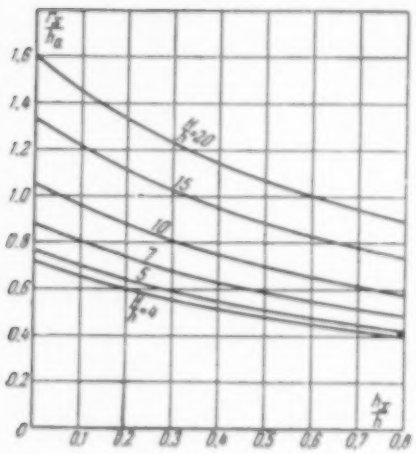

FIG. 1.

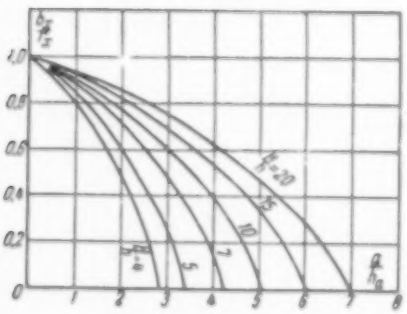

FIG. 2.

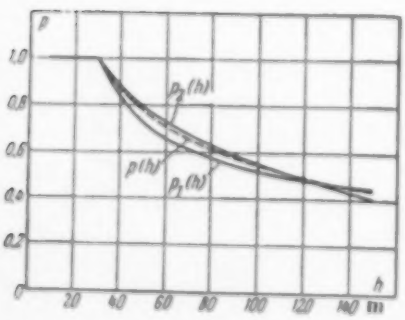

FIG. 3.

The nomogram can also be used in a different way. Set the dividers to the distance between the point $a = 60$ m and the point of intersection of the curves $h_x = 15$ m and $h_a = 49 - 15 = 34$ m. With this distance as radius and with point $a = 60$ m as the centre determine the point at which the ordinate is intersected; this is seen to be at $b_x = 25$ m. It follows then that the given lightning conductor would protect an object for which $b_x = 25$ m.

Example 2. Determine the necessary active height of a single lightning conductor placed in the centre of a structure having a cylindrical form with the diameter 40 m and the height 6 m.

With radius equal to the distance from the origin ($a = 0$) to the point $r_x = b_x = 20$ m, determine the point of intersection with the curve $h_x = 6$ m. The curve $h_a = 16$ m which also passes through this point gives the desired value for the active height of the conductor.

Example 3. Find the radius of the protective zone at the level of $h_x = 26$ m for a single lightning conductor 120 m high placed on the chimney of a power station.

With origin as centre and radius equal to the distance from the origin to the point $h_x = 26$ m on the curve for $h = 120$ m, determine the point of intersection with the ordinate; this is found to be $b_x = r_x = 59.5$ m, which is the required value for the radius of protection.

The nomogram has been constructed on the assumption that the distance a between two lightning rods is given, which is normally the case in practice. In these exceptional cases when the distance is to be determined, it may be quickly found using a simple geometrical construction.

From the middle of the line joining the given points b_x (on the ordinate) and h_a

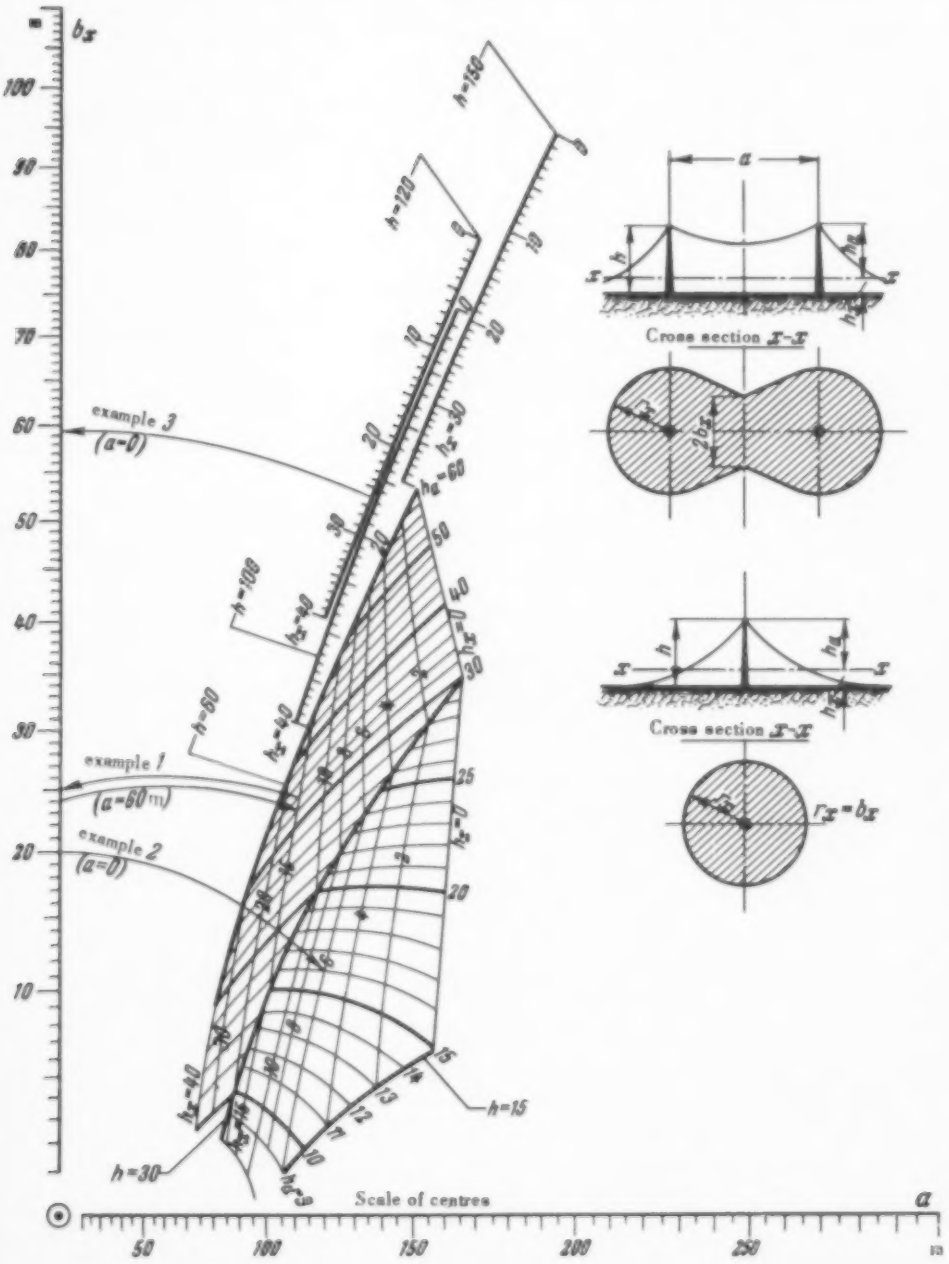

FIG. 4. The nomogram for determining protective zones of rod lightning conductors.

and h_x (the intersection of the corresponding curves) drop the perpendicular on the scale of centres. The point of intersection with this scale gives the required distance between the two lightning rods.

In conclusion it should be mentioned that the Code of Practice considers but in a small degree the critical observations regarding simplification of the contour of the protective zone [5]. In the present edition of the Code it would be desirable to approximate the curvilinear generatrix of the "cone" of the protective zone by a number of straight lines. This should considerably simplify graphical constructions.

REFERENCES

1. *The Code of practice on protection from overvoltages of a.c. electrical installations for 3 - 220 kV. Gosenergoizdat* (1954).
2. A.A. Akopyan; *Proceedings All-Union Electrotechnical Institute* VOL. 36, *Gosenergoizdat* (1940).
3. *The code of practice on protection from overvoltages of a.c. electrical installations for 3 - 220 kV. Gosenergoizdat* (1946).
4. L.M. Lopshits; *A Nomogram for determining protective zones of lightning conductors up to 60 m high. Elektrichestvo*, No. 10 (1947).
5. I.S. Stekol'nikov *et al; Lightning protection of industrial structures and buildings. Izd. Akad. Nauk SSSR* (1951).

1958

958

1958

TWO-COMMUTATOR ROTARY AMPLIFIER*

I.N. CHUPIATOV and V.F. BAIKO

Obraztsov Institute of Railway Transport
Engineers, Leningrad

(Received 4 March 1957)

Rotary amplifiers are used in various cases of electro-drive in order to improve the quality of regulation.

At present there are a few types of rotary amplifiers differing in their mode of operation and in their working characteristics. Of these, rotary amplifiers with a cross-field are most frequently used in industry and transport. Nevertheless, in certain cases, these amplifiers do not satisfy requirements and cannot be used in automatic control systems.

Therefore, the study of the properties of other amplifier systems is of considerable interest.

In the present article, we consider the mode of operation and the fundamental working characteristics of a two-commutator rotary amplifier which in foreign literature is called "magnavolt". The two-commutator rotary amplifier of this type has not yet found application in our national automatic control systems. Its physico-technical and working characteristics are not elucidated in our technical and scientific literature.

Mode of operation of the amplifier

The two-commutator rotary amplifier differs essentially in principle from amplifiers with an axial field and from those with cross-field as well.

The rotary amplifier in question has, like any ordinary d.c. machine, a yoke on which are fixed main poles and interpoles. But the armature of this amplifier, unlike those of ordinary machines, has two windings, calculated for different numbers of poles. The armature windings are connected to separate commutators, thus they form two independent electrical circuits. In the slots of the armature, the windings are placed in four layers, since every winding has two layers. The characteristic property of the amplifier is its method of excitation. The magnetic circuit of the amplifier consists of the superimposed magnetic circuits of two machines, designed

* *Elektrichestvo* No. 1, 1 – 5, 1958 [Reprint Order No. EL. 40].

or different numbers of poles, the ratio of the number of poles of the two combined machines being always equal to two.

The windings of the armature are calculated according to the number of poles of the combined machines.

We consider the principle of action of an amplifier with the number of poles of the combined magnetic circuit equal to $2p = 2$ and $2p = 4$, respectively. On the yoke of such an amplifier, there are four cores of the main poles, on which two excitation windings are placed, forming a two-pole and a four-pole magnetic circuit.

The winding producing a two-pole m.m.f. (two-pole magnetization) is placed on all four cores of the yoke poles and is fed from an independent source. The current in this excitation winding produces the polarity of the poles according to the sequence N-N-S-S., i.e. a two-pole magnetic system is formed. This excitation winding is called a control winding of the amplifier. There may be two or more such windings on the cores of the stator, according to the use of the amplifier and according to the requirements of the system in which it works.

The second excitation winding is placed on the same four cores and is fed from the two-pole armature winding. This excitation winding produces a four-pole m.m.f. (four-pole magnetization) with the polarity sequence N-S-N-S.

Four-pole armature winding of the amplifier ensures the required voltage at the output, U_{out}, and is designed in accordance with the load parameters.

The electric circuit of the amplifier may be represented by the equivalent circuit of two machines (Fig. 1). The first, a two-pole machine, is separately excited and ensures the amplification of the first stage. The four-pole excitation winding acts as a load for the first machine and ensures the second stage of amplification. Thus, the amplifier in question is a two-stage amplifier. The total amplification factor of the amplifier is equal to the product of the amplification factors of its two stages.

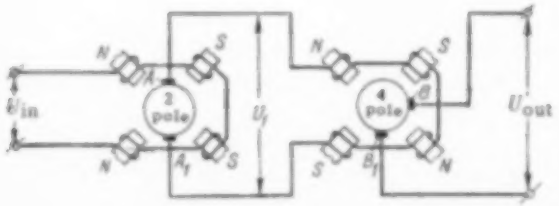

FIG. 1. The equivalent circuit of a two-stage amplifier.

Besides the above-mentioned windings, the amplifier may also have two or four-pole windings for self-excitation. The presence of this winding increases the total amplification factor.

The complete diagram of the electric and magnetic circuit of a two-commutator rotary amplifier is shown in Fig. 2.

For a better understanding of the principle of a two-stage amplifier and its properties, it is necessary to consider the mutual influence of a two-pole and four-pole m.m.f., acting in a single magnetic circuit.

A four-pole excitation system has no influence on the e.m.f. of the two-pole armature winding, since the sides of the sections of this winding are situated by poles of the same polarity.

The two-pole m.m.f. produces a distortion in the distribution of the four-pole m.m.f. The degree of distortion depends on the magnitude of the two-pole m.m.f. and on the degree of saturation of the magnetic circuit of the amplifier. Since, in a two-stage amplifier, the m.m.f. of the control winding (two-pole m.m.f.) is usually very small in comparison with the four-pole m.m.f., its influence is insignificant.

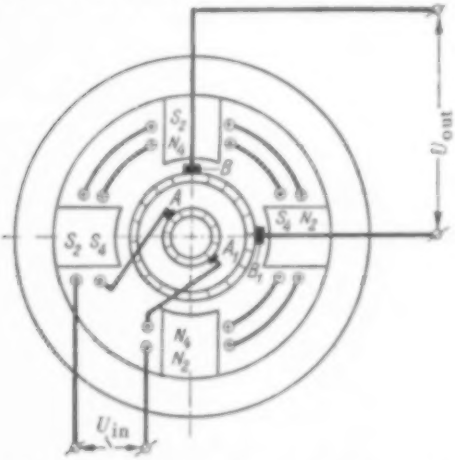

FIG. 2. Electric and magnetic networks of a two-stage amplifier.

But even insignificant distortion of the four-pole m.m.f. under the influence of two-pole excitation necessitates the use of the wave-winding of the armature for a four-pole system, and this excludes the formation of equalizing currents.

In the case of saturation of the magnetic circuit of the machine, the influence of the two-pole magnetic system on the e.m.f. of the four-pole armature winding is practically removed.

Commutation

The presence of two commutators in a two-stage amplifier should be considered as a disadvantage in comparison with other types of rotary amplifiers. Nevertheless, the conditions of current commutation of the armature windings of the amplifier may be quite satisfactory. The current commutation of the two-pole armature winding is practically independent of the load, and usually does not require the addition of interpoles in a two-pole magnetic system.

Since the power of the two-pole armature winding is comparatively small, "commutation by resistance" is quite satisfactory. For a four-pole armature winding only two interpoles can be provided, just as for an ordinary four-pole small-power machine. In this machine two interpoles of the four-pole magnetic system are placed on the line $n - n'$ (Fig. 3), perpendicular to the two-pole magnetic neutral axis $m - m''$. If an interpole mechanism is required in the two-pole magnetic system, then these two poles are established on the two-pole magnetic neutral $m - m'$.

In this case the excitation of the interpoles along the axis $m - m'$ should be from a common source; i.e., their excitation windings should be fed by the current

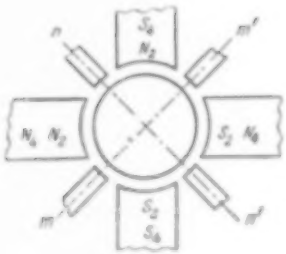

FIG. 3. Magnetic network of a two-stage amplifier with interpoles.

of the four-pole armature winding.

The calculation of the m.m.f. of the amplifier interpoles does not differ from analogous calculations of the ordinary d.c. machines. It is necessary to point out that the presence in a two-stage amplifier of a separate armature winding for each amplification stage simplifies the commutation problem, since there is the possibility of the choice of the voltage of the two-pole armature winding, and consequently of the winding parameters.

The three-stage amplifier

The two-commutator rotary amplifier may be made as a three-stage amplifier, as diagramatically shown in Fig. 4.

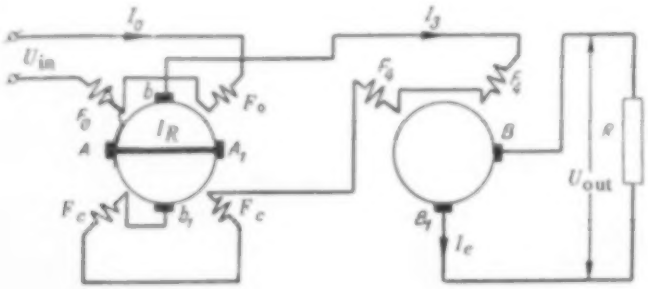

FIG. 4. The equivalent circuit of a three-stage amplifier.

The three-stage amplifier differs in construction from the two-stage machine in that an additional pair of brushes, b - b_1, is fixed on the commutator of the two-pole armature winding, these brushes being placed perpendicular to the line of the brushes A - A_1. Brushes A - A_1 are placed, as stated above, on the two-pole magnetic neutral axis (m.n.a.). Brushes A - A_1 are short-circuited. Two windings are connected to the brushes b - b_1, the winding of the four-pole excitation system F_4 and the compensation winding F_C, which is fixed on the same cores as the control winding F_0. The role of the four-pole excitation winding F_4 of the amplifier has already been discussed; the action of the compensation winding is to compensate for the armature reaction, occuring along the longitudinal axis of the two-pole system. From the circuit of a three-stage amplifier, shown in Fig. 4, it is clear that the properties of a two-stage amplifier with a cross-field are used for the first two stages of amplification. The flux of the control winding F_0, produced by the current I_0, induces an e.m.f. in the two-pole armature winding, which induces a current I_2 in the network of the short-circuited brushes A - A_1. The current of the two-pole armature winding induces a flux in the direction of the cross-axis of the two-pole magnetic system, which in its turn induces an e.m.f. in the same armature winding.

Hence, a current I_3 is produced in the network of brushes b - b_1. The current I_3 induces m.m.f. F_4 which determines the output voltage U_{out} and the load current I_e.

The total power amplification factor of a three-stage amplifier is:

$$K_p = \frac{U_{out} \cdot I_e}{U_{in} \cdot I_o}$$

In a three-stage amplifier, the addition of two brushes on the commutator, and of the compensation winding F_c on the poles, does not increase the size of the machine in comparison with a two-stage amplifier. This also permits a considerable increase of the power amplification factor.

The work of a two-stage two-commutator rotary amplifier in transient conditions

The analysis of transient conditions in a two-stage amplifier of the type in question is carried out, certain assumptions being made. These are usually accepted for the analysis of transient conditions in multi-stage amplifiers.

The initial equations for a two-stage amplifier, when a constant voltage U_{in} is applied to one of its control windings, are:

(a) equations for the balance of e.m.f.'s:

$$U_{in} = i_1 r_1 + w_1 p\Phi_1;$$
$$c_1 n\Phi_1 = r_2 i_2 + w_2 p\Phi_2;$$
$$E_{out} = c_2 n\Phi_2;$$

(b) conditions for the balance of m.m.f.'s:

$$a_1\Phi_1 = i_1 w_1;$$
$$a_2\Phi_2 = i_2 w_2,$$

where i_1 – the current in the control winding, i_2 – the current in the four-pole field winding, w_1 and w_2 – the number of turns in the two- and four-pole field windings, r_1 and r_2 – resistances of the two- and four-pole field windings; c_1 and c_2 – constants of the amplifier, a_1 and a_2 – factors of proportionality between m.m.f. and the magnetic flux, Φ_1 and Φ_2 – two- and four-pole magnetic fluxes, E_{out} – e.m.f. at the output of the amplifier.

The solution of this equation gives:

$$E_{out}(p) = U_{in} \frac{k_1 k_2}{(1 + pT_1)(1 + pT_2)},$$

where $k_1 = \frac{w_1 c_1 n}{r_1 a_1}$ – amplification factor of the first stage;

$k_2 = \frac{w_2 c_2 n}{r_2 a_2}$ – amplification factor of the second stage;

$T_1 = \frac{w_1^2}{a_1 r_1}$ – time constant of the two-stage field network;

$T_2 = \frac{a_2^2}{a_2 r_2}$ — time constant of the four-pole field network.

Thus, a two-stage amplifier behaves as an inertial amplifying link of the second order and is characterized by the equation analogous to the equation of a rotary cross-field amplifier with a full compensation of the axial armature reaction.

Tests of an experimental model of an amplifier

For the experimental investigation of fundamental working chacteristics of a two-stage amplifier a special experimental model of such an amplifier was made in the electric machines laboratory of the Leningrad Institute of Railway Transport Engineers.

The amplifier has the following nominal chacteristic: $P = 2$ kW; $U = 50$ V; current $I = 40$ A; $n = 2850$ r.p.m. The amplifier was made on the base of a PN-17.5 d.c. machine. On the armature, on its two sides, are fixed two commutators, one of which is connected to the two-pole and the other to the four-pole winding. The fundamental data of the amplifier are given in the appendix.

The static and dynamic characteristics were recorded during the test.

Fig. 5 shows the characteristics of the no-load running of the first stage (curve 1), and of the second stage (curve 2). From these characteristics, the saturation of the magnetic system of the amplifier and its zone of insensitivity can be deduced.

In Fig. 6 a characteristic of the amplifier on load is shown, recorded at a constant resistance of the load $R_l = 1.6\,\Omega$. From these characteristics the dependence of the poweraamplification factor on R_{out} is obtained (Fig.7). It is necessary to point out that the power amplification factor of this experimental model of a two stage amplifier is comparatively small, owing to defects in the manufacture of the experimental model.

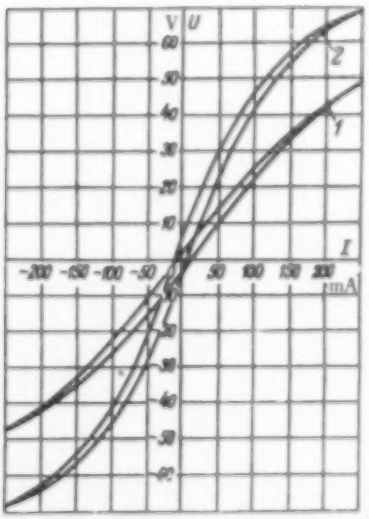

FIG.5. Characteristics of no-load running of the first (1) and second (2) stages of the test-model of the amplifier.

Preliminary tests of a three-stage amplifier have shown that its power amplification factor, in comparison with a two-stage amplifier, is increased considerably more than 20 times.

The dynamic characteristics were determined by measuring the rate of increase of the voltage at the output of the amplifier, after connecting one of its control windings to a source of constant voltage.

Fig. 8 shows the oscillograms of the voltage variation at the output of the amplifier, in no-load conditions, and during its work on load. Control power was equal to 2 W. The rate of voltage-increase per second was more than five times the nominal value of the voltage. This figure is quite permissible for many systems of automatic control, in which similar amplifiers can be used.

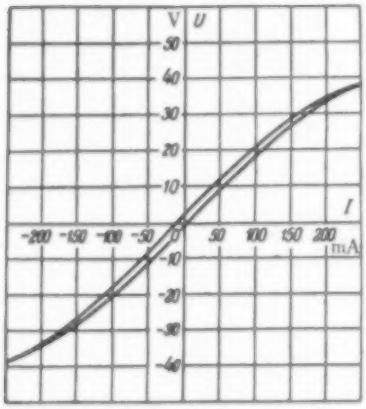

FIG. 6. The load characteristics of the test-model of the amplifier taken at a constant resistance $R_l = 1.6\ \Omega$

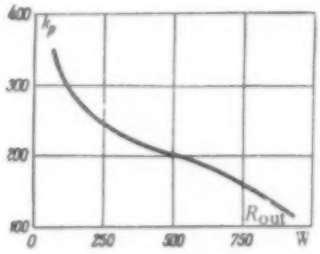

FIG. 7. Power amplification factor K_p as a function of the power at the output of the amplifier.

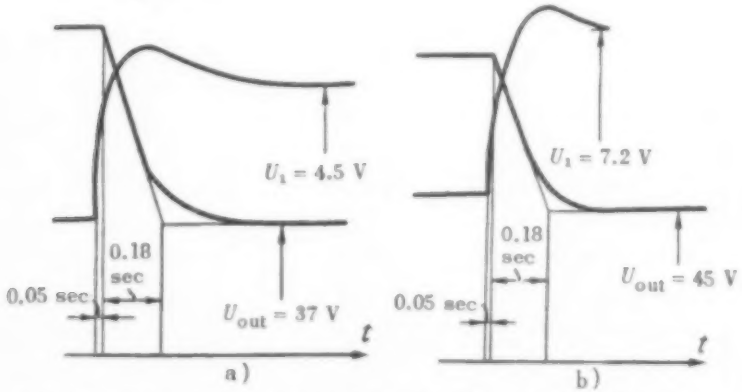

FIG. 8. Oscillograms of the amplifier voltage in no-load conditions (a), and under load (b).

(a) $\left(\frac{dU_1}{dt}\right)_{max} = 90$ V/sec.; $\left(\frac{dU_{out}}{dt}\right) = 250$ V/sec.

(b) $\left(\frac{dU_1}{dt}\right)_{max.} = 144$ V/sec.; $\left(\frac{dU_{out}}{dt}\right) = 205$ V/sec.

U_1 – voltage at the output of the first stage; U_{out} – voltage at the output of the second stage.

Conclusions

(1) The power obtained from such a machine equals up to 50 – 55 per cent of that of a machine of the normal type and of the same size.

(2) The specific features and the most important problems in the design of an

amplifier are:

(a) determination of the optimum ratio of the volumes of the armature slot, occupied by the first and the second stage windings;

(b) the determination of the optimum ratio of the areas of the slot opening occupied by the field windings of the corresponding stages of an amplifier. Obviously, the static and dynamic properties of an amplifier will depend on these ratios and on the degree of utilization of its size for the power supplied.

For better determination of the qualitative induces of the amplifiers of the type in question, in comparison with the figures for other types, a more detailed analysis and comparative tests of different amplifiers are needed.

Such investigations will enable classification of the different types of amplifiers according to the requirements imposed upon them in different systems of automatic control. A very important advantage of the amplifiers in question, in comparison with amplifiers with an axial field, is the possibility of their use in conditions of variable load resistance, without any additional mechanisms.

1958

Appendix

Fundamental numerical data

Armature diameter $D_a = 135$ mm; the length of the armature $l_a = 135$ mm; the number of slots $Z = 20$; the number of commutator segments for a four-pole system ($2p = 4$) $K_1 = 59$; for a two-pole system ($2p = 2$), $K_2 = 60$. Air gap under the main poles $\delta = 1.5$ mm.

The data of the two-pole armature winding

Two-pole armature winding is laid in the lower part of the slot and occupies 38 per cent of its volume. Number of conductors in a slot – 24; the number of windings in a section $w_s = 4$; area of the cross-section of the winding $q = 1.21$ mm²; slot pitch – $y_s = 10$; armature winding resistance – $R_a = 0.90\ \Omega$.

Four-pole field winding of the amplifier

Number of turns per pole $w_4 = 72$; area of copper cross-section of the winding $q_4 = 2.99$ mm²; winding resistance $R_4 = 0.93\ \Omega$; time constant $T_4 = 0.112$ sec.

First control winding

Number of turns per pole $w_{01} = 485$; area of the copper cross-section of the winding $q_{01} = 0.152$ mm²; winding resistance $R_{01} = 100\ \Omega$, time constant $T_{01} = 0.069$ sec.

Second control winding

Number of turns per pole $w_{02} = 485$; area of the copper cross-section $q_{02} = 0.152$ mm², winding resistance $R_{02} = 100\ \Omega$, time constant $T_{02} = 0.069$ sec.

Translated by S. Szymanski, Dipl. Ing.

REFERENCES

1. A. Vallini; Rotary amplifiers, *L'Energia, Elettrica* (1953).
2. M.G. Say (Editor); *Rotary amplifiers* (1954).

THE THEORY OF THE ELECTRICAL CIRCUIT FOR THE THREE-PHASE ORE-REDUCTION FURNACE*

N.A. MARKOV

Kuibyshev Industrial Institute

(Received 4 February 1957)

In the ore-reduction arc furnace the arcs burn under a layer of hard charge substances. The conducting charge produces a charge current circuit in the furnace, parallel to the arc. In addition, the ore-reduction furnace has a layer of slag and melt separating the arc from the pool of metal, and which is connected in series with the arc [1].

Fig. 1 is a representative diagram for the electrical circuit of an installation with a three-phase ore-reduction furnace. In this diagram the resistance of the arc, the charge and the layer are replaced by resistances, and the resistances of the supply circuit by resistances and inductive reactances. The resistances of the arcs and charge for the separate circuit phases are connected to two parallel star connexions. The furnace may also contain charge resistances connected in mesh between the electrodes of the separate furnace phases. This impedance mesh may be replaced by an equivalent star connexion, which is also connected in parallel with the arc resistance star connexions.

Both the arc resistances and those of the charge and the layer of melt alter during operation of the furnace.

When all the furnace phases are loaded equally and the circuit is symmetrical, the values characterizing the electrical working conditions of the furnace are linked by the following equations:

$$V = ir + L.di/dt + i_d R_s + u_d; \quad (1)$$

$$V = ir + L.\ di/dt + i_{sh} R_{sh}; \quad (2)$$

where V is the phase voltage of the circuit, i is the total electrode current, r is the supply circuit resistance, L is the supply circuit inductance, R_s is the layer resistance, R_{sh} is the charge resistance and u_d is the arc voltage; in the conditions in an ore-reduction furnace, this may be assumed not to depend on the current and to be linearly dependent on arc length.

* *Elektrichestvo* No. 1, 10 – 13, 1958 [Reprint Order No. EL 41].

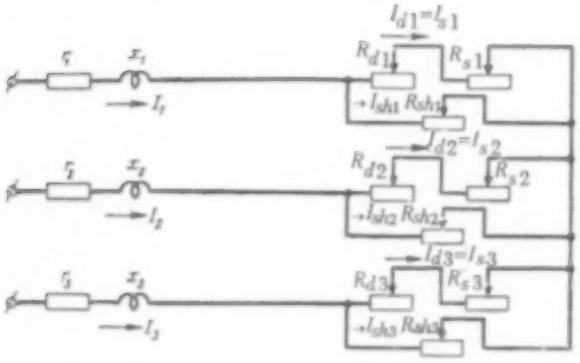

FIG. 1. Equivalent for a three-phase ore-reduction furnace electrical unit.

If there is no layer of melt ($R_c = 0$), the voltages between the ends of the arc and the charge are identical and remain unchanged in magnitude if the arc length is constant. Therefore, when the charge resistance alters and the arc length is constant, the total electrode current remains unchanged and all that occurs is redistribution of the current between the arc and the charge [1].

If there is no layer of melt ($R_c = 0$), the voltages between the ends of the arc and the charge are identical and remain unchanged in magnitude if the arc length is constant. Therefore, when the charge resistance alters and the arc length is constant, the total electrode current remains unchanged and all that occurs is redistribution of the current between the arc and the charge [1].

For the total electrode current, we have

$$i = i_d + i_{sh} = i_d + \frac{ud}{R_{sh}}, \tag{3}$$

and for the melt layer current:

$$i_s = i_d. \tag{4}$$

The curve for the voltage across the ends of the charge and of the arc, approximately equal to the furnace voltage, will, depending on time, in a given case be sinusoidal with a truncated top and small excitation and extinction spikes (Fig. 2).

The size of the angle $\alpha = \omega t_1$, which defines the moments of arc excitation and extinction, depends on the charge resistance and the charge current. The lower the resistance of the charge and the higher the current in it, the larger the angle α and also the interval of time between arc extinction and excitation.

It follows from the curves in Fig. 2, that the relationship between the currents in the charge for different charge resistances and constant arc voltage is determined by the equation:

$$\frac{I_{sh1}}{I_{sh2}} = \frac{\sin \omega t_1}{\sin \omega t_2}. \tag{5}$$

If the arc voltage is of square form, the arc current will be:

$$i = \frac{V}{z}\sin(\omega t + \varphi - \psi) + \frac{u_d}{r}\left(\frac{2e^{-\frac{r}{L}t}}{1+e^{-\frac{r\pi}{\omega L}}} - 1\right). \qquad (6)$$

The arc current curve is practically sinusoidal, particularly in the three-phase circuits of an ore-reduction furnace with no neutral conductor, since there are no third and multiples-of-three harmonic components in the current curve for a symmetrical circuit.

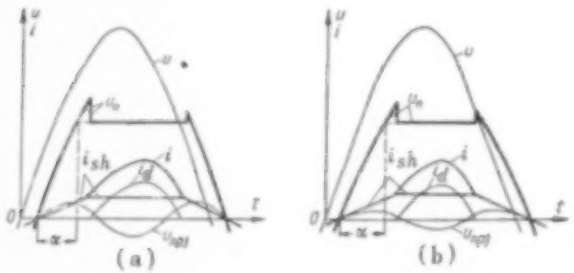

FIG. 2. Curves for furnace voltages and currents for different charge resistances. (a) for $R_{sh}1$; (b) for $R_{sh}2 < R_{sh}1$.

The curve for the current in the charge during arc burning is of square form, similar to the arc potential curve; when the arc is extinguished, the curve for the current in the charge is of sinusoidal form [2]. The curve for the total current may be obtained as the sum of the arc and charge current curves (Fig. 2).

Let us resolve the curve for the voltage across the ends of the arc and charge into Fourier series.

Between 0 and α the change in this curve is expressed by the equation

$$y_1 = mA\sin x$$

and between α and $\frac{\pi}{2}$ by the equation

$$y_1 = A,$$

where A is the height of the square part of the curve and mA is the sine curve amplitude of the sinusoidal part of the curve; it follows that the amplitudes of the harmonic components are determined from the equation

$$A_k = \frac{4}{\pi}\left(\int_0^{\alpha} mA\sin x\sin kx\,dx + \int_{\alpha}^{\frac{\pi}{2}} A\sin kx\,dx\right) =$$

$$= \frac{4A}{\pi}\left[\frac{m}{2(1-k)}\sin(1-k)\alpha - \frac{m}{2(1+k)}\sin(1+k)\alpha + \frac{1}{k}\cos k\alpha\right],$$

and that the voltage across the ends of the charge and the arc may be represented as follows:

$$u_n = \frac{4A}{\pi}\left[\left(-\frac{m}{4}\sin 2\alpha + \cos\alpha\right)\sin x + \left(\frac{m}{4}\sin 2\alpha - \right.\right.$$
$$- \frac{m}{8}\sin 4\alpha + \frac{1}{3}\cos 3\alpha\Big)\sin 3x + \Big(\frac{m}{8}\sin 4\alpha - \qquad (7)$$
$$\left.\left. - \frac{m}{12}\sin 6\alpha + \frac{1}{5}\cos 5\alpha\right)\sin 5x + \ldots\right].$$

The presence of a layer of melt alters the correlation between the electrical values of the circuit, and changes the aspect of the curve for the voltage across the charge.

In this case the voltage across the charge (the furnace voltage) will be:

$$u_n = u_d + i_d R_s \tag{8}$$

and the current in the charge will be:

$$i_{sh} = u_n / R_{sh} = (u_d + i_d R_s) / R_{sh} \tag{9}$$

If the resistance of the charge alters at the same time as the currents in the charge and in the arc are redistributed, the furnace voltage also will change, and so in consequence will the total current.

The presence of a layer of melt can therefore be gauged from the changes in furnace voltage where there are changes in the charge resistance, for example when charging the furnace. If, for example, the resistance of the charge is increased for fixed electrode positions, this will reduce the current in the charge and increase the current in the arc, and will in consequence raise the furnace voltage, according to equation (8), from u_{n1} to u_{n2}. At the same time, with circuit voltages and supply circuit resistances unchanged, the total current will drop from I_1 to I_2 according to the equation

$$u_n = -Ir + \sqrt{(V^2 - I^2 x^2)} \tag{10}$$

The difference between these furnace potentials is:

$$u_{n1} - u_{n2} = (I_{d1} - I_{d2}) R_s = (I_1 - I_2 - I_{sh1} + I_{sh2}) R_s,$$

and in consequence

$$R_s = (u_{n1} - u_{n2}) / (I_1 - I_2 - I_{sh1} + I_{sh2}) \tag{11}$$

Since the curve for arc current is almost sinusoidal for a symmetrical circuit, the curve for voltage drop in the layer will also be almost sinusoidal. Therefore the curve for furnace voltage against time will, disregarding the arc excitation and extinction spikes, be depicted by two sine curves of different amplitudes and periods: the sine curve for voltage drop in the charge and that for voltage drop in the layer (Fig. 3).

Let us resolve this curve into Fourier series. Since the alteration in this curve between 0 and α is expressed by the equation:

$$y_1 = mA \sin x$$

and between α and $\pi/2$ by the equation:

$$y_2 = A + nA \sin lx,$$

where nA is the amplitude of the sine curve for voltage drop in the layer, and since $l = (\pi - 2\alpha)/\pi$, the relationship of the arc burning time interval to a half-cycle, therefore the amplitudes of the harmonic components are determined by the equation:

$$A_k = \frac{4}{\pi}\left[\int_0^{\alpha} mA \sin x \sin kx\, dx + \int_{\alpha}^{\pi/2} (A + nA \sin lx) \sin kx\, dx\right] =$$

$$= \frac{4A}{\pi}\left\{\frac{m}{2(1-k)}\sin(1-k)\alpha - \frac{m}{2(1+k)}\sin(1+k)\alpha + \frac{1}{k}\cos\alpha + \right.$$

$$+ \frac{n}{2(l-k)}\left[\sin(l-k)\frac{\pi}{2} - \sin(l-k)\alpha\right] -$$

$$\left. - \frac{n}{2(l+k)}\left[\sin(l+k)\frac{\pi}{2} - \sin(l+k)\alpha\right]\right\}.$$

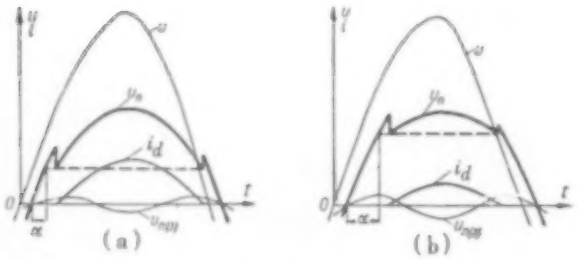

FIG. 3. Curves for furnace voltages for different layer and charge resistances. (a) for $R_s 1$; (b) $R_s 2 < R_s 1$.

Therefore the furnace voltage may be represented as follows:

$$u_a = \frac{4A}{\pi}\left\{\left\{\left[-\frac{m}{4}\sin 2\alpha + \cos\alpha \quad + \frac{n}{2(l-1)}\left(\sin\alpha + \sin\frac{2\alpha^2}{\pi}\right) - \right.\right.\right.$$

$$\left. - \frac{n}{l+1}\left[\sin\alpha - \sin 2\alpha\left(1 - \frac{\alpha}{\pi}\right)\right]\right\}\sin x \quad + \left\{\left[\frac{m}{4}\sin 2\alpha - \frac{m}{8}\sin 4\alpha + \frac{1}{3}\cos 3\alpha + \right.\right.$$

$$+ \frac{n}{2(l-3)}\left[\sin\alpha + \sin 2\alpha\left(1 - \frac{\alpha}{\pi}\right)\right] +$$

$$\left.\left. + \frac{n}{2(l+3)}\left[\sin\alpha + \sin 2\alpha\left(2 - \frac{\alpha}{\pi}\right)\right]\right\}\sin 3x +$$

$$+ \left\{\left[\frac{m}{8}\sin 4\alpha - \frac{m}{12}\sin 6\alpha + \frac{1}{5}\cos 5\alpha \quad + \frac{n}{2(l-5)}\left[-\sin\alpha + \sin 2\alpha\left(1 + \frac{\alpha}{\pi}\right)\right] - \right.\right.$$

$$\left.\left. - \frac{n}{2(l+5)}\left[\sin\alpha - \sin 2\alpha\left(3 - \frac{\alpha}{\pi}\right)\right]\right\}\sin 5x + \ldots\right\}.$$

Since the curve for total current is depicted, as is the furnace voltage curve, by two sine curves, both with a layer present and without a layer, the total current may

in both cases be represented by a series of the same type as (12), the value of A being equal to the ordinate up to a horizontal straight line drawn through the point of intersection of the sine curves (Fig. 3).

The shape of the total current curve in an ore-reduction furnace does not therefore depend solely on the shape of the arc potential curve, as is the case with a steel melting furnace, but also on the correlation of arc, charge and layer resistances.

If the circuit is three-phase with no neutral conductor, as is the case in a three-phase ore-reduction furnace, with a symmetrical circuit there are no third and multiples-of-three harmonic components in the current curve.

Where the circuit is non-symmetrical, third and multiples-of-three harmonic current-components appear in the circuit even where there is no neutral conductor.

For example, if the arc lengths and potentials differ in individual phases of the circuit, currents with third and multiples-of-three harmonics will pass in these phases, their values being determined from the equations:

$$I_{(3\ldots)1}=(u_{(3\ldots)1}-u_{(3\ldots)0})\,y_1;\qquad I_{(3\ldots)2}=(u_{(3\ldots)2}-u_{(3\ldots)0})\,y_2;$$

$$I_{(3\ldots)3}=(u_{(3\ldots)3}-u_{(3\ldots)0})\,y_3; \tag{13}$$

$$U_{(3\ldots)0}=\frac{u_{(3\ldots)1}\,y_1+u_{(3\ldots)2}\,y_2+u_{(3\ldots)3}\,y_3}{y_1+y_2+y_3},$$

where $u(3\ldots)1$, $u(3\ldots)2$ and $u(3\ldots)3$ are the voltages of the third and multiples-of-three harmonics of the first, second and third phases, and y_1, y_2, and y_3 are the conductivities of the separate phases, including the arc conductivities.

These currents will supplement the currents for the separate phases and distort the current curves of these phases.

The third harmonics will reach their maximum during two-phase short-circuiting of arcs in operation, when $u(3\ldots)2 = 0$, $u(3\ldots)3 = 0$ and the phase currents for $y = y_1 = y_2 = y_3$ are as follows:

$$I_{(3\ldots)1}=\frac{2}{3}u_{(3\ldots)1}\,y;\qquad I_{(3\ldots)2}=\frac{1}{3}u_{(3\ldots)1}\,y;\qquad I_{(3\ldots)3}=\frac{1}{3}u_{(3\ldots)1}\,y. \tag{14}$$

The determination of the size of the voltage between the neutral points of a furnace and furnace transformer with respect to the resistances of the charge and the layer is of practical interest, since this voltage can easily be measured in a working furnace and used for determining the resistance of the charge.

This voltage is formed by third and multiples-of-three harmonic voltage components and occurs where there are electric arcs in a circuit even when the circuit is completely symmetrical.

Its value is arrived at from the equation:

$$u_0=\sqrt{u_3^2+u_9^2+u_{15}^2+\ldots}, \tag{15}$$

where u_3, u_9, u_{15} etc. are the third, ninth, etc. voltage components for different circuit phases.

The form taken by the curve for this potential depends on the shape of the furnace potential curve.

Its value for different correlations between charge, arc and layer resistances may be calculated by the equations given above.

Fig. 4 shows curves for the relationship between this voltage and the charge current, drawn on the basis of calculations made for different charge and layer resistances. We can see that as the charge current increases the voltage of the third and multiples-of-three harmonics decreases, while the reduction follows different courses depending on the resistance of the layer.

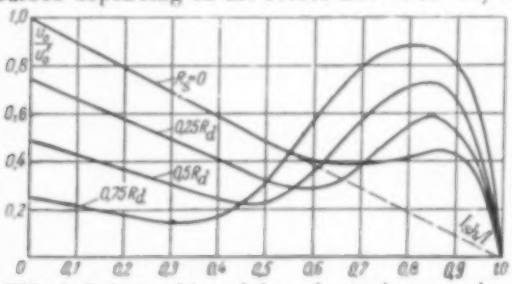

FIG. 4. Relationships of the voltages between the furnace and transformer neutral points to the charge current for a symmetrical circuit.

When the charge current is varied between 0 and 60 per cent of the total current, i.e. within the charge-current limits encountered in practice, the relationship of the voltage between the furnace and transformer neutral points, where no layer is present, is very close to linear and may be expressed as:

$$u_0 = u_0'(1 - I_{sh}/I), \qquad (16)$$

where u_0' is the voltage between neutral points without a charge ($R_{sh} = \infty$, $I_{sh} = 0$), and I = the total electrode current.

If there is no charge, then since the arc voltage curve is of square form, the voltage value u_0' will be one third of that at the arc ends. The arc voltage may be measured in the furnace when there is no layer, or may be calculated by equation (10) from the measured total furnace current.

The u_0 line can easily be drawn from equation (16) through two points: (a) the first point: $I_{sh} = 0$, $u_0 = \frac{1}{3} u_d$; (b) the second point: $I_{sh} = I$, $u_0 = 0$.

The curves in Fig. 4 and equation (16), may be used for determining values for charge resistance from electrical instrument measurements.

Fig. 5 is a circuit for the connexion of the electrical measuring instruments required for the determination of charge and layer resistances in a furnace.

To determine the charge resistance, where the furnace is symmetrically charged the voltage between the neutral points, the total current and the furnace potential must be measured. The charge current and charge resistance are determined from the upper curve in Fig. 4 by the equation:

$$R_{sh} = u_n/I_{sh}. \qquad (17)$$

The charge current may also be calculated from the equation:

$$I_{sh} = (1 - u_0'/\frac{1}{3}u_n)\, I. \tag{18}$$

If there is no charge, the resistance of the layer is determined from the readings of a voltmeter connected between the neutral points of furnace and transformer, by the well-known equation:

$$R_s = (u_n - 3u_0)/I. \tag{19}$$

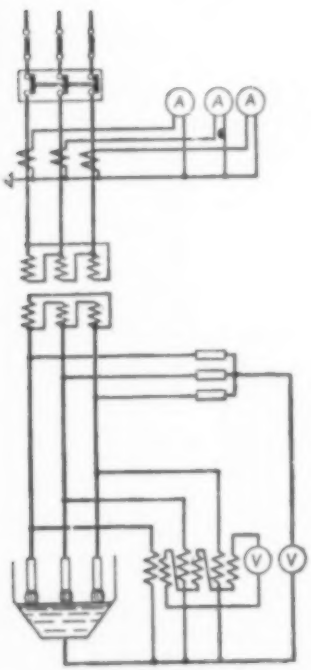

FIG. 5. Diagram for measuring charge and layer resistances.

However, where a charge is present, the resistance of the layer cannot be determined by this method, since the value of the potential u_0 depends on the charge resistance. In this case, if the charge resistance has been determined, the charge current can be calculated, and the resistance of the layer may be determined from the curves in Fig. 4 for a measured value of u_0 and the calculated charge current. Charge and layer resistances may only be determined by this method for voltage u_0 where the circuit is fully symmetrical and the furnace charging uniform.

Conclusions

(1) The non-sinusoidal nature of the curves for the furnace potential and the current in the electrical circuits of ore-reduction furnaces caused by the existence of charge and layer resistances has features distinguishing these curves from those for the electrical circuits in steel-melting furnaces.

(2) The problems of the theory of ore-reduction furnace electrical circuits which have been analysed enable us to increase the accuracy of the procedure for calculating these circuits; it becomes possible to calculate working currents and operating short-circuit currents, furnace characteristics and supply circuit impedances, the sinusoidal nature of the current curves being allowed for.

(3) The method proposed for determining the charge and layer resistances enables us to determine them from readings given by instruments set up outside the furnace.

Translated by J.H. Dixon

REFERENCES

1. S.I. Tel'nyi; Regulirovanie elektricheskovo rezhima raboty rudnotermicheskikh pechei (Control of the electrical conditions in operating ore-reduction furnaces), *Sborn. nauch. trud. Kuibyshevskovo industrial'novo inst.* No. 3 (1950).
2. S.I. Tel'nyi and I.T. Zherdev, Shuntirovannaia duga v elektricheskikh ferrosplavnykh pechakh (The shunted arc in electric ferroalloy furnaces). *Teor. i prakt. metallurg.* No. 9 (1937).

THE UNIVERSAL CHARACTERISTICS OF THE DYNAMIC BRAKING OF ASYNCHRONOUS MOTORS*

V.I. KLIUCHEV

Moscow Power Institute

(Received 29 April 1957)

The existing methods used for calculating the mechanical characteristics of the dynamic braking of asynchronous motors according to a scheme with separate excitation from a d.c. circuit are founded on the use of the motor magnetization curve $E_1 = f(I\mu)$. Use of the magnetization curve is made necessary by the saturation of the magnetic circuit which takes place in the great majority of cases in practice.

The saturation is allowed for in analytical methods of calculation by the use of a non-linear or piecewise-linear approximation of the magnetization curve. As a rule sufficient closeness of approximation over a wide range of magnetizing current values is not obtained, nor at the same time are correlations convenient for the calculation produced. Analytical methods of calculation have not therefore been applied in practice.

The graphic analysis method of calculation [2-4], which is based on direct use of the motor magnetization curve and equations (1) and (2) below, is at present the method most widely used in practice:

$$I_E^2 = \frac{E_1^2}{x_\mu^2}\left[1 + x_\mu \frac{x_\mu + 2x_2'}{\frac{R_2'^2}{s^2} + x_2'^2}\right]; \qquad (1)$$

$$M = \frac{3}{9{,}81\omega_0} \frac{E_1^2}{\frac{R_2'^2}{s^2} + x_2'^2} \frac{R_2'}{s}, \qquad (2)$$

where I_E is the rated stator alternating current phase in amperes, equivalent to the direct current I_n, relating to the generated magnetizing force of the stator winding; E_1 is the atator phase e.m.f., in volts; I_μ is the magnetizing current in amperes; $x_\mu = E_1 / I_\mu$, the inductive reactance of magnetization, in ohms; x_2' is the reduced

* *Elektrichestvo* No. 1, 14 – 18, 1958 [Reprint Order No. EL 42].

rotor winding leakage inductive reactance, in ohms; $R_2' = r_2' + R_{d2}'$, the full reduced resistance of the rotor phase, in ohms; r_2' is the reduced resistance of the rotor winding phase, in ohms; $s = \omega/\omega_0$, the slip in dynamic braking; and M is the moment, in kg m.

The values of E_1 being known, $x\mu$ is determined from the magnetization curve; the slip is then found from equation (1). The corresponding value for the moment M is determined from equation (2). Calculations are made for points, and to draw the mechanical characteristic $M = f(s)$ takes a great time, particularly when calculating the static characteristics of dynamic braking in automatic control systems.

In this connexion, efforts to obtain universal mechanical characteristics in relative units, generalized for the greatest possible number of series of asynchronous motors, are of great practical interest. Much work was done in this direction at the Moscow Power Institute [2, 3].

It was shown to be possible, on the basis of analysis of the magnetization curves for isolated sizes in various series, to generalize the magnetization curves in relative units for motors in a given series to an accuracy of ± 5 per cent; it was found to be impossible to generalize the magnetization curves for different series with acceptable accuracy. At the same time, analysis of the parameters showed that it is not possible to generalize either the basic parameters or various combinations of them, even for motors in a single series, let alone for those in every series. Thus attempts to simplify the calculations by using universal curves have not yet led to the required results.

Analysis of the works indicated draws one to conclude that the relative units system adopted at present [2, 4] must be renounced if we are to obtain universal curves which are suitable for calculations of dynamic braking for motors in different series. A relative units system must be found which, when employing universal characteristics, will allow us to take into account the features of a particular machine both regarding its parameters and its magnetization curve. The first step in this direction was taken by Prof. A.T. Golovan in his published works. Dynamic braking characteristics are adduced in [1] in relative units which make it possible to take a number of specific motor characteristics into account; the applicability of these characteristics however, as the author remarks, is limited to low-power motors. The present article puts forward universal characteristics which can be used in the majority of cases in practice.

Generalization of the magnetization curves is based on a system of relative units in which the open circuit current I_0, for $V_{1\phi} = V_{1\phi N}$, and the stator phase e.m.f. $E_{1\phi 0}$ corresponding to this current are taken as the basic quantities of the magnetizing current and e.m.f. Here the difference between the magnetization curves for separate sizes and series is governed on the one hand by discrepancy in the magnetization curve shapes, and on the other hand by different levels of saturation of the magnetic circuit at specified voltage. It is impossible to eliminate the difference between the shapes of the characteristics by selecting other basic quantities; there are however grounds for supposing that this difference may not be important. The influence of the second feature can be fully eliminated if we take as basic quantities for each

specific motor the rated e.m.f. E_{1p} and the rated open circuit current I_{0p} corresponding to that e.m.f. in conditions where the magnetic circuit is saturated to an equal degree:

$$E_{1p} = b_e E_{1\phi 0}; \; I_{0p} = b_i I_0. \tag{3}$$

Where a magnetization curve for $e = f(i\mu)$ exists which corresponds to the rated basic quantities, it is possible to proceed to the characteristic $e_p = f(i\mu_p)$ corresponding to the calculated basic quantities by using the following relationships:

$$e_p = \frac{E}{E_{1p}} = \frac{1}{b_e} e; \; i_{\mu p} = \frac{I_\mu}{I_{0p}} = \frac{1}{b_i} i_\mu. \tag{4}$$

Thus universal dynamic braking characteristics calculated on the basis of some magnetization curve assumed as basic, may be used for specific motors with an accuracy determined by the degree to which the shapes of the magnetization curves coincide. The magnetization curve for the motor in question may serve as the basis for the selection of the coefficients b_e and b_i. However, in the majority of cases the person performing the calculations is not in possession of these data, and to obtain them is a very laborious process. The conclusion mentioned above that the $e = f(i\mu)$ magnetization curves can be generalized for motors of individual series is therefore of great practical interest.

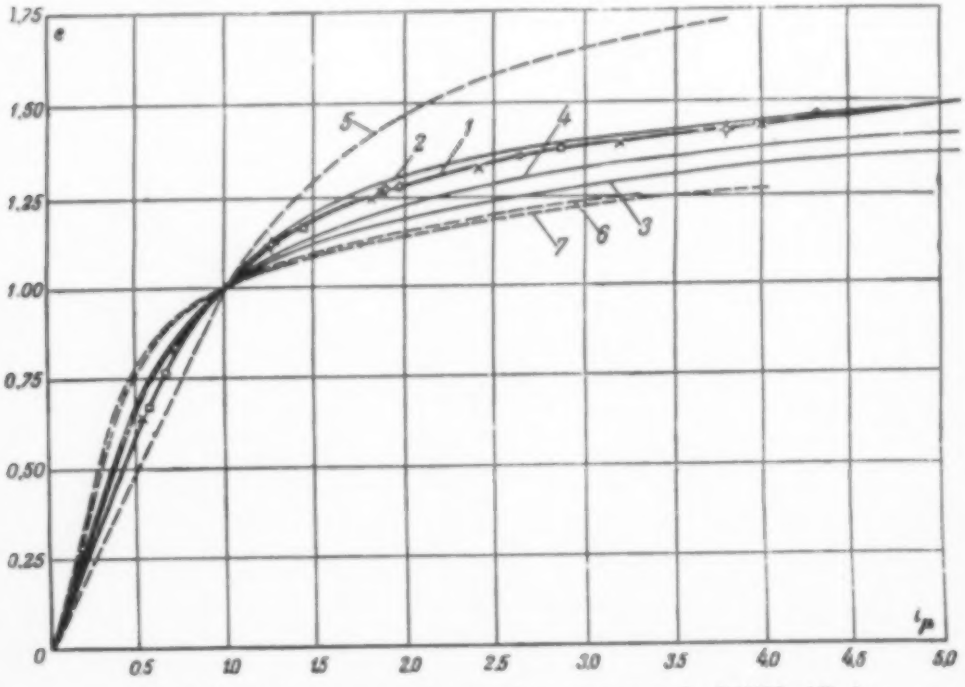

FIG. 1. Magnetization curves for asynchronous motors. 1 - FAMSO, AT, A; 2 - AM, DA; 3 - MT; 4 - MTK; 5 - KT-55/1003; 6 - AK61-6; 7 - AK61-4. ———— generalized relationships; — — — — relationships obtained experimentally.

1958

Generalized $e = f(i\mu)$ curves for series MT, MTK, AM [2] and FAMSO,DA, AT and A [3] are shown in Fig. 1. The $e = f(i\mu)$ curve may be used to advantage as the basic magnetization characteristics for FAMSO, AT and A series motors, the curve being common to this group of series. The values of the coefficients b_e and b_i selected from a state of equal saturation are set out in Table 1.

TABLE 1.

	FAMSO AT & A	DA, AM	MT	MTK	KT-55/1003	AK 61-1, AK 61-6
b_e	1.00	1.03	0.86	0.93	1.30	0.79
b_i	1.00	1.06	0.70	0.84	1.52	0.50

Points on the $e_p = f(i\mu_p)$ curves, calculated on the basis of equations (4) using the coefficients set out in Table 1, are plotted in Fig. 1. Over the whole range of magnetizing current these points lie in practice on the $e = f(i\mu)$ curve taken as the basic curve; this confirms that universal characteristics calculated from a basic curve can be used with equal accuracy for motors of all series enumerated.

Series AK and KT, whose generalized curves are lacking, are represented as examples by the experimental magnetization curves for the AK 61-4, AK 61-6 and KT-55/1003 motors. The values of b_e and b_i used for calculating the corresponding points on the $e_p = f(i\mu_p)$ curves for these motors are given in Table 1. These curves also practically coincide with the basic characteristic $e = f(i\mu)$. Thus, when the appropriate basic quantities are selected, on the one hand the limits within which the magnetization curves can be generalized become wider and on the other hand calculations from universal dynamic braking characteristics, where a magnetization curve exists for a given type of machine, become more accurate.

We will adopt the following basic unit system from now on:

$$e_p = \frac{E_1}{b_e E_{1\varphi 0}}; \quad i_{\mu p} = \frac{I_\mu}{b_i I_0}; \quad x_{\mu d} = \frac{e_p}{i_{\mu p}} = \frac{E_1}{b_e E_{1\varphi 0}} \times \times \frac{b_i I_0}{I_\mu} = \frac{x_\mu}{b_\mu x_0}; \quad i_E = \frac{I_s}{b_i I_0}; \quad x'_{2d} = \frac{x'_2}{b_\mu x_0}. \tag{5}$$

Using (5), equation (1) becomes:

$$i_E^2 b_i^2 I_0^2 = \frac{e_p^2 b_e^2 E_{1\varphi 0}^2}{x_{\mu d}^2 b_\mu^2 x_0^2} \times \left(1 + x_{\mu d} b_\mu x_0 \frac{x_{\mu d} b_\mu x_0 + 2x'_{2d} b_\mu x_0}{\frac{R_2'^2}{s^2} + x_{2d}'^2 x_0^2 b_\mu^2} \right).$$

From this we can obtain the following equation for the universal characteristic $e_p = f(i_E, s_0)$ by simple transformations

$$e_p^2 = \frac{i_E^2 x_{\mu d}^2}{1 + x_{\mu d} \frac{x_{\mu d} + 2x'_{2d}}{1/s_0^2 + x_{2d}'^2}}, \tag{6}$$

where $s_o = s/s_p$, the relative slip, and $s_p = R_2' / b_\mu x_o$, the calculated slip.

In a similar way we can obtain from equation (2) an equation for the universal characteristic $m = f(e_p, s_o)$:

$$m = \frac{s_o e_p^2}{1 + s_o^2 x_{2d}'^2}, \qquad (7)$$

where $m = M/M_p$, the relative moment value, and $M_p = 0.306/\omega_o b_e b_i \times I_\beta^2 x_o$, the calculated moment value in kg m.

With the aid of the magnetization curve, relationships (6) and (7) establish the link between the relative values for the moment m, the slip s_o and the direct current i_E for a given value of the parameter $x_{2}'_d$ tabulated in Table 2.

TABLE 2.

Series	$x_{2}'_d$	
	Minimum	Maximum
MT	0.045	0.10
FAMSO	0.035	0.07
DA	0.040	0.09
AT, AM	0.025	0.06

The values of x_{2d}' lie between 0.025 and 0.1, while the lower values correspond to high-speed high-power motors. Taking this into account and using equations (6) and (7) and the magnetization characteristic selected above, two groups of universal $m = f(s_o)$ characteristics were calculated for a constant i_E, these groups corresponding to the intermediate values of x_{2d}' of 0.04 and 0.08 (Fig. 2). Comparison of the curves corresponding to these values of x_{2d}' confirms that to disregard the value of x_2', as is recommended in a number of published works, for low and average power machines, may involve errors of 10-12 per cent in determining the moment. On the other hand it is evident that the groups of curves shown in Fig. 2 enable us to take the effect of this parameter sufficiently accurately into account.

The value of the stator current I_n, ensuring the specified maximum braking moment M_{max} for a motor may be determined from the universal characteristics $m_{max} = f(i_E)$, x_{2d}' being a constant, given in Fig. 3. For this purpose the relative value for the moment $m_{max} = M_{max}/M_p$ must be determined; the corresponding relative stator current i_E must then be found from the curves in Fig. 3.

The direct current magnitude is calculated from the equation

$$I_n = k_{sx} b_i I_o i_E,$$

where $k_{sx} = I_n/I_E$, a coefficient depending on the stator winding circuit diagram [1,4].

The $M = f(s)$ characteristic, where i_E is constant, is calculated from the corres-

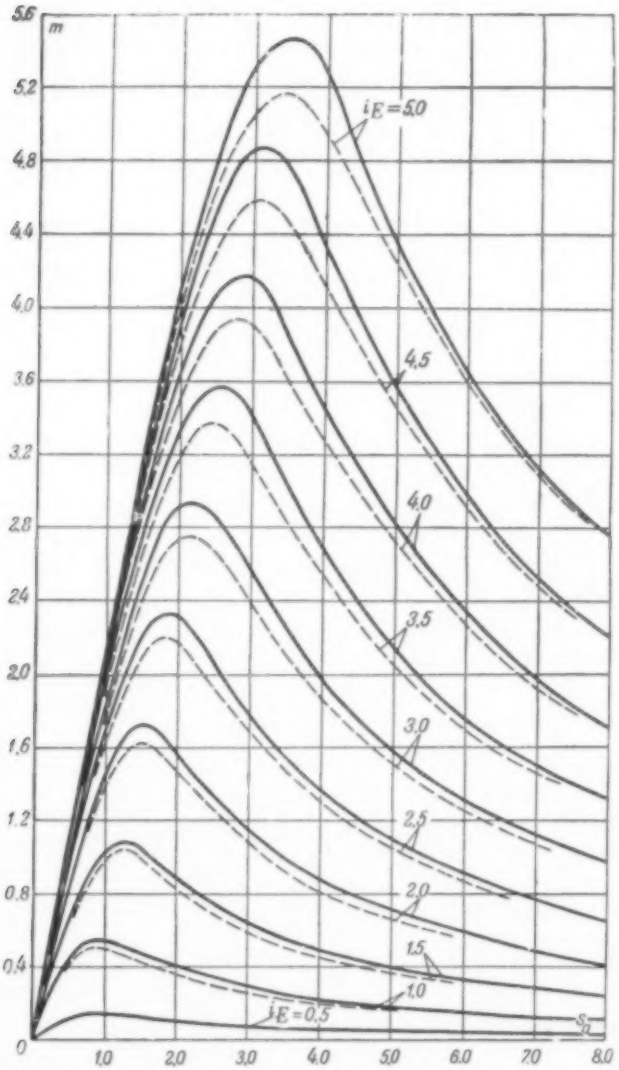

FIG. 2. Universal mechanical characteristics of the dynamic braking of asynchronous motors; —— for $x'_{1d} = 0.04$; – – – – for $x'_{1d} = 0.08$.

ponding universal $m = f(s_o)$ curve (i_E constant) from the following equations:

$$M = mM_p = m \frac{0{,}306}{\omega_0} b_e b_i I_0^2 x_0; \qquad s = s_o s_p = s_o \cdot \frac{R'_2}{b_\mu x_0}.$$

If it is necessary to determine the additional resistance of the rotor circuit R'_{d2}, for which the unknown characteristic passes through specific points M_1 and s_1, the corresponding slip s_{01} is determined, with the aid of the relative moment value $m_1 = M_1 / M_p$, from the universal characteristics.

The additional resistance R'_{d2} is calculated from the equation

$$R'_{d2} = b_\mu x_0 \frac{s_1}{s_{01}} - r'_2.$$

The static characteristics in control systems acting on the stator current magnitude during dynamic braking can be calculated in a minimum of time from universal characteristics. If for example $I_n = f(s)$, then this relationship can be expressed, using the correlations given above, in relative units by $i_E = f(s_0)$, and the points for the mechanical characteristics of control systems can be determined directly from the $m = f(s_0)$ curves (where i_E is constant).

It is necessary to dwell briefly on the recommendations met in technical literature, according to which the mechanical characteristic for the dynamic braking of an asynchronous motor can be deduced, for known values of maximum moment and the slip corresponding to them, from the well known simplified equation for the mechanical characteristics of asynchronous motors:

$$M = \frac{2M_{max}}{\frac{s}{s_{max}} + \frac{s_{max}}{s}}. \qquad (8)$$

Fig. 4 shows the $M = f(s)$ characteristics (where i_E is constant) for MT 31-6 motors, calculated using the universal curves according to the parameters for this motor given in [4], the characteristics obtained by equation (8) and also the corresponding experimental curves. We can see from comparison of the curves that saturation alters the shape of the characteristic; the error in determining the moment may reach 20-30 per cent for a given slip; calculations from equation (8) should there be considered to be approximate. The initial data necessary for calculation may be obtained from the curves given in Fig. 3.

Just as when using the initial graphic analysis method, it is necessary to know a number of motor parameters, r_1, r'_2 and I_0 in order to make calculations using universal curves. The effect of errors in the determination of each of these parameters on the accuracy of the calculations varies. For example, the value of r_1 is necessary for calculations for a d.c. circuit, and a certain amount of inaccuracy in its determination has no material effect. Errors in determining r'_2 involve inaccuracy in computation of the slip corresponding to a given moment value. The greater the additional resistance of the rotor circuit R'_{d2} the less the inaccuracy. Inaccuracy in determining the open circuit current I_0 involves the highest error in calculation, since it is used for determination of the moments M and the direct current I_n. Therefore calculations must be based, in important cases, on reliable motor parameter values, and their determination from catalogue data can only be recommended for rough calculations.

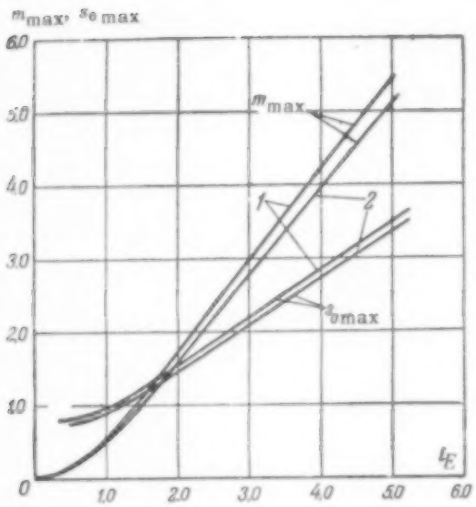

FIG. 3. The relationships $m_{max} = f(i_E)$ and $s_{\theta\,max} = f(i_E)$ for constant x'_{1d}. 1 - where $x'_{1d} = 0.04$; 2 - where $x'_{1d} = 0.08$.

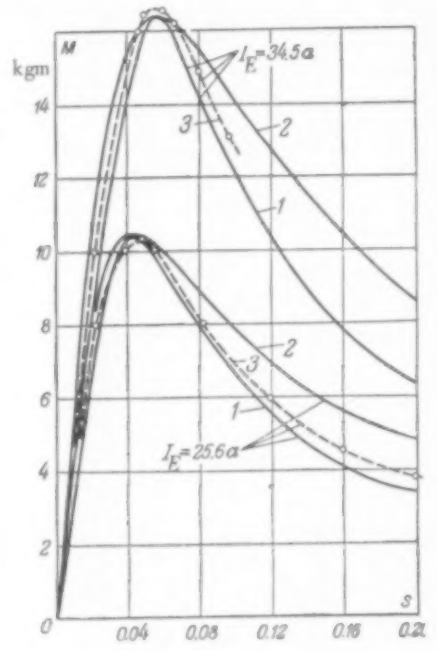

FIG. 4. The dynamic braking mechanical characteristics for the MT-31-6 motor. 1 - calculated from universal characteristics; 2 - calculated from equation (8); 3 - experimental curves.

When using the generalized magnetization curves given in Fig. 1, calculation of dynamic braking from universal characteristics cuts down the labour involved by many times and provides the same accuracy as is given by calculation from the initial equations (1) and (2) checked experimentally [2, 3]. At the same time, the great advantage of universal characteristics is that thay may also be used directly for the known magnetization curve for a specific motor or for a generalized curve for a series not given in Table 1. To do this, values for the coefficients b_e and b_i providing maximum coincidence between the $e_p = f(i_{\mu p})$ curve and the magnetization curve taken as basic must be selected. Thus the proposed curves can, in the majority of cases, in practice facilitate calculation of the static chacteristics of the braking of asynchronous motors.

Translated by J.H. Dixon

REFERENCES

1. A.T. Golovan; *Elektroprivod (Electric drive)*. Gosenergoizdat (1947).
2. A.T. Golovan, I.P. Barbarash, A.P. Kuvaeva and V.I. Yakovlev; *Issledovanie i razrabotka metoda rascheta dinamicheskovo tormozheniia asinkhronnykh dvigatelei (Investigation and development of a method for calculating the dynamic braking of asynchronous motors)*, Moscow Power Institute (1954).

3. A.T. Golovan, I.I. Levina, and V.I. Kliuchev; *Metodika rascheta dinamicheskovo tormozheniia shakhtnykh pod'emnykh mashin (Procedure for calculating the dynamic braking of mine hoist machines)*, Moscow Power Institute (1954).
4. S.N. Veshenevskii; *Raschet kharakteristik i soprotivlenii dlia elektrodvigatelei (Calculation of characteristics and impedances for electric motors)*, Gosenergoizdat (1954).

1958

ARCING SHORT-CIRCUITS ON 400 kV TRANSMISSION LINES AND METHODS OF DEALING WITH THEM*

A.S. MAIKOPAR and N.N. BELIAKOV

Central Scientific and Research Electrotechnical Laboratory,
Moscow Electric Station

(Received 19 September 1957)

On 400 kV transmission lines with a solidly earthed neutral, we have to expect mainly single-phase short-circuits to earth. As opposed to the lines with lower voltages, the restoring of the electric strength of the path of the arc after switching off the phase becomes more difficult on 400 kV lines because of appreciable influence of the current at the point of damage caused by capacitive and electromagnetic connections between the disconnected phase and the working phases. The supply current which will flow at the point of the fault, after automatically switching off the faulty section of the line, will sustain the electric arc for a certain time. The next reclosing can be done only after the extinction of the arc and restoration of the electric strength. This circumstance not only defines the placing of protective relays but also exerts an influence on the total lay-out of switchgear on the 400 kV lines. In particular, the problem of connecting shunting reactors directly to the line or through the circuit-breakers is strictly connected with the extinguishing of the sustained current arc. Several works are known dealing with research on the sustained current arcs [1-5]. Nevertheless, they do not give a clear idea of the range of sustained currents, for which it is possible to use single-phase automatic reclosing. As a result of these works, it is assumed that the extinguishing of the sustained current arc is possible for the currents of the order of 12-15 A.

Research into powerful open arcs, carried out by the C.S.R.E.L., has shown that an electric arc is capable of self-extinction even for currents of a few hundred ampres, if the conditions exist for a substantial increase of its length [6]. On this basis the investigations of the sustained current conditions were undertaken. Experiments on a 6 kV model have shown that the extinction of the sustained current arc for gradients of 5-15 kV/m occurs for currents up to 75-100 A, and experiments on a 220 kV grid 750 km long have shown the possibility of

* *Electrichestvo* No.1, 19-25, 1958 [Reprint Order No. EL 43].

extinction of the sustained current arc in the real conditions for currents of 30 A, [7]. Further experiments have been carried out on the 400 kV line from Kuibyshev Hydroelectric Power Station Moscow. The results are given in this article.

The values of the sustained currents and the restoring voltages at the place of flash-over determine to a considerable degree the time of burning of the arc.

In considering various separate cases, used for calculations, it is necessary to bear in mind that in the case of a single-phase automatic reclosing, the phenomenon of the sustained current is conditioned by the presence on the sound phases of the voltage of industrial frequency and of the working current, and, in the case of three-phase reclosing, by the presence of voltages varying in time on the sound phases during their capacitive discharge into the earth.

If a voltage transformer is connected to the 400 kV line, then the discharge of the line into it will have an aperiodic character. For a section of the line 200-500 km long the time constant of the aperiodic discharge is about 0.01 sec. The process of the discharge will be practically finished in 0.05 sec and will not produce any appreciable sustained current phenomenon. Therefore, in future, there is no need to consider this case. If the voltage transformer and the reactor are connected to the line, then the discharge process will be determined by the ratio of the capacitance of the line and the parameters of the reactor, in so far as the resistance of the reactor is smaller than the resistance of the voltage transformer by a few orders of magnitude. In this case, there will be an oscillatory discharge, and the constants of the discharge process will vary according to the length of the disconnected section. These constants are calculated by known formulae. The data, necessary for calculations of the amplitude values of the discharge current, proper frequency and time constant of discharge as a function of the length of the 400 kV line, are given in Table 1.

TABLE 1

Element of the electro-transmission	Values for one phase				
	Resistance of the positive sequence R (Ω)	Inductance of the positive sequence L (H)	Mutual inter-phase inductance M (H)	Phase capacitance with respect to earth C_0 (μF)	Interphase capacitance C_1 (μF)
Line (for 1 km)	0.2	0.93×10^{-3}	0.86×10^{-3}	8.6×10^{-3}	1.28×10^{-3}
Shunting reactor	5.3	3.4	–	–	–

As can be seen from the graphs on Fig.1, the values of the parameters characterizing the discharge of the line in relation to the length of the section vary rather

considerably. Nevertheless, the current of discharge and its proper frequency are of the same order as the working current of the 400 kV line and its working frequency.

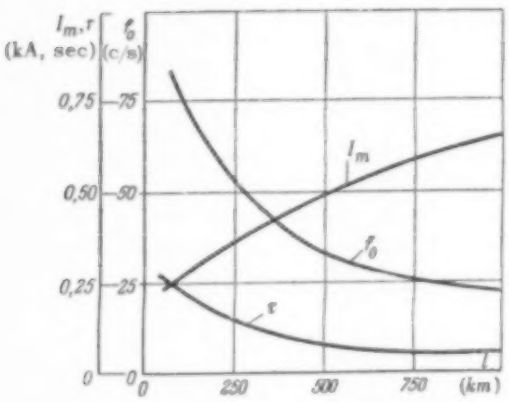

FIG.1. The values of the amplitudes of the discharge current I_m, time constant of the discharge τ and the proper frequency f_0 at the discharge of the line through the shunting reactor as a function of the length of the disconnected section.

The time constant of the discharge τ is equal to a fraction of a second; therefore we have to reckon with the fact that the voltage on the sound phases of the line and the discharge current will maintain sustained current conditions at the faulty place through the disconnected phase for 1 sec or more.

Thus, calculation of the sustained currents and of the recovery voltages should be done for two cases: switching off one phase and switching off all three phases in the presence of a reactor. The general formulae for these quantities are deducted on the basis of the simplified circuit of the line element with distributed constants, as shown in Fig.2. In this diagram, two sound phases are replaced by an equivalent single phase, the voltage along it being assumed constant. This assumption enables us to exclude consideration of the inductance and the resistance of the equivalent phase. The mutual inductance between the sound phases and the disconnected phase of the section is accounted for by the introduction into the faulty phase of the c.m.f. of the mutual inductance.

The differential equation of the line element has the following form:

$$\left.\begin{aligned} -\frac{\partial \dot{U}}{\partial l} &= j\omega L\dot{I} + j\omega M\dot{I}_A; \\ -\frac{\partial \dot{I}}{\partial l} &= j\omega C_0\dot{U} + (\dot{U} - \dot{U}_A)j\omega C, \end{aligned}\right\} \qquad (1)$$

where $\dot{U}_A = 0.5\,\dot{U}_f$; $I_A = I_f$; $C = 2C_1$;

$\dot{U}_A$ and I_A are the voltage and current in the phase equivalent to the two sound phases;

$\dot{U}_f$ and $\dot{I}_f$ are the voltages and currents in the sound phases; and

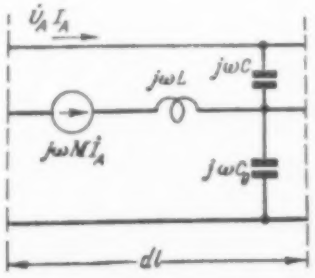

FIG.2. The diagram of the element of the line with distributed parameters for the calculated example.

$\dot{U}$ and $\dot{I}$ are the voltage and current in the disconnected phase.

Solving simultaneously the equations (1) for the section of the line of length l, we have:

$$\begin{aligned}\dot{U}_2 &= \dot{U}_1 \operatorname{ch}\gamma l - \dot{I}_1 Z_c \operatorname{sh}\gamma l + \dot{U}_A \frac{a}{\gamma^2}(1-\operatorname{ch}\gamma l) - \dot{I}_A \frac{j\omega M}{\gamma}\operatorname{sh}\gamma l;\\ \dot{I}_2 &= -\frac{\dot{U}_1}{Z_c}\operatorname{sh}\gamma l + \dot{I}_1 \operatorname{ch}\gamma l + \dot{U}_A \frac{a}{Z_c\gamma^2}\operatorname{sh} l - \dot{I}_A \frac{j\omega M}{Z_c\gamma}(1-\operatorname{ch}\gamma l),\end{aligned} \tag{2}$$

where $a = -\omega^2 LC$; $\gamma = j\omega\sqrt{L(C_0+C)}$; $Z_c = \frac{j\omega L}{\gamma}$;

$\dot{U}_1$ and $\dot{I}_1$ refer to the beginning of the section; and $\dot{U}_2$ and $\dot{I}_2$ refer to the end of the section.

Let us divide the section of the line in question into two parts: x and l-x. Let us establish for each of them the boundary conditions:

For the beginning of the part x: $\dot{U} = \dot{U}_1$; $\dot{I} = 0$; for the end of the part x: $\dot{U} = \dot{U}_x$; $\dot{I} = \dot{I}_x$; for the beginning of the part $l-x$: $\dot{U} = \dot{U}_x'$; $\dot{I} = \dot{I}_x'$; for the end of the part $l-x$: $\dot{U} = \dot{U}_2$; $\dot{I} = 0$; At the junction of two parts: $\dot{U}_x = \dot{U}_x'$; $\dot{I}_x = -\dot{I}_x'$

Using equations (2) and the boundary conditions we get the following expressions: for the recovery voltage on the disconnected phase

$$\dot{U}_x = \dot{U}_A \frac{C}{C_0+C} + j\dot{I}_A \frac{M}{\sqrt{L(C_0+C)}} \times \frac{\frac{1-\cos\gamma x}{\cos\gamma x} - \frac{1-\cos\gamma(l-x)}{\cos\gamma(l-x)}}{\tan\gamma x - \tan\gamma(l-x)}; \tag{3}$$

for the magnetization current

$$\dot{I}_x = -j\dot{U}_A \frac{C}{\sqrt{L(C_0+C)}}[\tan\gamma x + \tan\gamma(l-x)] + \dot{I}_A \frac{M}{L}\cdot\frac{\cos\gamma(l-x)-\cos\gamma x}{\cos\gamma(l-x)\cos\gamma x}.$$

As can be seen from formulae (3), voltage $\dot{U}_X$ and current $\dot{I}_X$ have two components: the first of them depends on the voltage on the sound phases and is due to the capacitive connexion between sound and faulty phases, and the second depends on currents in the sound phases and is due to the mutual inductance.

On the basis of data given in Table 1, we obtain the distribution of the components of the recovery voltage and of the sustained current for different lengths of the disconnected section of the line in the case of an automatic single-phase reclosing after break. The value of the current I_A is assumed equal to 700 A.

The plotting of graphs of distribution in Figs 3 and 4 is done in such a way that the ordinate axis corresponds to the middle of the disconnected section, and the variable coordinate to the faulty place.

From graphs in Fig. 3 and 4, it is seen that the capacitive component of the recovery voltage does not vary along the section; we can also assume that the capacitive component of the sustained current remains constant along the section.

1958

Inductive components of the sustained current and of the recovery voltage are equal to zero when the short-circuit occurs at the central point of the section, and for short-circuits at the ends of the section they have maximum values. The inductive component of the voltage has a positive value when the short-circuit occurs at one end of the section, and a negative one when it occurs at the other end of the section. The value of the resultant of the inductive and capacitive components depends upon the angle between the current, which produces them, and the voltage on the sound phases; the maximum value of the resultant also occurs at the end of the section.

The above method may also be used for calculations of the sustained current and of the recovery voltage in the case then a shunting reactor is connected at the end of the section of the line. Since, however, the maximum values of these quantities are of primary importance, we give below the formulae for calculations in the case when a short-circuit occurs at the end of the section opposite to that where the shunting reactor is connected. The boundary condition for this case will be: at the end of the section in which the fault occurred $U = U_d$; $I = 0$; at the end of the section with a reactor $U = I_{2j} X_p$; $I = I_2$ where $X_p = \omega L_p$ – inductive reactance of the reactor.

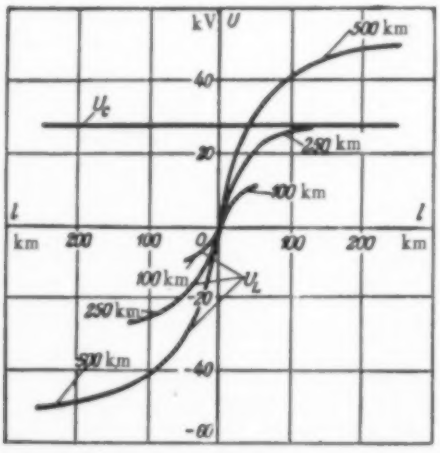

FIG.3. Capacitive U_c and inductive U_l component of the voltage on the disconnected phase (in the absence of the reactor).

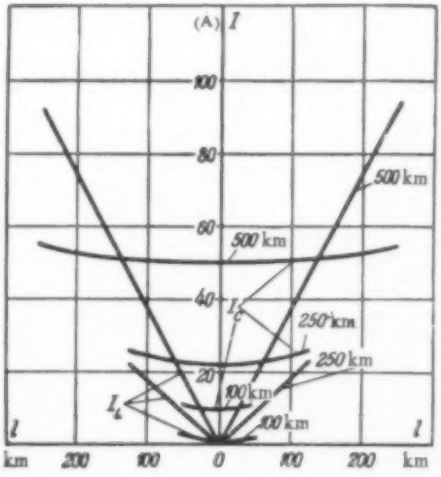

FIG.4. Capacitive I_c and inductive I_l components of the sustained fault current when one phase is disconnected (in the absence of the reactor).

Using equations (2) and the boundary conditions we get:

$$\left.\begin{aligned}
\dot{U}_d &= \dot{U}_A \frac{C}{C_0+C} \frac{\sin\gamma l - \frac{Z_c}{x_p}(1-\cos\gamma l)}{\sin\gamma l - \frac{Z_c}{x_p}\cos\gamma l} + \\
&+ jI_A \frac{M}{\sqrt{L(C_0+C)}} \frac{1-\cos\gamma l - \frac{Z_c}{x_p}\sin\gamma l}{\sin\gamma l - \frac{Z_c}{x_p}\cos\gamma l}; \\
I_n &= -j\dot{U}_A \frac{C}{\sqrt{L(C_0+C)}} \frac{\sin\gamma l - \frac{Z_c}{x_p}(1-\cos\gamma l)}{\cos\gamma l - \frac{Z_c}{x_p}\sin\gamma l} + \\
&+ I_A \frac{M}{L} \frac{1-\cos\gamma l + \frac{Z_c}{x_p}\sin\gamma l}{\cos\gamma l + \frac{Z_c}{x_p}\sin\gamma l}
\end{aligned}\right\} \quad (4)$$

Here, the recovery voltage and the sustained current also have two components each, one of the components being capacitive and the other inductive.

For calculation of the resultant values of the current and voltage, despite the previously assumed values of different parameters, $\cos\phi$ of the transmission was taken equal to unity, which approximately corresponds to the conditions of normal power. Fig.5 shows the results of calculations for the cases when the reactors are present and when they are absent.

In the case of a single-phase automatic reclosing after the break and in the absence of a reactor, the recovery voltage varies within the limits 30-60 kV according to the length of the section. In the case when a reactor is present, its inductance and interphase capacitance appear as if connected in series; because of this, voltage resonance is possible, and, hence, a considerable increase of voltage on the faulty phase. Equating to zero the denominator of one of the terms for the voltage (4), we find that the resonance occurs for the length of the section

$$l_{res} = \frac{1}{\omega\sqrt{L(C_0+C)}} \tan^{-1}\frac{Z_c}{\omega L_p}.$$

Calculations show that $l_{res} = 290$ km. Although, in fact, resonance over-voltage is limited by the saturation of the reactor and the discharge, nevertheless it is necessary to reckon with a considerable increase of voltage. In the presence of a reactor, the sustained current also reaches a considerably higher value than in its absence.

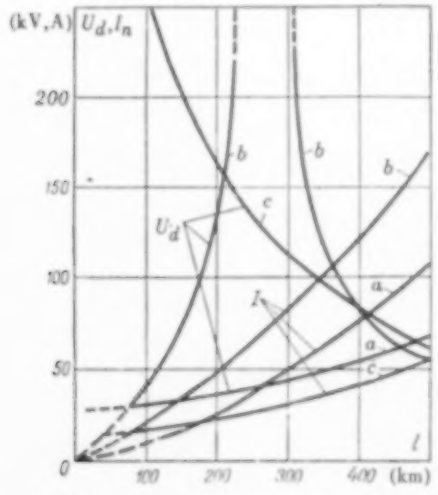

FIG.5. The sustained current and the recovery voltage on the disconnected phase for a point of the end at the section: (a) one phase disconnected, reactor absent; (b) one phase disconnected, reactor present; (c) three phases disconnected, reactor present.

1958

In calculating the sustained current and the recovery voltage for conditions at the three-phase automatic reclosing after break, the values of the discharge current and of the proper frequency of the discharge for each length of the section were taken in accordance with graphs in Fig.1. Voltage on the sound phases was assumed to be equal to the nominal, the damping of the discharge current was disregarded, angles between vectors of the discharge currents and voltages of the sound phases were taken equal to 90 el. deg. The results of calculations are given on Fig.5. The sustained current was a little smaller, and the recovery voltage bigger than for conditions in the case of a single-phase automatic reclosing in the absence of a reactor. The sustained current in the case of a single-phase automatic reclosing in the presence of a reactor was approcimately equal to 0.3 A/km, and in the same case, in the absence of a reactor, to 0.2 A/km. In the case of the three-phase automatic reclosing in the presence of a reactor, the current equalled 0.1 A/km.

The diagram of the 400 kV line Kuibyshev - Moscow, during the experiments carried out by the C.S.R.E.L., is shown on Fig.6. Wind during these experiments was weak.

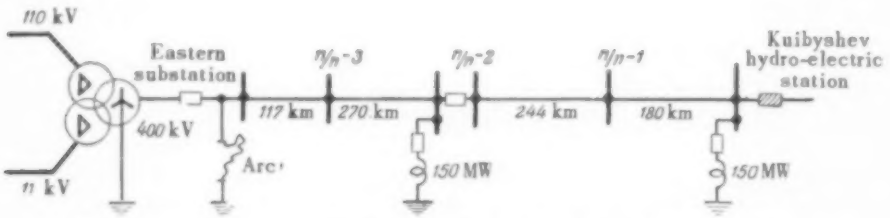

FIG.6. The diagram of the 400 kV Kuibyshev - Moscow line during the experiments with extinction of the sustained faulty current arc.

Arcing short-circuit on the group of insulators of the suspension type was produced by means of a copper wire of 1 mm² cross-section. After fixing the wire, all three phases were switched on and the arc was struck.

The damaged phase was disconnected by a breaker after 0.14 sec, and after this, the sustained current arc remained. The voltages of all three phases, the current of one sound phase, the short-circuit current and the sustained current were recorded by a magneto-electric ossillograph. The photographs of the arc were taken by a cine-camera at the rate of 32 frames/sec. Cine - frames of the experiment on the section of the line 815 km long, in the absence of reactors, are given in Fig.7, and the oscillograms of this experiment in Fig.8.

During the short-circuit stage, the arc on the film appears as a luminous cloud; later the luminous gases, surrounding the arc disperse and the patch of the sustained current arc can be clearly seen; this path gradually becomes longer, bending sideways and upwards, at the expense of thermal forces of the previous short-circuit and due to its own thermal effect; after this comes extinction.

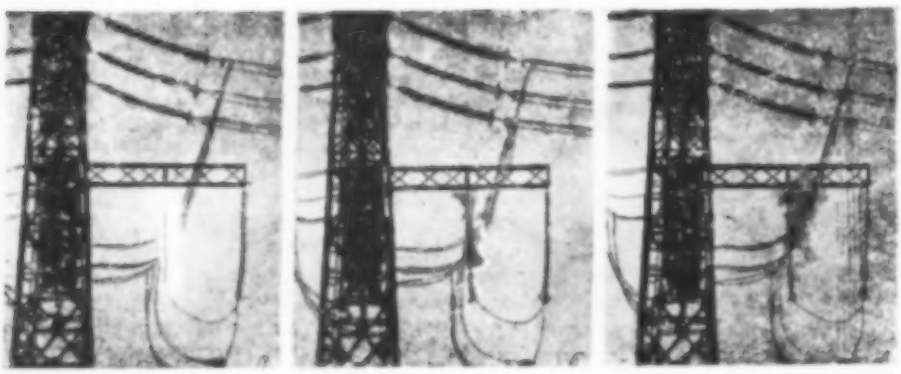

FIG.7. Separate cine-frames of the single-phase short-circuit with the following sustained current arc: (a) short-circuit arc; (b) the sustained current arc before the beginning of extinction; (c) cooling of gases after extinction of the sustained current arc.

1958

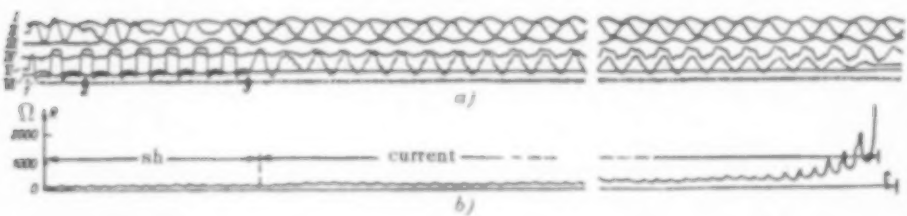

FIG.8. Oscillogram of the experiment (a) and the graph of the resistance of the path of the arc (b) on the single-phase short-circuit and switching off one phase. I – voltage of the "yellow" phase U_y. II – current of the "yellow" phase I_y. III – voltage of the "green" phase U_g. IV – voltage on the arc (of the "red" phase) U_r. V – current I_{sh}. VI – short-circuit current I_{sh} (1) the beginning of the short-circuit; (2) connecting of the sound phase with a delay; (3) switching off the "red" phase (the end of the short-circuit).

As can be seen from the oscillogram in Fig.8, after switching off, the sustained current flows through the discharge channel; the current gradually decreases with the lengthening of the channel and the voltage increases on the arc gap. The resistance of the path of the sustained current arc, whose graph of variation is plotted using the oscillogram data, shows a steady increase during the whole process. This arc dies away due to the steady decrease of current caused by the increasing resistance of the path. This process of extinction occurred in all experiments and is typical for the sustained current arc. The extinction of open powerful arcs occurred in a similar way in all the experiments performed by Burgsdorf [6]. In a few cases in these experiments, single restrikes may be observed, these being peculiar to arcs in capacitive networks.

The oscillogram of the experiment on switching-off all three phases on a section of the line 117 km long, without a reactor, is shown in Fig.9a. In this case, the discharge of the sound phases of the line and the sustained current correspond-

ing- to it have an aperiodic character. The discharge lasts only 1.5-2 periods of industrial frequency; therefore, reclosing with a delay of 0.3 sec proves successful.

The oscillograms of the experiment on switching off all three phases on a section of the line 635 km long with the reactor are shown in Fig.9b. In this case, the discharge of sound phases through the reactor, after they have been switched off, proceeds at a frequency of 31 c/s per sec and with small damping, and this agrees with calculations. The curve of the sustained current has an irregular shape, and the extinction of the arc occurs during 0.2 sec. The reclosing after 0.3 sec also proves succesful.

Table 2 shows the results of the experiments carried out on the line from Kuibyshev to Moscow. The experimental values of the sustained current are taken after the first half period after switching off the short-circuit, and the voltage on the disconnected phase is taken at its established value.

In all experiments, the short-circuit current was equal to 2.000 A, and the time of short-circuit 0.14 sec.

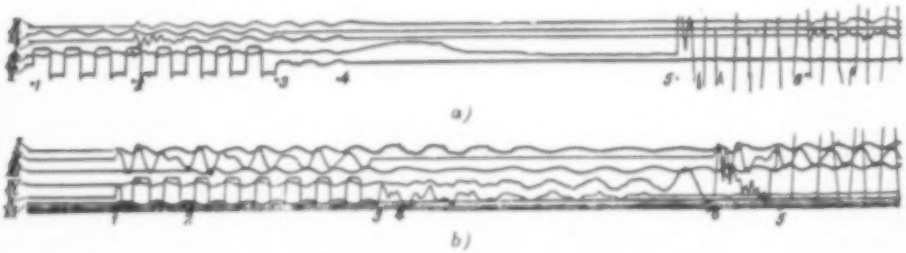

FIG.9. Oscillograms of the experiments with the three-phase switching off and reclosing. (a) section of the line with a voltage transformer; (b) section of the line with a voltage transformer and reactor. I – voltage of the "yellow" phase U_y; II – current of the "yellow" phase T_y; III – voltage of the "green" phase U_g; IV – voltage of the arc (of the "red" phase) U_r; V – current I_{sa}; VI – short-circuit current I_{sh}. (1) the beginning of the short-circuit; (2) reclosing of the sound phase with a delay; (3) switching off the "red" phase (the end of the short-circuit); (4) switching off the "yellow" and "green" phases; (5) reclosing of the "red" phase; (6) reclosing of the "yellow" and "green" phases.

The data of the table show a satisfactory coincidence of calculated and measured values of the sustained currents and recovery voltages on the disconnected phase.

Experimentally obtained values of the times of arc extinction in relation to the sustained current for a single-phase automatic reclosing are plotted in Fig.10 as dots. As can be seen from this graph, these points show a considerable dispersion, due to the characteristic instability of the arc.

It is necessary to point out that the experiments were carried out on the line without load, and without the sustained current component, due to the inter-phase

TABLE 2

Kind of experiment	Length of the line (km)	Reactors on phases	Capacitive component of the: Voltage on the disconnected phase (kV) Calculated	Voltage on the disconnected phase (kV) Measured	Sustained current (A) Calculated	Sustained current (A) Measured	Time of burning of sustained current arc (sec)
Single phase A.R.	117	—	28	28	15	17	0.05
" "	391	Y,G	28	28	40	38	0.26
" "	391		28	28	40	38	0.34
" "	391		28	28	40	38	0.38
" "	391		28	28	40	38	0.59
" "	635		28	28	67	62	0.25
" "	635		28	28	67	62	0.33
" "	635		28	28	67	62	0.40
" "	815		28	28	82	80	0.35
" "	815		28	28	82	80	0.76
" "	815		28	28	82	80	1.60
" "	391	Y,G,R	100	92	25	25	0.22
" "	391		100	92	25	25	0.24
" "	391		100	92	25	25	0.25
" "	635		45	50	47	45	0.84
" "	635		45	50	47	45	1.10
" "	635		45	50	47	45	1.88
Three phase A.R.	117	—	—	—	—	—	0.02*
" "	635	Y,G,R	—	—	—	36	0.1
" "	635		—	—	65	25	0.15
" "	635		—	—	65	75	0.20
" "	635		—	—	65	35	0.08**
" "	635		—	—	65	70	0.16***

* Reclosing succesfully done after 0.3 sec.
** " " " " 0.27 sec.
*** " " " " 0.26 sec.

mutual inductance. If the experiments were carried out on the line with a normal load, the sustained current would have been greater.

Taking into account the maximum durations of time for arc extinction and considering an additional interval of time of the order 0.05 sec, necessary for the recovery of the electric strength of the path after the arc extinction, we can assume, as an approximation, that the sustained current and the duration of the currentless interval for the single-phase automatic reclosing of the line without a reactor, are linearly dependent (straight line on Fig.10). Therefrom we can derive the relationship between the currentless interval and the length of the disconnected section, if the relationship between the length of the section and the sustained current has been determined earlier (see Fig.7). The corresponding approximate formula is

$$t_{Sfar} = 0.003\, l$$

where t_{Sfar} is the necessary currentless interval for the single-phase automatic reclosing (sec) and l is the length of the section (km)

With the reactor, which causes an increase in the recovery voltage, the necessary currentless interval will be appreciably longer than that obtained by formula (6).

In conditions approaching resonance the sustained current arc may remain unextinguished.

So far as the 400 kV line from Kuibyshev to Moscow is concerned, such conditions may occur on the section between the switching points 3 and 2, of length

1958

274 km, and on the section between switching points 2 and 1, of length 244 km, if resonance occurs, as was found earlier, on the length of the disconnected 290 km section.

The resonant increase of the voltage on the disconnected phase can be dangerous for the insulation of the connected transformers and for the shunting reactor. The real value of the over-voltage may be found only experimentally.

For the successful use of the single-phase automatic reclosing on the sections considered of the line from Kuibyshev to Moscow, it is possible, for the single-phase short-circuit, to switch off the shunting reactor simultaneously with switching off the faulty phase. In designing 400 kV lines it is necessary to choose such distances between the switchgears that the conditions for the resonant increase of voltage should not arise when switching off one phase.

If the shunting reactors are sufficiently reliable and damage to them is less probable than serious damage to the line itself, excluding the possibility of its reclosing after break, then we can omit the breaker in the network of the reactor.

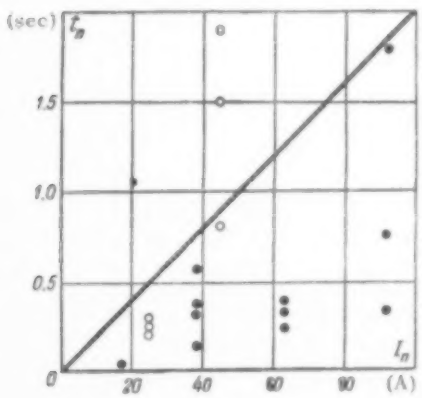

FIG.10. Experimentally found durations of the arc extinction in relation to the current:
● – on the section of the line without a reactor, ○ – on the section of the line with a reactor.

For the three-phase automatic reclosing with a reactor, the durations of arc extinction show a considerable dispersion, but the maximum duration does not exceed 0.2 sec. Therefore, in this case, we may successfully use the so-called quick-acting automatic reclosing, for which the interval is determined by the time of the separation of the arc breaking contacts of the air breaker and their consequent reclosing, this time being equal to 0.27-0.3 sec, as it was during the performed experiments.

In the conditions of dynamic stability of the electro-transmission it is desirable that the currentless interval for the three-phase automatic reclosing should be very small. Nevertheless, the further decrease of the interval of the quick-acting automatic switch-on is inadmissible with shunting reactors, since the relation between the maximum time of the burning of the sustained current arc (0.2 sec), and the maximum interval (0.3 sec) had a limiting value in the experiments. For deionization and the recovery of the electric strength of the path of the arc only 0.1 sec is left.

If, simultaneously with the disconnection of the three-phases of the line, we disconnect the three phases of the shunting reactor as well, then the interval of

the quick-acting automatic reclosing will not be limited by the sustained current arc. In this case, the duration of the pause will be determined by the time of deionization and of the recovery of the electric strength of the path of the short-circuit arc. According to the published data, this time does not exceed 0.2 - 0.25 sec for a large range of short-circuit currents. Taking into consideration that for the 400 kV Kuibyshev - Moscow transmission line, the three-phase short-circuit current varies within the limits 1 - 10 kA, the reduction of the interval of the quick-acting automatic reclosing, the reactor being disconnected, may be brought down to the value of 0.25 sec. The possibility of the further reduction of the interval should be confirmed by additional experiments.

It is necessary to point out that on the section of the line between Moscow and switching point 3, where the reactor is absent, and the extinction of the sustained current arc takes only 0.05 sec, we may successfully use the single-phase quick-acting reclosing.

In conclusion it is necessary to point out that the effectiveness of the automatic reclosing on the 400 kV lines, judging from the experience gained from the exploitation of the 154 kV and 220 kV lines, having analogous electrical and mechanical characteristics, should be high. According to CSREL data, for the period from 1945 to 1954, on the lines with steel cables and the protective angle of 20° or less, there occurred about seventy cases of break - down. Damage due to lightning did not occur. 45 per cent of break-downs were of short duration (dirt, damp insulation in marshy regions, various deposits), and in 55 per cent of cases the break-downs were due to serious and lasting damage, followed by the conductors falling to the ground. It follows that approximately half of the short-circuit cases may be handled without prolonged disconnection of the line.

The authors wish to thank V.V. Burgsdorf for his valuable advice and help given during their work and colleagues who participated in the experiments.

Translated by S. Szymanski

REFERENCES

1. E. Mory; *Bull S.E.F.*, 8 (1945).
2. A. Amstat; *B.B.M.* 7/8 (1948).
3. E. Harrington and E. Starr; *Trans. Amer. Inst. Elect. Engrs. 2* (1949).
4. A. Matthey-Doret and A. Leuthold; *B.B.M.*, 9 (1954).
5. L. Norlin; *Tech. Tijdschro*, 40 (1953).
6. V.V. Burgsdorf; *Elektrichestvo*, No.10 (1948).
7. A.S. Maikopar; *Trud. TsNIEL (CSREL)*, No.2 (1953).

1958

EARTHWIRE EARTHING SYSTEMS FOR LONG POWER-TRANSMISSION LINES*

N.A. MEL'NIKOV,

All-Union External Power Engineering Institute

A.I. GERSHENGORN and A.N. SHERENTSIS

Teploelektroproekt

(Received 13 July 1957)

At present, the lightning-protection wires of power transmission lines of all voltages are securely earthed at each tower.

During the design of long-distance 220-400 KV lines, it was established that a considerable amount of electrical energy can be lost via earth-wires earthed at many points. These losses are due to the presence of currents in the closed circuits of the wire-tower earthing systems, as a result of the electromagnetically induced e.m.f. in the earthwires. With the most widely adopted lightning-protection system using two earthwires, which are interconnected through the towers, the current obtained is greater than with one earthwire, in which case the circuit is completed only through earth.

Since the energy losses in the earthwires can reach considerable magnitudes, it is worthwhile considering the question of isolating them completely or partially from earth.

It should be pointed out that studies have been made in the U.S.S.R. in recent years on the question of using, as lightning-protectors, current-carrying conductors intended for supplying power to small-scale consumers [1], for driving electric motors when carrying out repair work on the line, melting ice-deposits and the like. The wires can also be used as communication wires, especially during erection of the power lines. In this connection, the need again arises to insulate the wires from earth. Isolation of the earthwire eases the conditions of repair work on the lines and also simplifies the measurement of the line-earth resistance at the towers.

Thus, the multiple earthing of earthwires could only be justified if the additional cost of isolating them were not covered by the saving in energy losses.

* *Ekektrichestvo* No. 1, 25-30, 1958 [Reprint Order No. EL 44].

An obligatory condition for the use of isolated earthwires is the maintenance of the same level of protection as is obtained with earthed wires. For this, the wires must be earthed through spark gaps which are bridged in the early stages of the leader stroke of a lightning discharge, to direct the latter on to the wire. Then when the spark gap has been bridged, the subsequent flow of the lightning current will proceed as with earthwires. Experimental work, carried out on a model, and also the experimental use of sections of 35 to 220 kV power lines with isolated earth wires, confirmed that the earthing of wires via spark gaps does not reduce their protective properties [2].

On the basis of the results of these investigations, the Technical Management of the Ministry for Power Stations decided to suspend the earthwires of 25 to 220 kV lines on insulators with spark gaps not exceeding 40 to 50 mm. The isolated earthwire system has since been extended somewhat to those sections of power lines, where the cables are used for reactive power take-off and consumer supply or the supply to protective relay circuits.

1958

Electrical energy losses in earthwires

If a 400 kV line, for example, 1,000 km long, erected on towers such as are used on the Kuibyshev Power Station - Moscow line, has two steel earthwires 70 mm² in section, earthed at each tower, then the earthwires form a closed circuit over each pitch between the towers and the e.m.f. set up in the earthwires at a line load of 1,000 MW (on two circuits) is 52V/km, the current in each earthwire 27 A, the total loss of power in the earthwires about 3MW (in the two circuits) and the yearly energy loss of the order of 10 million kWh (Appendix 1a).

In a 350 MW transmission with the two 220 kV lines, 360 km long, the power loss in similar earthwires is 380 kW, and the yearly energy loss about 1.8 kWh.

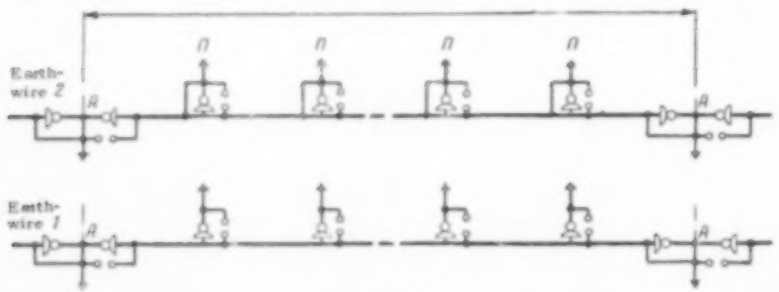

FIG. 1.

If the cost is taken as 10 kopecks per kWh, complete isolation of the earthwires in these lines would give a yearly saving of 1 million roubles in the first case and 180,000 roubles in the second. The saving due to isolating the earthwires on lower voltage lines would be considerably less, since such lines are comparatively short and the working currents are less.

If one of the earthwires is divided into sections, corresponding to the distance between strain towers, and each of these sections is isolated, as shown in Fig. 1. (earthwire), the closed earthwire circuit will be eliminated; current can flow only in the other earthwire and will return through earth. Since the distance between towers on long lines is quite considerable [3], we can ignore the current flowing at the ends of the sections and consider the earthwire-tower earthing system as a single-conductor earthwire-earth line. This system of earthing the wires gives a considerable reduction of the additional energy losses in the line, compared with the system of earthing both earthwires at many points. If this system is used on the 400 and 220 kV lines discussed above, the additional energy loss is reduced by 1.8 times (Appendix 1b).

Further reduction of the losses can be achieved by similarly dividing the second earthwire into sections and isolating them. In this case, in determining the loss on the distance between strain towers, the earthwire-tower circuit must be considered with full reference to the flow of current to earth at the separate towers (Appendix 1c). For example, in the 400 and 220 kV lines discussed above, this system of earthing the wires gives a reduction of approximately 3 times in the additional energy losses, compared with the system of earthing both wires at many points.

In accordance with the decision of the Technical Management of the MES, the distance between strain towers on 220 and 400 kV lines with receiving substiutions must not exceed 10 and 15 km respectively, whereas for lines with switching stations or stations of limited circuit-breaking capacity, this distance is not limited. The length of each section of earthwire in the latter case is determined by the distance between angle-strain towers and may exceed 20 to 30 km.

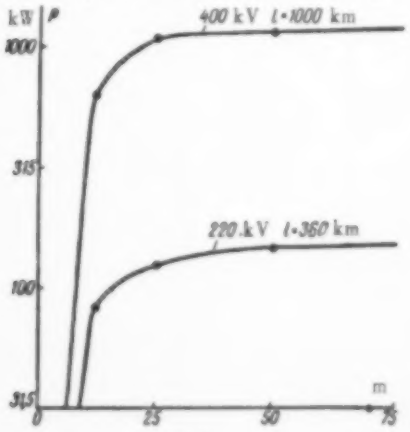

FIG. 2.

Fig. 2 shows the relationship between additional power losses in the earthwires and the section length with earthwires earthed at many points; the section length is plotted as the number of intermediate spans and the losses are plotted on a logarithmetic scale.

It follows from Fig. 2 that even at a section length of km, the additional energy losses with earthwires earthed at many points are considerable. This is explained by the fact that the current flow at the ends of the earthwire-tower circuits occurs over a relatively short length. At medium lengths of section, earthed at many points, the currents flowing

in the earthwires are almost equal to those in earthwires of unlimited length, earthed at many points. Therefore, to eliminate additional losses of energy, it is also advantageous to avoid the use of sectionalized earthwires earthed at many points.

Earthwire isolation

If an earthwire is to be completely isolated, the insulator must be selected for the maximum voltage which can be set up in the earthwire in service. This voltage is that produced by the capacitative linkage between the earthwire and the line conductors (Appendix II).

Furthermore, the earthwire insulator must withstand the voltage set up by the longitudinal e.m.f., induced in the earthwire due to short-circuits on the line. This e.m.f. will be a maximum for an asymetric short-circuit to earth.

The e.m.f. induced in the earthwire of a three-phase line, when a single-phase short-circuit occurs in phase a, can be expressed by the following formula (Appendix Ia):

$$\dot{E} = j0.145 \cdot I_a \log \frac{D_{am}}{D_e}.$$

This formula is equally valid for each of the earthwires on a line.

The maximum voltage due to the capacitative linkage, on the length between two towers, under normal working conditions, is 31 kV on 400kV lines, and 9 kV on 220 kV lines. Thus, the earthwire insulators on 400 kV lines may consist of strings of three insulators of the type P-4.5, and on 220 kV lines, of a single insulator of the same type.

Complete earthwire isolation on 400 kV lines is undesirable, since it complicates the tower design for these lines. In addition, the setting up of high voltages in the earthwires may make the use of such lines somewhat more difficult.

The total e.m.f. induced in an earthwire when there is a single-phase short circuit on the line, depends on the uninterrupted length of earthwire. Over the length of a complete transposition cycle, which may be taken as 250 km for a 400kV line the total longitudinal e.m.f. at a current of 5,000A may reach the comparatively high value of 45kV.

The size of the spark gap must be such as to ensure isolation of the earthwire under normal working conditions, whilst retaining the lightning-protection properties of the earthwire and ensuring self-extinction of the supplementary current arc after the spark gap has been bridged. For 400kV lines the required spark gap size must be determined experimentally.

The value of the total longitudinal e.m.f. can be reduced by dividing the earthwire into sections of shorter length. With a section length of earthwire earthed at one point equal to say 10km (distance between strain towers), the total longitudinal e.m.f. must not lead to voltages in the earthwire exceeding 1kv relative to earth. In this case also, the earthwire insulators on 400kV lines can consist of a single insulation of type P-4.5, with a 25 mm spark gap in parallel. In that case, the earthing system under consideration will be analogous, as regards its lightning-protection effect, to that used on 110 and 220 kV lines for equipment with reactive power take-off, and additional experimental confirmation of the lightning-protection effect of the earthwires is unnecessary. Reduction of the length of earthwire sections is also necessary, as will be shown below, on grounds of safety.

A current will flow from an earthwire earthed at one point through the earthing connexion to earth, owing to the capacitative linkage between the earthwire and line conductors, and a voltage difference with respect to earth will be set up at the corresponding tower or at several towers, connected to the other earthed wire.

The current in the earthwire earthing connection will be a maximum when the line is operating under unbalanced phase conditions. To determine it, it is sufficient to use the Maxwell equations for many conductor systems (Appendix II). The required current is

$$I = j\omega\dot{q}_m,$$

where $\dot{q}_m$ is the charge on the earthwire, obtained from the combined solution of the system of Maxwell equations, which are set up under the assumption that the voltage in the cable is zero.

Calculations show that, over the distance between switching stations in a 400kV line, the current in the earthwire under unbalanced phase conditions may attain 12 A, so that the voltage on the tower, at a resistance of 10 Ω in the tower footing, may attain 120, which cannot be allowed from safety considerations. The current flowing in the earthwire over the distance between strain towers is less than 1.5 A; the voltage on the tower in this case does not exceed the permitted value even in the absence of a connection between it and the next tower through the other earthwire.

Comparison of earthwire earthing systems

A cost comparison, on the basis of the calculations made, established that the expense of isolating the earthwires on both 400 kV and 220 kV lines will be recovered within one year. Thus, the economic advantage of eliminating the earthing of the earth wires at many points throughout the length of 400 and 220 kV lines is quite obvious.

In connexion with increasing the resistance to current flow by isolating the

earthwires, doubts arose during the design of the 400kV Kuibyshev-Moscow line, as to whether the selector devices on the single-phase circuit-breakers would operate normally in cases of a single-phase short-circuit. This consideration resulted in the decision not to divide both earth wires into sections corresponding to the distance between strain-towers, each section earthed at one point only.

The system adopted for earthing the earth-wires on the Kuibyshev-Moscow transmission line is shown in Fig. 1. It satisfies all the specified requirements; namely, reduction of additional losses of electrical energy, reduction of the additional costs of isolating the earth wires and retention of stable operation of the automatic control equipment. Earth wire 1 of each circuit is isolated by means of a single insulator of type P-4.5 and divided into line sections corresponding to the distance between strain-towers; each section is earthed at one point (at one of the strain towers). Earth wire (2) is divided into sections of the same length, earthed at each intermediate tower and at one strain tower. At the other strain tower, earth wire (2) is isolated by one insulator. To increase the degree of lightning protection for the 400 kV equipment at the approaches to substations and intermediate switching points, both earth wires on each circuit are directly earthed over a 5km section.

No diminution of lightning protection has been observed since the Kuibyshev-Moscow line has been in operation.

The doubt mentioned above, that the protective relay and automatic equipment would operate incorrectly, is not supported by experimental operation of transmission lines which have been working for a long time without earth wires. It must therefore be further recommended that on long 220 and 400 kV lines, the two earth wires on all the lines should be isolated, and divided into sections corresponding to the distance between strain-towers, since this system is the most economical.

It should be noted that earth wire (2) in Fig. 1, although earthed at each tower, is suspended on single insulators of type P-4.5 with spark gaps. On the Kuibyshev-Moscow line, this makes it possible to proceed to the system of isolating both earth wires.

The above calculations of the voltages which may arise in earthwires show that it is essential to earth the earthwire sections directly at one point on 400 kV lines. As for the earthwires on 220 kV lines, it is possible not to earth them, but merely to provide spark gaps.

It should be noted that to divide earth wires into sections and earth each at one point prevents their use as current-carrying conductors.

If only one earth wire is erected on a line, then to reduce additional energy losses it is also recommended to divide this into sections corresponding to the distance between strain-towers.

1958

Appendix 1. Determination of energy losses

a) *Earthwires forming a two-conductor short-circuit loop.*

The flow of current in the line conductors induces an e.m.f. in the earthwires. At a frequency of 50 c/s, the induced e.m.f. in the earthwire [4] is

$$\dot{E}_e = j0.145 \sum_{p=1}^{3} I_p \log \frac{D_{pe}}{D_r},$$

where D_{pe} is the distance between the phase conductor and the earth wire,

D_r is the depth of the equivalent earth return current (5);

I_p is the current in phase p.

As is well known, under normal symmetrical conditions of operation, the currents flowing in the different phase conductors are related as follows:

$$I_a = aI_b = a^2 I_c,$$

so that the e.m.f. induced in earth wire T_1 (Fig. 3) is:

$$\dot{E}_e = j0.145 I_a \left(a^2 \log \frac{D_{be}}{D_{ae}} + a \log \frac{D_{ce}}{D_{ae}} \right),$$

and in earthwire T_2:

$$\dot{E}'_e = j0.145 I_a \left(a^2 \log \frac{D_{be}}{D_{ae}} + \log \frac{D_{ce}}{D_{ae}} \right),$$

where I_a is the current in phase a conductor;

D_{ae} is the distance between the phase a conductor and the earthwire;

D_{be} is the same for phase b;

D_{ce} is the same for phase c.

It is assumed that the earth wires and conductors are arranged symmetrically on the tower with respect to the vertical axis.

If the earthwires are earthed at each tower on the line, then over each span the e.m.f. induced in the earthwires will produce currents in the earth-wires, towers and earth, since there are earthed wire-tower circuits.

The biggest energy loss will be due to currents flowing in the short-circuit loop formed by the earthwires.

The current in this loop is;

$$I_e = \frac{\dot{E}_e - \dot{E}'_e}{2Z_e},$$

Here Z_e is the impedance of the earth wire;

$$Z_e = r_e + j0.145 \ln \frac{D_e}{r_{e.e}},$$

where D_e is the distance between the earth wires;

r_{ee} is the equivalent radius of cross section of the earth wire [5].

The active power loss over 1km length of the loop is

$$\Delta P_e = -\mathrm{Re}(\dot{E}_e - \dot{E}'_e) I_e =$$

$$= 1.5 \left(0.145 \cdot I_a \log \frac{D_{ce}}{D_{ae}}\right)^2 g,$$

where

$$g = \frac{r_e}{r_e^2 + \left(0.145 \log \frac{D_e}{r_e}\right)^2}.$$

The approximate yearly loss of energy in the earthwires of a two-circuit line can be found in the normal way.

$$\Delta A = 2\Delta P_e l\tau,$$

where τ is the loss time from the loading curve at some average point (hr);

l is the length of the line, in km.

In its final form the formula for determining losses is:

$$\Delta A = \frac{3\left(0.145 I \log \frac{D_{ce}}{D_{ae}}\right)^2 r_e}{r_e^2 + \left(0.145 \log \frac{D_e}{r_e}\right)^2} \tau l,$$

where I is the load on one circuit of the line at some average point (A).

b) Earthwire – earth loop

Since the resistance of an earthwire – earth loop between towers is considerably greater than the footing resistances at the ends, particularly at substations

and switching-points, where this resistance is at most 0.5 Ω, the earthwire – tower loops can be regarded as short-circuits. Then the e.m.f. is

$$\dot{E}_e = \dot{E}_e - I_e Z_e = \dot{E}'_e + I_e Z_e = \frac{\dot{E}_e + \dot{E}'_e}{2},$$

and the impedance of the earthwire-earth loop is

$$Z_{e.e} = \frac{r_e}{2} + 0.05 + j0.145 \log \frac{D_e}{r_e},$$

where

$$r_e = \sqrt{D_e r_{a.e}}$$

and the current of the loop is

$$I_n = \frac{\dot{E}_e}{Z_{e.e}}.$$

The active power loss over 1km of the line is

$$\Delta P_n = -\operatorname{Re} \hat{E}_e I_n$$

and the energy loss is

$$\Delta A = 2\Delta P_n \tau l = 2\left(0.145 \frac{I_n}{2} \log \frac{D_{be}^2}{D_{ae} D_{ce}}\right)^2 \times \times \frac{(0.5 r_e + 0.05)}{(0.5 r_e + 0.05)^2 + \left(0.145 \log \frac{D_e}{r_e}\right)^2} \tau l.$$

If the line has only one earthwire earthed at many points, then

$$\Delta A'_n = 2\left(0.145 I \log \frac{D_{ce}}{D_{ae}}\right)^2 \times \times \frac{r_e + 0.05}{(r_e + 0.05)^2 + \left(0.145 \log \frac{D_e}{r_{e.e}}\right)^2} \tau l.$$

To determine the loss in the earthwire-earth loop it is borne in mind that long-distance power transmission lines are constructed with extended transposition cycles.

c) Earthwires - towers earthing system on sections between strain-towers

If a section earthed at many points is limited to the distance between strain-towers and is not electrically connected to other earthwire sections, then to calculate the energy losses it is necessary to take into account the flow of current in the whole earthwire-tower system [5].

Let an earthwire earthed at many points have n spans, i.e. earthed at $n+1$

towers; the footing resistances of the towers can be taken to be identical and equal to R, whilst the resistance of the earthwire - earth loop for each span is

$$Z_{n.m} = Z_{me}\, l_m,$$

where l_m is the span length.

A chain of this type is active, uniform and finite.

The current in the span of earthwire between towers k and $k+1$ is

$$I_{k,\,k+1} = -I_{n-k-1,\,n-k} = \frac{E_m}{Z_m}\left(1 - B\,\frac{A^{k-n} + A^{-k-1}}{1-B}\right),$$

where A is the coefficient of voltage drop at each successive tower in an infinitely long chain:

$$A = \frac{Z^2}{RZ_{n.m}};$$

Z is the input resistance of an infinitely long chain with identical parameters for each unit:

$$Z = -\frac{Z_{n.m}}{2} + \sqrt{\left(\frac{Z_{n.m}}{2}\right)^2 + Z_{n.m}R};$$

B is the ratio between the currents at the two ends of a given finite chain, forming part of an infinitely long chain:

$$B = \frac{Z}{Z_{n.m}}A^n(1-A).$$

The active power loss in the chain considered is:

$$\Delta P = \sum_{k=0}^{n-1} P_{k,\,k+1} = E_m^2 \operatorname{Re}\frac{1}{Z_{n.m}}\left(n - 2B\,\frac{\sum_{k=0}^{n-1} A^{k-1}}{1-B}\right) =$$

$$= E_m^2 \operatorname{Re}\frac{1}{Z_{n.m}}\left[n - \frac{2B(1-A^{-n})}{(1-B)(1-A^{-1})A}\right].$$

The energy loss for the entire two-chain line is

$$\Delta A = 2\Delta P \tau N = 2E_m^2 \operatorname{Re}\frac{1}{Z_{n.m}} \times$$

$$\times\left[n - \frac{2B(1-A^{-n})}{(1-B)(1-A^{-1})A}\right]\tau N,$$

where N is the number of strain towers for one circuit of the line; approximately:

$$N = \frac{l}{l_a}.$$

where l_a is the distance between strain-towers.

Appendix II. Determination of the voltage on an isolated earthwire.

If the effect of the earth is replaced by the effect of mirror-image conductors with the same voltage but opposite sign, then each circuit of the line gives a system of six conductors with given voltages relative to earth, and the earthwire under consideration is in the electrical field thereby produced.

The charges q_a, q_b and q_c on the conductors can be found from the corresponding Maxwell equations [6]. In the case of a symmetrical system, in which the conductors are arranged in a right-handed sequence and symmetrical horizontally on the tower (Fig.3), the system of equations can be written in the following simplified form [4]:

$$\dot{U}_a = \frac{\dot{q}_a h_1 + \dot{q}_b h_2 + \dot{q}_c h_3}{2\pi\varepsilon_0};$$

$$a^2\dot{U}_a = \frac{\dot{q}_a h_2 + \dot{q}_b h_1 + \dot{q}_c h_2}{2\pi\varepsilon_0};$$

$$a\dot{U}_a = \frac{\dot{q}_a h_3 + \dot{q}_b h_2 + \dot{q}_c h_1}{2\pi\varepsilon_0},$$

where

$$h_1 = \log\frac{2H}{r_p}, \quad h_2 = \log\frac{D'_{ab}}{D_{ab}}, \quad h_3 = \log\frac{D'_{ac}}{D_{ac}};$$

$D_{ab} = D$ is the distance between phase a and b conductors;

$D_{ac} = 2D$ is the distance between phase a and c conductors;

D'_{ab} is the distance between phase a conductor and the mirror image of phase b conductor;

D'_{ac} is the same for phase c.

As a result of the combined solution of the equations we obtain:

$$\dot{q}_a = 2\pi\varepsilon_0\dot{U}_a\frac{h'}{h}, \quad \dot{q}_b = 2\pi\varepsilon_0\dot{U}_a\frac{h''}{h}, \quad \dot{q}_c = 2\pi\varepsilon_0\dot{U}_a\frac{h'''}{h},$$

where

$$h = \begin{vmatrix} h_1 & h_2 & h_3 \\ h_2 & h_1 & h_2 \\ h_3 & h_2 & h_1 \end{vmatrix}; \quad h' = \begin{vmatrix} 1 & h_2 & h_3 \\ a^2 & h_1 & h_2 \\ a & h_2 & h_1 \end{vmatrix};$$

$$h'' = \begin{vmatrix} h_1 & 1 & h_3 \\ h_2 & a^2 & h_2 \\ h_3 & a & h_1 \end{vmatrix}; \quad h''' = \begin{vmatrix} h_1 & h_2 & 1 \\ h_2 & h_1 & a^2 \\ h_3 & h_2 & a \end{vmatrix}.$$

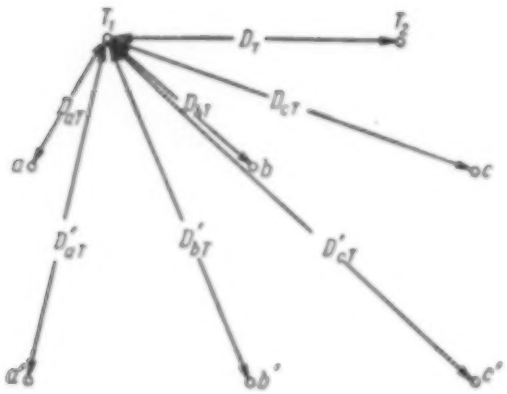

FIG. 3

Assuming that the earthwires are thin and arranged accurately along equipotential surfaces, the voltage in them relative to earth can be found:

$$\dot{U}_m = \frac{1}{2\pi\varepsilon_0} \sum_{k=a}^{c} \dot{q}_k \log \frac{D'_{mk}}{D_{mk}}.$$

Change in the order of sequence of the phases leads to conjugate values for the voltage in the earthwire.

The voltage in an earthwire when the line is operating under unbalanced phase conditions depends on the condition of the conductor which is out of the circuit. If the conductor is isolated then one must first determine some average voltage which will be produced in this conductor over the entire length of the transposition cycle, and then use the original equations to determine the charges q_a, q_b and q_c. If the conductor is connected to earth, the voltage in it can be taken as zero.

Translated by E. Bishop

REFERENCES

1. G.N. Baskakov; *Emkostnyi otbor moshchnosti ot vysokovol'tnykh linii elektroperedachi (Capacitative Power Take-off From High-voltage Transmission Lines)* Gosenergoizdat (1950).
2. A.I. Dolginov, I.G. Smirnov and V.D. Iurenkov; Earthing lightning-protection wires via spark-gaps, *Elektrichestvo*, No. 4 (1952).
3. A.I. Gershengorn, N.A. Mel'nikov and A.N. Sherentsis, The transposition of long transmission lines, *Elektrichestvo* No. 1 (1953).
4. N.A. Mel'nikov; *Raschety rezhimov raboty setei elektricheskikh sistem, (Calculation of Operating Conditions for the Circuits of Electrical Systems)*, Gosenergoizdat (1950).
5. N.F. Margolin; *Toki v zemle (Earth Currents)*, Gosenergoizdat (1947).

1958

6. P.A. Ionkin and G.V. Zeveke; *Osnovy elektrotekhniki (Fundamentals of Electrical Engineering)*, Gosenergoizdat (1956).

EXPERIMENTAL DETERMINATION OF PARAMETERS OF ELECTRO - TRANSMISSION: KUIBYSHEV HYDRO - ELECTRIC POWER STATION – MOSCOW*

D.E. ARTEM'EV and S.S. SHUR

Science and Research Institute for Direct Current

(Received 15 April 1957)

1958

For purposes of research, calculations, designing etc., it is necessary to know the parameters of electro-transmission not only for a frequency of 50 c/s, but also for frequencies within the range of variation of free oscillations in different transient processes and abnormal conditions.

The experiments the results of which are discussed in this article were conducted on two sections of the southern grid of the transmission line from Kuibyshev hydro-electric power station to Moscow; that is, Moscow - Vladimir, with a length of 117 km, and Moscow - Arzamas with a length of 391 km.

Let us mention the main characteristic features of the line from Kuibyshev hydro-electric station to Moscow.

The phases of this line are divided into three components, situated at the apices of an equilateral triangle with a distance between the components of $2d = 40$ cm. A mark ACO - 480 cable is used for the line. The diameter of each on the three conductors is $2a = 302$ mm. The total cross-section of aluminium is in the phase 1,440 mm². The distance between phases is $D = 10.5$ m; the height of the cables above the earth is 21.85 m; the mean value of the sag equals 11.9 m and the mean length of the span equals 450 m. On each section of the line, that is between any two switchgear points ot sub-stations, there is a full cycle transposition. The line is protected by two steel lightning-cables of 70 mm² cross-section; one of them is earthed through the towers along the whole length of the line, and the second one is insulated by arcing gaps. The angle of the protection cone is equal to about 17°. The earthing resistance of most of the towers varies within the range 2-6 Ω. The dependence of the parameters of the transmission line on the frequency may be determined by two methods:

(1) by measuring these parameters in stabilized conditions when feeding the line from a generator with a large variation of frequency;

(2) by measurements in unstabilized conditions of the discharge of a battery of

Elektrichestvo No. 1, 31 – 38, 1958 [Reprint Order No. EL 45].

capacitors into networks consisting of feeders of the line and earth ("method of damped oscillations").

The first method has the advantage that it is simple to use for interpreting experimental data. It disadvantages are that it is complex and expensive, that highly specialized equipment is required and that the exact measurement of resistance is difficult.

The second method has the advantages that it is simple to use, the equipment is readily available and reliable experimental data for determination of inductive reactances and resistances can easily be obtained. Its disadvantages are a rather cumbersome process of interpreting experimental data, and the necessity of arranging additional experiments for determination of capacitances of the system, since the error in finding them by the method of damped oscillations may be of the order of 10-15 per cent.

Taking into account the above advantages and disadvantages of the two methods, and the fact that for frequencies of less than 10 c/s per sec and height of the cables above the earth not exceeding a few tens of meters, the capacitances of the system are practically independent of the frequencies [1], and it is expedient to combine the two methods. We determine the proper and relative capacitances of the transmission system by the first method with a frequency of 50 c/s per sec and rated voltage. Inductive reactances and resistances for positive and zero sequences of the line, in a given range of frequencies, are measured by the second method.

Interphase capacitances and phase capacitances with respect to earth may be determined from the experiment, diagrammatically shown in Fig. 1. To ensure accuracy of the measurements, it is necessary to fulfil two conditions:

(1) the wave length of the section of line on test should be much less than $\frac{\pi}{2}$;

(2) the voltage graph during the test must not be distorted by the presence of higher harmonics. The more accurately these conditions are satisfied, the greater is the accuracy of the equations:

$$C_{11}+2C_{12}=\frac{I_A}{\omega l U_A}; \quad C_{12}=\frac{I_{BC}}{2\omega l U_A}, \tag{1}$$

where C_{11} is the capacitance of the phase with respect to earth per unit length of the line and C_{12} the interphase capacitance per unit length of the line.

The experiments made on the discharging of a battery of capacitors into the network consisting of phases of line and earth, enable us to determine the parameters of the equivalent circuit, representing the section of the line in question.

If the line is closed at one end and has a battery of capacitors at the other, then it may be shown, in the case of free oscillations of the system, that all harmonics with an index $k > 1$ are damped, approximately in accordance with the law $\exp(-R_k t/L_k)$ and harmonics with the index $k = 1$, in accordance with the law $\exp(R_1 t/2L_1)$; i.e. much more slowly, since for $k > 1$, because of the presence of skin - effect, $R_1/2L_1 < R_k/2L_k$. Therefore, after 2 - 3 half-periods of oscillations of

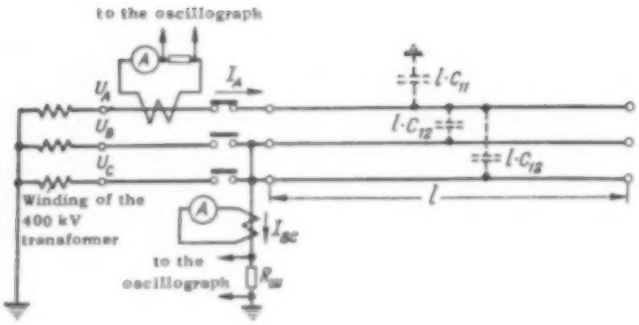

FIG. 1. Diagram for measurement of inductances of the line.

the lowest frequency, all high harmonics of the free oscillations, having index $k > 1$, will die out and the curve of discharge will practically become a damped sinusoid. Therefore, starting from a certain half-period, the line may be represented with sufficient accuracy by a single equivalent network, drawn for the lowest frequency of free oscillations, as shown in Fig. 2.

The equation characterizing the circuit in Fig. 2 will have the form:

$$C_n L_n R_d C_{bat} p^3 + [L_n (C_n + C_{bat}) + R_n C_n R_d C_{bat}] p^2 + \\ + [R_n C_n + (R_n + R_d) C_{bat}] p + 1 = 0. \tag{2}$$

It is easy to show that, if the relations $R_d < R_n$ and $10\, C_n < C_{bat}$ are satisfied, then, up to the value of the operator $p \leq (-0.2 + j1)\, 10^3$ equation (2) may be replaced by a simpler one:

$$p^2 + 2\alpha p + \omega_0^2 = 0, \tag{3}$$

where

$$\alpha = \frac{1}{2L_n}\left[R_n + R_d \frac{C_{bat}}{C_n + C_{bat}}\right]; \quad \omega_0^2 = \omega^2 + \alpha^2 = \frac{1}{L_n (C_n + C_{bat})}. \tag{4}$$

The error resulting from this simplification will be less than 1 per cent. The ratio of two adjacent maxima of the curve will be equal to $\exp(2\pi\alpha/\omega)$, whence

$$\alpha = \frac{\omega}{2\pi} \ln \frac{i_{max}^{(k)}}{i_{max}^{(k+1)}}. \tag{5}$$

On the basis of this discussion, we may formulate the following requirements, which must be satisfied to ensure the reliability of experimental results:

(1) resistances of connecting leads, earthings etc. should be small in comparison with the total resistance to be measured;

(2) capacitance of the battery should be at least to the order of one magnitude greater than

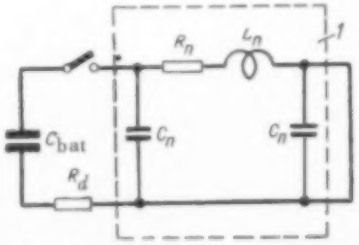

FIG. 2. Network of the experiment damped oscillations. 1. π - form equivalent circuit of the lines; R_d - total resistance of the connecting conductors and earthings.

1958

the total capacitance of the line;

(3) discharge currents should be sufficiently large, so that any occasional influences may be disregarded, and small enough, so that we may consider earthing resistances as linear and constant. The most suitable current to meet these conditions will be the current within the range of a few tens to a few hundreds of amperes.

Having found the discharge frequency ω from the oscillographs and the ratio of two adjacent maxima of the curve $i^{(k)}_{max} / i^{(k+1)}_{max}$ we determine by formulae (4) and (5) the resistance and inductive reactance of the circuit shown in the equivalent circuit diagram of the section of the line on test.

The parameters of the equivalent circuit Rn, Ln and Cn are expressed by the wave-length λ and wave impedance Z_B of the line, and, consequently, by the line parameters per unit length of the line.

In the case in question, the equivalent circuit of the line on test is set up for the operator $p = -\alpha + j\omega$; i.e. for a damped oscillations process. Because of this, the usual formulae relating line parameters per unit length and lumped parameters of the equivalent circuit R_n and L_n with quantities λ and Z_B, should be transformed. Deduction of these formulae is given in Appendix I. Only the final results and the order of calculation of the line parameters per unit length of the circuit in question are given here for the frequency ω and damping α.

We shall ignore the influence of the resistance on reactances of the equivalent circuit; it is well known that this simplification does not cause errors exceeding a fraction of 1 per cent, even for lines with a length of 60 – 70 el.deg. In this case, reactive components of the impedance and admittance of the equivalent circuit of the line network in question may be written in such a form:

$$j\omega L_n = jZ_B \sin\lambda; \quad j\omega C_n = j\frac{1}{Z_B}\tan\frac{\lambda}{2}, \tag{6}$$

where

$$Z_B = \sqrt{\frac{L}{C}}, \quad \lambda = \omega l\sqrt{LC};$$

L and C being inductance and capacitance per unit length of the line circuit on test.

By cross-multiplication of the first equation of (6) by the second equation of (4), we have

$$\frac{1}{C_n + C_{bat}} = \frac{\omega^2 + \alpha^2}{\omega^2}\frac{\lambda}{lC}\cdot\sin\lambda. \tag{7}$$

Multiplying equation (7) by the second equation of (6), and, substituting into the resulting expression the value $1/C_n + C_{bat}$ from equation (7), we obtain the following transcendental equation for the determination of λ:

$$\frac{\alpha^2}{\alpha^2 + \omega^2} = \cos\lambda - \frac{C_{bat}}{lC}\lambda\cdot\sin\lambda, \tag{8}$$

where C is a capacitance per unit length of the line, independent of a and ω, determined experimentally using asymmetrical idling.

For known λ and C, it is easy to find the inductance per unit length of the circuit in question:

$$L(a;\ \omega) = \frac{\lambda^2}{l^2 \omega^2 C}. \tag{9}$$

The resistance component of the impedance of the equivalent circuit (Fig. 2) is

$$R_a(a, \omega) = \mathrm{Re}[Z_{Ba} \sinh \lambda_a] \tag{10}$$

Formulae for determination of $Z_{Ba} = z_{Ba} e^{j\theta}$ and $\lambda_a = m + jn$ are given in appendix I.

Expanding expression (10), we have the transcendental equation

$$\frac{R_a(a, \omega)}{Z_{Ba}} + \sin\theta \sin n \cosh m = \cos\theta \cos n \sinh m \tag{11}$$

for determination of the resistance $R(a, \omega)$ per unit length of the circuit of the line on test.

The phenomena of skin effect, determining the dependence of line parameters on the frequency – other conditions being equal – differ for oscillations with constant amplitude, whose operator is $p = j\omega$, from damped oscillations, whose operator is $p = (-\alpha + j\omega) = (-\eta + j)\omega$. The method of damped oscillations gives the corresponding parameters per unit length of the circuit in question.

Let us consider the relationship between parameters $R(a, \omega)$ and $L(a, \omega)$ for circuits phase-phase and phase-earth, and parameters of positive and zero sequences of the transmission line for the undamped process.

Having the results of the experiment of the battery discharge into the network phase-phase, we can, by formulae (8), (9) and (11), directly determine products of active resistance and inductance of the positive sequence by a double length of the section of the line on test, $R_1(a, \omega)\ 2l$ and $L_1(a, \omega)\ 2l$. The active resistance for the positive sequence for an undamped process can be calculated using the value of the active resistance for the positive sequence, obtained from formula (II, 17) for a given damped process.

The inductance of the positive sequence may be represented as a sum of two inductances: external L_e and internal L_i. The first one, L_e, is determined by geometric dimensions and depends neither on frequency nor on damping. For a three-phase transposition line with one phase divided into three components and with horizontal conductors, L_e may be found from the formula:

$$L_e = \frac{\mu_0}{2\pi} \ln \frac{D_1}{a_{\mathrm{equ}}}, \tag{12}$$

where

$$D_1 = \sqrt[3]{2}D;\ a_{\mathrm{equ}} = \sqrt[3]{4ad^2}.$$

1958

The influence of damping on the internal induction L_i may be found from formulae (II,18).

Calculations by formulae (II,17) and (II,18) show that the calculation of damping when $\eta < 0.2$, within the range of frequencies 10 - 200 c/s, is practically superfluous, since the corresponding correction is only of the order of a small fraction of 1 per cent of the active resistance and of inductance for the positive sequence.

From the results obtained experimentally by the discharge of the battery into the phase-earth network, we determine the active resistance, equal to the sum $R_1(a;\omega) + R_2(a;\omega)$, and the inductance, equal to the sum $L_i(a;\omega) + L_2(a;\omega) + L_2$, where $R_2(a;\omega)$ and $L_2(a;\omega)$ are the active resistance and inductance, introduced into the line by an imperfectly conducting earth; L_2' is the inductance of the network phase-earth, assuming perfect earth conduction.

Inductance L_2' is calculated from the following formula, which is derived from formulae (II,13) when $s = 3$.

$$L_2' = \frac{\mu_0}{2\pi(1+\delta)} \ln \frac{2h_{equ}}{a_{equ}},$$

where

$$\delta = \frac{a(h_2 - h_1)}{2d^2}; \qquad h_{equ} = \sqrt[9]{h_2 h_1^2}. \tag{13}$$

Formulae for calculation of $R_2(\omega)$ and $L_2(\omega)$ for given values of $R_1(\omega)$ and $L_1(\omega)$ are given in Appendix II. It can be seen from formulae (II,19) and (II,20), that the ratio of the active resistances $\frac{R_{er}(a;\omega)}{R_{er}(\omega)}$ depends only on damping, characterized by parameter η. The ratio of the inductances $\frac{L_{er}(a;\omega)}{L_{er}(\omega)}$ depends on damping and on the parameter $\varkappa$, the value of which depends on an unknown quantity σ_e, specific earth conductance. Therefore, to be able to use expression (II,20), it is necessary to determine $\varkappa$, and consequently σ_e, from an auxiliary transcendental equation. This equation is derived by a transformation, leading to expression (II,20); when $s = 3$, we can ignore all terms in this equation with $\varkappa$ raised to a power greater than unity, since the error will not exceed 0.5 per cent. The equation has the following form:

$$\frac{\sqrt{2}}{3}\left[\sqrt{\sqrt{1+\eta_i^2} - \eta_i} - \eta_i \sqrt{\sqrt{1+\eta_i^2} + \eta_i}\right] \varkappa - \\ - \ln \varkappa = \frac{2\pi(1+\delta)}{\mu_0} L_{er}(a;\omega) - \eta_i \psi - 0{,}6166. \tag{14}$$

Equation (14) may have one or two roots, but only the smaller root has a real meaning.

After having found values $R_2(\omega)$ and $L_2(\omega)$, we can determine the parameters of the zero sequence from relations

$$R_0(\omega) = R_1(\omega) + 3R_2(\omega); \quad L_0(\omega) = L_i(\omega) + 3[L_2(\omega) + L_2'], \tag{15}$$

where L_2' is the inductance of the circuit three phases-earth, assuming a perfect earth conductance.

Inductance L_2 is calculated by the formula

$$L_2 = \frac{\mu_0}{2\pi(1+b)} \ln \frac{D'_{equ}}{D_{equ}}, \qquad (16)$$

where

$$D_{equ} = \sqrt[4]{a_{equ} D^2}.$$

The asymmetrical idling experiment was carried out on the Moscow - Vladimir section of the line from Kuibyshev hydro-electric power station to Moscow, at the rated line voltage. A scheme of the experiment is shown in Fig. 1.

The wave-length for this section at the frequency of 50 c/s is approximately equal to $0.75\,\pi/2$; consequently, voltages at the beginning and end of the idle phase differed one from the other by less than 0.5 per cent. The use of formulae (1) is therefore justifiable.

Table (1) shows the result, obtained by reading index instruments and from oscillographs, one of which is shown for purposes of illustration in Fig. 3.

TABLE 1.

Experiment	U_A (kV)	I_A (A)	I_{BC} (A)	C_{11} (μF / km)	C_{12} (μF / km)	C_{work} (μF / km)
27*	230	91.4	17.7	0.00872	0.001047	0.01187
		96.0	18.25	0.00922	0.001077	0.01244
28*	225	89.9	16.7	0.00884	0.001011	0.01186
		94.5	17.1	0.00935	0.001033	0.01245

* The first line gives the results obtained from oscillographs (first harmonic), and the second line those obtained by the reading of instruments.

The working capacitance of the line was calculated by the formula

$$C_{work} = C_{11} + 3C_{12}. \qquad (17)$$

As is seen from the oscillograph in Fig. 3 there all small per cent distortions present in the current of the order of 5 - 6 per cent are caused by the presence of higher harmonics. Because of this, capacitances calculated from index readings are slightly too large. Therefore, those values of capacitance calculated from the fundamental harmonic of current and voltage are accepted as the mean values (Table 5).

The experiments with damped oscillations were carried out on the phase - phase circuit on the Moscow - Vladimir section and phase - earth circuits on two sections, Moscow - Vladimir and Moscow - Arzamas.

During the experiments, the capacitances of batteries varied from 15 to 650 μF. The sum of resistances of earthing and of connecting conductors (R), was on the Moscow end of the line 0.51 Ω, Vladimir 0.8 Ω and in Arzamas 0.24 Ω. Phases not

used in the experiment were disconnected from both ends. The amplitudes of the discharge currents varied from 25 to 230.

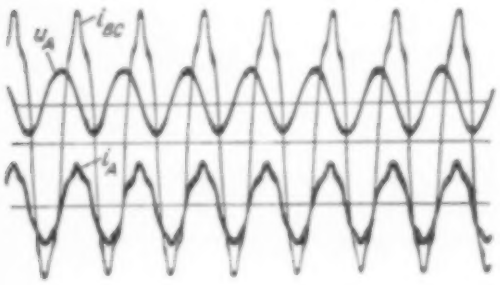

FIG. 3. The oscillographs of currents and voltages obtained from the experiment of asymmetrical idle running.

From the above conditions of these experiments, it follows that the use of the above formulae was justifiable.

For purposes of illustration, Fig. 4 shows oscillographs obtained from experiments with damped oscillations.

The results of experiments of the discharge of a battery of capacitors into the phase - phase network are given in Table 2. The experiments were carried out at temperatures of 0 - 2° C.

TABLE 2.

f (c/s)	α (1/sec)	Parameters of the positive sequence	
		$L_1(\omega)$ (μH/km)	$R_1(\omega)$ (Ω/km)
14.3	9.51	0.968	0.0207
17.4	9.54	0.967	0.0207
24.9	9.46	0.964	0.0206
35.3	10.1	0.955	0.0217
60.2	11.67	0.944	0.0251
77.0	12.59	0.935	0.0268
90.3	13.51	0.930	0.0289
118.7	15.05	0.928	0.0327

Graphs of dependence R_1 and L_1 on frequencies, plotted using the data of Table 2 are shown in Fig. 5. The external inductance L_e, calculated by formula (12), is also shown in this figure (horizontal dotted line). The difference $L_1(\alpha, \omega) - L_e = L_i$ gives the value of the internal inductance of the bundle of three conductors, which is necessary for the calculations.

The results of the discharge of a battery of capacitors into the phase-earth network are given in Table 3 (Moscow - Arzamas section) and in Table 4 (Moscow - Vladimir section) and the corresponding graphs in Fig. 5 and 6.

For the frequency 50 c/s the inductances of the positive and zero sequences were also measured under static conditions of short-circuit. The results obtained were very near to those obtained by the method of damped oscillations for the same frequency.

Table 5 gives the values

TABLE 3.

f (c/s)	α (1/sec)	$R_1(\alpha;\omega) + R_{er}(\alpha;\omega)$ (Ω/km)	$L_i(\alpha;\omega) + L_2' + L_e(\alpha;\omega)$ (μH/km)	Parameters of the zero sequence	
				$R_0(\omega)$ (Ω/km)	$L_0(\omega)$ (μH/km)
7.3	6.41	0.03385	1.850	0.0571	3.979
13.9	7.91	0.04143	1.830	0.0783	3.918
20.1	10.72	0.05425	1.754	0.1155	3.685
34.4	15.75	0.07968	1.718	0.1866	3.559
48.3	20.2	0.10440	1.679	0.2553	3.479

of the parameters of the line from Kuibyshev HEPS to Moscow, obtained experimentally at the frequency of 50 c/s. For comparison, it also gives values of these parameters, calculated by the Carson formulae and from the Maxwell equations, with and without consideration of the earthed steel cable. The values calculated, disregarding the earthed cable, are taken from those of the project of electrotransmission, designed by the *Teploelektroproekt* (Electric power and heat generating project). As can be seen from Table 5, the values of inductance of the positive sequence and of the partial capacitance of the phase with respect to earth are near to the values assumed in the design.

The interfacial capacitance obtained experimentally differs from the value assumed for the design by 24 per cent, but practically coincides with that obtained from calculations, taking into account the earthed cable. Therefore, the experimental value of the working capacitance is near enough to that used for design calculations.

T The experimental value of the active resistance of the positive sequence exceeds the value taken for

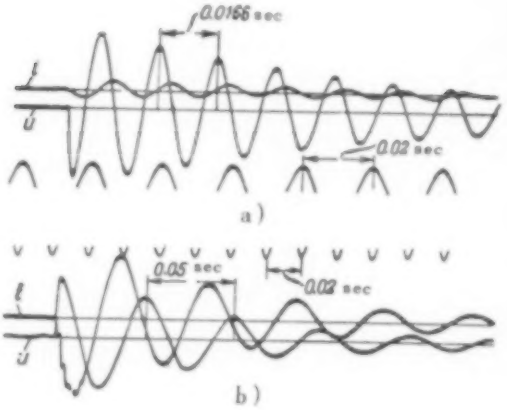

FIG. 4. The oscillographs of current and voltage obtained from the experiment with damped oscillations. (a) discharge of the battery into the network phase - phase; (b) discharge of the battery into the network phase - earth.

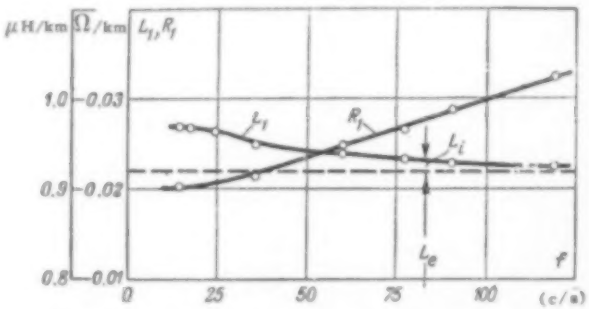

FIG. 5. Dependence of parameters of the positive sequence on the frequency.

TABLE 4.

f (c/s)	α (1/sec)	$R_1(\alpha;\omega)+R_{ef}(\alpha;\omega)$ (Ω/km)	$L_1'(\alpha;\omega)+L_2'+L_e(\alpha;\omega)$ (μH/km)	Parameters of the zero sequence	
				$R_0(\omega)$ (Ω/km)	$L_0(\omega)$ (μH/km)
13.5	11.57	0.0550	1.883	0.1137	4.040
14.5	12.10	0.0576	1.888	0.1212	4.056
17.9	13.15	0.0628	1.850	0.1365	3.951
26.1	16.37	0.0772	1.760	0.1781	3.667
37.5	21.07	0.0939	1.700	0.2395	3.511
52.9	29.02	0.1471	1.685	0.3681	3.474
65.1	35.46	0.1710	1.648	0.4359	3.379
84.6	42.41	0.1999	1.602	0.5147	3.253
100.8	56.61	0.2630	1.573	0.6857	3.172
135.5	70.78	0.3115	1.486	0.8447	2.920

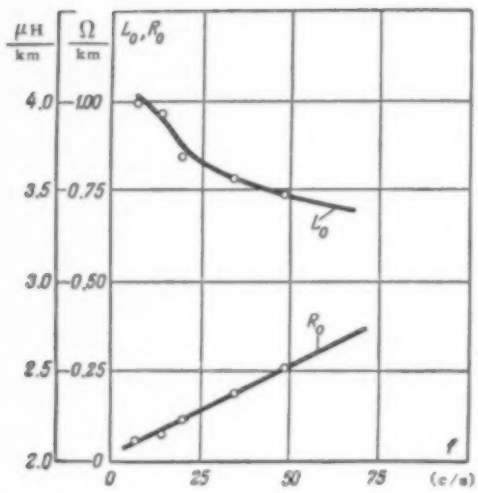

FIG. 6. Dependence of parameters of the zero sequence on the frequency for the Moscow - Arzamas section of the line.

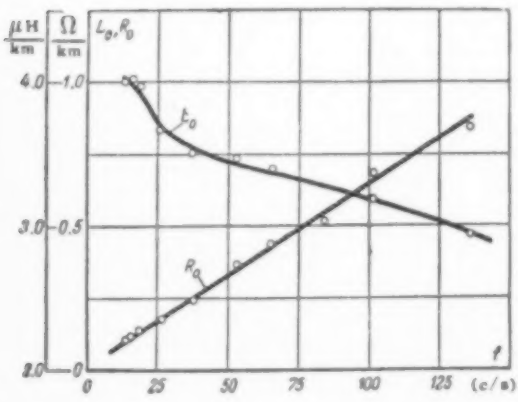

FIG. 7. Dependence of parameters of the zero sequence on the frequency for the section of the line from Moscow to Vladimir.

design purposes approximately by 7.5 per cent, and this can be attributed to the influence of tie beams, terminal fittings and other parts fixed on split feeders of the line. Measurements taken in the Science and Research Institute for direct current and in the central science and research laboratory of the Moscow Electric Station have shown that tie-beams and other fittings are a source of additional losses in the line.

Experimental values of the active resistance of the zero sequence differ considerably from those assumed in the design project and differ slightly less from those obtained from calculations, considering the influence of the steel cable. From this, the influence of the earth conductance is also clearly seen on different sections.* According to Carson's theory, this should not occur at low frequencies. The dependence of line parameters on frequency, found from experiments, is sufficiently near to the dependence given by Carson [for low frequencies $R_0(\omega)$ is practically a straight line]. Evidently, Carson's assumption about unbound and homogeneous earth is valid for high frequencies and good for the determination of the character of the function $R_0(\omega)$, but is inadmissible for purely quantitative calculations for frequencies within the range of a few hundred c/s.

* According to regulations [2], the earth conductance on the Moscow - Vladimir section is approximately equal to 65×10^{-9} $1/\Omega$ cm, and on the Moscow - Arzamas section to 35×10^{-9} $1/\Omega$ cm.

TABLE 5.

Description of parameter	Value of the parameter obtained from experiment	Value of the parameter obtained from calculations	
		Taking into account the earthed steel cable	From the transmission design
Partial phase capacitance with respect to earth C_{11} (μF/km)	0.00878	—	0.00867**
Interphase capacitance C_{12} (μF/km)	0.001030	0.001060	0.001276
Working capacitance C_{work} (μF/km)	0.01187	0.01185	0.01250
Active resistance of the positive sequence R_1 (Ω/km)	0.0236	—	0.0220
Inductance of the positive sequence L_1 (μH/km)	0.946	—	0.948
Active resistance of the zero sequence R_0 (Ω/km)			
for section 117 km long	0.365	0.282/0.359*	0.171
for section 391 km long	0.257	0.275/0.348*	
Inductance of the zero sequence L_0 (μH/km)			
for section 117 km long	3.466	3.410	2.970
for section 391 km long	3.446	3.560	

* Value in the numerator for steel cable resistance R cable = 2.0 Ω/km, in the denominator for R cable = 1.5 Ω/km.

** Taking into account the steel cable.

As can be seen from Table 5, the inductance of the zero sequence, calculated by Carson's formulae, taking into account the influence of the steel cable, is sufficiently accurate for practical purposes.

With the variation of frequency from 10 to 130 c/s, the active resistance of the

positive sequence increases approximately 1.5 times, and that of the zero sequence 8 to 10 times. Inductances, as could be expected, increase less (by 20 - 25 per cent), therefore, in practical calculations and in research, we can disregard variation of inductance with frequency, if the wave - length of the line for a given frequency is not too near to $\pi/2$. It is desirable to take into consideration the variation of the active resistances with frequency, particularly for the determination of surge currents and voltages.

Thus, with free oscillations, damping manifests itself in effect only by the influence on the active resistance of the zero sequence. Nevertheless, increase of R_0 due to damping is small, and for practical calculations we may use the simplest formula (II,19).

In conclusion, it is necessary to point out that the experimental data discussed are related only to the region of comparatively low frequencies. For calculation of transient processes in long-distance lines it may be necessary to know the resistances at higher frequencies, of the order of hundreds of c/s. For determination of these resistances it may be expedient to perform additional experiments.

The authors express their gratitude to the employees of the transmission line from Kuibyshev hydro-electric station to Moscow, to E.P. Belov and to P.I. Gedinia for their daily help in carrying out these experiments.

Appendix I.

Expressions for wave resistance and wave length of the line during the damped sinusoidal process.

Let the process occurring in the line correspond to the law

$$\dot{U}e^{(-\alpha+j\omega)t} \text{ and } \dot{I}e^{(-\alpha+j\omega)t}. \tag{I,1}$$

Substituting expressions (I,1) into the equation of a long-distance line, after simple transformations we have:

$$\frac{d^2\dot{U}}{dx^2} - \gamma^2\dot{U} = 0; \quad \frac{d^2\dot{I}}{dx^2} - \gamma^2\dot{I} = 0, \tag{I,2}$$

where

$$\gamma^2 = (R - \alpha L + j\omega L)(g - \alpha C + j\omega C). \tag{I,3}$$

From expressions (I,2) and (I,3) it is seen that the transformation of the known formulae, giving the relation between parameters λ_α and Z_B for a damped wave $\exp[(-\alpha + j\omega)t]$ and undamped sinusoidal oscillations, consists in replacing R by $R^1 = R(\alpha, \omega) - \alpha L(\alpha, \omega)$ and g by $bg' = g - \alpha C$. Let us perform this substitution.

$$\begin{aligned} Z_{B\alpha} &= z_{B\alpha}[\cos\vartheta + j\sin\vartheta] \approx \sqrt{\frac{R - \alpha L + j\omega L}{-\alpha C + j\omega C}}, \\ \lambda_\alpha &= m + jn \approx l\sqrt{(R - \alpha L + j\omega L)(-\alpha C + j\omega C)}. \end{aligned} \tag{I,4}$$

In expressions (I,4) it is taken into consideration that, as a rule, $10\,g < \alpha\,C$.

Separating on the right-hand side of expressions (I,4) the real and imaginary terms, we have the components of the wave impedance:

$$Z_{Bs} = \sqrt[4]{\frac{(R-\alpha L)^2+\omega^2 L^2}{C^2(\alpha^2+\omega^2)}}; \quad 2\vartheta = \tan^{-1}\frac{-\omega R}{L(\alpha^2+\omega^2)-\alpha R} \tag{I,5}$$

and the components of the wave length

$$\left.\begin{matrix} m \\ n \end{matrix}\right\} = l\sqrt{\frac{C}{2}} \times$$
$$\times \sqrt{\mp L(\omega^2-\alpha^2) \mp \alpha R + \sqrt{(\alpha^2+\omega^2)[(R-\alpha L)^2+\omega^2 L^2]}}. \tag{I,6}$$

Remembering that for frequencies $f > 5\text{-}7$ c/s the inequality $(R-\alpha L) \ll \omega^2 L^2$ holds good, it is easy to reduce formulae (I,6), to a form more convenient for calculations. For this purpose, we expand the internal square root in the formulae (I,6), into the power series

$$\frac{\omega^2(R-2\alpha L)^2}{[L(\omega^2-\alpha^2)+\alpha R]^2} \ll 1.$$

Restricting ourselves to the first two terms of the expansion we have

$$m = \frac{\omega l\sqrt{C}}{2}\cdot\frac{R-2\alpha L}{\sqrt{L(\omega^2-\alpha^2)+\alpha R}}; \quad n = \frac{l\sqrt{C}}{2}\sqrt{\frac{4[(\omega^2-\alpha^2)L+\alpha R]^2+\omega^2(R-2\alpha L)^2}{L(\omega^2-\alpha^2)+\alpha R}}. \tag{I,7}$$

Appendix II

The relation between parameters of the transmission line for the sinusoidal processes dying away with time.

The solution of the problem is applicable to the three-phase line with phases divided into three conductors (Fig. 8) for a sinusoidal time-attenuated process.

$$e^{pt} = e^{(-\eta+j)\omega t}, \quad 0 \leqslant \eta < 1, \tag{II,1}$$

It is convenient to carry out this solution exactly by the methods of Grinberg and Bonshtedt [1], ignoring the influence of the proximity of phases; i.e., representing a system of s conductors-earth, as s separate conductor-earth systems, and to find field components in air and in earth by superimposing s fields, corresponding to s separate conductor-earth systems. In future we shall use the following notation: medium 1 – conductors, medium 2 – air, medium 3 – earth. Remaining notations are clear from Fig. 8, or are given in the text.

Expressions for field components of the conductor-earth system inside any of the three media (conductor, air, earth), for sinusoidal processes are derived in [1]. The derivation of these expressions for processes of type (II,1) shows that they will have the same form, the only difference being that $j\omega$ should be replaced by

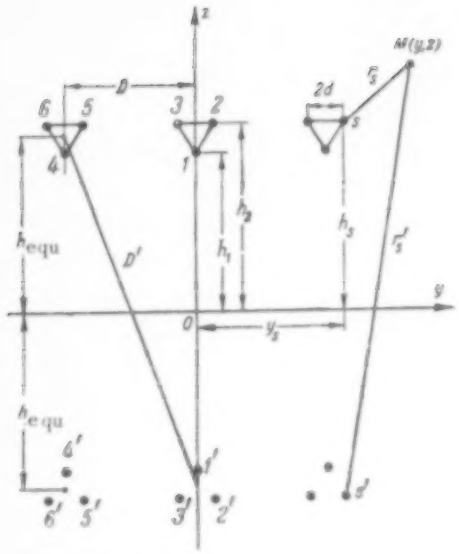

FIG. 8. Layout of the conductors of the line.

$p = (-\eta + j)\omega$. Therefore, we shall not give this derivation; we shall write only these expressions of field components, which are the constants of integration of the Maxwell equations obtained from boundary conditions of the given problem. We shall also give the equations for determination of the complex propagation constant, which will be necessary for further discussion.

The intensity of the electric field in air may be represented in such a form as this:

$$\overline{E}^{(2)} = \overline{E}^{(2)\,0} - \overline{E}_1^{(2)}, \qquad \text{(II,2)}$$

where $\overline{E}_1^{(2)}$ is the intensity of the secondary electric field in air, due to the presence of earth; $\overline{E}^{(2)\,0}$ is the intensity of the electric field of the conductor, situated in an infinitely homogeneous medium (air).

The components of the field intensity of separate conductors along the z axis are given by the following expressions written in the Gauss system of units.

$$E_{sz}^{(2)\,0} = -\frac{jq}{m_2^2} C \frac{\partial}{\partial z} H_0(m_2 r_s). \qquad \text{(II,3)}$$

$$E_{sz}^{(2)} = \frac{2qC}{\pi m_2^2} \int_0^\infty \frac{\varepsilon_3' \gamma_2 - \varepsilon_2' \gamma_3}{\varepsilon_3' \gamma_2 + \varepsilon_2' \gamma_3} e^{-\gamma_s (z+h_s)} \cos \nu (y - y_s)\, d\nu,$$

where (II,4)

$$\gamma_i = \sqrt{\nu^2 - m_i^2}; \quad \operatorname{Re} \gamma_i > 0;$$

$$m_i = \sqrt{k_i^2 - \zeta^2}, \quad \operatorname{Im} m_i > 0;$$

$$k_i = -j \frac{p}{C} \sqrt{\varepsilon_i' \mu_i}, \quad \operatorname{Im} k_i > 0.$$

$\varepsilon_i' = \varepsilon_i + \dfrac{4\pi\sigma_i}{p}$ is the complex dielectric constant; σ_i is the specific electric conductance of the ith medium; H_0 is the Hankel function of the first kind of zero order.

The resultant field in the second medium (air) will be determined if we add the component fields of all nine conductors.

The constant of integration C is expressed by the parameters of the system and by the current in one conductor I_1:

$$C = \frac{l_1 m_2 z_1'}{2ra z_1} \times \frac{1}{H_1(m_2 a) + \frac{2(h_2 - h_1)}{\sqrt{d^2 + (h_2 - h_1)^2}} H_1(m_2 \sqrt{d^2 + (h_2 - h_1)^2}}. \qquad (II,5)$$

Using the above quoted method of Grinberg and Bonshedt we can deduce the following equation for the approximate determination of the complex propagation constant q of the system in question:

$$\left(\frac{m_2}{k_2}\right)^2 \frac{1}{1+\delta}\left(\ln\frac{2h_1}{a} + \sum_{s=2}^{9} \ln\frac{\sqrt{y_s^2 + (h_s + h_1)^2}}{\sqrt{y_s^2 + (h_s - h_1)^2}}\right) = \frac{1}{1+\delta}\sum_{s=1}^{9} F_s - \frac{1}{ak_1}\frac{J_0(ak_1)}{J_0'(ak_1)}, \qquad (II,6)$$

where

$$\delta = \frac{2a(h_2 - h_1)}{d^2 + (h_2 - h_1)^2}; \quad F_s = 2\varkappa_2' \int_0^\infty \frac{\gamma_1\gamma_0 - \nu^2}{k_3^2\gamma_2 + k_2^2\gamma_3} e^{-\gamma_0(h_1 + h_s)} \cos \nu y_s d\nu.$$

The calculation of the integral F_s, within the limits $\omega < 10^9$, $\sigma_3 > 10^7$, with an error not exceeding 0.25 per cent, gives as the first approximation

$$F_s = 2\left\{-\frac{(h_1 + h_s)^2 - y_s^2}{[(h_1 + h_s)^2 + y_s^2]^2} \cdot \frac{1}{k_3^2} + \frac{1}{2}\frac{1}{\varkappa_s'}\left[\frac{\pi}{2} Y_1(\varkappa_s') - \right.\right.$$

$$\left. - \sum_{n=1}^{\infty} (-1)^{n-1} \frac{(\varkappa_s')^{2n}}{1^2 \cdot 3^2 \ldots (2n-1)^2 (2n+1)}\right] + \frac{1}{2}\frac{1}{\varkappa_s''}\left[\frac{\pi}{2} Y_1(\varkappa_s'') - \qquad (II,7)$$

$$\left. - \sum_{n=1}^{\infty} (-1)^{n-1} \frac{(\varkappa_s'')^{2n}}{1^2 \cdot 3^2 \ldots (2n-1)^2 (2n+1)}\right]\right\},$$

where

$$\varkappa_s' = k_2[y_s - j(h_1 + h_s)], \quad \varkappa_s'' = k_2[-y_s - j(h_1 + h_s)].$$

$Y_1(x)$ is the Bessel function of the second kind and of the first order.

Let us determine the parameters of the zero sequence per unit length of the line.

The equations for the long-distance line for time-damped sinusoidal processes, ignoring the active conductance of the earth, can be written in the following form:

$$jqU = \left(R_0' + \frac{p}{c^2} L_0'\right) I; \quad pC_0' U = jqI, \qquad (II,8)$$

where R_0', L_0', C_0' are active resistance, inductance and capacitance, respectively, per unit length of the line, when the currents flowing in all conductors are in the

same phase. The total current flowing in all conductors of the line $I = 9 \sum I_1$, voltage

$$U = -\int_0^{h_1-a} E_z^{(2)}|_{y=0}\, dz. \tag{II,9}$$

Let us substitute into equation (II,9) expressions (II,3) and (II,4) for the components of the field intensity. For frequencies $\omega \leqslant 10^6$, earth conductance $\sigma_3 \geqslant 10^7$, the height of the conductors above the earth being of the order of a few tens of metres, we can derive the following expression for the voltage:

$$U = \frac{jqI}{9p}\,\frac{1}{1+\delta}\left[\ln\frac{2h_1}{a} + \frac{1}{2}\sum_{s=2}^{9}\ln\frac{y_s^2+(h_s+h_1)^2}{y_s^2+(h_s-h_1)^2}\right]. \tag{II,10}$$

The error in using formula (II,10) will not exceed 0.5 per cent.

From the second equation of (II,8), taking into consideration (II,10), we have

$$C_0' = \frac{9(1+\delta)}{2\left[\ln\frac{2h_1}{a} + \frac{1}{2}\sum_{s=2}^{9}\ln\frac{y_s^2+(h_s+h_1)^2}{y_s^2+(h_s-h_1)^2}\right]}. \tag{II,11}$$

Substituting into the first equation (II,8) expressions (II,10) and (II,11), we have the equation which, in view of (II,6), is reduced to this form:

$$c^2R_0' + pL_0' = \frac{2p}{9(1+\delta)}\left[\ln\frac{2h_1}{a} + \frac{1}{2}\sum_{s=2}^{9}\ln\frac{y_s^2+(h_s+h_1)^2}{y_s^2+(h_s-h_1)^2}\right] - \tag{II,12}$$

$$-\frac{2p}{9(1+\delta)}\sum_{s=1}^{9}F_s + \frac{1}{9}\,\frac{2p}{ak_1}\cdot\frac{J_0(ak_1)}{J_0'(ak_1)}.$$

Equation (II,12), can be written in the form

$$Z_0' = pL_2' + Z_{er} + Z_1,$$

where L_2' is the external inductance, of the line assuming ideal earth conductance

$$L_2' = \frac{1}{C_0'}; \tag{II,13}$$

Z_{er} is the total impedance, introduced into the line by non-ideal earth conductance:

$$Z_{er} = -\frac{2p}{9(1+\delta)}\sum_{s=1}^{9}F_s. \tag{II,14}$$

Z_1 is the total impedance of line conductors for time attenuated alternating current (impedance of the positive sequence):

$$Z_1 = \frac{1}{9}\,\frac{2p}{ak_1}\,\frac{I_0(ak_1)}{I_0'(ak_1)}. \qquad \text{(II,15)}$$

For practical calculations it is convenient to use the following formulae for determination of the active resistance and inductance of the zero sequence:

$$R_0 = 3R_0' = \frac{1}{3}(R_1 + R_{er}); \qquad L_0 = 3L_0' = \frac{1}{3}(L_i + L_{er} + L_2). \qquad \text{(II,16)}$$

Dependences of resistances R_1 and R_2, and of inductances L_i and L_2 on the damping parameter η, may be conveniently represented as the dependence on damping of the ratios of these values to the corresponding values (say R_1', R_2'; L_i', L_2'), measured when damping is absent, i.e. when $\eta = 0$. For real lines, when radius, height of conductors above earth and frequency of the process are not too large, formulae (II,14) and (II,15) may be considerably simplified, if we expand into the power series the transcendental functions of these equations and restrict ourselves to a few terms of expansion. In this case, the error will not exceed 0.5 per cent. For $m = \frac{1}{4}\,a^2\omega\,\mu_0\sigma_1 < 2$, the following expressions can be obtained for active resistance and internal inductance of the conductor:

$$\frac{R_i(x;\,\omega)}{R_1(\omega)} = 1 + \eta_i^2\,\frac{m^2}{12} + \eta_i(1+\eta_i^2)\,\frac{m^3}{24} + \quad \eta_i^2(1+4\eta_i^2)\,\frac{m^4}{240} - \eta_i(1+\eta_i^2)(8-5\eta_i^2)\,\frac{m^5}{862}; \qquad \text{(II,17)}$$

$$\frac{L_i(x;\,\omega)}{L_i(\omega)} = 1 + \eta_i\,\frac{m}{3} + \eta_i^2\,\frac{m^2}{8} - \quad \eta_i(5-8\eta_i^2)\,\frac{m^3}{180} - \eta_i^2(5-3\eta_i^2)\,\frac{m^4}{240}. \qquad \text{(II,18)}$$

For $X < 9.3$ and distances between the conductors of adjacent phases not exceeding the distances between the conductor and earth, for active resistances and inductances in the line to earth, we can use the formulae:

$$\frac{R_g(x;\,\omega)}{R_g(\omega)} = \frac{4}{\pi}(1+\eta_i^2)\,\phi; \qquad \frac{L_g(x;\,\omega)}{L_g(\omega)} = 1 + \frac{2\eta_i\phi}{1 - 2\ln\frac{\gamma\rho x}{2}} - \qquad \text{(II,19)}$$

$$- \frac{2\sqrt{2}}{3}\,\frac{x}{1 - 2\ln\frac{\gamma\rho x}{2}}\left[1 - \frac{2\eta_i\phi}{1 - 2\ln\frac{\gamma\rho x}{2}} - \sqrt{1-\eta_i} + \eta_i\sqrt{1+\eta_i}\right]. \qquad \text{(II,20)}$$

where $\phi = \tan^{-1}\sqrt{\dfrac{\sqrt{1+\eta_i^2}+\eta_i}{\sqrt{1+\eta_i^2}-\eta_i}}$; $x = 2h_{equ}\sqrt{\omega\mu_0\sigma_2}$;

$\rho = \dfrac{D'_{equ}}{2h_{equ}}$; $D'_{equ} = \sqrt[9]{2h_{equ}(D')^8}$; $h_{equ} = \sqrt[9]{h_2 h_1^8}$.

1958

If the formulae (II,19) and (II,20) are used, the error will not exceed 0.5 per cent.

REFERENCES

1. G.A. Grinberg and B.E. Bonshteot; Asnovy tochnoi teorii volnovogo polga linuu peredachi (Basis of an accurate theory of the wave field of transmission lines), *Zh. tekh. fiz.*, 24, 1 (1954).
2. *Pravila ograhdeniia sooruzherii soiazi u signalizatsii ot vrednogo deistviia ustanovok silnogo toka (Rules for the protection of communication installations and the indication of faults).*

PARTIAL CAPACITIES (CONDUCTIVITIES) OF A SYSTEM OF ELECTRODES AND SEPARATE FLUXES OF THE RESULTANT FIELD *

E.A. MEEROVICH and V.K. RED'KIN

Moscow

(Received 25 April 1957)

1958

The point of view has been put forward that partial fluxes of the electrical displacement vectors in charged conductors, in the general case, are numerically equal to the charges in the partial capacities. This point of view is erroneous, and in engineering calculations it can lead to inaccuracies.

Let us consider the electrostatic field of n conducting charged bodies in a linear dielectric medium (Fig. 1).

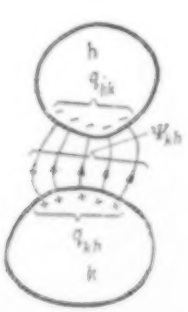

FIG. 1.

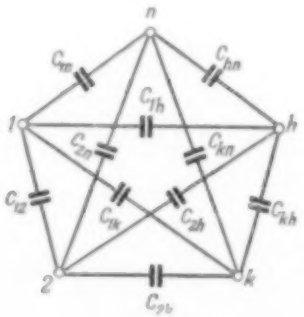

FIG. 2.

The following symbols are used:

- q_k the excess charge on body k;
- ϕ_k the potential of the body;
- D the lectrical displacement vector;
- S_k the surface area of body k;
- ψ_k the flux due to the electrical displacement vector across the surface area S_k;

* *Elektrichestvo* No. 1, 54-57, 1958 [Reprint Order No. EL 46].

ψ_{kh} the partial flux due to the electrical displacement vector across surface area S_k, linked only to area S_h;
q_{kh} that part of the charge on body k, relating to the partial flux ψ_{kh};
C_{kh} the partial capacitance between k and h.

The flux of the electrical displacement vector across the surface of body k equals the excess charge on this body:

$$\psi_k = q_k.$$

The partial flux ψ_{kh} resides on parts of the surfaces of bodies k and h, on which there are charges, equal in magnitude and opposite in sign, $q_{kh} = -q_{hk}$.

Let the sign of the partial flux ψ_{kh} correspond to the sign of the charge on that portion of the body k on which this charge resides. In this case the following equations are valid:

$$q_{kh} = \Psi_{kh} \text{ and } \Psi_{kh} = -\Psi_{hk},$$

whilst the fluxes of the electrical displacement vectors and the excess charges are determined by the equations:

$$\left.\begin{aligned} \Psi_k &= \sum_{h=1}^{n} \Psi_{kh}, \ (h \neq k); \\ q_k &= \sum_{h=1}^{n} q_{kh}, \ (h \neq k). \end{aligned}\right\} \tag{1}$$

The excess charges on the bodies can also be determined from the equations containing the partial capacities:

$$q_k = \sum_{h=1}^{n} C_{kh} (\varphi_k - \varphi_h), \ (h \neq k). \tag{2}$$

To equations (2) there corresponds an equivalent circuit in the form of a closed network (Fig. 2), the elements of which are condensers equal to the partial capacities of the system of bodies.

This network may be regarded as analogous to the system of n bodies in the sense that if to each body there corresponds a given node, and if the excess charge on each body equals the sum of the charges on the plates of the condensers connected to the node representing that body, the potential difference between any two bodies will be identical to the potential difference between the nodes corresponding to those bodies. On the other hand, if the potential differences between nodes and between the bodies to which they correspond are

equal, then the excess charge on each body will equal the sum of the charge on the plates of the condensers connected to the node representing this body.

Another system of indices is sometimes used in literature to denote the partial capacitances. It is normally used in those cases when the fields of bodies are considered in the presence of the earth. The earth is regarded as the $(n+1)$th body, of infinitely large size and at zero potential [1, p.85]. In this case the partial capacities of the bodies relative to earth are denoted by two identical indices (C_{kk}) and are called self-capacities, whereas the other partial capacities (C_{kh}) are called mutual.

Since the set of bodies under consideration need not include a body of infinite size and the potential may be taken as zero at any desired point, the partial capacities will not be divided into self and mutual in this paper. It should be noted that the index system has no effect on subsequent deductions.

From equations (1) and (2) if follows that

$$\sum_{h=1}^{n} q_{kh} = \sum_{h=1}^{n} C_{kh}(\varphi_k - \varphi_h), \quad (h \neq k). \tag{3}$$

However a number of authors consider that there is also a further relationship, as follows:

$$\Psi_{kh} = q_{kh} = C_{kh}(\varphi_k - \varphi_h). \tag{4}$$

This is equivalent to the assertion that the partial fluxes of the electrical displacement vectors are numerically equal to the corresponding terms on the right hand side of equations (2), i.e. to the charges on the corresponding condensers in the equivalent circuit.

For example, it is stated [1, p. 86] that the separate terms on the right hand side of the equations containing the partial capacities determine the respective parts of the displacement fluxes emanating from the charged bodies. Thus, for example, that part of the flux emanating from the first body equal to $C_{11}(\varphi_1 - 0)$ represents the total number of unit tubes of flux passing from the first body to the surface of the earth. Another part of the same flux, equal to $C_{12}(U_1 - U_2)$ represents the total number of unit tubes of flux passing from the first body to the second and so on. In fact, a similar assertion is made in [2, 3].

No less definite statements are found in foreign publications. For example in [4] formulae are given for calculating the partial capacities in the equivalent circuit, which correspond to relationship (4):

$$C_{10} = \frac{q_{10}}{\varphi_1 - \varphi_0}; \quad C_{12} = \frac{q_{12}}{\varphi_1 - \varphi_2}; \quad C_{02} = \frac{q_{02}}{\varphi_0 - \varphi_2}.$$

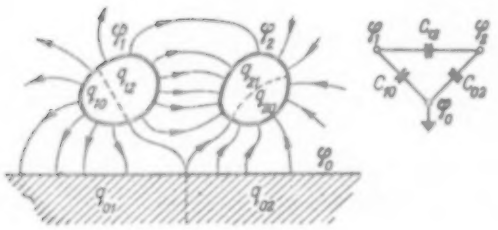

FIG. 3.

This relationship is illustrated in Fig. 3 taken from [4] *.

We shall show that this point of view is erroneous. We assume that the medium is uniform, the sum of all the charges on the bodies is zero, all the surfaces S_k are smooth and none of them completely encloses any other surface.

Under these conditions the following propositions may be established for a system of n charged bodies.

1. On the surfaces of the bodies which have a maximum or minimum potential in the given field, the values of the modulus of the electrical displacement vectors exceed some positive number. The validity of this proposition follows from the general theory of harmonic functions [5].

2. None of the partial capacities is zero. This corresponds to the Maxwell proposition [6] that the mutual electrostatic induction coefficients of a system of bodies are negative if the condition is observed that none of the surfaces completely encloses any other surface.

The second proposition is easily derived.

In fact, the partial capacities are equal to the mutual electrostatic induction coefficients, with the signs reversed. To determine the partial capacities C_{kh}, relating to body k, it is necessary, for example, to impart to it a potential of ϕ_k; and to the remaining bodies a potential of ϕ, equal on them all, but such that $\varphi_* \neq \varphi_k$. Then, in accordance with the first proposition, all the charges ϕ_{kh} will differ from zero.

In these conditions, we have for the partial capacities:

$$C_{kh} = \frac{q_h}{\varphi_* - \varphi_k} > 0.$$

Without disturbing the general nature of the proof, we shall further consider fields in which the bodies, except k and h, can be replaced by a single body Σ (Fig. 4).

* Fig. 3 (also corresponds to Fig. 4-9, in [2].

The method of proof will be by *reductio ad absurdum*. Assume that equation (4) is valid whatever potentials the bodies are at. Take the case when the potentials are different for each body, i.e.

$$\phi_k \neq \phi_{\underset{\sim}{k}} \neq \phi_{\underset{\sim}{\Sigma}} \text{ whilst } \phi_k > \phi_{\underset{\sim}{\Sigma}} \text{ and } \phi_{\underset{\sim}{k}} > \phi_{\underset{\sim}{\Sigma}}.$$

Since none of the partial capacities is equal to zero, the following picture must be set up of the flux distribution. Two partial fluxes emanate from the surface of each body, whilst the total number of partial fluxes is equal to three, since $|\psi_k| = |\psi_{\underset{\sim}{k}\underset{\sim}{k}}|$. The partial fluxes emanating from the body with a potential intermediate between those of the other two will clearly have opposite directions relative to the normal direction outwards from the surface of the body in question.

The selected potential distribution can be regarded as resulting from the superimposition of two conditions, shown schematically in Fig. 4a, b, the values e' and e'' of the e.m.f. being taken as follows:

$$e' = \varphi_k - \varphi_{\underset{\sim}{\Sigma}}; \quad e'' = \varphi_{\underset{\sim}{k}} - \varphi_{\underset{\sim}{\Sigma}}.$$

In each of these cases two bodies in the system are at the same potential, and consequently there is no partial flux between them.

According to the first proposition, it follows that for any value of $(\phi_{\underset{\sim}{k}} - \phi_{\underset{\sim}{\Sigma}})$ a value of $(\phi_k - \phi_{\underset{\sim}{\Sigma}})$ can be found such that the value of the modulus of the electrical displacement vectors at any points on the surfaces $S_{\underset{\sim}{k}}$ and S_k will be greater for the condition of Fig. 4b, than for that of Fig. 4a. In that case, after superimposition, the electrical displacement vector will not change direction relative to the normal direction outwards from one of the surfaces; in other words, the flux distribution corresponds to Fig. 4c, and is not in accordance with the assumption made.

Thus on the bases of equation (4) we have reached a contradiction, proving that this equation is not valid.

The result obtained is to some extent analogous to those obtained in considering the magnetic field due to a number of current-carrying coils [7, 8, 9]. The idea existed earlier that the dispersal fluxes, figuring in transformer calculations, can be found directly from the picture of the flux-coupling of the resultant magnetic field. In actual fact, there is generally no correspondence between the real partial flux distribution and the representation of the separate dispersion fluxes.

The use of an equivalent circuit makes the calculations easier. Having found the partial capacities by one method or another and built up from them the equivalent circuit, it is possible to calculate the input capacities on the part of any two bodies, to find the distribution of excess charges and potentials on the bodies and so on. All the calculation methods for electrical networks are applicable to the equivalent circuit.

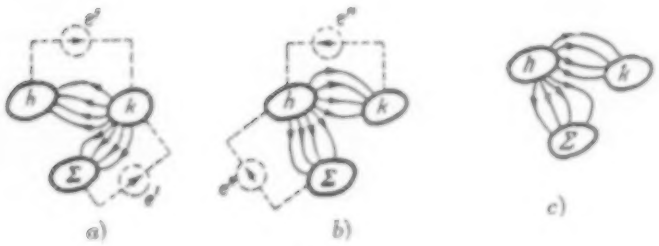

FIG. 4.

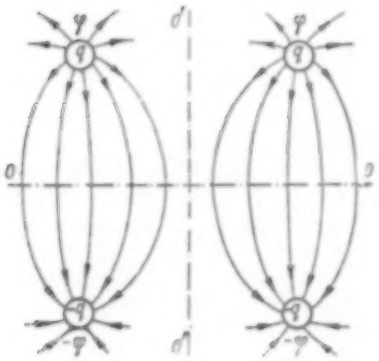

FIG. 5.

The partial capacities can be found from equations (2), in which the values of the excess charges and potentials are substituted. Since the total number of unknown capacitances in $\frac{1}{2}n\,(n-1)$, whereas only $(n-1)$ equations correspond to each condition, it is necessary to consider a number of conditions which can be the most convenient.

In the special case when the charges on all the bodies other than k are equal, the value of the charge on these bodies is numerically equal to the electrical displacement vector flux. For each such condition, the partial capacitances relative to body k are found directly from equation (4).

Calculation of the stationary field of the electric current in a system of electrodes in a conducting medium is carried out in an analogous manner, if it is assumed that the electrodes have infinite conductance. Since there is an analogy between current fields and charge fields, such fields can be used as models for each other; the analogues of the electric displacement vector fluxes will be the currents flowing in the conducting medium, the partial conductances will correspond to partial capacities, and so on. Consequently, all the preceding arguments relating to partial capacities and fluxes can be related to partial

conductances and currents. The equivalent circuit in this case will be a closed network in which the node potentials correspond to the electrode potentials and the elements are partial conductances.

Example Consider the plane-parallel electrostatic field of four circular conductors (Fig. 5). Assume that all the conductors have the same cross-section, and that their centres are at the corners of a rectangle. All values will relate to unit length of the conductors in a direction normal to the plane of Fig. 5. The medium is taken to be uniform.

In this case, equations (2) take the form:

$$q_1 = C_{12}(\phi_1 - \phi_2) + C_{13}(\phi_1 - \phi_3) + C_{14}(\phi_1 - \phi_4);$$

. . . . . .

. . . . . .

whilst none of the partial capacities is equal to zero.

We shall study the condition in which:

$$\phi_1 = \phi_2 = \phi \ ;$$
$$\phi_3 = \phi_4 = -\phi \ .$$

In this condition the line of symmetry O-O is the intercept of the equipotential surface, whilst the line of symmetry O′-O′ is the intercept of the surface of equal electrical displacement vector flux. Since there can be no unit tubes of displacement across the line O′-O′, the resultant field contains only two partial fluxes, equal in magnitude:

$$\Psi_{14} = \Psi_{23} = q = (C_{14} + C_{13})\, 2\phi \ .$$

If the formulae (4) are assumed correct, then, for example, to calculate the partial capacity C_{14} we have:

$$\Psi_{14} = q = 2C_{14}\phi \ .$$

Thus the error in calculating C_{14} from formula (4) is determined by the value of the partial capacity C_{13}.

Translated by E. Bishop

REFERENCES

1. L.R. Neiman and P.L. Kalantarov; *Teoreticheskie osnovy electrotekhniki (Theoretical Principles of electro-technology)*, III, 4, Gosenergoizdat (1954).
2. G.V. Zeveke and P.A. Ionkin; *Osnovy elektrotekhniki* (Principles of Electro-technology) 1, Gosenergoizdat (1955).
3. A.V. Netushil and K.M. Polivanov; *Osnovy elektrotekhniki (Principles of Electro-technology)*, 3, Gosenergoizdat (1956).
4. E. Weber; *Electromagnetic Fields*, New York, 1 (1950).
5. V.I. Smirnov; *Kurs vysshei matematiki (Course of Higher Mathematics)* GITL IV, 3 (1953).
6. Maxwell; *Electricity and magnetism*, Oxford, 1 (1904).

1958

7. Hemmeter; *A. f. E.*, 32, 167 (1927).
8. E.G. Markvardt; *Elektromagnitnye raschety transformatorov* (Electromagnetic Transformer Calculations), ONTI (1938).
9. E.A. Meerovich; "On the problem of electromagnetic dispersion in transformers", *Izv. ENIN Akad. Nauk SSSR*, 1, 1-2 (1935).

THE HEAT EMISSION OF RECTIFIER STACKS MADE OF LARGE SELENIUM CELLS*

F.F. SOKOLOV

Scientific Research Institute of Cinema Photography

1958

Special thermal tests have been carried out here to calculate the heat emitted by rectangular selenium plates of large dimensions, particularly under forced-draught cooling; the results of these tests are given below.

Method of testing

The cells were heated by losses of forward currents when passing d.c. through the stacks, The stacks consisted of cells specially selected in order as far as possible to exclude non-uniform heating owing to differences in cell characteristics. Losses were measured by the voltmeter-ammeter method. The excess heating was measured by copper-constantan thermocouples soldered to the cells (the mean of six cell-stacks). The excess heating was measured 15 mm from the upper edge of the cells (the point of maximum heat of a cell). Where cooling was natural, the stacks were set 150 mm above the test-bench. With forced-draught cooling, the stacks were set up in a container-duct of cross-section 365 × 312 mm. An electric motor and fan were installed at the top; the cooling air velocity could be regulated over a wide range. The stacks were installed in such a way as to fill the entire cross-section of the container. The air velocity was measured by vane anemometer in the bottom opening of the container. These tests were reduced, when processing the results, to the air velocity between the cells.

Natural cooling

Tests were made on stacks of selenium cells, 6 to 18 mm apart, on 100 × 200 and 100 × 300 mm aluminium base-plates. The heat emission data were determined for cell excess temperatures of from 0 to 40°C, and with a surrounding air temperature of about 20°C. All the thermal regimes were repeated for two stack positions: "vertical" (the long side of the cell being vertical) and "horizontal" (the long side horizontal). The experimental data obtained are given in Figs. 1 and 2 in the form of graphs for the relationship between r, the excess heating of the cells and the specific

* *Elektrichestvo* No. 1, 58 – 63, 1958 [Reprint Order No. EL 47].

losses q (W/dm²).

Analysis of the results obtained enables us to draw the conclusion that the heat emissivity of the rectangular cells tested is better than the known data for circular cells [2, 3, 4]. The improvement in heat emission should be attributed primarily to the difference in materials: the data for circular cell-stacks were mainly obtained when testing rectifiers on steel base-plates; in my case aluminium plates with better heat-conductivity were tested, this reducing the amount by which the most heated parts of cells (at the top) were overheated, while somewhat raising the overheating of the less-heated parts. In addition, the parameter of rectangular cells is greater than that of circular cells and, as we know, the regions of a cell close to the periphery are the more effective as to heat emission [3].

For the purpose of generalization, the experimental data on the heat emission of stacks of rectangular cells were expressed in dimensionless form [5]. The logarithmic coordinate curve in Fig. 3 expresses the graphical relationship of the Nousselt number:

$$Nu = \frac{\alpha b}{\lambda}$$

to the product of the three numbers:

The Grasshof:

$$Gr = \frac{\beta g b^3 \tau}{\nu};$$

The Prandtl:

$$Pr = \frac{\nu}{a}$$

and the dimensionless number:

$$\frac{b}{H},$$

where α is the coefficient of heat emission of the surface of the cell, (kcal/m²/hr/°C);
λ is the coefficient of heat conductivity, f the cooling medium, (kcal/m/hr/°C);
β is the coefficient of volumetric expansion of the cooling medium (/°C);
ν is the coefficient of kinometric viscocity of the cooling medium (m²/sec);
a is the coefficient of temperature conductivity of the cooling medium (m²/sec);
g is the gravitational acceleration (m/sec²);
b is the gap between cells (m);
and H is the cell height (m).

A temperature of 35° was taken as the specific temperature, in making calculations for the physical constants used in the numbers; this temperature of 35° corresponds to 30°C mean excess cell temperature and a surrounding medium temperature of 20°C.

If we substitute the following values for the constants:

$$\lambda = 0.0225; \qquad \beta = \frac{1}{273}; \qquad \nu = 17.1 \cdot 10^{-6}; \qquad a = 2.33 \cdot 10^{-5}$$

and for the convenience express b and H in mm and α in W/dm²/°C, the equations for calculating the numbers are simplified:

$$Nu = 3.82 \alpha b; \tag{1}$$

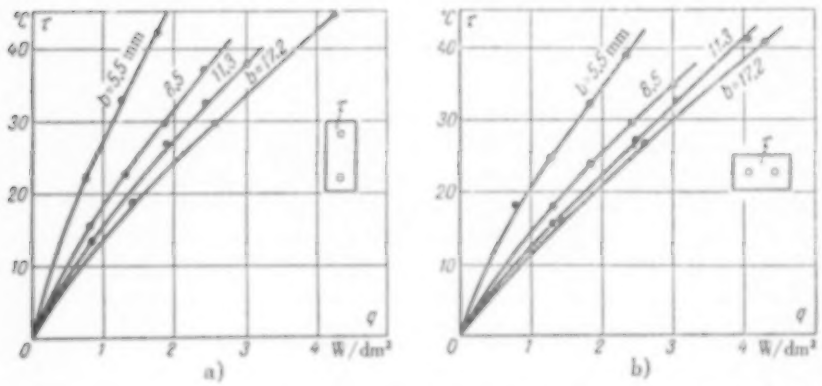

FIG. 1. The heat emission of 100 × 200 mm selenium cells, naturally cooled in stacks with different gaps (b is the gap between cells). (a) vertical and (b) horizontal cell arrangement.

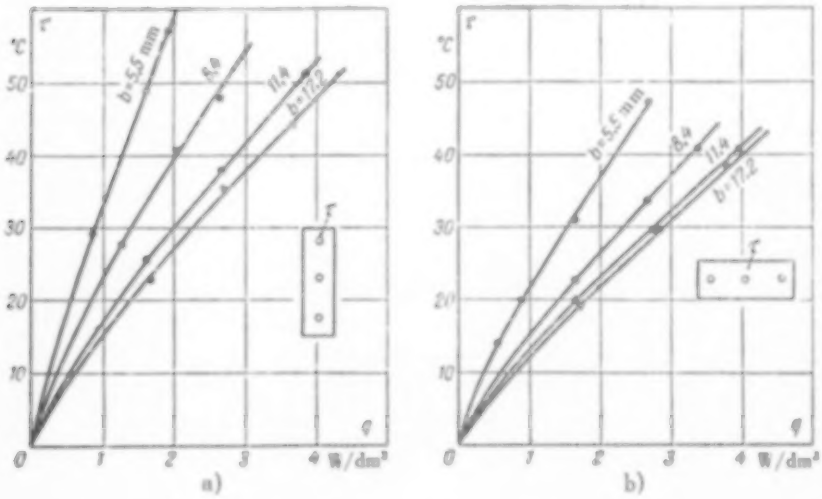

FIG. 2. The heat emission of 100 × 300 mm selenium cells, naturally cooled in stacks with different gaps (b is the gap between cells). (a) vertical and (b) horizontal cell arrangement.

$$Nu = 3.82\, \alpha\, \beta$$

$$Gr\, Pr\, \frac{b}{H} = \frac{0.089 b^4 \tau}{H}. \qquad (2)$$

The curve in Fig. 3 is drawn according to equations (1) and (2) by substituting the values for b, H, τ and $\alpha = q/\tau$ from the curves in Figs. 1 and 2.

It is clear from the curve that the results of my tests on stacks with cells of dimensions 100 × 200 and 100 × 300 mm (in the vertical and horizontal positions)

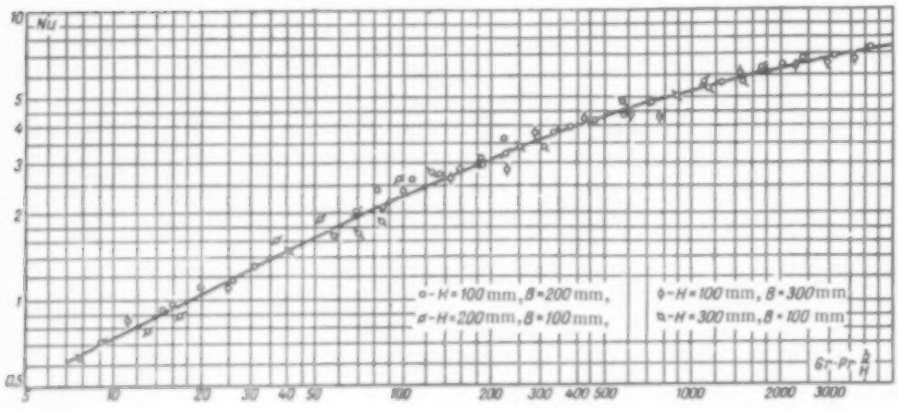

FIG. 3. Heat emission of selenium stacks composed of rectangular cells naturally cooled, in numerically generalized arrangement.

6 - 18 mm apart fit quite well on one curve (the error does not exceed 10 - 12 per cent). This result may be counted fully satisfactory particularly if we take into account that in the preceding analysis the proportion of the heat emission falling to radiation was not deducted,* for convenience in making use of the data obtained, and also that the test results combined by processing were obtained using selenium stacks which differed considerably in geometrical dimensions.

The generalized relationship represented in Fig. 3 can clearly be applied successfully to other stacks composed of rectangular cells of dimensions almost the same as those of the tested stacks, and with any gap encountered in practical cases in calculations for separated stacks cooled naturally. The generalized relationship obtained may also be applied in principle to cases of the heat emission of stacks in other mediums, for example in oil (by substituting appropriate values for the physical constants in the dimensionless numbers).

When the stacks are arranged in any specific layout (in a housing, together with other parts, several stacks beneath one another, etc.) the heat emission conditions obtained for separately arranged stacks (Figs. 1 - 3) may alter substantially. In these cases other methods for the thermal calculation [3], and the data obtained with forced-draught cooling, should be used.

* Specially conducted experiments have shown [3] that 12 - 16 per cent of the total heat emission fell to radiation in selenium stacks with natural cooling. The assumption made for the excess temperatures in the narrow range in which I was interested is therefore fully justifiable.

Forced draught cooling

Stacks of 100 × 300 mm cells were tested in two series. In the first series (Fig. 4a) the stacks were arranged with the long sides of the cells vertical, tests being carried out with gaps of 6, 12 and 18 mm between cells. In the second series (Fig. 4b) the stacks were arranged with their long sides horizontal, tests being carried out with a gap of 12 mm between cells, but for one, two and three stacks arranged above one another (stacked); the excess heat was measured for the cells in the upper stack.

Tests were carried out with air velocities up to about 5 m/sec. The data obtained were processed in the form of the graphical relationship between the heat emission coefficient α and the air velocity between plates ω. Tests were made for stack excess temperatures of close to 30°C and at surrounding air temperatures of about 20°C.

The test-results show that the coefficient of heat emission for identical cooling-air velocities depends to a great extent on the gap between cells (Fig. 4a), the height of the cell (comparing the mean curve in Fig. 4a and the upper curve in Fig. 4b) and on the number of stacks set one above the other (Fig. 4b).

1958

The conclusion can be drawn, from analysis of the experimental data obtained, that the heat emission data obtained for stacks of cells 300 mm high can also be applied to stacks of cells of different heights if a correction is made for the excess heating of the cooling air corresponding to the difference between the cell heights. Let us examine the thermal balance of a rectifier cooling-channel under set conditions.

The thermal energy liberated into the channel from the walls of the cells (per unit of cell width), $Q = 2qH$;
the same energy is carried away with the cooling air

$$Q = b\omega\gamma c_p \tau_v,$$

whence

$$\tau_v = \frac{2qH}{b\omega\gamma c_p},$$

where q is the specific loss in the cells (W/dm²), H is the height of the cell (mm), τ_v is the mean excess temperature of the air in the cooling channel at height H (°C), b is the width of the cooling channel (mm), ω is the velocity of the cooling air (m/sec), γ is the specific gravity of the air (kg/mm³), and c_p is the thermal capacity of the air in kcal/kg/°C.

Substituting the values $\gamma = 1.164$ and $c_p = 0.242$, and taking 1 kcal/sec as being equal to 4184 W, we get:

$$\tau_v = \frac{0.17qH}{b\omega} \ (^\circ\mathrm{C}). \tag{3}$$

If α_n, the coefficient of heat emission of the cells, is known by experiment (for example from Fig. 4b) for a given stack of cells of height H_n for any conditions, and

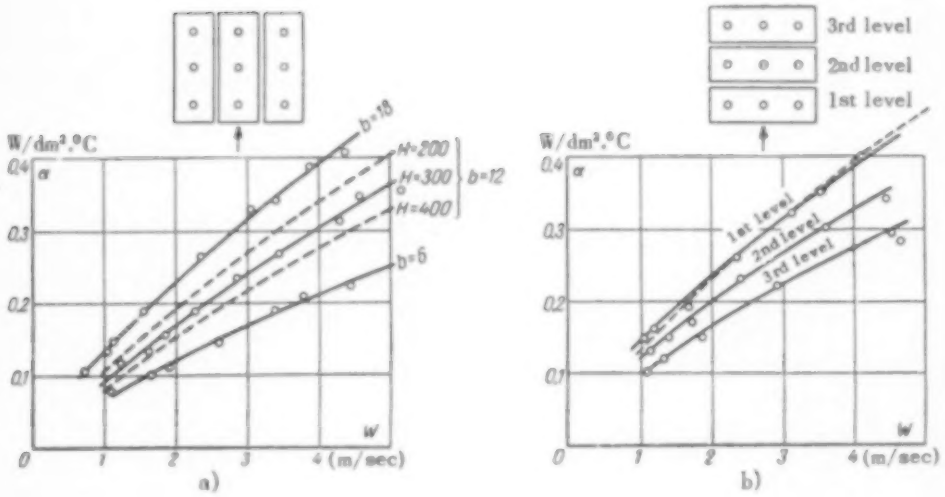

FIG. 4. Heat emission of forced-draught air-cooled selenium stacks of 100 × 300 mm rectangular cells. (a) "vertical" stacks with 6, 12 and 18 mm gaps b between cells (the dotted curves are calculated heat emission curves for stacks of heights H = 200 and 400 mm with a 12 mm gap b between cells); (b) "horizontal" stacks with 12 mm gaps b between cells; stacks arranged in 1st, 2nd and 3rd levels (the dotted curve is that for the heat emission of a stack of height H = 100 mm, calculated by equation (5) from data for a stack of H = 300 mm).

so for any given specific load q, we also know the excess temperature of the cells

$$\tau_n = \frac{q}{\alpha_n}, \tag{4}$$

then the excess temperature of cells of height H_m can be found for the same load q from (3) and (4) as follows:

$$\tau_m = \tau_n + \tau_{v(m-n)} = \frac{q}{\alpha_n} + \frac{0{,}17q\,(H_m - H_n)}{b\omega},$$

where $\tau_{v(m-n)}$ is the excess temperature of the cooling air in the rectifier channel at a height H_m-H_n above the lower edge of the cell.

Consequently the coefficient of heat emission for cells of height H_m

$$\alpha_m = \frac{q}{\tau_m} = \frac{1}{\frac{1}{\alpha_n} + \frac{0{,}17\,(H_m - H_n)}{b\omega}}. \tag{5}$$

Equation (5) enables us to determine the coefficients a_m for stacks of height H_m, which may be either less or more than H_n, from the coefficients of heat emission a_n obtained experimentally for stacks of height H_n.

Heat emission curves are drawn according to this equation in Fig. 4a, from data for stacks of height 300 mm, for stacks of cells 200 and 400 mm in height (the gap $b = 12$ mm, the dotted curves). To confirm the correctness of these calculations, a heat emission curve is drawn in Fig. 4b from the same data for a stack with cell height 100 mm (dotted); this curve coincides extremely well with the experimental curve (unbroken line) obtained with cells of height 100 mm.

Equation (5) does not take into account the phenomenon of thermal conductivity in the body of a cell which, generally speaking, should also be taken into consideration when determining the relationship between heat emission and height of cell. However, as specially conducted experiments showed, this factor is not of great importance. Fig. 5 shows isotherms (lines of identical excess temperature) for a selenium cell on an aluminium base of dimensions $1 \times 100 \times 300$ mm, in a stack with 18 mm gaps, with an air velocity of 3.6 m/sec, specific load of 9.8 W/dm² and surrounding air temperature of 22°C; the isotherms are drawn for the excess temperatures measured at 10 points on the cell (see the measurement points on Fig. 5). The temperature gradient, with a general downward direction, is clearly visible in the illustration; however, calculations show that the levelling effect of the thermal conductivity is not great, owing to the small thickness of the cell, and may be ignored. Thus only about 2.4 per cent of the heat liberated above the line AA is transmitted downwards across the section AA, and correspondingly less than 2 per cent across the section BB.

On comparing the mean curve in Fig. 4a (single level arrangement, gap 12 mm, height 300 mm) with the lower curve in Fig. 4b (the same gap of 12 mm but three-level arrangement, and total height also 300 mm), it can be concluded that, other things being equal, for a multi-step arrangement the coefficient of heat emission is somewhat reduced (by roughly 10 per cent in the given specific case). To some extent the reason for this is the difference noted above in the heat conductivity conditions in the body of a cell; in addition very probably there are other factors which I have not examined connected with the conditions under which the air flows in the channels between cells (stagnant zones, etc).

On analysing the particular experimental relationships, given in Fig. 4, between the coefficient of heat emission and parameters such as cell height, width of gap between cells and number of levels, it is easy to satisfy oneself that for a given air velocity these relationships are of an almost linear nature and therefore lend themselves well to interpolation for other close values of the parameters. The data obtained can thus be used in the thermal calculations for rectifiers of the most varied designs, also in the comparative analysis of different types of rectifier for different specific cases.

Let me give an example to illustrate the use of the heat emission data obtained for forced draught cooling. The cost and dimensions of very powerful selenium recti-

1958

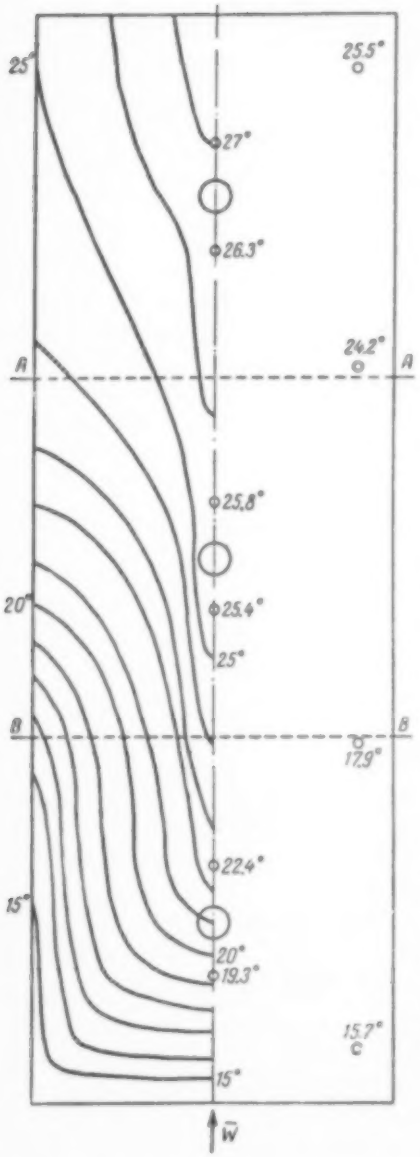

FIG. 5. Excess temperature isotherms for a selenium cell on an aluminium base, dimensions 1 × 100 × 300 mm, in a stack with 18 mm gaps, air velocity 3.6 m/sec, specific load 9.8 W/dm², surrounding air temperature 22° C.

fiers are the most important characteristics of their design.

We can assume as a first approximation that the cost of a rectifier is directly proportional to the area S of the selenium cells; this can easily be expressed through Q, the losses in the rectifier or, if we introduce η the efficiency of the rectifier, through the rectifier output power P (*el*):

$$S = \frac{Q}{a\tau} = \frac{P\left(\frac{1}{\eta} - 1\right)}{a\tau}. \qquad (6)$$

It follows from this that for a given rectifier output P the area of the cells, and also the cost of the rectifier, are in inverse proportion to a, the coefficient of heat emission (since τ, the excess temperature of the cells, and η are given by the technical data for the selenium cells).

Turning to the rectifier dimensions, it can be affirmed that, besides the height, the plan area of the rectifier is of particular interest, for with forced draught cooling this area determines the fan output, and to a great extent its dimensions and power.*

Fig. 6 gives a network of intersecting curves drawn from the data in Fig. 4a and compiled using equation (5), showing how the height of the cells H and the gap between cells b affects alterations in a, the coefficient of heat emission for the cells, and A, the "field" coefficient of heat emission; A is expressed by:

$$A = \frac{a2H}{b + \delta},$$

where δ is the thickness of a cell, usually 1mm for large cells.

* Losses due to friction are usually low in the general fan pressure balance; fan power is therefore little dependent on the height of the cells.

For specific losses, or from output power and efficiency, the coefficient A enables us easily to determine the area of the field occupied by a rectifier (its vertical projection), S_n(dm²):

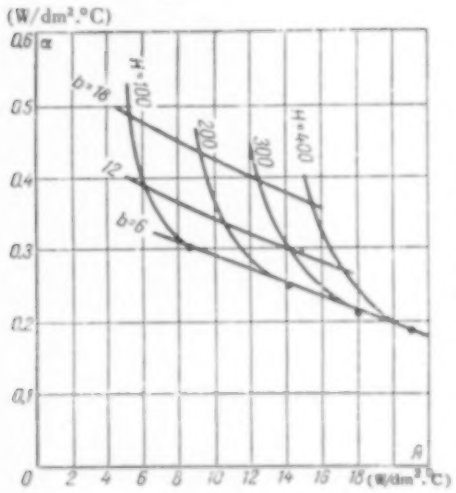

FIG. 6. Relationship of α, the coefficient of heat emission, and A, the coefficient of specific load of the rectifier vertical projection, to b, the gap between cells.

$$S_n = \frac{Q}{A\tau} = \frac{P\left(\frac{1}{\eta} - 1\right)}{A\tau}. \qquad (7)$$

Thus the graph in Fig. 6 has ordinates α which are in inverse proportion to the area of the cells (and so to their cost); the abscissae A are in inverse proportion to the vertical projection area of the rectifier; these facts facilitate selection of the most acceptable compromise between these parameters with relation to the specific requirements in the case of calculations for different rectifiers.

It is also quite evident from Fig. 6 how important it is to use large-dimension cells when constructing powerful rectifiers; for acceptable rectifier dimensions can only be obtained by increasing the height of a rectifier (or by increasing the number of levels which is, however, worse than was shown in Fig. 4) and simultaneously increasing the gap b; this is equivalent to sufficiently increasing the specific field load (the coefficient A) without materially reducing the utilization of the elements (the coefficient α).

Translated by J.H. Dixon

REFERENCES

1. F.F. Sokolov; Iz. Opyta ekspluatatsii selenovykh vypriamitelei (Experience in the operation of selenium rectifiers), *Elektrichestvo* 3 (1953).
2. V.G. Komar; Raschet selenovykh vypriamitelei (Calculations for selenium rectifiers), *Elektrichestvo* 9, 46 (1946).
3. F.F. Sokolov; *Teplovoi raschet selenovykh vypriamitelei (Thermal calculations for selenium rectifiers)*, Moscow, NIKFI, dissertatsiia (1949).
4. V.G. Komar; *Rabota poluprovodnikovykh vypriamitelei v tsepiakh upravleniia (The operation of semi-conductor rectifiers in control circuits)*, Gosenergoizdat (1952).
5. M.A. Mikheev; *Osnovy teploperedachi (The fundaments of heat transfer)*, Gosenergoizdat, 53–78 (1947).

THE USE OF 220 kV LINES WITH SPLIT CONDUCTORS*

A.N. ZEILIGER and B.P. NOVGORODTSEV

Leningrad Teploelektroproekt Department**

(Received 4 October 1957)

This article presents the results of the technical and economic comparison of 220 kV lines with split conductors and transmission lines of the same voltage without split conductors.***

As we know, there are two purposes in splitting the conductors in 220 kV lines: (1) to increase the carrying capacity of long-distance lines when the transmitted power is limited by voltage drop or by their stability limits; (2) to reduce the number of parallel lines when the rated load of one line exceeds the economic load of the maximum gauge single conductor available.

In the first case, a single large section conductor is replaced by two or more conductors of smaller section with the same total conductor section per phase. In the second case, the single conductor is replaced by two or more conductors whose total cross-section per phase exceeds the maximum cross-section of the single conductor. In the first case the reactance of the line can be reduced at the expense of making its mechanical part somewhat more costly; carrying capacity is thereby raised. In the second case the reactance of the single line with split conductors and the reactance losses in it are considerably higher than in lines consisting of the corresponding number of parallel lines containing single conductors of the same total cross-section.

However, the splitting of conductors is not the only method of ensuring the required electrical transmission properties. Increase in the carrying capacity and reduction in the reactance losses in long-distance lines may also be obtained by the use of compensating installations; reduction in the number of parallel lines may be achieved by the use of double-circuit lines. In view of this, the question of the expediency of using split conductors for 220 kV electric power transmission

* *Elektrichestvo* No. 2, 9-12, 1958 [Reprint Order No. EL 48].

** *"Teploelektroproekt"*: "Electric Power and Heat Generating Project".

*** The article has been compiled from the results of work done by the authors with K.P. Kriukov and S.N. Ruzanov at the Leningrad Teploelektroproekt Department.

lines in different cases must be solved on the basis of the technical and economic comparison of different transmission line design variants. In this comparison, the following must be taken into account as well as the cost of the mechanical part of the line: the cost of the compensating installations installed on the power line itself, or in the power transmission system, to compensate the additional reactance and reactance losses, where a line of high reactance is used.

Analysis of the problem of the expediency of splitting conductors has been made for three groups of 220 kV electric power transmission lines. The first group comprises lines whose total conductor single phase cross-section is (for aluminium) 480 mm². The economic load corresponding to this cross-section is about 200 MVA at an economic current density of 1 amp/mm². Single circuit lines with single ASO-480 conductors and split 2 × ASO-240 conductors belong to this group. The second group comprises lines of a total conductor cross-section of 960 mm² (economic load about 400 MVA). Single circuit lines with 2 × ASO-480 split conductors and double circuit lines with single ASO-480 conductors belong to this group. The third group comprises lines of a total conductor cross-section of 1920 mm² (economic load about 800 MVA). Double circuit lines with 2 × ASO-480 split conductors belong to this group.

1958

Calculations for the supports and foundations for all these lines have been made for climatic regions I and II. The rated wind velocity was taken as 25 m/sec. The wind velocity in the zone 30-50 m above the earth was taken as 110 per cent of the velocity in the first zone. The supports were made of type St-3 steel and low-alloy type NL-2 steel. The latter was used in every case where it resulted in reduction of the weight of the support. The stresses permitted for the type St-3 steel were, according to the *Rules for the Construction of Electrical Engineering Installations*, with the emergency stress permitted for intermediate supports, reduced to 2000 kg/cm².

The permitted tension, compression and bending stresses in NL-2 steel components were taken as being: for normal conditions, 2250 kg/cm², and for emergency conditions 2600 kg/cm² (anchorage supports), and 2800 kg/cm² (intermediate supports).

The normal condition support plans were made in accordance with the *Rules for the Construction of Electrical Engineering Installations*. The conductor breaking stress at intermediate supports was reduced for lines without split conductors to 0.75, and for lines with split conductors to 0.6 times the reduced breaking stress for the full phase. This reduction was taken into account in making the calculations for all the types of support, except the "barrel" type twin-circuit support which was supplied until the relative MES Technical Directorate instruction came into force. Twin-circuit "barrel" type supports were designed for the total reduced conductor breaking stress.

In cases where breaking conductors may fall on to part of the support structure, it was specified that supports with releasing terminals were to be reinforced by clamping terminals.

When comparing lines with releasing and clamping terminals, it was taken into consideration that the distances between the anchorage supports of the former must not exceed 10 km; the distance between anchorage supports in the second case is unlimited; ie., supports of the anchorage type are only used for important crossings.

When designing the foundations, a pressure of 2 kg/cm² on the ground, ground weight of 1.6 tons/m³ (when calculating for excavation) and 1.8 tons/m³ (when calculating for compression) were allowed. It was assumed that the ground water-level was below the base of the foundation and that the angle of slope of the ground was less than 35°. Concrete type 200 was used for built-up foundations.

The most economic variants for the construction of the different types of lines (single circuit or double circuit with single or split conductors) were taken for comparison.

The development work by Teploelektroproekt showed that the most suitable metal supports for double-circuit 220 kV lines are supports of the "barrel" type with clamping terminals, made of low-alloy steel. According to the working drawings, the weight of an intermediate support with clamping terminals is only 375 kg, or 5 per cent, greater than that of an intermediate support with releasing terminals. This is explained by the fact that normal conditions are assured when calculating for the support body cords, and therefore, the assortment of body cords is identical in both cases. For the lattice-work of the body, conductor breaking conditions in clamping terminals on the upper cross-arm are taken for calculations in the case of releasing terminals, and conductor breaking conditions in clamping terminals on the middle cross-bar in the case of clamping terminals. Since the number of anchorage supports is lower on lines with clamping terminals than on lines with releasing terminals, practically identical weights of metal are used per kilometre of line in both cases. The greater reliability of lines with clamping terminals during operation forces us to give preference to this type of line.

Till recently "wine-glass" or "hinged portal" type supports were used for single circuit 220 kV lines. However, the work by Teploelektroproekt on developing new types of support, designed for the suspension of type ASO-480 zero conductors in climatic regions I and II, have proved that the Crimea type support is the most economical. The use of low-alloy steel for these supports considerably reduces the amount of metal used, while the use of this steel for 220 kV portal-type supports provides practically no economy.

The weights of intermediate supports for the three types compared and the

amounts of metal and concrete used per km of line are given in Table 1.

The foundation reinforcement is included in the amount of metal used per kilometre of line. The amounts of metal and concrete used are taken for the most economical variants of the lines (those on "hinged portal" and "wine-glass" type supports with releasing terminals, and those on Crimean type supports with clamping terminals).

TABLE 1

Type of support	Calculated span	Weight of support (kg)		Material used per km of line	
		with releasing terminals	with clamping terminals	metal (tons)	concrete (m^3)
"Hinged portal"	400	4300	5800	17.3	17.8
"Wineglass"	450	4900	6200	16.9	8.5
Crimean	450	4500	4800	13.6	8.0

1958

It was also established, when developing supports for single circuit lines with split conductors, that Crimean type supports are the most economical. We used 16.7 tons of metal and 10.6 m^3 of concrete per kilometre of line on Crimean type supports, 21.7 tons and 15.5 m^3 respectively per kilometre of line on "hinged portal" type supports, and 22.4 tons and 15.0 m^3 respectively per kilometre of line on "wineglass" type supports, using A-P type anchorage and corner supports.

We will now therefore compare single circuit lines on Crimean type supports and double circuit lines on "barrel" type supports. It is conditionally assumed that all the lines being compared have the following: intermediate supports with clamping terminals, 90 per cent; intermediate corner supports (2-20°), 5 per cent; and corner supports (20-60°), 5 per cent. K, the coefficient of utilization, is taken as being 0.9 for all the lines being compared.

Fig. 1 provides a schematic representation of the supports of the lines being compared. Table 2 gives the technical and economic figures. The costs per kilometre of line are given in comparative figures.

It is evident from comparison of lines in the first group that a single circuit line with single type ASO-480 conductors (line (*a*)) is cheaper than a single circuit line with split conductors of type 2×AS-240 (line (*b*)). This is explained by the fact that the wind pressure on the line and the sag of the conductors in line (b) is higher than in line (a), leading to reduction in the economic span and

an increase in the metal and concrete used per kilometre in line (b), and therefore to an increase in the cost of this line per kilometre.

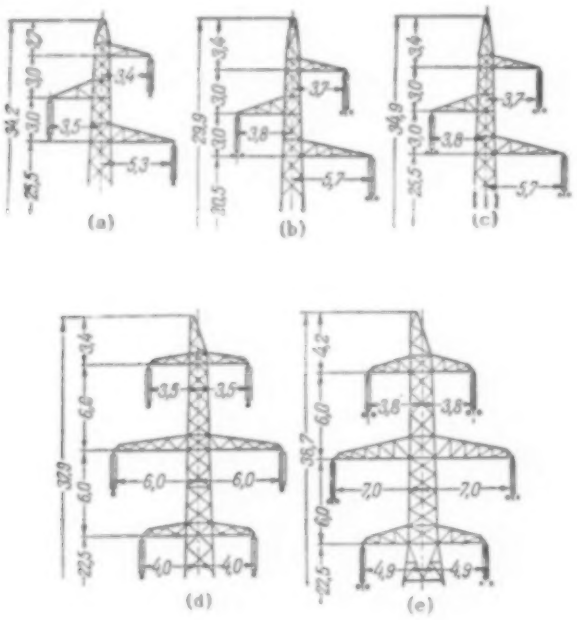

FIG. 1. Schematic representation of the supports of the lines being compared.

TABLE 2

Line lettering (see Fig. 1.)	Conductor types	Supports	Calculated span (m)	Expenditure per km of line		Cost of 1 km of line (1000 roubles).
				Metal (tons)	Concrete (m^3)	
Line (a)	ASO-480	Crimean type	450	13.6	8.0	154.8
Line (b)	2 × AS-240	Crimean type	340	15.6	10.4	172.8
Line (c)	2 × ASO-480	Crimean type	450	16.7	10.6	246.3
Line (d)	ASO-480	"Barrel" type (narrow body)	400	21.2	12.4	262.7
Line (e)	2 × ASO-480	"Barrel" type (wide body)	400	27.6	15.3	383.3

It should be noted that comparisons between single circuit lines with single and split conductors made abroad have produced the same results. For example, it was established in Sweden that a single circuit 220 kV line with split conductors is 18 per cent more costly than a single circuit line with single conductors.

The total wind pressures on the conductors of single circuit lines with 2×ASO-480 split conductors (line (c)) and on those of double circuit lines with single ASO-480 conductors are identical, since in both cases six conductors of the same type are suspended from the supports. However, the double circuit support is heavier than the single circuit support, owing to its greater height and greater number of cross-arms. The amount of metal used for 1 km of double circuit line is therefore greater than that for 1 km of single circuit line. More concrete is used for double circuit lines, also because of the greater height from which the conductors are suspended and their consequently greater moment. Thus, the double circuit line with single conductors is more costly than the single circuit line with split conductors.

It was stated above that the double circuit supports examined were calculated for total reduced conductor breaking stress, and Crimean type supports for 0.75 times the reduced stress. When converting to the new calculation conditions, the weight of the "barrel" type intermediate supports is reduced, and in consequence the difference between the costs of the lines being compared becomes less.

It should be noted that single circuit lines with split conductors are only cheaper than double circuit lines with single conductors in cases where Crimean type supports with a triangular arrangement of conductors are used. Single circuit lines with split conductors on portal-type supports, with the conductors horizontally arranged, are more costly than double circuit lines on "barrel" type supports.

Of the lines in the third group, with a total cross-section of the conductors of 1920 mm² per phase, we can compare a single double-circuit line with split conductors on wide-bodied "barrel" type supports (line (e)), with two single circuit lines with split conductors or two double circuit lines with single conductors. The amount of metal used for one double circuit line with split conductors is 17 per cent less than the amount used for two single circuit lines, and 35 per cent less than that used for two double circuit lines; the amounts of concrete used are respectively 27 and 38 per cent less, and the costs 22 and 26 per cent less.

In order to make a full technical and economic comparison of the various 220 kV lines, taking into account the expenditure on compensating installations, a number of factors for 220 kV lines with single and split conductors are given in Table 3. The line reactance losses were determined, starting from the utilization factor, in accordance with the economic current density at an average voltage level of 230 kV.

It is evident from Table 3 that, for identical rated loads, the reactance losses are different for the lines being compared.

The vast majority of present-day electric power systems have no excess reactive power, and each increase in the line reactance losses makes it desirable as a rule to install additional compensating devices of corresponding capacity. Table 3 provides the capacity of the additional compensating devices which must be installed, to ensure identical reactive power equalization, on the electric power lines under comparison. The additional compensating installations are as a rule installed in the power system receiving-end circuits in the form of synchronous or static compensators.

In cases where the reactance of a line must be compensated in order to raise its carrying capacity, part of the capacity of the compensating devices may be arranged in the form of longitudinal compensation. The use of any system of compensation has no effect on the results of the technical and economic comparison, since the total of the compensating device capacities and their specific costs are not materially affected in either case.

Comparison of the economic figures for the lines, taking the expenditure on additional compensating devices into account, is made in Table 4.

Comparison of the lines in Group I shows that, even when the cost of the compensating devices is taken into account, the total cost of electric power transmission by single conductors is lower than that for split conductors.

Comparison of the lines in Group II shows that the costs of the additional devices for compensating the increased reactance losses of lines with split conductors cover the difference in the cost of the mechanical part of the lines; in this connexion, single circuit lines with split conductors of large section are less economic than double circuit lines with single conductors of the same section. In addition, double circuit lines with single conductors are more reliable and convenient to operate than single circuit lines with split conductors. Therefore it may prove expedient to use single circuit lines with split conductors only in particular isolated cases, for example, with the simultaneous installation of two parallel lines in power systems with no excess reactive power.

Comparison of the lines in Group III shows that the use of double circuit lines with split conductors is economically very effective, since it enables us to reduce the number of parallel lines. The use of double circuit lines with split conductors can be recommended in every case where the transmission of such high power on a single double-circuit line is permissible from the point of view of power supply reliability.

CONCLUSIONS

1. Phase-splitting, on 220 kV lines, into two or more conductors of smaller

TABLE 3

Name of factor	Group I		Group II		Group III	
	Single circuit line, ASO-480 conductor	Single circuit line, 2 × AS-240 conductors	Single circuit line, 2 × ASO-480 conductors	Double circuit line, ASO-480 conductor	Two double circuit lines, ASO-480 conductors	Double circuit line, 2 × ASO-480 conductors
Economic loading (MVA)	200	200	400	400	800	800
Resistance (Ω/km)	0.064	0.064	0.032	0.032	0.016	0.016
Inductive reactance (Ω/km)	0.4	0.314	0.304	0.2	0.1	0.152
Capacitive susceptance, (1/Ω/km)	2.75×10^{-6}	3.6×10^{-6}	3.7×10^{-6}	5.5×10^{-6}	11×10^{-6}	7.4×10^{-6}
Inductive losses at economic load (kVAR)	302	237	920	605	1210	1840
Capacitive power, for V_{av} = 230 kV (kVAR)	-145	-190	-196	-291	-582	-392
Total reactance losses (kVAR)	157	47	724	314	628	1448
The capacity of the additional compensating installations necessary to equalize the reactive capacity of lines in each group (kVAR)	-110	-	-410	-	-	-820

1958

TABLE 4

Name of factor	Group I		Group II		Group III	
	Single circuit line, ASO-480 conductor	Single circuit line, 2×AS-240 conductors	Single circuit line, 2×ASO-480 conductors	Double circuit line, ASO-480 conductor	Two double circuit lines, ASO-480 conductors	Double circuit line, 2×ASO-480 conductors
Cost of line (1000 roubles /km)	154.8	172.8	246.3	262.7	525.4	383.3
Cost of installing additional compensating devices (costing 75 roubles/kVAR) 1000 roubles/km	8.2	-	30.8	-	-	61.6
Total costs (10 roubles/km)	163.0	172.8	277.1	262.7	525.4	444.9

section, for the purpose of reducing the reactance of lines, is not economically justifiable, since a similar effect may be achieved at lower cost by the use of compensating devices.

2. The splitting of each phase of a single circuit 220 kV line into two conductors of greater section, in order to raise the total conductor cross-section, results in most cases in an increase in the total capital outlay, including the cost of compensating appliances, in comparison with double-circuit 220 kV lines. In view of this, the use of single circuit 220 kV lines with split conductors of larger cross-section is not as a rule expedient.

3. The use of double-circuit 220 kV lines with split conductors of large cross-section is economically justifiable, since the capital expenditure for erecting such lines is considerably lower than that for the erection of two parallel double-circuit lines with single conductors.

Translated by J.H. Dixon

1958

CALCULATIONS OF SHORT-CIRCUITS IN UNBALANCED PHASE TRANSMISSION SYSTEMS*

G.G. KOSTANIAN

Tbilisi Scientific Research Institute of Building and Hydroelectrics

(Received 22 June 1957)

As a result of researches carried out in recent years, calculations of complicated asymmetric faults in electrical systems have been materially simplified. Thanks to this research, it is now possible to study combinations of any asymmetric faults at two points in a system, and in particular combinations of short circuits in systems with unbalanced phase transmission [1, 2]. However, calculations of such faults, particularly in complex systems with ring connexions, are none the less laborious and can be materially simplified if treated as an extension of calculations dealing with a fault at one point of the system.

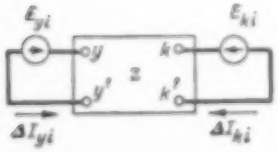

FIG. 1. Circuit for any sequence at a phase break.

Actually, all the changes introduced by the second fault in each sequence of the circuit can be represented, as shown in Fig. 1, by two e.m.f.'s only: E_{ki}, the e.m.f. at the point of the first fault, and E_{yi}, the e.m.f. at the point of the second fault. The resulting components of current and voltage in the sequences of the circuit can be found by superimposing the components calculated for a fault at one point of the circuit on to the components determined from the circuit of Fig. 1. This approach to calculations of asymmetric faults at two points in a circuit makes it possible to use the methods and results already obtained in calculations for faults at one point of a circuit; the changes introduced by the second fault are taken into account in these circuits by the e.m.f.'s E_{ki} and E_{yi}.

The basic ideas of the proposed method are described below, as applied to the calculation of various combinations of short-circuits in unbalanced phase transmission systems. One of the special types of fault at two points in the system is considered, namely various combinations of short-circuit at one point in the system with a break on one phase at another point.

From now on, values referring to the short-circuit branch will be denoted by the

* *Elektrichestvo* No.2, 13–18, 1958 [Reprint Order No. EL 49].

subscript k, those referring to the break branch by y; to the corresponding phases, by A and B respectively; to the corresponding sequences, by 1, 2 and 0; and to any sequence, by i. The superscript (3) denotes that the value in question refers to the case of a three-phase short-circuit; (1.1) to the case of a short to earth on two phases; (1) to the case of a short to earth on one phase.

The problem of calculating the components of the two e.m.f.'s referred to above is considerably simplified by the method proposed in this paper of transferring all the e.m.f.'s operating in the system to the one branch being studied.

Consider the relationship between the e.m.f.'s E_y and the current in the branches of the passive quadripole shown in Fig. 2.

In the presence of a single e.m.f. in the branch $y-y'$, the current in the branch $k-k'$ is

$$I_k = \frac{\alpha E_y}{z_y} = \frac{\beta E_y}{z_k} = pE_y, \tag{1}$$

where $1/z_y = g_y$; $1/z_k = g_k$, the intrinsic conductivities in branches $y-y'$ and $k-k'$ respectively; $\rho = g_{yk} = g_{ky}$, the mutual conductivity between the branches $y-y'$ and $k-k'$; $\alpha = g_{ky}/g_y$; $\beta = g_{yk}/g_k$ are coefficients.

The coefficients α, β and ρ are values which are reciprocals of the known coefficients of quadripoles. They depend only on the parameters of the quadripole, and are related as follows :-

$$\beta = \frac{z_k}{z_y}\alpha = \rho z_k. \tag{2}$$

The coefficient β shows what fraction of the total e.m.f. in the branch $y-y'$ is equal to the e.m.f. in branch $k-k'$, and what fraction of the current in branch $k-k'$ is equal to the current in branch $y-y'$. This assumes that the e.m.f. occurs only in branch $y-y'$ and the current source only in the branch $k-k'$. The coefficient α, on the other hand, shows what fraction of the e.m.f. in branch $k-k'$ is equal to the e.m.f. in branch $y-y'$ and what fraction of the current in branch $y-y'$ is equal to the current in branch $k-k'$.

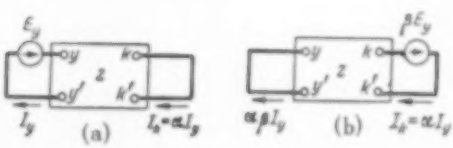

FIG. 2. Relationships between currents and e.m.f.'s in a passive quadripole, on transferring them from one branch to another.

The transfer of e.m.f. E_y from branch $y-y'$ to branch $k-k'$, as shown in Fig. 2, does not change the current in branch $k-k'$.

As applied to an active quadripole, expression (1) determines the component of current due to e.m.f. E_y, whilst the full current in branch $k-k'$ of such a quadripole is found by superimposing the currents due to all the e.m.f.'s (at an e.m.f. $E_y = 0$) on to the current due to e.m.f. E_y. In this case, expression (2) and the assumption that when e.m.f. E_y is transferred to branch $k-k'$ the current in the latter is unchanged,

1958

are valid not only for the passive quadripole shown in Fig. 1 but also for an active quadripole with other e.m.f.'s in its branches in addition to E_y.

Extending this to active networks, it can be shown to be valid to account for the effect of an e.m.f. in branch $n-n'$ on the current in any other branch $p-p'$ by taking E_n from branch $n-n'$ and transferring the fraction which is numerically equal to $g_{np}/g_p\, E_n$ over to branch $p-p'$, where g_{np} is the mutual conductivity between branches $n-n'$ and $p-p'$ and g_p is the intrinsic conductivity of branch $p-p'$.

The coefficients β, ρ and α between the branches containing two faults in the circuits of two separate sequences can be measured on a calculating machine, e.g. by methods known from the theory of quadripoles, or found from the results of previous short-circuit calculations. Below is given only the latter method of determining them, as applied to the calculations of a short-circuit with a phase break.

The circuits and expressions from which to start out in the determination of coefficients β_i, ρ_i and α_i for the individual sequences are shown in Table 1.

The data required for determining the coefficients are taken from the results of a calculation of any type of asymmetric short circuit in branch $k-k'$, in the absence of a fault in branch $y-y'$.

The coefficients β_i and ρ_i are the most interesting, since they enter into the expressions determining E_{yi} and E_{ki}, whereas the coefficient α_i does not figure in these expressions.

Coefficient α_i has only subordinate value and serves to simplify the calculation of the circuit conductivities of the sequences at the point of phase rupture, which is of most importance in calculating complex circuits with ring connexions.

For example, the sum of the circuit conductivities of all the sequences can be determined using this coefficient as follows:-

$$g_{y\Sigma} = \frac{1}{z_{y1}} + \frac{1}{z_{y2}} + \frac{1}{z_{y0}} = \frac{\rho_1}{\alpha_1} + \frac{\rho_2}{\alpha_2} + \frac{\rho_0}{\alpha_0}. \tag{3}$$

The sums of coefficients β_i and α_i, given in Table 1, merit particular attention; to determine them we need the total currents in the phases when one phase is short-circuited and the total e.m.f.'s in the phase when two phases are shorted to earth. These sums define the connexion between the components of current and e.m.f. in the calculations which are to be made.

The equations relating currents and e.m.f.'s, given in the circuit of Fig. 1, can be put in the following form:-

$$\Delta I_{yi} = I^{*}_{yi} - I_{yi} = \rho_i \Delta E_{ki} - \frac{E_{yi}}{z_{yi}}; \tag{4}$$

$$\Delta I_{ki} = I^{*}_{ki} - I_{ki} = \rho_i E_{yi} - \frac{\Delta E_{ki}}{z_{ki}}, \tag{5}$$

where I^{*}_{yi} and I^{*}_{ki} are the current components in branches $y-y'$ and $k-k'$ after phase

TABLE 1.

Initial Circuits	Expressions for coefficients in the circuits: Direct sequence	reverse sequence	zero sequence	Expressions for finding the sums of coefficients
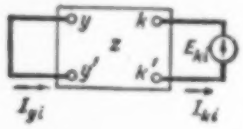 Circuit *A* Any asymmetric short-circuit between k - k' in the condition prior to phase rupture in section y - y′	$\beta_1 = \frac{I_{y1} - I_y^{(3)}}{I_{k1} - I_k^{(3)}}$	$\beta_2 = \frac{I_{y2}}{I_{k2}}$	$\beta_0 = \frac{I_{y0}}{I_{k0}}$	$\beta_1 + \beta_2 + \beta_0 = \frac{3\left(I_{yA}^{(1)} + \beta_1 I_k^{(3)} - I_y^{(3)}\right)}{I_{kA}^{(1)}}$ $a^2\beta_1 + a\beta_2 + \beta_0 = \frac{3\left(I_{yB}^{(1)} - a^2\beta_1 I_k^{(3)} - aI_y^{(3)}\right)}{I_{kA}^{(1)}}$
	$\rho_1 = \frac{I_{y1} - I_y^{(3)}}{E_{k1}}$	$\rho_2 = \frac{I_{y2}}{E_{k2}}$	$\rho_0 = \frac{I_{y0}}{E_{k0}}$	$\rho_1 + \rho_2 + \rho_0 = \frac{3\left(I_{yA}^{(1.1)} - I_y^{(3)}\right)}{E_{kA}^{(1.1)}}$ $a^2\rho_1 + a\rho_2 + \rho_0 = \frac{3\left(I_{yB}^{(1.1)} - a^2 I_y^{(3)}\right)}{E_{kA}^{(1.1)}}$
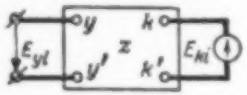 Circuit *B* Any asymmetric short-circuit between k - k' with three-phase cut-off section y - y′.	$\alpha_1 = \frac{E_{y1}}{E_{k1}}$	$\alpha_2 = \frac{E_{y2}}{E_{k2}}$	$\alpha_0 = \frac{E_{y0}}{E_{k0}}$	$\alpha_1 + \alpha_2 + \alpha_0 = \frac{3E_{yA}^{(1.1)}}{E_{kA}^{(1.1)}}$ $a^2\alpha_1 + a\alpha_2 + \alpha_0 = \frac{3E_{yB}^{(1.1)}}{E_{kA}^{(1.1)}}$

Note: 1. In the circuits, only e.m.f. currents and frequencies at the point of short-circuit are noted. E.m.f. currents and frequencies of the generators are excluded from the direct sequence circuits.

2. Phase *A* is taken as the main phase in the indices.

1958

rupture in the sequence circuits; I_{yi}, I_{ki} are the corresponding values before phase rupture; z_{yi}, z_{ki} are the intrinsic resistances of the branches y-y' and k-k' in the sequence circuits.

Equations (4) and (5) are valid for each sequence and are not limited by the conditions of short-circuit in branch k-k' or of phase break in branch y-y'.

As applied to the faults under consideration, E_{yi} can signify the component of e.m.f. at the phase break point and ΔE_{ki}, ΔI_{ki} and ΔI_{yi} the changes in the components of e.m.f. and current produced by the phase break. The relationships between these values (boundary conditions) are given in Table 2. They are analogous to the known boundary conditions characterizing the relationships between the currents and voltages in separate sequences with asymmetric short circuits and phase breaks. As regards ΔI_{ki} and ΔE_{ki}, they are determined only by the type of fault in branch k-k'; ΔI_{yi} and ΔE_{yi} are determined both by the type of fault in branch y-y' and by the conditions under which the fault arises.

Equations (4) and (5) can be limited by the special conditions of various combinations of short-circuits and phase ruptures; for each combination it is necessary to solve twelve equations, six of which are given by equations (4) and (5), the other six by the special limiting conditions for the short circuit or phase break, as shown in Table 2. The simplest solution to this problem is obtained by using the known complex substitution circuits in place of the short-circuit and in place of the phase break, transferring all the effective e.m.f.'s caused by the phase break, first into the short-circuit branch and then into the phase break branch.

Fig. 3a shows the complex substitution circuit in place of a short to earth on phases B and C. Figs. 3b, 4b show the same circuits after subtracting the currents and e.m.f.'s acting before the break, and transferring the e.m.f. E_{yi} to the circuit branch. These circuits determine the current and e.m.f. at the point of short-circuit, due to the phase break.

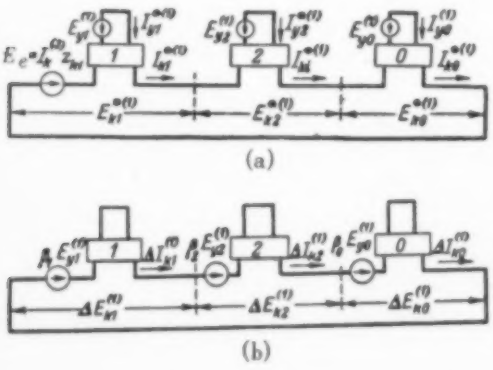

(a)

(b)

FIG. 3.

In finding the current in the circuit of Fig. 3b and the voltage in that of Fig. 4b it can be shown that:

$$\Delta I_{k1}^{(1)} = \Delta I_{k2}^{(1)} = \Delta I_{k0}^{(1)} = \frac{B_1 E_{y1} + \beta_2 E_{y2} + \beta_0 E_{y0}}{z_{k1} + z_{k2} + z_{k0}} = nE_{y0}; \tag{6}$$

$$\Delta E_{k1}^{(1.1)} = \Delta E_{k2}^{(1.1)} = \Delta E_{k0}^{(1.1)} = \frac{\rho_1 E_{y1} + \rho_2 E_{y2} + \rho_0 E_{y0}}{\frac{1}{z_{k1}} + \frac{1}{z_{k2}} + \frac{1}{z_{k0}}} = mE_{y0}, \tag{7}$$

where n and m are coefficients which are determined, for a break on any phase, by

TABLE 2.

In short-circuit branch (branch k-k' in Fig. 1).		In phase rupture branch (branch y-y′ in Fig. 1).	
Type of fault	Boundary conditions	Phase broken	Boundary conditions
Three-phase to earth	$\Delta E_{k1} = \Delta E_{k2} = \Delta E_{k0} = 0$	A	$I_{yA} + \Delta I_{y1} + \Delta I_{y2} + \Delta I_{y0} = 0$ $E_{y1} = E_{y2} = E_{y0}$
Two-phase (phases B and C) to earth	$\Delta E_{k1} + \Delta I_{k2} + \Delta I_{k0} = 0$ $\Delta E_{k1} = \Delta E_{k2} = \Delta E_{k0}$	B	$I_{yB} + a^2\Delta I_{y1} + a\Delta I_{y2} + \Delta I_{y0} = 0$ $a^2E_{y1} = aE_{y2} = E_{y0}$
Single-phase (phase A) to earth	$\Delta I_{k1} = \Delta I_{k2} = \Delta I_{k0}$ $\Delta E_{k1} + \Delta E_{k2} + \Delta E_{k0} = 0$	C	$I_{yC} + a\Delta I_{y1} + a^2\Delta I_{y2} + \Delta I_{y0} = 0$ $aE_{y1} = a^2E_{y2} = E_{y0}$

Note: 1. Phase A is taken as the main phase.
2. In interphase damage without earthing short-circuits, in the expressions cited $\Delta E_{k0} = 0$; $\Delta I_{k0} = 0$.

the coefficients β and ρ and by the phase differences between E_{y1}, E_{y2} and E_{y0}. Expressions for the coefficients n and m, for various combinations of short-circuit and phase rupture are shown in Table 3.

Having used the complex substitution circuit in place of the phase break in an analogous manner, we obtain*:

$$E_{y0} = E'_{y0} + E''_{y0} = \frac{I}{g_{y\Sigma}} + E''_{y0}, \tag{8}$$

where E_{y0} is the e.m.f. at the phase rupture point in the zero sequence circuit; I is the current in the phase to be broken, before the rupture; $g_{y\Sigma} = 1/z_{y1} + 1/z_{y2} + 1/z_{y0}$ is the sum of the conductivities of all the sequence circuits at the phase rupture point; E''_{y0} is the component of e.m.f. E_{y0}, due to the voltage changes at the short-circuit point resulting from the phase break.

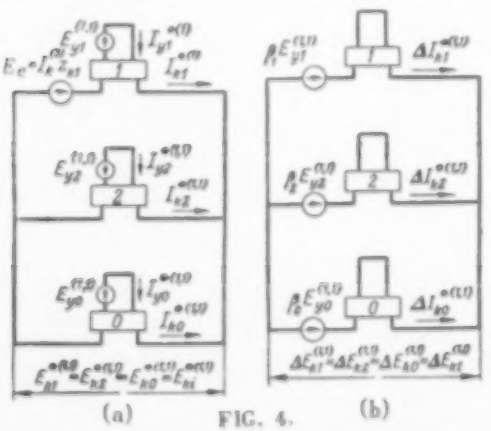

(a) (b)

FIG. 4.

If phase A is broken

$$E''_{y0} = \frac{\rho_1\Delta E_{k1} + \rho_2\Delta E_{k2} + \rho_0\Delta E_{k0}}{g_{y\Sigma}};$$

and if phase B,

$$E''_{y0} = \frac{a^2\rho_1\Delta E_{k1} + a\rho_2\Delta E_{k2} + \rho_0 E_{k0}}{g_{y\Sigma}}.$$

* Equation (8) can also be obtained by solving equation (4) together with equations defining the boundary conditions for the phase break (Table 2).

TABLE 3.

Type of short-circuit to earth	Phase broken	Expressions for coefficients	
		Δ	m and n
Three phase	A	$\Delta_A^{(3)} = 0$	—
Two phase (B and C)	A	$\Delta_A^{(1.1)} = -\frac{(\rho_1 + \rho_2 + \rho_0)^2}{g_{k\Sigma}}$	$m_A = \frac{\rho_1 + \rho_2 + \rho_0}{g_{k\Sigma}}$
	B	$\Delta_B^{(1.1)} = \Delta_A^{(1.1)} + \frac{3(\rho_1\rho_2 + \rho_2\rho_0 + \rho_1\rho_0)}{g_{k\Sigma}}$	$m_B = \frac{a\rho_1 + a^2\rho_2 + \rho_0}{g_{k\Sigma}}$
Single phase (A)	A	$\Delta_A^{(1)} = \frac{(\beta_1 + \beta_2 + \beta_0)}{z_{k\Sigma}} - \left(\frac{\beta_1^2}{z_{k_1}} + \frac{\beta_2^2}{z_{k_2}} + \frac{\beta_0^2}{z_{k_0}}\right)$	$n_A = \frac{\beta_1 + \beta_2 + \beta_0}{z_{k\Sigma}}$
	B	$\Delta_B^{(1)} = \Delta_A^{(1)} - \frac{3(\beta_1\beta_2 + \beta_1\beta_0 + \beta_2\beta_0)}{z_{k\Sigma}}$	$n_B = \frac{a\beta_1 + a^2\beta_2 + \beta_0}{z_{k\Sigma}}$

Note: Phase C in any form of short-circuit has no special characteristics in relation to phase B; for this reason combinations which include an interruption of phase C are not cited.

Equation (8) is not limited by the conditions of the short circuit in the branch. For a three-phase short-circuit, $E''_{y0} = 0$, and equation (8) takes the following form:

$$E_{y0} = \frac{I^{(3)}}{g_{y\Sigma}},$$

where $I^{(3)}$ is the current in the phase to be broken (before the break) in a three-phase short-circuit. For other forms of short-circuit, $E''_{y0} \neq 0$ and takes various values, depending on the combination of short-circuit and phase rupture.

For any combination of short-circuit and phase break, equation (8) can be written in the following form:-

$$E_{y0} = \frac{I}{g_{y\Sigma} + \Delta}, \tag{9}$$

where Δ is a coefficient determined by the boundary conditions of the short-circuit and phase break and having the dimensions of conductivity. Values of Δ, obtained as a result of the combined solution of equations (6) - (8) for various combinations of short-circuit and phase rupture, are given in Table 3.

Given the values of E_{y0}, $\Delta I_{k0}^{(1)}$ and $\Delta E_{k0}^{(1.1)}$, we can find their values for straight and reverse sequence circuits (Table 2), and determine $\Delta E_{ki}^{(1)}$ and $\Delta I_{ki}^{(1.1)}$ according

to equation (5), and ΔI_{yi} according to equation (4), for all the sequence circuits. This completes the calculation of the current and e.m.f. components shown in Fig. 1.

Thus, all the current and e.m.f. components shown in Fig. 1, for any combination of short-circuit and phase break, can be expressed in terms of E_{y0} and the coefficients g_{ki}, g_{yi}, ρ_i, β_i. Together with this it can be seen from equation (9) that, whatever the combination of short circuit and phase break, E_{y0} is always determined only by the magnitude and direction of the current in the break phase and by coefficients $g_{y\Sigma}$ and Δ, which have the dimensions of conductivity. Current I depends on the e.m.f. in the circuit prior to the phase break, whilst the sum of $(g_{y\Sigma} + \Delta)$ is determined independently of the e.m.f. parameters of the circuit.

If only the inductive resistance is taken into account, the coefficient Δ for any combination of faults considered, is in phase with $g_{y\Sigma}$ and can be regarded as a correction to the conductivity $g_{y\Sigma}$, accounting for the special features of various combinations of faults. In the general case $\Delta_A^{(1)} \neq \Delta_B^{(1)} \neq \Delta_A^{(1.1)} \neq \Delta_B^{(1.1)}$.

In fact this correction accounts for the changes in the e.m.f. E_{y0} due to a phase rupture, with various forms of short-circuit. In cases of rupture in the phase damaged by the short-circuit, these changes are small. Calculations show that if $2z_{ki} < z_{yi}$, even under the most unfavourable conditions, Δ does not exceed 4 per cent of the conductivity $g_{y\Sigma}$ and drops rapidly as β_1, β_2 and β_0 fall. Thus in practical calculations of E_{yi} for any combination of phase breaks, with a short circuit at $2z_{ki} < z_{yi}$, a coefficient Δ can be assumed to be zero.

It should be noted that the combinations of faults considered are of great practical interest, since they introduce the maximum change in the e.m.f. and current values before the break.

Calculations of these combinations can be simplified still further if we neglect not only ΔE_{ki}, but also the inequality between the direct and reverse sequences. In this case expression (4) takes the form:-

$$I_{yi} = I_{yi} - q_i I, \tag{10}$$

where I is the current in the break phase prior to rupture; q_i are coefficients in the direct (q_1), reverse (q_2) and zero (q_0) sequence circuits, depending only on $k = z_{y0}/z_{y1}$ and on which phase is broken; if phase A,

$$q_1 = q_2 = kq_0 = \frac{k}{2k+1};$$

and for a break in phase B,

$$a^2 q_1 = a q_2 = k q_0 = \frac{k}{2k+1}.$$

By analyzing expression (10), it can be shown that in real circuits I^*_{y0} cannot exceed 0.6 I in a three-phase short-circuit and 0.6 I-I_{y0} in a single- or two-phase short-

circuit to earth. On this basis it can be found, without any calculation, whether deliberate incomplete phase transmission endangers the protective relays or whether more detailed calculation is required to examine their safety.

Expression (10) makes it possible to find without trouble the significant values of the components for combinations giving the maximum distortion, and, for $2z_{ki} < z_{yi}$, to determine them to the accuracy normally allowed for practical calculations.

Example It is required to find the current and voltage components for a short to earth in phases A and B at point k, with a simultaneous break in phase A in the y-y' branch. The data required for this determination are given in Fig. 5.

Replace the given combination of faults by another, easier to consider: namely, shorts to earth in phases B and C with a break in phase B in the y-y' branch. The return step from this combination to that given is not difficult, since for this the current and voltage vectors found must be rotated through 120°.

In order to simplify the example and working, we assume that the circuit contains only active resistances.

The coefficients α_i, β_i and ρ_i, and their sums as in the expressions in Table 1 are:

$$\beta_1 = 0.25;\ \beta_2 = 0.25;\ \beta_0 = 0.5;\ \rho_1 = 0.5;\ \rho_2 = 0.25;$$
$$\rho_0 = 1;\ \alpha_1 = 0.66;\ \alpha_2 = 0.66;\ \alpha_0 = 1;\ \rho_1 + \rho_2 + \rho_0 = 1.75;$$
$$\rho_1\rho_2 + \rho_1\rho_0 + \rho_2\rho_0 = 0.875;\ a\rho_1 + a^2\rho_2 + \rho_0 = 0.5 - 0.25a^2.$$

The resistances at the point of rupture in the separate sequence circuits are:

$$z_{y1} = \frac{\alpha_1}{\rho_1} = 1.33\ \Omega;\quad z_{y2} = \frac{\alpha_2}{\rho_2} = 2.66\ \Omega;\qquad z_{y0} = \frac{\alpha_0}{\rho_0} = 1\ \Omega.$$

The total conductivities of the sequence circuits at the point of phase rupture and the point of short-circuit are:

$$g_{y\Sigma} = 2.12 = \frac{1}{\Omega};\qquad g_{k\Sigma} = \frac{I_k^{(2)}}{E_k^{(1.1)}} = 5\,\frac{1}{\Omega}.$$

The total coefficient Δ for the combination of faults considered (Table 3) is:

$$\Delta_B^{(1.1)} = -0.086 \cdot \frac{1}{\Omega}.$$

The e.m.f. of the zero sequence, according to expression (9), is:

$$E_{y0} = \frac{I_B^{(1.1)}}{g_{y\Sigma} + \Delta_B^{(1.1)}} = -1\,053\,a^2 + 147.$$

The e.m.f.'s in the direct and reverse sequences, taking into account the boundary conditions of the phase break, are:

$$E_{y1} = aE_{y0} = -147\,a^2 - 1\,200;\ E_{y2} = a^2E_{y0} = 1\,053 + 1\,200\,a^2.$$

The change in e.m.f. at the point of short-circuit, according to equation (7) is:

$$\Delta E_{k1}^{(1.1)} = \frac{ap_1 + a^2 p_2 + p_0}{E_{y\Sigma}} E_{y0} = (-165a^2 + 38).$$

The resultant e.m.f. at the point of short-circuit is:

$$E_{ki}^{*} = E_{ki} + \Delta E_{ki} = 438 - 165\,a^2.$$

The change in current at the point of short circuit, according to expression (5) is:

$$\Delta I_{k1} = 257a^2 - 524;\ \Delta I_{k2} = 301 + 465a^2 \text{ и } \Delta I_{k0} = 223 - 722\,a^2.$$

The resultant current at the point of short-circuit is:

$$I_{k1}^{*} = 676 + 257\,a^2;\quad I_{k2}^{*} = 465\,a^2 - 99;\quad I_{k0}^{*} = -722a^2 - 577.$$

The change in current at the point of the phase break, according to expression (4) is:

$$\Delta I_{y1} = 28a^2 + 884;\ \Delta I_{y2} = -493a^2 - 406 \text{ and}$$

$$\Delta I_{y0} = 838a^2 - 185.$$

The resultant current at the point of phase break is:

$$I_{y1}^{*} = -1166 + 28\,a^2;\quad I_{y2}^{*} = -306 - 493\,a^2;\quad I_{y0}^{*} = 215 + 888\,a^2.$$

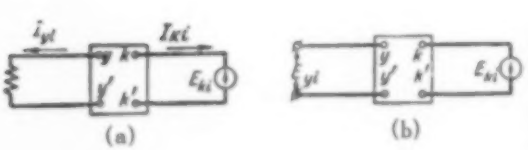

FIG. 5. (a) branch y - y′ included; $I_{y1} = 2050$ A; $I_{y2} = 100$ A; $I_{y0} = 400$ A; $I_{k1} = 1200$ A; $I_{k2} = 400$ A; $I_{k0} = 700$ A; $E_{k1} = E_{k2} = E_{k0} = 400$ V; $Z_{k1} = 0.5\ \Omega$. $Z_{k2} = 1\ \Omega$; $Z_{k0} = 0.5\ \Omega$; $I_k^{(3)} = 2000$ A; $I_y^{(3)} = 2200$ A. (b) branch y - y′ excluded; $E_{y1} = E_{y2} = 95$ V; $E_{y0} = 143$ V; $E_{k1} = E_{k2} = E_{k0} = 143$ V.

The amount of calculation required to find the values needed is quite independent of the complexity of the circuit. In this respect the proposed method differs usefully from all the other known methods, in which the calculations become more complicated as the circuit becomes more involved.

To find z_{yi} in the absence of calculations shown by the scheme *B* in Table 1, it is possible to use the data given in Fig. 6. Fig. 6a corresponds to a short-circuit at one end of branch y-y′, and Fig. 6b at the other.* On the basis of these data it is possible to find the intrinsic resistance of the y-y′ branch in the absence of a short circuit in the system, if the following expression is used:-

$$z_y' = \frac{ab}{b - ac},$$

* As applied to the direct sequence circuit, the data shown in Fig. 6 denote the currents and voltages due solely to the e.m.f. at the point of short-circuit, assuming that the generator e.m.f. is zero. These currents and voltages are found by the superimposition of the conditions for any asymmetric short-circuit on those for a three-phase short circuit.

where

$$a = \frac{z_n^2}{z_n - \frac{U_k''}{I_k''} + \frac{U_k' U_k''}{U_k' I_k''}}; \quad b = \frac{U_k'}{I_y'}; \quad c = \frac{I_y'}{I_k'}.$$

The changes produced by a short-circuit in the value of intrinsic resistance for the y-y' branch can be taken into account, bearing in mind that:

$$\frac{1}{z_y} = \frac{1}{z_y'} + \frac{\beta^2}{z_k},$$

where β shows what fraction of the total current at the point of short-circuit constitutes the current in the y-y' branch (Table 1); z_k is the resistance introduced at the point of short-circuit.

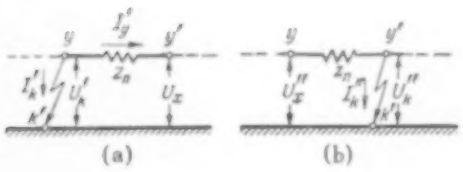

FIG. 6.

Conclusions

The described method of calculation affords: (1) substantial simplification of the calculation of asymmetric faults by use of the results of calculations of short circuits in full-phase conditions. The changes brought about by unbalanced phase transmission are expressed in terms of the current for the full-phase condition and are independent of the e.m.f. parameters of the system; (2) simplification of calculations in systems with deliberately selected coefficients of current distribution. This refers in particular to combinations of any complex faults not considered in the paper, to the calculation of short circuits in power systems in connexion with changes in the generator e.m.f. and so on; (3) simplification of the calculation of complex asymmetric faults, when carried out on computing machines, by the superimposition of current components determined for full-phase conditions on to the current components due to the e.m.f.'s E_{yi} and ΔE_{ki}.

Translated by E. Bishop

REFERENCES

1. N.N. Shchedrin and S.A. Ul'ianov; *Zadachi po raschetu korotkikh zamykanii (Problems in the Calculation of Short-Circuits)*, Gosenergoizdat, (1955).
2. A.B. Chernin; *Korotkie zamykaniia pri nepolnofaznykh rezhimakh elektricheskikh setei (Short-Circuits in Unbalanced Phase Conditions in Electric Circuits)*, Gosenergoizdat, (1952).

A NEW CIRCUIT FOR HIGH-SPEED PULSE CONTROL IN SYSTEMS CONTAINING IONIC INVERTERS*

D.P. MOROZOV, M.G. CHILIKIN, N.G. LYSENKOV and L.M. TVERDIN

(Received 22 July 1957)

1958

Modern electric drive is characterized by wide use of controlled ionic inverters. The use of control systems containing magnetic and electronic amplifiers ensures the development of high-quality electric drive systems satisfying the increased demands made on automatic control for precision and speed of effective action.

The introduction of ionic inverters in the electric drive systems of metallurgical shops, where a large number of different systems using controlled mercury rectifiers as inverters operate, is most significant. Practical experience in the operation of these installations has been accumulated both here and abroad. Our design and scientific research organizations have developed various different systems for grid control by ionic inverters (systems containing peak transformers and chokes, etc.).

The rectified voltage is regulated, in systems in use at present which contain ionic inverters, by the phase displacement of the control peaks. The ionic inverter mean rectified voltage is determined from the well-known equation $V_d = V_{d0} \cos \alpha$. A number of intricate and important units are used for changing the grid control system firing angle: grid supply and phase shift systems, and systems summing, shaping and amplifying the control signals [1-3]. The use of modern grid control systems enables us to exercise control by means of powerful mercury rectifiers with high-speed rectified voltage build-up [3].

Study of the systems containing ionic inverters used at present and the experience accumulated in their operation permits us to formulate the following basic tasks which must now be performed in order that these installations may be put to wider use.

(1) The improvement of $\cos \phi$ and the efficiency of systems with a wide range of rectified voltage control.

(2) Increase in the speed of effective action of control systems, this increase

* *Elektrichestvo* No.2, 22-27, 1958 [Reprint Order No. EL 50].

being particularly important for powerful rolling mills and other important industrial plant.

(3) Further increase in the operating reliability of installations containing ionic inverters, and maximum simplification of the control system, as a necessary condition for the use of these inverters.

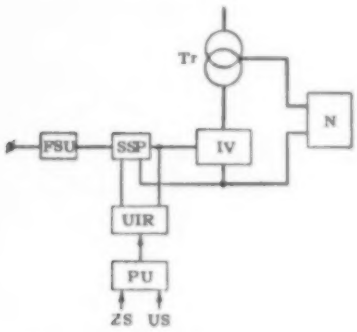

FIG.1. Diagram of the principle of high-speed pulse regulation. Tr - transformer; IV - ionic valve; N - load; FSU - phase-shifting appliance; SSP - grid feed system; UIR - pulse regulation unit; PU - intermediate installation; ZS - specified signal; US - controlling signal.

The grid control systems containing ionic inverters used at present do not fully satisfy these requirements. Where the rectified voltage regulation range is wide, the phase-shifting and summing units are complicated and definitely sluggish.

Regulation of rectified voltage by altering the firing angle over a wide range considerably worsens the power factor, this making the introduction of ionic inverters in powerful installations difficult.

The authors of this article have developed and investigated several variants of a new way of regulating the mean rectified voltage of an ionic inverter (Fig.1).

The basis on which the system operates is the pulse method of regulating the mean rectified voltage; here, change in the regulated quantity is caused not by phase displacement of the positive control peaks, but by how frequently and for how long the ionic inverter is applied.

Pulsatory ionic inverter working conditions are obtained by introducing a new unit into the grid control circuit. The main purpose of this unit is to blank-off and trigger the ionic inverter in accordance with the required regulation conditions. The principle components of this unit are the controlled low-power valves which ensure the blanking-off and triggering of the ionic inverters at the necessary intervals and for the necessary lengths of time. Magnetic or mechanical appliances can be used in place of the controlled valves. All these installations must satisfy the condition of low voltage drop when the control peaks fed to the ionic inverter are applied.

Let us examine the working of this system in the example of an installation with a 3-phase mercury rectifier (Fig.2), in order to clarify the principle on which the proposed new high-speed pulse regulation system operates.

When there is no control signal V_{vkh} on the grids of the pulse regulation high-speed unit control valves UV, these valves are blanked off by the blanking

voltage V_{sm} (the bias voltage).

The positive triggering peaks, produced by the mercury rectifier in the grid control circuit, are fed to its grids in the usual way. The mercury rectifier is opened and the rectified voltage determined by α, the angle of regulation.

When a control signal V_{vkh}, sufficient for triggering, is fed to the grids of the valves UV, these valves fire and clip the positive pulses fed to the grids of the rectifier RV. The mercury rectifier is blanked-off.

The cessation of the input signal V_{vkh} corresponds to the blanking-off of the valves UV and the triggering of the mercury rectifier.

Depending on the frequency of transmission and the duration of the signals fed to the grids of the valves UV, rectified voltage pulses of the corresponding frequency and duration are produced at the output of the ionic inverter. The mean mercury rectifier rectified voltage depends on the time of conduction and the spacing, where α is constant.

The new ionic inverter high-speed pulse control unit may be introduced into certain systems in use for regulating ionic inverters by various means, depending on the nature and purpose of the systems.

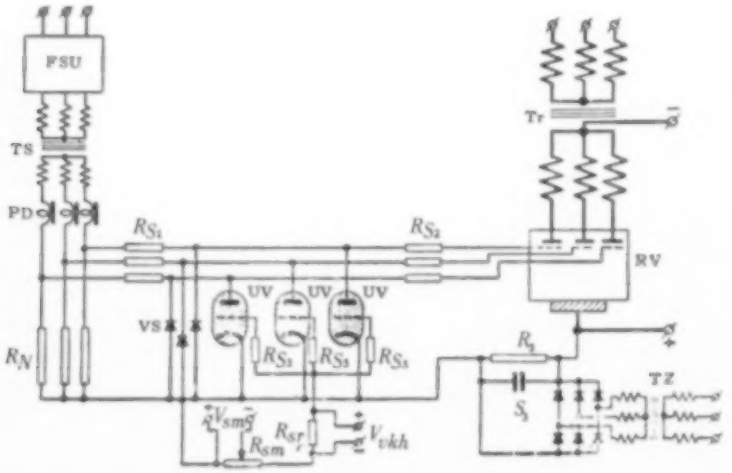

FIG.2. Circuit illustrating the principle of pulse regulation of rectified voltage. Tr - transformer; RV - mercury rectifier; FSU - phase-shifting appliance; TS - grid transformer; PD - peak choke; RN - load resistance; R_{S1}, R_{S2} - grid resistances; VS - semiconductor rectifiers; TZ - mercury rectifier locking voltage unit transformer; R_3 - locking potential unit resistance; UV - controlled valves of the pulse control unit; R_{S3} - grid resistance in the controlled valve grid circuits; R_{sm} - grid bias; R_{sr} - comparing resistance in the controlled valve grid circuits.

In the new system, the rectified voltage can be regulated both where $\alpha \neq 0$ and where $\alpha = 0$. In the first case, the high-speed impulse regulation unit is made an additional link in the circuits in use. In the second case, the phase-shifting appliance may be removed from the circuit and all the necessary signals fed only to the pulse regulation unit.

The control signal V_{vkh}, the frequency and duration of which correspond to the specified mean rectified voltage, may be obtained:

(a) from the independent switchgear, for instance, a mechanical switch with conducting plates and slide contact (an open circuit regulating system), or

(b) from intermediate gear providing equalization of the specified and regulated magnitudes (a closed regulating system).

Oscillation or electronic regulators, also magnetic amplifiers, can be used as the intermediate equipment, working on the input of the pulse regulation unit. The summing of the various signals, their comparison with the specified value, and also the shaping of the signal supplied to the input of the pulse regulation unit, are performed in the intermediate equipment.

In a number of cases, the intermediate equipment may be omitted. In these circuits the control signals are fed direct to the pulse regulation unit.

A number of circuits using the high-speed pulse regulating unit were investigated in the laboratories of the Moscow Power Institute Industrial Undertaking Electrical Equipment. In particular, the circuit shown in Fig.3 was examined. The circuit provides forced generator voltage build-up, generator voltage "cut-off", and the maintenance of a specified voltage; the control signal is fed directly to the high-speed impulse regulation unit.

A PN-550 type generator was used; $P_N = 88\,\text{kW}$, $V_N = 230\text{V}$, $I_n = 383\text{A}$, $n_N = 1440$ rev/min an RM-200 mercury rectifier with grid supply unit was used, and the controlled valves were TR 1-2.5/2 thyratrons.

In the supply circuit, feed to the field windings of the generator was accomplished by the inclusion of a two-pole contactor K. A negative potential, exceeding their blanking-off potential, was fed to the grids of the valves UV by a potentiometer P. Whilst starting the motor, the rectifier RV was open and a voltage $a_0 V_{vN}$ (a_0 being the forcing coefficient) was applied to the field windings of the generator. The controlled valves were blanked-off until the generator voltage had reached a value such that $| V_{sm} | - | V_{vkh} | \leqslant | V_{otn} |$, where V_{otn} is the triggering voltage for UV. The valves UV come into operation. The positive peaks fed to the grids of the rectifier RV are cut off, and extinguished. The current in the generator field windings begins to drop. The generator field winding self-induction e.m.f. will maintain the current in the discharge resistance and at one of the mercury rectifier anodes (until the anode current passes zero). Reduction of the generator voltage causes reduction in the signal V_{vkh}; UV thereupon is extinguished and RV comes

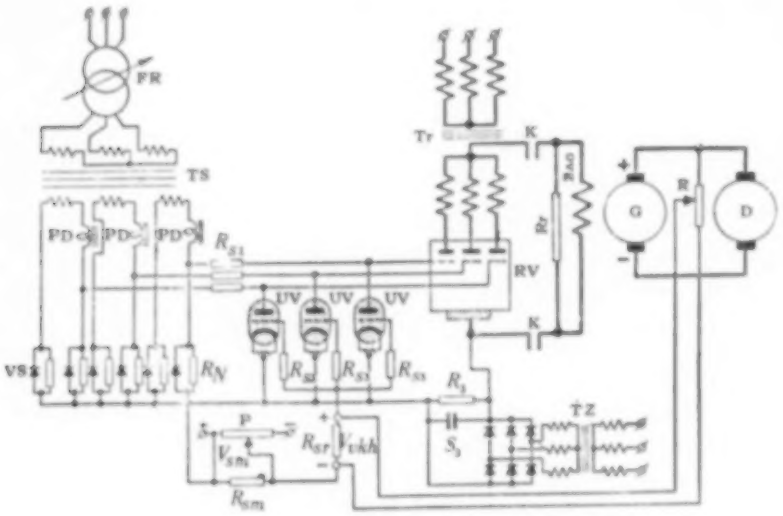

FIG.3. Diagram illustrating the principle of the pulse regulation of generator excitation current in a generator-motor system.

into action. Thus, the mercury rectifier is working on a system of impulses and the generator voltage is maintained at a specified level, fluctuating around its mean value.

The "cut-off" voltage is determined by the bias voltage V_{sm} and $\beta = \frac{V_{vkh}}{V_g}$ (Rheostat R contact position).

The control circuit (Fig.3) is extremely simple, notwithstanding the complicated tasks which it performs. Ideal voltage "cut-off" is very simply accomplished. The change in time of generator voltage, generator excitation current and field winding voltage for various levels of voltage regulation are shown in the oscillographs in Fig. 4-6. The recording in Fig. 4 shows the process of transition to the rated generator excitation current and voltage. The ultimate values for these quantities are equal to 0.66 of the rated values in the recording in Fig. 5, 0.33 in

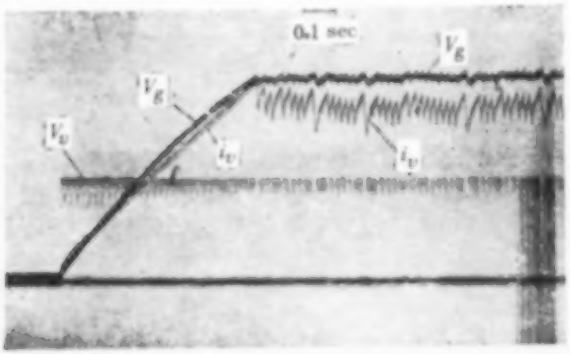

FIG.4. Oscillograph recording of the transitional generator excitation process where the forcing coefficient $a_0 = 2$; $i_{vu} = i_{vn}$.

Fig.6. In spite of the considerable deviations of thyratron-actuating characteristics and the lack of an intermediate appliance ensuring a steep signal front at the input of the pulse regulation unit, the circuit provides small generator voltage fluctuations at various excitation levels.

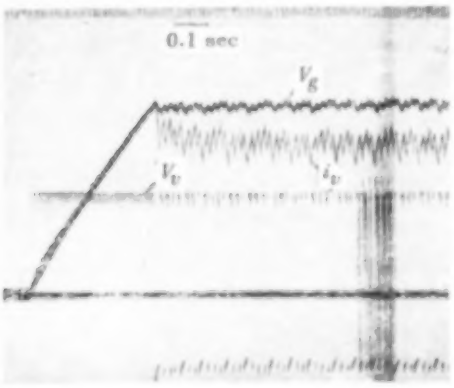

FIG.5. Oscillograph recording of the generator excitation transitional process for forcing coefficient $a_0 = 2$; $I_{vu} = 0.66\ I_{vn}$.

Since regulation of the rectified voltage takes place at a firing delay angle $\alpha = 0$, the circuit ensures a high power coefficient and efficiency. The circuit is quick-acting; the operating time is determined solely by the time taken by the thyratrons UV to fire and extinguish. Their firing time is practically zero; the time they take to extinguish depends on the moment at which the signal is fed to the fired thyratron and cannot, for a three-phase circuit, exceed 8.33×10^{-6} sec (for a six-phase rectifier it is 66.6×10^{-6} sec).

It must be noted that the qualitative and quantitative factors of the new circuit are subject to further theoretical and experimental research. It will also be necessary to study a number of physical phenomena and processes which accompany the working of the new regulation circuit. The preliminary results show that the new circuit can be employed in various intricate electrical drive circuits requiring: (a) a wide range of regulation; (b) speedy action; (c) precise regulation with high power coefficients and efficiencies.

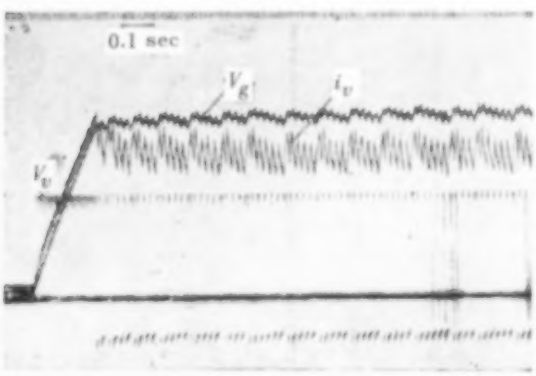

FIG.6. Oscillograph recording of the generator excitation transitional process for forcing coefficient $a_0 = 2$; $i_{vu} = 0.33\ I_{vn}$.

Ionic inverters operating in pulse systems may be used for the supply of: (a) electric motor and generator starter circuits, and (b) electric motor armature circuits.

Without enumerating all the possible types of mechanism for which the new high-speed pulse regulation circuit may be used, we will give some examples to illustrate its use.

Fig.7 shows the principles of the control of the generator-motor system for a reversing blooming mill stand. The generator and motor field windings are supplied from ionic inverters operating in impulse systems. Reversing of the motor is accomplished by changing the generator excitation polarity, using a reversing switch. The motor rotation rate is regulated up to basic by the effect on the ionic inverter feeding the generator excitation circuit, and above basic by the effect on the ionic inverter feeding the motor excitation circuit.

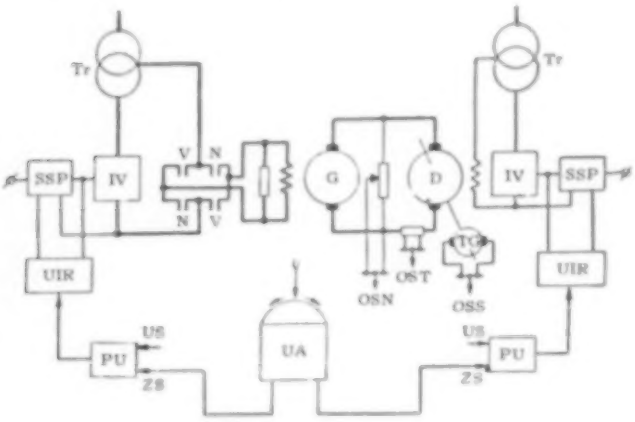

FIG.7. Diagram illustrating the principle of the pulse control of the excitation of large machines from ionic inverters in the generator-motor system of a reversing mill. Tr - transformer; IV - ionic valves; G - generator; D - motor; TG - tacho-generator; V,N - reversing contacts "forward", "back"; UA - controlling gear; SSP - grid supply system; UIR - pulse regulation unit; PU - intermediate installation; ZS - specified signal; US - controlling signal; OSN - voltage feed-back; OSS - rotation feed-back; OST - current feed-back.

There are no complicated phase-shifting devices in the diagram for control using mercury rectifiers. All the control functions in the steady-running and transitional states are performed by the pulsatory regulation unit. Although the pulsatory control unit can be made on the basis of magnetic appliances (high-speed magnetic amplifiers and relays, etc.) the use of thyratrons may be considered a sufficiently reliable solution. We know that thyratrons are widely used in practice at home and abroad (in the U.S.A. and Germany) in electric drive control circuits. Certain designs of thyratron being introduced into industry at the present time are very reliable and hard-wearing (service life of 15,000 hr). The elimination of phase-shifting and other intricate units simplifies and improves mill control circuits in comparison with existing circuits, and facilitates their operation.

The mercury rectifiers in the given circuit operate with an angle of regulation $\alpha = 0$. Calculations show that for constant electrical motor or generator field winding times $T_v = 3 - 4$ sec, forcing coefficient $\alpha_s = 3 - 4$ and tolerated regulated quantity variations (generator voltage, field current, motor rate) of 4 - 5 per cent of the rated values, the resting and working times of the mercury rectifier RV vary between 0.04 and 0.1 sec (in a three-phase rectification system this corresponds to the firing or misfiring of six to fifteen anodes in succession). The extinction of the rectifier RV in pulsatory ionic excitation circuits is determined by the discharge

resistance selection condition:

$$k_p < \frac{\alpha_0 \pi}{m \sin \frac{\pi}{m}},$$

where $k_p = R_p / r_v$, R_p is the discharge resistance in the field winding circuit, and m is the number of rectification phases.

For the rectifier RV pause and firing-period intervals indicated above, the impulse system of this rectifier hardly worsens the shape of the circuit current curves, and ensures that cos ϕ is close to unity. Where the anodes fire and misfire in quicker rotation, the coefficient of power is affected by the worsened shape of the current curve and the firing of the last (prior to extinction of RV) anode in the transformer secondary e.m.f. negative value region. However, in this case also, the power coefficient is considerably higher in impulse control circuits than in RV continuous control circuits. In an experimental installation with frequent rotation of anode firing and misfiring, pulsatory RV control improved cos ϕ (for identical conditions), in comparison with continuous control by up to 60-70 per cent (0.34 to 0.58; 0.51-0.72; 0.62-0.85, etc).

The simplicity, economy and precision with which the regulated value is maintained (less than 1 per cent when T_v = 3-4 sec), and high-speed action enable us also to recommend pulsatory RV control circuits for the excitation of the principle electrical machinery in the generator-motor transmission systems of powerful continuous mills (reconstructed and under construction), and of less powerful plant.

The use of ionic inverters operating in impulse systems for supplying the armature circuits of blooming mill motors is shown in Fig.(8). The motor is reversed in this circuit by a switch in the motor armature circuit. The introduction of an impulse regulation unit into the control circuit hardly makes this circuit more complicated in view of the simplicity of the proposed unit, and enables the armature to be supplied at reduced rates of rotation (up to basic rate), with a regulation angle $\alpha = 0$. At the lowest motor rotation rates, in order to reduce the armature current pulsations and improve motor working conditions, it is advantageous to work at $\alpha = \cos nt \neq 0$, but at lower regulation angles than in the case of continuous RV control. The employment of a pulse regulation unit ensures a high power coefficient and is more advantageous than intricate circuits with artificial anode communication, non-symmetrical control, etc.

The proposed pulse control by mercury rectifiers feeding the motor armature can be very widely applied (with or without phase-shifting equipment) in the electric drive systems of less powerful plant, (rolling mill auxiliary mechanisms, metal-working machines, etc.), where the motors work under better conditions. It should be possible, in order to confirm the proposal that an RV impulse system may be employed for the supply to a motor armature, to refer to the details given in

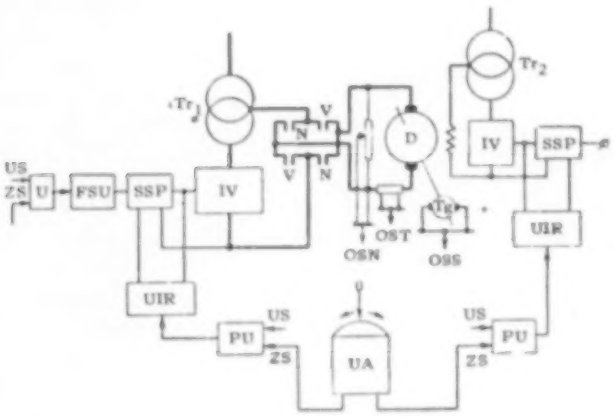

FIG.8. Diagram illustrating the principle of reversing mill motor feed from a mercury rectifier using pulse regulation. Tr_1 - main inverter transformer; Tr_2 - motor excitation circuit ionic inverter transformer; D - motor; IV - ionic valves; SSP - grid feed system; FSU - phase-shifting appliance; U - amplifier; UIR - pulse regulation unit; PU - intermediate installation; US - controlling apparatus; ZS - specified signal; US - controlling signal; OSN, OST, OSS - voltage, current and rate feed-backs; V, N, - reversing contacts, "forward", "back".

foreign literature [4], on practical experience abroad of the use of mercury rectifiers working in a system of impulses in the electric drives of the pressure roll and other auxiliaries in powerful rolling mills.

Finally, yet one more important field for the employment of the pulse regulating unit must be indicated: that is, the electric drive of continuous mills, (the armature and excitation circuits of the motor supplied from mercury rectifiers), where speedy action and precision of regulation are required with a narrower range of regulation (narrower than, for example, in a blooming mill).

The use of pulse regulation in circuits where synchronous motor field windings are supplied from ionic inverters is of great interest.

Conclusions

The practical introduction of powerful controlled rectifiers for electric drive is a progressive trend in the development of automatic regulated industrial installations. Considerable reduction in capital outlay, increased labour productivity and lower power consumption are associated with this.

The reconstruction and modernization of installations already in use should be undertaken incorporating ionic inverters just as these are used in installations now being constructed.

The new system of high-speed pulse regulation described in this article will result in the fulfilment of the highest technical and economic production standard, in installations using ionic inverters. These standards are primarily high coefficients of power and efficiency, and the high speed and comparative simplicity of the automatic control circuit.

Translated by J.H. Dixon

1958

REFERENCES

1. I.L. Kaganov; *Elektronnye i ionnye preobrazovateli (Electronic and ionic inverters)*, III, Gosenergoizdat (1956).
2. F.I. Butaev and E.L. Ettinger; *Ventil'nyi elektroprivod (Valve electric drive)*, Gosenergoizdat (1951).
3. E.L. Ettinger, B.M. Gutkin and P.M. Borodavchenko; Sovremennye skhemy ventil'novo elektroprivoda (Modern valve electric drive circuits), *Elektrichestvo* 9 (1956).
4. F. Holters; Stromrichteranlagen fur Walzwerksantriebe, *AEG M:* 44, 9-10, 364 (1954).

THE CONTROLLED PHASE-TYPE COMPOUND WINDING OF SYNCHRONOUS GENERATORS WITH CORRELATION AS TO VOLTAGE *

O.M. KOSTIUK and V.E. RYBINSKII

Ukr. S.S.R. Electrical Engineering Institute of the Academy of Sciences

(Received 21 February 1957)

1958

The controlled compound winding of synchronous motors and generators with correlation as to voltage is at present widely used. At the same time, the possibilities of improving the compounding circuits by achieving a relationship between the excitation of synchronous machines and not only the stator current, but also the stator voltage, taking the phase angle between them into account (phase compound winding), and also by achieving circuits with parameters which change under the action of an automatic corrective device, have been under examination for quite a long time.

In 1945, circuits for controlled (not phase) compound winding were developed by Moscow Regional Power System Administration, and simultaneously by the Moscow Electric Power Institute and the State Trust for the Organization and Efficiency of Electric Power Plants. Control was accomplished by the excitation of an intermediate transformer [1], or shorting choke [1, 2], in a normal compound winding circuit. An electronic voltage corrective device was used for this purpose in both the articles referred to. The shortcoming of this circuit is the lack of automatic regulation in low generator load conditions. In the second circuit they used what was, essentially, an additional corrective device creating a supplementary voltage drop at the shunt rheostat, to eliminate this shortcoming. This made the construction of the regulator more complicated.

For the first time, controlled phase compound winding with electro-mechanical corrective devices was then achieved on a 35 MW turbo-generator at Kievenergo [3,4].

Controlled phase compound winding was thereafter used to improve a circuit with electronic and ionic regulators [5], but this circuit was not widely adopted owing to the comparative complexity of the regulators themselves.

* *Elektrichestvo* No. 2, 27-34, 1958 [Reprint Order No. EL 51].

A phase (uncontrolled) compound-winding circuit for self-exciting generators of low power was developed in 1940 at the Lenin All-Union Electrical Engineering Institute [6]. In recent years, circuits for the phase combination of controlled compound winding with the field current, not controlled from the voltage [7 and 8], have been used for this purpose. The circuit for the phase combination of uncontrolled compound winding with the field current controlled from the voltage should be noted [9].

Controlled compound winding was also achieved for low-power generators with mechanical exciters, but in these circuits there is no automatic regulation in low generator load conditions, and the voltage regulation accuracy is not high [10].

This article sets out briefly the results of the development of a system for the automatic regulation of synchronous generator excitation, with phase compound winding controlled from the stator current and voltage. The industrial production of the regulators described in the article commenced in 1956.

Circuit and principle of operation

Fig. 1 contains diagrams showing the principles on which generators with mechanical exciters operate.

The main compount of the regulator is an all-mains transformer for controlled-phase compound winding, which in construction is a transformer-type magnetic amplifier. Fig. 2 is a schematic diagram of the all-mains transformer for low-voltage generators.

All the transformer windings are sited around the central bars of two III-shaped magnetic circuits (1), while the a.c. windings cover both magnetic circuits, and the field windings (2) cover each magnetic circuit individually. The primary series winding (3) is connected to the stator current circuit, phase *A* for example; the primary parallel winding 4 is connected to the stator voltage through an additional resistance of choking coil.

Taking into account the possibility of non-symmetrical generator states, it is desirable to perform compound winding on the current of at least two stator phases. A second series winding (5), connected for example to phase *B*, is provided for this purpose. The geometric sum or difference of the magnetizing forces in windings (3) and (5) is obtained, depending on the connexion polarity. With three-phase compound winding, thers may be a third series winding connected to phase *C*. The polarity of the two windings must then correspond to the sum of the magnetizing forces, and that of the third to the difference between them. This type of double or triple connexion of a single all-mains transformer is more expedient than the corresponding use of two or three separate transformers, one for each phase.

An e.m.f proportional to the resultant magnetizing force of the series and parallel primary windings is induced in the secondary (output) winding (6) of the

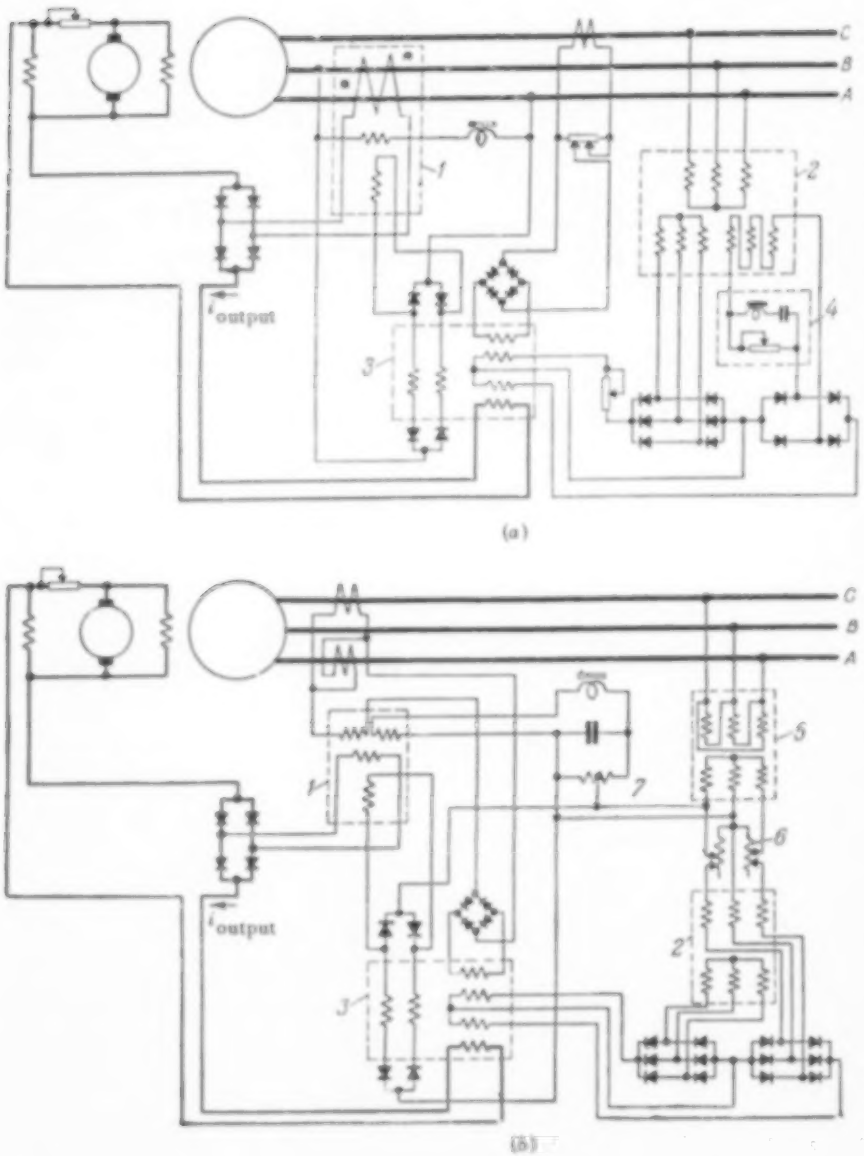

FIG. 1. Circuit for controlled phase compound winding with electro-magnetic voltage corrector.

(a) – for low-voltage synchronous generators; (b) – for high-voltage synchronous generators; 1 – all-mains controlled phase compound winding transformer; 2 – measuring device saturable transformer; 3 – magnetic amplifier; 4 – tuned circuit for frequency correction; 5 – voltage transformer; 6 – adjusting compensator; 7 – step-up compensator.

1958

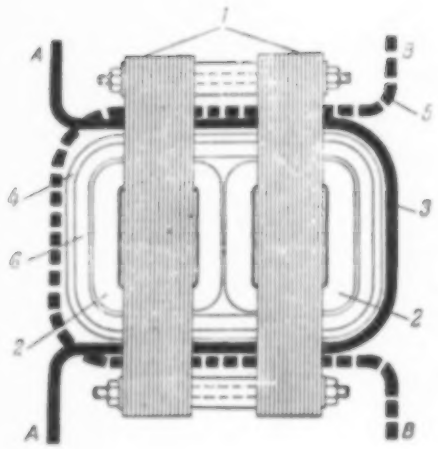

FIG. 2. Core and winding distribution in the all-mains controlled phase compound winding transformer.

all-mains transformer. The secondary transformer winding current is rectified and fed to the exciter-excitation circuit (Fig. 1).

It is expedient to connect a filler-type condenser in parallel with the magnetizing winding (2) (Fig. 2).

The phases to which the transformer parallel winding must be connected are determined with respect to the circuit diagram for the series windings of the all-mains controlled phase compound winding transformer and to the type of additional resistance in the parallel winding circuit (choke or rheostat). The phases selected must be such that, for an almost inductive load, where $\cos \phi = 0$, the magnetizing forces in the primary windings, which are proportional to the stator current and voltage, coincide as to direction, while for a load, where $\cos \phi = 1$ they should be displaced by an angle of 90° and the magnetizing force proportional to the stator voltage must lag.

The most expedient and constructionally convenient circuit is that of the double connexion for the difference in magnetizing forces of two phases. When connecting for the sum of the magnetizing forces of two phases, there will be no forced excitation in these phases on short circuit.

The electro-magnetic voltage corrective device has a three-phase measuring appliance at its input side, which acts on the single-phase intermediate magnetic amplifier. The output side of the voltage corrective device is connected to the field winding of the all-mains transformer. The possibility of additional correction of voltages as to frequency, by means of a tuned circuit connected to the non-linear component circuit, has been foreseen for low-power generators (Fig. 1 a). In this case, to reduce the size of the tuned circuit, the non-linear component circuit is made on the frequency tripler system.

The regulator shown in Fig. 1 b has been developed for powerful high-voltage generators. To increase the available regulation power and further improve the dynamics of the regulator, double-circuit regulation may be introduced; here a magnetic amplifier, counter-connected to an additional de-magnetizing field winding in the exciter, is also controlled from the corrective device measuring appliance. No additonal correction for frequency is required for powerful generators or for generators working in parallel in a powerful electric power system.

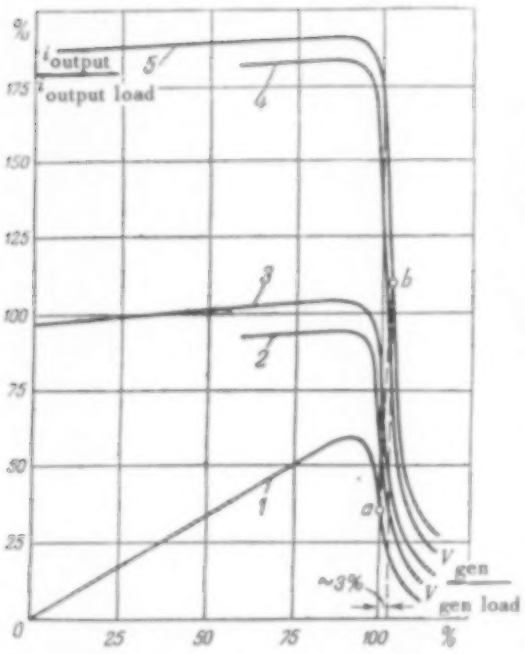

FIG. 3. The relationship between regulator output current and voltage. 1 – Generator open circuit; 2 – High power factor, $I_{gen} = 0.5\ I_{gen\ load}$; 3 – Low power factor, $I_{gen} = 0.5\ I_{gen\ load}$; 4 – high power factor, $I_{gen} = I_{gen\ load}$; 5 – low power factor, $I_{gen} = I_{gen\ load}$.

Owing to the development of a phase compound-winding circuit, the amplification coefficient of the voltage corrective device may be considerably less than for simple compound winding. In this connexion, the lag of the magnetic amplifier and control circuit of the all-mair s transformer is also less than the lag in electro-magnetic voltage correctors; this increases regulation stability. In this case, there is no need for additional regulator stabilization appliances; this simplifies the regulator circuit and still further increases the difference between its speed of action and that of the electro-magnetic correctors at present in use, in which a flexible negative feed-back (a stabilizing transformer) slows down the regulation.

The resultant regulator working characteristics are given in Fig. 3 for various generator states. For generator short-circuit and low loads, automatic regulation is accomplished by voltage compound winding (curve 1). The relationship between the regulator output current and the generator voltage, load current and power factor is characterized by a set of curves (2-5), from which it is clear that generator excitation increases with reduction of the power factor.

The spring feed-backs from the stator current and the regulator output current necessary for adjusting the regulator to the required statism and also for increasing the accuracy of the voltage regulation are provided in the regulator circuit (Fig. 1). In installations where very high voltage correction accuracy is not required, the stator current feed-back need not be used. In addition, it is possible to amplify or weaken the magnetic amplifier internal positive feed-back by using the normal additional external feed-back from the amplifier output current (not shown in Fig. 1).

Additional magnetic amplifier feed-back alters the steepness of the characteristics in Fig. 3. Increase in accuracy, and also decrease in regulation stability, correspond to the increase in steepness, which is limited by the possibility

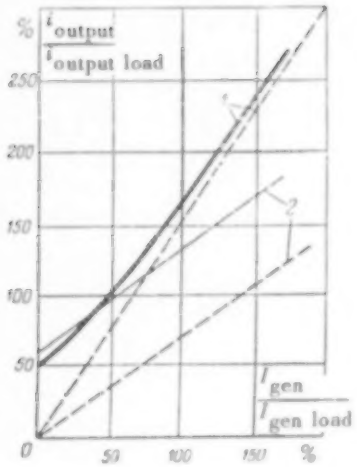

FIG. 4. Relationship between regulator output current and stator current in forcing conditions for steady reduction of 15 per cent in voltage (unbroken curves) and steady three-phase generator short circuit (dotted).
1 – controlled phase compound winding;
2 – normal compound winding with slow-acting electro-magnetic corrector (UK and EMK).

of a relay effect. Feed-back from the stator current is connected with polarity such that curves (2-5) are displaced to the left of curve 1.

In the case of feed-back from the stator current, the feed-back from the regulator output current is connected with polarity such that curves 1-5 are displaced to the right and their steepness increased. Here, accuracy of voltage correction increases with changes in the frequency and heating of the generator and exciter. Feed-back from the regulator output current also changes the phase sensitivity of the regulator; here the high and low power factor curves are displaced vertically in relation to one another.

The type of feed-back is selected when adjusting the regulator with respect to the generator and exciter parameters and the voltage correction requirements.

It is also clear from Fig. 3 that the regulator described without additional feed-backs can easily ensure adjustment with regative statism.

For example, if the regulator output current is altered, in different generator conditions, between open circuit and full load with a low power factor, the negative regulation statism between values *a* and *b* is about 3 per cent. In order, for example, to produce positive regulation statism, it is necessary for curves (2-5) to be displaced to the left of curve (1). This can be achieved by feed-backs.

It should be emphasized that the widespread idea that positive statism is necessary is based on the premise that a regulator setting of that sort ensures parallel working stability. Meanwhile we know that, from the point of view of maintaining constancy of voltage at the receiving terminal, it is most expedient to use a negative statism setting for automatic voltage regulators. The existence of the equalizing connexions, described below, enables us to recommend the negative statism adjustment of regulators as being more correct in

principle; this adjustment is easily achieved without introducing any additional equipment into the circuit.

Positive statism adjustment is easily achieved, on the other hand, in regulators of the compensator type, reacting to differences in the quantity being regulated. To create negative statism, essentially, a regulator compound winding is used; this, however, requires additional equipment.

Fig. 4 shows the forcing capacity characteristic of a regulator at generator voltage drops of 15 and 100 per cent (short circuit). Similar characteristics for a type UK-EMK regulator are plotted for comparison (simple compound winding with an electro-magnetic voltage corrector), on the assumption that, in the second case, the component of the resultant regulator current determined by the corrective device for a rated generator state, is 30 per cent. It is clear from Fig. 4 that the forcing capacity of the regulator being described is considerably higher. This is associated with the fact that it is necessary for this regulator, at rated voltage, other things being equal to take an all-mains transformer coefficient of transformation such as to compensate the field effect, which may be regarded as an additional transformer error. Therefore, with a drop in voltage, when the transformer magnetization is sharply reduced, the compounding coefficient quickly increases; this is a feature characteristic of controlled compound winding circuits.

1958

The increased forcing capacity, which has been indicated for the regulator described, makes the reactive load distribution stability condition more difficult, when generators are working in parallel. In order to achieve reliable stability, particularly for the generator voltage bus-bars when they are working in parallel, it is desirable that there should be an equalizing coupling between the generators working in parallel. This is achieved by the parallel connexion, either directly or through a spacing transformer, of sections, of the secondary windings themselves, of the all-mains transformers. In many cases, this circuit is more expedient than the use of equalizing connexions between the excitation circuits. In the proposed circuit, the excitation circuits are not electrically connected, and the possibility of using the coefficient of transformation in the equalizing circuit enables us to operate various types of generator in parallel. The elasticity of the equalizing coupling can be regulated at will by a small impedance connected in series.

It is possible, for low voltage generators, to confine ourselves to only one equalizing conductor between the primary (parallel) windings of the all-mains transformers on the choking coil side (Fig. 1a), since in this case the equalizing coupling closes the primary commutation circuit of the generators working in parallel.

It should be pointed out that the compound winding and voltage correction circuit described, is very valuable for self-exciting synchronous generators. In this case, in order to ensure the necessary compound winding capacity, all-mains transformers may be connected to the three phases. If additional frequency

correction is not applied, the voltage corrector may be still more simply constructed in the form of a saturable choke and rectifier. The choke is connected to the generator through a step-down transformer. The core of the choke should preferably be of permalloy (a type UTT-6 current transformer is used as the choke in the regulator we have constructed), but satisfactory results may also be obtained when using high quality electrical engineering steel. In this circuit the corrector is practically without inertia.

For comparatively powerful generators, controlled phase compound winding may be combined with uncontrolled phase compound winding, ensuring 70-80 per cent of the required excitation capacity. This makes it possible greatly to reduce the size of the all-mains controlled phase compound-winding transformers.

Basic relationships

Let us examine the steady working conditions for a phase compound winding circuit with all-mains transformers, assuming as a preliminary that the compound winding is uncontrolled.

Using the super-imposition principle, we can find the current in the secondary winding of the all-mains transformer:

$$I_2 = \sqrt{I_{2k}^2 + I_{2kh}^2 + 2I_{2k}\, I_{2kh} \cos\gamma}\,, \tag{1}$$

where I_{2k} and I_{2kh} are the currents in the transformer secondary winding for short circuit (at the specified stator current and open circuit conditions, and γ is the angle between the currents I_{2k} and I_{2kh}.

Currents I_{2k} and I_{2kh} are determined as follows:

$$I_{2k} = \sigma_k\, I_1 \omega_{i1}/\omega_{2e};\; I_{2kh} = \sigma_{kh}(V/z_e)\,/(\omega_{u_1}/\omega_2) \tag{2}$$

where I_1 is the current in the all-mains transfomer primary winding,

V is the generator voltage (Fig. 1a), or the voltage on the secondary side of the compensator (Fig. 1b),

σ_k and σ_{kh} are coefficients allowing for the all-mains transformer current errors for generator short-circuit and open circuit conditions,

ω_{i1}, ω_{v1}, ω_2 are the number of turns in the series and parallel primary windings and the secondary (output) winding of the all-mains transformer,

ω_{2e} is the equivalent number of secondary winding turns in short-circuit conditions (taking into account the effect of the primary parallel winding),

z_e is the equivalent resistance of the compound winding circuit due to voltage in open circuit conditions.

The values of ω_{2e} and z_e are determined from the following equations:

$$w_{2e} = \sqrt{w_2^2 + \left(\frac{r'_v}{\nu_k z_n}\right)^2 + 2w_2 \frac{r'_v}{\nu_k z_n} \cos\xi}\,; \tag{3}$$

$$z_e = \sqrt{\left(r_n + \frac{r'_v}{k_h}\right)^2 + x_n^2}\,, \tag{4}$$

where

$$r'_v = \frac{\beta_i}{\beta_u} \times \frac{\omega_u^2 1}{\omega_2^2} r_v\,,$$

the load resistance at the output side of the compound winding circuit, reduced to the number of windings in the all-mains transformer primary parallel winding (β_i and β_u are relationships of the mean rectified current and voltage values to the effective values for alternate current and voltage at the rectifier);

$z_n = r_n + jx_n$, the resistance in the all-mains transformer primary parallel winding circuit,

ξ is the difference between the impedance angles of the all-mains transformer primary parallel winding circuit and secondary winding circuit,

and ν_k and ν_{kh} are coefficients allowing respectively for the difference between the different voltage drops in the all-mains transformer secondary and primary parallel windings and the transformer voltage error in open circuit conditions.

The current fed to the all-mains transformer primary parallel winding circuit in generator short-circuit conditions is determined by the equation:

$$I_{nk} = (r_v/z_n)\,(\omega_2/\omega_u)\,I_{2k} \tag{5}$$

Fig. 5 gives the vector diagram for the case where an all-mains transformer is connected with the difference in currents between two generator phases and its linear voltage. The direction of the vector I_{2kh} is determined by the impedance angle ψ of the equivalent resistance z_e, the direction of the vector I_{2k} by the angle α which allows for the angular error of the all-mains transformer as regards the current reaching its primary parallel winding circuit (the direction OM is parallel to the vector $I_{1a} - I_{1b}$).

When the angle π alters, the end of the vector I_2 moves along the time curve which represents a circle of radius I_{2k}, its centre lying at the ends of the vector I_{2kh}.

The basic relationships of the linearized phase compound winding circuit which have been obtained can also be applied to controlled compound winding with the proviso that the magnetic state of the all-mains transformer is specified,

1958

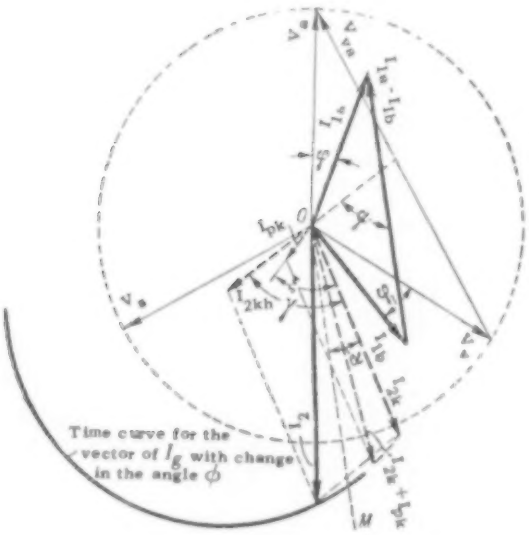

FIG. 5. Phase compounding vector diagram.

taking into account the constant magnetization corresponding to the specific generator voltage. The values of the parameters σ_k, σ_{kh}, ν_k, ν_{kh}, ψ and α must correspond to the given regime.

The sensitivity of the phase compound winding circuit $dI_2/d\phi$ depends on the correlation of the currents I_{2k} and I_{2kh} and the initial phasing angle, generally equal to $\gamma + \phi$. For each phase compound winding circuit this angle is a constant quantity.

On increase of this angle, the phase sensitivity rises, but, as analysis and tests showed, where the initial phasing angle exceeded 90° there was intensification of the undesirable non-linearity of the synchronous generator external characteristics, when loaded at a high power factor. It is expedient, therefore, to limit the initial phasing angle roughly between 70° and 110°.

Phase sensitivity is still not unduly lowered at the lower limit, and at the upper limit the non-linearity of synchronous generator external characteristics is within the tolerated limits.

A phase compound winding-circuit sensitivity ensuring that the external characteristic of the generator being regulated is independent of the power factor may be called normal. For astatic adjustment of a circuit for the automatic regulation of excitation, the phase sensitivity must approximate to the normal value. If adjustment with negative statism is being made (back regulation, to compensate for the voltage drop in the circuit supplying the consumer), it is expedient to have phase sensitivity above normal. Then the negative statism will be higher with inductive generator loading and with lower operating load; this is a requisite for

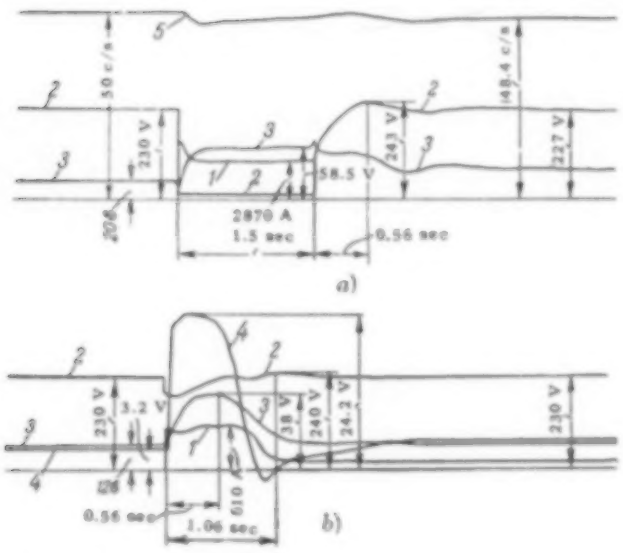

FIG. 6. Oscillograph recording of transitional processes.
(a) three-phase short circuit of MS-126-4 generator;
(b) short-circuited induction motor started from MS-126-4 generator, engine power about 30 per cent of generator power.
1 – generator current; 2 – generator voltage; 3 – generator excitation voltage; 4 – generator exciter excitation voltage; 5 – frequency.

obtaining a better approximation of astatic characteristics at the consumer's end or at a nodal point in the circuit.

Test results

Production models of the regulator were made according to the controlled phase compound winding circuit described. The Electrical Engineering Institute of the Ukr. S.S.R. Academy of Sciences assisted by the "Elektroprivod" (Moscow) Central Design Bureau, tested the regulators on MS-126-4 (150 kW) and MS-92-4 (50 kW) synchronous generators working separately and in parallel.

The external characteristics of the generators being regulated deviated with wide variations in the power factor between 0.1 and 0.8 (inductive load), by not more than ± 1 per cent from the mean value. Adjustment corresponded to a negative statism of 1-2 per cent. The phase sensitivity of the compounding circuit was above normal, since with low power factors, the negative statism was higher than with high power factors.

The generator operation was extremely stable when working in parallel, where there were equalizing couplings. Opening the equalizing coupling shortly disrupted the stability in an aperiodic manner, one of the generators passing to

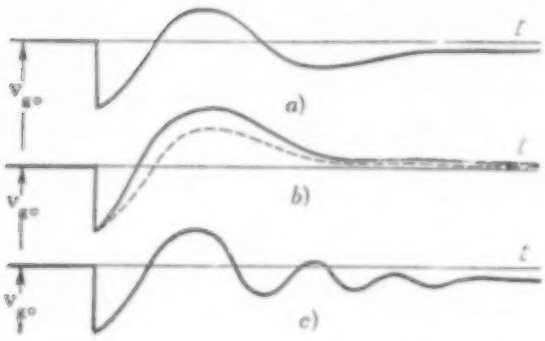

FIG. 7. Typical transitional processes in a circuit with weak damping without special equipment for changing statism (generator and exciter).
(a) compensation type regulator with artificial damping.
(b) controlled compound winding without artificial damping.
(c) compensation type regulator without artificial damping.

conditions with a capacitive power factor.

Oscillograph recordings were made of the transitional processes when static loads (about 50 and 100 per cent of the rated power of a generator with high and low power factors) were cut in and out, when starting short-circuited induction motors (about 30 and 90 per cent of the generator rated power), and for a number of generator short-circuits lasting for up to 1.5 sec.

Oscillograph recordings, for cases of the short-circuiting of a 150 kW generator and the starting of an induction motor connected to that generator, are given in Fig. 6; it is evident from these that the regulator ensures high-speed action and that the transitional processes are of a favourable nature. The low regulator lag is typified by the fact that the voltage at the regulator output (at the exciter shunt excitation winding) rose practically simultaneously with the stator current, and then in addition rose, owing to the removal of the excitation of the corrector, to maximum value in about 0.2 sec.

Tests made on a 50 kW generator with self-excitation through a regulator of the type described showed that the nature of the transitional processes is still more favourable in this case.

Fig. 7a shows the change in voltage when a static load is applied to a generator fitted with a compensation voltage regulator, with positive regulator statism and no special equipment for altering the statism. Fig. 7b shows a similar transitional process for the regulator described with natural negative statism. We can see from comparison of the curves that, in the second case, the first normal regulated voltage value is reached quicker, and the nature of the transitional process is more favourable.

Where sufficiently effective means of damping, which complicate the design of compensation regulators, are not available, the transitional process shown in Fig. 7c is typical of these regulators; here, the time for the first restoration of voltage is somewhat shorter, but the oscillations are more intense.

The transitional process on reduction in the compound winding coefficient is shown by the dotted line in Fig. 7b. Here the over-regulation is reduced, but so is the forcing capacity of the regulator. It should be emphasized that over-regulation for a single shock, and the consequent sufficiently fast aperiodic steadying of the conditions, may be regarded, when we consider the essential factors which make the post-shock conditions more difficult, as a favourable form of transitional process. Such factors are respective loads, for example, the alternate running of motors, changes in the slip of induction motors(which are braked on initial reduction of voltage and accelerated when it is subsequently restored) etc.

The considerations set forth were well supported by the tests. In particular on eliminating the short circuit of a 150 kW generator running idle, the over-regulation was 19.5 per cent of the rated voltage, but when a loaded 40 kW induction motor had previously been connected, this over-regulation was reduced to 5.6 per cent (Fig. 5a). Similar tests were successfully carried out on a MS-1250-750 (1000 kW) generator. A regulator constructed according to the circuit in Fig. 1b was tested on a 25 MW type T2-25-2 turbo-generator.

Translated by J.H. Dixon

1958

REFERENCES

1. N.I. Sokolov and N.V. Chernobrokov; Kompaundirovanie vozbuzhdeniia sinkhronnykh generatorov v Mosenergo (The compounding of synchronous generator excitation at Mosenergo), *Elektricheskie stantsii*, 4, 5 (1946).
2. I.I. Kodkind; Reguliator napriazheniia dlia kompaundirovannykh sinkhronnykh generatorov (A voltage regulator for compounded synchronous generators), *Elektricheskie stantsii*, 4, 5 (1946).
3. V.L. Inosov and L.V. Tsukernik; Kompaundirovannoe vozbuzhdenie sinkhronnykh generatorov s elektromekhanicheskym korrektorom napriazheniia(The compounded excitation of synchronous generators with an electro-mechanical voltage corrector) *Elektricheskie stantsii;* 4, 5 (1946).
4. L.V. Tsukernik; Metodika rascheta kompaundirovaniia sinkhronykh generatorov s elektromekhanicheskym korrektorom (The procedure for calculating the compounding of synchronous generators with an electro-mechanical corrector) *Sborn nauch-tekhnich. statei elektrotekh. Akad. Nauk. Ukr. S.S.R.*, No. 1 (1948).
5. G.R. Gertsenberg; Avtomaticheskie reguliatory napriazheniia sistemy VEI (VEI system of automatic voltage regulators) *Sborn. "Avtomatika i telemekhanika v energosistemakh"*, Gosenergoizdat (1950).
6. S.B. Iuditskii; *Sinkhronnye mashiny s poluprovodnikovymi vypriamiteliami (Synchronous machines with semiconductor rectifiers)*, Gosenergoizdat (1954).
7. H.F. Storm; A static magnetic exciter for synchronous generators, *Trans. Amer. Inst. Elect. Engrs.* 70 (1951).

8. A. Lang; Samoreguliruemye sinkhronnye generatory bez mashinnykh vozbuditelei (Self-regulating synchronous generators without mechanical exciters), *ETZ-A* 10 (1955).
9. P.A. Meshchaninov; Fazovaia skhema kompaundirovaniia s elektromagnitnym korrektorom (A phase compounding circuit with electro-magnetic corrector), *Elektricheskie stantsii*, 4 (1955).
10. N.A. Nechaev; Avtomaticheskii reguliator vozbuzhdeniia dlia generatorov maloi energetikoi (An automatic excitation regulator for low power generators). *Energetik*, 12 (1955).

TRANSISTOR AMPLIFIERS OF THE ALLOY TYPE *

A.A. MASLOV

(Received 23 September 1957)

An ordinary flat transistor amplifier consists of two electron- or hole-conducting junctions, situated in a single monocrystal and separated by a distance w; this distance should be considerably less than the diffusion length at the non-base carriers in the middle region. If a triode is made in such a way that an electron semiconductor, conventionally denoted by n, is fixed in the middle and a hole semiconductor, denoted by p, on the sides, then such a triode is called a p-n-p type as opposed to the triode of the n-p-n type, in which the mid section is the hole type of semiconductor. As is generally known, the semiconductor amplifier is connected in a circuit in such a way, that a forward biased voltage is applied to one junction; this junction is called the emitter junction. To the other junction a reverse biased voltage is applied; this junction is called the collector. The mid-part of the triode between the two junctions is called the base or the base region.

The circuit of a p-n-p triode is shown on Fig. 1. Consider the mode of operation of the p-n-p type amplifier. The emitter is biased on the forward direction and in certain conditions it will cause the injection of holes into the base region. Since the width of the base w is considerably less than the diffusion length of the holes in this region, the holes injected into the n region will be diffused to the collector and only a part of them will recombine with electrons in the base layer. The collector is biased in the reverse direction; the electric field is in such a direction that it will attract holes which entered in the base region. Consequently, these holes will reach the output network of the collector and produce the current of the output signal. If the value of the emitter current varies, the value of the current in the collector network will vary as well. Usually triodes are constructed in such a way that a considerable part of the emitter current enters the collector network. Therefore we can assume that the change in the emitter current is approximately equal to the change in the collector current, i.e.

$$\Delta I_e \approx \Delta I_c .$$

* *Electrichestvo* No. 2, 46-51, 1958 [Reprint Order No. EL 52].

Since the collector junction has a reverse bias and consequently a high load impedance, the change of current in the collector occurs in a network of high resistance, and this will produce a large change of voltage, tens of times greater than the change of the voltage in the emitter network, which produced the change in the emitter current. As a result, there will be a voltage and power gain, which can be taken from the load resistance. To get a good gain it is necessary that ΔI_c should differ from ΔI_e as little as possible. The ratio $I_c/I_e = \alpha$ is called the current amplification or current gain of a crystal triode. The current amplification depends on the quantities given below.

1. Emitter efficiency

The current flowing through the emitter junction has two components: the hole, and the electron components. In amplifying operations of the *p-n-p* triode only the hole component of the current takes part. The ratio of the change of the hole component (ΔI_{eh}) to the total emitter current (ΔI_e) is called the emitter efficiency and is designated γ. Obviously

$$\gamma = \frac{\Delta I_{eh}}{\Delta I_e}. \text{ By simple calculations we can find that } \gamma = 1 - \frac{w\sigma_b}{L_e\sigma_e}$$

where σ_b is the base region conductance

σ_e is the emitter region conductance, and

L_e is the diffusion length of the non-base hole carriers in the emitter region. In order that γ should be near to unity it is necessary that

$$w\,\sigma_b \ll L_e\,\sigma_e\,.$$

2. The ability of the base region to transfer the holes leaving the emitter to the collector (β)

This quantity is determined as the ratio of the change of the hole component of the collector current to the change of the hole component of the emitter current,

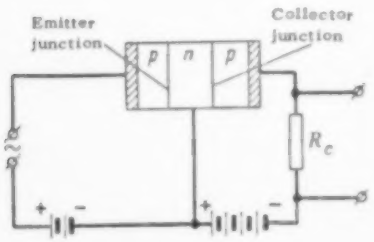

FIG. 1. *p-n-p* triode in a common base network

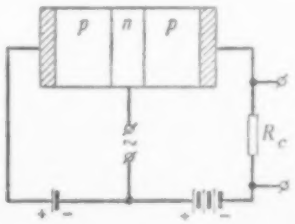

FIG. 2. *p-n-p* triode in a common emitter network

$$\beta = \frac{\Delta I_{eh}}{\Delta I_{eh}}$$

The losses in the base are caused by a partial recombination of holes with electrons. Obviously, to keep β near to unity it is necessary that $w \ll L_h$. The value of β can be calculated from the expression:

$$\beta = \frac{1}{\cosh(w/L_d)}$$

3. Collector efficiency α

The holes which have entered the collector region come under the influence of the accelerating field and can cause an avalanche process of hole increase. For the flat alloy triodes normally $\alpha^* = 1$.

The current gain will be determined by the product of the three above-mentioned factors $\alpha = \gamma \beta \alpha^*$. We have neglected here possible losses in the outer network and the influence of the frequency on the amplifying properties of the triode. Therefore, α will be the current gain for low frequencies and for the short-circuited collector junction. The factor α is an important physical characteristic of a triode and does not depend on the method of connexion in the circuit. The current gain for real circuits will be different. The circuit in Fig. 1 is called the circuit with a common base. This circuit has a small input and a large output resistance. The current gain of this circuit is less than α. This is true only for a short-circuited collector junction, i.e. when $R_c = 0$, $K_i = \alpha$. Two other methods of connecting a triode are possible. Fig. 2 shows a triode with a common emitter. This is characterized by large input and output resistances. Input and output voltages are of the opposite phase. This circuit gives the largest amplification. The factor K_i for $R_c = 0$ has the value

$$k \frac{\alpha}{1 - \alpha}.$$

1958

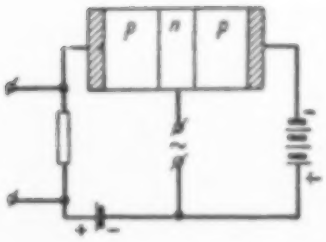

FIG. 3. p-n-p triode in a common collector network

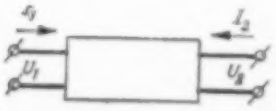

FIG. 4. Four-terminal network

Since normally $a > 0.9$ K_i, is large, this circuit is mainly used for flat apparatus. In Fig. 3 we see a circuit with a common collector. It has high input and low output resistance. The current gain for $R_c = 0$ is

$$k_i = \frac{1}{1-a} .$$

Omitting discussion of the processes occuring inside the triode we can consider it as an active four-terminal network, whose diagram is shown in Fig. 4. To describe the influence of such a four-terminal network on the external network it is necessary to know four quantities: input (U_1) and output (U_2) voltages, and input (I_1) and output (I_2) currents. Obviously, we can consider any two of these quantities as independent variables, and two other as dependent, which are determined by the independent variables and by the parameters of the four-terminal network.

We assume that $U_1 = f(I_1)$ and $U_2 = f(I_2)$. A change in the current by ΔI_1 and ΔI_2 will cause a change of voltage ΔU_1 and ΔU_2, hence

$$\Delta U_1 = \frac{\partial U_1}{\partial I_1}\Delta I_1 + \frac{\partial U_1}{\partial I_2}\Delta I_2; \tag{1}$$

$$\Delta U_2 = \frac{\partial U_2}{\partial I_1}\Delta I_1 + \frac{\partial U_2}{\partial I_2}\Delta I_2. \tag{1a}$$

If we assume that changes of currents and voltages are small in comparison with values U_1, U_2, I_1, I_2, and this is valid for low signal levels, then the assumption of the linear dependence of ΔU_1, ΔU_2 on ΔI_1, and ΔI_2 is justifiable; consequently

$$\frac{\partial U_1}{\partial I_1} = Z_{11}; \quad \frac{\partial U_1}{\partial I_2} = Z_{12}; \quad \frac{\partial U_2}{\partial I_1} = Z_{21}; \quad \frac{\partial U_2}{\partial I_2} = Z_{22}.$$

Then equation (1) will be:

$$\Delta U_1 = Z_{11}\Delta I_1 + Z_{12}\Delta I_2; \tag{2}$$

$$\Delta U_2 = Z_{21}\Delta I_1 + \Delta Z_{22} I_2. \tag{2a}$$

These four resistances determine entirely the behaviour of the triode in a circuit. There is no difficulty in finding these resistances by direct measurement. Using the values of these resistances and solving the equations for the four-terminal network, we can determine the current and power gain of the triode in any circuit in which it may be connected.

To find the value Z_{11} it is necessary that I_2 should be equal to zero, i.e. it can be measured with the open circuit output. To determine Z_{12}, we measure ΔU_1 and ΔI_2 with the open-circuit input. In exactly the same way, having measured ΔU_2, ΔI_1, and ΔI_2 with the open-circuit input and short-circuited output, we can determine Z_{21} and Z_{22}. Therefore, this network is called a network of no-load operation, or briefly, a network of Z-parameters. Its disadvantage consists

in using the short-circuited output. But usual conditions of operation are near to short-circuit conditions at the output, since the collector junction resistance is large in comparison with the load resistance. Moreover, at high frequencies, the collector capacitance becomes appreciable, and it is difficult to realize no-load conditions. It is more convenient to use a network of admittances, determined by the following equations of the four-terminal network.

$$\Delta I_1 = y_{11}\Delta U_1 + y_{22}\Delta U_2;$$
$$\Delta I_2 = y_{21}\Delta U_1 + y_{22}\Delta U_2.$$

To determine y parameters it is necessary to make ΔU_1 and ΔU_2 alternately equal to zero, i.e. to produce short-circuit conditions; this method being very convenient for high frequencies. This system of parameters is called the short-circuit system or the system of y parameters. Its disadvantage consists in using a short-circuit at the input, and this does not correspond to the actual conditions in the working of a triode.

Obviously, it would be convenient to choose such parameters in such a way as to measure them in conditions of the open-circuit input and short-circuited output. For this purpose, using the assumed linear relationship of currents and voltages, we estblish the following two equations of the four-terminal network.

$$\Delta U_1 = h_{11}I_1 + h_{12}\Delta U_2;$$
$$\Delta I_2 = h_{21}I_1 + h_{22}\Delta U_2,$$

where h_{11}, h_{12}, h_{21} and h_{22} are coefficients of proportionality. Such a system is very convenient since to determine the coefficients we have to produce conditions of open-circuit input $\Delta I_1 = 0$ and of short-circuited output $\Delta U_2 = 0$; and these conditions are similar to the conditions of the normal working of the triode. Moreover, these parameters have a quite definite physical meaning:

h_{11} is the input impedance with output short-circuit;
h_{12} is the voltage feedback ratio;
h_{21} is the current amplification with output short-circuit; and
h_{22} is the output admittance with input open-circuit.

The most widely used triode made by our industry for low power radio networks is the triode model P-6. Its construction is shown on Fig. 5. This triode is a *p-n-p* type amplifier; it is made by fusion of indium into a germanium lamina of dimensions 2.3 x 2.3 mm. The original germanium has resistance of 1 – 2 Ω cm and a diffusion length $\geq$ 0.4 mm.

This triode is made in five types. Limiting operation values of these triodes are given in Table 1, and their basic electrical characteristics in Table 2. In Table 2 electrical data are given for normal operation conditions in a network with a common base.

For calculation of the output cascade stage it is necessary to know the input and output triode characteristics.

1958

TABLE 1. Limiting values of the triodes model P-6 at $t = 20°C$.

Parameters	P6A	P6B	P6C	P6D	P6E
Collector voltage with respect to the base U_c max with $I_e = 0$ (V)	−30	−30	−30	−30	−30
Collector voltage with respect to the emitter U'_c max (V)	−15	−20	−20	−15	−20
Reverse emitter voltage U_e max with $U_b = 0$ (V)	−30	−30	−30	−20	−30
Collector current I_c (mA)	50	50	50	50	50
Emitter current (with $U_e = 5$ V) (mA)	50	50	50	50	50
Junction temperature t_j (°C)	>100	>100	>100	>100	>100
Collector dissipation P_c max (mW)	150	150	150	150	150

TABLE 2. Fundamental electrical characteristics of the triode model P-6 for $t = 20 + 5°C$ in the common base network.

Parameter	P6A	P6B	P6C	P6D	P6E
Output admittance (with input open-circuited) h_{22} (MΩ)	1.0	0.7	0.7	0.7	0.7
Current amplification (with output short-circuited) h_{21}	0.92	0.93	0.965	0.98	0.97
Input insistance (with output short-circuited) h_{11} (Ω)	27	27	27	27	27
Voltage feedback ratio (input open-circuited) $h_{12} \times 10^{-4}$	0.4	2.0	2.0	3.0	2.0
Collector capacitance C_c (pF)	30	30	30	30	30
Collector reverse current I_{c_0} (μA)	5	3	3	3	3
Emitter reverse current I_{e_0} (μA)	5	3	3	3	3
Temperature rise R_t (°C/mW)	0.3	0.3	0.3	0.3	0.3

Fig. 6 shows average input characteristics of the triode model P6D for $U_c = -5$ V with indication of possible deviations from mean values, and Fig. 7 shows output characteristics for the same group of triodes.

TABLE 3. Fundamental electric characteristic of the flat germanium triode model P4.

Triode model	P4A	P4B	P4C	P4D	P4E
$f\,a$ (kc/sec)	100	100	100	100	100
Power gain kp (dB)	20	23	—	27	30
Current gain (common emitter network)	$\geqslant 5$	8 . . . 20	$\geqslant 10$	10 . . . 20	$\geqslant 20$
Power given to the load in class P_{out} (W)	10	10	10	10	10
Collector "zero" current, for $U_c = 10$ V (mA)	$\leqslant 0{,}5$	$\leqslant 0{,}4$	$\leqslant 0{,}4$	$\leqslant 0{,}4$	$\leqslant 0{,}4$
Voltage drop between emitter and collector for $I_c = 2$A, $I_B = 300$ mA (V)	—	$\leqslant 0{,}5$	$\leqslant 0{,}5$	—	—
Limiting collector voltage (common emitter network) for $U_B = 0$ (V)	—50	—60	—35	—50	—50
Limiting collector current (A)	5	5	5	5	5
Limiting collector dissipation with a heat dissipating device keeping the temperature of the triode frame not over 50°C (W)	$\geqslant 20$	$\geqslant 25$	$\geqslant 25$	$\geqslant 25$	$\geqslant 25$
Coefficient of non-linear distortion	0,15	0,10	—	0,10	0,10

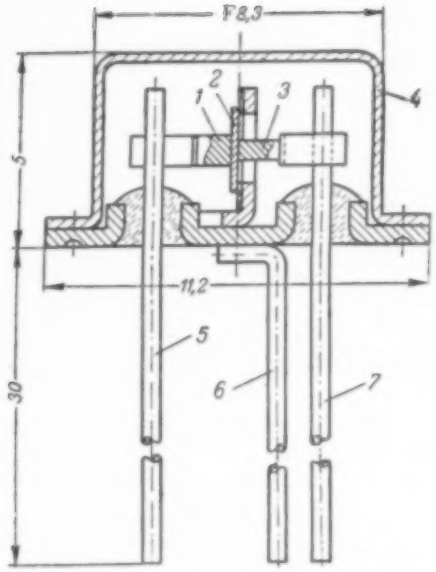

FIG. 5. Germanium triode, model P6.
1 – collector electrode;
2 – germanium crystal;
3 – emitter electrode;
4 – housing;
5 – collector;
6 – base;
7 – emitter

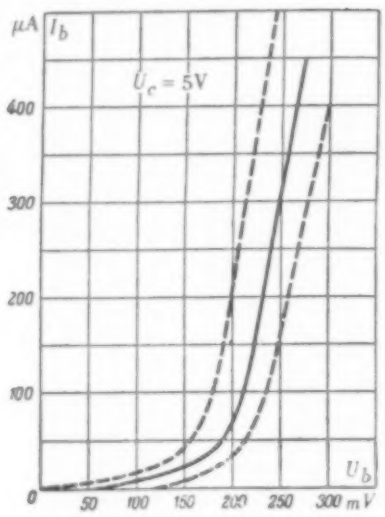

FIG. 6. Input characteristics of the P6G triode for U_c = – 5V in a common emitter network
———— – averaged parameters;
– – – minimum and maximum parameters.

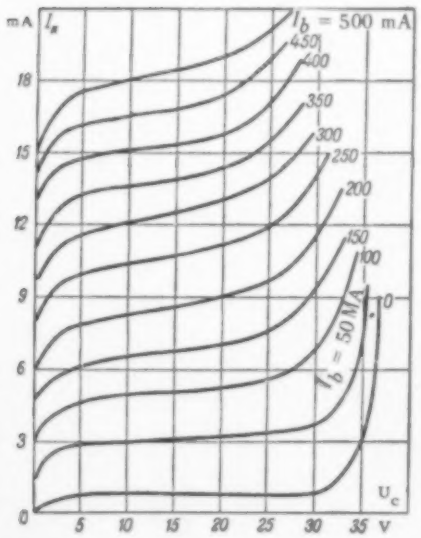

FIG. 7. Averaged input characteristics of the P6G triode in a common emitter network.

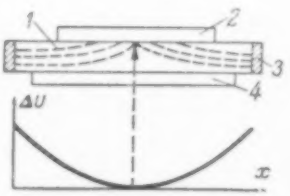

FIG. 8. Voltage drop caused by the electron current.
1 – lines of the electron current in the base;
2 – emitter;
3 – base contact;
4 – collector.

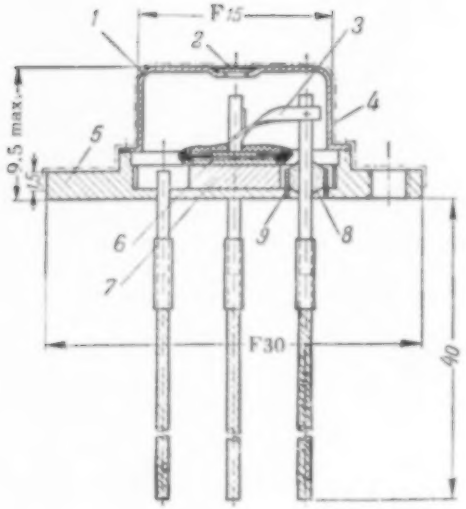

FIG. 9. Germanium triode model P-4
1 – housing;
2 – disc;
3 – lead;
4 – black paint;
5 – flange;
6 – junction;
7 – washer;
8 – insulator;
9 – tube.

1958

Powerful semiconductor triodes

The increase in power of triodes plays an important role in widening the scope of the application of semiconductor instruments. This problem, however, meets with many serious limitations; because of this, it has yet not been possible to produce a triode of more than 100 W dissipation without forced cooling.

The main difficulty in making powerful triodes is non-uniform current distribution in the emitter. This can be explained thus: in the *p-n-p* triode base there is always, besides the hole current, flowing from the emitter and reaching the collector, an electron current as well, caused by recombination of holes in the base. This current flows in the direction from separate points of the base to the base contact and is parallel to the surface of the emitter. Since germanium has a sufficient resistance, this current creates an electric field in the base directed from the centre to the periphery. Lines of the electron current in the base and the drop in the voltage caused by the current are shown in Fig. 8. Under the influence of this field, holes leaving the emitter are pushed towards the periphery. In consequence, non-uniform emitter current distribution occurs. This phenomenon causes the lowering of the current gain in the triode.

The larger the diameters of the emitter and collector, the more important this becomes. Therefore, although increasing the power of the triode, we cannot at the same time considerably increase the electrode diameters for improving conditions of heat dissipation in the collector junction.

Using germanium with a longer life expectancy, and thus lowering the base current and bringing the emitter efficiency nearer to unity by subsituting special alloys for indium, we can reduce the value of the electron current and, consequently, reduce the non-uniformity in the emitter current distribution.

Industry produces powerful triodes of the P3 type with dissipation 3.5 W, of the P201 type with dissipation 10 W and of the P4 type with dissipation 25 W as well as other models.

Fig. 9 shows the construction of the P4 triode. Its fundamental electrical parameters are given in Table 3.

To increase the emitter efficiency, an alloy of indium with 1 per cent of gallium is used instead of indium. Since gallium has a coefficient of separation 100 times greater than indium, the addition of 1 per cent of indium reduces the resistance of *r*-germanium, formed after recrystallization, by one half. To reduce the recombination rate in the base, ordinary *n*-germanium is used with diffusion length not less than 1.2 mm.

With the elimination of factors producing non-uniform current distribution in the emitter, the production of the alloy triodes with dissipation up to 100 W is now possible.

Translated by S. Szymanski

A STUDY OF THE SYNCHRONIZATION PROCESS IN COMPOUND EXCITED MOTORS *

V.I. INOSOV and V.E. KRUTIKOVA

(Received 7 February 1957)

In the processes of starting and synchronizing a synchronous motor, the major role is played by the damping cage, the design of which must be based on analysis of the motor synchronization process. The present paper gives the results of a study of the synchronization process in compound excited motors [1,2]; they may also be extended to other types of compound synchronous motor.

The motion of the rotor of a synchronous machine is described by the nonlinear differential equation:

$$\frac{M}{\omega}\delta'' + \frac{D(\delta,\delta')}{\omega}\delta' + P_e(\delta,\delta') = P_0, \qquad (1)$$

where

- δ is the angle of lag of the rotor;
- M is the constant of inertia of the rotor, in sec;
- D is the damping coefficient in relative units, which is a function of the angle and its first differential;
- P_e is the electrical torque of the machine (stator) in relative units, this depending on the angle and its differential;
- P_0 is the load on the machine shaft;
- ω is the angular speed of rotation of the machine.

A study of the synchronization process in a motor involves analysis of this equation in the range where the machine is slipping slightly; except for the method of numerical integration, this analysis can only be carried out by studying the trajectory of the motion in the phase-plane.

Two methods are known for carrying out such an investigation: the isocline method [3, 4] and the construction of separatrices [5, 6]. Both methods are notable in that they are comparatively very laborious. Thus, in the isocline method it is necessary to seek and plot the geometrical locations of points of equal slope on the integral curves, whereas the separatrix construction involves calculating

* *Elektrichestvo* No. 2, 56-59, 1958 [Reprint Order No. EL 53].

successive intervals by the trajectory method, and therefore takes up a considerable amount of time.

In the present investigation, the co-ordinate grid method was used. The construction of integral curves by this method is carried out as follows. Writing $\delta' = d\delta/dt = y$, we find from equation (1) the tangent of the angle of slope of tangents to the trajectory of rotor motion on the phase-plane:-

$$\tan \alpha = \frac{d_y}{d\delta} = \frac{[P_0 - P_e(\delta, y)]\,\omega}{My} - \frac{D(\delta, y)}{M}. \qquad (2)$$

For the various points on the phase-plane lying at the corners of the co-ordinate grid (δ_i, y_i) the values of tan α_i are determined and plotted on the plane in the form of arrows (Fig. 1).

Approximate rotor-motion trajectories are constructed, in accordance with the slope of the arrows; the shape of the curves provides a qualitative solution to the problem; i.e., it establishes whether the motor will get into synchronism. Since the direction of slipping does not reverse between the moment of starting and that of reaching synchronism, it is sufficient to construct the trajectories in the lower half-plane only. The synchronization criterion for a motor is the reduction of rotor slip after one complete pole-pitch has been slipped (in the range of small degrees of slip); i.e. the reduction of the absolute value of y at the end of an interval $(\pi; -\pi)$ as compared with its value at the start of the interval.

Trajectories of rotor motion, constructed by this method and calculated by the successive interval method, using an electronic computer, agree reasonably well.

The completeness and carefulness of an analysis of the synchronization process are determined by the degree to which other factors influencing the damping coefficient and the electromagnetic torques P_e of the machine are taken into account. However, the attempt to take into account all the factors involved in the complicated synchronization process in compound excited motors in general would have no practical significance, because of the immensity of the task. Thus, for a start, calculations were made to elucidate the magnitude of the effects of various factors on the synchronization process, so as to decide which factors could be neglected. The conclusions reached were checked by experiment. As a result of the preliminary calculations and experimental work it was established that one could ignore the saturation of the machine and the presence of valves in the rotor circuit, since the test showed that in the compound excitation circuit the rotor current does not change direction during synchronization. The transient process on switching the motor on to the rectifier was also ignored. The effect of the remaining factors was accounted for as follows.

The relationship between the damping coefficient and the angle of rotor lag and slip was taken in accordance with the Zhdanov formula [7]:

$$D = U^2 \left[\frac{x_d - x'_d}{x_d x'_d} \cdot \frac{T'_d}{1 + (yT'_d)^2} \sin^2 \delta + \right.$$
$$+ \frac{x'_d - x''_d}{x'_d x''_d} \cdot \frac{T''_d}{1 + (yT''_d)^2} \sin^2 \delta + \qquad (3)$$
$$\left. + \frac{x - x''_q}{x_q x''_q} \cdot \frac{T''_q}{1 + (yT''_q)^2} \cos^2 \delta \right].$$

The electrical torque P_e of the machine was determined as the sum of three terms taking into account the reactive moment of the machine, the effect of currents induced in the rotor winding, and the synchronous moment (allowing for the active resistance of the stator) respectively; thus:

$$P_{e1} = U^2 \frac{x_d - x_q}{x_d x_q} \sin 2\delta; \qquad (4)$$

$$P_{e2} = -\frac{U^2}{2} \cdot \frac{x_d - x'_d}{x_d x'_d} \cdot \frac{(yT'_d)^2}{1 + (yT'_d)^2} \sin 2\delta; \qquad (5)$$

$$P_{e3} = \frac{E_d^2}{\sqrt{r^2 + x_d^2}} \sin \alpha + \frac{E_d U}{\sqrt{r^2 + x_d^2}} \sin (\delta - \alpha), \qquad (6)$$

where $$\alpha = 90^\circ - \tan^{-1} \frac{x_d}{r}.$$

The existence of a series component of excitation in the circuit of normally-adjusted compound excited motors, with and without regard to the angle of lag of the rotor in respect of the rotor current in relation to the damping cage was correspondingly taken into account by introducing the relationship between the e.m. f. E_d and the angle δ:

$$E_d = \frac{1}{2} [(1 + n) + (1 - n) \cos \delta] U; \qquad (7)$$

$$E_d = \frac{1}{2} \left[(1 + n) + (1 - n) \frac{\cos (\varphi + \delta)}{\sqrt{1 + (yT''_d)^2}} \right] U, \qquad (8)$$

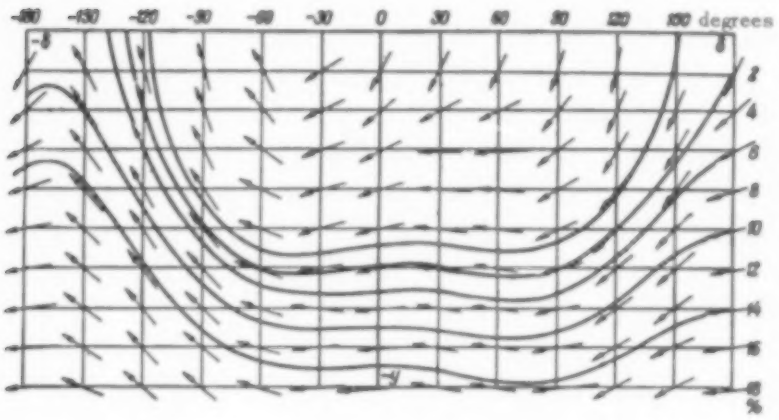

FIG. 1. Trajectories of rotor motion, calculated by the co-ordinate grid method for a motor of the following parameters:- $x = 1.6$; $\kappa'_d = 0.312$; $\kappa_q = 0.95$; $M = 1.27$ sec; $T'_d = 0.08$ sec.

Where n – is the ratio of the growth of e.m.f. E_d to the series component of excitation, as angle δ varies from 0 to π:

$$\psi = \cos^{-1} \frac{1}{\sqrt{1+(yT''_d)^2}}.$$

The value of n is determined by the compounding coefficient K and the synchronous reactance x_d:

$$n = \frac{x_d + k}{x_d - k}.$$

From equations (3) to (8) it follows that the expression for tan α can be written as a sum of the form:

$$\tan \alpha = \Sigma F_1(y) F_2(\delta),$$

where $F_2(\delta)$ are simple trigonometric functions.

Values of $F(y)$, calculated for any y value whatever, remain invariant as angle δ varies; these calculations are thus not laborious and can be completed in a short time.

From a comparison of rotor motion trajectories calculated for a series of cases, it could be established that lag in the change of magnetic flux in the rotor, relative to the change of excitation current due to the present of compounding, had an adverse effect on the conditions of synchronization of the machine, since it is equivalent to negative damping. This deduction was confirmed by experimental

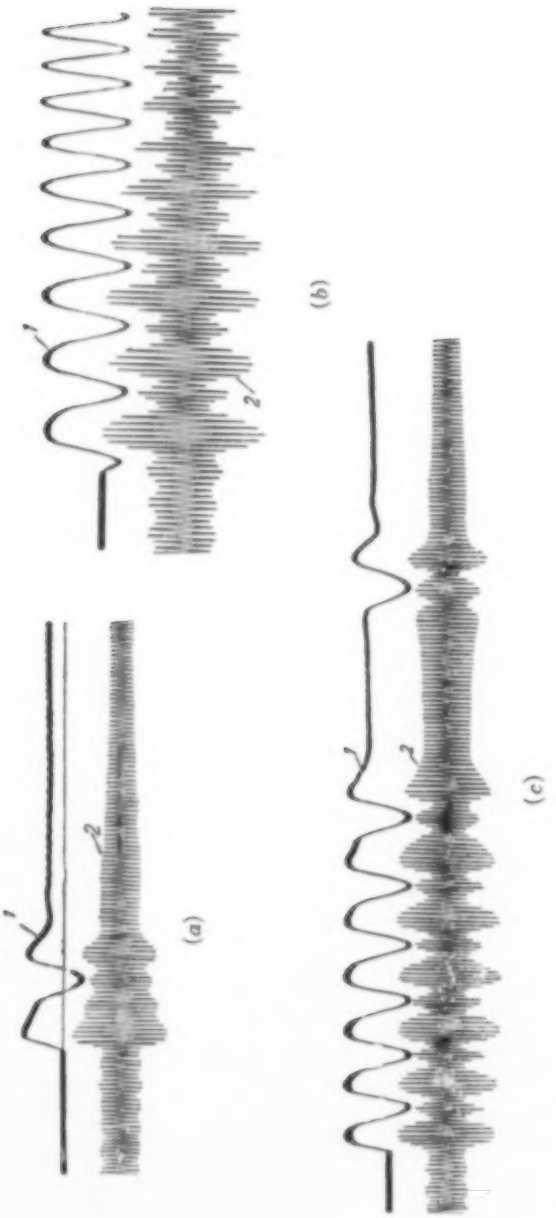

FIG. 2. Oscillograms of synchronization of type SG – 4.5 motor:
1 – rotor current; 2 – stator current.
Rotor current: (a) 6.0 A; (b) 7.0 A; (c) 8.1 A.

1958

tests which showed that, in the presence of compounding, a machine which falls out of synchronism is very rapidly retarded almost to a standstill, whereas with constant excitation it either pulls itself back periodically into synchronism or rotates asynchronously with a small amount of slipping.

Synchronization conditions are also adversely affected by active resistance in the stator circuit, and if the latter is considerable, there is an optimum level of excitation for synchronization of the machine.

The existence of an optimum level of excitation is confirmed by the oscillographs shown in Fig. 2. The motor gets back into synchronism in the very first cycle of oscillation (Fig. 2a), at a certain value of excitation current. At a lower excitation current the motor does not get into synchronism. As the excitation current is increased the synchronization time is extended (Fig. 2b), and at a still higher excitation current, synchronization is not achieved (Fig. 2c).

The effect of the active stator resistance on the synchronization process of the machine and the optimum excitation level can also be established analytically. Let the excitation (non-compounded) of the machine operate in a stable asynchonous condition. In this case the sum of the mean values of electromagnetic torques acting on the rotor must equal the torque due to the shaft load. The mean value of the torque P_e is:-

$$P_{e.m} = \frac{E_d^2}{\sqrt{r^2 + x_d^2}} \sin \alpha,$$

and the torque at the motor shaft is:

$$P_0 = D_m s - \frac{E_d^2}{\sqrt{r^2 + x_d^2}} \sin \alpha,$$

where s is the slipping in the machine:

$$\sqrt{r^2 + x_d^2} = Z_{11}.$$

The critical slipping, at which the machine will synchronize itself, is found from the well known Edgerton formula [8]:

$$s_{cr} = \frac{245}{n_c} \sqrt{\frac{P_{max}}{fGD^2}},$$

where n_c is the synchronous speed of the motor;
$P_{max} = UE_d/x_d$ is the maximum motor power output;
GD^2 is the moment of gyration of the motor;

f is the frequency.

Substituting the value of critical slipping in the formula, we obtain the limiting power output for conditions of synchronization at the shaft of a synchronous motor (non-compounded), taking into account the effect of its active resitance:

$$P_{synred} = \frac{245}{n} D_{mp} \sqrt{\frac{UE_d}{x_d \sum GD^2}} - \frac{E_d^2}{\sqrt{r^2 + x_d^2}} \sin \alpha. \qquad (9)$$

Equating to zero the differential of this expression (with respect to E_d) and bearing in mind that $\sin \alpha = r/x_d$ we find that the maximum load torque at which synchronization is still possible will be for the value of E_d equal to

$$E_d = \sqrt[3]{\left(\frac{245 D_{mp}}{4 n_c R}\right)^2 \frac{U x_d}{\sum GD^2}}$$

On the basis of the work carried out it must be concluded that compounded synchronous motors should be synchronized with the compounding switched out. This eliminates the "negative damping" effect and reduces the active resistance of the machine. If a compound excited motor is synchronized with the compounding in action (which simplifies the starting device), then, as the phase-plane studies and the experimental tests have shown, in this case, to determine the limiting load torque for synchronization, it is also possible to use the Edgerton formula to find the correct level of compounding, accepting references [1, 2] to the effect that

$$P_{max} = \frac{U_2}{4a} - b,$$

where a and b are coefficients defining the loss ΔP in the motor, as a function in the motor, as a function of the current I, according to the formula $\Delta P = I^2 + b$.

This deduction has been checked experimentally and shows good agreement with experiments. Thus, a 3.6 kW motor, designed on the basis of an SG-4.5 generator, came into synchronism at 70 per cent nominal load. In this case the maximum load torque found from formula (9), at which the motor can still be synchronized, is 66 per cent of nominal. An 11.8 kW motor, designed on the basis of an MSA-72/4 generator, synchronized at 68 per cent of nominal loss, and the calculation from formula (9) gives the same value of the torque, namely 68 per cent.

Translated by E. Bishop

1958

1. V.L. Inosov and V.E. Krutikova; A Synchronous compound excited motor, *Elektrichestvo*, No. 6 (1956).
2. V.L. Inosov; A synchronous compound excited motor and the theory of its operation, *Sborn. trud. inst. elektrotekh. Akad. Nauk SSSR*, 14 (1956).
3. A.A. Andronov and S.E. Khaikin; *Teoriia kolebanii (Theory of oscillation)*, United Scientific and Technical Press (1937).
4. K.M. Polivanov; *Fizicheskie osnovy elektrotekhniki (Physical principles of electrotechnology)* (1950).
5. V.L. Inosov and V.E. Krutikova; A study of the synchronization conditions of excited generators, brought asynchronously into circuit, *Sborn. trud. inst. elektrotekh. Akad. Nauk SSSR*, 13 (1956).
6. Dzh. Stoker; *Nelineinye Kolebaniia v mekhanicheskykh i elektricheskikh sistemakh (Non-linear oscillations in mechanical and electrical systems)* Izdatel'stvo inostrannoi lit., Moscow (1953).
7. P.S. Zhdanov; Synchronization of machines after disturbances of stability. *Elektrichestvo* No. 6 (1934).
8. H.E. Edgerton and P. Fourmarier; Synchronization of open-pole motors, *Elect. Engng.* (1932).

THE PERFORMANCE OF CURRENT-MEASURING TRANSFORMERS UNDER INCREASED POWER OUTPUT CONDITIONS *

V.S. BURTAKOV and M.I. GLAZOV
Moscow Power Institute

(Received 8 October 1957)

In the operation of protective relay circuits, at a variable actuating current, the current transformers operate with high load resistances under conditions which differ markedly from normal, since the circuit-breaker cut-out coils and the rapid-saturation transformers are usually connected to their secondary coils. The inductances in the current transformer cores under such conditions are not hundreds of gauss, as under normal conditions, but reach 15 to 25 kG. Thus, the current transformer cores are highly saturated and the magnetization current is sharply increased, resulting in a noticeable drop in the secondary current, i.e. in an increased error. This refers particularly to built-in current transformers with small transformation ratios. Reduction of the secondary current also results in a relative reduction of the power output of the transformer.

The power output of a current transformer depends on both the value of the current passing through the transformer and the value of the load resistance. For each current value a load resistance can be found which corresponds to maximum transformer power output. In particular, at currents of the order of the nominal rating, this maximum occurs at load resistances of the order of 1 Ω.

In cases when the cut-out coils of the circuit-breakers are connected in series with the relay (on the main cores of the current transformers), it is necessary, for calculation of the relay setting, to know the transformer errors when their power output is near maximum. These errors must also be known in the design of circuits with rapid-saturation current transformers, which are in the open circuit condition and thus have high resistances at the instant when the relay operates.

The present paper considers the stabilizing conditions of current transformer operation and the conclusions which are of value in the calculation of protective circuits with an operation time which is sufficient for attenuation of the transient process in the current transformer.

* *Elektrichestvo* No. 2, 59-61, 1958 [Reprint Order No. EL 54].

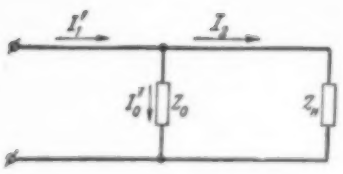

FIG. 1. Simplified equivalent circuit for current transformer.

A current transformer can be replaced by an equivalent non-linear resistance Z_0 (Fig.1), the value of which is determined so as to correspond to the dynamic magnetization curve. The source of supply to the current transformer can be regarded as a source of infinite power and the secondary winding resistance can be ignored, since in circuits on operative a.c. it is much smaller than the load resistance.

In the calculations, errors in the current transformer angle are usually ignored, since, as experiments show, with the normal inductive load on protective relay circuits this error is small. Curves of power output against load resistance are constructed for various values of primary current. From these results are found the maximum values of power output for the transformer, and the optimum load resistances and errors corresponding to these outputs.

If the magnetic flux in the transformer is sinusoidal, the transformer power output can be expressed mathematically by the following relationship:-

$$S = U_2 I_2 \equiv B H_2, \tag{1}$$

where $B \equiv U_2$ is the amplitude value of the inductance, found from the dynamic magnetization curve;

$H_2 = \frac{I_2 w_2}{l_m}$ is the partial secondary magnetic field intensity (w_2 is the number of turns in the secondary coil; L_m is the mean length of the magnetic path).

We denote the partial primary magnetic field intensity by the value

$$H_1 = \frac{I_1 w_1}{l_m},$$

where w is the number of turns in the primary winding of the current transformer.

Since
$$H_2 = H_1 - H_0, \tag{2}$$

we find that the power output S to the load is proportional to the shaded rectangular area in Fig. 2.

It can be seen from Fig. 2 that for a fixed value of primary intensity H_1, as the inductance increases, the power output of the transformer first increases and then falls, reaching zero at $H_0 = H_1$.

The maximum power output value is found from the condition:-

$$\frac{dS}{dH_0} = 0.$$

Taking (1) and (2) into account, we obtain

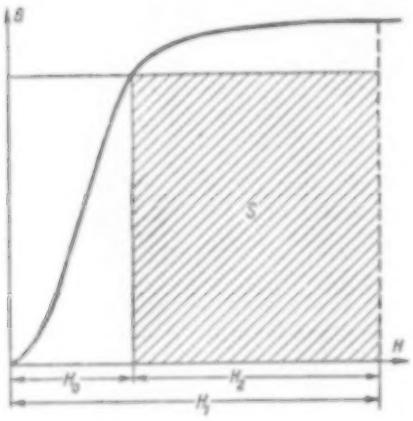

FIG. 2.

$$\frac{dB}{dH_0}(H_1 - H_0) - B = 0. \tag{3}$$

Introducing the following rotations:-

$\mu_\partial = \frac{dB}{dH_0}$ the differential magnetic permeability;

$\mu_n = \frac{B}{H_0}$ the nominal magnetic permeability,

we find the optimum value of intensity H_0 corresponding to maximum power output at a given value of H_1:

$$H_{0.\text{opt}} = \frac{1}{1 + \frac{\mu_{H.\text{opt}}}{\mu_{\delta\,\text{opt}}}} H_1, \tag{4}$$

where $\mu_{H\,\text{opt}}$ and $\mu_{\delta\,\text{opt}}$ are the magnetic permeabilities

for $H_0 = H_{0\cdot\text{opt}}$

To construct this relationship (Fig. 3) it is necessary to postulate $H_{0\cdot\text{opt}}$ values, to find on the magnetization curve the corresponding values of $\mu_{H.\text{opt}}$ and $\mu_{\delta\,\text{opt}}$ and to calculate the value of H_1.

It can be shown that the optimum load resistance is proportional to the tangent of the angle of slope of the tangent to the magnetization curve at the point corresponding to maximum S. Actually, from equation (3), we can obtain:

$$\frac{dB}{dH_0} = \frac{B}{H_2} \equiv \frac{U_2}{I_2} = z_2. \tag{5}$$

The error of a current transformer at maximum power output can be found

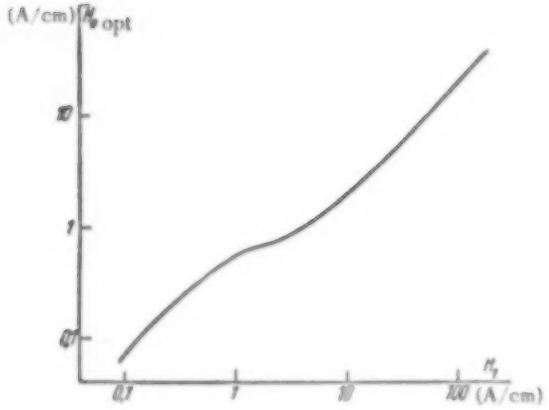

FIG. 3. Relationship between $H_{0.opt}$ and H_1 for a type TPF-10 current transformer (core 0.5).

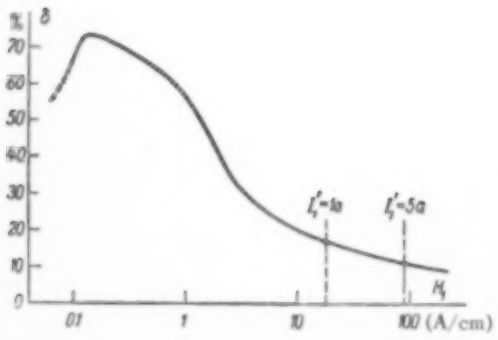

FIG. 4. Error of type TPF-10 current transformer (core 0.5), under maximum power output conditions.

from formula (4), taking into account the fact that the ratio of the currents shown is equal to the ratio of the corresponding intensities:-

$$\delta^0/_0 = \frac{100}{1 + \frac{\mu_{H.opt}}{\mu_{\delta opt}}}.$$

The character of the relationships between $\mu_{H.opt.}$, $\mu_{\delta \cdot opt}$ and the intensity H_1 is determined by the relationship $\delta = f(H_1)$. In the initial part of the magnetization curve $\mu_{\delta opt.}$ increases more rapidly than $\mu_{H.opt.}$ and therefore as H_1 increases the transformer error increases (Fig. 4). The maximum error (δ = 60 - 70 per cent) corresponds to the part of the magnetization curve which can be normally replaced by a parabola (B = 10 to $10^3 G$). When the field strength is increased further, $\mu_{\delta opt.}$ increases more slowly than $\mu_{H.opt.}$ and correspondingly δ starts to fall. Reduction of the error continues also after passing the $\mu_{\delta opt.}$ and $\mu_{H opt.}$ maxima, since $\mu_{\delta opt.}$ falls more rapidly than $\mu_{H.opt.}$ At high values of intensity the error increase again (not shown in Fig. 3), reaching 50 per cent in the limit.

Current transformers in protective relay circuits on operative a.c. operate

within definite limits of inductance value. At currents near the nominal rating the inductances under maximum power output conditions have values of the order of 10^4G and the errors for various transformer designs are within the range of 20 to 30 per cent. At high currents, the errors under maximum power output conditions fall to 10 per cent. The inductances to which corresponds the subsequent increase in errors up to 50 per cent are considerably in excess of the inductance values at which current transformers operate.

Thus the previous opinion, regarding the high values (of the order of 50 per cent and more) of the errors of current transformers operating under maximum power output conditions, must be regarded as incorrect.

Translated by E. Bishop

1958

A STUDY OF THE EFFECT OF NOZZLE PARAMETERS ON ARC EXTINGUISHING BY A COMPRESSED AIR JET *

R.A. MIKAELIAN

(Lenin All-Union Electro-technology Institute)

(Received 1 March 1957)

The present paper gives results obtained in an experimental investigation of arc-extinguishing nozzles of various designs made from insulating and conducting materials. In order to obtain a clearer picture of the characteristics of various arc-extinguishing jets, these investigations were carried out in a model arc-extinguishing chamber with a lateral blast.

The chamber contained 0.2 g of air compressed to 1.5 atm. Air from the chamber flowed through the nozzle for a period of 0.016 sec. The diameters of the fixed and moving arc-extinguishing contacts were 16 and 10 mm, respectively. The contacts were of copper. The value of the restoring voltage (effective value) at the opened circuit-breaker contacts was 6 kV. The frequency of self-oscillation in the short-circuit loop was 20,000 c/s.

It was established experimentally that the relationships obtained on the model between the nozzle parameters and the magnitude of the current which can be broken can be increased proportionately and thus extended to actual circuit-breakers.

Comparison of nozzles made from ceramic materials showed that "cardioride" nozzles were the most arc-resistant. During repeat experiments the working surface of this nozzle became gradually coated with a vitreous conducting mass. After approximately fifty breaks at a current of 400 A, the nozzle cracked and ceased extinguishing the arc. Nozzles made from other ceramic materials could only break the circuit for a smaller number of times.

Marble nozzles survived fourteen to sixteen breaks at a current of 400 A after which arc-extinguishing capacity was rapidly lost.

When nozzles were made of conducting materials it was found impossible to carry out more than six or seven breaks, after which the working surface of the nozzle built up, preventing the moving contact from passing into the nozzle any longer.

* *Elektrichestvo* No. 2, 61-63, 1958 [Reprint Order No. EL 55].

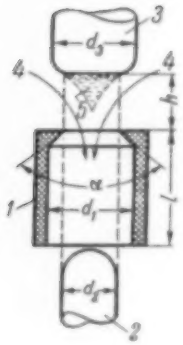

FIG. 1. Plexiglas nozzle of optimum arc-extinguishing capacity.
1. nozzle;
2. moving contact;
3. fixed contact;
4. direction of compressed air flow;
5. stagnant region.

1958

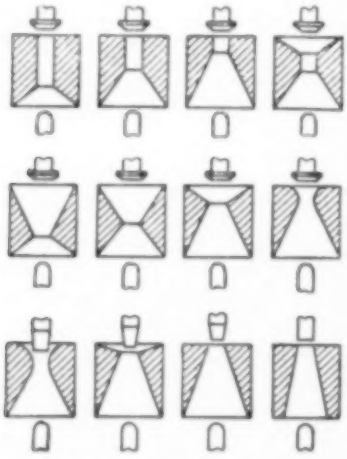

FIG. 2. Plexiglas nozzles, studied for arc-extinguishing capacity.

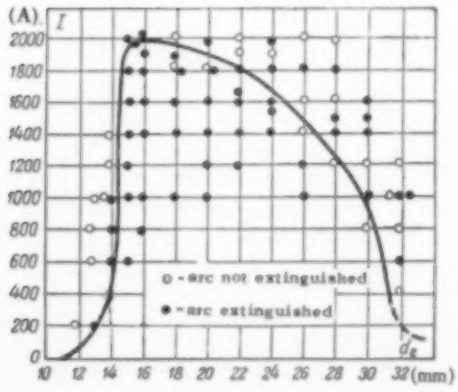

FIG. 3. Relationship between current which can be broken and internal diameter of cylindrical section of nozzle. (open circles – arc not extinguished) (black circles – arc extinguished)

Nozzles made from materials which evolve gases under the influence of the high arc temperature wore out after twenty to thirty breaks at a 400 A current, with a large amount of soot deposit.

Nozzles as shown in Fig. 1 were found to be very durable. A nozzle of this type made of plexiglass has a considerably greater arc-extinguishing capacity than other nozzles investigated (Fig. 2), which were made of more heat-resistant materials than plexiglass.

The basic parameters of nozzles (Fig. 1) are: the angle α of the conical funnel, the internal diameter d_1 of the cylindrical section of the nozzle funnel, the radius of curvature r of the nozzle edge and the position of the fixed contact above the nozzle. We shall consider each of these parameters individually.

It was established experimentally that the most successful arc extinction takes place in the case when at the very start of extinction the air flow is determined by the area of the nozzle opening and not by the area of the annular gap between the moving contact and the nozzle. To ensure this condition it is essential for the angle of the conical section of the nozzle to have the maximum possible value. In order to avoid mechanical breakdown of the tip the angle taken was $\alpha = 120°$. If nozzles are made from mechanically stronger material, this angle can be increased.

The internal diameter of the cylindrical section of the nozzle is selected in such a way that the area of the annular section between the moving contact and the inner nozzle wall is not less than that of the nozzle exit opening. This condition follows directly from the experimental curve shown in Fig. 3. The curve shows that the maximum value of the current which can be broken at a nozzle exit opening diameter of 10.5 mm is reached when the internal diameter of the cylindrical section of the nozzle is 16 mm. As this diameter is reduced, the arc-extinguishing capacity of the nozzle falls sharply. Increase of the internal diameter of the cylindrical section of the nozzle beyond 16 mm has comparatively little effect on the arc-extinguishing capacity.

The radius of curvature of the nozzle tip has a substantial influence on the magnitude of the current which can be broken. The results of tests with varying radii of curvature in the range from $r = 0$ to $r = 5$ mm, at a constant value of 16 mm for the internal diameter in the cylindrical portion of the nozzle, are shown in Fig. 4.

This relationship, showing that as the radius of curvature of the nozzle tip is reduced the arc-extinguishing capacity is improved, does not agree with the results of investigations by a number of other authors. In particular it has been shown that the breaking power of a nozzle which is good from a streamlining point of view and free from eddying is better than that of a nozzle with sharp edges [1].

It might be supposed that a nozzle with sharpened edges could not undergo any large number of breaks, since the edge sharpness will reduce the already low

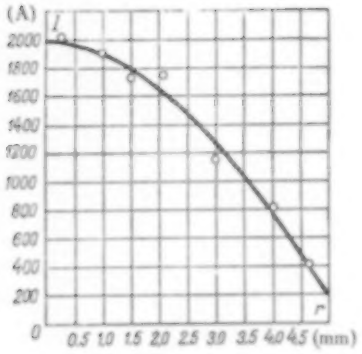

FIG. 4. Relationship between current which can be broken and radius of curvature of nozzle edge.

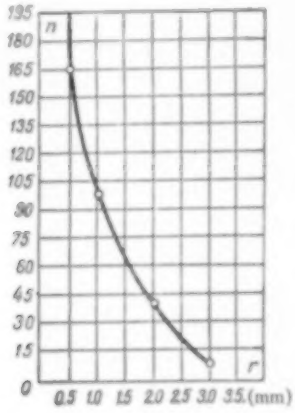

FIG. 5. Relationship between number of successful breaks at a current of 1 kA and radius of curvature of nozzle edge.

heat resistance of the nozzle material, (the decomposition temperature of plexiglass is about 150°C). However, experiments did not confirm this supposition, as Fig. 5 shows: as the radius of curvature of the edge is increased, the number of successful breaks is reduced.

The nozzle shown in Fig. 1 was able to break currents at short circuit values of the order of 4 kA (Fig. 6). The high arc resistance of a nozzle with sharp edges can be explained on the grounds of the formation of air eddies which, encircling the sharp edge, protect the latter from destruction by the incandescent arc gases. The positive effect of sharp nozzle edges on the magnitude of the current which can be broken may also be explained by the tearing from them of streams of cold air into the arc column which must substantially increase the intensity of the cooling effect.

On the basis of the results presented, it can be confirmed that improvement in the arc-extinguishing properties of nozzles made from insulating materials and extension of their service life can be obtained by using nozzles with sharp edges.

A relationship was also found by experiment, between the magnitude of the current which can be broken and the distance between the fixed contact and the nozzle. The maximum current-breaking value corresponds to the optimum distance $h_{opt.} = 2.7$ mm.

In this case the area of the nozzle exhaust opening $f_1 = \pi d_2^2/4$, and the area of the cylindrical surface $f_2 = \pi d_2 h$, through which the air enters the nozzle, are equal. Here, it is assumed that the area of the annular section $f_3 = (\pi/4)(d_1^2 - d_2^2)$ exceeds both these values.

If the distance between the fixed contact and the jet is below the optimum, then f_2 is the critical area. Since in this case $f_2 < f_1$, the air flow through the

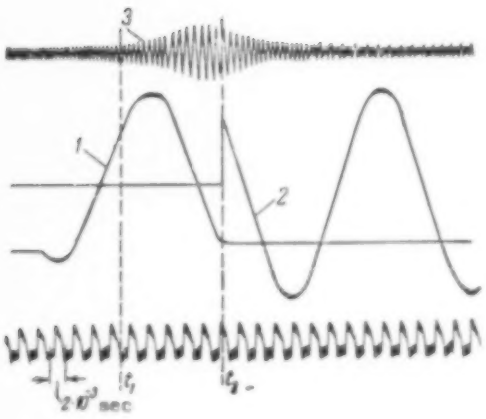

FIG. 6. Oscillagraph of current-breaking, using nozzle with sharp edges.
1. current (I = 4.2 kA);
2. voltage at circuit breaker contacts (U = 6 kV);
3. air pressure in chamber (P_{max} = 1.4 atm). 2 x 10^{-3} sec

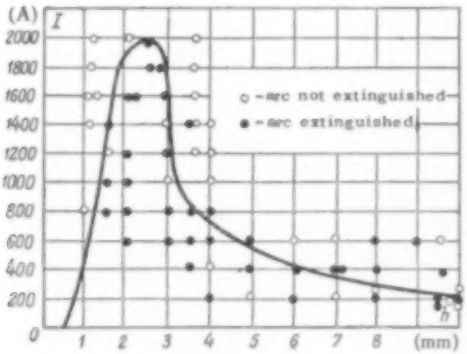

FIG. 7. Relationship between current which can be broken and distance between fixed contact and nozzle.

nozzle is reduced, lowering the value of current which can be broken (Fig. 7).

If the distance is increased beyond the optimum, f_1 becomes the critical area. This results in a fall in the radial component of the air stream velocity and so in a reduction in the penetration of cold air particles into the arc column. As a result, the arc is less intensely cooled. Moreover, in this case, there is a considerable increase in the "stagnant" region of incandescent gases (Fig. 1), which reduces the electric strength between the contacts.

This work was carried out under the direction of Prof. G.V. Butkevich, to whom the author extends his sincere thanks.

Translated by E. Bishop

REFERENCES

1. O. Mayr; *Hohe-leistungschalter ohne Öl*, *ETZ*, No. 31, 759 (1934).